

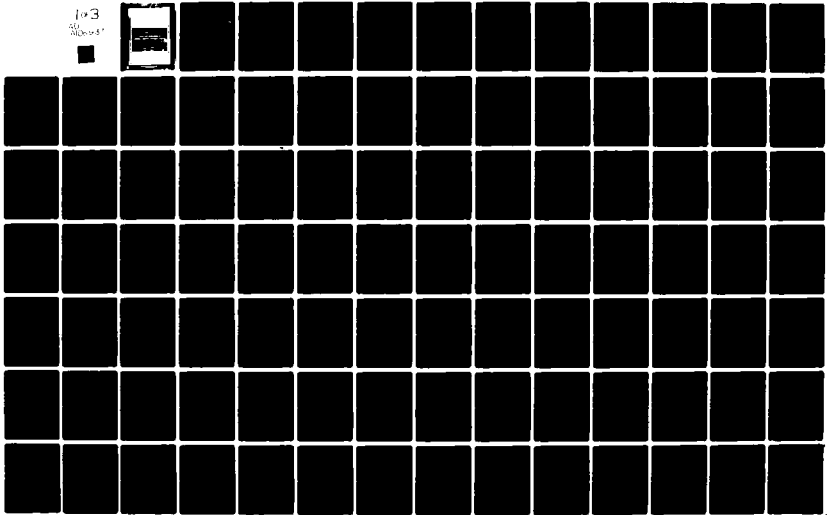
AD-A106 937

ADVISORY GROUP FOR AEROSPACE RESEARCH AND DEVELOPMENT--ETC F/G 1/4
THEORY AND APPLICATIONS OF OPTIMAL CONTROL IN AEROSPACE SYSTEMS--ETC(U)
JUL 81 P KANT
AGARD-AG-251

UNCLASSIFIED

NL

103
5/1/81



LEVEL

AGARD-AG

AD A106937

AGARDograph No. 28

Theory and Applications of Optimal Control in Aerospace Systems

INFORMATION STATEMENT
Approved for Public Release
Distribution Unlimited

DTIC
SELECTED
NOV 1 0 1967

FILE

EXTENT AND AVAILABILITY
OF THIS COVER

NORTH ATLANTIC TREATY ORGANIZATION
ADVISORY GROUP FOR AEROSPACE RESEARCH AND DEVELOPMENT
(ORGANISATION DU TRAITE DE L'ATLANTIQUE NORD)

DTIC
UNCLASSIFIED
NOV 10 1981

14/ AGARDograph No. 251

6

**THEORY AND APPLICATIONS OF OPTIMAL CONTROL
IN AEROSPACE SYSTEMS**

Edited by

10
Dr Pieter/Kant

Head of Space Department
National Aerospace Laboratory
Postbus 153
8300 AD Emmeloord
The Netherlands

11/3 81

THE MISSION OF AGARD

The mission of AGARD is to bring together the leading personalities of the NATO nations in the fields of science and technology relating to aerospace for the following purposes:

- Exchanging of scientific and technical information;
- Continuously stimulating advances in the aerospace sciences relevant to strengthening the common defence posture;
- Improving the co-operation among member nations in aerospace research and development;
- Providing scientific and technical advice and assistance to the North Atlantic Military Committee in the field of aerospace research and development;
- Rendering scientific and technical assistance, as requested, to other NATO bodies and to member nations in connection with research and development problems in the aerospace field;
- Providing assistance to member nations for the purpose of increasing their scientific and technical potential;
- Recommending effective ways for the member nations to use their research and development capabilities for the common benefit of the NATO community.

The highest authority within AGARD is the National Delegates Board consisting of officially appointed senior representatives from each member nation. The mission of AGARD is carried out through the Panels which are composed of experts appointed by the National Delegates, the Consultant and Exchange Programme and the Aerospace Applications Studies Programme. The results of AGARD work are reported to the member nations and the NATO Authorities through the AGARD series of publications of which this is one.

Participation in AGARD activities is by invitation only and is normally limited to citizens of the NATO nations.

The content of this publication has been reproduced directly from material supplied by AGARD or the authors.

Published July 1981

Copyright © AGARD 1981
All Rights Reserved

ISBN 92-835-1391-6



Printed by Technical Editing and Reproduction Ltd
Herford House, 7-9 Charlotte St, London, W1P 1HD

PREFACE

Modern control theory has for a long time been largely the domain of mathematicians and control theoreticians. Engineering applications were rare and partial, for a part due to the inaccessibility of the theory to the practical engineer, but mainly because of the lack of computing power available to process the estimation and control algorithms resulting from the theory. In the course of the sixties and especially in the seventies the digital computer made enormous advances resulting in a reduction in size, power and cost by several magnitudes. Moreover, successful attempts were made to develop efficient algorithms which could be implemented in moderate-size onboard computers.

As a result of these developments, realisation of the potential benefits of modern control has come within grasp and several applications in the aerospace field can be witnessed to-day.

The present Agardograph is an attempt to present a picture of the advances in modern control as applied to aerospace system design. The Agardograph is divided into three parts. Part one deals with some basic concepts of control theory, part two contains a number of chapters on practical design techniques developed from the theory, and finally part three describes a number of design examples and practical applications in real systems.

The editor wishes to thank all contributors to this Agardograph for their efforts and patience when changes to the original manuscripts were required. The assistance and encouragement of his colleagues and the executive staff of the AGARD Guidance and Control Panel are greatly appreciated. They were of great help in the lengthy process of soliciting the contributions and compiling the publication.

IR. PIETER KANT

Accession For	
NTIS Grant	<input checked="" type="checkbox"/>
DTIC TAB	<input type="checkbox"/>
Unannounced	<input type="checkbox"/>
Justification	<input type="checkbox"/>
By _____	
Distribution/	
Availability Codes	
Avail and/or	
Special	
A	

CONTENTS

	Page
PREFACE by Ir. P.Kant	iii
	Reference
<u>PART I – THEORY</u>	
AN OVERVIEW OF OPTIMAL CONTROL IN AEROSPACE SYSTEMS by A.E.Bryson, Jr.	1
THEORY OF STOCHASTIC OPTIMAL CONTROL – SOME BASIC NOTIONS by G.Campion	2
AN INTRODUCTION TO STOCHASTIC OPTIMAL CONTROL THEORY by R.F.Stengel	3
<u>PART II – DESIGN TECHNIQUES</u>	
DESIGN CONSIDERATIONS FOR OPTIMAL FLIGHT CONTROL SYSTEMS by F.R.Gill	4
DESIGN TECHNIQUES FOR MULTIVARIABLE FLIGHT CONTROL SYSTEMS by C.A.Harvey and R.E.Pope	5
PRACTICAL DESIGN AND REALIZATION OF A DIGITAL ADAPTIVE FLIGHT CONTROL SYSTEM by V.Krebs and U.Hartmann	6
CONTROL LAW DESIGN FOR TRANSPORT AIRCRAFT FLIGHT TASKS by V.Adam and H.Leyendecker	7
CONTROL DESIGN OF FLEXIBLE SPACECRAFT by R.E.Skelton	8
<u>PART III – APPLICATIONS</u>	
OPTIMUM CLIMB AND DESCENT TRAJECTORIES FOR AIRLINE MISSIONS by H.Erzberger	9
APPLICATION OF NONLINEAR SYSTEMS INVERSES TO AUTOMATIC FLIGHT CONTROL DESIGN – SYSTEM CONCEPTS AND FLIGHT EVALUATIONS by G.Meyer and L.Cicolani	10
MANAGEMENT OF REDUNDANCY IN FLIGHT CONTROL SYSTEMS USING OPTIMAL DECISION THEORY by R.C.Montgomery	11
OPTIMAL CONTROL IN THE LUNAR MODULE DIGITAL AUTOPILOT by W.S.Widnall	12
APPLICATION OF OPTIMAL CONTROL TECHNIQUES TO TACTICAL MISSILE GUIDANCE by C.F.Price	13
DEVELOPMENT OF MULTIVARIABLE CONTROLLERS FOR AIRCRAFT TURBINE ENGINES by R.L. De Hoff, S.M.Rock and M.M.Akhter	14

AN OVERVIEW OF OPTIMAL CONTROL IN AEROSPACE SYSTEMS

by
 Arthur E. Bryson, Jr.*
 Stanford University
 Department of Aeronautics and Astronautics
 Stanford, California 94305, USA

1. INTRODUCTION

Optimal control started nearly 300 years ago with Isaac Newton and John Bernoulli when they invented the calculus of variations (COV). The calculus of variations was developed further by Euler and Lagrange in the 18th century, by Hamilton, Jacobi, Weierstrass, and Bolza in the 19th century, and by Bliss, Caratheodory, McShane, Bellman, Pontryagin, and others in this century. However, it was the digital computer in the 1950's that made the calculus of variations a practical tool for synthesis of optimal control logic. Optimal control concepts and algorithms are now used not only in the field of automatic control but also in fields of structural optimization, econometrics, and operations research.

2. AREAS OF APPLICATION IN AEROSPACE SYSTEMS

For convenience, we divide the areas of application of optimal control in aerospace guidance and control into four categories:

- Performance,
- Navigation,
- Guidance, and
- Control.

2.1 Performance

Aerospace designers are always concerned with getting optimal performance from their vehicles. Optimization of flight paths is a direct extension of Bernoulli's brachistochrone ("shortest time") problem.

One of the earliest optimal flight path problems was stated by Hohman (Ref. 1) in the 1920's. He also gave the solution, namely that a minimum fuel transfer between two circular orbits is obtained by applying thrust impulses at the periapsis points of a tangent elliptical orbit. Also, in the 1920's Goddard (Ref. 2) formulated the sounding rocket problem, which was partly solved by Hamel (Ref. 3), and more completely by Tsien and Evans (Ref. 4). They showed that minimum fuel for a given final altitude is obtained by using a thrust impulse that brings the rocket up to a velocity where thrust approximately equals drag plus weight, followed by a slowly changing thrust period, and then a coasting period. In the late 1940's Hestenes (Ref. 5), at the Rand Corporation, discussed the application of the COV to the problem of maximum airplane range. In 1957, Bellman introduced the concept of "dynamic programming", a feedback view of the COV, that really started the modern developments in optimal control (Ref. 6). In the late 1950's, Okhotsimskii and Eneev (Ref. 7) and Breakwell (Ref. 8) gave digital computer solutions to the problem of minimum fuel rocket trajectories from the earth's surface to orbit injection. In 1960, Kelley introduced the idea of a gradient algorithm for numerical solution of COV problems (Ref. 9). In 1962, digital computer solutions, using a gradient algorithm, were given for minimum time-to-climb flight paths for a supersonic airplane with terminal constraints on velocity and flight path angle (Ref. 10). Also, in 1962, the first book on applications of optimal control to aerospace problems appeared, edited by Leitmann (Ref. 11). It was followed in 1963 by Lawden's book (Ref. 12) on optimal space trajectories.

In the years since then, the design of algorithms has become a challenging field of intellectual endeavor (Ref. 13). As a result, optimization algorithms have been greatly improved so that synthesis of optimal flight paths for spacecraft, boosters, and aircraft is nearly routine in government and in industry. One of the interesting recent contributions is by Erzberger (Ref. 14) who demonstrates an algorithm for on-board determination of the flight path of an airplane to minimize "direct operating cost", a linear combination of fuel and time of flight. This algorithm will be used in the flight control computer of the Boeing 767 (See also Part III, Chapter 1 of this Agardograph).

2.2 Navigation

Optimal navigation merges concepts from the calculus of variations with those from statistics and random processes.

Navigation is the science of estimating the position of a vehicle from observations of celestial objects, objects in the vicinity, and from observations of velocity and acceleration. A navigation "fix" is made when the number of observations is equal to the number of unknowns; e.g., two star sightings from a ship determine its latitude and longitude. If more observations are made, the position is "over-determined" and some form of data-weighting must be used to arrive at a best estimate of position. Gauss introduced the idea of "least-square fits" in the 19th century and showed how observations could be used recursively to update the six elements in the ephemeris of a planet or the moon (Ref. 15). The concepts of random processes were developed in this century by Einstein, Markov, Kolmogorov, Wiener, Kalman, and many others (Ref. 16).

Wiener, in particular, extended the idea of minimizing a finite sum of squared errors

with static constraints to the minimization of an integral of squared errors with dynamic constraints, using the concept of continuous white noise (Ref. 17). This minimization is a calculus of variations problem, and in 1961 Kalman and Bucy (Ref. 18) gave an elegant recursive solution to it (the Kalman-Bucy Filter, or KBF) for the case where the dynamic constraints can be written as a set of first order coupled ordinary differential equations. This filter concept, combined with cheap reliable digital computers, has had an enormous impact on aerospace navigation, guidance, and control. For navigation it permits the combination of all kinds of continuous and/or discrete observations to give a continuous best estimate of position and velocity.

The basic inertial navigation scheme uses an ad hoc concept developed by Schuler that is quite similar to the more general concept used in the KBF. Measured specific force components are combined with calculated components of gravitational force and kinematics to estimate velocity and position. When an inertial measurement unit (IMU) is aligned or updated using other observations of velocity and/or position, this is done rationally and conveniently using a KBF (see e.g. Ref. 19).

One problem in the use of KBF's in aerospace systems has been "divergence" which appears to be caused primarily by unmodeled process noise so that the filter gains become too small. Some methods of preventing divergence are discussed later in this paper and in (Ref. 20).

2.3 Guidance

Guidance may be regarded as a feedback version of performance. As such it combines navigation (to estimate present position and velocity) with a feedback law for actuating thrusters or aerodynamic control surfaces that accelerate the vehicle in a manner to take it to the desired destination.

Booster guidance to orbit injection is a prime example. Ground radar measurements, supplemented perhaps by an onboard IMU, give position and velocity. A ground computer continuously calculates the present desired pitch angle of the booster to take it efficiently from there to orbit injection. This angle is transmitted to the booster and the onboard control system continuously changes the pitch angle to the desired value. The guidance law used in the ground computer may be developed using optimal control concepts. A neighboring optimum guidance law can be developed in conjunction with the determination of the nominal optimal path, using concepts of the second variation (Ref. 21) or differential dynamic programming (Refs. 22, 23).

Missile guidance to intercept moving targets may be developed using linear-quadratic-gaussian (LQG) techniques, a central part of optimal control theory. For short ranges, it merges with attitude control.

Minimax strategies for missiles and fighters may someday be developed using "differential game" theory, which, at present, are limited due to computer capacity and the complexity of these 3-D problems (Ref. 24).

2.4 Control

Control differs from guidance only in having shorter time scales. Control traditionally has meant attitude control whereas guidance was concerned with translation of the center of mass along a flight path. Thus "guidance" is implemented by "control". Optimal control has all the elements of optimal guidance plus elements of feedback regulator (or servomechanism) theory. In the 19th century, Routh gave the first precise statements on necessary conditions for stability of dynamic systems, but most of feedback regulator technology was developed in this century by Bryant, Sperry, Nyquist, Black, Bode, Wiener, Kalman, and many others.

One of the major triumphs of optimal control is linear-quadratic-gaussian (LQG) synthesis of feedback logic (Refs. 25, 26). A linear-gaussian stochastic model of the system is developed first, then an integral-quadratic performance index is selected. Using methods of the calculus of variations a set of optimal regulator gains and a set of optimal filter (KBF) gains are determined. By feeding back estimated state, an optimal compensator is formed (see e.g. Ref. 27). This technique really comes in to its own for controlling multi-input, multi-output systems. It has been used for attitude and translational control of spacecraft, satellites, aircraft, helicopters, boosters, missiles, remotely-piloted-vehicles, hydrofoils, ships, submarines, etc. There are, however, some things to beware of in using LQG synthesis. We have already mentioned one of the main difficulties, filter divergence, but another is sensitivity to system parameters. If one or more significant parameters in the linear-gaussian stochastic model of the system are uncertain or vary slowly with time it is important to investigate the sensitivity of closed-loop system stability to these parameters (Ref. 28). Methods have been developed for designing feedback control logic that is minimally sensitive to specified parameters. This is discussed below and in reference 29.

Lastly, as space and aircraft structures get larger, elastic deformation and fuel slosh frequencies get lower and creep into the controller bandwidth. Care must be taken not to destabilize these modes with the feedback law (see e.g. Ref. 30). In some instances active damping of these modes may be desirable as in flutter suppression (Ref. 31).

3. DESIGN OF OPTIMAL TIME INVARIANT ESTIMATORS

The optimal estimator for a linear plant excited by gaussian white noise, using measurements containing additive gaussian white noise, is the Kalman-Bucy filter (KBF) of reference 18. It is inherently a time-varying filter, even for a time-invariant plant with time-invariant noise densities (a stationary stochastic system). However, for a stationary system that is observable with the given measurements, the KBF becomes time-invariant in a

short time after initialization. Surprisingly, this steady-state KBF is usually not the best time-invariant estimator for the system. In fact, some of the estimate errors may grow with time, a phenomenon called divergence.

Divergence may be understood for a time-invariant linear system if we think about it in modal co-ordinates. The time-varying filter gain for any stable observable mode that is undisturbed by process noise will asymptotically tend to zero since the estimate-error variance tends to zero. Thus, the steady-state KBF will estimate this mode "open-loop". If this mode is neutrally stable (real part of the eigenvalue equal to zero), the initial estimate-error in the mode will not attenuate if we use only the steady-state KBF. Even if we use the exact time-varying gain, this gain will asymptotically tend to zero and modeling errors (which are inevitable) will soon produce an error in the estimate of this modal co-ordinate. This behaviour is masked in non-modal co-ordinates since (usually) none of the filter gains tends to zero.

One straightforward way to prevent divergence is to ensure that all neutrally-stable and marginally-stable modes are disturbed by the process noise model even if this requires the addition of unrealistic noise terms such as noise in kinematic equations. Another way is to de-stabilize the undisturbed neutrally-stable modes since the gain on an undisturbed, unstable mode does not tend to zero for a KBF. Perhaps the most rational way (but also the most complicated way) is to use a nonlinear programming algorithm to select constant filter gains that minimize the weighted trace of the error-covariance matrix subject to estimate-error eigenvalue constraints (see Ref. 20).

An example (treated in Ref. 20) is a constant-gain filter to estimate the lateral motions of an aircraft using measurements of heading angle (from a magnetic compass) and roll rate (from a roll rate gyro) and only one process noise source, lateral wind gusts. All modes are observable but the heading mode (eigenvalue equal to zero) is completely undisturbed by lateral wind gusts, and the spiral mode (often marginally stable or only slightly unstable) is only slightly disturbed by lateral gusts. The steady-state KBF does not estimate the heading modal co-ordinate at all and the time-constant of the estimate-error decay for the spiral modal co-ordinate may be several minutes. Small changes in the KBF gains will fix this difficulty so that the time-constants for estimate-error decay of these two modes will be only a few tens of seconds while producing only modest increase in the error variances.

4. DESIGN OF OPTIMAL TIME-INVARIANT COMPENSATORS

The optimal compensator (in the sense of minimizing the expected value of a quadratic performance index) for a linear plant excited by gaussian white noise, using measurements containing gaussian white noise is comprised of

a) the KBF which estimates the state variables of the plant, and
 b) feedback of linear combinations of these estimated states to the controls.
 The optimal feedback gains are time-invariant for a time-invariant plant with long operating times. This compensator is inherently time-invariant even for a time-invariant plant with time-invariant noise densities, since the KBF is inherently time-varying (see previous section). However, if the plant and the noise densities are time-invariant, the KBF asymptotically becomes time-invariant so the compensator also becomes time-invariant. Surprisingly this steady-state compensator is usually not the best time-invariant compensator for the system, for the reasons given in the previous section (divergence of the KBF).

Even if the KBF is modified to avoid divergence, the resulting compensator may prove to be unsatisfactory because of its sensitivity to small changes in the plant parameters. Methods for designing optimal time-invariant compensators with sensitivity constraints are discussed below.

5. DESIGN OF OPTIMAL TIME-INVARIANT COMPENSATORS FOR PLANTS WHOSE PARAMETERS VARY OVER A SPECIFIED RANGE

A requirement for many control systems is that the closed-loop system remain stable over a specified range of plant parameters. This requirement may arise from either of two considerations:

a) Some plant parameters are uncertain but are known to be in a certain range.
 b) The closed-loop system is being designed to operate with a fixed compensator over a range of operating conditions and hence over a specified range of values of plant parameters.

Closed-loop stability over the specified range of plant parameters may be regarded as a constraint in the design of a fixed compensator. Other performance criteria might include:

a) Attenuation of response to disturbances.
 b) Rapid and accurate response to command inputs.
 c) Rapid and accurate tracking response.

An approach to the design of parameter-insensitive systems that also give good response is discussed in reference 29. These compensator parameters are determined (for a chosen order of dynamic compensator) to minimize a weighted sum of several quadratic performance indices (QPI's) where one QPI is evaluated with nominal values of the plant parameters and the other QPI's are evaluated at the limits of the specified parameter ranges. Nonlinear programming techniques are used to find the optimal compensator parameters. Performance degrades as the design range of plant parameters increases. This is shown symbolically in figure 1.

Performance improves and parameter insensitivity degrades as the compensator order is increased for a given set of measured outputs. Thus estimated-state feedback, which corresponds to a compensator of order equal to the order of the plant, gives the best performance but has the poorest parameter insensitivity characteristics.

6. REFERENCES

- 1 Hohmann, W., "Die Erreichbarkeit der Himmelskörper", Oldenbourg, Munich, 1925.
- 2 Goddard, R.H., "Rockets", Smithsonian Institute, 1919; reprinted Amer. Rocket Soc., 1946.
- 3 Hamel, G., "Über eine mit dem Problem der Rakete Zusammenhängende Aufgabe der Variationsrechnung", ZAMM, Vol. 7, No. 6, 1927, pp. 451-452.
- 4 Tsien, H.S. and Evans, R.C., "Optimal Thrust Programming for a Sounding Rocket", Journ. Amer. Rocket Soc., Vol. 21, No. 5, 1951, pp. 99-107.
- 5 Hestenes, M.R., "A General Problem in the Calculus of Variations with Applications to Paths of Least Time", Rand Corp. Rpt. RM-100, 1950.
- 6 Bellman, R., "Dynamic Programming", Princeton University Press, 1957.
- 7 Okhotsimskii, O.E. and Eneev, T.M., "Some Variational Problems Connected with the Launching of Artificial Satellites of the Earth", Journ. Brit. Interplan. Soc., Vol. 16, No. 5, 1958.
- 8 Breakwell, J.V., "The Optimization of Trajectories", SIAM Journal, Vol. 7, 1959 (also North Amer. Aviation Rpt. AL-1706, August 1957).
- 9 Kelley, H.J., "Gradient Theory of Optimal Flight Paths", Jour. Amer. Rocket Soc., Vol. 30, No. 10, 1960, pp. 947-954.
- 10 Bryson, A.E. and Denham, W.F., "A Steepest-Ascent Method for Solving Optimum Programming Problems", Jour. Appl. Mech., Vol. 29, June 1962.
- 11 Leitmann, G. (Ed.), "Optimization Techniques", Academic Press, New York, 1962.
- 12 Lawden, D.F., "Optimal Trajectories for Space Navigation", Butterworths, London, 1963.
- 13 Knuth, D.E., "The Art of Computer Programming", Addison-Wesley, Reading, Mass., 1968 (2nd edition 1973).
- 14 Erzberger, H., McLean, J.D. and Barman, J.F., "Fixed-Range Optimum Trajectories for Short-Haul Aircraft", NASA TN D-8115, December, 1975.
- 15 Gauss, K.F., "Theory of the Motion of the Heavenly Bodies Moving about the Sun in Conic Sections", transl. by C.H. Davis, Dover, New York, 1963.
- 16 Wax, N., "Collected Papers on Noise and Stochastic Processes", Dover, New York, 1954.
- 17 Wiener, N., "The Interpolation and Smoothing of Stationary Time Series", MIT Press, Cambridge, 1949.
- 18 Kalman, R.E. and Bucy, R., "New Results in linear Filtering and Prediction", Trans. ASME, Vol. 83D, 1961.
- 19 Leondes, C. (Ed.), "Theory and Applications of Kalman Filtering", AGARDograph 139, February 1970.
- 20 Bryson, A.E., "Kalman Filter Divergence and Aircraft Motion Estimators", Jour. Guid. & Control, Vol. 1, No. 1, 1978, pp. 71-79.
- 21 Kelley, H.J., "Guidance Theory and Extremal Fields", Proc. I.R.E., 1962, p. 75.
- 22 Dyer, P. and McReynolds, S.R., "The Computation and Theory of Optimal Control", Academic Press, New York, 1970.
- 23 Jacobson, D.H. and Mayne, D.Q., "Differential Dynamic Programming", Elsevier, New York, 1970.
- 24 Isaacs, R., "Differential Games", Wiley, New York, 1965.
- 25 Athans, M. (Ed.), "Special Issue on Linear-Quadratic-Gaussian Problem", IEEE Trans. Auto. Control, Vol. 16, December 1971.
- 26 Kwakernaak, H. and Sivan, R., "Linear Optimal Control Systems", Wiley-Interscience, New York, 1972.
- 27 Bryson, A.E., "Some Connections Between Modern and Classical Control Concepts", Jour. Dyn. Sys., Meas., Control, Vol. 101, June 1979, pp. 91-98.
- 28 Gelb, A. (ed.), "Applied Optimal Estimation", MIT Press, Cambridge, 1974, Ch. 7 on "Suboptimal Filter Design and Sensitivity Analysis".

- 29 Vinkler, A., Wood, L.J., Ly, U.L. and Cannon, R.H., "Minimum Expected Cost Control of Linear Systems with Uncertain Parameters-Application to Remotely-Piloted Vehicle Flight Control Systems", AIAA Guidance and Control Conf., Boulder, Colo., August, 1979.
- 30 Yocum, J.F. and Slafer, L.I., "Control System Design in the Presence of Severe Structural Dynamics Interaction", Jour. Guid. & Control, Vol. 1, No. 2, 1978, pp. 109-116.
- 31 Rogers, K.L., Hodges, G.E. and Felt, L., "Active Flutter Suppression - A Flight Test Demonstration", Jour. Aircraft, Vol. 12, June 1975, pp. 551-556.

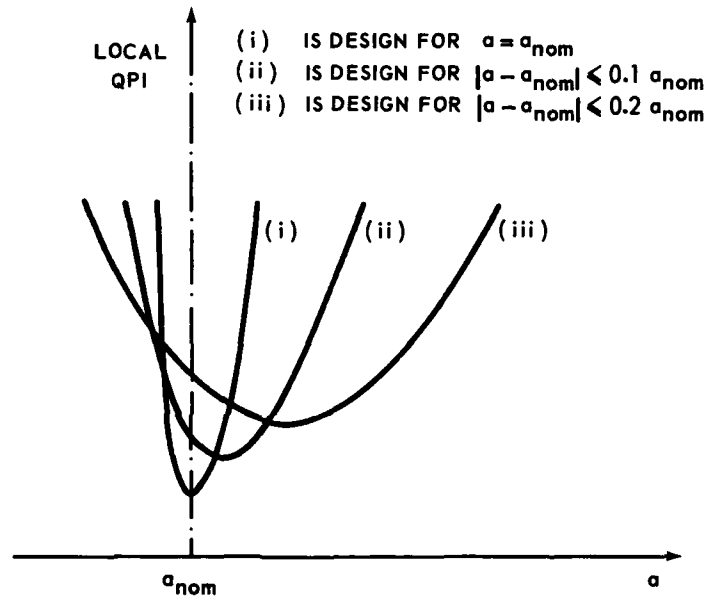


Fig. 1 Local quadratic performance index vs. plant parameter, a

THEORY OF STOCHASTIC OPTIMAL CONTROL
SOME BASIC NOTIONS

by

GUY CAMPION

Chercheur qualifié FNRS

Université Catholique de Louvain
Bâtiment Stévin
Place du Levant, 2
B-1348 Louvain-la-Neuve
BELGIUM.

ABSTRACT

The optimal control problem for stochastic systems is described in details. Several classes of policy are defined and compared. The corresponding solutions are deduced from Bellman's principle and discussed in connection with the concept of "dual effect" of the control. After the derivation of the optimal closed-loop solution for the linear quadratic gaussian problem, several algorithms are proposed for the nonlinear problem and discussed in the perspective of their implementation in aerospace applications.

TABLE OF CONTENTS

1. Introduction
 2. Problem formulation
 - 2.1 System description
 - 2.2 Some types of control policies
 3. Solution structure
 - 3.1 Derivation of the optimal controllers
 - 3.2 Dual effect of the control-Probing and Caution
 - 3.3 Certainty equivalence property and separation property
 4. Optimal control of linear quadratic systems
 5. Extensions of the linear quadratic gaussian theory
 - 5.1 Non linear systems
 - 5.2 Effect of modelling errors
 - 5.3 Adaptive control
 6. Conclusions
- Appendices
- A. Kalman filter equations
 - B. Closed-loop optimal control for the linear quadratic problem.

Figures

References.

LIST OF SYMBOLS

$x(k)$	n -dimensional state vector at time k
$u(k)$	p -dimensional control vector applied at time k
$v(k)$	n -dimensional noise affecting the dynamic at time k
$z(k)$	m -dimensional measurement vector available at time k
$w(k)$	m -dimensional noise affecting the observation at time k
X_0^k	sequence of the state vectors from time 0 to time k ($x(j) 0 \leq j \leq k$)
U_0^k	sequence of the control vectors from time 0 to time k ($u(j) 0 \leq j \leq k$)
Z_0^k	sequence of the measurement vectors from time 0 to time k ($z(j) 0 \leq j \leq k$)
$f(k,x,u)$	function of $(N \times R^n \times R^p) \rightarrow R^n$ describing the dynamics
$h(k,x)$	function of $(N \times R^n) \rightarrow R^m$ describing the observation process
$Q(k)$	covariance matrix of the plant noise at time k
$R(k)$	covariance matrix of the measurement noise at time k
C	cost function
$\theta(x)$	terminal cost function
$L(k,x,u)$	cost function
I_k	information state at time k
$J(N-k)$	cost-to-go for the k remaining steps
$\hat{x}(k k)$	estimate of the state vector at time k
$P(k k)$	error covariance matrix of the estimate at time k
p.d.f.	probability density function
OL	open loop
F	feedback
qF	q measurement feedback
OL	closed-loop
OLO	open-loop optimal
CLO	closed-loop optimal
OLOF	open-loop optimal feedback.

1. Introduction

In modeling any aerospace system the engineer first defines variables characterizing the problem (the state variables) and then try to connect these variables via causal relationships deduced from physical laws. After a simulation based on this model he is able to determine how well it can predict the evolution of the physical system. In most cases this prediction is not exact. At this point the engineer can try to elaborate a more sophisticated model in order to reach a better concordance. He may or may not succeed. If he does not that may be because the system is influenced by physical perturbations which are actually unpredictable, i.e. for which causal relationships do not exist. On the other hand it is also possible that the concordance between the observation of the physical system and of the mathematical model is corrupted by random errors in the instruments used to observe the system, or by imprecision introduced by the transmission of this information (for example the quantization error introduced by the digital coding of the measurements). These two kinds of random perturbation are referred to as "noises" (noise on the dynamical model and noise on the observations) and it is possible to determine their statistics by repeated experimentation. Finally, due to the complexity of the system, the engineer has maybe to consider only a reduced order model, neglecting deliberately high order modes, to make possible the treatment of the model on the available computer (for example small size on-board computer). In this simplification the effects of the neglected modes have to be considered as unpredictable noises. In order to take into account these random noises or errors in the elaboration of the model use is made of the "stochastic processes theory". The purpose of this chapter is to discuss a particular aspect of this theory (e.g. the optimal control of stochastic systems) in the perspective of aerospace applications. The mathematical background of this theory has been developed and discussed in many publications (see, for example, [1] to [7]).

Two main problems occur in the investigation of stochastic processes: the estimation problem and the optimal control problem. The estimation problem is stated as follows. Consider a physical system, possibly corrupted by random perturbations, and producing outputs which are observable but also corrupted by noises. The purpose of the estimation problem is to elaborate, on the basis of a mathematical model, a suitable policy in order to generate the "best" estimation, in some statistical sense, of the state of the system by processing the outputs. The problem structure is given in fig. 1. Kalman was the first to propose an optimal recursive solution, for the linear gaussian problem, with the

classical "Kalman filter" ([8], [9]). Many books and papers were published in this domain (see, for example, [10]). The second problem, which is in fact the subject of this chapter, concerns the optimal control of stochastic systems. Consider the same physical system but assume it is possible to influence its evolution via some input variable. The purpose of the problem is to elaborate a suitable policy in order to produce the input variable minimizing some performance index. The problem structure is given in fig. 2. This problem can be considered as a generalization of the optimal deterministic control problem. Well-known contributions to the optimal stochastic control are the works of Bellman ([11]), Feld'baum ([12]), Aoki ([13]), Meditch ([14]), Aström ([15]).

The problem of estimation and control of stochastic systems is, of course, very crucial in aerospace applications. Many examples can be found in the literature, e.g. lateral control for automatic landing for DC8 ([16]), lateral and longitudinal control systems for CCV-B52 ([17]). These methods have been widely used in spacecraft applications and will be developed in the future. For example the attitude control of the future large space structures is based on these modern control methods ([18]).

The purpose of this paper is to present the theoretical background of the stochastic optimal control theory, to show the general structure of the solution and to underline how difficult it is to implement it in the general case. As the theory will be reviewed in the perspective of aerospace applications the mathematical developments will be omitted, as well as the historical evolution of the theory. What is intended is a good understanding of the problem in order to make possible the comparison and the discussion of practical optimal and suboptimal solutions. As the aerospace systems are generally described as lumped systems characterized by differential equations (or by difference equations in the discrete time formulation), we restrict ourselves to the consideration of lumped stochastic systems. On the other hand only the discrete-time formulation will be considered, although a substantial literature has been published concerning continuous-time systems. There are three main reasons to justify this restriction. Firstly the discrete-time formulation avoids some mathematical difficulties related to the stochastic differential calculus and permits therefore to explain more comprehensively the basis of the theory. The second reason is that measurements are often taken at discrete times (radar, starscanner ...). The third reason is that, due to the complexity of the problem, digital computers are necessary to generate the solution. The discrete-time formulation is therefore particularly suitable for the practical implementation of the solution algorithms.

The paper is organized as follows. In section 2, the general formulation of the problem is presented and some classes of control policies are discussed and compared, according to the amount of information used in their elaboration. In section 3 the optimal solutions corresponding to these classes are deduced from Bellman's principle. The "certainty equivalence" property and the "separation" property are discussed with respect to the "dual effect" of the control. In section 4 the optimal solution for the linear quadratic gaussian problem is presented in details while in section 5 some classical extensions to non linear problems are discussed in the perspective of their implementation in aerospace systems.

2. Problem formulation

2.1 System description

Consider an aerospace system characterized by some variables, referred to as "state-variables" (for example, position, velocity, angles of attitude, angular velocity...), with some control variables (for example thrusters, control surfaces...), and with output variables (radar outputs, accelerometer, gyrooutputs...). Assume furthermore that a mathematical model has been elaborated for the evolution of these variables. Examples of modelisation can be found in [19] (ch.5) (lateral and longitudinal autopilot, roll attitude controller for a missile). This last simple example is now presented in details.

We want to design a feedback controller for a missile using hydraulic powered ailerons that keeps the roll attitude ϕ , close to zero, while staying within the physical limits of aileron deflection δ and aileron deflection rate $\dot{\delta}$. Considering a reduced order model where the roll attitude motion is decoupled from the other attitude motions, the mathematical model reduces to

$$\begin{aligned}\dot{\delta} &= u \\ \dot{\omega} &= -\frac{1}{\tau} \omega + \frac{E}{\tau} \delta + \text{noise} \\ \dot{\phi} &= \omega\end{aligned}\quad (2.1)$$

where u is the command signal to aileron actuators
 ω is the roll angular velocity
 τ is the roll time-constant
 and E is the aileron effectiveness

Defining the state vector x as

$$x(t) = \begin{bmatrix} \delta(t) \\ \omega(t) \\ \phi(t) \end{bmatrix}, \quad (2.2)$$

eq. (1.1) can be rewritten as

$$\dot{x}(t) = \begin{bmatrix} 0 & 0 & 0 \\ \frac{E}{\tau} & -\frac{E}{\tau} & 0 \\ 0 & 1 & 0 \end{bmatrix} x(t) + \begin{bmatrix} 1 \\ 0 \\ 0 \end{bmatrix} u(t) + \text{noise} \quad (2.3)$$

Assuming, in addition, that the roll angle ϕ can be measured with some accuracy, the output equation can be written as

$$z(t) = [0 \quad 0 \quad 1] x(t) + \text{noise} \quad (2.4)$$

where $z(t)$ is the output variable.

In the general case the system is described by a discrete-time dynamical equation of the following form

$$x(k+1) = f[k, x(k), u(k)] + v(k) \quad (2.5)$$

In this expression

$x(k)$ is the state vector (of dimension n) at time k
 $u(k)$ is the control vector (of dimension p) applied at time k
 $v(k)$ is the additive noise at time k
 $f[\cdot, \cdot, \cdot]$ is a function of $(N \times R^n \times R^p) \rightarrow R^n$.

We assume that the system is observed via the following measurement equation

$$z(k) = h[k, x(k)] + w(k) \quad (2.6)$$

In this expression,

$z(k)$ is the observation vector (of dimension m) at time k
 $w(k)$ is the additive measurement noise at time k
 $h[\cdot, \cdot]$ is a function of $(N \times R^n) \rightarrow R^m$

In our roll attitude controller example, consider a discretization of the time with a given sample period T . The discrete-time equations are now written as

$$x(k+1) = Ax(k) + Bu(k) + G(v(k)) \quad (2.7)$$

where $A = \begin{bmatrix} 1 & 0 & 0 \\ E[1-e^{-T/\tau}] & e^{-T/\tau} & 0 \\ E[T-\tau+te^{-T/\tau}] & \tau[1-e^{-T/\tau}] & 1 \end{bmatrix} \quad (2.8)$

$$B = \begin{bmatrix} T \\ E[T(1-e^{-T/\tau}) + (1-e^{-T/\tau})] \\ E[T^2 - T\tau(1-e^{-T/\tau}) - \tau^2(1-e^{-T/\tau})] \end{bmatrix} \quad (2.9)$$

and $G = \begin{bmatrix} 0 \\ 1 \\ 0 \end{bmatrix} \quad (2.10)$

The output equation is given by

$$z(k) = Hx(k) + w(k) \quad (2.11)$$

where

$$H = [0 \quad 0 \quad 1]$$

It is assumed, in general, that the a priori probability density function (p.d.f.) of the initial state $x(0)$ is given ($p[x(0)]$) and that the two noise sequences, $\{v(k)\}$ and $\{w(k)\}$, are white, uncorrelated, uncorrelated with the initial state, gaussian, with zero mean and covariance matrices equal respectively to $Q(k)$ (semi-definite positive) and $R(k)$ (positive definite). These assumptions concerning the statistics of the noises may seem rather restrictive but they are made in order to avoid difficulties in the derivation of the equations and to keep an implementable form for the solution structure. The structure of the system, as given in fig. 3, is a particular case of fig.2 relative to (2.5) and (2.6). The model structure is assumed to be known and we are concerned only by the design of the "controller black box" appearing below the dashed line.

There is an infinite number of ways to generate the control variable. The choice is nevertheless constrained by the objectives of the control action and by restrictions on the control as well as on the state variables. These control policies belong to the class of admissible controls and it is reasonable to try to select, from this class, the control which is the "best" one with respect to some prespecified performance measure. For deterministic systems this performance index to be minimized is a given function of the state and the control variables. For stochastic systems such a function is itself random "variable" so it is not appropriate to consider its minimization. This performance index is therefore transformed into a deterministic quantity by taking its expected value, extended to all possible initial vectors and all possible noise sequences, $\{v(k)\}$ and $\{w(k)\}$, according to their given statistics. As conclusion, the optimal stochastic control problem consists in the elaboration of the best admissible control policy minimizing a performance index defined as

$$E[C(N)] \quad , \quad (2.12)$$

where

$$C(N) \triangleq C[x_0^N, u_0^{N-1}] = \theta[x(N)] + \sum_{k=0}^{N-1} L[k, x(k), u(k)] \quad . \quad (2.13)$$

In this relation,

$\theta(\cdot)$ is the terminal cost contribution and is a non negative convex function $R^n \rightarrow R$
 $L(\cdot, \cdot, \cdot)$ is the cost contribution relative to the evolution of the state variables and control variables

N is the number of stages of the process and is fixed a priori.

This $C(N)$ is a function of the state and control variables sequences.

$$\begin{aligned} x_0^N &\triangleq \{x(0), \dots, x(N)\} \\ u_0^{N-1} &\triangleq \{u(0), \dots, u(N-1)\} \end{aligned} \quad (2.14)$$

The controller block appearing in fig. 3 has now to be designed in order to elaborate the policy minimizing the performance index defined in (2.13).

In the roll attitude controller example, we want to obtain, after a given time interval (N sample periods) a roll angle, a roll angle velocity and an aileron deflection as close as possible to zero. It is the reason why we select a terminal cost function penalizing the terminal offsets of these variables according to three weighting coefficients (a_1, a_2, a_3)

$$\theta[x(N)] = a_1 \delta^2(N) + a_2 \omega^2(N) + a_3 \phi^2(N) \quad . \quad (2.15)$$

On the other hand, as we have to stay within acceptable limits of roll angle, aileron deflection and aileron deflection rate, it is suitable to construct a performance index penalizing, during the evolution of the system, the offsets of ϕ , δ and u from zero.

$$L(k, x, u) = \frac{\phi^2(k)}{\phi_0^2} + \frac{\delta^2(k)}{\delta_0^2} + \frac{u^2(k)}{u_0^2} \quad (2.16)$$

where ϕ_0 is the maximum acceptable value of ϕ
 δ_0 is the maximum available value for δ
 u_0 is the maximum available value for u .

This simple example of construction of a performance index gives some insight in the meaning and choice of the cost function.

2. Some types of control policies.

Suppose that, at time k , $u(k)$ has to be selected. The only information concerning the past evolution of the system, available at time k , consists in the sequence of control variables actually applied up to time $(k-1)$:

$$u_0^{k-1} \triangleq \{u(0), \dots, u(k-1)\} \quad ,$$

and of the sequence of observation vectors, up to time k :

$$z_0^k \triangleq \{z(0), \dots, z(k)\} \quad .$$

As the control has, of course, to be causal, i.e. non anticipative, the optimal control must be an explicit function of these data

$$u(k) = \psi[u_0^{k-1}, z_0^k] \quad (2.17)$$

As this point, ψ could be a random function of the past data. Feld'baum has investigated this possibility ([12]) and its conclusion was that this does not improve the results for the cases he considered. We shall therefore restrict ourselves to deterministic control policies, i.e. to policies where the control, at time k , is generated as a deterministic function of the past data. The problem consists in the suitable choice of the form of this function.

Different classes of deterministic control policies will be defined according to the amount of information used in their elaboration. We now define notations characterizing this information. We first characterize the "a priori" information with

- a) The knowledge about the *dynamics*, from time r up to time l , i.e. the knowledge of the functions $f(k, \dots)$ for k varying from r to l .

$$D_r^l \triangleq \{f(k, \dots) | r \leq k \leq l\} \quad (2.18)$$

- b) The knowledge about the *measurement* program, from time r up to time l , i.e. the knowledge of the functions $h(k, \dots)$, for k varying from r to l .

$$M_r^l \triangleq \{h(k, \dots) | r \leq k \leq l\} \quad (2.19)$$

- c) The knowledge about the structure of the *performance index*, i.e.

$$C(N)$$

- d) The knowledge about the *statistics* of the initial state and of the noise sequences. With the assumptions made in 2.1 concerning the noises this information reduces to

$$S_0 \triangleq \{p[x(0)]\} \text{ concerning the initial state,} \quad (2.20)$$

$$S_Q^k \triangleq \{Q(0), \dots, Q(k)\} \text{ concerning } \{v(k)\}, \quad (2.21)$$

$$S_R^k \triangleq \{R(0), \dots, R(k)\} \text{ concerning } \{w(k)\}. \quad (2.22)$$

For convenience we define a new amount of information related to the a priori statistics :

$$S^k \triangleq \{S_0, S_Q^{N-1}, S_R^k\}. \quad (2.23)$$

We now characterize the "on-line" information, consisting, at time k , in the control variables actually applied from time 0, up to time $(k-1)$:

$$U_0^{k-1} \triangleq \{u(r) | 0 \leq r \leq k-1\} \quad (2.24)$$

and in the outputs of the system, actually observed from 0 up to k :

$$Z_0^k \triangleq \{z(r) | 0 \leq r \leq k\}. \quad (2.25)$$

According to the amount of information actually used four main types of control policies have classically been defined. They are :

- 1) The *Open-loop* (OL) control policy.

In this class the controller is elaborated mainly from the "a priori" information. Incomplete use is made of the on-line information and, particularly, no measurement knowledge is exploited. The control has the following form :

$$u^{OL}(k) = u^{OL}[D_0^{N-1}, S_0, S_Q^{N-1}, C(N), U_0^{k-1}] \quad (2.26)$$

- 2) The *Feedback* (F) control policy.

In this class use is made, in addition, of the measurement information up to the present time, but no knowledge about the future observations is available. At every time the on-line information is fed back into the controller but no subsequent feedback is anticipated. The controller has the following form :

$$u^F(k) = u^F[D_0^{N-1}, S^k, C(N), M_0^k, U_0^{k-1}, Z_0^k], \quad (2.27)$$

- 3) The *q-measurement Feedback* (qF) control policy.

In this class use is made, in addition, of the knowledge about the observations for the q next stages, i.e. of the h functions and of the statistics of the measurement noises for the q next stages, although the corresponding observations, of course, are not yet available. The controller has the following form :

$$u^{qF}(k) = u^{qF}[D_0^{N-1}, S^{k+q}, C(N), M_0^{k+q}, Z_0^k, U_0^{k-1}] \quad (2.28)$$

- 4) The *closed-loop* (CL) control policy.

This class is a generalization of the qF policy class. More precisely the information concerning the next observations is available for the $(N-k)$ next stages. The controller has the following form :

$$u^{CL}(k) = u^{CL}[D_0^{N-1}, S^N, C(N), M_0^N, Z_0^k, U_0^{k-1}] \quad (2.29)$$

The algorithms proposed in the literature belong to one of these four principal classes. As the amount of information used in the elaboration of the controller becomes more important from the OL class to the CL class it can be expected that the "best" policy belongs to the CL control class. The superiority of the CL class will be discussed in section 3 in connection with the concept of "dual control". At this point it must be

noted that the F class, the qF class and the CL class differ only in the availability of the knowledge about future observations, while in the OL class no use at all is made of the observations, past, present or future. We now show how it is possible to derive theoretically the best controller for each of these four classes.

3. SOLUTION STRUCTURE.

1) Derivation of the optimal controllers.

For the derivation of the optimal controller structure for the four proposed classes use will be made of the well-known Bellman's principle of optimality ([11],[20]) stating that the optimal policy has the following basic property. At any given time, whatever the present state and the previous control actions are, the remaining control variables must constitute an optimal policy with respect to the present state. For deterministic systems the state can be considered as known while in the stochastic case this state is, in general, imperfectly known. What is available, at time k , concerning the state is some statistical knowledge namely the conditional probability density function of the state, given some information. This information is called "information state" by Striebel ([21]) and will be noted I_k^{OL} (respectively $I_k^{\text{OL}}, I_k^{\text{F}}, I_k^{\text{qF}}, I_k^{\text{CL}}$ for the four considered classes). These information states represent in fact the amount of information used in the elaboration of the controller and have been defined in relations (2.26), (2.27), (2.28) and (2.29). With this notation we can use an unified formulation for the derivation of the solution structure for the four classes.

As, according to Bellman's principle, for each remaining period the policy has to be optimal with respect to the actual information state, the optimal policy elaboration begins, classically, with the optimal choice of the last control. Assume therefore that, at time $(N-1)$, with an information state I_{N-1} , $u(N-1)$ has to be chosen. This last control is selected in order to minimize the expected value of the cost, conditioned in the information state I_{N-1} , without regard to the past controls, i.e.

$$\min_{u(N-1)} E\{C(X_0^N, U_0^{N-1}) | I_{N-1}\} \quad (3.1)$$

At time $(N-2)$, the control $u(N-2)$ is then obtained in such a way that it minimizes the expected value of the above expression conditioned on I_{N-2} . i.e.

$$\min_{u(N-2)} E\{\min_{u(N-1)} E\{C(X_0^N, U_0^{N-1}) | I_{N-1}\} | I_{N-2}\} \quad (3.2)$$

Proceeding similarly backward in time up to time 0, we obtain the optimal policy and the corresponding optimal value of the performance index, noted $J^0(N)$ (respectively $J^{\text{OLO}}(N)$, $J^{\text{FO}}(N)$, $J^{\text{qFO}}(N)$ and $J^{\text{CLO}}(N)$):

$$J^0(N) = \min_{u(0)} E\{\dots \min_{u(N-2)} E\{\min_{u(N-1)} E\{C(X_0^N, U_0^{N-1}) | I_{N-1}\} | I_{N-2}\} \dots | I_0\} \quad (3.3)$$

With the assumptions made in 2.14 concerning the form of the performance index it is possible to rewrite (3.3) under the following form of the usual stochastic dynamic programming equation :

$$J^0(N-k) = \min_{u(k)} E\{L(k, x(k), u(k)) + J^0(N-k-1) | I_k\} \quad (3.4)$$

where $J^0(N-k)$ is called the "cost-to-go" for the remaining $(N-k)$ stages and is a function of I_k . The terminal condition is given by

$$J^0(0) = E\{\theta[x(N)] | I_N\} \quad (3.4)$$

This last formulation shows that, for a given class, the optimal solution is completely characterized by the knowledge of the sequence of the $J^0(N-k) | I_k$, for k varying from N to 0. Suppose that, at time k , $J^0(N-k-1) | I_{k+1}$ is an available function of I_{k+1} . The optimal control at time k is then obtained by the condition of minimization (3.4), where the conditional expected value has to be extended to all the I_{k+1} , according to their statistics conditioned on the actual available information state I_k . These $J^0(N-k)$ have to be generated recursively according to eq.(3.4) with terminal condition 3.5. The fundamental difficulty of the stochastic optimal control problem consists precisely in the practical construction of the sequence of the $J^0(N-k)$.

It will now be shown how to specialize this general formulation of the solution structure for the four proposed classes.

a) Open-Loop policy

For this class the information state I_k^{OL} consists in

$$I_k^{\text{OL}} \triangleq \{D_0^{N-1}, S_0, S_Q^{N-1}, C(N), U_0^{k-1}\} \quad (3.6)$$

It follows that

$$I_k^{\text{OL}} = I_{k-1}^{\text{OL}} \cup \{u(k-1)\} \quad (3.7)$$

The expression (3.2) can therefore be rewritten as

$$\min_{u(N-2)} E\{\min_{u(N-1)} E\{C(X_o^N, U_o^{N-1}) | I_{N-2}^{OL}, u(N-2)\} | I_{N-2}^{OL}\} \quad (3.8)$$

As the expression

$$\min_{u(N-1)} E\{C(X_o^N, U_o^{N-1}) | I_{N-2}^{OL}, u(N-2)\}$$

is a function of I_{N-2}^{OL} , its expectation, conditioned on I_{N-2}^{OL} , coincides with it and (3.8) can be written as

$$\min_{u(N-2)} \min_{u(N-1)} E\{C(X_o^N, U_o^{N-1}) | I_{N-2}^{OL}, u(N-2)\} \quad (3.9)$$

The process can be reproduced. As conclusion, the optimal cost for the N stages problem, $J^{OLO}(N)$ is given by

$$J^{OLO}(N) = \min E\{C(X_o^N, U_o^{N-1}) | I_o^{OL}, U_o^{N-1}\} \quad (3.10)$$

where the minimization is taken with respect to the sequence U_o^{N-1} . The optimal open-loop control sequence is obtained from this minimization subject to eq(2.5). This problem is, in fact, a static problem because all the controls can be obtained before the process starts.

The formulation (3.4) can also be used in order to derive the solution structure. The terminal condition (3.5) can be rewritten as

$$J^{OLO}(0) = E\{\theta[x(N)] | I_N^{OL}\} = \int \theta[x(N)] p[x(N) | I_N^{OL}] dx(N) \quad (3.11)$$

In this relation the conditional p.d.f. $p[x(N) | I_N^{OL}]$ can be obtained using the Markov property of the system

$$p[x(N) | I_N^{OL}] = \int p[x(N) | x(N-1), Q(N-1)] \dots p[x(1) | x(0), Q(0), u(0)] p[x(0)] dx(N-1) \dots dx(0) \quad (3.12)$$

The expression of $J^{OLO}(N-k)$ is then obtained recursively by (3.4) where

$$E\{L[k, x(k), u(k) | I_k^{OL}]\} = \int L[k, x(k), u(k)] p[x(k) | I_k^{OL}] dx(k) \quad (3.13)$$

with $p[x(k) | I_k^{OL}]$ obtained as in (3.12), and

$$E\{J^{OLO}(N-k-1) | I_k^{OL}\} = J^{OLO}(N-k-1) | I_k^{OL}, u(k) \quad (3.14)$$

as $u(k)$ has to be obtained deterministically from I_k^{OL} . It is easy to verify that this formulation is equivalent to (3.10).

b) Feedback policy

For this class the information state J_k^F consists in

$$J_k^F \triangleq \{D_o^{N-1}, S_o, S_Q^{N-1}, S_R^k, U_o^{k-1}, Z_o^k\} \quad (3.15)$$

In (3.3) the expression $\min_{u(N-1)} E\{C(X_o^N, U_o^{N-1}) | I_{N-1}^F\}$ is, in fact, a function of I_{N-2}^F , $z(N-1)$, $h(N-1, \dots)$, $R(N-1)$ and $u(N-2)$. As in the feedback policy no information is assumed to be available about future measurement, it is impossible to evaluate at time $(N-2)$, given I_{N-2}^F , the expected value of this expression conditioned on I_{N-2}^F . This difficulty arises because the problem is not well defined: no specific assumption has been made regarding the subsequent feedback. A classical method to avoid the difficulty consists in considering that no subsequent feedback will be available in the future time. This assumption defines the open-loop optimal feedback (OLOF) policy. This corresponds to replacing the quantity

$$\min_{u(N-1)} E\{C(X_o^N, U_o^{N-1}) | I_{N-1}^F\} \text{ by } \min_{u(N-1)} E\{C(X_o^N, U_o^{N-1}) | I_{N-1}^{OL}\}$$

which is not a function of $z(N-1)$ so it becomes possible to evaluate its expected value conditioned on I_{N-2}^F . That means, in other words, that $u(N-2)$ is chosen as the OL optimal control, for the problem defined on the last two stages. This process can be reproduced and the OLOF control is defined in general as follows.

Suppose that $u^{OLOF}(k)$ has to be chosen at time k with I_k^F available. Define first the sequence of OL optimal controls to be applied from time k up to time $(N-1)$, based on the available I_k^F . This sequence, noted $(U^{OLO})_k^{N-1}$ is a function of I_k^F .

$$(U^{OLO})_k^{N-1} = (U^{OLO})_k^{N-1} [I_k^F] \triangleq \{u^{OLO}(l|k) | l = k, \dots, N-1\} \quad (3.16)$$

and is generated according to the following condition

$$J^{OLO}(I_k^F) \triangleq \min_{U_k^{N-1}} E\{C(X_o^N, U_o^{N-1}) | I_k^F\} \quad (3.17)$$

The OLOF policy consists in applying at time k the control $u^{OLO}(k|k)$, which is the first control of this sequence. Processing then the next observation, $z(k+1)$, redefine I_{k+1}^F .

recompute the sequence $(U^{OLO})_{k+1}^{N-1}$, choose $u^{OLO}(k+1|k+1)$ and so on. The resulting sequence of controls is defined by

$$(U^{OLO})_0^{N-1} = \{u^{OLO}(k|k) | k=0, \dots, N-1\} \quad (3.18)$$

This OLOF policy has been proposed by Dreyfus ([22]) and OLOF algorithms can be found in the works of Spang ([23]), Aoki ([13]) and Farison ([24]). There are other feedback policies, namely the policies based on the certainty equivalence property or on the separation property. As these policies are frequently used in practical applications they will be exposed and discussed in details later.

As the q-measurement feedback policy is an intermediate between the F policy and the CL policy, the CL policy will be first discussed and it will be shown later how the qF policy follows from it.

c) Closed-loop policy.

For this class the information state I_k^{CL} consists in

$$I_k^{CL} \triangleq \{D_0^{N-1}, S_0, S_Q^{N-1}, S_R^N, M_0^N, U_0^{k-1}, Z_0^k\} \quad (3.19)$$

In (3.3) the expression

$$\min E\{C(X_0^N, U_0^N) | I_{N-1}^{CL}\}$$

is a function of I_{N-2}^{CL} , $z(N-1)$, $h(N-1, \cdot)$, $R(N-1)$ and $u(N-2)$. As in the CL policy knowledge about the future measurement is available, it is possible to evaluate, at time $(N-2)$, the conditional expected value of this expression given I_{N-2}^{CL} . The formulation (3.2), (3.3) can therefore be used and

$$J^{CLO}(N) = \min_{u(0)} E\{\dots \min_{u(N-2)} E\{\min_{u(N-1)} E\{C(X_0^N, U_0^{N-1}) | I_{N-1}^{CL}\} | I_{N-2}^{CL}\} \dots | I_0^{CL}\} \quad (3.20)$$

In order to obtain more comprehensible expressions the incomplete notation $\{U_0^{k-1}, Z_0^k\}$ is generally used in the literature, instead of the complete information state I_k^{CL} , as defined in (3.19), with the implicit assumption that the conditional expected values have to be evaluated in the CL frame.

The nested structure of the expectations and minimizations in (3.20) shows that this solution structure anticipates subsequent feedback. Whenever a control is computed in eq. (3.20) we have to evaluate expectations conditioned on the subsequent measurements. At this is done at each step the resulting control depends on the future observation program and the associated statistics.

The formulation of eq. (3.4) and (3.5) can also be used. With the incomplete notation convention for the information state mentioned earlier it follows

$$J^{CLO}(N-k) = \min_{u(k)} E\{L[k, x(k), u(k)] + J^{CLO}(N-k-1) | Z_0^k, U_0^{k-1}\} \quad (3.21)$$

with the terminal condition

$$J^{CLO}(0) = E\{\theta[x(N)] | Z_0^N, U_0^{N-1}\} = \int \theta[x(N)] p[x(N) | Z_0^N, U_0^{N-1}] dx(N) \quad (3.22)$$

d) The q-measurement Feedback policy.

For this class the information state consists in

$$I_k^{qF} \triangleq \{D_0^{N-1}, S_0, S_Q^{N-1}, S_R^{k+q}, M_0^{k+q}, U_0^{k-1}, Z_0^k\} \quad (3.24)$$

The qF control sequence is obtained, similarly to the OLOF, as the sequence of the first controls for the partially CL control sequences for the problem defined on the time interval $[k, N]$, with the assumption that no measurement will be available after $k+q$. At each step k it is necessary to define a new problem on the time interval (k, N) , to compute the partially CL sequence for this problem and then to select the first control of this sequence. This is in fact a "finite-horizon closed-loop" control since at each step it takes into account the measurement program and the corresponding statistics for the q subsequent steps.

As said before, since the CL policy uses more completely the available information, it can be expected that the best control belongs to this class. We will now try to give more insight into this property. The following qualitative discussion is based on the introduction of the concepts of "dual effect" of the control, and of "probing" and "caution".

2) Dual effect of the control-probing and caution.

Feld'baum ([12]) was the first to point out that the control can have two effects on a stochastic system: a direct effect on the evolution of the state variables but also in addition, an indirect effect on the future state uncertainty, that means that the control can result in learning about the state of the system. This is referred to as "the dual effect" of the control. The control is said to have no dual effect of order r ($r \geq 2$)

if the expected future uncertainty (i.e. the central moments of order 2 to r) is not affected by the control with probability one. The system is then said to be "neutral". Conversely, if one of these r-th central moments is affected by the control sequence with non zero probability the system presents the dual effect. It must be noted that the presence or the absence of the dual effect is an intrinsic property of the dynamic system and of the corresponding observation process.

On the other hand the controller can present two properties referred to as "probing" and "caution".

a) Probing or active information storage.

If the structure of the system is such that the control presents the dual effect, i.e. if the control has an influence on the future uncertainty on the state, this situation can be exploited in order to enhance the estimation and ultimately to improve the overall performance. It is clear that only a CL control (and partially a qF control) can take benefit of this effect, because it anticipates the future feedback. If the system is not neutral the CL control will "probe" to improve the estimation, and presents therefore the capability of "active learning", while a F control, even though it "learns" about the system by processing the past measurements does not actively "help" the learning.

b) Caution

In a stochastic system, because of the presence of uncertainties on the initial state, on the dynamics and on the measurements, the controller has to be "cautious" in order to avoid to increase the effect of these uncertainties on the performance index. An OL controller, for example, has to be quite cautious because it assumes no future feedback and does not therefore permit corrective action on the evolution of the uncertainty. At the opposite a CL controller can be less cautious because it "knows" that observations will be available in the future and that it will therefore be possible to control the evolution of the uncertainty. The performance is therefore better for a CL control than for an OL control. Dreyfus ([22]) gives an example of a neutral system for which the CLO control produces a better performance than the OLOF control : the OLOF control ignores that measurements will be available in the future so the predicted uncertainty is greater for the OLOF control than for the CLO control with the consequence that the OLOF control has to be too cautious.

We now introduce two particular control policies belonging to the feedback class. As they are widely used they are investigated in details. On the other hand, the properties on which these policies are based are strongly related to the concept of dual effect of the control.

3) Certainty Equivalence Property and Separation Property.

The certainty equivalence (CE) is said to hold if the CLO control has the same structure as the optimal control for the corresponding deterministic optimal control problem defined by the same dynamical equation and same performance index but where all the random variables have been replaced by their expected values. Suppose that the optimal control for this deterministic problem (deterministic optimal-DO) has, at time k, the form

$$u^{DO}(k) = \psi[k, x(k)] . \quad (3.24)$$

The CE property holds if

$$u^{CLO}(k) = \psi[k, \hat{x}(k|k)] , \quad (3.25)$$

where

$$\hat{x}(k|k) = E[x(k) | Z_o^k, U_o^{k-1}] . \quad (3.26)$$

It will be seen in section 4 that this property holds for linear systems with quadratic cost and gaussian additive noises.

The CE property is, in general, not valid but a control policy frequently used is elaborated by assuming that the CE property holds. The resulting control, called certainty equivalent control, is obtained as follows. Evaluate first the deterministic optimal control for the corresponding deterministic problem without process noise and with complete state knowledge and replace than $x(k)$ by its estimate, i.e.

$$u^{CE}(k) = \psi[k, \hat{x}(k|k)] . \quad (3.27)$$

The problem is partitioned into two decoupled subproblems :

- optimal estimation of the state
 - elaboration of the optimal control for the deterministic problem.
- The controller structure is given in fig. 4. It must be noted that for non linear systems the solutions of these subproblems are not trivial and that only approximate solutions are available in general. In most cases this control policy is not optimal because the CE property does not hold in general. It must be noted, in addition, that this policy belongs to the feedback class rather than to closed-loop class, because no use is made of the future measurement program in the elaboration of the controller.

The separation property is a generalization of the CE property. A control is said to present the separation property if it depends on the observations only through the

estimation of the state, $\hat{x}(k|k)$, i.e. if its structure is of the following form

$$u^{CLO}(k) = \phi[k, \hat{x}(k|k)] , \quad (3.28)$$

where the ϕ function can be different of ψ defined in (3.25), as the function characterizing the optimal control for the corresponding deterministic problem. As in the CE property discussion a separation control policy can be defined even if the separation property does not hold. Here also the problem can be partitioned in two subproblems :

- optimal estimation of the state
- elaboration of the controller using as input the estimation of the state.

It is clear that the CE property is a particular case of the separation property. An example of system where the separation property holds, but not the CE property is given in [25].

When the CE property holds it is clear that nothing can be gained by anticipating the subsequent observations. In this case the CLO policy reduces to be OLOF policy because no use is made of future measurements. This is not true for the separation property. The fact that the separation property holds does not necessarily imply that CLO control belongs to the feedback class, because the ϕ function defined in (3.28) can depend on the future evolution of the uncertainty.

It is not possible, at the moment, to investigate, in general, the relationship between CE or separation property and the presence or absence of the dual effect in the control. Only results corresponding to particular classes of problems are available. Bar-Shalom and Tse ([26]) have shown, for example, the following result. Consider a stochastic linear system with quadratic cost but non linear measurement equation. For this system the CE property holds if and only if the control has no dual effect, i.e. if the system is neutral. The generalization of this result is also given by the same authors ([27]) and concerns stochastic systems with linear dynamics non linear measurement equation, quadratic cost but non gaussian noises. In this case the CE property holds if and only if the control has no dual effect of second order, i.e. if the conditional covariance matrix of the estimation error is independent of the past control sequence. These results constitute in fact extensions of the properties of the linear quadratic gaussian problem which will now be investigated in details, as an illustration of the above theory.

4. OPTIMAL CONTROL OF LINEAR QUADRATIC SYSTEMS.

Consider, as a particular case of the general problem defined in section 2, a linear system with quadratic cost, that means that in eq. (2.5) and (2.6) $f(k,x,u)$ and $h(k,x)$ have respectively the form

$$f(k,x,u) = A(k)x + B(k)u , \quad (4.1)$$

and

$$h(k,x) = H(k)x , \quad (4.2)$$

and that the performance index introduced in (2.13) has the following form

$$C(N) \triangleq \frac{1}{2} x^T(N) S x(N) + \sum_{k=0}^{N-1} \left[\frac{1}{2} x^T(k) L_1(k) x(k) + \frac{1}{2} u^T(k) L_2(k) u(k) \right] \quad (4.3)$$

with S and $L_1(k)$ symmetric semi-definite positive ($n \times n$) matrices and $L_2(k)$ symmetric semi-definite positive ($p \times p$) matrix. The properties of the noises are the same as in section 2 while the a priori p.d.f. of the initial state is assumed to be Gaussian with mean $\hat{x}(0)$ and covariance matrix $P(0)$.

Two preliminary remarks can immediately be made.

- a) The estimation problem related to this system admits an exact solution by use of the Kalman filter. It is well-known (see for example [7]) that the conditional p.d.f. of the state, given the past measurements and a control sequence, is gaussian with a mean and a covariance matrix generated recursively by the Kalman filter, i.e.

$$p[x(k)|Z_0^k, U_0^{k-1}] = N[\hat{x}(k|k), P(k)] , \quad (4.4)$$

with

$$\hat{x}(k|k) \triangleq E[x(k)|Z_0^k, U_0^{k-1}] \quad (4.5)$$

and

$$P(k|k) \triangleq E\{[x(k) - \hat{x}(k|k)][x(k) - \hat{x}(k|k)]^T | Z_0^k, U_0^{k-1}\}$$

The recursive expressions of $\hat{x}(k|k)$ and $P(k|k)$ are given in Appendix A. As this conditional p.d.f. is gaussian it is characterized only by its first two moments. As the evolution of the covariance matrix is independent of the control sequence this system does not present the dual effect of the control and is therefore a neutral system.

- b) On the other hand the corresponding deterministic optimal control problem admits an exact solution. It is well-known (see for example [14]) that the optimal control $u^{DO}(k)$ is a linear function of the state vector, i.e.

$$u^{DO}(k) = K_c(k)x(k) , \quad (4.6)$$

where the control gain matrix $K_c(k)$ is given by

$$K_c(k) = -[L_2(k) + B^T(k) \pi(k+1) B(k)]^{-1} B(k) \pi(k+1) A(k) \quad (4.7)$$

The $(n \times n)$ matrix $\pi(k)$ is given recursively by a backward Riccati equation

$$\pi(k) = L_1(k) + K_c^T(k+1) L_2(k) K_c(k+1) + [A(k) + B(k) K_c(k+1)]^T \pi(k+1) [A(k) + B(k) K_c(k+1)] \quad (4.8)$$

with the terminal condition

$$\pi(N) = S \quad (4.9)$$

In addition the minimal cost corresponding to a given initial state $x(0)$ is given by

$$J(N) = \frac{1}{2} x^T(0) \pi(0) x(0) \quad (4.10)$$

The structure of the CLO solution for the stochastic problem is also well-known. It can be shown, by application of the theory of section 3, that the CLO solution is of the following form :

$$u^{CLO}(k) = K_c(k) \bar{x}(k|k) \quad (4.11)$$

with the control gain matrix $K_c(k)$ given in (4.7). The performance index is given by

$$J^{CLO}(N) = \frac{1}{2} \bar{x}(0)^T \pi(0) \bar{x}(0) + \alpha(0) \quad (4.12)$$

where $\pi(0)$ results, as in the deterministic problem, from a backward evolution governed by the Riccati equation (4.8) with terminal condition (4.9). The scalar $\alpha(0)$ results also from a backward evolution independent of the control sequence (see Appendix B). As the controller has exactly the same structure as in the deterministic problem, with $x(k)$ replaced by its estimate the CLO control presents the certainty equivalence property. The only effect of the noises is to increase the value of the performance index via the term $\alpha(0)$.

According to what was said in section 3 the OLOF policy coincides with the CLO policy because the system is neutral (CE property). The OLO policy can be deduced similarly to the CLO policy. The solution structure is identical. The only difference is that $\bar{x}(k|k)$ and $P(k|k)$ are replaced by the characteristics of the prediction estimate $\bar{x}(k|0)$ and $P(k|0)$ i.e.

$$\bar{x}(k|0) = E[x(k) | U_0^{k-1}] \quad (4.13)$$

and

$$P(k|0) = E\{[x(k) - \bar{x}(k|0)][x(k) - \bar{x}(k|0)]^T | U_0^{k-1}\} \quad (4.14)$$

More precisely the OLO control at time k is given by

$$u^{OLO}(k) = K_c(k) \bar{x}(k|0) \quad (4.15)$$

and the performance index by

$$J^{OLO}(N) = \frac{1}{2} \bar{x}(0)^T \pi(0) \bar{x}(0) + \beta(0) \quad (4.16)$$

where $K_c(k)$ and $\pi(0)$ are obtained as in the CLO solution (and as in the deterministic optimal^c solution), while $\beta(0)$ results from the same backward evolution equation as in the CLO solution, but where $P(k|k)$ is replaced by $P(k|0)$. The superiority of the CLO solution on the OLO solution results from the fact that $\beta(0)$ is greater than $\alpha(0)$ because it is evaluated on the basis of prediction covariance matrices greater than filtering estimation matrices.

As the roll attitude control problem described in section 2.1 (eq.(2.7) to (2.11)) has a linear structure, the optimal solution presents the separation property and is obtained, as exposed in the present section, in two steps. The first step consists in the optimal estimation of the state vector

$$x(k) = \begin{bmatrix} \delta(k) \\ \omega(k) \\ \phi(k) \end{bmatrix} \quad (4.17)$$

by use of the Kalman filter (App. A). In order to implement the filter the a priori probability density function of the initial state, characterized by its mean and covariance matrix, has to be specified on the basis of the a priori information about this state, and the perturbations on the dynamics and the measurements have to be defined, namely the noise covariance matrices which in this case present the following form

$$Q(k) = \begin{bmatrix} 0 & 0 & 0 \\ 0 & q(k) & 0 \\ 0 & 0 & 0 \end{bmatrix} \quad \text{and} \quad R(k) = r(k) \quad (4.18)$$

The choice of adequate values of $q(k)$ and $r(k)$ is based on the physical information available about these perturbations. The second step consists in the optimal control. The form of the optimal controller is given in eq (4.11) with a controller gain given recursively by eq. (4.7) to (4.9). In these expressions the weighting matrices S , $L_1(k)$ and $L_2(k)$ are chosen according to the form of the cost function defined by (2.15) and

$$(2.16) : \quad S = \begin{bmatrix} a_1 & 0 & 0 \\ 0 & a_2 & 0 \\ 0 & 0 & a_3 \end{bmatrix}, \quad L_1(k) = \begin{bmatrix} 1/\delta_0^2 & 0 & 0 \\ 0 & 0 & 0 \\ 0 & 0 & 1/\phi_0^2 \end{bmatrix} \quad \text{and } L_2(k) = \frac{1}{u_0^2}$$

The flowchart of the solution is given in fig. 5.

The assumption concerning the noise sequences can be somewhat weakened without invalidating the CE property. Root has shown ([28]) that the CE property holds even if the noises are non gaussian, and Tse that it still holds if the measurement noise is not white but gaussian. Other cases have been given in section 3.3. Unfortunately the linear quadratic gaussian problem is the only class where it is easy to derive the exact solution. We now present suboptimal algorithms proposed for non-linear problems and we discuss them with respect to their implementability in aerospace applications.

5. EXTENSIONS OF THE LINEAR QUADRATIC GAUSSIAN THEORY.

The linear quadratic gaussian theory is now extended in 3 directions : the optimal control of non-linear problems, the study of the effect of modelling errors and the adaptive control theory.

5.1 Non-linear systems.

As said in section 3.1 the CLO solution of the general non-linear problem is completely characterized by the sequence of the $J^{CLO}(N-k)$ functions, which are functions of the information states I^{CL} , and are generated recursively according to Bellman's principle (eq (3.3) and (3.4)). For CL policies, each of these $J^{CLO}(N-k)$ can be considered as a functional defined on the set of the probability density functions of the state at time k, given past controls and measurements, i.e. of $p[x(k)|Z_0^k, U_0^{k-1}]$, with the implicit assumption that the a priori information, as defined in section 2.2, is completely available. In order to elaborate the complete solution it is necessary to generate this sequence of functionals. In most cases an analytical solution does not exist (except for the linear quadratic gaussian case where the conditional p.d.f. of the state is gaussian and is characterized by its first two moments), and only suboptimal algorithms are proposed.

In a first class of algorithms it is intended to generate a recursive approximation of the $J^{CLO}(N-k)$ functions. A first method, due to Alspach ([30]), is based on the approximation of the conditional probability density function of the state by use of the gaussian sum approximation technique. Following this approach this p.d.f. is represented as a superposition (a "mixture") of elementary gaussian distributions ([31] - [33]). The parameters of these distributions are generated recursively by a set of Kalman filters working in parallel. This representation of the state p.d.f. is then used in the evaluation of the expectations appearing in (3.3) and (3.4). The complexity of the algorithm results from the fact that a large number of terms have to be considered in the gaussian sum. Nevertheless this method takes into account the eventual dual effect of the control and seems therefore to be, at the moment, one of the best approximations of the CLO solution, although its implementation is tedious and computer-time consuming.

A second algorithm is due to Bar-Shalom, Tse and Meyer ([34],[35]). In this method, a simplification is introduced in the recursive evaluation of the $J^{CLO}(n-k)$ by considering that the conditional probability density function of the state is characterized by its first two moments, even if the estimation is performed using a sophisticated method as the gaussian sum approximation. By consideration of a perturbation problem around nominal trajectories it is possible to minimize the expectation appearing in (3.4). This solution shows also the possible influence of the control on the future uncertainty of the state so the dual effect of the control is taken into account. This algorithm is easier to implement but can be less effective because only the first two moments of the density functions are considered and because the performance depends on the choice of the nominal trajectories.

A third algorithm is due to Campion ([36]) and consists in a gaussian sum approximation of the $J^{CLO}(N-k)$ under the form

$$\exp[-J^{CLO}(N-k)] = \sum_{i=1}^M a_i(k) \exp[-\frac{1}{2}[\lambda(k) - \lambda_i(k)]^T \pi_i(k) [\lambda(k) - \lambda_i(k)]] \quad (5.1)$$

where $\lambda(k)$ is the vector of the parameters characterizing $p[x(k)|Z_0^k, U_0^{k-1}]$. This vector is, in general, of infinite dimension and has therefore to be truncated. The evolution of the parameters $a_i(k)$, $\lambda_i(k)$ and $\pi_i(k)$ satisfies backward recursive equations deduced from (3.4). In this algorithm the computer time requirements are also important although the greatest part of the computational work can be achieved off-line, before starting the process, independently of the initial condition.

It is clear, from these descriptions that these algorithms are not easily implementable with on-board computers. For practical realizations implementable suboptimal algorithms are derived from the certainty equivalence property (see 3.3), with, possibly correction terms in order to compensate as much as possible the fact that this solution

does not present the dual effect of the control. As the original problem is partitioned into two decoupled subproblems (the estimation problem and the deterministic control problem) the implementation of the certainty equivalent solution supposes that the solutions of these two problems are available. The estimation of the state can be obtained using the linearized Kalman filter, or the extended Kalman filter, or by a more sophisticated method (see, for example [7],[10],[37]). On the other hand, even for deterministic systems, it can be difficult to obtain the closed-loop optimal policy when the system is not linear (see, for example [9]).

Jacob and Patchell ([39]) and Hughes ([40]) propose a controller based on the certainty equivalence property but a modification is introduced in order to take into account the concepts of caution and probing defined in section 3.2. The caution is included to reflect the knowledge the system has about the state : when the uncertainty decreases the controller can be less "cautions". On the other hand, in order to reflect the influence that the controller can have on the future evolution of the uncertainty, a probing signal is superposed to the certainty equivalent solution. Jacobs and Patchell propose a small known increment with alternating sign, while Hughes suggests a threshold probing signal, so the control signal is prevented to become smaller (in absolute value) than a prespecified level. The introduction of an additional probing signal is motivated by numerical studies in which phenomena called "Turn-off" and "Escape" were observed ([41]) - ([43]). Turn-off is defined to appear when the state estimate becomes small and causes the control to be small for a long period. During this method, because of the lack of control, some state variable are not yet controlled and can behave unsatisfactorily. The use of a probing signal prevents or terminates turn-off. Escape is said to occur when the control becomes very large and causes unsatisfactory system behaviour. Caution can eliminate this phenomena.

5.2 Modelling errors.

In order to make possible the implementation of an optimal controller with small on-board controller one has to consider simple mathematical model, ideally a low order linear model. Because of this simplification divergence can occur between the physical system and the mathematical model. These errors, referred to as "modelling errors", are of three kinds.

1. The physical system can present non linear characteristics.
2. Even if the physical system do not present nonlinearities, the physical parameters are maybe not perfectly known or may be subject to slow change (for example the inertia characteristics of a satellite with unknown thermal deformations).
3. In a low-order model the higher order modes are deliberately neglected. These modes can affect the outputs of the system (this phenomenon is known as the "observation spillover") and on the other hand, are also influenced by the control variables designed on the basis of the low order modes only. This phenomenon, referred to as the "control spillover", can cause unsatisfactory behaviour of the system. The effect of this mode truncation is under intensive investigation, specially for the future large space structures ([18]).

Methods of reduction of the effect of the third modelling error can be found in [18], specially in [44]. The best method to reduce the effects of the first two kinds of errors is to implement an adaptive controller. This particular aspect of optimal control is now quickly described in section 5.3.

5.3 Adaptive control.

Even if a linear mathematical model is realistic, the solution structure of the optimal control problem becomes non linear if the parameters of the model are not known exactly or are not selected optimally. That can be seen on the roll attitude controller example introduced in section 2.1. Suppose, for example, that the roll time-constant τ is not known with a good accuracy, producing an unsatisfactory behaviour of the system. Defining an augmented state vector x_a

$$x_a = \begin{bmatrix} x \\ \tau \end{bmatrix}, \quad (5.2)$$

the dynamical equation of the augmented system becomes

$$x_a(k+1) = \begin{bmatrix} x(k+1) \\ \tau(k+1) \end{bmatrix} = \begin{bmatrix} A[\tau(k)] & 0 \\ 0 & I \end{bmatrix} x_a(k) + \begin{bmatrix} B[\tau(k)] \\ 0 \end{bmatrix} u(k) + \begin{bmatrix} Gv(k) \\ 0 \end{bmatrix} \quad (5.3)$$

which is non linear in the variable $x_a(k)$.

It can be possible to identify these unknown parameters before applying effectively the control variables. There are many identification methods (see, for example, [45]). If it is not possible, an adaptive controller has to be designed, i.e. a controller structure where the parameters are adapted following the evolution of the unknown parameters uncertainty. The most used method is the "model reference" adaptive control, introduced by Landau ([46]). In this method the controller is designed for a linear reference model, but the parameters of this model and of the controller are adapted following the evolution of the system. This technique can also be used if the physical system presents non linearities. This adaptive control approach, which is an intermediate between non linear control and linear control, is promised to a wide development, specially for aerospace

applications, but a complete discussion of its properties and possibilities is outside the subject of this chapter.

6. Conclusions.

1. As the complexity of the optimal controller increases dramatically if a non-linear or an high order model is considered, one has interest to design the controller on the basis of a low order linear mathematical model. In order to prevent unsatisfactory behaviour it can be necessary to modify somewhat the solution based on this model (see section 5). Such a solution is of course suboptimal but presents the advantage to be implementable with on-board computers.
2. It is worthwhile, nevertheless, to develop more sophisticated algorithms. As they are closer to the optimal solution they produce a reference for the comparison with the suboptimal solutions. These algorithms are not implementable for on-line applications but they are usefull for ground simulations. On the other hand it is important to have a clear understanding of the mechanism of elaboration of the optimal control and, particularly, of the concept of dual effect of the control (section 3.2), because this discussion gives the reasons why a certainty equivalent controller can behave unsatisfactorily, and can be helpfull for the a priori detection of situations where a more sophisticated method has to be implemented.

APPENDIX A : Kalman filter equations.

For the linear system described by (4.1) and (4.2) the mean and covariance matrix of the conditional p.d.f. of the state are given recursively by the Kalman filter equations.

- a) The prediction p.d.f. $p[x(k+1)|z_0^k, u_0^k]$ is gaussian with a mean $\bar{x}(k+1|k)$ and a covariance matrix $P(k+1|k)$ given by

$$\bar{x}(k+1|k) = A(k)\bar{x}(k|k) + B(k)u(k) \quad , \quad (A.1)$$

and

$$P(k+1|k) = A(k)P(k|k)A^T(k) + Q(k) \quad . \quad (A.2)$$

- b) The conditional p.d.f. $p[x(k+1)|z_0^{k+1}, u_0^k]$ is still gaussian with a mean $\bar{x}(k+1|k+1)$ given by

$$\bar{x}(k+1|k+1) = \bar{x}(k+1|k) + K(k+1)[z(k+1) - H(k+1)\bar{x}(k+1|k)] \quad , \quad (A.3)$$

and

$$P(k+1|k+1) = [I_n - K(k+1)H(k+1)]P(k+1|k) \quad , \quad (A.4)$$

where I_n is the identity matrix of order n and where the Kalman gain $K(k+1)$ is given by

$$K(k+1) = P(k+1|k)H^T(k+1)[H(k+1)P(k+1|k)H^T(k+1) + R(k+1)]^{-1} \quad (A.5)$$

APPENDIX B : Closed-loop optimal control for the linear quadratic gaussian problem.

Following eq. (3.5) the terminal condition for the backward evolution of the J^{CLO} is written

$$J^{CLO}(0) = \int \left[\frac{1}{2} x^T(N) S x(N) \right] p[x(N)|I_N^{CL}] dx(N) \quad . \quad (B.1)$$

As the conditional p.d.f. of the state is gaussian, with mean $\bar{x}(N|N)$ and covariance matrix $P(N|N)$, the relation (B.1) can be rewritten as

$$J^{CLO}(0) = \frac{1}{2} \bar{x}^T(N|N) \pi(N) \bar{x}(N|N) + \alpha(N) \quad , \quad (B.2)$$

where

$$\pi(N) = S \quad , \quad (B.3)$$

and

$$\alpha(N) = \frac{1}{2} \text{tr}[SP(N|N)] \quad . \quad (B.4)$$

We now show that, in general, $J^{CLO}(N-k)$ can be expressed as

$$J^{CLO}(N-k) = \frac{1}{2} \bar{x}(k|k) \pi(k) \bar{x}(k|k) + \alpha(k) \quad (B.5)$$

where the weighting matrix $\pi(k)$ and the scalar $\alpha(k)$ are independent of the control sequence and of the actual realization.

Suppose that $J^{CLO}(N-k-1)$ has this form. From eq. (3.4) $J^{CLO}(N-k)$ is obtained as

$$J^{CLO}(N-k) = \min_{u(k)} E \left\{ \frac{1}{2} x^T(k) L_1(k) x(k) + \frac{1}{2} u(k) L_2(k) u(k) + \frac{1}{2} \bar{x}(k+1|k+1) \pi(k+1) \bar{x}(k+1|k+1) + \alpha(k+1) \middle| I_k^{CL} \right\} \quad (B.6)$$

We now evaluate separately the terms of the above conditional expectation.

a) $E \left[\frac{1}{2} x^T(k) L_1(k) x(k) \middle| I_k^{CL} \right] = \frac{1}{2} \bar{x}^T(k|k) L_1(k) \bar{x}(k|k) + \frac{1}{2} \text{tr}[L_1(k) P(k|k)]$ (B.7)

b) $E \left[\frac{1}{2} u^T(k) L_2(k) u(k) \middle| I_k^{CL} \right] = \frac{1}{2} u^T(k) L_2(k) u(k)$, (B.8)

because $u(k)$ is assumed to be selected through a deterministic policy.

- c) The expression of $\bar{x}(k+1|k+1)$ is given in (A.3). As the innovations sequence (i.e. the

sequence of $\{z(k) - H(k)\hat{x}(k|k-1)\}$ is a white gaussian sequence with zero mean and a covariance matrix given by $[H(k)P(k|k-1)H^T(k) + R(k)]$, it is independent of the previous estimates and the expected value

$$E\left[\frac{1}{2} \hat{x}(k+1|k+1)\pi(k+1)\hat{x}(k+1|k+1) \Big| I_k^{CL}\right]$$

is given by

$$\frac{1}{2}[A(k)\hat{x}(k|k) + B(k)u(k)]^T \pi(k+1)[A(k)\hat{x}(k|k) + B(k)u(k)] + \frac{1}{2} \text{tr}\{\pi(k+1)[H(k+1)P(k+1|k)H^T(k+1) + R(k+1)]\} \quad (B.8)$$

d) As the quantity $\alpha(k+1)$ is assumed to be independent of the actual realization it is but a deterministic quantity coinciding with its expected value. The minimization condition (B.6) is therefore equivalent to the following condition

$$\min_{u(k)} \left\{ \frac{1}{2} u^T(k)L_2(k)u(k) + \frac{1}{2}[A(k)\hat{x}(k|k) + B(k)u(k)]^T \pi(k+1)[A(k)\hat{x}(k|k) + B(k)u(k)] \right\}, \quad (B.9)$$

which has the same form as in the deterministic problem. The optimal control is therefore given by

$$u^{CLO}(k) = K_c(k)\hat{x}(k|k), \quad (B.10)$$

where the control gain $K_c(k)$ is given by

$$K_c(k) = -[L_2(k) + B^T(k)\pi(k+1)B(k)]^{-1} B(k)\pi(k+1)A(k). \quad (B.11)$$

With this expression of $u^{CLO}(k)$, $J^{CLO}(N-k)$ can be rewritten as

$$J^{CLO}(N-k) = \frac{1}{2} \hat{x}(k|k)\pi(k)\hat{x}(k|k) + \alpha(k), \quad (B.12)$$

where

$$\pi(k) = L_1(k) + K_c^T(k+1)L_2(k)K_c(k+1) + [A(k) + B(k)K_c(k+1)]^T \pi(k+1)[A(k) + B(k)K_c(k+1)],$$

and

$$\alpha(k) = \alpha(k+1) + \frac{1}{2} \text{tr}[L_1(k)P(k|k)] + \frac{1}{2} \text{tr}\{\pi(k+1)[H(k+1)P(k+1|k)H^T(k+1) + R(k+1)]\}$$

It must be noted that the relation (B.12) is the same as (4.8) corresponding to the deterministic problem.

Fig. 1 : The estimation problem

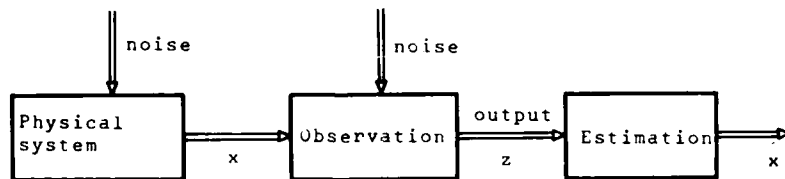


Fig. 2 : The control problem (1)

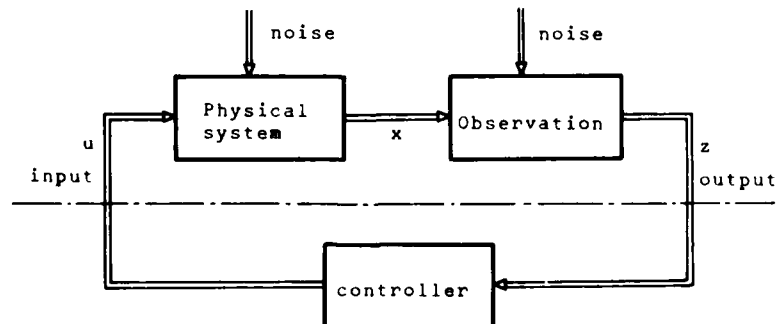


Fig. 3 : The control problem (2)

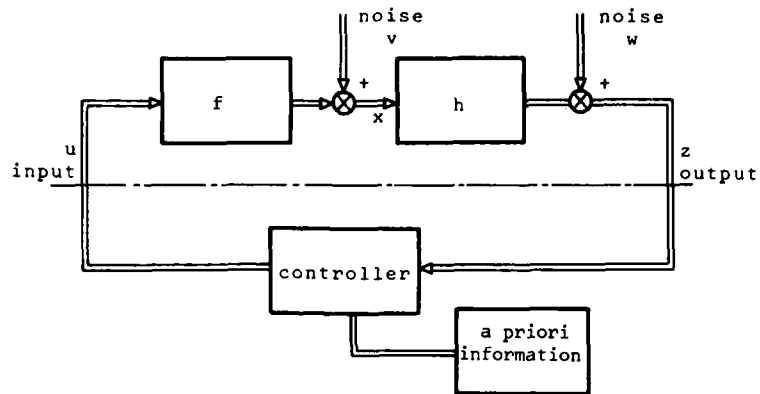


Fig. 4 : The Certainty equivalence control

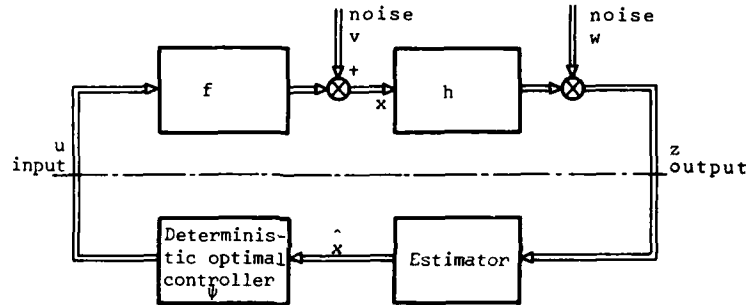
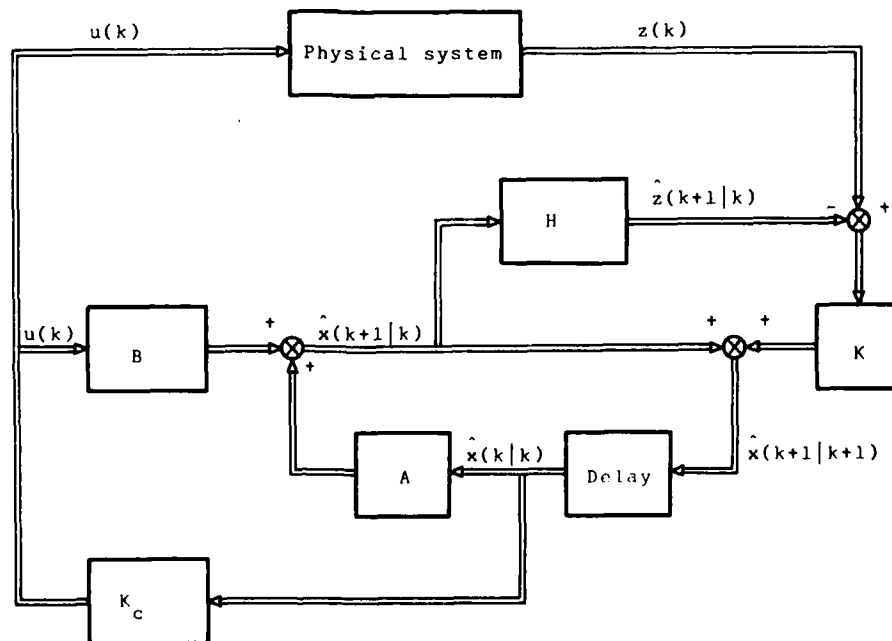


Fig. 5 : Linear-quadratic-gaussian problem



- [1] J.H. LANING & R.H. BATTIN "Random processes in Automatic Control", Mc Graw-Hill, New York, 1956.
- [2] H.J. KUSHNER "Introduction to Stochastic Control", Holt, New York, 1971.
- [3] J.L. DOOB "Stochastic Processes", Wiley, New York, 1953.
- [4] A. PAPOULIS "Probability Random variables and Stochastic processes", Mc Graw Hill, New York, 1965.
- [5] E. PARZEN "Stochastic processes", Holden Day, San Francisco, 1962.
- [6] A.T. BHARUCHA-REID "Elements of the theory of Markov Processes and their Applications", Mc Graw Hill, New York, 1960.
- [7] A.H. JAZWINSKI "Stochastic Processes and Filtering Theory", Academic Press, New York, 1960.
- [8] R.E. KALMAN "On the general theory of control systems", Proc. 1st IFAC Congress Moscow 1960.
- [9] R.E. KALMAN "A new Approach to linear filtering and prediction problems", J. of Basic Engineering, March 1960, 35-45.
- [10] G. CAMPION, M.Z. DAJANI & P.Y. WILLEMS "Non linear Estimation. A survey". Proceedings Euromech 38 Symposium, Springer Verlag, 1974.
- [11] R.E. BELLMAN "Adaptive Control Processes", Princeton Univ. Press, Princeton, New Jersey, 1961.
- [12] A.A. FELD'BAUM "Optimal Control Systems", Academic Press, New York, 1965.
- [13] M. AOKI "Optimization of Stochastic Systems", Academic Press, New York, 1967.
- [14] J.S. MEDITCH "Stochastic Optimal Linear Estimations and Control", Mc Graw Hill, New York, 1969.
- [15] K.J. ASTROM "Introduction to Stochastic Control Theory", Academic Press, New York, 1970.
- [16] W.E. HOLLEY, A.E. BRYSON "Wind Modeling and lateral control for automatic landing", J. of Spacecraft and Rockets, Vol. 14, n°2, Feb. 77, 65-72.
- [17] R.V. GRESSANG, D. ZONARS "Modern Aerospace Systems", Control and Dynamics Systems (Edited by C.T. Leondes), vol. 13, 1977.
- [18] Proc. of the 2d VPI and SU/AIAA Symposium on Dynamics and Control of Large Flewible Spacecraft. Blacksburg, Virginia, June 1979.
- [19] A.E. BRYSON & Y.C. HO "Applied Optimal Control", Wiley, 1975.
- [20] R.E. BELLMAN "Adaptive Control Processes : A guided tour", Princeton Univ. Press, Princeton, New Jersey, 1961.
- [21] C. STRIEBEL "Sufficient Statistics in the optimal control of stochastic systems", J. Math. Anal. and Applications 12, 576 (1965).
- [22] S.E. DREYFUS "Dynamic Programming and the calculus of Variations", Academic Press, New York, 1965.
- [23] H.A. SPANG "Optimum Control of an unknown linear plant using Baeyesian Estimation of the error", IEEE Trans. on Autom. Control, vol. AC 10, 80 (1965).
- [24] J.B. FARISON, R.E. GRAHAM & A.C. SKELTON "Identification and Control of Linear Discrete Systems", IEEE Trans. on Autom. Control, AC 12, 438, (1967).
- [25] J. SPEYER, J. DEYST & D. JACOBSON "Optimization of Stochastic Linear Systems with additive measurement and Process noise using experimental performance criteria", IEEE Trans. on Autom. Control, AC-19, 358 (1974).

- [26] Y. BAR-SHALOM & E. TSE "Dual effect, certainty equivalence and separation in Stochastic Control", IEEE Trans. on Autom. Control, AC 19, 494 (1974).
- [27] Y. BAR SHALOM & E. TSE "Concepts and Methods in Stochastic Control", Control and Dynamic Systems, vol. 12, 1976 (Edit. by C.T. Leondes)
- [28] J.G. ROOT "Optimum Control of non Gaussian linear stochastic system with inaccessible state variables", SIAM J. Control 7-317 (1969).
- [29] E. TSE "On the Optimal control for linear systems with incomplete information", Report ESC-R-412. Electronic Systems Laboratory, MIT Cambridge Massachussets, 1970.
- [30] D.L. ALSPACH "Dual control based on approximate a posteriori density functions", IEEE Trans. on Autom. Control, AC 17-1972.
- [31] D.L. ALSPACH "A Bayesian approximation technique for Estimation and Control of time-discrete stochastic systems", Ph.D. Dissertation, Univ. of California, San Diego, 1970.
- [32] H.W. SORENSON & D.L. ALSPACH "Recursive Bayesian estimation using gaussian sums", Automatica, vol. 7 (1971), pp. 465-479.
- [33] D.L. ALSPACH & H.W. SORENSON "Non linear Bayesian Estimation using Gaussian sum Approximation", IEEE Trans. on Autom. Control, AC-17, n° 4, Aug. 1972.
- [34] E. TSE, Y. BAR-SHALOM & L. MEIER "Wide-sense Adaptive dual control for non linear Stochastic Systems", IEEE Trans. on Autom. Control, vol. AC 18, n° 2, 1973.
- [35] Y. BAR-SHALOM, E. TSE & R.E. LARSON "Some Recent advances in the development of closed-loop stochastic control and Resource Allocation algorithms", Proceeding of the IFAC Stochastic Control Symposium, Budapest, 1974.
- [36] G. CAMPION "Optimal control of non-linear stochastic systems by approximation of the optimal cost functional", Proc. 18th IEEE Conference on Decision and Control, San Diego, 1979.
- [37] "Theory and Applications of Kalman filtering", Edited by C.T. LEONDES, Agardograph 139(1970).
- [38] O.L.R. JACOBS & S.M. LANGDON "An optimal extremal control system", Automatica, 6, (1970).
- [39] O.L.R. JACOBS & J.N. PATCHELL "Caution and Probing in Stochastic Control", Int. Journal of Control 16 (1972).
- [40] D.J. HUGHES "Studies in Stochastic Control Theory", Ph.D. Dissertation, University of Oxford, 1974.
- [41] D.J. HUGHES & O.L.R. JACOBS "Turn-off, escape and probing in non-linear stochastic control", Proc. IFAC Symposium on Stochastic Control, Budapest, 1974.
- [42] K.J. ASTROM & B. WITTENMARK "Problems of Identification and Control", J. Math. Analysis and Appli., vol. 34, n° 1, April 1971.
- [43] B. WITTEN MARK "On the turn-off phenomena in adaptive control", Lund Inst. Tech., Report 7105, sept. 1971.
- [44] J.R. SESAK, P. LIKINS & T. CORADETTI "Flexible Spacecraft Control by Model error sensitivity suppression", Proc. of the 2d VPI/AIAA Symposium on Dynamics and Control of Large Flexible Spacecraft, Blacksburg, June 1979.
- [45] P. EYKHOFF "System Identification : Parameter and State Estimation", John Wiley, New York 1974.
- [46] I.D. LANDAU "Adaptive Control : the model reference approach", Marcel Dekker - New York 1978.

AN INTRODUCTION TO
STOCHASTIC OPTIMAL CONTROL THEORY

Robert F. Stengel
Princeton University
Flight Research Laboratory
Department of Mechanical and Aerospace Engineering
Princeton, N. J. 08544 U.S.A.

SUMMARY

The design of control logic that commands a dynamic system to a desired output or that augments the system's stability is facilitated if objectives are expressed in a quantitative criterion, because the optimization of this criterion establishes a feasible design point for control. If the information which the control logic must use is uncertain or if the dynamic system is forced by random disturbances, one can hope to optimize only the expected value rather than the actual value of this criterion. The methodology for design is based upon stochastic optimal control theory, the topic of this chapter. After introducing the dynamic models of interest, optimal control and estimation are presented separately. Limitations of this approach are addressed, and the unified design of linear stochastic optimal controllers for analog and digital implementations is described. The principal benefit of stochastic optimal control theory is that it provides an engineering framework within which practical control design can be accomplished for complex dynamic systems.

INTRODUCTION

Optimal control theory is that body of information which describes the application of forces to a system for the purpose of maximizing some measure of performance or minimizing a cost function. The nature of the control is stochastic if, in addition to the controlling forces, the system is forced by random disturbances, if the parameters of the system are subject to random variation, if initial conditions are random, or if any measurements used to formulate the control are subject to random errors. All control systems are intended to optimize some criteria, whether or not the criteria are stated explicitly, and there is some degree of uncertainty in any control system implementation. Consequently, stochastic optimal control theory has broad application to practical systems, as demonstrated by the remaining papers in this volume.

The apparent dichotomy between "optimal" control and "practical" control is linked more closely to style than substance, as optimal control design can be a very practical process. One impediment to understanding is the definition of what we mean by "optimal". Whereas there is a class of problems in which a single, unequivocal optimum can be defined, e.g., minimum time, fuel, or cost, there is an even greater class in which the selection of weights in the cost function is arbitrary. These weights have no small effect on the numerical solution, and the analyst may purposely digress from theoretically "best" weights in order to make the solution more "robust", i.e., more insensitive to parameter variations. In such instance, optimality, *per se*, is less important than the fact that optimization provides a systematic procedure for "trading off" system performance and control activity within established limits. This in itself is a most practical quality. Therefore, let us define "optimal" as "tending toward the optimum", recognizing that some deviation from the optimum is acceptable, if not unavoidable, in practical application.

Aerospace systems are dynamic, and the evolution of their motions in time is of particular interest; hence, the criteria to be optimized are expressed naturally in terms of final values and time-integrals of the motion and control variables. Nevertheless, stability, input-output characteristics, parameter sensitivity, and modal response are of great practical concern, so frequency-domain equivalents are useful. The power of time-domain formulations is related to their generality; optimal controls for nonlinear time-varying systems are specified (if not calculated) readily, and the simplifications afforded by linearity and time-invariance are accommodated in a single theoretical framework. When both linearity and time-invariance can be assumed, frequency-domain concepts aid interpretation and, in some cases, computation. This chapter presents stochastic optimal control theory from a time-domain viewpoint, providing frequency-domain perspectives where possible.

What follows can not include all methodologies for all optimization problems. It is an interpretation of the theoretical underpinnings of optimization techniques commonly applied to aerospace problems. While it is hoped that this chapter may provide new insights or clarifications of stochastic optimal control theory, the theory itself has been developed earlier. The reader who is interested in greater detail should refer to [1] to [14], which are principal sources of material for this chapter.

After reviewing general models of dynamic systems and some basic characteristics of the mathematics, the theory of deterministic nonlinear optimal control is presented. The notion of neighboring-optimal trajectories as prototypes for feedback control is

introduced, as is the need for estimation that arises in some cases. Optimal filtering and prediction for discrete-time systems are presented, with continuous-time estimation developed as the limiting case for vanishingly small sampling interval. The separation theorem and its limitations are discussed, and the chapter concludes with details of linear, time-invariant stochastic optimal controllers.

MODELS OF DYNAMIC SYSTEMS

Stochastic optimal control is to be applied to a dynamic system that consists of a physical process and its observation. Elements of the physical process can be arranged in five distinct families, which identify their respective roles in the process, and the observation contains two families of variables. Each family is represented by an ordered set (or column vector) of scalar quantities, with dimension appropriate to the system:

<u>Vector</u>	<u>Description</u>	<u>Dimension</u>
\underline{p}	Parameters	l
\underline{u}	Controllable Inputs	m
\underline{w}	Uncontrolled Inputs (Disturbances)	s
\underline{x}	Physical States	n
\underline{y}	Process Outputs	r
\underline{n}	Measurement Errors	r
\underline{z}	Observations	r

The relationships between these variables are illustrated by Fig. 1.

These seven categories of variables serve distinct purposes in the dynamic system. The vector of parameters, \underline{p} , scales the process's response to inputs and to its own motions. The forces on the process (or inputs) that can be controlled are contained in \underline{u} , while those which are beyond control are contained in \underline{w} . The state vector, \underline{x} , represents the dynamic condition of the process, i.e., the fundamental response to inputs. The process structure is such that \underline{x} "feeds back" into the system (through physical effects), and this feedback can modify process response in several ways, e.g., by shifting the steady-state characteristics, causing oscillations, stabilizing the process, and so on. The output vector, \underline{y} , can contain none or all of the above (\underline{p} , \underline{u} , \underline{w} , and \underline{x}), selected components of each vector, or transformations of these vectors, depending upon the process and its instrumentation. In general, the output can not be measured exactly, so the observation, \underline{z} , is some combination of the output, \underline{y} , and measurement error, \underline{n} . Any dynamic effects associated with control actuation or measurement sensing are assumed to be contained in the physical process.

Open-loop optimal control can be applied only if the dynamic system is characterized by adequate controllability, and closed-loop optimal control (including stochastic control) requires adequate observability as well. A system is controllable at time t_0 , if there is a control history, $\underline{u}(t)$, $t_0 \leq t \leq t_f < \infty$, which transfers each element of an arbitrary initial state, $\underline{x}(t_0)$, to zero at t_f . If there is an independent physical path between every component of \underline{x} and at least one element of \underline{u} , then the process is likely to be completely controllable. (There must be adequate control "power" as well.) The path can be either direct or indirect, as long as it can be distinguished from possibly redundant paths. A system is observable at t_0 if the output history, $\underline{y}(t)$, $t_0 \leq t \leq t_f < \infty$ is adequate to reconstruct $\underline{x}(t_0)$. If there is an independent physical path between every component of \underline{x} and at least one element of \underline{y} , then the process can be said to be completely observable. Again, the path can be direct or indirect, but it must be non-identical to all other paths. Conditions that must be satisfied for complete controllability and observability can be found in [1]-[3], [6]-[8]. These definitions say nothing about the potential quality of control or observation -- they merely indicate whether or not the structures for control and observation exist.

In most cases, the physical process is only partially controllable and observable, either as a consequence of the physical process itself or because limited resources prevent implementation of complete control and observation. Such a process can be separated into four parts -- those sub-processes which are both completely controllable and observable, those which are one but not the other, and those which are neither.

From a practical point of view, complete controllability and observability are not required if the uncontrolled or unobserved states are well-behaved. For example, adequate rigid-body control of an aircraft need not depend on controlling or observing well-damped aeroelastic, fuel sloshing, or external stores modes. If an uncontrolled sub-process is stable, i.e., bounded disturbance inputs produce bounded response, the sub-process is said to be stabilizable, and its effects can not cause the process to diverge. If an unobservable sub-process is stable, it is said to be detectable, as bounds on the observed states can be estimated. Partial controllability and observability may be acceptable, but sub-processes which are not stabilizable and/or not detectable must be avoided. Closed-loop control can be applied only to those elements which are both controllable and observable.

Physical processes normally are continuous functions of time, so it is appropriate to model the evolution of their motions by differential equations. Although some processes

are best described by partial differential equations, we will restrict our view to ordinary differential equations, noting that numerical approximations to the former can be achieved with the latter. The solution variables for these equations are contained in the state vector, $\underline{x}(t)$, the focal point of estimation and control. In an increasing number of applications using digital computers, control settings are calculated and measurements are made at discrete (often periodic) instants of time. Difference equations that are equivalent to the original differential equations can be found, and continuous-time stochastic optimal control solutions are paralleled by discrete-time results.

For either continuous-time or discrete-time models, the dynamic equations can be classified as in Fig. 2. If the dynamic coefficients are changing rapidly with time, in comparison with the time scale of motions, the dynamic model must be time-varying; if the coefficients are relatively constant, a time-invariant model will suffice. If motions evidence the superposition characteristic, i.e., doubling the input doubles the output, then linear models can be used; if not, the dynamic model must be nonlinear. A non-linear, time-varying dynamic system can be described by an n-component vector differential equation representing its dynamics, an r-component algebraic (or transcendental) equation representing the output, and an r-component equation representing the observation:

$$\frac{d\underline{x}(t)}{dt} = \underline{\dot{x}}(t) = \underline{f} [p(t), \underline{x}(t), \underline{u}(t), \underline{w}(t), t] \quad (1)$$

$$\underline{y}(t) = \underline{h} [p(t), \underline{x}(t), \underline{u}(t), \underline{w}(t), t] \quad (2)$$

$$\underline{z}(t) = \underline{j} [\underline{y}(t), \underline{n}(t)] = \underline{y}(t) + \underline{n}(t) \quad (3)$$

The vector, \underline{f} , contains an element for each element of \underline{x} ; each element of \underline{f} is the appropriate scalar equation that defines the time-rate-of-change of its corresponding component of \underline{x} . The dimension of the output function, \underline{h} , is not governed by the dynamics of the process; it may be larger or smaller than the state dimension, and there is some freedom in its choice. The nonlinear complexities of observation normally can be absorbed in Eq. (2), and observation error is added in Eq. (3).

Solutions of nonlinear, time-varying differential equations require direct integration, either by numerical or analog computation. The resulting time histories describe the evolution of motions for given controls, disturbances, and initial conditions; each change in any of these quantities leads to a new state trajectory.

Small perturbations from a nominal trajectory can be modeled by linear approximation. To do this, both sides of Eq. (1) to (3) are expanded in Taylor series, and terms beyond the first degree are neglected. The zeroth-degree terms generate the nominal solution, and the first-degree terms govern the perturbation solution. The model variables are assumed to be separable into nominal and perturbation components denoted by $()_0$ and $\Delta ()$, respectively. The nominal, nonlinear equations are

$$\dot{\underline{x}}_0(t) = \underline{f}[p_0(t), \underline{x}_0(t), \underline{u}_0(t), \underline{w}_0(t), t] \quad (4)$$

$$\underline{y}_0(t) = \underline{h}[p_0(t), \underline{x}_0(t), \underline{u}_0(t), \underline{w}_0(t), t] \quad (5)$$

$$\underline{z}_0(t) = \underline{y}_0(t) + \underline{n}_0(t) \quad (6)$$

Assuming parameter variations are not perturbed, the corresponding linear, time-varying equations are

$$\Delta \dot{\underline{x}}(t) = \underline{F}(t)\Delta \underline{x}(t) + \underline{G}(t)\Delta \underline{u}(t) + \underline{L}(t)\Delta \underline{w}(t) \quad (7)$$

$$\Delta \underline{y}(t) = \underline{H}_x(t)\Delta \underline{x}(t) + \underline{H}_u(t)\Delta \underline{u}(t) + \underline{H}_w(t)\Delta \underline{w}(t) \quad (8)$$

$$\Delta \underline{z}(t) = \Delta \underline{y}(t) + \Delta \underline{n}(t) \quad (9)$$

where the Jacobian matrices,

$$\underline{F}(t) = \frac{\partial \underline{f}}{\partial \underline{x}} (n \times n), \underline{G}(t) = \frac{\partial \underline{f}}{\partial \underline{u}} (n \times m), \underline{L}(t) = \frac{\partial \underline{f}}{\partial \underline{w}} (n \times s) \quad (10)-(12)$$

$$\underline{H}_x(t) = \frac{\partial \underline{h}}{\partial \underline{x}} (r \times n), \underline{H}_u(t) = \frac{\partial \underline{h}}{\partial \underline{u}} (r \times m), \underline{H}_w(t) = \frac{\partial \underline{h}}{\partial \underline{w}} (r \times s) \quad (13)-(15)$$

are evaluated at $[\underline{x}_0(t), \underline{u}_0(t), \underline{w}_0(t), p_0(t), t]$. The Jacobian matrices express the linear sensitivity of \underline{f} and \underline{h} to small perturbations in \underline{x} , \underline{u} , and \underline{w} . Even if $p_0(t)$ is

constant, these matrices are likely to vary in time as long as the nominal input variables ($\underline{u}_0, \underline{w}_0$) and solution variable (\underline{x}_0) vary in time. The linear, time-invariant case rigorously occurs only with constant nominal inputs, when the state has reached equilibrium, or if there is no functional dependence of the Jacobian matrices on the changing variables.

The dynamic equations have been expressed as a vector set of first-order differential equations because these provide the most flexibility for computation and analysis. A large body of dynamic analysis, particularly that related to structures, is based on linear second-order equation sets, which can easily be converted to first-order "state-space" notation. Using the modal coordinate vector, $\Delta \underline{q}$, the second-order equations are

$$M\Delta \ddot{\underline{q}} + C\Delta \dot{\underline{q}} + K\Delta \underline{q} = D\Delta \underline{u} \quad (16)$$

where, M, C, K, and D are the mass, damping, spring, and forcing matrices, respectively. This equation can be put in the first-order form

$$\Delta \dot{\underline{x}} = F\Delta \underline{x} + G\Delta \underline{u} \quad (17)$$

by first defining

$$\Delta \underline{x} = \begin{bmatrix} \Delta \underline{q} \\ \Delta \dot{\underline{q}} \end{bmatrix} \triangleq \begin{bmatrix} \Delta \underline{x}_1 \\ \Delta \underline{x}_2 \end{bmatrix} \quad (18)$$

then forming

$$F = \begin{bmatrix} 0 & I \\ -M^{-1}K & -M^{-1}C \end{bmatrix} \quad (19)$$

and

$$G = \begin{bmatrix} 0 \\ -M^{-1}D \end{bmatrix} \quad (20)$$

If the Jacobian matrices are constant, an equivalent frequency-domain model is easily formed. The Laplace transforms of Eq. (7) and (8), neglecting initial conditions, are

$$(sI - F)\Delta \underline{x}(s) = G\Delta \underline{u}(s) + L\Delta \underline{w}(s) \quad (21)$$

$$\Delta \underline{y}(s) = [H_x(sI - F)^{-1}G + H_u]\Delta \underline{u}(s) + [H_x(sI - F)^{-1}L + H_w]\Delta \underline{w}(s) \quad (22)$$

where s is the Laplace operator. Equation (22) is seen to contain transfer function matrices between the inputs, $\Delta \underline{u}(s)$ and $\Delta \underline{w}(s)$, and the output, $\Delta \underline{y}(s)$.

While a comparable difference equation is not easily specified for the nonlinear dynamic equation, the linear, time-varying differential equation has a straightforward discrete-time equivalent. The time-varying difference equation

$$\Delta \underline{x}(t) = \phi(t, t_0)\Delta \underline{x}(t_0) + \int_0^t \phi(t, \tau)[G(\tau)\Delta \underline{u}(\tau) + L(\tau)\Delta \underline{w}(\tau)] d\tau \quad (23)$$

propagates the state precisely from one sampling instant, t_0 , to the next, t , using the state transition matrix, $\phi(t, t_0)$ [6]. For a linear, time-invariant system with stepwise-constant inputs and periodic sampling, Eq. (23) can be put in the form

$$\Delta \underline{x}_{k+1} = \phi(T)\Delta \underline{x}_k + \Gamma(T)\Delta \underline{u}_k + \Lambda(T)\Delta \underline{w}_k \quad (24)$$

where T is the sampling interval, k is a sampling index, and

$$\phi(T) = e^{FT} = I + FT + \frac{1}{2!}F^2T^2 + \dots \quad (25)$$

$$\Gamma(T) = (\phi - I)F^{-1}G = [I + \frac{1}{2!}FT + \frac{1}{3!}F^2T^2 + \dots]GT \quad (26)$$

$$\Lambda(T) = (\phi - I)F^{-1}L = [I + \frac{1}{2!}FT + \frac{1}{3!}F^2T^2 + \dots]LT \quad (27)$$

The equilibrium response of linear, time-invariant models is shown below to be useful in the design of non-zero set point regulators using stochastic optimal control theory. Starting at the nominal equilibrium, a constant input perturbation, $\Delta \underline{u}_p$ or $\Delta \underline{w}_p$, would disturb the state from its nominal value. The perturbation equilibrium value, $\Delta \underline{x}_p$, is defined by Eq. (7), with $\Delta \dot{\underline{x}} = 0$:

$$\Delta \underline{x}_p = -F^{-1}(G\Delta \underline{u}_p + L\Delta \underline{w}_p) \quad (28)$$

provided F^{-1} exists. The corresponding output is found by substituting $\Delta \underline{x}_p$, $\Delta \underline{u}_p$, and $\Delta \underline{w}_p$ in Eq. (8). Alternatively, if desired values of m components of the output, $\Delta \underline{y}_m$, are specified, Eq. (7) and (8) can be solved simultaneously to find $\Delta \underline{x}_p$ and $\Delta \underline{u}_p$. With $\Delta \underline{x} = 0$ and $H_w = 0$,

$$\begin{bmatrix} \Delta \underline{x}_p \\ \Delta \underline{u}_p \end{bmatrix} = \begin{bmatrix} F & G \\ H_{x_m} & H_{u_m} \end{bmatrix}^{-1} \begin{bmatrix} -L\Delta \underline{w}_p \\ \Delta \underline{y}_m \end{bmatrix} = S \begin{bmatrix} -L\Delta \underline{w}_p \\ \Delta \underline{y}_m \end{bmatrix} \quad (29)$$

requiring the existence of an additional inverse matrix, S [15]. The corresponding discrete-time perturbation equilibrium involves Eq. (24) and (8) with $\Delta \underline{x}_{k+1} = \Delta \underline{x}_k$; however, it can be shown that the solution is identical to Eq. (29), as might be expected.

OPTIMAL TRAJECTORIES AND NEIGHBORING-OPTIMAL SOLUTIONS

Conditions for Optimality

We begin by considering optimal control strategies for dynamic systems whose parameters, disturbances, and initial conditions are known without error. By convention, the control history, $\underline{u}^*(t)$, $t_0 \leq t \leq t_f$, that minimizes a cost function, J_{NL} , is to be found. The cost function considered here consists of two parts, a scalar algebraic function of the final state, $\phi[\underline{x}(t_f)]$, and a scalar integral function of the state and control:

$$J_{NL} = \phi[\underline{x}(t_f)] + \int_0^{t_f} L[\underline{x}(t), \underline{u}(t)] dt \quad (30)$$

The choice of $\phi[\cdot]$ and the integrand, $L[\cdot]$, dictates the nature of the optimizing solution, and there is some flexibility in expressing a particular cost as a terminal or integral function. In the example of an aircraft trajectory with fixed terminal cost function, $\phi[\underline{x}(t_f)]$, choosing $L[\cdot] = 1$ specifies a minimum-time problem, while choosing $L[\cdot] = \text{fuel flow rate}$ leads to a minimum-fuel problem. Alternatively, the state can be augmented to include a fuel mass component, and the minimum-fuel problem can be specified by redefining $\phi[\underline{x}(t_f)]$.

Equation (30) is minimized subject to the dynamic constraint provided by the system's differential equation:*

$$\dot{\underline{x}}(t) = \underline{f}[\underline{x}(t), \underline{u}(t), \underline{w}(t), \underline{p}(t), t], \text{ with } \underline{x}(t_0), \underline{w}(t), \underline{p}(t) \text{ given} \quad (31a)$$

or

$$\underline{f}[\cdot] - \dot{\underline{x}}(t) = 0, \quad t_0 \leq t \leq t_f \quad (31b)$$

Because Eq. (31b) always equals zero, it can be adjoined to the integral cost function without changing the value of J_{NL} or the minimizing control; however, Eq. (31b) is a vector relationship and the integral cost is a scalar. Defining the n -component vector of Lagrange multipliers, $\underline{\lambda}(t)$ (also called the adjoint or costate vector), the scalar product $\underline{\lambda}^T[\underline{f}[\cdot] - \dot{\underline{x}}(t)]$ is formally added to $L[\cdot]$. The solution equations for $\underline{\lambda}$ determine the optimal control.

Defining the scalar Hamiltonian, $H[\underline{x}(t), \underline{u}(t), \underline{\lambda}(t), t]$,

$$H[\underline{x}(t), \underline{u}(t), \underline{\lambda}(t), t] = L[\underline{x}(t), \underline{u}(t)] + \underline{\lambda}^T(t)\underline{f}[\underline{x}(t), \underline{u}(t), t] \quad (32)$$

Eq. (30) can be written as

$$J_{NL} = \phi[\underline{x}(t_f)] + \int_0^{t_f} \{H[\underline{x}(t), \underline{u}(t), \underline{\lambda}(t), t] - \underline{\lambda}^T(t)\dot{\underline{x}}(t)\} dt \quad (33)$$

Following [1], the second term in the integrand can be integrated by parts:

* Constraints on the state or control at interior points, end points, or over the entire interval also can be addressed. These constraints can specify that the variable(s) equal given value(s) or that they are merely bounded by such values.

$$J_{NL} = \phi[\underline{x}(t_f)] - [\underline{\lambda}^T(t_f)\underline{x}(t_f) - \underline{\lambda}^T(t_0)\underline{x}(t_0)] + \int_{t_0}^{t_f} \{H[\cdot] + \underline{\lambda}^T(t)\underline{x}(t)\} dt \quad (34)$$

Necessary conditions for a minimum value of J_{NL} with respect to the control are formed by requiring that the sensitivity of J_{NL} to any control variations, $\Delta \underline{u}(t)$, and associated state variations, $\Delta \underline{x}(t)$, be zero on the minimizing path. From Eq. (34), the first variation in J_{NL} can be expressed as

$$\begin{aligned} \Delta J_{NL} &= \Delta J_{IC} + \Delta J_{control} \\ &= \underline{\lambda}^T(t_0)\Delta \underline{x}(t_0) + \int_{t_0}^{t_f} \left[\left(\frac{\partial H}{\partial \underline{x}} + \underline{\lambda}^T \right) \Delta \underline{x} + \frac{\partial H}{\partial \underline{u}} \Delta \underline{u} \right] dt + \left\{ \frac{\partial}{\partial \underline{x}} \phi[\underline{x}(t_f)] - \underline{\lambda}^T(t_f) \right\} \Delta \underline{x}(t_f) \end{aligned} \quad (35)$$

where the first term is the cost function's variation due to changes in the initial state and the remaining terms are the result of changes in control. $\Delta J_{control} = 0$ for arbitrary values of $\Delta \underline{x}$ and $\Delta \underline{u}$ only if three conditions are satisfied:

$$\dot{\underline{\lambda}}(t) = - \frac{\partial H^T(t)}{\partial \underline{x}} = - \frac{\partial L^T(t)}{\partial \underline{x}} - F^T(t)\underline{\lambda}(t) \quad , \quad t_0 \leq t \leq t_f \quad (36)$$

$$\underline{\lambda}(t_f) = \left\{ \frac{\partial}{\partial \underline{x}} \phi[\underline{x}(t_f)] \right\}^T \quad (37)$$

$$\frac{\partial H^T(t)}{\partial \underline{u}} = \frac{\partial L^T(t)}{\partial \underline{u}} + G^T(t)\underline{\lambda}(t) = 0 \quad , \quad t_0 \leq t \leq t_f \quad (38)$$

The adjoint vector is obtained by integrating Eq. (36) backward in time from the end condition specified by Eq. (37), with all time functions evaluated along the optimal (nominal) trajectory. Equation (38) is then a direct expression of the cost function's stationarity: on the optimal path, the sensitivity of the Hamiltonian to small changes in the control is zero. These three equations are called the Euler-Lagrange equations.

It is necessary for the Euler-Lagrange equations to be satisfied on the optimal path, but these equations guarantee only stationarity, not optimality. While the minimum may be indicated, it also is possible that J_{NL} has been maximized or forced to an inflection point by the control. As described in [1], three sufficiency conditions must be satisfied to guarantee a minimum. 1) The Hamiltonian must be convex ($H_{uu} > 0$) in the interval, indicating that the solution has reached a "valley" rather than a "ridge line" or "ledge". For controllable systems without terminal constraints, this condition usually is sufficient to guarantee optimality. If the ($m \times m$) matrix H_{uu} is singular, minimizing controls may still exist, but time derivatives of H_u , as well as H_u itself, must equal zero in the interval. 2) The solution must be "normal", i.e., small changes in terminal constraints lead to neighboring optimal solutions. A system that is not completely controllable is likely to be "abnormal" in this respect. 3) There must be no conjugate (or focal) points. Finding the path which yields the minimum distance from any point on the globe to the equator provides an example: the north and south poles are conjugate points because there are an infinite number of such paths.

If the nonlinear system equations have low order and simple structure, it may be possible to find analytic closed-form solutions to the optimizing equations; however, in most cases, it is necessary to resort to iterative numerical techniques for solution. These are discussed briefly in the next section.

Numerical Optimization

Iterative techniques for finding the optimal control history, $\underline{u}^*(t)$, $t_0 \leq t \leq t_f$, and the corresponding state trajectory, $\underline{x}^*(t)$, must provide solutions of the n -component differential equation [Eq. (36)], subject to initial conditions for the state, $\underline{x}(t_0)$, and final conditions for the adjoint vector, $\underline{\lambda}(t_f)$. The optimal trajectory is very much a function of how the control vector is defined; changing the components of $\underline{u}(t)$ is likely to change the numerical values of $\underline{x}^*(t)$. Solutions to the two-point boundary-value problem can be found using extremal fields (dynamic programming), neighboring extremals, penalty functions, quasilinearization, and gradient methods [1], [11]. The principal distinctions between these methods are which equations and conditions are nominally satisfied by the problem formulation itself and which must be forced to solution by the iteration. A particular appeal of the gradient methods is that the dynamic system equation is solved exactly on each iteration, with the control being perturbed from step to step. In other words, the algorithm simulates the system's dynamic response with varying control histories from one iteration to the next, and the physical effects of the

optimization are quite visible at each step.

A schematic of gradient (or steepest-descent) optimization is shown in Fig. 3. The process begins with the specification of initial conditions and a nominal control history. Note that a simulation program is an inherent part of the process and that the adjoint vector is integrated back from the final point on each iteration. In most cases, sufficiency need not be verified for every iteration, so this computation is optional. The choice of a stopping condition is somewhat arbitrary. If the minimizing value of J_{NL} is known (for example, it would be zero with a path-following cost function), the iteration can stop when the computed cost is acceptably close to its known value. Otherwise, the iteration can stop when some scalar function of the control gradient,

$$H_u(t), \text{ e.g., } \left(\int_{t_0}^{t_f} [H_u(t)H_u^T(t)]dt \right) / (t_f - t_0), \text{ is acceptably close to zero.}$$

The choice of the $(m \times m)$ control-gradient weighting matrix, $K_k(t)$, in the control adjustment equation,

$$\underline{u}_{k+1}(t) = \underline{u}_k(t) - K_k(t)H_{u_k}^T(t) \quad (39)$$

is critical for rapid convergence to the minimizing control. If $K(t)$ is too small, convergence may require a large number of iterations; if it is too large, convergence may not occur at all. In the neighborhood of the optimal trajectory, $H_{uu}(t)$ should be greater than zero (by convexity); if $K_k(t) = H_{uu}^{-1}(t)$, the iteration becomes a Newton-Raphson algorithm. In practice, $H_{uu}(t)$ can be difficult to calculate precisely, and the calculated value may not be convex during early iterations. Efficient constant values of K_k (which may change from one iteration to the next but are constant on each iteration) can be found from auxiliary integrals of the trajectory [1] or by numerical search, as in [16].

It should be recognized that the amount of computation associated with iterative numerical optimization is immense, and it rarely will be practical to solve these equations in "real time", i.e., during the actual time interval, (t_0, t_f) . Indeed, even if the computing "power" to effect such a solution is available, uncertainties regarding disturbances in (t, t_f) and variations in the target time and state may invalidate the optimality of the instantaneous control shortly after it is applied. The principal value of such solutions, to date, has been to identify nominal trajectories and control histories prior to application. In addition to providing valuable planning information for vehicle and actuator sizing, fuel loading, etc., the pre-calculated optimal trajectories and controls can determine time-varying set points for feedback controllers, e.g., the neighboring-optimal control laws described in the next section. An interesting alternative is to define an "extremal field" of optimal paths in order to implement nonlinear guidance and control laws based upon the principles of dynamic programming. [17]

Neighboring-Optimal Solutions

The linear perturbation models introduced in an earlier section can be put to use to examine the effects of small variations in initial conditions and terminal cost on the optimal trajectory and controls. We formally consider the second variation of the cost function for the nonlinear system, $\delta^2 J_{NL}$, identifying it as the cost function for the associated linear perturbation model (Note that optimality guarantees that the first variation is zero on the optimal path):

$$J_{NL} \{[\underline{x}(t_0) + \Delta \underline{x}(t_0)], [\underline{x}(t_f) + \Delta \underline{x}(t_f)]\} \approx J_{NL}[\underline{x}(t_0), \underline{x}(t_f)] + \delta^2 J_{NL}[\Delta \underline{x}(t_0), \Delta \underline{x}(t_f)] \quad (40)$$

Taking second variations on the right side of Eq. (30),

$$\delta^2 J_{NL} = J_L = \frac{1}{2} \Delta \underline{x}^T(t_f) \phi_{xx}(t_f) \Delta \underline{x}(t_f) + \frac{1}{2} \int_{t_0}^{t_f} \left\{ [\Delta \underline{x}^T(t) \Delta \underline{u}^T(t)] \begin{bmatrix} L_{xx}(t) & L_{xu}(t) \\ L_{ux}(t) & L_{uu}(t) \end{bmatrix} \begin{bmatrix} \Delta \underline{x}(t) \\ \Delta \underline{u}(t) \end{bmatrix} \right\} dt \quad (41)$$

subject to the linear dynamic constraint,

$$\Delta \dot{\underline{x}}(t) = F(t) \Delta \underline{x}(t) + G(t) \Delta \underline{u}(t), \quad \Delta \underline{x}(t_0) \text{ given} \quad (42)$$

$F(t)$ and $G(t)$ are defined by Eq. (10) and (11), evaluated along the optimal path. Perturbations from the nominal optimal solution are

$$\Delta \underline{x}(t) = \underline{x}(t) - \underline{x}_N^*(t) \quad (43)$$

$$\Delta \underline{u}(t) = \underline{u}(t) - \underline{u}_N^*(t) \quad t_0 \leq t \leq t_f \quad (44)$$

A notational change is introduced in the quadratic cost function,

$$J_L = \frac{1}{2} \Delta \underline{x}^T(t_f) P(t_f) \Delta \underline{x}(t_f) + \frac{1}{2} \int_{t_0}^{t_f} \left\{ [\Delta \underline{x}^T(t) \Delta \underline{u}^T(t)] \begin{bmatrix} Q(t) & M(t) \\ M^T(t) & R(t) \end{bmatrix} \begin{bmatrix} \Delta \underline{x}(t) \\ \Delta \underline{u}(t) \end{bmatrix} \right\} dt \quad (45)$$

and the corresponding Hamiltonian can be written as

$$H(t) = \frac{1}{2} [\Delta \underline{x}^T(t) Q(t) \Delta \underline{x}(t) + 2 \Delta \underline{x}^T(t) M(t) \Delta \underline{u}(t) + \Delta \underline{u}^T(t) R(t) \Delta \underline{u}(t)] + \Delta \underline{\lambda}^T(t) [F(t) \Delta \underline{x}(t) + G(t) \Delta \underline{u}(t)] \quad (46)$$

The Euler-Lagrange equations, Eq. (36) to (38), are

$$\Delta \dot{\underline{\lambda}}(t) = -Q(t) \Delta \underline{x}(t) - M(t) \Delta \underline{u}(t) - F^T(t) \Delta \underline{\lambda}(t) \quad (47)$$

$$\Delta \underline{\lambda}(t_f) = P(t_f) \Delta \underline{x}(t_f) \quad (48)$$

$$0 = M^T(t) \Delta \underline{x}(t) + R(t) \Delta \underline{u}(t) + G^T(t) \Delta \underline{\lambda}(t) \quad (49)$$

Equation (49) can be rearranged to solve for the control,

$$\Delta \underline{u}(t) = -R^{-1}(t) [M^T(t) \Delta \underline{x}(t) + G^T(t) \Delta \underline{\lambda}(t)] \quad (50)$$

and this relationship can be substituted in Eq. (42) and (47) to express the linear two-point boundary value problem as

$$\Delta \dot{\underline{x}}(t) = [F(t) - G(t)R^{-1}(t)M^T(t)] \Delta \underline{x}(t) - G(t)R^{-1}(t)G^T(t) \Delta \underline{\lambda}(t), \quad \Delta \underline{x}(t_0) \text{ given} \quad (51)$$

$$\Delta \dot{\underline{\lambda}}(t) = [-Q(t) + M(t)R^{-1}(t)M^T(t)] \Delta \underline{x}(t) - [F(t) - G(t)R^{-1}(t)M^T(t)]^T \Delta \underline{\lambda}(t), \quad \Delta \underline{\lambda}(t_f) \text{ given} \quad (52)$$

Because $\Delta \underline{x}(t)$ and $\Delta \underline{\lambda}(t)$ are adjoint, Eq. (48) applies not only at the final time but during the entire interval:

$$\Delta \underline{\lambda}(t) = P(t) \Delta \underline{x}(t), \quad t_0 \leq t \leq t_f \quad (53)$$

Then Eq. (50) can be expressed as an optimal feedback control law,

$$\begin{aligned} \Delta \underline{u}^*(t) &= -R^{-1}(t) [G^T(t)P(t) + M^T(t)] \Delta \underline{x}(t) \\ &= -C(t) \Delta \underline{x}(t) \end{aligned} \quad (54)$$

where $C(t)$ is the time-varying ($m \times n$) control gain matrix.

The ($n \times n$) matrix $P(t)$ remains to be found. Differentiating Eq. (53), incorporating Eq. (51) to (53), and rearranging terms, a nonlinear differential equation for $P(t)$ can be derived:

$$\begin{aligned} \dot{P} \Delta \underline{x} &= \Delta \dot{\underline{\lambda}} - P \Delta \dot{\underline{x}} \\ &= [(-Q + MR^{-1}M^T) \Delta \underline{x} - (F - GR^{-1}M^T)^T \Delta \underline{\lambda}] - P[(F - GR^{-1}M^T) \Delta \underline{x} - GR^{-1}G^T \Delta \underline{\lambda}] \\ &= [(-Q + MR^{-1}M^T) - (F - GR^{-1}M^T)^T P] \Delta \underline{x} - P[(F - GR^{-1}M^T) - GR^{-1}G^T P] \Delta \underline{x} \end{aligned} \quad (55)$$

Cancelling $\Delta \underline{x}$ on both sides of the equation leads to a matrix Riccati equation for P :

$$\dot{P} = -(F - GR^{-1}M^T)^T P - P(F - GR^{-1}M^T) + P(GR^{-1}G^T)P + (-Q + MR^{-1}M^T), \quad P(t_f) \text{ given} \quad (56)$$

The solution for $P(t)$ and, therefore, for $C(t)$ is seen to be independent of $\Delta \underline{x}(t)$; hence, the control law defined by Eq. (54) is linear. Variations in $\Delta \underline{x}(t_0)$ or $\Delta \underline{x}(t_f)$ have no effect on $C(t)$, although the linear-optimal [or linear-quadratic (LQ)] control history obviously is affected by state perturbations.

From Eq. (44), the total control is formed as the sum of the nominal and perturbation optimal controls:

$$\begin{aligned} \underline{u}(t) &= \underline{u}_N^*(t) + \Delta \underline{u}^*(t) \\ &= \underline{u}_N^*(t) - C(t) [\underline{x}(t) - \underline{x}_N^*(t)] \end{aligned} \quad (57)$$

The prototype neighboring-optimal control law is illustrated in Fig. 4. This diagram reflects Eq. (57), and it introduces the notion that an alternative to time-scheduling of \underline{x}_N^* , \underline{u}_N^* , and C can be considered. When t_f is not fixed and is of secondary importance, it may be desirable to choose a scalar function, n , of the state with fixed end point as the scheduling variable. This scalar function must be monotonic in time, so as not to introduce singularities in the scheduling, and it also can be used to reduce the order and complexity of the original optimization, as demonstrated in [1], [16], [17], and several other references. Range, R , and specific energy, E , are examples of functions that have proven to be suitable scheduling variables for flight path optimization;* just as "time-to-go", $(t-t_f)$, is often a more pertinent independent variable than time, t , "range-to-go" and "energy-to-go" can be employed in actual implementation.

Equation (57) indicates that the total control approaches its nominal value as the actual state approaches its optimal value. This result apparently assures that the total control is optimal, i.e., that the dynamic system is forced to follow the optimal trajectory. If, however, there are disturbances not modelled in Eq. (31) or the actual system differs from the dynamic model, Eq. (57) may not be up to the task, and $C(t)$ may not be optimal.

The optimal treatment of disturbances and system variations depends on whether they are deterministic (certain) or random (uncertain) and, in the latter case, whether they are random constants or random processes (continually changing in time). From Eq. (17), disturbances, $\Delta w(t)$, that are certain and, therefore, known can be opposed by perturbing the control an additional amount, $\Delta u_d(t)$, such that $G(t)\Delta u_d(t) = -L(t)\Delta w(t)$. A rocket launch through a known vertical wind profile could be treated in this fashion. Known parameter variations should be taken into account in calculating $C(t)$.

Random disturbances and parameter variations pose a different problem because the cost functions presented earlier can not be minimized with certainty. At best, we can hope to minimize some statistical measure of the cost, and this implies that statistical characteristics of the random processes are known. A reasonable approach, as presented in [1], [3], [4], [10], [12]-[14], is to minimize the expected value (or average value) of the cost, conditioned on the statistics of the random processes. Random disturbances and parameter variations are treated in the same manner, i.e., both can be modelled as "process noise". Although conditions for stochastic optimality of nonlinear systems have been discussed in the literature, the most useful results apply to linear systems with zero-mean gaussian process noise. The fortuitous result for this case is that the LQ gain matrix defined by Eq. (54) is optimal without qualification. Equation (57) is the stochastic neighboring-optimal control law for a linear system forced by zero-mean random processes, although the minimum value of the cost function is greater than it would be without random forcing [1].

Solving the problem of random constant disturbances or parameter variations is more involved because the induced error does not average zero during the interval. Two possible solutions are estimation of the constant and integral compensation. Assuming the disturbance or parameter is observable, the state can be augmented to include the random constant, and an estimate of the constant can be based upon observation of the system. The estimate then is used in the same way as its deterministic equivalent. Recognizing that the random constant would prevent $[\underline{x}(t) - \underline{x}_N^*(t)]$ from reaching null, an integral of the state error could be added to Eq. (57), leading to asymptotic convergence of the actual and optimal states. These approaches are shown to be similar in [18].

Figure 4 implies direct feedback of the state in neighboring-optimal control, but it should be recalled that the state may not be measured directly and that available measurements may be corrupted by error (Fig. 1). In such instance, Eq. (57) must use an estimate of the state, $\hat{\underline{x}}(t)$, which is derived from the observation, $\underline{z}(t)$. If the statistics of the measurement errors are known, that estimate can be optimal in some sense. For example, estimators which minimize the root-mean-square error between $\hat{\underline{x}}(t)$ and $\underline{x}(t)$ or which maximize the probability that $\hat{\underline{x}}(t)$ and $\underline{x}(t)$ are the same can be found. (These two estimators are identical for a wide class of problems.) By the separation theorem, the controller and estimator can be optimized separately [19]; however, contrary to early suppositions, the stochastic optimal control law that results is not guaranteed to have satisfactory stability and performance. These issues are addressed in later sections. The next section presents a number of important aspects of optimal estimation.

OPTIMAL ESTIMATION

Given k equally valid but "noisy" measurements of a constant scalar quantity, it would be reasonable to simply average the measurements to produce an estimate of the constant. Such an estimate is optimal in the sense that it minimizes the sum of the squared

* Specific energy is the sum of kinetic and potential energy per unit mass.

errors between the measurements and the constant, i.e., it is a "least-squares" estimate. If prior knowledge of the measurement errors indicated that some measurements were better than others, this could be taken into account in the estimate, and the better measurements could be weighted more heavily in the averaging process. The proper weighting factors could be determined by penalizing the poorer measurements in the squared-error criterion, leading to a weighted-least-squares estimate of the constant. An additional measurement could be incorporated in the estimate by repeating the computation with $(k+1)$ terms, but it is possible to get an identical estimate using a recursive weighted-least-squares algorithm that sums the prior estimate and the measurement update with suitable weighting.

If the variable to be estimated is not a scalar constant but a vector that is varying in time, this algorithm can be extended to account for the passage of time and for an underlying linear stochastic dynamic process, resulting in the discrete-time Kalman-Bucy Filter, often shortened to Kalman filter. The equivalent continuous-time Kalman filter is obtained in the limit as the time interval between samples approaches zero. The extended Kalman filter is, in effect, a neighboring-optimal estimator, combining linear measurement updates with nonlinear observations and propagation of the state. The optimal predictor uses the system model to project current optimal estimates ahead in time. These filters and predictors can be employed to provide the optimal estimates required for stochastic optimal control.

Least-Squares Estimates of Constant Vectors

Constant vectors can be treated as easily as constant scalars, so we begin with the linear observation equation,

$$\Delta \underline{z} = H \Delta \underline{x} + \Delta \underline{n} \quad (58)$$

where the constant vector, $\Delta \underline{x}$, has dimension n , the measurement vector, $\Delta \underline{z}$, has dimension $k_1 \geq n$, H is a $(k_1 \times n)$ observation matrix, and the error vector has dimension k_1 . This equation is analogous to Eq. (8) and (9), with $H = H_x$ and $H_u = H_w = 0$.

A scalar quadratic (or mean-square) cost function of the residual, i.e., the error between $\Delta \underline{z}$ and the estimate, $\Delta \hat{\underline{x}}$, is formed:

$$\begin{aligned} J &= \frac{1}{2} (\Delta \underline{z} - H \Delta \hat{\underline{x}})^T (\Delta \underline{z} - H \Delta \hat{\underline{x}}) \\ &= \frac{1}{2} (\Delta \underline{z}^T \Delta \underline{z} - \Delta \underline{z}^T H \Delta \hat{\underline{x}} - \Delta \hat{\underline{x}}^T H^T \Delta \underline{z} + \Delta \hat{\underline{x}}^T H^T H \Delta \hat{\underline{x}}) \end{aligned} \quad (59)$$

The optimal estimate minimizes J , and it is found from the necessary condition for a functional minimum [1], [7]:

$$\frac{\partial J}{\partial \Delta \hat{\underline{x}}} = (H^T H \Delta \hat{\underline{x}} - H \Delta \underline{z})^T = 0 \quad (60)$$

Solving for $\Delta \hat{\underline{x}}$, the least-squares estimator is written as

$$\Delta \hat{\underline{x}} = (H^T H)^{-1} H^T \Delta \underline{z} \quad (61)$$

No reference to the statistical properties of $\Delta \underline{z}$ is made in this equation. A solution can be found with $k_1 = n$; however, for averaging to occur, k_1 must be greater than n .

To verify that Eq. (61) averages the measurements, assume that $\Delta \underline{x}$ is a scalar and that $\Delta z_k = \Delta x + \Delta n_k$, $k = 1$ to k_1 . Then H is a $(k_1 \times 1)$ matrix of ones, and $(H^T H)^{-1} = 1/k_1$.

The product $H^T \Delta \underline{z}$ merely sums the measurements, which are divided by k_1 to produce the estimate.

Now suppose that some measurements are better than others, i.e., that the statistics of Δn vary from one element to the next. If each scalar residual is normalized by the magnitude of its expected value, e_k , the normalized residual vector can be expressed as $N(\Delta \underline{z} - H \Delta \hat{\underline{x}})$, where N is a diagonal $(k_1 \times k_1)$ matrix with elements $1/e_k$. The corresponding cost function is

$$\begin{aligned} J &= \frac{1}{2} (\Delta \underline{z} - H \Delta \hat{\underline{x}})^T N^T N (\Delta \underline{z} - H \Delta \hat{\underline{x}}) \\ &= \frac{1}{2} (\Delta \underline{z} - H \Delta \hat{\underline{x}})^T R^{-1} (\Delta \underline{z} - H \Delta \hat{\underline{x}}) \\ &= \frac{1}{2} (\Delta \underline{z}^T R^{-1} \Delta \underline{z} - \Delta \underline{z}^T R^{-1} H \Delta \hat{\underline{x}} - \Delta \hat{\underline{x}}^T H^T R^{-1} \Delta \underline{z} + \Delta \hat{\underline{x}}^T H^T R^{-1} H \Delta \hat{\underline{x}}) \end{aligned} \quad (62)$$

$R = (N^T N)^{-1}$ is a diagonal matrix with elements e_k^2 , i.e., a matrix of the expected squared errors of the residuals. Differentiating with respect to $\Delta \hat{\underline{x}}$,

$$\frac{\partial J}{\partial \Delta \underline{x}} = (H^T R^{-1} H \Delta \underline{x} - H^T R^{-1} \Delta \underline{z})^T = 0 \quad (63)$$

and the weighted-least-squares estimator for constant $\Delta \underline{x}$ is

$$\Delta \underline{x} = (H^T R^{-1} H)^{-1} H^T R^{-1} \Delta \underline{z} \quad (64)$$

This equation is a "batch processing" algorithm, in that all measurements are processed at once to provide the estimate. If new measurements become available, they can be incorporated without a complete recalculation of the prior result. Given k_1 measurements and the resulting estimate,

$$\Delta \underline{z}_1 = H_1 \Delta \underline{x} + \Delta \underline{n}_1 \quad (65)$$

$$\Delta \underline{x}_1 = (H_1^T R_1^{-1} H_1)^{-1} H_1^T R_1^{-1} \Delta \underline{z}_1 \quad (66)$$

The new measurement, $\Delta \underline{z}_2$, with dimension k_2 , is

$$\Delta \underline{z}_2 = H_2 \Delta \underline{x} + \Delta \underline{n}_2 \quad (67)$$

R_2 is a $(k_2 \times k_2)$ matrix containing the expected squared errors in the new measurement. The cost function for all $(k_1 + k_2)$ measurements [Eq. (62)] can be partitioned as

$$J = [(\Delta \underline{z}_1 - H_1 \Delta \underline{x}_1)^T (\Delta \underline{z}_2 - H_2 \Delta \underline{x}_2)^T] \begin{bmatrix} R_1^{-1} & 0 \\ 0 & R_2^{-1} \end{bmatrix} \begin{bmatrix} (\Delta \underline{z}_1 - H_1 \Delta \underline{x}_1) \\ (\Delta \underline{z}_2 - H_2 \Delta \underline{x}_2) \end{bmatrix} \quad (68)$$

and the estimate following incorporation of all the data is derived from $\partial J / \partial \Delta \underline{x}_2 = 0$:

$$\Delta \underline{x}_2 = (H_1^T R_1^{-1} H_1 + H_2^T R_2^{-1} H_2)^{-1} (H_1^T R_1^{-1} \Delta \underline{z}_1 + H_2^T R_2^{-1} \Delta \underline{z}_2) \quad (69)$$

Defining

$$P_1 = (H_1^T R_1^{-1} H_1)^{-1} \quad (70)$$

and using the matrix inversion lemma [6],

$$(P_1^{-1} + H_2^T R_2^{-1} H_2)^{-1} = P_1 - P_1 H_2^T (H_2 P_1 H_2^T + R_2)^{-1} H_2 P_1 \quad (71)$$

Eq. (69) can be written as

$$\begin{aligned} \Delta \underline{x}_2 &= \Delta \underline{x}_1 - P_1 H_2^T (H_2 P_1 H_2^T + R_2)^{-1} H_2 \Delta \underline{x}_1 \\ &\quad + P_1 H_2^T [I - (H_2 P_1 H_2^T + R_2)^{-1} H_2 P_1 H_2^T] R_2^{-1} \Delta \underline{z}_2 \end{aligned} \quad (72)$$

Noting that $(H_2 P_1 H_2^T + R_2)^{-1} (H_2 P_1 H_2^T + R_2) = I$, Eq. (72) can be reduced to

$$\begin{aligned} \Delta \underline{x}_2 &= \Delta \underline{x}_1 + P_1 H_2^T (H_2 P_1 H_2^T + R_2)^{-1} (\Delta \underline{z}_2 - H_2 \Delta \underline{x}_1) \\ &= \Delta \underline{x}_1 + K_2 (\Delta \underline{z}_2 - H_2 \Delta \underline{x}_1) \end{aligned} \quad (73)$$

where K_2 is the recursive weighted-least-squares estimator gain matrix. Although the derivation is complex, the result is quite simple, because the new estimate is based on the old estimate plus a gain matrix times a residual. Equation (73) looks like a digital filter, and measurements taken over a period of time could update the estimate as they occur. Redefining k as a time index and letting the observation vector at time k have r components, the recursive mean-value estimator is

$$\Delta \underline{x}_k = \Delta \underline{x}_{k-1} + K_k (\Delta \underline{z}_k - H_k \Delta \underline{x}_{k-1}) \quad (74)$$

with

$$K_k = \hat{P}_k H_k^T (H_k \hat{P}_{k-1} H_k^T + R_k)^{-1} \quad (75)$$

and

$$\hat{P}_k = (\hat{P}_{k-1}^{-1} + H_k^T R_k^{-1} H_k)^{-1} \quad (76)$$

K_k is an $(n \times r)$ gain matrix, while \hat{P}_k is an $(n \times n)$ matrix that represents the estimation error at the k th sampling instant.

Keep in mind that these equations estimate a constant vector, and the gain matrix normally gets smaller as more measurements are made. If least-squares estimation is to be applied to the states of a dynamic system over a period of time, the estimated quantities may not be constant, and a vanishing gain matrix will not account properly for the information contained in later measurements. There must be mechanisms for including effects of the system model and its inputs (both controlled and uncontrolled) on $\Delta \hat{x}_k$ and \hat{P}_k . Before doing this, however, more substance must be given to statistical descriptions of the random processes which contribute to estimation uncertainty.

Probability, Random Processes, and the Propagation of Uncertainty

Probability theory describes the relative frequency of occurrence of a variable's numerical values. For a real scalar variable, x , the probability that its numerical value lies in the range $(-\infty, +\infty)$ is one. The probability density function of x , $p(x)$, indicates which numerical values are more (or less) likely than others, and its integral over $(-\infty, +\infty)$ is one:

$$\int_{-\infty}^{\infty} p(x) dx = 1 \quad (77)$$

The expected value (or expectation) of a function of x , $g(x)$, is the integral of the product of $g(x)$ and $p(x)$ over the range:

$$E[g(x)] = \int_{-\infty}^{\infty} g(x) p(x) dx \quad (78)$$

The expected value of x is its mean value, m_x ,

$$E[x] = \int_{-\infty}^{\infty} x p(x) dx = m_x \quad (79)$$

while the expected value of the squared error between x and m_x is its mean squared error or variance, σ_x^2 :

$$E[(x - m_x)^2] = \int_{-\infty}^{\infty} (x - m_x)^2 p(x) dx = \sigma_x^2 \quad (80)$$

The square root of the variance, σ_x , is the standard deviation of x from m_x .

A gaussian (or normal) probability density function is defined completely by its mean and variance,

$$p(x) = \frac{1}{\sqrt{2\pi} \sigma_x} e^{-(x - m_x)^2 / 2\sigma_x^2} \quad (81)$$

and it reaches its maximum value, i.e., the point of maximum likelihood, when $x = m_x$. The corresponding multivariate gaussian probability density function of the n -component vector, \underline{x} , is

$$p(\underline{x}) = \frac{1}{(2\pi)^{n/2} |P|^{1/2}} e^{-(\underline{x} - \underline{m})^T P^{-1} (\underline{x} - \underline{m}) / 2} \quad (82)$$

where \underline{m} is the vector of mean values, P is the $(n \times n)$ covariance matrix of \underline{x} , and $|P|$ is its determinant. The diagonal elements of this symmetric matrix are the variances of the components of \underline{x} , and the off-diagonal covariances represent the degree of correlation between the components ($-1 \leq \rho_{ij} \leq 1$):

$$P = E[(\underline{x} - \underline{m})(\underline{x} - \underline{m})^T]$$

$$= \begin{bmatrix} \sigma_{x_1}^2 & \rho_{12} \sigma_{x_1} \sigma_{x_2} & \dots & \dots \\ \rho_{12} \sigma_{x_1} \sigma_{x_2} & \sigma_{x_2}^2 & \dots & \dots \\ \dots & \dots & \dots & \dots \\ \dots & \dots & \dots & \sigma_{x_n}^2 \end{bmatrix} \quad (83)$$

A scalar random process, or stochastic process, is an ensemble of random continuous-time functions, $x_i(t)$, $i=1$ to ∞ , each of which has a probability function, $p(x_i, t)$, that may vary with time. The value of $x_i(t)$ at a specific time, t , is a random variable. The statistics of a random process are formally averaged over the entire ensemble of trials, although it is understood that an infinity of trials is rarely (if ever) available. If ensemble statistics do not vary in time, the process is stationary; if ensemble statistics and time-averaged statistics are interchangeable, the process is ergodic.

The significance of the gaussian probability density function is that it characterizes a large percentage of naturally occurring random variables, and it is particularly amenable to stochastic analysis and computation. One reason that the gaussian distribution is so common is that random variables often are the sum of many random effects, and, by the central limit theorem [7], the distribution of such a sum tends to become gaussian as the number of effects becomes large no matter what the distributions of the original effects. As a corollary, gaussian inputs to linear systems produce gaussian outputs; because each random process is fully characterized by its mean value and covariance matrix, analysis can be based upon these quantities rather than more complex characterizations. Mean values, $\underline{m}(t)$, can be propagated by deterministic linear dynamic equations, e.g., Eq. (7) and Eq. (24), and covariance matrices, $P(t)$, can be propagated by equivalent difference or differential equations, to be presented below.

Stochastic optimal control normally deals with vector processes that are nonstationary, i.e., mean values, covariances, and any other pertinent statistical measures are likely to vary in time. A process can be said to have reached stochastic equilibrium if all statistical measures are stationary. The assumption of ergodicity may become important if experimental samples are used to estimate statistical parameters. Similar definitions can be applied to random sequences, the discrete-time equivalents of random processes.

The frequency content, or time correlation, of a random process is an additional statistical measure of importance. If the power spectral density, or frequency spectrum, of a stationary process has a constant value, Ψ_0 , over all frequencies in $(-\infty < \omega < +\infty)$, the process is called white noise [7]. As a consequence, two samples of continuous-time white noise, $x(t)$ and $x(t - \tau)$, are completely uncorrelated unless τ is identically zero; the corresponding autocorrelation function,

$$\psi_{xx}(\tau) = E[x(t)x(t + \tau)] \quad (84)$$

is a Dirac delta function of τ , $\delta(\tau)$, scaled by Ψ_0 [7]:*

$$\psi_{xx}(\tau) = \Psi_0 \delta(\tau) \quad (85)$$

By analogy to optics, a stationary random process whose power spectral density varies with frequency is called colored noise. The corresponding autocorrelation function typically consists of a symmetric combination of exponential and sinusoidal functions of τ , with maximum (finite) value at $\tau = 0$.

There is an essential quandary associated with continuous-time white noise that does not carry over to discrete-time white noise. Because the variance of a stationary process equals its autocorrelation function at $\tau = 0$, continuous-time white noise with finite power spectral density, Ψ_0 , has an infinite variance [Eq. (85)]. Nevertheless, just as response to an impulse function can be well-defined and useful in deterministic systems analysis, the response to white noise has significance in stochastic analysis. One reason is that system dynamics normally cause adjacent continuous signals to be correlated, so the output autocorrelation function is not singular. The variance of a stationary random sequence also is defined by $\psi_{xx}(0)$; however, $\psi_{xx}(0) = \Psi_0$ (without the delta function) for discrete-time white noise, so its variance is finite [12]. In the "digital" (discrete-time) filter developments which follow, the white random sequences that are assumed to drive the system and corrupt the measurements are represented by covariance matrices; for "analog" (continuous-time) filters, white random processes are represented by spectral density matrices.

* The Dirac delta function is infinite at $\tau = 0$ and zero when $\tau \neq 0$. Its integral over all time is one.

The propagation of uncertainty is introduced most easily for the linear discrete-time case. Beginning with Eq. (7), it is assumed that the controlled input, Δu_k , is known and that the disturbance is a time-varying random sequence with covariance matrix, Q'_k , and zero mean value. The mean value is propagated by the equation itself,

$$E[\Delta x_k] = E[\phi_{k-1} \Delta x_{k-1} + \Gamma_{k-1} \Delta u_{k-1} + \Lambda_{k-1} \Delta w_{k-1}] \quad (86a)$$

or

$$\Delta \underline{m}_k = \phi_{k-1} \Delta \underline{m}_{k-1} + \Gamma_{k-1} \Delta u_{k-1} + \Lambda_{k-1} (0) \quad (86b)$$

The covariance propagation is defined by squaring Eq. (7) and taking expectations throughout. The Δu_k terms drop out, as there is no uncertainty in them, to yield

$$E[(\Delta \underline{x} - \Delta \underline{m})_k (\Delta \underline{x} - \Delta \underline{m})_k^T] = E\left\{[\phi_{k-1} (\Delta \underline{x} - \Delta \underline{m})_{k-1} + \Lambda_{k-1} \Delta w_{k-1}] \cdot [\phi_{k-1} (\Delta \underline{x} - \Delta \underline{m})_{k-1} + \Lambda_{k-1} \Delta w_{k-1}]^T\right\} \quad (87a)$$

or, with $P_k = E[(\Delta \underline{x} - \Delta \underline{m})_k (\Delta \underline{x} - \Delta \underline{m})_k^T]$,

$$P_k = \phi_{k-1} P_{k-1} \phi_{k-1}^T + \Lambda_{k-1} Q'_{k-1} \Lambda_{k-1}^T \\ \triangleq \phi_{k-1} P_{k-1} \phi_{k-1}^T + Q_{k-1} \quad (87b)$$

The expected value of $(\Delta \underline{x} - \Delta \underline{m})_{k-1} \Delta w_{k-1}$ is zero because the disturbance is white noise and, therefore, not correlated with any other variable. The covariance matrix of the "process noise" can account for random parameter variations as well as disturbances, following earlier comments.

ϕ and Γ are functions of the sampling interval, T ; as $T \rightarrow 0$, the propagation equations for continuous-time models are obtained. For small T ,

$$\Delta \underline{m}_k = (I + F_{k-1} T) \Delta \underline{m}_{k-1} + G_{k-1} T \Delta u_{k-1} \quad (88)$$

In the limit, $(\Delta \underline{m}_k - \Delta \underline{m}_{k-1})/T \rightarrow \dot{\Delta \underline{m}}(t)$, $\Delta \underline{m}_{k-1} \rightarrow \Delta \underline{m}(t)$, and $\Delta u_{k-1} \rightarrow \Delta u(t)$, leading to

$$\dot{\Delta \underline{m}}(t) = F(t) \Delta \underline{m}(t) + G(t) \Delta u(t) \quad (89)$$

Similarly, Eq. (87b) is

$$\frac{P_k - P_{k-1}}{T} = F_{k-1} P_{k-1} + P_{k-1} F_{k-1}^T + F_{k-1} P_{k-1} F_{k-1}^T + \frac{Q_{k-1}}{T} \quad (90)$$

As $T \rightarrow 0$, this becomes

$$\dot{P}(t) = F(t)P(t) + P(t)F(t) + Q(t)\delta(t-\tau) \quad (91)$$

Equations (86) and (87) provide the mechanisms for incorporating system dynamics in the discrete-time weighted least-squares estimator derived earlier, while Eq. (89) and (91) do the same for the continuous-time case.

Kalman Filters and Predictors

A filter uses past and current measurements to estimate the expected value of the current state. A predictor uses the same information to estimate the expected value of the future state. A smoother uses the same information to estimate the expected values of the current and all past states. In the context of stochastic optimal control, we want to know where the system is and where the system (or its target) is going; filters and predictors provide information that is relevant to feedback and command, and it is these that will be discussed presently. Smoothers provide more precise data processing because all interior estimates are based upon future as well as past and current measurements. They should be applied in "post-flight" trajectory determination, evaluation, calibration, and analysis; however, they have little application to "real-time" control and are not treated here.

The linear discrete-time Kalman filter performs five functions in recursive fashion:

- 1) State Estimate Extrapolation (Propagation)
- 2) Covariance Estimate Extrapolation (Propagation)
- 3) Filter Gain Computation
- 4) State Estimate Update
- 5) Covariance Estimate "Update"

The first two of these were introduced in the previous section, while the last three follow directly from weighted-least-squares estimation. Given the state estimate from a previous iteration, (1) uses the physical process model to propagate the estimate of the state mean to the next sampling instant without regard to new measurements; (2) does the same thing for the state covariance matrix, assuming that "process noise" of known covariance is forcing the system. The result enters the computation of the optimal gains for incorporating new measurements. The filter gain computation (3) weights prior knowledge of measurement error covariance with state estimate covariance on a purely statistical basis, i.e., the actual measurements have no effect on the gain computation. These measurements correct the state propagation in (4), adding the product of the gain matrix and the measurement residual to the physical estimate of the state provided by (1). A similar correction is made to the covariance estimate; however, actual measurements have no effect on the covariance "update" (5). It is assumed that the measurement errors are described by random processes with known covariance.

The five equations corresponding to these functions are summarized using $\hat{(\)}$ to denote an estimated (expected) rather than actual value, the subscript to denote the sampling instant, $(-)$ to indicate an estimate computed before the measurement is incorporated, and $(+)$ to indicate the fully updated estimate [7]:

State Estimate Extrapolation

$$\hat{\Delta z}_k(-) = \phi_{k-1} \hat{\Delta z}_{k-1}(+) + \Gamma_{k-1} \Delta u_{k-1}, \quad \hat{\Delta z}_0(+) \text{ given} \quad (92)$$

Covariance Estimate Extrapolation

$$\hat{P}_k(-) = \phi_{k-1} \hat{P}_{k-1}(+) \phi_{k-1} + Q_{k-1}, \quad \hat{P}_0(+) \text{ given} \quad (93)$$

Filter Gain Computation

$$K_k = \hat{P}_k(-) H_k^T [H_k \hat{P}_k(-) H_k^T + R_k]^{-1} \quad (94)$$

State Estimate Update

$$\hat{\Delta z}_k(+) = \hat{\Delta z}_k(-) + K_k [\Delta z_k - H_k \hat{\Delta z}_k(-)] \quad (95)$$

Covariance Estimate "Update"

$$\begin{aligned} \hat{P}_k(+) &= [\hat{P}_k^{-1}(-) + H_k R_k^{-1} H_k]^{-1} \\ &= (I - K_k H_k) \hat{P}_k(-) \quad (\text{see [7]}) \end{aligned} \quad (96)$$

The filter described by Eq. (92) to (96) is optimal only if ϕ_k , Γ_k , H_k , Q_k , and R_k are known precisely. These matrices may be time-varying, i.e., varying from one sampling instant to the next. Even if they are constant, there is a starting transient associated with the filter computation. In other words, if the filter is not initialized at stochastic equilibrium, it is a time-varying filter. With constant system and covariance matrices, once stochastic equilibrium is reached, $\hat{P}_k(+) = \hat{P}_{k-1}(+)$, $K_k = \text{constant}$, and the optimal estimate can be made using Eq. (92) and (95) alone. The optimal filter's structure and performance depend on the definition of the observation vector; for a given state vector, changing the number or quality of the measurements affects the complexity of computations and the precision of state estimates. Multiple dissimilar measurements can provide a degree of "analytic redundancy" [20], allowing the full state to be estimated even though measurements have been degraded or lost. In such case, the optimal filter is defined by these five equations, but the definitions of Δz , H , and R are altered to account for changes in the measurement. Requirements for observability must be satisfied in any event.

Optimal prediction of the future state is based upon extrapolation of $\hat{\Delta z}_k(+) to a future time using the dynamic system model [Eq. (92)]. The prediction time interval need not be the same as the sampling interval used for estimation, as long as ϕ and Γ are redefined accordingly. From Eq. (93) it should be clear that the uncertainty in the predicted state is greater than that of the current state estimate.$

The number of discrete-time filter equations could be reduced to three by substituting Eq. (92) in Eq. (95) and Eq. (93) in Eq. (96). $\hat{P}_k(-)$ is no longer available for the

K_k computation; however, [7] presents a suitable alternate form:

$$K_k = \hat{P}_k (+) H_k^T R_k^{-1} \quad (97)$$

Although the three-equation formulation does not necessarily involve less computation, it provides a good starting point for obtaining the continuous-time Kalman filter using the limiting arguments of the previous section:

State Estimate Extrapolation and Update

$$\dot{\hat{x}}(t) = F(t)\hat{x}(t) + G(t)\Delta u(t) + K(t)[\Delta z(t) - H(t)\hat{x}(t)], \quad \hat{x}(t_0) \text{ given} \quad (98)$$

Covariance Estimate Extrapolation and "Update"

$$\begin{aligned} \dot{\hat{P}}(t) &= F(t)\hat{P}(t) + \hat{P}(t)F^T(t) + Q(t) - \hat{P}(t)H^T(t)R^{-1}(t)H(t)\hat{P}(t), \\ \hat{P}(t_0) &\text{ given} \end{aligned} \quad (99)$$

Filter Gain Computation

$$K(t) = \hat{P}(t)H^T(t)R^{-1}(t) \quad (100)$$

Direct derivations of the continuous-time estimation equations contend with the mathematical difficulties of "white noise" using the calculi of Ito and Stratonovich, as in [12] - [14]. Whereas, Eq. (92) to (96) can be solved sequentially in the order shown, the continuous-time equations [Eq. (98) to (100)] must be solved concurrently for optimal estimation. The general statements made earlier about discrete-time estimators apply here as well. In particular, constant-coefficient systems can reach stochastic equilibrium with constant filter gains, leaving only Eq. (98) to be integrated for optimal estimation. Optimal prediction is obtained by integrating Eq. (98) to the prediction time with no further measurements, using $\Delta \hat{x}(t)$ as an initial condition.

Comparison of the optimal filter gain computations [Eq. (99) and (100)] with the optimal control gain computations [Eq. (56) and (54), with $M(t)=0$] reveals a mathematical duality [1]. The filter covariance is computed using a matrix Riccati equation that is the same as Eq. (56) with F^T replacing F , H^T replacing G , time running forward rather than backward, and Q and R representing spectral density matrices rather than state and control weighting matrices. Unlike the corresponding control gain computation, optimal filter gains can be realized in "real time", with no knowledge of the final state. Duality allows the same computer algorithms to be applied in obtaining control and estimator gains, and it facilitates the extension of analytical results from one problem to the other.

As shown below, linear estimators are consistent with the neighboring-optimal controllers discussed earlier, but it is instructive to consider the extension of the Kalman filter to nonlinear dynamic systems before proceeding. Because Eq. (98) serves to propagate the time-varying expected value of the state using linear dynamics originally presented as Eq. (7), the estimator can be applied to nonlinear models by using nonlinear dynamics [Eq. (1)] instead, i.e.,

$$\dot{\hat{x}}(t) = f[\hat{x}(t), u(t)] + K(t)\{z(t) - h[\hat{x}(t), u(t)]\} \quad (101)$$

$K(t)$ is obtained from Eq. (99) and (100), with the various matrices defined as before. The estimate obtained from this extended Kalman filter is optimal only to the extent that assumptions regarding the statistics of inputs, noise, and states are not violated. The performance of such filters can be improved, at the expense of increased computation, by using statistical linearization (i.e., random-input describing functions) to characterize the matrices in Eq. (99) and (100) [7]. Furthermore, hybrid filters can be formulated to process discrete-time measurements with continuous-time dynamic models.

If some of the parameters, $p(t)$, of the physical process are subject to uncertainty, the extended Kalman filter can be used to provide on-line estimation of the unknown parameters. These parameter estimates are of value in updating control strategies as well as state estimates. In such case, the state vector and dynamic equations are augmented to include the random parameters and their assumed relationships with the remainder of the process, and Eq. (99) to (101) are applied as before. The estimation problem is necessarily nonlinear even if the original physical process is linear because products of the original states and the unknown parameters, i.e., the new state components, destroy the linear superposition characteristic. Thus, the sensitivity matrices, Eq. (10) to (15), must be continuously redefined during the estimation, and the filter can be expected to reach stochastic equilibrium only in rare instances.

Uncertainties in the initial conditions or the statistics of disturbances and measurement errors also can be estimated on line, but the extended Kalman filter is not particularly appropriate for this job. Maximum likelihood hypothesis testing provides a better solution. In this approach, a bank of optimal estimators -- each of which is

formulated under a different hypothesis regarding the system's initial conditions, statistics, or parameters -- is applied to the measurements, and the estimate whose likelihood of correctness is greatest determines which hypothesis is to be accepted [9]. The instantaneous state estimate can be obtained either from the associated filter or as a sum of all the filters' outputs, each weighted by its probability of correctness.

An estimate of the probability (or likelihood) that each hypothesis is correct is propagated from one instant to the next using Bayes's Rule. For hypothesis A, the likelihood of correctness at the k^{th} sampling instant is estimated from the likelihood at the previous instant,

$$p_k(A) = a_k(z_k|A)p_{k-1}(A) \quad (102)$$

where z_k represents the set of all measurements through the k^{th} instant and $a_k(z_k|A)$ is the probability that these measurements would have occurred under hypothesis A. The process is replicated for hypotheses B, C, and so on.

Maximizing the natural logarithm of the likelihood is equivalent to maximizing the likelihood itself, and it is a simpler computation. With the gaussian assumption [Eq. (82)], the logarithm of $a_k(z_k|A)$ is a quadratic function of the residual, $\theta_k[\cdot]$, and the multiplication of Eq. (102) is replaced by addition:

$$\ln[p_k(A)] = \theta_k[(z_k - H_k \hat{x}_{k-1})|A] + \ln[p_{k-1}(A)] \quad (103)$$

In principle, an infinite bank of filters would be required to account for a continuum of hypotheses; in practice, a small number of filters (on the order of a half dozen or less) may be adequate to track the most likely hypotheses.

Contrary to the assurances implied by optimality, the estimates produced by optimal estimators may diverge from reality for a number of reasons, e.g., modeling error or uncertainty, incomplete observability, and numerical error (roundoff, truncation, or ill-conditioning). Methods of limiting divergence include enhancement of the estimator's "robustness" by altering its assumed noise statistics or structure [21] - [23], integral compensation of filter residuals [24], and use of square-root or "U-D" algorithms to compute filter gains [25] - [26]. Broad discussions of causes of divergence and possible solutions are contained in [7] and [8].

STOCHASTIC NEIGHBORING-OPTIMAL CONTROL

The Prototype for Linear-Quadratic-Gaussian (LQG) Control

At this point, we can return to the closed-loop control problem, as methodologies for obtaining optimal estimates of the state from the measurements have been specified. Figure 5 presents a schematic of a stochastic neighboring-optimal control law that has three parts: the nominal trajectory and control generator, a linear-optimal filter, and the linear-optimal feedback control logic. The first part results from prior nonlinear optimization and is scheduled as discussed in a previous section. The second part subtracts the nominal measurement from the actual measurement to obtain the perturbation measurement, $\Delta z(t)$, which is the input for a linear estimator. The resulting perturbation estimate, $\Delta \hat{x}(t)$, is multiplied by the feedback gain matrix, $C(t)$, to produce a linear-optimal control perturbation, $\Delta u^*(t)$. This is summed with the nominal optimal control, $u_N^*(t)$, that drives the dynamic system. If the neighboring-optimal estimation and control gains are based upon linear models driven by gaussian processes and controlled to minimize quadratic costs, a linear-quadratic-gaussian (LQG) control law is the natural outcome of the design.

The nominal trajectory may be altered to achieve a continually changing objective, e.g., rendezvous with or impact on a moving target. Determining where the target is or will be at some future time requires additional filtering or prediction. Whereas linear estimation of the controlled system's deviation from the nominal path is consistent with neighboring-optimal control, optimum estimation of the target's state may require nonlinear processing. Nevertheless, practical considerations may dictate a simpler approach. For example, a proportional navigation (constant or compensated line-of-sight) scheme may use a linear estimator, absorbing nonlinear target dynamics in the assumed process "noise" with little degradation of accuracy but great reduction in computation.

The combination of target tracking and estimation of the controlled system's state introduces the more general notion of an estimator (or bank of estimators) whose order is not the same as or whose structure differs from that of the controlled system. The deterministic neighboring-optimal controller (Fig. 4) introduces no new dynamic modes, because the feedback law is a linear combination of the actual states; therefore, the closed-loop dynamic system is described by an n^{th} -order differential (or difference) equation. A full-state linear-optimal estimator is itself an n^{th} -order differential (or difference) equation, so the prototype stochastic closed-loop system is of order $2n$. Adding a target estimator further increases system order.

Alternatively, some characteristic of the controlled system may be handled best by increasing the order of the estimator. For example, coherent vibrational or aeroelastic modes may not require active control yet may degrade the utility of rigid-mode motion sensors. Increasing the assumed measurement noise decreases the bandwidth of the optimal filter, possibly resulting in unacceptably low phase margins in the closed-loop system. The classical control approach of notch filtering provides more precise control of phase characteristics, and including known resonant modes in the optimal filter has similar effect.

There also could be good reason to employ estimators with order less than n . Some measurements may be effectively noise-free, and full- or augmented-state estimation may be unnecessary. Reduced-order or decoupled estimators then would provide suitable alternatives for practical implementation, as discussed in a later section.

Certainty Equivalence and Separation

Invoking the certainty-equivalence principle or the separation theorem allows optimal control and estimation gains to be derived independently; however, the limitations of these concepts must be noted. As summarized in a number of this chapter's references, "certainty-equivalence" indicates that the control gains for the uncertain (stochastic) system can be computed as if the feedback information were certain, i.e., as if $\Delta \hat{x}(t) = \Delta x(t)$. "Separation" addresses the computation of estimation as well as control algorithms. When these synonymous principles apply, the expected value of the stochastic system's cost function is minimized with control strategies that take no account of estimation error and estimator gains that are unaffected by control strategy.

The separation theorem does not apply to all control problems, and even when conditions for its application are met, there is no guarantee that stability, response, and sensitivity characteristics will be satisfactory. The separation theorem applies to the LQG problem, including the stochastic neighboring-optimal controller presented here, and to systems that are nonlinear in the control or the observation [19]. If second-degree perturbation effects are considered in neighboring-optimal control, the separation theorem does not apply [27]. The nonlinear terms introduce multiplicative disturbances and noise that couple the actions of control and estimation gains in minimizing the expected value of the cost function. Multiplicative disturbances are akin to parameter uncertainty, leading to another circumstance in which the separation theorem does not formally apply; mismatch between actual system dynamics and those assumed in the estimator.

Of more fundamental concern is the possibility that the LQG controller may have negligible tolerance to parameter variations [28]. This problem is discussed in the next section, where it is shown that enhancing the robustness of the estimator at the expense of increased estimation error restores the system's stability margin.

LINEAR, TIME-INVARIANT (LTI) SYSTEMS AND STOCHASTIC EQUILIBRIUM

To this point, it has been assumed that the physical process to be controlled is nonlinear and that the associated linear perturbation model has time-varying coefficients. Stochastic equilibrium is unlikely to occur because input statistics and parameters may be continually changing. Nevertheless, the salient features to be addressed in control system design often can be captured by linear, time-invariant (LTI) models.

In many cases, the nominal state and control $\{x_N(t) \text{ and } u_N(t)\}$ are determined without regard to optimality, deriving instead from physical conditions of nonlinear equilibrium determined on an *ad hoc* basis. Deviations from this nominal condition, including "retrimming" to a new equilibrium, may be small enough to be well approximated by linear models. Furthermore, if the system parameters, $p(t)$, and the equilibrium are slowly changing, the transient behavior and stability characteristics of the process can be portrayed by a succession of time-invariant models.

Even if an LTI model provides an adequate description of system motions and observations, the previous sections clearly show that optimal control and estimation gains are time-varying. The gains, $C(t)$ and $K(t)$, depend on the Riccati matrices, $P(t)$ and $\hat{P}(t)$, which are solution variables of differential equations. In both cases, the time variation of gains takes the form of a transient which begins at the integration starting point, i.e., the final time for control and the initial time for estimation.

A simple scalar open-loop example illustrates that the time scales of the Riccati equation transients often are comparable to that of the associated dynamic system. With time constant, τ , the unforced scalar system is

$$\Delta \dot{x}(t) = -\left(\frac{1}{\tau}\right)\Delta x(t) \quad , \quad \Delta x(t_0) = \Delta x_0 \quad (104)$$

In the limit, as control and observation weightings become large, the homogeneous solutions to Eq. (56) and (99) are,

$$p(t) = p(t_f) e^{2(t-t_f)/\tau} \quad , \quad t_f \geq t \geq t_0 \quad (105)$$

$$\hat{p}(t) = \hat{p}(t_0) e^{-2(t-t_0)/\tau}, \quad t_0 \leq t \leq t_f \quad (106)$$

respectively, and the time constants for solution are $\tau/2$ in both cases. Thus, if $(t_f - t_0)$ is large compared to τ , and if the p^2 terms introduced by control and observation are stabilizing, the control and estimation Riccati solutions are essentially at equilibrium for the major part of the interval. The period following the estimator gain transient and preceding the control gain transient is one of stochastic equilibrium, i.e., the coefficients of the dynamic system and the stochastic optimal controller are constant. As a practical matter, it may be acceptable to employ constant gains throughout the interval in order to simplify the control implementation and its analysis.

LTI controllers and estimators are discussed in the remainder of this section, with the particular objectives of describing some of their fundamental properties, as well as some of the structural and modeling alternatives that can be employed in solving particular problems. It should be recognized that although the design process is linear, the choices of weighting matrices and logical structures often are dictated by unmodeled nonlinearities, e.g., the operating ranges of sensors and control surfaces, the needs and opinions of human pilots, and so on. Furthermore, not all random processes are gaussian, and not all error sources are random. As a consequence, stochastic controller design remains an iterative process, in which evaluation of interim results by computation and analysis plays an important part.

Design of Continuous-Time Linear-Quadratic (LQ) Regulators

An LQ regulator is a linear-optimal constant-coefficient controller that forces an LTI system to a zero or non-zero set point. In the context of the original problem, a zero set point lies on the nominal nonlinear equilibrium trajectory, $[\underline{x}_N(t), \underline{u}_N(t)]$, while a non-zero set point connotes some deviation, $[\Delta \underline{x}_p, \Delta \underline{u}_p]$ from the nominal equilibrium. Both alternatives are treated by defining the state and control perturbations from the set point,

$$\Delta \tilde{\underline{x}}(t) = \Delta \underline{x}(t) - \Delta \underline{x}_p \quad (107)$$

$$\Delta \tilde{\underline{u}}(t) = \Delta \underline{u}(t) - \Delta \underline{u}_p \quad (108)$$

and minimizing the quadratic cost function

$$J = \frac{1}{2} \int_0^{\infty} \left\{ \begin{bmatrix} \Delta \tilde{\underline{x}}^T(t) & \Delta \tilde{\underline{u}}^T(t) \end{bmatrix} \begin{bmatrix} Q & M \\ M & R \end{bmatrix} \begin{bmatrix} \Delta \tilde{\underline{x}}(t) \\ \Delta \tilde{\underline{u}}(t) \end{bmatrix} \right\} dt \quad (109)$$

subject to the dynamic constraint

$$\dot{\Delta \tilde{\underline{x}}}(t) = F \Delta \tilde{\underline{x}}(t) + G \Delta \tilde{\underline{u}}(t) \quad (110)$$

From Eq. (54), the continuous-time LQ regulator is

$$\begin{aligned} \Delta \tilde{\underline{u}}(t) &= -R^{-1} \left[G^T P + M^T \right] \Delta \tilde{\underline{x}}(t) \\ &= -C \Delta \tilde{\underline{x}}(t) \end{aligned} \quad (111)$$

where P is the $(n \times n)$ equilibrium solution of Eq. (56) (with arbitrary initial conditions) and C is the $(m \times n)$ constant control gain matrix. The set point is reintroduced to the controller by substituting Eq. (107) and (108) in Eq. (111):

$$\Delta \underline{u}(t) = \Delta \underline{u}_p - C[\Delta \underline{x}(t) - \Delta \underline{x}_p] \quad (112)$$

If the set point represents the desired value of an m -component output vector, $\Delta \underline{y}_p$, as in Eq. (29) (i.e., $k = m$), $\Delta \underline{x}_p$ and $\Delta \underline{u}_p$ are algebraic functions of $\Delta \underline{y}_p$ and any constant disturbance, $\Delta \underline{w}_p$,

$$\Delta \underline{x}_p = -S_{11} L \Delta \underline{w}_p + S_{12} \Delta \underline{y}_p \quad (113)$$

$$\Delta \underline{u}_p = -S_{21} L \Delta \underline{w}_p + S_{22} \Delta \underline{y}_p \quad (114)$$

where S is partitioned as

$$S_{11} = F^{-1} (-GS_{21} + I) \quad (115)$$

$$S_{12} = -F^{-1} GS_{22} \quad (116)$$

$$S_{21} = -S_{22}H_x F^{-1} \quad (117)$$

$$S_{22} = (-H_x F^{-1}G + H_u)^{-1} \quad (118)$$

The deterministic LQ regulator (Fig. 6) can be expressed as

$$\Delta \underline{u}(t) = C_F \Delta \underline{y}_p + C_B \Delta \underline{x}(t) + C_D \Delta \underline{w}_p \quad (119)$$

with the forward, feedback, and disturbance gain matrices defined by substituting Eq. (113) and (114) in Eq. (112):

$$C_F = (S_{22} + CS_{12}) \quad (120)$$

$$C_B = -C \quad (121)$$

$$C_D = -(S_{21} + CS_{11})L \quad (122)$$

Once C is determined, C_F and C_D become deterministic functions of the system. Conversely, C is unaffected by the choice of set point or the presence of disturbances. The LQ regulator has zero "hangoff" from the output set point, $\Delta \underline{y}_p$, if system parameters are known and disturbances are measured without error; however, parameters often are uncertain, disturbances rarely are measured, and steady-state errors are likely to occur.

Stability of the open-loop LTI system* is dictated by the eigenvalues (or roots) of F, which are the n complex-valued solutions to the characteristic equation,

$$\Delta_{OL}(s) = |sI - F| = 0 \quad (123)$$

The eigenvalues express the natural frequencies, damping ratios, and time constants of the system's normal modes of motion [6]. Asymptotic stability is guaranteed if all the eigenvalues of F have negative real parts.

The characteristic equation of the closed-loop system

$$\Delta \dot{\underline{x}}(t) = (F + GC_B)\Delta \underline{x}(t) + GC_F \Delta \underline{y}_p + (L + GC_D)\Delta \underline{w}_p \quad (124)$$

which results from using Eq. (119) as the control law is

$$\Delta_{CL}(s) = |sI - (F + GC_B)| = 0 \quad (125)$$

Regardless of the stability of the open-loop system, the deterministic continuous-time LQ regulator guarantees closed-loop stability if the following four conditions are met [4]:

- 1) R is a positive definite matrix
- 2) $(Q - MR^{-1}M^T)$ is a positive semi-definite matrix
- 3) $\{(F - GR^{-1}M^T), (Q - MR^{-1}M^T)^{\frac{1}{2}}\}$ is an observable pair
- 4) $\{(F - GR^{-1}M^T), G\}$ is a stabilizable pair

This stability result assumes that the proper F and G are used in the calculation of C; nevertheless, the control law has been shown to be remarkably tolerant to parameter variations, which effectively change the gain and phase characteristics of the multiloop system. The LQ regulator is shown to provide $\pm 60^\circ$ phase margin and infinite loop gain margin, as well as guaranteed stability with 50% gain reduction, for scalar and multi-input controls in [4] and [29], respectively.

The locus of roots for the LQ closed-loop system can be expressed as a function of the quadratic weighting matrices if we consider the 2n eigenvalues of the closed-loop LTI system and its adjoint [Eq. (51) and (52), with constant matrices]. The eigenvalues are solutions to the equation

$$\Delta_{SA}(s) = |sI - F| = 0 \quad (126)$$

where, from Eq. (51) and (52),

$$F = \begin{bmatrix} (F - GR^{-1}M^T) & (-GR^{-1}G^T) \\ (-Q + MR^{-1}M^T) & (-F + GR^{-1}M^T)^T \end{bmatrix} \quad (127)$$

* A system is asymptotically stable if all components of the state approach their equilibrium values as $t \rightarrow \infty$. If one or more state components diverge, the system is unstable.

The eigenvalues of F are found to be symmetric about the imaginary axis, i.e., half have negative real parts and half have positive real parts. If the four necessary conditions described above are met, the stable (negative) eigenvalues describe the LQ closed-loop system whether or not the open-loop system is stable and independent of the magnitudes of Q , R , and M . The right-half plane eigenvalues describe the adjoint system, which is stable for time running in reverse. Put another way, the n stable eigenvalues of F are the eigenvalues of $(F + GC_p)$, which are solutions to Eq. (125).

The asymptotic behavior of the closed-loop roots as R approaches infinity or becomes vanishingly small are of interest. In the latter case, the "cost" of control is "cheap", so the speed of response is rapid. For scalar control and full state feedback, [3] shows that p eigenvalues approach the transmission zeros of $(sI - F)^{-1}G$ as R becomes small, where p is the number of zeros. The remaining $(n-p)$ eigenvalues go to infinity in a Butterworth configuration, described in [3]; thus, the corresponding modes become very fast. Similar asymptotic behavior is experienced with multiple controls.

As R approaches infinity, the cost of control increases, so a "minimum control energy" solution is obtained in the limit. If F is stable, the minimum-energy solution is no control at all; C approaches zero, and all eigenvalues approach their open-loop positions. If one or modes of F are unstable, C cannot go to zero and still guarantee closed-loop stability; the minimum-energy control forces the unstable roots to their left-half-plane "mirror images" and allows the stable roots to approach their open-loop values.

The LQ regulator may be unduly conservative in the case of very unstable open-loop roots because it tends to make the corresponding closed-loop modes very stable, even with minimum-energy control. Ad hoc gain reduction (within the 50% limit) can reduce excessive stability margin. As an alternative, a prescribed degree of reduced stability could be achieved by including $e^{2\alpha t}$, $\alpha < 0$, in the integrand of the cost function [Eq. (109)]. This is equivalent to computing gains for a system matrix $(F + \alpha I)$ [4] that is more stable than the actual matrix, F .

The quadratic weighting matrices (Q , M , and R) can be selected to achieve various purposes, e.g., state-control perturbation tradeoff [1], pole placement [3], output regulation [3], and implicit model following [30], as well as neighboring-optimal control. All of these options produce control laws described by Eq. (119) and Fig. 6. The quadratic integrand of Eq. (109) is normalized to maximum allowable mean-square values of the state and control by specifying the diagonal elements of Q and R to be the inverses of these maximum values (M and the off-diagonal elements of Q and R are zero). This is an effective means of adjusting the speed of response and the relative magnitudes of state and control perturbations, but it has relatively weak effect on overshoots in the transient response. Overshoot can be addressed using state-rate weighting [31], in which a term of the form, $\Delta \dot{x}^T Q_x \Delta \dot{x}$, is included in the cost function. From Eq. (110), the corresponding increments in state, cross-product, and control weighting are:

$$\begin{aligned} \begin{bmatrix} \Delta Q & \Delta M \\ \Delta M^T & \Delta R \end{bmatrix} &= \begin{bmatrix} F^T \\ G^T \end{bmatrix} Q_x \begin{bmatrix} F & G \end{bmatrix} \\ &= \begin{bmatrix} F^T Q_x F & F^T Q_x G \\ G^T Q_x F & G^T Q_x G \end{bmatrix} \end{aligned} \quad (128)$$

Output or command weighting, $\Delta \dot{y}^T Q_y \Delta \dot{y}$, is obtained in similar fashion using Eq. (8),

$$\begin{bmatrix} \Delta Q & \Delta M \\ \Delta M^T & \Delta R \end{bmatrix} = \begin{bmatrix} H_x^T Q_y H_x & H_x^T Q_y H_u \\ H_u^T Q_y H_x & H_u^T Q_y H_u \end{bmatrix} \quad (129)$$

For constant set point,

$$\Delta \dot{y} = H_x (F \Delta \dot{x} + G \Delta \dot{u}) \quad (130)$$

output rate weighting can be specified by analogous manipulations.

The closed-loop system can be forced to be dynamically similar to a model system of order n ,

$$\Delta \dot{x}_M = F_M \Delta x_M \quad (131)$$

by specifying that the mean-square error between modelled and actual state rates be minimized. The implicit model-following weighting matrix is

$$\begin{bmatrix} \Delta Q & \Delta M \\ \Delta M^T & \Delta R \end{bmatrix} = \begin{bmatrix} (F - F_M)^T Q_M (F - F_M) & (F - F_M)^T Q_M G \\ G^T Q_M (F - F_M) & G^T Q_M G \end{bmatrix} \quad (132)$$

where Q_M weights state-rate errors. The quadratic cost function [Eq. (109)] can be defined as an aggregate of the various weighting types, the only restriction being that the net values of Q , M , and R satisfy the four conditions for stability.

If reduced-order control of low-frequency modes is the primary goal, or if control actuator rates are limited, it may be desirable to restrict the bandwidth of control outputs. These objectives can be accommodated by adding a control rate penalty to the cost function,

$$J = \frac{1}{2} \int_0^{\infty} \left\{ \begin{bmatrix} \Delta \dot{\underline{x}}^T & \Delta \dot{\underline{u}}^T & \Delta \dot{\underline{v}}^T \end{bmatrix} \begin{bmatrix} Q & M_1 & 0 \\ M_1^T & R_1 & 0 \\ 0 & 0 & R_2 \end{bmatrix} \begin{bmatrix} \Delta \underline{x} \\ \Delta \underline{u} \\ \Delta \underline{v} \end{bmatrix} + \Delta \dot{\underline{u}}^T R_3 \Delta \dot{\underline{u}} \right\} dt \quad (133)$$

and augmenting the dynamic system to include control actuator dynamics, as well as a new control variable, $\Delta \underline{v}$:

$$\begin{bmatrix} \Delta \dot{\underline{x}} \\ \Delta \dot{\underline{u}} \end{bmatrix} = \begin{bmatrix} F & G \\ D_x^u & D_u \end{bmatrix} \begin{bmatrix} \Delta \underline{x} \\ \Delta \underline{u} \end{bmatrix} + \begin{bmatrix} 0 \\ G_v^u \end{bmatrix} \Delta \underline{v} \quad (134)$$

There are two cases of interest. In the first, the linear dynamics of the actuator are significant: D_u contains the time constants of the actuators and possible coupling between them, D_x^u reflects loading of the actuators by the state variables, $G_v^u = -D_u$, and $\Delta \underline{v}$ is the commanded value of control position, i.e., $\Delta \underline{v} \triangleq \Delta \underline{u}_c$. The cost function is put in standard form by substituting the lower rows of Eq. (134) for $\Delta \underline{u}$ in Eq. (133), and the perturbation control law becomes

$$\Delta \dot{\underline{u}}_c(t) = -C_1 \Delta \underline{x}(t) - C_2 \Delta \underline{u}_c(t) \quad (135)$$

The term $\Delta \underline{u}_c(t)$ could be obtained from measurements of control position, or it could be constructed by integrating the lower rows of Eq. (134). In the second case, actuator dynamics are negligible; then $D_x^u = D_u = 0$, $G_v^u = I$, and $\Delta \underline{v} \triangleq \Delta \underline{u}$. The control rate is commanded, and the LQ regulator is

$$\Delta \dot{\underline{u}}(t) = -C_1 \Delta \underline{x}(t) - C_2 \Delta \underline{u}(t) \quad (136)$$

Taking the Laplace transform and performing minor manipulation

$$\Delta \underline{u}(s) = -(sI + C_2)^{-1} C_1 \Delta \underline{x}(s) \quad (137)$$

Because it is a "strictly proper rational matrix" (more poles than zeros), $(sI + C_2)^{-1}$ can be recognized as a low-pass filter matrix. The controller attenuates high frequency components of $\Delta \underline{x}(s)$, which in turn reduces the feedback from higher order modes, lessens disturbance and measurement noise effects, and smoothes the commands to control actuators. Note, however, that Eq. (136) and (137) describe a perturbation controller; changes in the set point are transmitted without filtering, as in Eq. (112).

Control rate weighting is seen to change the structure of the LQ regulator, adding m integrators as part of the control reconstruction or low-pass filters. Integral compensation also can be added explicitly, providing an "autotrimming" feature that accounts for parameter variations and bias disturbances. Pure integrals of the output vector $\Delta \underline{y}$ ($k \leq m$) result in infinite "D.C." (zero frequency) gain in the associated open-loop transfer functions, reducing the low frequency sensitivity of the closed-loop system. Also referred to as "Type 1" compensation [31], the output integrators eliminate steady-state "hangoff" without direct measurement and compensation of disturbances.

For constant set point, the perturbation output integral is,

$$\Delta \underline{y}_I(t) = \Delta \underline{y}_I(t_0) + \int_{t_0}^t \Delta \underline{y}(t) dt, \quad \Delta \underline{y}_I(t_0) = 0 \quad (138)$$

the cost function is,

$$J = \int_0^{\infty} \left\{ \begin{bmatrix} \Delta \tilde{x}^T & \Delta \tilde{\xi}^T & \Delta \tilde{u}^T \end{bmatrix} \begin{bmatrix} Q_1 & 0 & M \\ 0 & Q_2 & 0 \\ M^T & 0 & R \end{bmatrix} \begin{bmatrix} \Delta \tilde{x} \\ \Delta \tilde{\xi} \\ \Delta \tilde{u} \end{bmatrix} \right\} dt \quad (139)$$

and the augmented state equation is

$$\begin{bmatrix} \dot{\Delta \tilde{x}}(t) \\ \dot{\Delta \tilde{\xi}}(t) \end{bmatrix} = \begin{bmatrix} F & 0 \\ H_x & 0 \end{bmatrix} \begin{bmatrix} \Delta \tilde{x}(t) \\ \Delta \tilde{\xi}(t) \end{bmatrix} + \begin{bmatrix} G \\ H_u \end{bmatrix} \Delta \tilde{u}(t) \quad (140)$$

The perturbation controller takes the form,

$$\Delta \tilde{u}(t) = -C_1 \Delta \tilde{x}(t) - C_2 \Delta \tilde{\xi}(t) \quad (141)$$

and its Laplace transform can be written as,

$$\Delta \tilde{u}(s) = -C_1 \Delta \tilde{x}(s) - C_2 \Delta \tilde{\xi}(s)/s \quad (142)$$

revealing the proportional-integral "Type 1" structure. Integral compensation and control-rate weighting are combined in the proportional-integral-filter ("PIF") controller, which evidences parameter insensitivity, bias disturbance rejection, and high frequency attenuation [32].

All of the continuous-time LQ regulators discussed here use the same solution equations to determine feedback gains and non-zero set points; hence, the criteria for closed-loop stability, steady-state response, and root locus properties apply throughout. The principal differences between the controllers derive from definitions of cost functions and augmented system dynamics. Consequently, in the discussion of digital control that follows, it is sufficient to address only the basic LQ regulator.

Digital Linear-Quadratic Regulators

The corresponding discrete-time optimization of a quadratic cost function subject to a linear, time-invariant dynamic constraint uses summations and difference equations rather than integrals and differential equations. The cost function is,

$$J = \frac{1}{2} \sum_{k=0}^{\infty} \left\{ \begin{bmatrix} \Delta \tilde{x}_k^T & \Delta \tilde{u}_k^T \end{bmatrix} \begin{bmatrix} \hat{Q} & \hat{M} \\ \hat{M}^T & \hat{R} \end{bmatrix} \begin{bmatrix} \Delta \tilde{x}_k \\ \Delta \tilde{u}_k \end{bmatrix} \right\} \quad (143)$$

and the dynamic constraint is, from Eq. (24),

$$\Delta \tilde{x}_{k+1} = \phi \Delta \tilde{x}_k + \Gamma \Delta \tilde{u}_k \quad (144)$$

The discrete-time LQ regulator takes the form,

$$\Delta \tilde{u}_k = -C \Delta \tilde{x}_k \quad (145)$$

where the control gain matrix is [33],

$$C = (\hat{R} + \Gamma^T P \Gamma)^{-1} (\Gamma^T P \phi + \hat{M}^T) \quad (146)$$

and P is the steady-state solution to the discrete-time matrix Riccati equation,

$$P_{k-1} = \phi^T P_k \phi + \hat{Q} - (\Gamma^T P_k \phi + \hat{M}^T)^T (\hat{R} + \Gamma^T P_k \Gamma)^{-1} (\Gamma^T P_k \phi + \hat{M}^T) \quad (147)$$

The discrete-time problem does not formally recognize the time between sampling instants, but \hat{Q} , \hat{M} , and \hat{R} can be defined in such a way that the discrete-time regulator minimizes the continuous-time cost function, subject to the constraint that the control is piecewise-constant between sampling instants.* If we simply multiplied Eq. (143) by the sampling interval, T, it would be an Euler (rectangular) integration of the continuous-time cost function [Eq. (109)], but a more precise approach is to specify that the

* In other words, the digital commands are converted to analog signals using a zero-order hold [3].

cost summation be equivalent to

$$J = \frac{1}{2} \sum_{k=0}^{\infty} \int_{t_k}^{t_{k+1}} \left\{ \begin{bmatrix} \Delta \hat{x}^T(t) & \Delta \hat{u}^T(t) \end{bmatrix} \begin{bmatrix} Q & M \\ M^T & R \end{bmatrix} \begin{bmatrix} \Delta \hat{x}(t) \\ \Delta \hat{u}(t) \end{bmatrix} \right\} dt \quad (148)$$

with $(t_{k+1} - t_k) = T$. Following [33], [34] shows that \hat{Q} , \hat{M} , and \hat{R} can be expressed as integrals of Q , M , R , and the system equations:

$$\hat{Q} = \int_0^T \phi^T(t) Q \phi(t) dt \quad (149)$$

$$\hat{M} = \int_0^T \left[\Gamma^T(t) Q \phi(t) + M \phi(t) \right] dt \quad (150)$$

$$\hat{R} = \int_0^T \left[R + \Gamma^T(t) Q \Gamma(t) + 2M \Gamma(t) \right] dt \quad (151)$$

With these definitions of the cost matrices, Eq. (145) becomes a sampled-data LQ regulator whose deterministic closed-loop response remains close to continuous-time LQ regulator response even with relatively long sampling intervals (compared to the system's natural periods of motion). Nevertheless, the system is essentially "open-loop" between sampling instants, as feedback information is processed only periodically; effects of measurement errors and disturbances are free to grow during the interval. Under the assumption that these effects are gaussian, Eq. (87) can be used to predict the growth of state uncertainty, and the sampling interval can be chosen to limit the uncertainty to an acceptable level [35]. If the uncertainty arises from parameter variations, there may be an absolute limit on the sampling interval beyond which no optimal solution can be found [36].

Design of Linear-Gaussian (LG) Estimators

Paralleling the previous two sections, we consider the estimation of the state perturbation about its set point, Δx_p , which is specified in Eq. (113). The LT^T system model is

$$\dot{\Delta \hat{x}}(t) = F \Delta \hat{x}(t) + L \Delta \hat{w}(t), \quad \Delta \hat{x}(t_0) \text{ given} \quad (152)$$

with $\Delta \hat{x}(t)$ specified by Eq. (108), and

$$\Delta \hat{w}(t) = \Delta w(t) - \Delta w_p \quad (153)$$

$\Delta \hat{w}(t)$ is assumed to be a white gaussian process with zero mean and spectral density matrix Q . The controlled input, $G \Delta \hat{u}(t)$, is neglected for simplicity; it can be restored as a deterministic factor at will. The measurement vector is

$$\Delta \hat{z} = H \Delta \hat{x} + \Delta \hat{n} \quad (154)$$

where $\Delta \hat{n}$ is a white gaussian process with zero mean and spectral density matrix R . The LG estimate, $\Delta \hat{x}(t)$, is obtained by integrating

$$\dot{\Delta \hat{x}}(t) = F \Delta \hat{x}(t) + K \left[\Delta \hat{z}(t) - H \Delta \hat{x}(t) \right], \quad \Delta \hat{x}(t_0) \text{ given} \quad (155)$$

The state estimate relative to the nominal (zero set point) condition is $[\Delta \hat{x}(t) + \Delta \hat{x}_p]$. The filter gain matrix is

$$K = \hat{P} H^T R^{-1} \quad (156)$$

where \hat{P} is the steady-state solution of Eq. (99):

$$0 = \hat{F} \hat{P} + \hat{P} \hat{F}^T + L Q L^T - \hat{P} H^T R^{-1} H \hat{P} \quad (157)$$

Collecting the $\Delta \hat{x}$ terms, the characteristic equation of the estimator [Eq. (155)] is

$$\Delta_E(s) = |sI - (F - KH)| = 0 \quad (158)$$

From [5], the estimator is guaranteed to be asymptotically stable if 1) $R > 0$, 2) $Q \geq 0$, 3) $[F, (LQ L^T)^{1/2}]$ is a stabilizable pair, and 4) $[F, H]$ is a detectable pair. As before, it

is assumed that the correct F and H are used to calculate K ; however, asymptotic stability of the estimate error is guaranteed if the gain and phase characteristics of the assumed and actual systems are sufficiently close [23]. Suppose that the noise-free defect in modeling for each observation, Δz_i , $i = 1$ to r , is represented by an amplitude ratio, A_i , and phase angle, ϕ_i :

$$\frac{\Delta z_{\text{actual}}}{\Delta z_{\text{assumed}}} = A_i e^{j\phi_i} \quad (159)$$

Stability is maintained for $\frac{1}{2} \leq A_i \leq \infty$ or $|\phi_i| \leq 60^\circ$.

The asymptotic behavior of the LG estimator's roots also is equivalent to that of the LQ regulator [3]. As the signal-to-noise ratio becomes large ($Q \gg R$), p eigenvalues approach the p transmission zeros of $H(sI - F)^{-1}L$ and the remaining $(n - p)$ eigenvalues go to infinity in a multiple Butterworth configuration. For low signal-to-noise ratio ($Q \ll R$), the n estimator eigenvalues approach positions representing the stable open-loop modes or the stable mirror images of unstable open-loop modes. Additional insight can be found in [37], which shows that the filter structure partitions asymptotically into r "fast", uncoupled first-order filters and an $(n - r)$ Luenberger observer [38] as measurement noise becomes small.

Although an observer is asymptotically stable, it can produce a steady error with constant input [39], and the same is true for the LG estimator. Setting $\Delta \hat{x} = 0$ and substituting Eq. (154) in Eq. (155),

$$\Delta \hat{x}_{SS} = - (F - KH)^{-1} K (H \Delta \hat{x}_{SS} + \Delta \hat{n}_{SS}) \quad (160)$$

Assuming the $\Delta \hat{n}_{SS} = 0$ and $r = n$, the steady-state estimate equals the actual steady-state only if $\Delta \hat{x}_{SS} = 0$ or $F = 0$. The latter is equivalent to specifying the dynamic system to represent Brownian motion, or integrated white noise [3]. The value of estimating the perturbation from the control set point (rather than from the nominal value) is apparent, for the control action should force $\Delta \hat{x}_{SS}$ to zero, eliminating the offset error. Alternatives to this approach include rescaling the estimate by $[-(F - KH)^{-1}KH]^{-1}$ or using the compensated filter [24].

There is substantial latitude for specifying the statistics of disturbance inputs and measurement noise. If all components are white, gaussian, and uncorrelated with other components, the spectral density matrices, Q and R , are diagonal. If disturbances are instantaneously correlated with each other or if measurement errors are coupled, Q and R are symmetric but not diagonal. If disturbance inputs are "colored", i.e., correlated in time as in a turbulence spectrum, the dynamic equation and state vector can be augmented to incorporate the assumed correlation [7]. Colored measurement noise is best handled by defining a derived measurement,

$$\Delta \hat{z}_1 = \Delta \hat{z} - E \Delta \hat{z} \quad (161)$$

whose measurement noise is self-correlated by E and, therefore, is correlated with the process noise, $L \Delta \hat{w}$. The LG estimator structure then is equivalent to Eq. (155), with $\Delta \hat{z}_1$ replacing $\Delta \hat{z}$ and K defined accordingly [40]. In addition to these alternatives motivated by random process statistics, it is possible to consider Q and R as design parameters which can be adjusted to achieve non-optimizing objectives, e.g., robustness [22]. In such case, the justification for using the LG estimator rather than a more general observer is that its stability properties are well-defined and its design algorithms are straightforward.

This discussion carries over to discrete-time LG estimators with little modification; furthermore, the earlier treatment of LTV discrete-time estimators is easily restricted to the LTI case. One important distinction is that even if the continuous-time disturbance spectral density matrix, LQI^T , is diagonal, the equivalent sampled-data covariance matrix, $\hat{A}Q\hat{A}^T$, is likely to be non-diagonal (but symmetric). This occurs because states not directly forced by $L\Delta \hat{w}$ are coupled to the disturbance through F and $\phi(T)$, both of which figure in the computation of \hat{A} [Eq. (27)]. This coupled forcing can have a material effect on the performance of the discrete-time filter.

"Aliasing" or "frequency folding" may limit the maximum acceptable estimation sampling interval [3], [41], [42]. A sampling interval of T sec corresponds to a sampling frequency of $1/T$ Hz or $2\pi/T$ rad/sec. From Shannon's theorem [43], at least two samples per cycle are required to reconstruct a sine wave of known amplitude (or phase) without ambiguity; hence, the dominant signal frequencies must be below $1/2T$ Hz to satisfy this criterion. If signals above $1/2T$ Hz are sampled, they are indistinguishable from sampled

signals below $1/2T$ Hz, i.e., they are "folded" into the properly defined frequency spectrum, causing irreversible "aliasing" errors in the sampled signal. In other words, a continuous spectrum in $0 < \omega < \infty$ is "mapped" into the discrete spectrum in $0 < \omega(\text{rad/sec}) < \pi/T$ by the sampling process.

Troubles in estimation can occur if the spectrum of $\Delta \hat{\underline{z}}(t)$ (which is sampled every T sec to produce $\Delta \hat{\underline{z}}_k$) has significant amplitude at frequencies beyond π/T rad/sec. In principle, one can distinguish between high frequency information (contained in $\Delta \hat{\underline{x}}$) and high frequency noise (contained in $\Delta \hat{\underline{n}}$) because the former could be modelled and estimated; however, even the minutest modelling errors -- including the use of finite-precision computation -- can turn the former into the latter. If the measurement originates in an "analog" sensor that either is noisy or sensitive to high frequency signals, e.g., an accelerometer that picks up unwanted structural vibrations, a high-roll-off analog low-pass filter should precede the sampling.

The Linear-Quadratic-Gaussian (LQG) Regulator

The LQ regulator and LG estimator are combined to form the LQG stochastic controller. This section summarizes continuous-time and sampled-data LQG regulators with non-zero set points, and it presents recent results regarding the properties of such systems.

With constant control gain matrix, C , and estimator gain matrix, K , which have been computed earlier, the continuous-time LQG control law (Fig. 7) is described by two equations:

$$\Delta \underline{u}(t) = S_{22} \Delta \underline{y}_p(t) - C \Delta \hat{\underline{x}}(t) \quad (162)$$

$$\begin{aligned} \dot{\Delta \hat{\underline{x}}}(t) = & F_E \Delta \hat{\underline{x}}(t) - G_E C \Delta \hat{\underline{x}}(t) \\ & + K \left\{ \Delta \underline{z}(t) - H_E \left[\Delta \hat{\underline{x}}(t) + S_{12} \Delta \underline{y}_p(t) \right] \right\}, \quad \Delta \hat{\underline{x}}(t_0) \text{ given} \end{aligned} \quad (163)$$

Perturbations are measured from the nominal condition (zero set point), the disturbance input is assumed to be unmeasured, and the deterministic control effect is introduced in the estimator. The physical model used for estimation (F_E, G_E, H_E) may differ from the actual system (F, G, H), but it is assumed here that $\Delta \hat{\underline{x}}$ is dimensionally equivalent to $\Delta \underline{x}$. The equilibrium response matrices are computed from Eq. (116) and (118) using F_E, G_E, H_E , and the H_x and H_u that correspond to the commanded input, $\Delta \underline{y}_p$. For design purposes, it is assumed that $\Delta \underline{y}_p$ is constant; however, the actual commanded input may vary in time.

Substituting Eq. (162) in Eq. (7) and noting that $\Delta \underline{z} = H \Delta \underline{x} + \Delta \underline{n}$, the $2n^{\text{th}}$ -order differential equation which describes the LQG closed-loop system is

$$\begin{aligned} \begin{bmatrix} \dot{\Delta \hat{\underline{x}}}(t) \\ \dot{\Delta \underline{x}}(t) \end{bmatrix} = & \begin{bmatrix} F & -GC \\ KH (F_E - G_E C - KH_E) \end{bmatrix} \begin{bmatrix} \Delta \hat{\underline{x}}(t) \\ \Delta \underline{x}(t) \end{bmatrix} + \begin{bmatrix} GS_{22} \\ -KH_E S_{12} \end{bmatrix} \Delta \underline{y}_p(t) \\ & + \begin{bmatrix} 0 \\ K \end{bmatrix} \Delta \underline{n}(t) + \begin{bmatrix} L \\ 0 \end{bmatrix} \Delta \underline{w}(t), \quad \begin{cases} \Delta \hat{\underline{x}}(t_0) \text{ given} \\ \Delta \underline{x}(t_0) \text{ given} \end{cases} \end{aligned} \quad (164)$$

The stability of this system is described by the roots of the characteristic equation

$$\left| sI - \begin{bmatrix} F & -GC \\ KH (F_E - G_E C - KH_E) \end{bmatrix} \right| = 0 \quad (165)$$

A dynamically equivalent description of the system, is obtained by replacing the state estimate, $\Delta \hat{\underline{x}}$, with the error in the estimate, $\Delta \underline{\epsilon} = \Delta \hat{\underline{x}} - \Delta \underline{x}$,

$$\begin{aligned} \begin{bmatrix} \dot{\Delta \underline{x}} \\ \dot{\Delta \underline{\epsilon}} \end{bmatrix} = & \begin{bmatrix} (F - GC) & -GC \\ [(F_E - F) - K(H_E - H) - (G_E - G)C] & [F_E - (G_E - G)C - KH_E] \end{bmatrix} \begin{bmatrix} \Delta \underline{x} \\ \Delta \underline{\epsilon} \end{bmatrix} \\ & + \dots \end{aligned} \quad (166)$$

If the estimator's model is exact, this reduces to

$$\begin{bmatrix} \dot{\Delta \underline{x}} \\ \dot{\Delta \underline{\epsilon}} \end{bmatrix} = \begin{bmatrix} (F - GC) & -GC \\ 0 & (F - KH) \end{bmatrix} \begin{bmatrix} \Delta \underline{x} \\ \Delta \underline{\epsilon} \end{bmatrix} + \dots \quad (167)$$

In this case, the stability matrix is upper-block-triangular; hence, the closed-loop eigenvalues of $\Delta \underline{x}$ are determined by $(F - GC)$, and the closed-loop eigenvalues of $\Delta \underline{\epsilon}$ are determined by $(F - KH)$. This affirms that the closed-loop LQ regulator and LG estimator error dynamics are uncoupled and stable when the actual and assumed parameters agree.*

The LQG regulator is guaranteed to be stable in the absence of parameter variation, but unlike the separate LQ regulator and LG estimator, it is not guaranteed to be tolerant to parameter variations. These alter the estimator error dynamics and cause them to couple into the state dynamics, as indicated by the lower row of Eq. (166). [28] presents a simple example in which an infinitesimal parameter variation of either sign gives rise to instability.

One might suspect that the transfer characteristics of the estimator cause the problem, and this turns out to be the case. Each input-output pair in the estimator has gain and phase characteristics that are affected by the choice of Q and R. Estimation bandwidth generally decreases as measurement noise intensity increases, reducing high frequency gain and increasing phase lag. Conversely, the bandwidth is increased by reducing the assumed measurement noise or increasing the assumed process noise. From the earlier discussion it is clear that if all the states are measured, the n estimator poles tend to infinity as the assumed process noise becomes very large, i.e., estimator response tends to become instantaneous [3] [37]; the remaining LQ regulator dynamics then recover their deterministic robustness. If all the states are not measured, the (n - r) estimator poles that approach finite transmission zeros may limit the robustness obtained by arbitrary increase in Q. Designing the LG estimator with the assumed process noise

$$Q(\rho) = Q_0 + \rho^2 G Q_1 G^T, \quad 0 < \rho < \infty \quad (168)$$

where ρ is an arbitrary adjustment parameter and Q_1 is any positive definite symmetric matrix, is shown to restore the phase margin for a scalar control example at the expense of decreased measurement noise rejection [22]. It would appear that if some parameters of F and G are more likely to vary than others, selective increases in process noise of the following form would address the problem directly:

$$\Delta Q(\rho) = \rho^2 \Delta F P_0 \Delta F^T \quad (169)$$

or

$$\Delta Q(\rho) = \rho^2 \Delta G C_0 P_0 C_0^T \Delta G^T \quad (170)$$

where ΔF and ΔG reflect the expected variations in F and G, and C_0 and P_0 are the results of LQ regulator design without parameter variations. (This approach remains to be investigated.)

Recognition of the importance of gain and phase margins in multiloop systems has led to a renewed interest in frequency domain techniques, including application to LQG problems [45] - [49]. Particular attention is directed to the frequency-dependent singular values** of various transfer function matrices in the control and estimation loop. For example, the "return difference" in a single input-single output system is directly related to the system's sensitivity to parameter variations. The "return difference matrix" has a similar interpretation for multiloop systems, and its maximum and minimum singular values characterize this sensitivity. Because they are scalar quantities, singular values are amenable to graphical techniques, including Bode-like "frequency response" plots. Furthermore, the minimization of quadratic cost functions is found to be equivalent to the minimization of associated singular values [49].

The sampled-data LQG control law is most easily described by three equations:

* This does not guarantee open-loop stability of the estimator, as might be desired in preliminary testing of control logic or following partial failure of control actuators [44]. If the loop between the estimator and the system is broken, Eq. (164) indicates that the eigenvalues of the estimator are defined by $(F - GC - KH)$. Although $(F - GC)$ and $(F - KH)$ are guaranteed to be stable, there is no guarantee that $(F - GC - KH)$ is stable. The problem is, of course, avoided if the deterministic effect of control is not included in the estimator.

** Singular values are the square roots of the eigenvalues of the product of the matrix times its complex conjugate transpose.

$$\Delta u_k = S_{22} \Delta y_{p_k} - C \Delta \hat{x}_k (+) \quad (171)$$

$$\Delta \hat{x}_k (-) = \Phi_E \Delta \hat{x}_{k-1} (+) - \Gamma_E C \Delta \hat{x}_{k-1} (+) \quad , \quad \Delta \hat{x}_0 (+) \text{ given} \quad (172)$$

$$\Delta \hat{x}_k (+) = \Delta \hat{x}_k (-) + K \left\{ \Delta z_k - H_E \left[\Delta \hat{x}_k (-) + S_{12} \Delta y_{p_k} \right] \right\} \quad (173)$$

This controller is formulated under the same assumptions employed for the continuous-time example. Its robustness properties parallel but are somewhat more restrictive than those of the continuous-time LQG controller, approaching the latter's stability margins asymptotically as the sampling interval becomes small [50].

CONCLUSION

Stochastic optimal control theory encompasses a wide range of mathematical and physical principles, only a few of which could be addressed here. As must be the case in any introductory or abbreviated treatment of a complex subject, selected facts, rules, and examples have been reviewed, but there are exceptions, alternate methods, and special cases which could not be included. The principle benefit to be derived from stochastic optimal control theory is that it provides a systematic way of describing feasible solutions that can be expanded or simplified to match the control design problem. The theory provides the equations and algorithms which generate answers once the system model and performance indices are specified; however, it cannot give *a priori* guidance as to which indices are good and what numerical values are satisfactory. It must rely on the user's good judgment to specify models and objectives properly, and it is quite literal in its response; ask the wrong question, and it most surely will give the wrong answer. Pose the problem accurately, and it provides a practical solution, no matter how counter-intuitive the solution may be. The challenge in applying stochastic optimal control theory is to match understanding of the methodology, knowledge of the system to be controlled, and reasonable expectations of optimal system performance.

REFERENCES

1. Bryson, A. E., Jr., and Ho, Y. C., Applied Optimal Control, Hemisphere Publishing Corp. (J. Wiley & Sons), Washington, 1975.
2. Athans, M., and Falb, P., Optimal Control, McGraw-Hill, Inc., New York, 1966.
3. Kwakernaak, H., and Sivan, R., Linear Optimal Control Systems, J. Wiley & Sons, Inc., New York, 1972.
4. Anderson, B. D. O., and Moore, J. B., Linear Optimal Control, Prentice-Hall, Inc., Englewood Cliffs, 1971.
5. Anderson, B. D. O., and Moore, J. B., Optimal Filtering, Prentice-Hall, Inc., Englewood Cliffs, 1979.
6. Brogan, W. L., Modern Control Theory, Quantum Publishers, New York, 1974.
7. Gelb, A., ed., Applied Optimal Estimation, M.I.T. Press, Cambridge, 1974.
8. Maybeck, P. S., Stochastic Models, Estimation, and Control, Volume 1, Academic Press, Inc., New York, 1979.
9. Schweppe, F. C., Uncertain Dynamic Systems, Prentice-Hall, Inc., Englewood Cliffs, 1973.
10. Athans, M., "The Role and Use of the Stochastic Linear-Quadratic-Gaussian Problem in Control System Design", IEEE Transactions on Automatic Control, Vol. AC-16, No. 6, Dec 1971, pp. 529-552.
11. Polak, E., "An Historical Survey of Computation Methods in Optimal Control", SIAM Review, Vol. 15, No. 2, April 1971, pp. 553-583.
12. Åström, K. J., Introduction to Stochastic Control Theory, Academic Press, New York, 1970.
13. Kushner, H. J., Stochastic Stability and Control, Academic Press, New York, 1967.
14. Davis, M. H. A., Linear Estimation and Stochastic Control, Halsted Press (J. Wiley & Sons), New York, 1977.

15. Stengel, R. F., "Equilibrium Response of Flight Control Systems", Proceedings of the 1980 Joint Automatic Control Conference, San Francisco, Aug 1980, pp. WP10(1-8).
16. Stengel, R. F., and Marcus, F. J., "Energy Management Techniques for Fuel Conservation in Military Transport Aircraft", AFFDL-TR-75-156, Feb 1976.
17. Stengel, R. F., "Optimal Guidance for the Space Shuttle Transition", AIAA Journal of Spacecraft and Rockets, Vol. 11, No. 3, Mar 1974, pp. 173-179.
18. Holley, W., and Bryson, A. E., Jr., "Multi-Input, Multi-Output Regulator Design for Constant Disturbances and Non-Zero Set Points with Application to Automatic Landing in a Crosswind", Stanford Univ. SUDAAR No. 465, Apr 1973.
19. Tse, E., "On the Optimal Control of Linear Systems", IEEE Transactions on Automatic Control, Vol. AC-16, No. 6, Dec 1971, pp. 776-785.
20. Deckert, J. C., Desai, M. N., Deyst, J. J., and Willsky, A. S., "F8-DFBW Sensor Failure Identification Using Analytic Redundancy", IEEE Transactions on Automatic Control, Vol. AC-22, No. 5, Oct 1977, pp. 795-803.
21. Bryson, A. E., Jr., "Kalman Filter Divergence and Aircraft Motion Estimators", AIAA Journal of Guidance and Control, Vol. 1, No. 1, Jan-Feb 1978, pp. 71-79.
22. Doyle, J. C., and Stein, G., "Robustness with Observers", IEEE Transactions on Automatic Control, Vol. AC-24, No. 4, Aug 1979, pp. 607-611.
23. Safonov, M. G., and Athans, M., "Robustness and Computational Aspects of Nonlinear Stochastic Estimators and Regulators", IEEE Transactions on Automatic Control, Vol. AC-23, No. 4, Aug 1978, pp. 717-725.
24. Athans, M., "The Compensated Kalman Filter, Proceedings of the 2nd Symposium on Nonlinear Estimation Theory and its Applications, Sept 1971, pp. 10-22.
25. Bierman, G. J., "A Comparison of Discrete Linear Filtering Algorithms", IEEE Transactions on Aerospace and Electronic Systems, Vol. AES-9, No. 1, Jan 1973, pp. 28-37.
26. Thornton, C. L., and Bierman, G. J., "Filtering and Error Analysis via the UDU^T Covariance Factorization", IEEE Transactions on Automatic Control, Vol. AC-23, No. 5, Oct 1978, pp. 901-907.
27. Gustafson, D. E., and Speyer, J. L., "Design of Linear Regulators for Nonlinear Stochastic Systems", AIAA Journal of Spacecraft and Rockets, Vol. 12, No. 6, June 1975, pp. 351-358.
28. Doyle, J. C., "Guaranteed Margins for LQG Regulators", IEEE Transactions on Automatic Control, Vol. AC-23, No. 4, Aug 1978, pp. 756-757.
29. Safonov, M. G., and Athans, M., "Gain and Phase Margin for Multiloop LQ Regulators", IEEE Transactions on Automatic Control, Vol. AC-22, No. 2, April 1977, pp. 173-179.
30. Tyler, J. S., Jr., "The Characteristics of Model-Following Systems as Synthesized by Optimal Control", IEEE Transactions on Automatic Control, Vol. AC-9, No. 4, Oct 1964, pp. 485-498.
31. Sandell, N. R., and Athans, M., "On Type-L Multivariable Linear Systems", Automatica, Vol. 9, No. 1, Jan 1973, pp. 131-136.
32. Stengel, R. F., Broussard, J. R., and Berry, P. W., "Digital Controllers for VTOL Aircraft", IEEE Transactions on Aerospace and Electronic Systems, Vol. AES-14, No. 1, Jan 1978, pp. 54-63.
33. Dorato, P., and Levis, A. H., "Optimal Linear Regulators: The Discrete-Time Case", IEEE Transactions on Automatic Control, Vol. AC-16, No. 6, Dec 1971, pp. 613-620.
34. Stengel, R. F., Seat, J. C., and Miller, G. E., "Digital Flight Control Research Using Microprocessor Technology", Office of Naval Research Report ONR-CR-300-003-1, May 1980.
35. Berman, H., and Gran, R., "Design Principles for Digital Autopilot Synthesis", AIAA Journal of Aircraft, Vol. 11, No. 7, July 1974, pp. 414-422.
36. Athans, M., Ku, R., and Gershwin, S. B., "The Uncertainty Threshold Principle: Some Fundamental Limitations of Optimal Decision Making under Dynamic Uncertainty", IEEE Transactions on Automatic Control, Vol. AC-22, No. 3, June 1977, pp. 491-495.
37. Stein, G., "Asymptotic Eigenstructures of Filters", Proceedings of the 1979 Conference on Decision and Control, Ft. Lauderdale, Dec 1979, pp. 297-301.
38. Luenberger, D. G., "An Introduction to Observers", IEEE Transactions on Automatic Control, Vol. AC-16, No. 6, Dec 1971, pp. 596-602.

39. Cooper, D. J., and Graham, A., "Errors in State Variable Reconstruction When an Observer is Subject to Constant Input Disturbances and Measurement Noise", IEEE Transactions on Automatic Control, Vol. AC-22, No. 1, Feb 1977, pp. 121-123.
40. Bryson, A. E., Jr., and Johansen, D. E., "Linear Filtering for Time-Varying Systems Using Measurements Containing Colored Noise", IEEE Transactions on Automatic Control, Vol. AC-10, No. 1, Jan 1965, pp. 4-10.
41. Mallinckrodt, A. J., "Aliasing Errors in Sampled Data Systems", AGARD Report 316, Paris, April 1961.
42. Bendat, J. S., and Piersol, A. G., Measurement and Analysis of Random Data, J. Wiley & Sons, New York, 1966.
43. Shannon, C. E., and Weaver, W., The Mathematical Theory of Communication, University of Illinois Press, Urbana, 1964.
44. Johnson, C. D., "State-Variable Design Methods May Produce Unstable Feedback Controllers", International Journal of Control, Vol. 29, No. 4, April 1979, pp. 607-619.
45. Ryraski, E. G., and Whitbeck, R. F., "The Theory and Application of Linear Optimal Control", AFFDL-TR-65-28, Jan 1966.
46. Harvey, C. A., Safonov, M. G., Stein, G., and Doyle, J. C., "Optimal Linear Control", Office of Naval Research Report ONR CR215-238-4F, Dec 1979.
47. Sandell, N. R., Jr. (ed), "Recent Developments in the Robustness Theory of Multi-variable Systems", Office of Naval Research Report ONR-CR215-271-1F, Aug 1979.
48. Whitbeck, R. F., "Wiener-Hopf Approaches to Regulator, Filter/Observer, and Optimal Coupler Problems", Office of Naval Research Report ONR-CR215-260-1, Jan 1980.
49. Safonov, M. G., Laub, A. J., and Hartmann, G. L., "Feedback Properties of Multi-variable Systems: The Role and Use of the Return Difference Matrix", to appear in IEEE Transactions on Automatic Control, 1981.
50. Stein, G., and Athans, M., "Robustness Properties of Discrete Time Regulators, LQG Regulators, and Hybrid Systems", M.I.T. Laboratory for Information and Decision Systems Report LIDS-FR-960, Oct 1979.

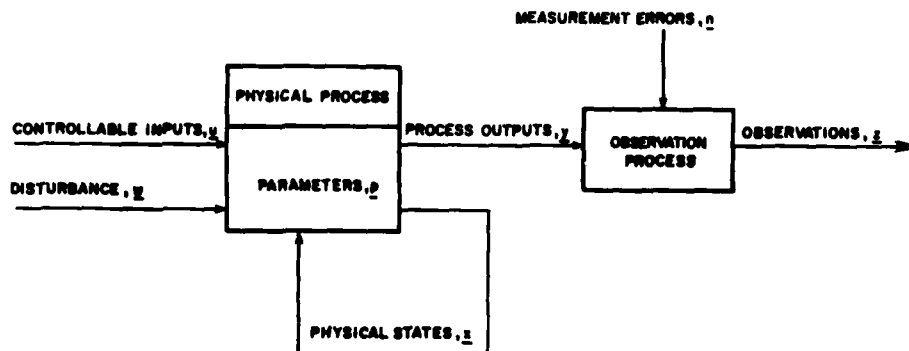


Figure 1. Elements of the Dynamic System.

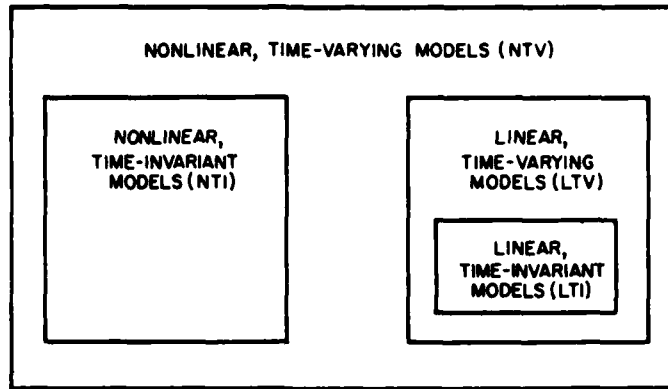


Figure 2. Classification of Dynamic Equations.

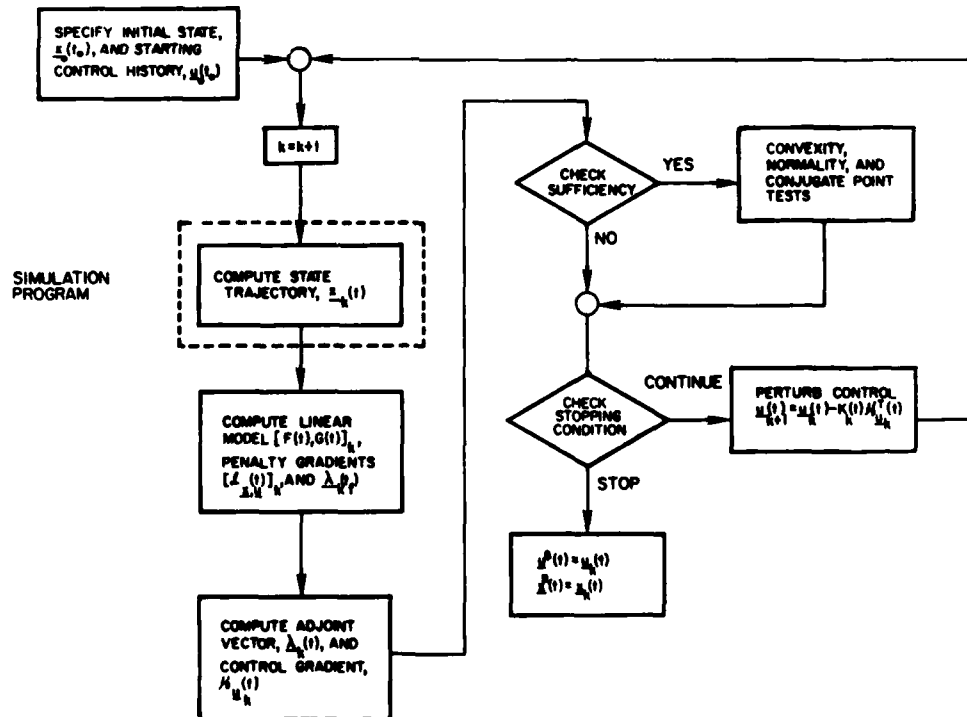


Figure 3. Gradient Method of Numerical Optimization.

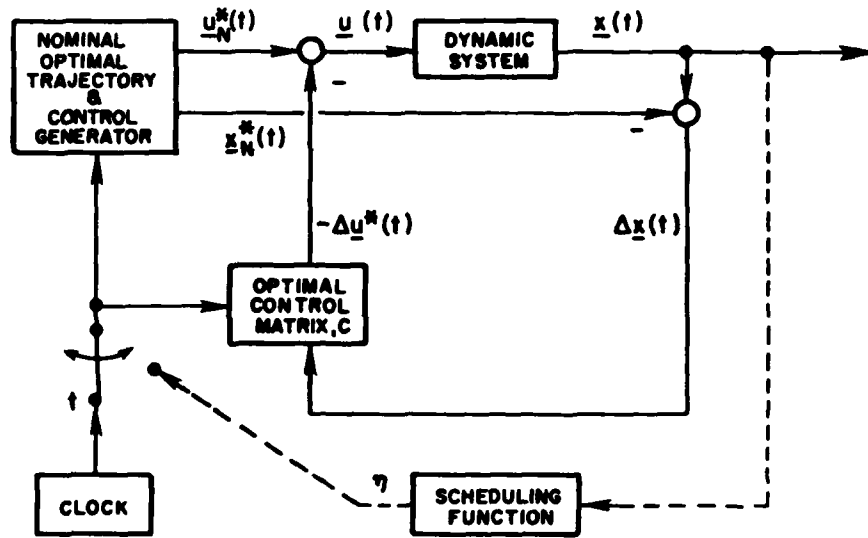


Figure 4. Prototype Neighboring-Optimal Control Law.

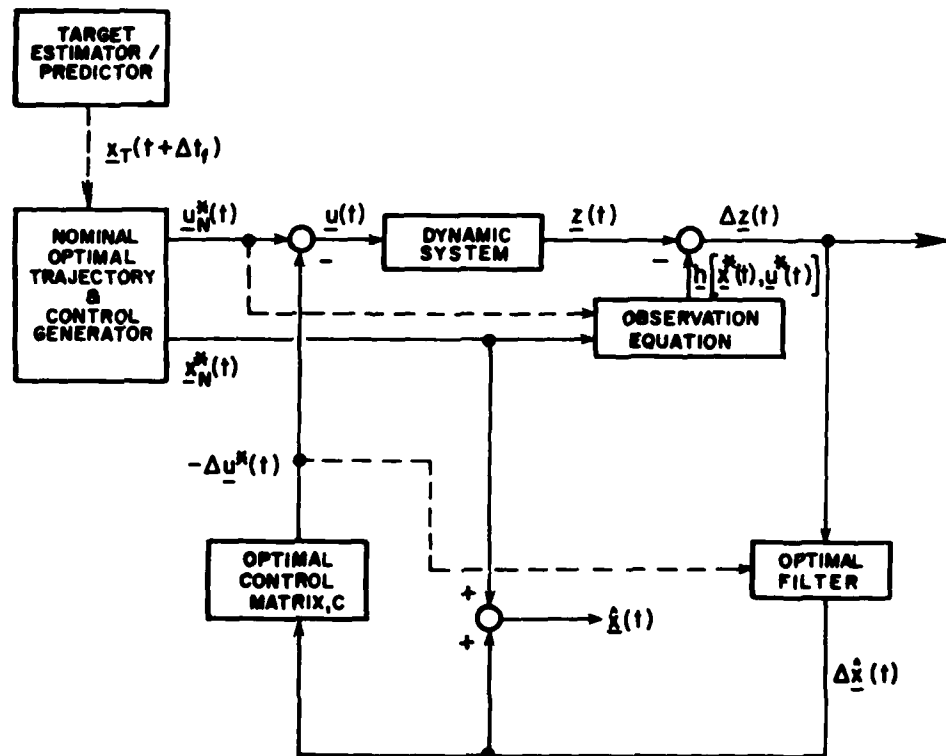


Figure 5. Stochastic Neighboring-Optimal Control Law.

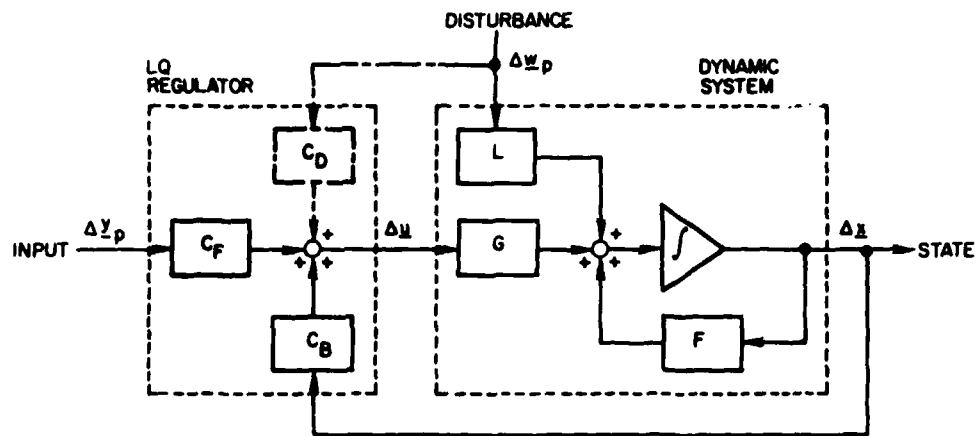


Figure 6. Non-Zero Set Point Linear-Quadratic (LQ) Regulator.

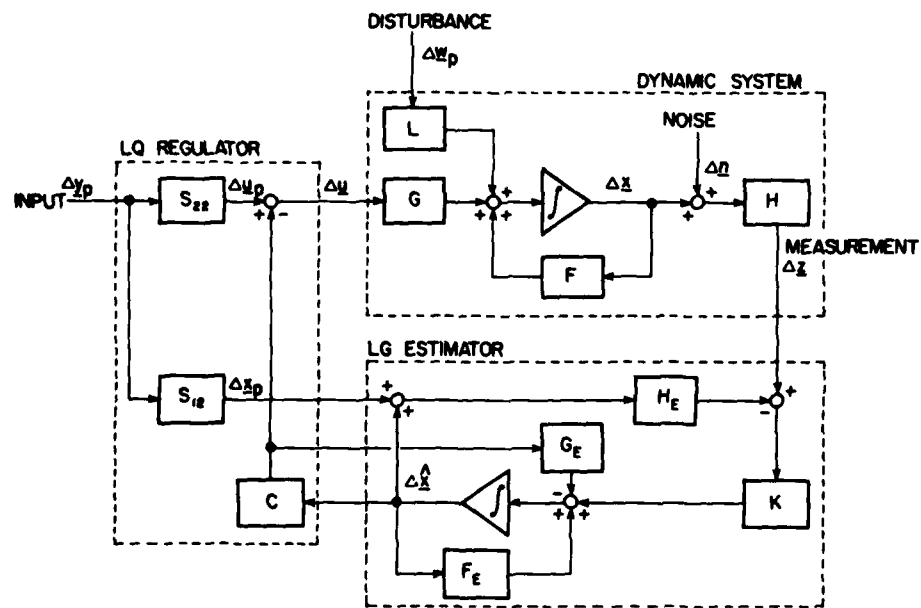


Figure 7. The Non-Zero Set Point Linear-Quadratic Gaussian Regulator.

DESIGN CONSIDERATIONS FOR OPTIMAL FLIGHT CONTROL SYSTEMS

F. R. Gill
 Flight Systems Department
 Royal Aircraft Establishment
 Farnborough, Hampshire, England

SUMMARY

This paper is a contribution to a proposed AGARDograph on "Theory and applications of optimal control in aerospace systems". Following a review of the several interacting factors affecting the design of control laws for any kind of Flight Control System (FCS), the modelling problem is discussed, including accuracy requirements for computer models of the aircraft, FCS, external disturbances and sensor noise. The state-of-the-art in designing the control and scheduling laws is surveyed and the limits of conventional control techniques are exposed. To overcome these limits, the use of selected nonlinear control techniques is discussed, including the concept of redundant adaptation with safeguards.

LIST OF SYMBOLS

A	$(n \times n)$ matrix of coefficients for aircraft or full system
B	$(m \times m)$ matrix of coefficients of control signal to control surfaces
B_a	control effectiveness
F	input filter control parameters
G	closed-loop control parameters
G_i	gearing of closed-loop (i)
G_{iA}, G_{iB}, G_{iC}	minimum, maximum and compromise values of G_i
G_a	part of G_i changed with aircraft characteristics
G_v	VICTOR gearing: $G_i = G_a \cdot G_v$
ΔG_L	error in G_i causing limit cycles or hazardous poor damping
ΔG_i	error in G_i
J	quadratic performance function
K	feedback gains from solution to the matrix Riccati equations
M	model parameters
$P(s)$	input command filter to give dead-beat response in \underline{x} to \underline{x}_c
$Q(s)$	input command filter for desired response of \underline{y} to \underline{p}_c
T_i	response time of closed-loop (i)
T_g	gust time constant
V	function used for parameter optimisation
\underline{d}	difference signal, $\underline{y} - \bar{\underline{y}}$
\underline{e}	closed-loop error signal
\underline{p}_c	pilot input command
\underline{u}^c	control signal input
\underline{v}	external disturbances
\underline{w}	sensor noise
\underline{x}	n -dimensional state vector
\underline{x}_c	command for change in state \underline{x}_i
\underline{x}_i	state used in closed-loop (i)
\underline{y}	output state vector
\underline{y}_1	components of \underline{y} representing primary aircraft motion
\underline{y}_2	other significant components of \underline{y}
\underline{y}_m	model response
$\underline{\theta}$	control parameters
$\underline{\theta}_a$	control parameters changed with aircraft characteristics
$\underline{\theta}_{op}$	values of $\underline{\theta}$ which minimise V
τ_i	time constant of simplified noise filter
λ_i	weight associated with i 'th component of V

1 INTRODUCTION

The main purpose of this paper is to review the problems faced in designing practical control laws for a full authority flight control system (FCS). A secondary aim is to expose limitations experienced with conventional (linear) control laws and suggest how these limitations may be reduced in future FCS.

In general, various control law design techniques are being developed by separate groups faced with solving particular problems using different facilities. The review in this paper is based on the particular experience of a group at RAE Farnborough and reflects the present but rapidly changing state-of-the-art within this group.

The design of the control laws for a fly-by-wire (FBW) aircraft is the basis for most of the discussion although reference is made, when appropriate, to other types of system. Referring to Fig 1, we require to:

- (a) select the closed-loop controller G in order to reduce the effects of external disturbances to acceptable values (regulator problem);
- (b) select the command input controller F in order to obtain acceptable aircraft response to a pilot command (tracking problem);
- (c) select how F and G are varied in order to compensate for variations in the aircraft characteristics across the flight and manoeuvre envelope, i.e. select the scheduling laws.

In order to achieve a satisfactory design of the control and scheduling laws, we need to specify flying qualities in terms of the required characteristics of the output y to both a pilot command and to external disturbances and sensor noise. We also need to define satisfactory models of the aircraft, sensors, FCS, external disturbances and sensor noise for simulation on the computer used for design and analysis purposes. These are discussed briefly in sections 2 and 3 as a background to the review of procedures used in the design of linear control laws, section 4, and a discussion of recent research into the use of nonlinear control laws, section 5.

Reference is made to many text books on classical¹ and modern control theory² and their application to FCS.

2 REVIEW OF FACTORS AFFECTING THE DESIGN OF CONTROL LAWS

As a background, we discuss first a number of issues which impinge on the design of control laws and which complicate the overall design, analysis and assessment problem.

2.1 Airworthiness requirements

The question of airworthiness is of greatest importance, and is discussed first. In the past, the signals to the control surfaces from the FCS have been limited in authority such that, if the control signal is incorrect, the resulting aircraft motion is not hazardous, and the pilot has time to disconnect the failed FCS. In many in-service systems, certain control systems have full authority and, in some future systems, loss of stabilising control signals could result in loss of aircraft, eg loss of the control which stabilises an otherwise statically unstable aircraft.

With the full authority FCS, a single failure may cause an undesirable and, perhaps, hazardous motion, which may then cause damage to or loss of the aircraft. A full authority FCS must be designed to automatically detect and isolate all such failures before the aircraft's motion is significantly affected, so that the average rate of aircraft loss due to all causes is not increased, i.e. between 10^{-6} and 10^{-5} pfh (per flight hour) for a combat aircraft in peacetime operations and between 10^{-7} and 10^{-6} pfh for a transport aircraft. Recognising that there are many different causes of aircraft damage or loss, some of which are unaffected by the FCS, the figure associated with each cause of FCS failure is in the region of 10^{-8} pfh or less, depending on how the overall target is partitioned. It is impossible to 'prove' that a system will meet such an integrity target (10⁸ hours equals about 10⁴ years) and we have to rely on 'engineering' judgement based on previous experience and rigorous analysis in order to obtain certification of full authority and especially full time FCS.

Much attention has been and continues to be given to surviving that class of failures associated with equipment malfunctions which can be detected and survived by using hardware redundancy techniques. There are, however, other kinds of failure which are not detected by hardware redundancy techniques alone. One of these is associated with inappropriate design or implementation of the flight control or scheduling laws. Such failures may not result in an immediate loss of the aircraft but, combined with the pilot's subsequent difficulty in completing his flight task under the experienced conditions, there may be an unacceptable increase in the risk of aircraft loss.

Inappropriate flight control or scheduling laws arise in a number of ways. For example, an inaccuracy in the aircraft model used during the design, combined with poor modelling of errors in the scheduling sensors, could lead to an error in the closed-loop gain sufficiently large to cause unacceptably poor damping and even instability. In order to avoid this hazardous situation, satisfactory gain margins must be applied.

This particular example indicates the need to model the aircraft and all components of the FCS as accurately as possible. Alternatively, more advanced control policies, such as self-adaptive techniques, are being developed so as to adjust automatically the control laws to behave in the required manner. With such policies, we would no longer need very accurate modelling of the aircraft for control law design purposes and, moreover, the number of different types of scheduling sensors could be reduced, resulting in a significant reduction in FCS hardware.

With the advent of digital FCS computers, the means of implementing these more complex nonlinear control laws is available. However, we are faced with the problem of detecting and isolating possible, although infrequent, failures of such complex functions. It is this question of integrity that has so far prevented the use of nonlinear control laws.

In the design of all functions programmed in the FCS computers, see Table 1, there are three interacting and conflicting requirements:-

- (a) minimise the amount of FCS hardware,
- (b) improve flying qualities through the use of more appropriate control and scheduling laws;
- (c) increase confidence that the airworthiness targets will be met.

Although this AIAA paper is mainly concerned with (b), we must keep in mind the other areas (a) and (c) in designing the 'optimal' practical system for a particular aircraft.

2.1 Specification of flying qualities

It is generally recognised⁵ that existing specifications of flying qualities are inadequate for the design of control laws aimed at achieving best possible performance for difficult flight tasks and severe environmental conditions. Existing specifications are based on experience with aircraft without full authority FCS and do not, therefore, embody the performance benefits of multi-loop feedback and feedforward control.

A chicken-and-egg situation arises. Realisable requirements can be formulated only after exhaustive pilot-in-the-loop simulation experiments, augmented by appropriate flight tests on a number of representative aircraft using representative control laws. On the other hand, design of the optimal control laws implies the need to specify optimal flying qualities in a fashion appropriate to the design technique applied. This situation is likely to remain for some time as further and more comprehensive experience is gained on the benefits - and problems - of flying an aircraft with a full authority multi-loop FCS.

The difficulties in specifying performance requirements are compounded by the fact that the control laws and, therefore, the flying qualities can be changed with flight task and environmental condition⁶. This is already done, of course, with in-service autopilots. With FBW aircraft, in order to reduce pilot's workload and eliminate the possibility of pilot error, such task-oriented control laws should be selected automatically whenever possible. However, pilot-selectable control laws may be advantageous for some flight tasks and/or for some system concepts.

The present trend, therefore, is to consider the flying qualities, control laws and FCS requirements for each difficult flight task under the most severe conditions, eg 'worst' gust. Table 2 lists some of the difficult flight tasks for a combat aircraft.

2.2 An interpretation of flying qualities requirements for the design of control laws

From the point of view of designing the control laws for each flight task, it is necessary to interpret formal specifications in terms of the design techniques to be applied. Referring to Fig 1, one method involves, firstly, defining outputs y_1 which are important for each task and, secondly, specifying a model M such that the differences between the actual response $y_1(t)$ and the model response

$$\underline{y}_m(t) = M \underline{p}_c(t) \quad (1)$$

are reduced to acceptable values for all pilot commands $\underline{p}_c(t)$ and all external disturbances $\underline{v}(t)$. The model M is a diagonal matrix which could be varied with flight task, and amplitude and/or rate of pilot command.

In many ways, a pilot's command can be viewed as a command for a change in trimmed output state \underline{y}_{01} . The outputs y_1 can often be selected such that the desired model response is dead-beat with a specified rise time and/or delay to a rapid pilot step command about any trimmed state. For such cases, $y_1(t)$ should follow $\underline{y}_m(t)$ with negligible overshoot provided this can be achieved sufficiently rapidly.

When the pilot makes no input, as in an autopilot hold mode, the main problem is to reduce the difference

$$\Delta y_1 = \underline{y}_{01} - \underline{y}_1 \quad (2)$$

to acceptable values for the 'worst' external disturbance $v_m(t)$, i.e. that yielding largest deviations from the required trimmed state, y_{01} . During the glide path hold mode, for example, y_1 includes height, airspeed and attitude and we are concerned with ensuring that deviations outside specified limits of these outputs are acceptable for any shape or size of wind gust or shear.

It is also useful to specify the behaviour of each $y_1(t)$ when the disturbance $v(t)$ reduces to zero. Ideally, each component of $\Delta y_1(t)$ should reduce to zero with little overshoot provided the decay is sufficiently rapid. This implies that the modes of motion associated with $y_1(t)$ are close to being critically damped.

In addition to the primary outputs y_1 , there are other important outputs y_2 which also need to be considered. Depending on the flight task and conditions, y_2 may include actuator activity, acceleration at the pilot's station and excessive loads. In general, we require to reduce y_2 to acceptable levels provided we can achieve the desired performance in terms of y_1 . Experience has shown, however, that it is also necessary to specify:

- (a) the minimal damping of all modes of motion formed by interaction between the FCS and the aircraft;
- (b) adequate gain and phase margins for each mode of motion.

These additional conditions, together with the need to minimise deviations in all components of $y = y_1 + y_2$ caused by sensor noise $w(t)$, often cause situations where compromises have to be made between the different components of y .

Pilot opinion, of course, remains a major factor in deciding how to specify y for each flight task and the relative importance of the components of y . As mentioned before, however, pilot opinion can be obtained only through pilot-in-the-loop simulations or flight experiments using previously defined and practically realisable control laws. For research work, we can define a range of control law options for comparative assessment and subsequent iteration through a design and assessment procedure. As a result of such research studies, pilots' opinions may change as improvements in achievable flying qualities are recognised and preconceived ideas in the designer's mind may change as features of the control laws which lead to the pilot achieving improved performance are exposed. For a new project aircraft, a more precise specification is desirable, based on the state-of-the-art at the time of project definition. However, with the possibility of being able to re-program the digital FCS computers during the lifetime of the aircraft, an update of the control laws is feasible as improved flying qualities specification become available or as the aircraft's mission(s) change. Much work is being done, at the present time, to update current flying qualities specifications.

2.4 Design, analysis and assessment procedure

The main stages in the design of the control laws and the assessment of both airworthiness and flying qualities of the aircraft plus FCS are shown as a flow chart in Fig 2. It is convenient to consider that part of the process which need not include the pilot-in-the-loop as a separate design/analysis package. It is shown within the dashed box of Fig 2.

As discussed above, a provisional statement of objectives is defined from available formal specifications of flying qualities and airworthiness requirements and from the results of experimental work proceeding elsewhere. This statement is provisional in the sense that changes may be made from the results obtained in subsequent stages of the design, analysis and assessment (pilot-in-the-loop) procedure on the control law, system algorithms, software and hardware aspects of the system. (The feedback paths are excluded from Fig 2 for clarity).

The current state-of-the-art on control law design is based on linear control theory^{1,2}. It is necessary to interpret requirements in terms of these design techniques and to linearise and otherwise simplify the models of aircraft, FCS and external disturbances (discussed further in section 3). Initial design studies are often made using as simple as possible models in order that the computer operator is not confused by the complexity of the problem. These are followed, of course, by further analysis with the simplifications removed, and eventually including all nonlinearities. At this point, the process is one of analysis rather than design, e.g. time responses to representative inputs and disturbances appraised. Several iterations through the design/analysis process may be necessary.

The resulting control laws, satisfactory from the objective viewpoint, are then assessed with the pilot-in-the-loop, using available simulators and, finally, flight tests in the aircraft. Adverse pilot comments, particularly in executing difficult flight tasks, together with performance measurements, may well lead to further iterations through the design, analysis and assessment loop.

Parallel developments of the multiplexed FCS leads to the need to include the effects of certain properties of the FCS in the analysis, pilot-in-the-loop simulation and flight tests. In particular, it is necessary to assess the effects of real hardware characteristics rather than the assumed models of the FCS, ideally using a comprehensive rig in conjunction with a pilot-in-the-loop simulator. The transient effects on FCS failures and problems associated with loss of parts of the FCS require careful assessment.

It should be noted that there is a need for rapid and inexpensive re-programming of the FCS computers during the development stages in order to allow for (inevitable) changes in the control laws. This requirement has system implications in that means must be found to establish airworthiness confidence for such rapid changes.

The main emphasis in this paper is on the design/analysis phases within the dashed box of Fig 2. This includes in section 5 an appraisal of the future use of nonlinear control laws for the following two main reasons:-

- (a) with conventional control laws, it is necessary to make inevitable compromises in view of the fact that different control laws are needed to reduce errors in different elements of $y (= y_1 + y_2)$ to acceptable values;
- (b) it is necessary to provide for unknown or incorrect values of parameters in the total system, eg through the application of adequate gain margin. With conventional techniques, this provision leads to larger errors in y_1 compared with a system which would automatically and safely correct for such errors.

The limitations of conventional control and scheduling laws emerges from a sensitivity analysis of the system's performance to changes in the characteristics of the aircraft, FCS and external disturbances. This is an important part of the design/analysis package. As discussed further in section 3, a particular objective of the sensitivity analysis is to define modelling requirements.

2.5 Design/analysis package

At RAE Farnborough, the design/analysis package, dashed box in Fig 2, is contained in an operator-interactive computer program called Time SIMulation (TSIM). In contrast to previous procedures that were based on separate programs, some on different computers, the interactive TSIM package represents a significant step forward, because the operator can quickly change the program and obtain results in a rapid sequence and in a digestible visual form from different and selectable sub-routines. For example, he can obtain in quick succession time histories for representative inputs and disturbances using linear (and simplified) equations and the full nonlinear equations of motion. The separate phases of design, sensitivity analysis and performance analysis shown in Fig 2 merge where the operator interacts continuously with the design/analysis package.

A simple simulation language has been defined which allows simulations to be written as a set of nonlinear equations in a Fortran program. This is linked to the main analysis package by a translator. When running, the analysis package is controlled interactively by commands typed in by the operator. He can command, for example, an automatic linearisation of the nonlinear equations about any datum he specifies, select which 'nodes' to ignore in simplifying the equations, and obtain outputs in tabular or graphical form on a VDU or print-out from any sub-routine of the analysis package. Changes to the equations of motion or to the characteristics of inputs and disturbances need not necessarily require a re-build of the TSIM package.

With an interactive procedure such as TSIM, the operator is an important part of the design/analysis loop. As such he needs to be very familiar with the chosen analysis technique and conversant with its limitations, bearing in mind that he is often dealing with systems of order 40 or more. It is also important to make the TSIM or similar computer package as simple as possible to operate so that the designer can concentrate his expertise on the design/analysis problem.

As a research tool at RAE, the TSIM package is being continuously modified as more complex problems are investigated and as experience is gained of new techniques. Some of the analysis tools currently available are listed in Table 3.

3 SOME ASPECTS OF THE MODELLING PROBLEM

For the design of the control laws and a first analysis of the aircraft's behaviour it is necessary to model on a suitable computer the aircraft's equations of motion, external disturbances and the characteristics of the FCS including sensor imperfections. The following brief comments on the problems of modelling are based on recent RAE experience.

3.1 Aircraft equations of motion

The nonlinear equations of motion of the aircraft plus its FCS can be written

$$\dot{x} = f(x, u) \quad (3a)$$

where x is an n -dimensional state vector and u is an m -dimensional control vector representing control signals applied to the control surfaces and other kinds of motivator. It is desirable for the form of these equations to be such as to facilitate linearisation and simplifications so that suitable approximations can be made for control law design purposes. In effect, this is part of a sensitivity analysis which establishes the more important modes of motion and associated closed loops.

Given the aircraft equations of motion, it is necessary to ensure that flying qualities are optimum for small perturbations at all points in the flight and manoeuvre

envelope. For this purpose, equation (3a) is linearised about representative flight conditions, yielding

$$\dot{\underline{x}} = A\underline{x} + B\underline{u} \quad (3b)$$

where A and B are $(n \times n)$ and $(m \times m)$ matrices of constant coefficients. The powerful techniques of linear control design and analysis are now applicable.

The results of this linear design remain satisfactory for manoeuvres which are slow relative to the variations in the coefficients of the A -matrix representing both the aircraft and its feedback control. For more rapid manoeuvres, the linear design is no longer satisfactory and it is necessary to design and analyse performance using the full nonlinear equations.

It is now widely recognised that it is necessary to write the equations of motion representing both rigid body and structural motion of the aircraft in a common form. This need arises because there is an increased coupling between all modes of aircraft motion and other modes introduced by the multi-loop feedback control. There has been and continues to be difficulty in obtaining appropriate values of the coefficients of the A -matrix representing structural modes of motion. Traditionally, structural mode equations have been written in a form compatible with both structural analysis techniques and methods of measuring coefficients for these equations. Translation of this available data into the required form is complicated but necessary in order to allow an integrated design.

3.2 Accuracy required for aircraft equations

Precautions must be taken, during the design of the control laws, to avoid possible inaccuracies in either the form of the aircraft model or the values of the coefficients. In the following discussion, we restrict attention to inaccuracies in the values of the coefficients for rigid body small perturbation motion, the simplest case being the simplified manoeuvre demand system shown in Fig 3.

Consider first the i 'th loop of the several closed loops depicted in Fig 3. There is a range of values of the gearing G_i

$$(G_i)_A \leq (G_i) \leq (G_i)_B, \quad i = 1, 2, 3, \dots, m < n \quad (4)$$

for which all modes are acceptably damped. The damping can be increased by decreasing the phase lag of the feedback signal x_i , or, equivalently, phase advancing x_i using a lead-lag filter or a sensor measuring \dot{x}_i (in state space, \dot{x}_i is equivalent to x_{i-1} , and thus phase advance is achieved by increasing G_{i-1}). Alternatively, the decrease in phase lag can allow an increase in $(G_i)_B$ for a given minimum damping.

The potential benefits of increasing G_i are twofold, both related to the associated decrease in the response time T_i of the mode associated with closed loop (i). First, there is a decrease in the deviations of x_i (and the associated y_i) caused by a particular external disturbance and, second, the output y_i can be made to track more accurately a pilot's command p_c . Conversely, there are two main disadvantages, an increase in the undesirable effects of sensor noise and a decrease in the gain margin of the closed loop (i).

The closed-loop gain is the product of G_i , the motivator effectiveness, and the equivalent gearing of the FCS equipment. Suppose that poor damping results if this overall closed-loop gain increases by some increment ΔG_L . For high frequency modes, such poor damping may result in hazardous limit cycles through the exceedence of hardware rate limits. It is therefore essential to ensure that variations ΔG_i in closed-loop gain are less than ΔG_L . Major contributions to ΔG_i include:

- (a) incorrectness or uncertainty in the model motivator effectiveness;
- (b) approximations in designing the scheduling laws;
- (c) errors in the FCS gearing and in phase delays which contribute to the gain margin;
- (d) errors in the models of the scheduling sensors.

A compromise gearing $(G_i)_C < (G_i)_B$ is selected from these and other considerations and this practical value limits achievable performance in terms of the response time T_i .

Given a maximum possible response time T_i for the i 'th closed loop, we next consider the accuracy requirements of the aircraft model for the response y_i to pilot command p_c . Referring to Fig 3, we restrict attention to a particular control law structure for which the input u_i into the i 'th closed loop is (assuming for the present that $G_{i+1} = 0$):

$$u_i = F_i(s)p_c = Q_i(s)P_i(s)p_c \quad (5)$$

where $P_i(s)$ is an approximation to the reciprocal of the transfer function between u_i and x_i , and $Q_i(s)$ is chosen to give the desired response in y_i to p_c . In effect we are defining a command x_c in the state x_i such that:

$$x_c = Q_i(s)p_c, \quad u_i = F_i(s)x_c \quad (6)$$

The transfer function between u_i and x_i can be written:

$$N(s)/D(s) \quad (6a)$$

where, in general, the order of the denominator is greater than the numerator. A practical form of filter $P_i(s)$ is:

$$P_i(s) = \frac{1}{N(s)} \quad (6b)$$

assuming that $N(s)$ includes the gain of the transfer function (6a). The response of x_i to x_c is then the same as the response of the output of $1/D(s)$ to u_i . Given an appropriate $Q_i(s)$, the problem reduces to obtaining accurate tracking of x_c to x_i which ideally requires:

- (i) critical damping of the mode associated with x_i ;
- (ii) a response time T_i less than the fastest expected response time of x_c (limited by choice of $(G_i)_c$);
- (iii) accurate knowledge of the numerator $N(s)$ of the transfer function between x_c and u_i .

The last condition (iii) leads to further accuracy requirements for aircraft modelling.

In many cases, a first order approximation for $P_i(s)$ is satisfactory but the parameters θ_a of this approximate $P_i(s)$ are complicated functions of the aircraft's coefficients in the A-matrix. In contrast to the closed-loop characteristics, which are affected almost entirely by the motivator effectiveness, accurate knowledge of several aerodynamic derivatives are required to compute θ_a with sufficient accuracy.

The problem is eased by several factors. First, large errors in θ_a do not affect stability in the closed loop although, if the errors are gross, pilot-induced oscillations (PIO) may result when the pilot increases the gain of his loop via his response to cues from the outside world. Second, the effects of errors in θ_a can be decreased by adding an integral loop, G_{i+1} in Fig 3.

The integrator (or leaky integrator) operates on the difference ($x_i - x_c$) so that the lower frequency mode associated with the integral loop ($i + 1$) is excited significantly only when there are significant errors in θ_a . Finally, the pilot is so adaptive that he will accept a wide range of response characteristics, initially preferring those experienced before. Performance may not be affected by such errors but the workload to achieve this performance will increase.

3.3 Modelling external disturbances

We restrict the discussion to variations in wind speed/direction, *ie* gusts, although other external disturbances are important in a final assessment, *eg* dropping a store, change in aircraft configuration, change in fuel disposition. During the initial design/analysis stages, it is desirable to use simple models of gusts in order to keep the problem as comprehensible as possible. The basis of such simplifications can be explained by continuing the discussion of the closed loops depicted in Figs 1 and 3.

Considering first the gust shape, we may define three types of gust (Fig 4). For the impulse-like gust (a), the steady state error in x_i is zero for all values of G_i . However, the transient error in x_i decreases with increasing G_i (other parameters being changed to maintain relative damping of all modes). This performance improvement is significant only if the gust decay time T_g is smaller than the closed-loop response time T_i . For relatively small T_g , undesirable motion of the system is experienced with no significant benefit in reducing x_i . For the step-like input (b), there is a steady state error in x_i which decreases as G_i is increased. Introduction of the integral term, closed loop ($i + 1$) in Fig 3, causes this steady state error to decrease to zero at a rate determined by the response time T_{i+1} of the ($i + 1$)th loop, $T_{i+1} < T_i$. As G_{i+1} is increased, T_{i+1} decreases with a resulting more rapid removal of the steady state error in x_i . There is, however, a maximum value of G_{i+1} above which relative damping is unacceptable but this maximum value increases as G_i is increased. For the ramp input (c), there is a steady state error in x_i even when the integral is applied. This steady state error decreases as the gearing G_{i+1} is increased. It should be noted that, for an impulse-like gust (a), increasing G_{i+1} increases the duration of the transient error in x_i due to unnecessary excitation of the long period mode associated with the ($i + 1$)th closed loop.

Suppose we find the closed-loop control parameters G which minimise the errors in the output y caused by the simplified gusts (a), (b) and (c). Experience has shown that G is insensitive to the shape of the gusts, *eg* to values T_g , T_i' and T_g'' . Indeed, the same result is obtained if we minimise errors in y caused by more complex models of gusts, *eg* von Karman or discrete gust spectra. The errors in y for a given G depend, of course, on the gust shape so that, for the assessment of performance, more representative gust models must be used.

Whether this empirical result is generally applicable is questionable but experience to date justifies simplification of the gust models for initial design/analysis

purposes. In fact, for linear control law design, further simplifications can be made since there are well established relationships between a system's response to an impulse, a step and a white noise input (as indicated by the transfer functions in Fig 4).

The gust models required for assessment, especially pilot-in-the-loop assessments, must be more accurate. In particular, the modelling of gusts as a stationary random process (eg von Karman spectra) draws the adverse comment from pilots that the simulation is unnatural, and this situation is unacceptable. For this reason, improved gust models are being sought, a discreet gust spectrum being one option⁶.

Another aspect of the assessment problem involves finding which gust shape by itself or in combination with other disturbances can cause a hazardous error in y . A hill-climbing procedure, similar to that used for parameter optimisation (section 4), can be applied to determine which gust shape in a family of gusts produces maximum y . We can then calculate the magnitude of this 'worst' gust shape which causes a hazardous situation and attempt to ascertain whether this event will occur more frequently than acceptable. It is interesting to note that, in general, different worst gusts are associated with different elements of y , (eg longitudinal displacement and rate of descent at touchdown due to gusts during an automatic landing).

3.4 Modelling FCS characteristics

There are three main issues in modelling FCS characteristics:

- (a) phase or time delays caused by FCS components;
- (b) noise, particularly sensor imperfections;
- (c) nonlinearities, eg actuation rate limit.

The need to attenuate high frequency sensor noise using some form of noise filter introduces a significant phase lag so that (a) and (b) must be discussed together.

3.4.1 Phase and time delays

The replacement of analogue by digital computers and the possible replacement of some sensors by their digital equivalents has led to the need for sampled-data analysis in the z-plane, rather than the customary continuous analysis in the s-plane. Although z-plane analysis is available in a design program such as TSIM, the current approach still usually involves an approximate linearisation of the model representing the digital processor so that the more familiar s-plane analysis can be used for initial studies. Subsequent analysis of sampled data effects are examined using z-plane analysis and time responses. In the interests of brevity, we exclude further discussion of problems arising from such sampled-data effects, assuming that the time delay and data staleness can be modelled as an analogue lag.

In addition to this computer lag, it is necessary to introduce an analogue filter immediately before A-D conversion in order to eliminate aliasing and, in some cases, another filter is needed after D-A conversion in order to reduce quantisation noise. Furthermore, there are problems in implementing on a digital computer the high frequency part of the complex filter used for attenuating unwanted structural modes which are detected by motion sensors such as rate gyros and have to be treated as noise. In practice, the analogue filter before A-D conversion is generally designed to include the high frequency part of this structural filter (and thus the overall FCS is effectively hybrid).

The phase delays of the actuation system and, in some cases, lags in the sensors, are partially compensated using a lead-lag filter as shown in Fig 3. Full compensation is not practical, partly because the filter must be realisable and also because allowance must be made for variations in the lags of the actuation system.

In broad terms, the phase lag of available FCS components, excluding the noise filter(s), is approximately equivalent to a first order filter of about 0.04 s time constant, equally divided between the computer with its associated filters and the actuation with its associated compensation.

It will be appreciated that, even for the linear model of the FCS, we are faced with a high order set of equations, the modes of which interact with each other and with the aircraft equations of motion. Simplification of these equations, as with the aircraft equations, must be made with caution but is useful in preliminary design studies and for purposes of examining the physical principles involved. The simplification in Fig 3, for example, has been chosen to illustrate numerous problems and techniques in this Chapter.

3.4.2 Sensor noise

Ideally, the sensor should measure the state x_i used in the feedback control (or the state required for scheduling). In addition to instrument noise, as measured under static conditions, sensors detect variations in other states x_j under dynamic conditions. Appropriate positioning of the sensors and corrections to the outputs of the sensors using data from other sensors are techniques used to reduce such non-instrumental noise. Some of these corrections require *a priori* knowledge of the motion detected by the sensor in the environment of the aircraft and such knowledge is often scarce. For example, there is uncertainty as to what airstream sensors measure at high incidence and low speed. Consequently, there is always some residual unwanted signals which must be treated as 'noise'.

The conventional method of reducing the effects of high frequency sensor noise is to introduce a noise filter. In Fig 3, this is represented as a first order lag, time constant τ_i , with phase lag approximately equal to that of a practical and more complex high order filter. For increased attenuation of high frequency noise, τ_i should be increased, the penalty being an increase in the phase lag of the i 'th closed loop, leading to the need to decrease G_i so as to maintain acceptable damping. It is useful, in fact, to consider varying G_i with $1/\tau_i$ 'slaved' such that relative damping of all modes remains acceptable. In many cases, the slaved $1/\tau_i$ is approximately proportional to G_i . Since flying qualities tend to improve with decreasing response time T_i and this decreases with increasing G_i , the control laws required to reduce the effects of high frequency sensor noise conflict with those required for improved flying qualities.

Lower frequency components of the noise are not significantly attenuated by the noise filter. In some cases, the effect of such noise components are, in fact, reduced by increasing G_i (and $1/\tau_i$) in the same way as low frequency external disturbances. In such cases, an additional integral loop (G_{i+1}) is required to reduce the effects of such noise, eg the effects of datum errors or drifts of one sensor are reduced by the correcting action of a second sensor.

For initial studies of the control laws, simplifications can be made similar to those discussed for gusts (see Fig 4). For detailed analysis and assessment purposes, more accurate models are required but are not always available, in contrast to the availability of comprehensive gust models. It should be noted that the undesirable effects of sensor noise are often as significant as the effects of gusts although the effects may be related to different components of the output y .

The relationship between the effects of external disturbances and of sensor noise is more readily understood with reference to the closed-loop error signal, e in Fig 1. There are frequency components of e , high relative to $1/\tau_i$, for which a decreased gearing G_i is beneficial and lower frequency components of e requiring an increased G_i . This conflict is the same for all causes of fluctuation in e , ie whether sensor noise or external disturbances.

3.4.3 Nonlinearities

In practice, several components of the FCS have nonlinear characteristics. The improvement in components and sub-systems in recent years has reduced the extent of many undesirable nonlinearities considerably and their effects are usually small. Nevertheless, there are a number of features that need careful consideration including:

(a) the suppression of the effects of external disturbances by the closed-loop control laws, especially those using powerful integral terms, can reduce significantly the authority available from a particular control surface for manoeuvre demand. A hazardous situation may arise if the pilot has no knowledge of the control authority available to him. In some cases, this situation can be eased by employing separate control surfaces for low and high frequency components.

(b) Although the amplitude and rate of change of control signals are not deliberately limited with full authority systems, there are practical limits, such as a rate limit in actuation systems. Exceeding such limits can lead to dangerous limit cycles and must therefore be avoided by the selection of the control laws and/or the development of appropriate hardware.

(c) The use of digital computers leads to sampled-data effects and, in some cases, to a 'staleness' of data through the use of data stored from one computer cycle to the next.

(d) Stick-feel characteristics with possible dead zones, hysteresis and other ergonomic features, both spurious and intentional, in the stick, rudder pedals etc.

4 ELEMENTS OF AN INTERACTIVE DESIGN/ANALYSIS PROCEDURE

With an interactive procedure such as TSIM, the computer operator is an important part of the design and analysis loop. It is important that he is fully familiar with:

- (a) the particular type of analysis (root locus, parameter optimisation, etc) and recognises its limitations;
- (b) the equations of motion of the aircraft and the FCS and takes account of nonlinearities and possible inaccuracies;
- (c) the provisional nature of the interpretation of flying qualities requirements, especially those for difficult flight tasks or severe environmental conditions.

We have discussed (b) and (c) in sections 2 and 3. In the following discussion of (a), we do not attempt to be rigorous since there are many excellent texts on the subject². The aim is to expose fundamental difficulties with available techniques and to show why, in practice, several analysis and design techniques are used in a complementary fashion.

Referring to Figs 1 and 3, we are concerned with the selection of multi-feedback loops G with associated feedforward control F , the parameters of which we combine as

the vector θ . With conventional control laws, the control parameters of the i 'th closed loop, eg (G_i , $1/\tau_i$), can be considered constant since their values are varied only as scheduled functions of aircraft state and such variations are usually but not always slow relative to the modes associated with the i 'th closed loop. This assumption of constant control parameters is necessary, of course, for the application of linear control theory.

4.1 Approach using optimal control theory

It is often useful to obtain an initial solution without assuming a control law structure. Instead, we are concerned with determining the optimal time history $u(t)$ of the control signals fed to the m control surfaces and other motivators. The linearised equations of motion of the aircraft alone can be represented by:

$$\dot{\underline{x}}(t) = \underline{A}\underline{x}(t) + \underline{B}\underline{u}(t) \quad (7)$$

where $\underline{x}(t)$ is an n -dimensional state vector (n th order linear aircraft equations), $\underline{u}(t)$ is an m -dimensional control vector, and \underline{A} and \underline{B} are matrices with constant coefficients.

The motions to be optimised are linear combinations of some but not necessarily all the states:

$$\underline{y}(t) = \underline{C}\underline{x}(t) \quad (8)$$

An optimal linear control can be defined² as the control vector $u(t)$ which transfers the system from an initial state $\underline{x}(t_0)$ to a final state $\underline{x}(t_f)$ and which minimises a quadratic performance function:

$$J = \int_{t_0}^{t_f} (\underline{y}^T(t)\underline{Q}\underline{y}(t) + \underline{u}^T(t)\underline{R}\underline{u}(t))dt + \underline{x}^T(t_f)\underline{P}_1\underline{x}(t_f) \quad (9)$$

subject to the constraints of equations (7) and (8). Here, \underline{Q} and \underline{R} are weighting matrices, usually diagonal.

The optimal regulator is generated by the linear control law:

$$\underline{u}(t) = -\underline{K}(t)\underline{x}(t), \quad \underline{K}(t) = \underline{R}^{-1}\underline{B}^T\underline{P}(t) \quad (10)$$

where $\underline{P}(t)$ satisfies the matrix Riccati equation:

$$-\dot{\underline{P}}(t) = \underline{C}^T\underline{Q}\underline{C} - \underline{P}(t)\underline{B}\underline{R}^{-1}\underline{B}^T\underline{P}(t) + \underline{P}(t)\underline{A} + \underline{A}^T\underline{P}(t) \quad (10a)$$

with

$$\underline{P}(t_f) = \underline{P}_1 \quad (10b)$$

As t_f becomes large, the solution $\underline{P}(t)$ approaches a steady state value independent of \underline{P}_1 . In practice, this is the usual requirement for FCS. Because of these asymptotic properties, the feedback matrix \underline{K} becomes independent of time.

Several methods are available for the numerical solution of these equations but most are unwieldy for large order systems. A relatively simple and straightforward solution⁷ results if we assume constant gains \underline{K} . The performance function to be minimised becomes an eigenvector ($n \times n$) matrix \underline{M} , the elements of which are numbers representing the response of each state x_i caused by an initial condition on each state x_j .

This approach is useful for a preliminary study of a new problem but its usefulness appears to be limited for a number of reasons including:

- (a) difficulties in selecting the weighting matrices \underline{Q} and \underline{R} ;
- (b) the solution requires feedback of all states (x_1 to x_n), some of which do not improve performance significantly and which must be estimated from a limited number of sensors;
- (c) the eigenvector matrix \underline{M} may not include all aspects of performance \underline{V} , the elements of which are numbers representing each output state y_i of \underline{y} due to representative disturbances on all states \underline{x} , aircraft and FCS;
- (d) although the solution is stable, the degree of damping and, in particular, gain margins are not implicit.

There has been, and continues to be, developments which reduce the above and other limitations at the expense of more complicated programs and conditions needed to obtain a realisable and stable solution. It is usually advantageous to employ alternative, although 'sub-optimal', design techniques to augment solutions from the matrix Riccati equations.

4.2 Parameter optimisation

After gaining some experience with a specific problem, the control law structure can be defined in terms of realisable filters between each motion sensor or pilot command and each motivator. The design problem becomes the selection of the parameter θ (combining G and F in Fig 1) which minimises a selected function (of outputs \underline{y} caused by a defined set of disturbances or inputs), *eg*

$$V = \int_{t_0}^{t_f} (\underline{y}^T \lambda \underline{y}) dt = \sum_{i=1}^N \lambda_i V_i \quad (11)$$

where λ is a weighting matrix assumed to be diagonal and N is the order of the aircraft and FCS equations. An iterative hill-climbing procedure is used to find θ_{op} which minimises V . Theoretically, the process may converge to a local minimum but, in practice, the initial guess of the optimum values of θ are close to the final values, especially when solutions using the matrix Riccati equations are available.

If the output \underline{y} does not include all state variables \underline{x} (now representing both aircraft and FCS equations, simplified or not), or if a specific value of relative damping $\zeta = \zeta_0$ is desired, a more appropriate function is:

$$V = \sum_{i=1}^N \lambda_i V_i + \delta [\zeta - \zeta_0] \quad (12)$$

where $\delta = 0$ if $\zeta \geq \zeta_0$ or δ is large if $\zeta < \zeta_0$. Such a constrained optimisation procedure has caused few problems other than the need, in general, to perform calculations for each V_i in the time domain and for the relative damping in the s -plane. However, most disturbances can be approximated to white noise for which the responses in \underline{x} or \underline{y} of linear systems are linearly related to their responses to initial conditions, and so can be calculated in the s -plane alone (see sections 3.3 and Fig 4). Consequently rapid calculations of each V_i can be obtained without employing lengthy time history calculations.

4.3 Conflict curves and the compromise constant control laws

The main difficulty with parameter optimisation is the selection of the diagonal weighting matrix λ in equation (11). Consider the simplest case when $N = 2$:

$$V = V_1 + \lambda_2 V_2 \quad (13a)$$

The optimum occurs when $\partial V / \partial \theta = 0$, *ie*

$$\lambda_2 = - \frac{\left(\frac{\partial V_1}{\partial \theta} \right)_{op}}{\left(\frac{\partial V_2}{\partial \theta} \right)_{op}} \quad (13b)$$

where the gradients are calculated at the optimum control state, θ_{op} . Equation (13) defines the value of λ_2 which should be used, but this requires an *a priori* solution of the problem.

This weighting dilemma is illustrated in Fig 5a by plotting V_1 against V_2 as the weight λ_2 in equation (13a) is changed in successive optimisations. When λ_2 is large, V_2 is a minimum employing parameter values θ_A (in many cases the gains of most of the components of θ_A are zero). When λ_2 is small, V_1 is just acceptable and V_1 is a minimum employing parameter values θ_B . Between these extremes, there is a compromise set of parameter values θ_C which is best selected by engineering judgement having first derived the conflict curve.

In the general case, the measurement matrix V is high order because the equations of motion include the FCS components and the control laws themselves. The conflict curve between two (or more) elements of V can be obtained using a constrained optimisation. The function to be minimised is:

$$V = V_1 + \delta_2 [V_2 - C_2] + \sum_{i=3}^N \delta_i [V_i - C_i] \quad (14)$$

where $\delta_i = 0$ when $V_i \leq C_i$ or δ_i is large when $V_i > C_i$. The result is a minimum value for V_1 with each V_i ($i = 2, \dots, 2n$) just less than the associated constraint C_i provided there is a solution for $V_i = C_i$. By changing the value of C_2 in successive applications of the constrained parameter optimisation, a conflict curve of V_1 against V_2 is obtained for which all other elements of V are forced to be less (usually, just less) than the assumed constant constraints.

A practical example is instructive. The pitch rate manoeuvre demand for an experimental FBW system in a Hunter aircraft⁸ involved a compromise between the effects of rate gyro noise (V_2) and the transient pitch rate error to a pitch rate command $q_c(V_1)$. In this simple case, we wished to minimise V_1 subject to the condition that actuator activity due to sensor noise was acceptable. Assuming a model of sensor noise and a model of the actuator, we defined:

$$V_1 = \int_0^T [q - q_c]^2 dt, \quad \text{for lagged step } q_c$$

$$V_2 = \frac{1}{T} \int_0^T \dot{n}^2 dt, \quad \text{for sensor noise } w$$

where T is very large and \dot{n} is elevator rate. We obtained the conflict curve V_1 vs V_2 , the points on which defined possible values of the control parameters. The models of the rate gyro noise and the actuator were then replaced by actual hardware and the compromise values θ_C selected as that for which V_1 was smallest subject to the condition that the real actuator motion caused by real gyro noise was acceptable. The author's finger placed on the actuator was used as the means to measure acceptable actuator motion!

4.4 Sensitivity to changes in aircraft or environment

In the above discussion of optimisation techniques, there has been no consideration of direct control of sensitivity aspects of performance, i.e. changes in the characteristics of the aircraft or FCS and changes in disturbance characteristics, gusts or sensor noise.

Consider, for example, the conflict curve V_1 vs V_2 where

$$V_1 = \int_0^T y_1^2(v) dt, \quad T \rightarrow \infty$$

$$V_2 = \int_0^T y_2^2(w) dt, \quad T \rightarrow \infty$$
(15)

i.e. the effects of gusts, v , against the effects of sensor noise, w . This conflict occurs in every closed loop although the outputs (y_1, y_2) may change from loop to loop. The conflict curve depends on the magnitude and, to a lesser extent, the frequency components of v and w . As an example, the change in the conflict curve for three magnitudes of the external disturbance v , assuming constant sensor noise w , is shown in Fig 5b.

When v is small, V_1 is negligible and we would select control parameters close to θ_A . When v is large, a more acceptable solution is close to θ_B , accepting a large value of V_2 . A more complex situation arises if the magnitudes of both v and w change.

This example illustrates a major difficulty closely associated with the weighting dilemma discussed above. With constant control parameters, an optimum can be defined only for constant values of the inputs and disturbances, e.g. 'average' models. For other values, the system is far from optimal. This limitation is unacceptable when we are seeking best performance for difficult flight tasks and for infrequent severe environmental conditions.

The situation is made more complicated if we introduce a gain margin ΔG_L of sufficient magnitude to ensure that V_2 in the above example remains fully acceptable for the worst combination of errors in the closed-loop gain (section 3.2). Because the gain margin decreases as we change from θ_A to θ_B , dashed line in Fig 5b, the compromise parameter values θ_C must be chosen, in many cases, to be θ_{C2} rather than θ_{C1} , i.e. applying a smaller nominal gearing than that decided from considerations of the conflicting elements of V alone, i.e. neglecting gain margin situations. The resulting decrease in the system's rate of response may be unacceptable in seeking improved performance for future aircraft throughout the flight and manoeuvre envelope.

5 THE FUTURE USE OF NONLINEAR CONTROL LAWS

As discussed in sections 3 and 4, many conflicts arise in the design of conventional control laws because:

- (a) the control parameters which minimise one aspect of performance differ from those which minimise other aspects. A compromise is necessary with conventional control laws with which parameters are essentially constant;

- (b) due allowance must be made for errors and variations, especially in terms of the gain margin ΔG_i in each closed loop.

The compromises obtained in designing conventional control laws usually yield satisfactory flying qualities except when the flight task is difficult and/or when severe environmental conditions are experienced.

Current research^{9,10} into selected nonlinear control policies is aimed at reducing the extent of such conflicts so that improved flying qualities can be achieved under all expected conditions. Although this work is still in progress, it was considered worthwhile to conclude this paper with a short discussion on the subject.

5.1 Variable integral control to optimise response

In the selection of the constant parameters in the closed loop control laws, eg G_i and $1/\tau_i$ of Fig 3, a compromise is made between two or more conflicting aspects of performance. Recent studies¹⁰ have established the feasibility of varying G_i as a function of on-line measurements of these conflicting aspects of performance. The parameter $1/\tau_i$ and other control parameters are slaved to the variation of G_i such that if G_i remains set at a value in the allowed range:

$$G_{iA} > G_i > G_{iB}$$

for any length of time, then damping and other aspects of performance are satisfactory.

The on-line measurements are derived from the error signal e , Fig 1, and separated by suitable filters into positive definite functions E_1 and E_2 measuring those frequency components that could be reduced by either increasing or decreasing G_i respectively. For example, we allow G_i to vary according to:

$$G_i(t) = \lambda_1 E_1(t) - \lambda_2 E_2(t) \quad (16)$$

where $\lambda_{1,2}$ are suitable weights. A number of precautions are necessary, including the use of an integral loop, G_{i+1} or its equivalent, so as to avoid prolonging the duration of large values of G_i . The latter condition has led to this technique being called¹⁰ VICTOR, Variable Integral Control To Optimise Response.

For most of the time, $E_1(t)$ is negligibly small for the flight task in hand, ie the low frequency components of the error signal e have negligible amplitude. The gearing G_i reduces to its minimum G_{iA} together with an associated increase in noise filter time constant. Consequently, the effects E_2 of high frequency components of inputs, external disturbances and noise are much smaller than with the compromise constant control laws, $G_{iA} < G_{iC}$. When E_1 increases due to pilot command, external disturbance or low frequency noise, G_i increases rapidly to its maximum $G_{iB} > G_{iC}$ for large E_1 . There is a more rapid decrease of E_1 than with the compromise constant control laws which leads to a rapid decrease of G_i to the minimum G_{iA} as E_1 approaches zero. Because the application of high values of G_i is transient, the corresponding increase in E_2 is transient and, therefore, acceptable. Referring to Fig 5b, we are allowing the control laws to change rapidly from G_A to G_B during the transient response to any input or disturbance.

5.2 Self-adaptive properties of VICTOR

The gain margin ΔG_i is large when $G_i = G_{iA}$, but as the gain is increased through the compromise value G_{iC} to the maximum value G_{iB} , the gain margin decreases. In a recent study¹⁰ of the pitch rate plus integral to elevator loop for a longitudinally unstable aircraft, the gain margin was 25 for $G_i = G_{iA}$ and 3 for $G_i = G_{iB}$.

It is convenient for the present and subsequent discussion on self-adaptive techniques to express the gearing G_i between the sensor and control surface as the product:

$$G_i = (G_a G_v) = (G_{a0} + \Delta G_a) G_v \quad (17)$$

where G_v is the VICTOR gearing and G_a is the control surface gearing which, ideally, compensates for the control surface effectiveness, B_a :

$$G_{a0} = \frac{1}{B_a}$$

We assume an error ΔG_a in G_a , bearing in mind that there are contributions to ΔG_a other than errors in B_a .

As G_v is increased, the situation can arise when the gain margin ΔG_i approaches ΔG_L , so that poor damping and hazardous limit cycling could occur. However, the second performance measure E_2 in equation (16) can be chosen to increase rapidly as the relative damping decreases so that the VICTOR gearing G_v is decreased. As a result, the system recovers rapidly from large errors ΔG_a in G_a .

The magnitude of E_2 may increase due to either an increase in sensor noise, or detection of high frequency external disturbances or deterioration of the FCS equipment, as well as incorrect compensation of the control surface effectiveness. It is hazardous, therefore, to estimate B_a in a self-adaptive manner from this technique alone.

Nevertheless, the onset of a large value of E_2 can be used to restrict the maximum value of G_{IB} until the correctness of G_a has been checked using more appropriate self-adaptive schemes (section 5.4).

5.3 Alternative self-adaptive schemes

In the design of conventional scheduling laws, a comprehensive model of the aircraft plus FCS is used to derive the laws by which selected parameters θ_a are varied as functions of the outputs of available scheduling sensors. The applied value of θ_a must allow for a tolerance $\Delta\theta_a$ equated to the expected worst combination of errors and variations in all factors contributing to both the closed-loop characteristics and the transfer function between the output y and pilot command u_c (section 3.2).

With explicit self-adaptive schemes¹¹, a simplification of this model is programmed in the PCS computers with a view to updating the parameters M of a simplified model from on-line measurements of the system's response to measurable inputs. Appropriate values of θ_a are computed from M using previously determined parametric relationships.

In effect, the model is fed by the same inputs as the system. The model output \tilde{y} is an estimate of the aircraft's response y . The difference signal:

$$d = y - \tilde{y}$$

is used to change the model parameters M in order to reduce the difference signal d . In some cases, it is possible to estimate the error ΔM in M so as to estimate $\Delta\theta_a$ and a safe value of θ_a .

In comparison with similar techniques used for the identification of the aerodynamic characteristics of aircraft, explicit adaptation differs in a number of ways, some of which are listed in Table 4. Of these differences, the most important is the need to ensure that gross errors in θ_a are avoided since these can lead to a hazardous situation. We restrict attention in this chapter to the question of reliable adaptation rather than survey the variety of algorithms available for accurate identification of M in the presence of noise.

Nearly all self-adaptive schemes so far investigated have been based on estimating the closed-loop gearing G_a , Fig 6b, and adjusting other components of θ_a in accordance with pre-selected parametric relationships. Such G_a -adaptation tends to be unreliable for three main reasons. Firstly, a grossly incorrect value of G_a can cause hazardous poor damping and limit cycles. Secondly, the difference signal d is insensitive to small errors in G_a leading to inaccurate identification. Thirdly, simplifications to the model of the aircraft lead to errors in G_a .

An alternative scheme based on estimating the input filter gearing k_a , Fig 6c, has been investigated recently. In contrast to G_a -adaptation, an adaptive scheme based on estimating k_a has the following advantages:

- (a) grossly incorrect values of k_a do not cause poor damping of the closed-loop and the self-adaptive loop recovers rapidly from a transient incorrect value of k_a ;
- (b) the difference signal d is relatively sensitive to small errors in k_a and can be made more sensitive if the closed-loop integral gearing is small during adaptation;
- (c) the model is simple and changes mainly through a change in closed-loop response time T_i which is related to the VICTOR gearing G_v .

Rapid and relatively accurate variations in k_a are, therefore, acceptable. Adjustments to other parameters, particularly G_a , could be made using pre-selected parametric relationships between k_a and other components of θ_a . It is preferable, however, to apply a number of additional precautions embodied in the concept of redundant adaptation with safeguards.

5.4 Redundant adaptation with safeguards

In order to explain this concept, we restrict attention to a specific case for the three parameters, the closed-loop gearing G_a , and the gearing k_a and time constant τ_a of a first order input filter, Fig 6a. Ideally, k_a is the reciprocal of the gain in the transfer function between x_c and x_i and depends in a known way on the VICTOR gearing G_v . The time constant τ_a is related to the zero of this transfer function.

Rapid and continuous k_a -adaptation is allowed for both pilot input commands and, if the latter has not occurred during the previous t_1 seconds, for a specially timed test signal. Estimates of G_a and τ_a are made from the current value of k_a using pre-selected parametric relationships and these estimates are compared with independent estimates of G_a and τ_a obtained from separate explicit self-adaptive schemes for G_a and τ_a . Agreement within a pre-selected tolerance leads to an update of G_a and τ_a , although the rate of change of G_a is made less than the expected maximum rate of change of the motivator effectiveness. Significant disagreement leads to a rapid decrease of the VICTOR gearing G_v for the short time t_2 necessary to apply the following special adaptation process.

The specially tuned test signal is applied at two values of the VICTOR gearing, one low and one high, so that the system's response characteristics are changed significantly. Two estimates for each of the three parameters k_a , G_a and τ_a are made independently. Agreement of all three within a pre-selected tolerance leads to an update of G_a and τ_a . In the unlikely event of a continuing disagreement, the gearing G_a is set at the lowest value.

Two further precautions are applied. Firstly, in the unlikely event of G_a being set on a grossly incorrect value, the VICTOR scheme causes the closed-loop gain to reduce automatically and rapidly, thus preventing a hazardous situation. Such an event initiates the above special adaptation process in order to distinguish whether the measure of noise effects (E_2) increased due to an increase in sensor noise or due to incorrect G_a . Secondly, limits are set to the maximum allowed excursions of the values of (G_a , k_a , τ_a). With a pilot-selectable, task-oriented control system, these maximum allowed excursions are changed such that, for flight tasks requiring maximum VICTOR gearings G_v , a tighter constraint is placed on the allowed self-adaptive variations.

This type of redundant adaptive concept fits in with the use of analytic redundancy schemes under development for detection of failures other than potential failures in the nonlinear control policies. Further consideration of this aspect of the subject is outside the scope of this paper although, as mentioned in section 2.1, these system aspects should be considered side-by-side with performance aspects in any practical design, analysis and assessment.

REFERENCES

- 1 J.J. D'Azzo and C.H. Houpis. Feedback control system analysis and synthesis. McGraw-Hill, 1960
- 2 H. Kwakernaak and R. Sivan. Linear optimal control systems. Wiley, 1972
- 3 B. Etkin. Dynamics of atmospheric flight. Wiley, 1972
- 4 F.R. Gill. Engineering of control systems and implications on control law design. Agard Lecture Series No.89, LS-89, June 1977
- 5 G.T. Black, D.J. Moorhouse and R.J. Woodcock. Proceedings of AFFDL Flying Qualities Symposium held at Wright State University. AFFDL-TR-78-171, 1978
- 6 J.G. Jones. Aircraft longitudinal ride bumpiness: an application of statistical discrete gust theory. RAE Technical Report 77020, 1977
- 7 D.E. Fry and D. Slatter. Design of aircraft flight control laws using the matrix Riccati equations. RAE Technical Report 75035, 1975
- 8 F.R. Gill and P.J. Fullam. The Hunter FBW experiment: recent experience and future implications. Agard CP-157, October 1974
- 9 F.R. Gill and D. McLean. A new model-reference adaptive scheme for aircraft flight control systems. Trans Inst. MC Vol.1 No.1, 1979
- 10 F.R. Gill. Nonlinear pitch rate to elevator control laws for a combat aircraft. RAE Technical Report 79075, 1979
- 11 J.R. Elliott. NASA's advanced control law program for the F-8 digital FBW aircraft. IEEE Trans. AC-22, October 1977

Acknowledgments

The author wishes to thank many of his colleagues at RAE for their help in preparing this paper, in particular Dr A. Jean Ross, D.E. Fry, M.R. Watts and J.S. Winter.

Table 1

Types of function programmed in an FCS computer

Function	Definition
Flight control laws	Provide appropriate feedback (<u>G</u>) and feedforward (<u>F</u>) control signals to each motivator from motion sensors and pilot's commands
Scheduling laws	Vary flight control laws as the aircraft characteristics change across flight envelope. Also, varies control laws with flight task
System algorithms	Provide acceptable FCS failure detection, isolation and survival capability

Table 2

Difficult flight tasks

1	Air-to-air tracking/high incidence manoeuvring
2	High speed, low level dash
3	Air-to-ground tracking
4	Approach and landing
5	Take-off

Table 3

Analysis techniques incorporated in TSIM

	Sub-routine	Comment
1	Time response	Applicable to both linear and nonlinear equations
2	Roots and root loci	s- and z-planes, and mixed continuous/discrete systems
3	Frequency response	
4	Parameter optimisation	Optional hill-climbing procedures. Discussed in section 4
5	Matrix Riccati equations	Discussed in section 4
6	Sensitivity analysis	Performance matrix evaluated as specified control and aircraft parameters are changed
7	Observer designs	

Table 4

Main differences between explicit self-adaptation and identification

Although the aircraft is 'identified' during self-adaptation, there are significant differences between self-adaptation and identification procedures with a new aircraft.

- (1) with self-adaptation, there is pre-knowledge of the relationship between the components of the aircraft model \bar{M} which leads to approximate parametric relationships between the components of $\bar{\theta}_a$;
- (2) the system, aircraft and FCS, is better behaved than the basic aircraft and, in particular, its response to a pilot command is accurately known;
- (3) the characteristics of the system can be changed in a defined manner, *eg* by varying the VICTOR gearing G_v ;
- (4) there is less store available in the FCS computers for on-line self-adaptation compared to ground-based computers with large store available for identification;
- (5) gross errors in the estimated $\bar{\theta}_a$ could be dangerous and must be avoided or otherwise prevented from causing a hazard;
- (6) special inputs must be small and infrequently used for self-adaptation whereas large signals are needed for identifying nonlinear characteristics of aircraft;
- (7) delays in updating $\bar{\theta}_a$ must be short compared with possible variations in the aircraft characteristics.

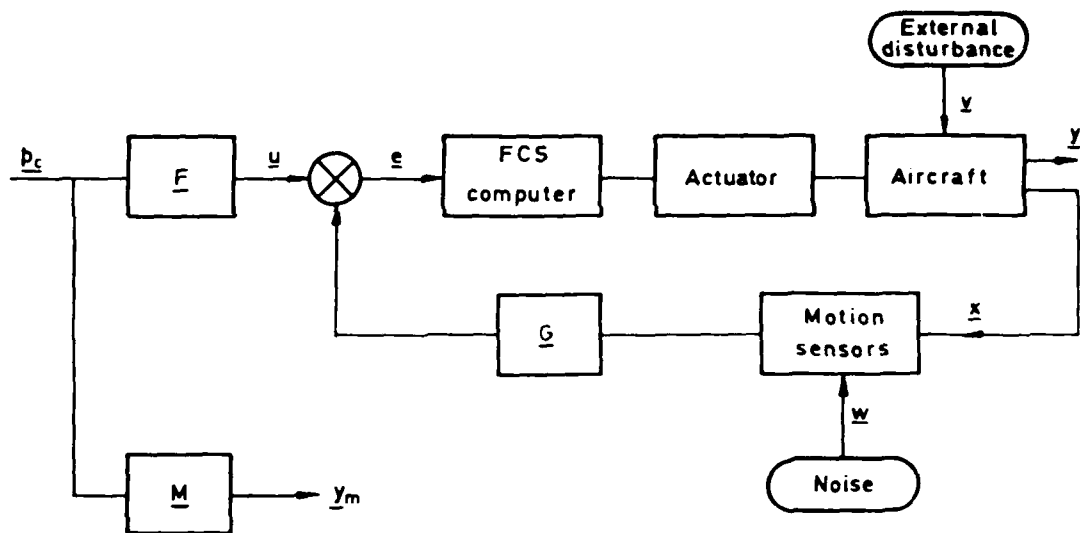


Fig 1 General form of control for a FBW system

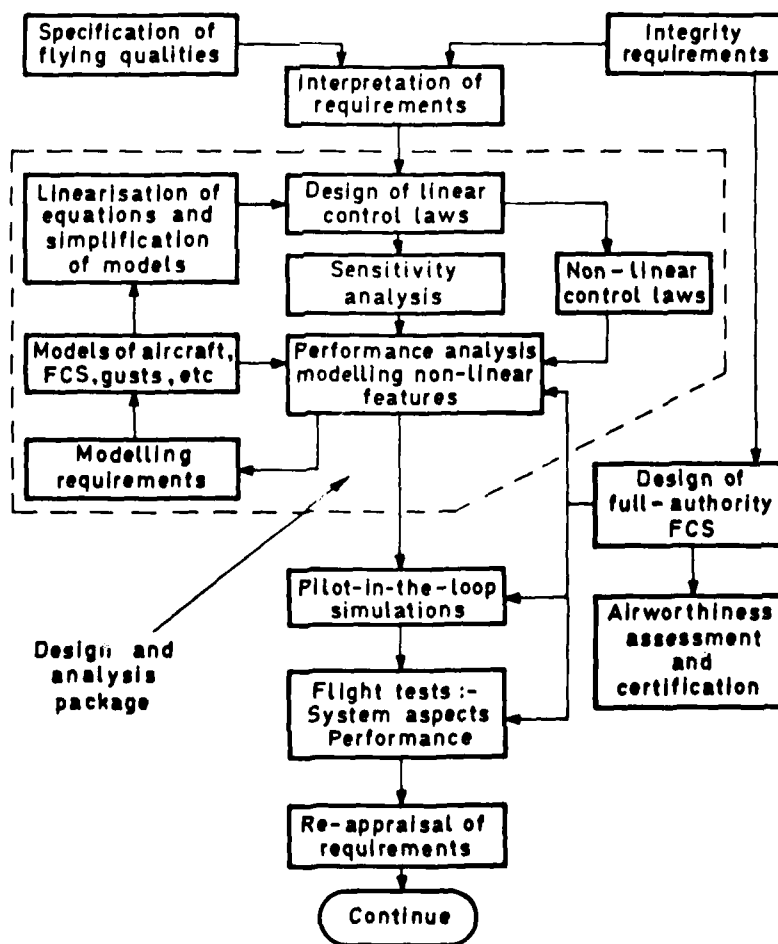


Fig 2 Stages in design, analysis and assessment

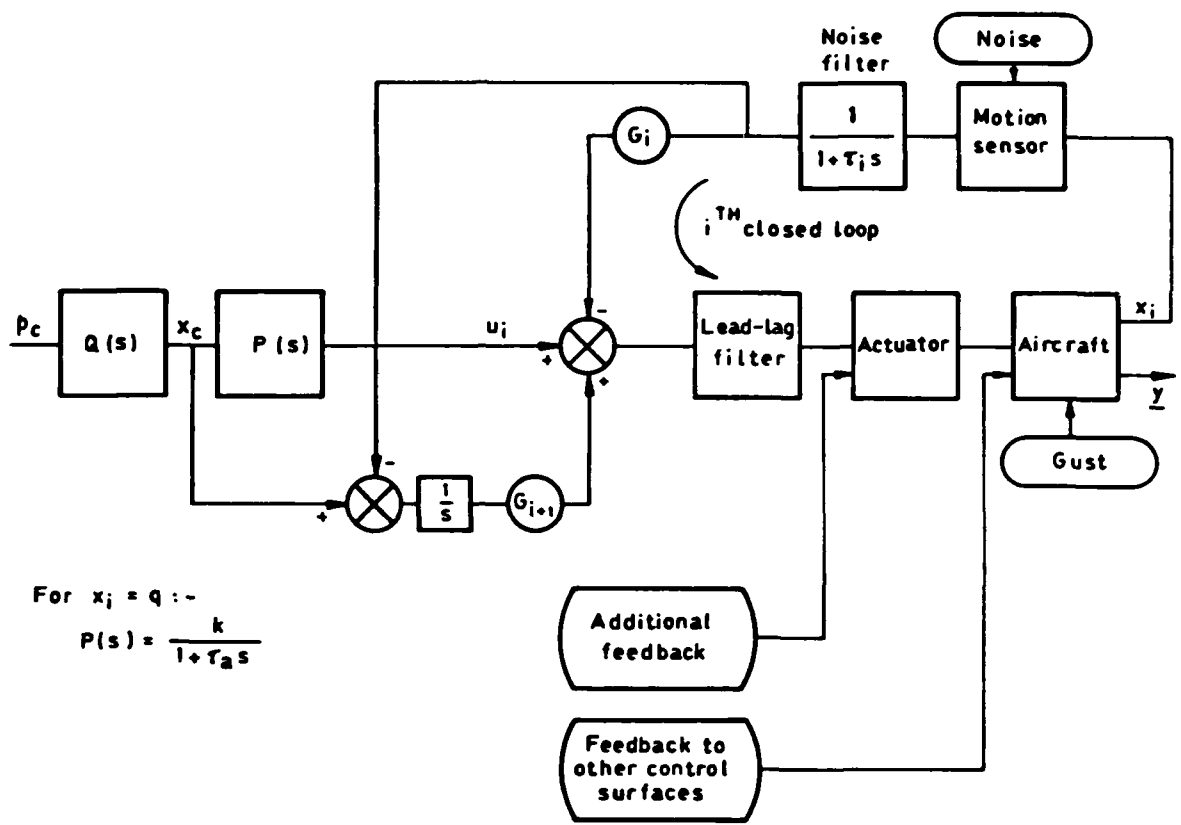


Fig 3 Simplified manoeuvre demand system

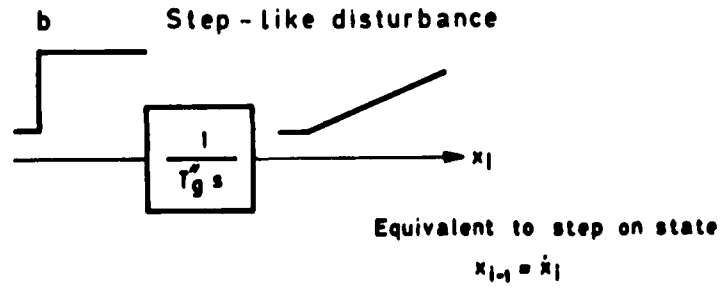
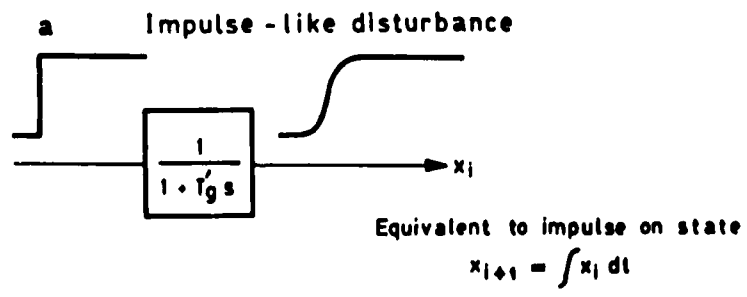
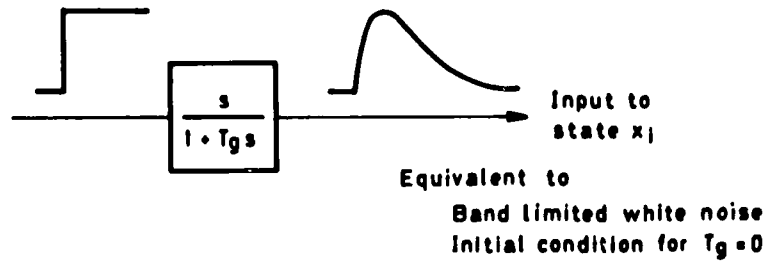
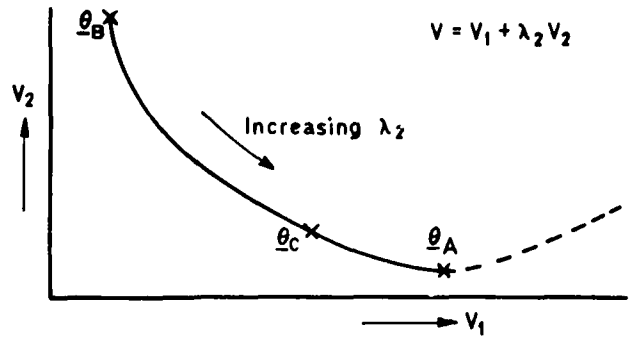
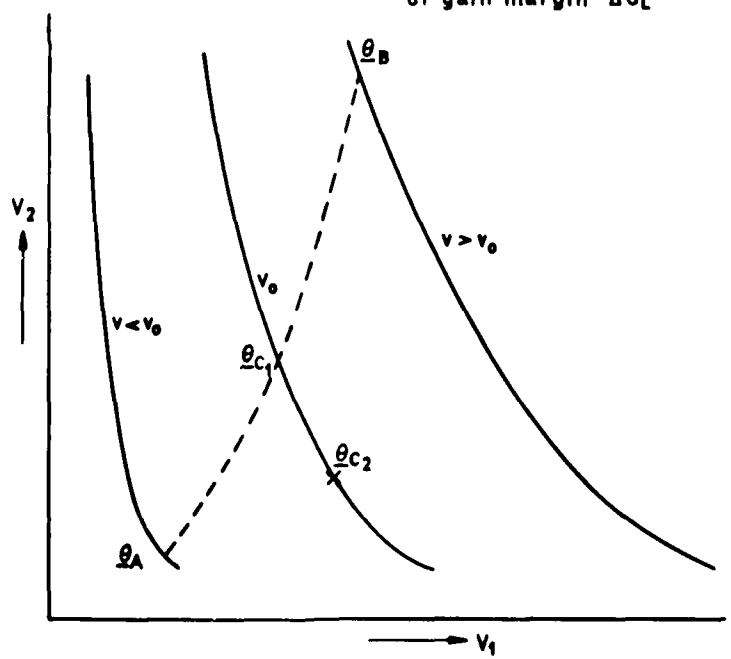


Fig 4a-c Simplified inputs for gusts and sensor noise



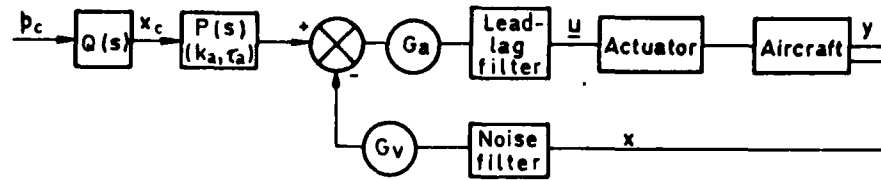
a The weighting dilemma

θ_{c1} : Compromise ignoring ΔG_L
 θ_{c2} : Compromise taking account of gain margin ΔG_L

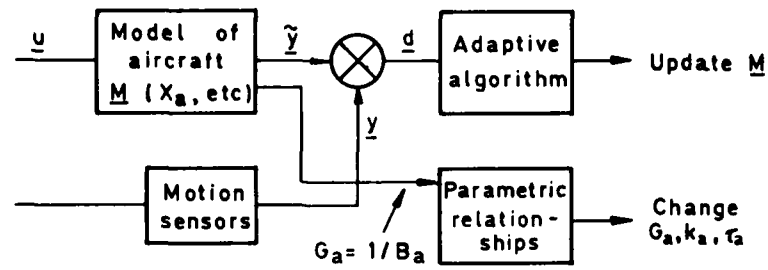


b Variation of conflict curve with v (constant w)

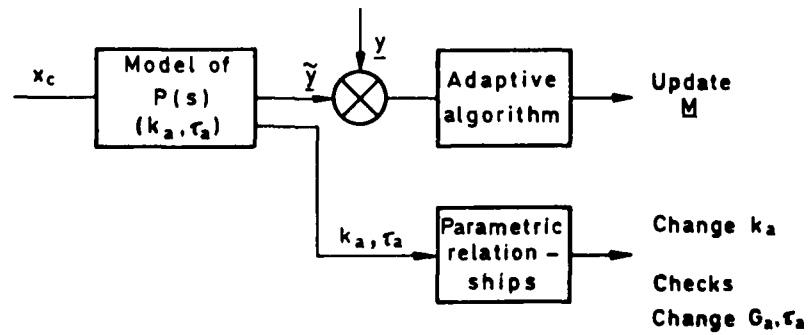
Fig 5a&b Typical conflict curves



a Main control loops



b G_a -adaptation



c Input filter adaptation

Fig 6a-c Redundant self-adaptive schemes

DESIGN TECHNIQUES FOR MULTIVARIABLE FLIGHT
CONTROL SYSTEMS

C. A. Harvey*
R. E. Pope

Honeywell Systems and Research Center
2600 Ridgway Parkway
Minneapolis, Minnesota 55413

SUMMARY

Modifications to airframe designs directed at increased maneuverability and reduced weight are placing stringent demands on flight control systems. This is particularly true for advanced fighter aircraft which may possess relaxed static stability, additional surfaces for direct force control, and active structural control requirements. Fly-by-wire systems, particularly digital systems, have provided the flexibility to not only accommodate but influence airframe design modifications and have led to the control configured vehicle (CCV) concept. These advances in air vehicle design and flight control system implementation have begun to overwhelm traditional design techniques which are most effective on aircraft applications with few surfaces, little dynamic coupling, separation between flight control and other avionics subsystem bandwidths and analog system implementations. This Chapter will describe and illustrate, through flight control design examples, new techniques which address 1) the multi-input closely coupled nature of advanced flight control applications and 2) digital implementation issues. The techniques described seek to exploit the advantages of traditional techniques in treating conventional feedback control design specifications and the simplicity of modern approaches for multi-variable control system design.

SYMBOLS

A	System matrix	p_s	Stability axis roll rate
B	Control matrix	P^s	Riccati matrix-optimal control
C	Measurement matrix	q	Robust estimator design parameter
C*	Linear combination of normal acceleration and pitch rate	Q	Weighting matrix
c	Collective	r	Left singular vector
dc	Differential collective	r_s	Stability axis yaw rate
E	Expected value	R	Matrix of left singular vectors; control weighting matrix
F	Kalman filter gains	r_{lim}	Rate limit
G(s)	Open-loop transfer function matrix	S	Riccati matrix - filter
gr	Rotor dynamics transfer function	s	Laplace operator
H(s)	Closed-loop transfer function matrix	u	Control vector
Hz	Hertz	U, V, G	Inverse Nyquist array matrix transformations
I	Identity index	v	Right singular vector
J	Performance index	V	Matrix of right singular vectors
J	$\sqrt{-1}$	x	System state vector
k	Loop gains	y	System measurement
K	Gain matrix	\dot{z}	Vertical velocity
L(s)	Perturbation matrix	z	Scalar variable analogous to inverse Nyquist variable; discrete plane operator
M	Relative maximum of closed-loop amplitude-frequency response	Z	Transform operator
β	Intermediate variable in calculation of z	ω	Frequency
η	Non-linearity input amplitude	σ	Singular value
δ	Control deflection	Σ	Diagonal matrix of singular values
ζ	Damping ratio	ρ	Scalar weighting parameter
λ	Eigenvalue	Λ	Diagonal matrix of eigenvalues
ϕ	Bank angle	ξ	System noise
θ	Sensor noise; pitch angle	Ξ	System noise covariance matrix
Θ	Measurement noise covariance matrix		

* Acknowledgment. The flight control system design techniques described in this chapter were developed under U.S. Office of Naval Research Contract # N00014-75-C-01444 and NASA Dryden Flight Research Center Contract # NAS4-2518. Honeywell's Systems and Control Technology section, primarily G. Stein, T. Cunningham, J. Doyle, R. Stone and G. Hartmann contributed extensively to the developments described through initial development and application of these techniques to numerous flight control design problems.

1.0 INTRODUCTION

A multivariable flight control system is one in which there are multiple interacting control loops. This interaction is dictated by the dynamic coupling resulting from the aircraft design. Until recently, aircraft were designed to minimize dynamic coupling.

For the design of flight control systems with little dynamic coupling, traditional or so called classical design and analysis techniques are more than adequate and provide key insights into the fundamental design issues of feedback control systems. The design and analysis techniques discussed in this chapter are directed at systems whose control loop interaction extend the utility of classical techniques to the point where they are not only cumbersome to use as design tools but produce flight control system designs with undesirable performance characteristics. The inadequacies of classical design techniques are by no means accepted facts. There has been continuous debate over the two last decades as to the utility of classical techniques versus the utility of non-classical or modern techniques.

It is useful to view the utility issue from the perspective of the flight control system application, particularly as flight control systems have evolved over the years. In depicting that history, the essential items to consider are

- the aircraft application
- the performance requirements
- the control approach

These items determine the utility of the design and analysis techniques.

The first row of Table 1 represents the aircraft application, performance requirements, control approach, and design and analysis techniques for early aircraft up through aircraft built in the 1950's. For these applications the airframe was designed to provide stability and control for the three attitude degrees of freedom and the propulsion system was designed for speed control. The control approach was open loop and design and analysis techniques were airframe oriented. Feedback control design techniques representative of classical techniques are shown for systems described by row 2 of Table 1. In this case also, the airframe was designed to provide 3 DOF attitude stability and control and the propulsion system provide speed control. Inadequate airframe designs or the promise of improved performance resulted in feedback systems which were used to augment stability. The most prevalent example of such a stability augmentation system is a yaw damper. The introduction of feedback control required additional design and analysis techniques, particularly those which addressed the stability characteristics of feedback control systems. Because the feedback control design was very simple, involving only one sensor variable and one surface command, classical techniques were very effective and led to the acceptance of stability margins as flight control system design specifications.

Additional demands were then placed on flight control systems in the form of command augmentation systems as shown in row 3 of Table 1. The airframe application still remained the same with or without a need for stability augmentation. Handling quality tests determined that command augmentation provided better handling qualities as exemplified by the acceptance of rate command systems or C* systems. Traditional design techniques were still very adequate for design since despite an increase in the number of sensor and surface pairs, the design could be performed one pair at a time because of the loose dynamic coupling.

The introduction of command augmentation, however, initiated the application of modern multi-variable techniques, particularly model following approaches. These techniques promised to facilitate flight control system design thus producing better designs. Despite the promise, they were not widely accepted by practical control system designers.

Fly-by-wire systems, particularly digital FBW systems, as shown in row 4 of Table 1, brought new issues to flight control design. New techniques were developed and utilized to insure that digital systems performed as closely as possible to their analog counterparts. In addition the availability of a digital computer and its associated "unlimited" computational capability on board the aircraft encouraged more application of modern techniques which promised better performance. Again these techniques were not widely accepted by practical control designers.

The systems described by row 4 of Table 1 represent the state of the art of today's production aircraft. Table 2 presents characterizations for current experimental and prototype aircraft and projected production systems. The introduction of the control configured vehicle (CCV) concept has had a dramatic effect on flight control systems. In a CCV aircraft, the flight control system is not merely augmenting stability or improving performance, but is providing a flight critical stabilizing and control function. The criticality of the flight control system in a CCV application has intensified the need for efficient and reliable design and analysis techniques. CCV aircraft, in themselves however, do not possess dynamic coupling levels which make classical design techniques intractable. In addition, classical techniques directly address stability issues and have therefore been much more attractive to a designer for CCV control designs.

Direct force control, made possible by additional surfaces and thrust vectoring of the propulsion system, as characterized by row 2 of Table 2 introduced a flight control design application that benefits from multivariable control techniques. In this application, it is difficult to eliminate closely coupled dynamics in the airframe design. Interaction with the propulsion system can magnify the coupling. For this application, the large number of control inputs and the close coupling of dynamics can easily overwhelm classical "one loop at a time" techniques.

The problem is projected to worsen with the integration of flight control and other avionics subsystems as shown in row 3 of Table 2 and Figure 1. In the sections that follow, we will discuss design and analysis techniques which have been developed to address these multivariable control problems. In the development of these techniques, which is still ongoing, the goal has been an efficient flight control design and analysis capability which addresses the following:

- i) multi-input closely coupled dynamic systems
- ii) conventional design specifications, particularly stability margin and high frequency attenuation
- iii) the impact of unmodeled or uncertain dynamics on system performance
- iv) digital realizations.

These items are addressed in varying degrees of detail in the techniques that are described and illustrated by design examples.

2.0 DISCUSSION OF TECHNIQUES

Various approaches exist for the design of multivariable flight control systems. This section presents a brief review of certain of these approaches followed by summary descriptions of the techniques with illustrative examples.

2.1 Review of Approaches

One approach is to use a classical single-input, single-output (SISO) technique for the design of one control loop at a time. In this approach the design of each individual loop is carried out on the basis of that loop's input-output pair and its effect on the input-output pairs for the other loops. This approach can be useful for certain problems, but its capability is severely limited for highly coupled multivariable systems. Furthermore, analysis of multivariable feedback systems with SISO techniques can give misleading results.

An approach to extending SISO techniques to multivariable systems makes use of approximate decoupling and the Inverse Nyquist Array methodology [2.1], [2.2]. This approach can be useful for systems that are sufficiently decoupled to be naturally diagonally dominant. But, forcing the loop dynamics to be diagonally dominant appears to impose undue restrictions on the design. Furthermore, the diagonalization or near diagonalization process can yield highly misleading conclusions concerning robustness with respect to design model uncertainty, by which we mean all the uncertainty between the design model and the actual operating system.

Another approach to extending SISO frequency domain techniques to multivariable systems uses the Characteristic Loci methodology [2.3], [2.4]. In this approach characteristic gain functions and characteristic frequency functions are defined in terms of appropriate matrix-valued rational functions of a complex variable to generalize the Nyquist-Bode and root locus methods used for SISO systems. This approach is appealing because of the mathematical insights that it can provide. But, it also can yield misleading conclusions concerning robustness with respect to design model uncertainty. Another drawback to this technique and the INA technique is that they are limited to square systems, that is, systems that have the same number of outputs as inputs. This could represent a severe limitation of the design process.

Alternatives to the frequency domain methods include the modal control approach and the linear-optimal approach. Both of these approaches commonly deal with state space formulations which permit treatment of non-square systems with ease. But, the deficiencies associated with these approaches are generally related to key issues that are most naturally expressed in frequency domain terms.

The modal control approach consists of choosing feedback gains so that the closed-loop system has desired eigenvalues and eigenvectors [2.5], [2.6]. This approach can be useful when design requirements can be easily expressed in terms of desired closed-loop modal characteristics. But, in many cases the system design requirements cannot be so simply expressed. This is especially true for design requirements associated with tolerance to design model uncertainty.

In the linear optimal control approach, controllers are determined that minimize a performance index which is the integral of a cost function. This cost function is a sum of quadratic terms in the states and controls. The controller uses feedback of all the states of the system or estimates of these states if all the states cannot be measured. This approach appears to be the most widely applicable,

but there are certain difficulties involved in its use. The first issue that arises is that of selecting appropriate weighting matrices for the cost function. A second issue that arises is that linear optimal controllers often have inadequate high frequency attenuation and excessive bandwidth. Another issue is the care required in the design of an estimator or observer so that the guaranteed stability margins of optimal full state feedback control are nearly preserved when the output of the estimator or observer is used in the feedback path.

A major deficiency in each of the above approaches is the lack of guaranteed robustness with respect to design model uncertainty. A viable approach to the analysis of this robustness is the use of singular values and certain characterizations of the design model uncertainty. Since there is no existing synthesis technique which corresponds directly to this analysis technique, it appears that such an analysis must be incorporated in the design process. That is, preliminary designs should be subjected to such an analysis, and if this analysis shows the design to be inadequate, then further iterations of the design should be made guided by the robustness analysis results.

2.2 Description of Linear-Multivariable Design Techniques and Illustrative Examples

The robustness of several of the illustrative examples will be analyzed using singular value analysis. So this method will be briefly summarized proceeding to the description of the design techniques.

As indicated above, a critical property of feedback systems is, their ability to maintain performance in the face of uncertainties. In particular, it is important that a closed-loop system remain stable despite differences between the model used for design and the actual plant. These differences result from variations in modeled parameters as well as plant elements which are either approximated, aggregated, or ignored in the design model. The robustness requirements of a linear feedback design are often specified in terms of desired gain and phase margins and bandwidth limitations associated with loops broken at the input to the plant actuators [2.7], [2.8]. These specifications reflect in part the classical notion of designing controllers which are adequate for a set of plants constituting a frequency-domain envelope of transfer functions [2.9]. The bandwidth limitation provides insurance against the uncertainty which grows with frequency due to unmodeled or aggregated high frequency dynamics.

The Nyquist or Inverse Nyquist diagram (polar plots of the loop transfer function) provides a means of assessing stability and robustness at a glance for SISO systems. Multivariable generalizations of the scalar Nyquist, Inverse Nyquist and Bode analysis methods can be developed from a basic result on robustness properties of linear systems expressed in terms of singular values.

Detailed discussions of the concepts of singular values and singular vectors are given in references [2.10] and [2.11]. For simplicity, these concepts will be briefly described here for square matrices, although the concepts apply to arbitrary matrices.

2.2.1 Singular values

The singular values σ_i of a complex $n \times n$ matrix A are the nonnegative square roots of the eigenvalues of A^*A where A^* is the conjugate transpose of A . The (right) eigenvectors v_i of A^*A and r_i of AA^* are the right and left singular vectors, respectively, of A . These may be chosen such that

$$\sigma_i r_i = A v_i, \quad i = 1, \dots, n \quad (1)$$

$$\sigma_1 \leq \sigma_2 \leq \dots \leq \sigma_n$$

and the $\{r_i\}$ and $\{v_i\}$ form orthonormal sets of vectors. The singular value decomposition of A is

$$A = R \Sigma V^* \quad (2)$$

where

$$R = [r_1, r_2, \dots, r_n], \quad V = [v_1, v_2, \dots, v_n] \quad (3)$$

and Σ is the diagonal matrix with diagonal elements $\sigma_1, \sigma_2, \dots, \sigma_n$. The minimum and maximum singular values have special significance and will be denoted here by $\underline{\sigma}(A)$ and $\bar{\sigma}(A)$ respectively. These singular values derive their special significance from the relations

$$\underline{\sigma}(A) = \min_{\|x\|=1} \|Ax\|, \quad \bar{\sigma}(A) = \max_{\|x\|=1} \|Ax\| \quad (4)$$

and $\bar{\sigma}(A)$ is the spectral norm of A . The singular values give an accurate measure of how close A is to being singular. The ratio $\underline{\sigma}/\bar{\sigma}$ is known as the condition number with respect to inversion. The eigenvalues of A generally fail to provide such an accurate measure. The magnitudes of the eigenvalues of A are bounded below by $\underline{\sigma}(A)$ and above by $\bar{\sigma}(A)$. But, the magnitude of the smallest eigen-

value can be much larger than $\underline{\sigma}(A)$, and the magnitude of the largest eigenvalue can be much smaller than $\bar{\sigma}(A)$. This key difference between singular values and eigenvalues is the reason that singular value analysis provides an adequate measure of robustness and that eigenvalue analysis is inadequate.

Now consider the linear feedback system shown in Figure 2 where $G(s)$ is the nominal loop transfer matrix and $L(s)$ is a perturbation matrix which is nominally zero and represents the deviation between $G(s)$ and the real plant. A reasonable measure of the robustness of this feedback system is the magnitude of the perturbation which may be tolerated without causing instability. Taking the magnitude of $L(s)$ to be its spectral norm, the following basic result was obtained by Doyle [2.12].

If a system, such as that shown in Figure 2, satisfies the following conditions:

- i) $G(s)$ and $L(s)$ are $n \times n$ rational square matrices
- ii) $\text{Det } G(s) \neq 0$
- iii) $L(s)$ is stable
- iv) The nominal closed loop system $H = G(I + G)^{-1}$ is stable

then the system is stable for all perturbations that satisfy

$$\underline{\sigma}(I + G^{-1}(s)) > \bar{\sigma}(L(s)) \quad (5)$$

for all s in the classical Nyquist D-contour consisting of the segment of the imaginary axis from $-jR$ to $+jR$ and the semicircle of radius R in the right half-plane with R chosen sufficiently large.

A similar result holds for a system with the perturbation shown in Figure 3. In this case the quantity $I + G(s)^{-1}$ in (5) is replaced by the quantity $I + G(s)$.

The singular values also have useful graphical interpretations. Consider the dyadic expansion

$$H^{-1} = I + G^{-1} = \sum_{i=1}^n \sigma_i r_i v_i^* \quad (6)$$

$$\sigma_1 \leq \sigma_2 \leq \dots \leq \sigma_n$$

where the σ_i , r_i and v_i are the singular values, and left and right singular vectors, respectively of $I + G^{-1}$. This is an alternative form of the singular value decomposition in equation (2).

It has been shown [2.13] that the eigenvalues and eigenvectors of a rational matrix are continuous (through generally not rational) functions of frequency. Since singular values and vectors are just special cases, $\sigma_i(j\omega)$, $r_i(j\omega)$ and $v_i(j\omega)$ are also continuous functions of ω .

Since

$$H = (I + G^{-1})^{-1} = \sum \frac{1}{\sigma_i} v_i r_i^* \quad (7)$$

the values $1/\sigma_1(j\omega)$ and $1/\sigma_n(j\omega)$ give the maximum and minimum possible magnitude responses to an input sinusoid at frequency ω . In this sense, a plot of these singular values vs. frequency may be thought of as a multivariable generalization of the Bode gain plot. Plots of this type will be referred to as σ -plots.

Another useful graphical interpretation analogous to the scalar Inverse Nyquist diagram may be constructed by noting that

$$\begin{aligned} G^{-1} &= \sum \sigma_i r_i v_i^* - I \\ &= \sum \sigma_i r_i v_i^* - \sum v_i v_i^* \\ &= \sum (\sigma_i r_i - v_i) v_i^* \\ &= \sum \beta_i g_i v_i^* \end{aligned} \quad (8)$$

where $\beta_i g_i = \sigma_i r_i - v_i$ with β_i real and $\|g_i\| = 1$ for all i .

Let z_i be defined implicitly as a function of σ_i and β_i by the quadratic equation

$$z_i^2 + (1 + \beta_i^2 - \sigma_i^2)z_i + \beta_i^2 = 0 \quad (9)$$

By plotting the $z_i(j\omega)$ ($i=1, \dots, m$) for frequencies of interest a plot analogous to the scalar Inverse Nyquist plot is generated. While phase does not have the conventional meaning on these plots, the more important notion of distance from the critical point preserves its importance. These plots will be referred to as z-plots.

Concepts such as M-circles are also obvious in this context. The minimum value of M is given by

$$M_m = \max_{\omega} (1/\sigma_1(j\omega)) \quad (10)$$

Similar results may be obtained for additive perturbations by working with $I + G$ rather than $I + G^{-1}$. In this case a diagram is generated which is analogous to the scalar Nyquist diagram.

Singular values offer no encirclement condition to test for right half-plane poles. But this is not a major deficiency because there are other simple techniques to assess the stability of the nominal system.

2.2.2 Deficiencies in Existing Approaches

The single-loop-at-a-time approach involves first of all the selection of loops. That is, for a system with a given number of inputs it is assumed that there are at least that many outputs of interest and the first question that arises is what outputs should be paired with the inputs. For some systems this choice is obvious from the system characteristics. In highly coupled systems the choice may be difficult. Once the pairs have been selected, it is necessary to choose the sequence of loop closures. This choice also can be clearly dictated for some systems, but not for others. The design then proceeds by closing one loop at a time, generally conducted in an iterative fashion. The robustness of the final closed loop system is then examined by breaking one loop at a time and determining the stability margins.

The following example illustrates that analyzing robustness by breaking one loop at a time can be very misleading. The example was chosen to demonstrate this point only and does not represent any particular physical system. In fact, the controller considered is not representative of a good single-loop-at-a-time design. The loop transfer matrix for the example is

$$G(s) = \frac{1}{s^2 + 100} \begin{bmatrix} s-100 & 10(s+1) \\ -10(s+1) & s-100 \end{bmatrix} \quad (11)$$

The open loop poles are at $\pm 10j$, and with identity feedback the closed loop poles are both at -1 . Single loop breaking analysis for either loop indicates that the phase margin is 90 and the gain margin is $\pm \infty$ db. For comparison, the corresponding z-plot is shown in Figure 4. It is not a plot of a rational function, so it may appear somewhat unusual. The important feature is the proximity of the plot to the critical point, -1 , which indicates a lack of robustness.

The discrepancy between these two robustness indications can be easily understood by considering a diagonal perturbation

$$L = \begin{bmatrix} k_1 & 0 \\ 0 & k_2 \end{bmatrix} \quad (12)$$

where k_1 and k_2 are constants.

Then regions of stability and instability may be plotted in the (k_1, k_2) plane as has been done in Figure 5. The open loop point corresponds to $k_1 = k_2 = 0$. Breaking each loop individually examines stability along the k_1, k_2 axes where robustness is good, but misses the close unstable regions caused by simultaneous changes in k_1 and k_2 . Thus, single loop analysis is not a reliable way of testing robustness.

The approach taken with the Inverse Nyquist Array (INA) methodology attempts to extend SISO techniques to multivariable systems. In this approach the key feature is the use of diagonal dominance of the INA. Computer-aided displays of the Nyquist plots of the elements of the inverse of the loop transfer matrix can be used to assess the closeness to decoupling. These plots can be examined, and the information obtained can be useful in the selection of appropriate input-output pairs. If diagonal dominance cannot be achieved by this selection process, the methodology suggest techniques for introducing compensation to achieve the desired dominance. Once the diagonal dominance of the INA is achieved, design of diagonal feedback is accomplished with SISO methods. References [2.1] and [2.2] are recommended for detailed descriptions of this approach.

The Characteristic Loci methodology uses multivariable generalizations of the open-loop gain as a function of frequency and the closed-loop characteristic frequency as a function of gain. In this technique an inner-loop is designed on the basis of characteristic frequency as a function of gain to serve as a starting point for an outer-loop design which provides sufficient feedback gain to insure satisfactory performance. This approach also uses computer-aided displays. In this case the displays of interest are the loci of characteristic gain and characteristic frequency. Detailed descriptions of this approach can be found in references [2.3] and [2.4].

The following simple example was constructed to illustrate deficiencies associated with the Inverse Nyquist Array and Characteristic Loci approaches.

Consider the system with loop transfer matrix

$$G(s) = \frac{1}{(s+1)(s+2)} \begin{bmatrix} -47s + 2 & 56s \\ -42s & 50s + 2 \end{bmatrix} \quad (13)$$

Assuming identity feedback, the closed-loop poles are at -2 and -4. This system may be diagonalized by introducing constant compensation. Let

$$U = \begin{bmatrix} 7 & 8 \\ 6 & 7 \end{bmatrix} \quad (14)$$

and

$$V = U^{-1} = \begin{bmatrix} 7 & -8 \\ -6 & 7 \end{bmatrix} \quad (15)$$

Then letting

$$\hat{G} = VGU = \begin{bmatrix} \frac{1}{s+1} & 0 \\ 0 & \frac{2}{s+2} \end{bmatrix} \quad (16)$$

the system may be rearranged so that

$$\begin{aligned} H &= G(I + G)^{-1} \\ &= U\hat{G}V(I + U\hat{G}V)^{-1} \\ &= U\hat{G}(I + \hat{G})^{-1}V \\ &= U \hat{G}(I + \hat{G})^{-1} V. \end{aligned} \quad (17)$$

This yields a diagonal system that may be analyzed by scalar methods. In particular under the assumption of identity feedback \hat{G} represents the new loop transfer matrix. Because U and V represent a similarity transformation, the diagonal elements of G are also the eigenvalues of \hat{G} so that the decoupling or dominance approach and eigenvalue or characteristic loci approach would generate the same Nyquist or Inverse Nyquist plot shown in Figure 6. Only a single locus is shown since the contours of $1/(s+1)$ and $2/(s+2)$ are identical. The tempting conclusion that might be reached from these plots is that the feedback system is very robust with apparent margins of $\pm \infty$ db in gain and 90° in phase. The closed-loop pole locations would seem to support this.

This conclusion, however, would be wrong. The z -plot for $I + G^{-1}$ is shown in Figure 7 and there is clearly a serious lack of robustness. The (k_1, k_2) - plane stability plot for this example is shown in Figure 8. Neither the diagonal dominance nor eigenvalue approaches indicate the close proximity of an unstable region. This failure can be attributed to two causes.

First, the eigenvalues of a matrix do not, in general, give a reliable measure of its distance (in a parametric sense) from singularity, and so computing the eigenvalues of $G(s)$ (or $I + G(s)$) does not give an indication of robustness. Using eigenvalues rather than singular values will always detect unstable regions that lie along the $k_1 = k_2$ diagonal, but may miss regions such as the one in Figure 8.

Second, when compensation and/or feedback is used to achieve dominance, the "new plant" includes this compensation and feedback. Because of this, no reliable conclusions may be drawn from this "new plant" concerning the robustness of the final design with respect to variations in the actual plant. It is important to evaluate robustness where there is uncertainty.

2.2.3 Modal Control

The modal control approach provides a method of finding feedback gains that yield certain desired closed-loop eigenvalues and eigenvectors. The modal concept is common to many flight control applications. For example, the lateral-directional axis of a fixed wing aircraft has three dominant modes (roll, dutch roll, and spiral) and the longitudinal axis has two dominant modes (short period and phugoid). Desired modal properties are often specified in terms of eigenvalues (frequencies, damping ratios, time constants) and associated coupling or decoupling of responses. Handling quality criteria for the lateral axis are expressed in such terms. The dutch roll mode should have an eigenvalue with desired frequency and damping ratio and an eigenvector that ideally contains nonzero components for sideslip and yaw rate only. The roll mode should have an eigenvalue corresponding to a desired time constant and an eigenvector which ideally has roll rate as its only nonzero component. The spiral mode should have a small

real eigenvalue and an eigenvector that ideally has only bank angle as its nonzero component. This approach can be used with state feedback or output feedback.

The details of this approach may be summarized as follows. Consider the linear multivariable feedback system

$$\dot{x} = Ax + Bu \quad (18)$$

$$y = Cx \quad (19)$$

$$u = -Ky \quad (20)$$

where the state vector, x , is n -dimensional, the control vector, u , is m -dimensional and the output vector, y , is p -dimensional, A , B , C , and K are matrices of appropriate dimensions, and it is assumed that

$$\text{Rank}(B) = m \quad (21)$$

$$\text{Rank}(C) = p \leq n \quad (22)$$

An eigenvalue-eigenvector pair for the closed-loop system is denoted as (λ_i, v_i) where

$$A_c v_i = \lambda_i v_i \quad (23)$$

and A_c is the closed-loop system matrix

$$A_c = A - BKC \quad (24)$$

Only certain pairs are achievable. An achievable pair satisfies

$$Av_i + Bw_i = \lambda_i v_i \quad (25)$$

where w_i is a vector with dimension = $\min(m, p)$.

In the case of state feedback, C may be chosen to be the identity, and (23) and (25) yield

$$w_i = Kv_i \quad (26)$$

Letting Λ be the diagonal matrix with elements λ_i on the diagonal, V be the matrix with its i^{th} column being the eigenvector v_i , and W be the $(m \times n)$ matrix with its i^{th} column being w_i , equation (25) yields

$$VA - AV = BW \quad (27)$$

and equation (26) yields

$$W = KV \quad (28)$$

which can be solved for K , i. e.

$$K = WV^{-1} \quad (29)$$

Complex eigenvector pairs can be rotated to provide a real matrix K . In the case of output feedback, equation (28) is replaced by

$$W = KCV \quad (30)$$

and if $p < n$, the matrix CV has rank less than n so that (30) cannot be solved for K in general. One method for resolving this difficulty is to select only p eigenvalue-eigenvector pairs with $\hat{\Lambda}$ denoting the $(p \times p)$ diagonal matrix of eigenvalues and \hat{V} denoting the $(n \times p)$ matrix of corresponding eigenvectors, and \hat{W} denote the corresponding $(w \times p)$ matrix. Then K is given by

$$K = \hat{W}(\hat{C}\hat{V})^{-1} \quad (31)$$

subject to

$$\hat{V}\hat{\Lambda} - A\hat{V} = B\hat{W} \quad (32)$$

In this case there is no constraint on the remaining $n-p$ eigenvalue-eigenvector pairs, and they could be undesirable.

The design procedure initially involves choosing portions of v_i in order to eliminate certain state responses from a mode while emphasizing others and letting other responses (control or compensation) react arbitrarily.

For Rank (B) = m, m free parameters can be specified, one of which is the eigenvalue. Equation (25) can be rewritten

$$A_{ci}q_i = [(A - \lambda_i I), B]q_i = 0$$

$$q = \begin{bmatrix} v_i \\ w_i \end{bmatrix} \quad (33)$$

q_i is therefore a null space mapping of A_{ci} . A convenient tool for finding the relationship between v_i and w_i is contained in the singular value decomposition of A_{ci} :

$$A_{ci} = X_i \Sigma_i Z_i^* \quad (34)$$

where X_i is an n-by-n matrix containing columns of orthogonal left singular vectors of A_{ci}

X_i is an n-by-n matrix containing columns of orthogonal left singular vectors of A_{ci}

Σ_i is an n-by-n+m matrix containing n singular values, σ 's, of A_{ci}

$$\Sigma_i = \left[\begin{array}{ccc|ccc} \sigma_1 & 0 & \dots & 0 & 0 & \dots & 0 \\ 0 & \sigma_2 & & & & & \\ \cdot & & \cdot & & & & \\ \cdot & & & & & & \\ \cdot & & & & & & \\ 0 & & & \sigma_n & & & \\ \hline & & & & 0 & \dots & 0 \\ & & & & 0 & \dots & 0 \end{array} \right] \quad \left. \vphantom{\Sigma_i} \right\} n$$

$$= \left[\begin{array}{c} \bar{\Sigma}_i \\ [0] \end{array} \right]; \quad \bar{\Sigma}_i \text{ is } n \times n \text{ diagonal}$$

Z_i is an n+m-by-n+m matrix containing n+m orthogonal right singular vectors of A_{ci}

By rearranging (34)

$$A_{ci}Z_i = X_i \Sigma_i \quad (35)$$

and noting that the last m columns of the $X_i \Sigma_i$ product are null, we find the appropriate null space for A_{ci} by using the last m columns of Z_i :

$$A_{ci} \bar{Z}_i = 0 \quad (36)$$

where \bar{Z}_i is defined as

$$Z_i = \left[\underbrace{Z_i}_n \quad \underbrace{\bar{Z}_i}_m \right] \quad n+m \quad (37)$$

The matrix \bar{Z}_i is a set of m orthonormal basis vectors spanning the null space of A_{ci} . Referring to (33), we have

$$q_i = \bar{Z}_i \alpha_i \quad (38)$$

where α_i is an m vector of linear coefficients not all of which can be zero.

Now we would like to select desired v_i and solve (33) for the corresponding w_i . This cannot be done in general if $m < n$, but an approximate solution can be obtained by minimizing a performance index

$$J = (v_{di} - v_i)^* Q (v_{di} - v_i) \quad (39)$$

subject to (33) where v_{di} is the desired eigenvector. By this process one can select arbitrarily the desired v_{di} and the resulting v_i which are attainable are the closest to those desired in the sense of (39). This can be accomplished by replacing v_i in (38) with $v_i = E \bar{Z}_i \alpha_i$ where

E is an n -by- $n+m$ matrix

$$E \triangleq \left[\begin{array}{c|c} \underbrace{I}_n & \underbrace{0}_m \end{array} \right]_n$$

and minimizing (39) with respect to α_i

$$\begin{aligned} \alpha_i &= \text{Arg min } J \\ &= (\bar{Z}_i^* E^T Q E \bar{Z}_i)^{-1} \bar{Z}_i^* E^T Q v_{di} \end{aligned} \quad (40)$$

the appropriate W_i is found using (38)

$$W_i = \bar{E} \bar{Z}_i \alpha_i = \bar{E} \bar{Z}_i (\bar{Z}_i^* E^T Q E \bar{Z}_i)^{-1} \bar{Z}_i^* E^T Q v_{di} \quad (41)$$

where \bar{E} is an m -by- $n+m$ matrix

$$\bar{E} \triangleq \left[\begin{array}{c|c} \underbrace{0}_n & \underbrace{I}_m \end{array} \right]_m$$

2.2.4 F-4 Design Example

As an illustrative example this method was applied to the design of an inner-loop control law for the F-4 lateral axis. The data for this example is taken from reference [2.14]. The state space representation of this example is in the form of equation (18) with

$$x = \begin{bmatrix} p_s \\ r_s \\ \beta \\ \phi \\ \delta_r \\ \delta_a \end{bmatrix} \begin{array}{l} \text{stability axis roll rate} \\ \text{stability axis yaw rate} \\ \text{angle of sideslip} \\ \text{bank angle} \\ \text{rudder deflection} \\ \text{aileron deflection} \end{array}$$

$$u = \begin{bmatrix} \delta_{rc} \\ \delta_{ac} \end{bmatrix} \begin{array}{l} \text{rudder command} \\ \text{aileron command} \end{array}$$

Matrices A and B are

$$A = \begin{bmatrix} -.746 & .387 & -12.9 & 0. & .952 & 6.05 \\ .024 & -.174 & 4.31 & 0. & -1.76 & -.416 \\ .006 & -.9994 & -.0578 & .0369 & .0092 & -.0012 \\ 1. & 0. & 0. & 0. & 0. & 0. \\ 0. & 0. & 0. & 0. & -20. & 0. \\ 0. & 0. & 0. & 0. & 0. & -10. \end{bmatrix}$$

$$B = \begin{bmatrix} 0. & 0. \\ 0. & 0. \\ 0. & 0. \\ \hline 0. & 0. \\ 20. & 0. \\ 0. & 10. \end{bmatrix}$$

Open Loop Poles

λ roll subsidence	=	-0.079
λ dutch roll	=	$-0.098 \pm j2.079$
λ spiral	=	-0.0063
λ rudder actuator	=	-20.0
λ aileron actuator	=	-10.0

From the point of view of fighter handling qualities, all four of the lateral axis closed loop roots have desired values which can be taken from MIL-F8785B, as is done, for example, in reference [2.14]. The desired roots are:

- a) Roll subsidence mode = -4.0
- b) Dutch roll mode = $-0.63 \pm j2.42$
- c) Spiral mode = -0.05

Desired eigenvectors were selected to pair with the desired eigenvalues, and the method described above was used to compute nearest attainable eigenvectors. The results are:

- a) Roll subsidence mode ($e^{-4t}v_1$)

Desired v_{d1}	=	[1. 0 0 a a a]
Attainable v_1	=	[1. -.007 0 -.25 .13 -.56]
- b) Dutch roll mode, real part ($e^{-.63t}(\cos 2.42t)v_2$)

Desired v_{d2}	=	[0 a 1. 0 a a]
Attainable v_2	=	[0 15.6 1. 0 7.86 -.103]
- c) Dutch roll mode, imaginary part ($e^{-.63t}(\sin 2.42t)v_3$)

Desired v_{d3}	=	[0 1. a 0 a a]
Attainable v_3	=	[0 1. 6.16 0 -9.49 14.6]
- d) Spiral mode ($e^{-.05t}v_4$)

Desired v_{d4}	=	[a a 0 1. a a]
Attainable v_4	=	[-.05 .037 0 1. -.0014 -.0079]

A few comments are in order to explain these choices. Consider, for example, the roll subsidence mode. The desired eigenvector is taken to be $v_{d1} = (1 \ 0 \ 0 \ a \ a \ a)$, which means that the mode should show up dominantly on roll rate, but not on yaw rate or sideslip (we want no sideslip buildup during turn entries). These are good basic handling quality considerations. The a's in the vector indicate that we do not care how much of the mode shows up on these components. Certainly, since $\phi = \int p_g dt$, some mode content has to be expected on element a_4 and, similarly, if the surfaces are actually controlling the mode, some mode content should also appear in a_5 and a_6 . The linear projection which best achieves these objectives is shown as v_1 above. Note that we can satisfy our desires almost perfectly.

Similar arguments also apply to the dutch roll mode. In this case we want no oscillatory dutch roll content on roll rate and bank angle. This is a key handling quality requirement for all well-behaved lateral control laws.

In the case of the spiral, we want the mode to be predominantly bank angle (corresponding to steady turns) with no substantial sideslip component. The latter is a basic turn coordination requirement.

A sample design was carried out with the modal approach assuming that the output, y , consisted of the first four states. This output posed little difficulty, since our desire is embodied in four eigenvalue-eigenvector pairs. There is some concern with the remaining two pairs. It is desired to have these poles not be too far left from their open loop values. This is not a problem in this case, since the trace of the open-loop system matrix is the same as the trace of the closed-loop system matrix. So the sum of the closed-loop eigenvalues is the same as the sum of the open-loop eigenvalues. Thus, for this example the sum of the remaining closed-loop poles is greater than their open-loop sum, and, in fact, each of these closed-loop poles is to the right of their open-loop values. The closed-loop values of λ_5 and λ_6 are -19.03 and -6.64 in comparison to open loop values of -20 and -10.

An initial condition response for the open-loop system is shown in Figure 9. A similar response is shown in Figure 10 for the closed-loop system. Dramatic improvement in reduced cross coupling between the roll and dutch roll modes is evident. Also evident is the improved dutch roll damping and the roll response time.

It is a simple matter to use this method to determine the effects of different sensor combinations and compensators. This makes it a useful tool for tradeoff studies. Unfortunately there is no robustness guaranteed so that this aspect of the design must be analyzed independently.

2.2.5 Linear Optimal Control

The linear optimal control approach has been extensively discussed in the automatic control literature. The synthesis procedure in this approach usually starts with a mathematical model of the form

$$\dot{x} = Ax + Bu + \xi \quad (42)$$

$$y = Cx + \theta \quad (43)$$

where ξ and θ represent system and sensor noise which are assumed to be gaussian, white, mutually independent, stationary, and zero mean with covariances,

$$\text{cov} \begin{bmatrix} \xi(t); \xi(\tau) \end{bmatrix} = \delta(t-\tau), \zeta \geq 0 \quad (44)$$

$$\text{cov} \begin{bmatrix} \theta(t); \xi(\tau) \end{bmatrix} = \theta \delta(t-\tau), 0 \geq 0 \quad (45)$$

The control law is obtained by minimizing a performance index of the form

$$J = E \int_0^{\infty} (x^T Q x + u^T R u) dt \quad (46)$$

The resulting control law is

$$u = -Kx = -R^{-1} B^T P \hat{x} \quad (47)$$

where P satisfies a Riccati equation and \hat{x} is an estimate of x given by

$$\dot{\hat{x}} = A\hat{x} + Bu + F(y - C\hat{x}) \quad (48)$$

with $F = SC^T_0^{-1}$ and S satisfies another Riccati equation. In a deterministic version of this approach where it is assumed that there is no noise and C is the identity, the control law is given by (47) with \hat{x} replaced by x . For this latter version it is known that the controllers possess guaranteed stability margins of at least -6db and + ∞ db in gain and at least 60° in phase at each input if R is chosen to be the identity. It is also known that these controllers have first order attenuation at high frequencies. This property can be a problem for many flight control applications. Controllers for the nondeterministic version generally have higher order attenuation at high frequencies but they do not possess any guaranteed stability margins.

One difficulty with this approach is that of relating the performance index to design specifications. A method for selecting the weighting matrices, Q and R , on the basis of desired modal characteristics is described in [2, 15]. This method is based on the asymptotic modal properties of optimal controllers as the weight on the control tends to zero. The designer can choose desired modes the same way as in the modal control approach and construct corresponding weighting matrices. The F-4 lateral-directional example was also treated by this method, and the resulting controller's closed-loop transient response was essentially the same as that shown in Figure 9. This controller does possess the guaranteed stability margins.

2.2.6 CH-47 Design Example

In another illustrative example this method was used in conjunction with singular value analysis of robustness. The example treats the longitudinal degrees of freedom of the CH-47 helicopter. In forward flight, this vehicle exhibits coupled pitch attitude and vertical motion dynamics which must be controlled by coordinated action of two inputs. This vehicle is a tandem rotor machine whose physical characteristics and mathematical models are given in [2, 16]. Control over vertical motions is achieved by simultaneous changes of blade angle-of-attack on both rotors (collective), while pitch and forward motions are controlled by changing blade angle differentially between the two rotors (differentially between the two rotors (differential-collective). These blade angle changes are transformed through rotor dynamics and aerodynamics into hub forces which then move the machine.

Our objectives will be to design a command augmentation control law which achieves tight, non-interacting control of the vertical velocity and pitch attitude responses. A small perturbation linearized aircraft model should prove adequate for this purpose and is available from [2.16]. The state vector consists of the vehicle's basic rigid body variables $x = (V, \dot{z}, q, \theta)$ (forward velocity, vertical velocity, pitch rate, pitch angle). Two integrators are appended to achieve integral control of the primary responses, and controls are the collective and differential collective inputs described above, $u = (c, dc)$. Hence, the design model is

$$\begin{aligned}\dot{x} &= Ax + Bu & A, B \text{ in [2.16]} \\ \dot{x}_5 &= -\dot{z} + \dot{z}_{\text{cmd}} \\ \dot{x}_6 &= -\theta + \theta_{\text{cmd}}\end{aligned}\tag{49}$$

The major approximations associated with this model are due to neglected dynamics of the rotors, to neglected nonlinearities in the blade angle actuation hardware, and to variations of the A, B matrices with operating point (flight condition variations). We will treat modeling errors due to these approximations as sources of the perturbation $L(s)$ in Figure 2 and will attempt to make controllers robust with respect to them.

Elementary dynamic and aerodynamic analyses of rotating airfoils, hinged at the rotor hub, indicate that lift forces will not be transmitted to the hub instantaneously with collective changes in blade angle-of-attack but will appear only when the cone angle of the rotor has appropriately changed. The dynamics of the latter have been shown to be damped second order oscillations with natural frequency equal to rotor speed and damping determined by somewhat uncertain aerodynamic effects [2.17]. Hence, rotor dynamics can be crudely represented by second order transfer functions

$$g_R(s, \zeta) = \frac{\omega_R^2}{s^2 + 2\zeta\omega_R s + \omega_R^2}\tag{50}$$

with $\omega_R = 25$ rad/sec and ζ conservatively confined to the range $0.1 \leq 1.0$. Because collective and differential-collective inputs both involve coning motions of the rotors, one such transfer function will appear in each control channel. Since these dynamics are neglected in equation (49), it then follows that any perturbed transfer function matrix computed from Figure 2 will have the form

$$\hat{G} = G(1 + L) = G \text{diag}(g_R),\tag{51}$$

and hence,

$$L = \text{diag}(g_R - 1)\tag{52}$$

$$\sigma[L] = \max_{\zeta} \left| \frac{s^2 + 2\zeta\omega_R}{s^2 + 2\zeta\omega_R s + \omega_R^2} \right|$$

The function was evaluated for a range of $s = j\omega$ values (with brute force maximization) and is shown by the solid lines in Figure 10.

Figure 10 also shows an alternate bound for $\bar{\sigma}[L]$ derived from a generalization of Safonov [2.18]. This bound is slightly more conservative than that given by the solid lines, but covers a larger class of perturbations corresponding to nonconstant ζ 's in the rotor dynamics.

In addition to the dynamics of rotors, each control channel contains nonlinearities which are neglected in the nominal design model. The most significant of these imposes the greatest dynamic constraint on performance, and is the rate limit on the control effect.

An approximate model for rate limits on the C-141 is

$$\dot{u} = R_{\text{lim}} \text{SAT} \left[\frac{94(u_c - u) R_{\text{lim}}}{R_{\text{lim}}} \right]$$

where $\text{SAT}(\cdot)$ denotes the standard saturation function. A more detailed model can be developed with Safonov's procedure, but the resulting bounds are not needed. These bounds will of course depend on the rotor dynamics, and the solid lines in Figure 10 depict the effect of the rate limit on the magnitude of $\bar{\sigma}[L]$ for the argument of the SAT function. The effect of the rate limit is most significant at frequencies. This is not surprising since the rate limit is a nonlinear effect which will have a significant effect on the system response at high frequencies.

The third major source of model uncertainty is the variation of A, B matrices with flight condition. Such "component" variation could again be translated into an overall bound for $L(s)$ via Safonov's procedure. In this case, however, the result would be unduly conservative because coefficient variations tend to be highly correlated and are not arbitrary dynamical operators. A more direct way to compute the bound is to compute the loop transfer matrix for a number of representative flight conditions and then compute the maximum (singular value) deviation. Results of this process are shown by the dotted line in Figure 11. We see the (initially surprising result that $\bar{\sigma}[L]$ becomes quite large at low frequencies. This happens because the basic helicopter's low frequency modes are stable at some flight conditions and unstable at others. Theoretically, $\bar{\sigma} G(j\omega)$ will approach infinity for frequencies and flight conditions where these modes cross the $j\omega$ -axis. This means that the perturbations exhibited by our plant are not necessarily stable and, hence, the stability-robustness result cited earlier fails to apply. We will see later that stable controllers can still be obtained and that the ability to incorporate unstable L's in a generalized multivariable stability robustness theory appears to be an important research topic. For the moment, however, our designs will be restricted to individual flight conditions for which the dotted L's in Figure 11 can be disregarded.

The uncertainty bounds shown in Figure 11 indicate that the robustness criterion given by equation (5) imposes a "multivariable bandwidth" limitation on the feedback loop. Magnitudes of $L(j\omega)$ tend to be large beyond certain frequencies which requires G^{-1} to be large and consequently G must be small. This is most readily illustrated with a single loop example where plots of the function $\underline{\sigma}[1+g^{-1}]$ reduce to the inverse closed loop frequency response, i. e.,

$$\underline{\sigma}[1+g^{-1}] = \left[\frac{1+g}{g} \right] = \left[\frac{1}{g_{cl}} \right] \quad (55)$$

The condition that $\underline{\sigma}[1+g^{-1}]$ be large then translates directly into the high-frequency "roll-off" requirement commonly imposed on classical control loops.

For illustrative purposes, single-loop and multi-loop designs will be described.

The vertical velocity and pitch attitude motions of the nominal CH-47 model at hover uncouple naturally into two non-interacting channels -- (z, x_5) controlled by (c), and (v, q, θ, x_6) controlled by (dc). The hover flight condition thus offers an attractive single-loop design case. Sigma plots for several trial pitch-motion controllers for this case are shown in Figure 12. These controllers were all designed with the linear-optimal methodology and correspond to the following cost functional:

$$J = \int_0^{\infty} \left[(57.3 x_6)^2 + \rho (dc)^2 \right] dt \quad (56)$$

with $\rho = 900., 9.0, 0.09,$ and $1.0,$ respectively, for the four trials. These weights were selected in accordance with the asymptotic procedure described in reference [2.19]. The asymptotic modes corresponding to these weights are a forward speed mode with an eigenvalue near the origin and a third order Butterworth pattern for the remaining modes. As expected, bandwidth of these controllers increases with decreasing ρ and eventually violates the stability-robustness constraint imposed by neglected rotor dynamics (for the moment we ignore rate limit and flight condition variations). That this violation actually produces instabilities was verified by computing closed-loop roots of the trial controllers in the presence of the rotor. Trial 3 is unstable! Our options are therefore to restrict bandwidth to approximately Trial 2 or to provide additional roll-off beyond the maximum 20 db/decade attenuation inherent in LQ-design [2.20]. The latter option is illustrated by Trial 4 which uses a ρ -value somewhat smaller than Trial 2 but includes a low-pass filter at $\omega=12$ rad/sec to help avoid the rotor resonance peak. Note that the closed loop frequency responses* are well-shaped for all pure LQ-trials and that Trial 4 achieves extra bandwidth at the expense of slightly larger M-peaks.

The beauty of singular values is that the above stability-robustness analyses carry over without change to multivariable systems. This is illustrated in Figure 13 with some two-channel trial designs at a 40 knot forward speed flight condition. These controllers are again of the LQ-type, this time using the cost function,

$$J = \int_0^{\infty} \left[(x_5)^2 + (57.3 x_6)^2 + \rho_1 (c)^2 + \rho_2 (dc)^2 \right] dt, \quad (57)$$

with $(\rho_1, \rho_2) = (10000, 900), (9.0, 9.0),$ and $(1.0, 1.0)$ for the three trials shown. The distinction between Figure 12 and 13 is that Figure 13 shows two sigma-plots for each trial, corresponding to the two singular values of $(1+G^{-1})$. For stability-robustness, the smaller of these values must fall above the sigma-plot of L at all frequencies. The larger value is unspecified. However, in order to maximize bandwidth "in all directions", it is reasonable to adjust the relative weights (ρ_1, ρ_2) such that the two singular values are approximately equal and then to push them jointly to as high a bandwidth as the $\bar{\sigma}[L]$ plot permits.

* According to (55), these are given by the sigma-plots of Figure 12 viewed "upside down".

(For the moment, we again use only neglected rotor dynamics for L.) This design philosophy is incorporated in the three trials of Figure 13. The first trial has low bandwidth and substantial differences between the two singular values. These differences are reduced and bandwidth is increased in the next trial. The third trial serves to maximize bandwidth by using additional roll-off filters in each control channel.

As seen from these trials, singular value analyses appear to offer a convenient way to maximize multivariable bandwidth subject to stability-robustness limitations. The next design step is to achieve reasonable command responses from the resulting feedback loop. One way to do this is to place a command shaping filter ahead of the loop. For feedback loops with integral control on the primary responses, such sophistication is often unnecessary because commands inserted at the integrators (as shown in equation (49)) produce good transients. This is the case here, as evidenced by the responses of Trial 3 to step attitude and step velocity commands shown in Figure 14. Note that the loops are tight, well damped, and non-interacting as desired.

So far we have ignored model uncertainties due to rate limits. This was done because there is no a priori way to select the parameter η for Figure 11, which is determined by the maximum magnitudes of signals in the closed loop. Clearly, for η sufficiently large all our trial designs would violate the resulting $\bar{\sigma}[L]$ bound. That such violations actually correspond to instabilities was verified by repeating the transient responses for Trial 3 with progressively larger attitude commands. Unstable behavior occurs for $\theta_{cmd} \geq 18$ degrees, with $\eta \approx 60$.

In order to improve robustness with respect to rate limits, the following iterative procedure may be used:

- 1) Assume a signal level limit $\eta \leq \eta_0$
- 2) Design $I + G^{-1}$ consistent with the resulting $\bar{\sigma}[L]$
- 3) Evaluate the actual maximum signal level, η_1 , by computing transient responses with worst case commands and/or initial conditions
- 4) If η_1 and η_0 are substantially different, return to step 1 with $\eta_0 = \eta_0 + \epsilon(\eta_1 - \eta_0)$ where ϵ is a design parameter. Otherwise STOP.

An illustration of the first iteration of this procedure is given in Figure 13 where the assumed signal level $\eta_0 = 20$. (The dashed $\bar{\sigma}[L]$ curve) yields a controller (Trial 2) whose actual signal level is $\eta_1 < 0.6$. The associated transient responses are slow but stable. To fine tune this design, a second iteration might be taken with $\eta_0 = 5$.

We noted earlier that $\bar{\sigma}[L]$ due to operating point changes becomes quite large at low frequencies because the helicopter's slow modes are not stable at all operating points. At intermediate and high frequency ranges, however, the uncertainty bounds are reasonably small (Figure 11). This suggests that if the loop transfer matrix $G(s)$ has sufficient low frequency gain to stabilize the slow modes under all conditions, then the design might well be stable even though the (sufficient) stability-robustness condition fails. This is in fact the case. Both trial design No. 2 and No. 3 remain stable at 8 representative flight conditions ranging from hover to 160 knot forward speed and from +2000 ft/min to -2000 ft/min ascent rates. The intuitive idea which underlies this result (sufficiently high low-frequency gain) may well provide needed insight toward a generalized multivariable robustness theory for unstable perturbations.

This example illustrates that the linear optimal approach may be combined with singular value analyses to provide a useful multivariable technique. In this illustrative example the use of a state estimator in the loop was not considered. But, in the general linear optimal approach the inclusion of such an estimator must be considered.

2.2.7 Robust Estimators

It was shown in reference [2.21] that multivariable linear-optimal regulators using full state feedback have impressive robustness properties, including guaranteed gain margins of -6 db and +6 db and phase margins of 60° in all channels. But, if observers or Kalman filters are used for state estimation in the implementation, there are no guaranteed margins. [2.22] Fortunately, an adjustment procedure is available [2.23] for use in the observer or filter design which makes it possible to essentially recover the guaranteed margins of full state feedback for minimum phase systems. This adjustment procedure involves the introduction of a scalar design parameter, q , with the property that as q tends to infinity the stability margins tend to the full state margins.

An example that illustrates this adjustment procedure is a linear optimal regulator designed for flutter suppression with the DAST (Drones for Aerodynamic and Structural Testing) wing. A single control surface input and two accelerometer outputs were used in the design. The model consisted of five flexure modes, five aerodynamic lags, a third order actuator, and a first order wind gust model.

The robustness of five controllers is summarized in Table 3 and Figure 15. The first controller is the full state feedback controller. The second uses a Kalman filter for state estimation. The remaining three use filters for state estimation derived using the adjustment procedure with different values of the design parameter, q . In addition to the stability margin data, the RMS control surface activity corresponding to an RMS gust input of one ft/sec is given as well as the controller bandwidth. The stability margins actually increase monotonically with q with an attendant increase in control surface activity. But, the control surface activity corresponding to the largest value of q was within the design specification limits and the stability margins for this value of q are significantly improved over the $q = 0$ case and are nearly as good as those of the full state feedback controller. As shown in the frequency response plots of Figure 15 the robust estimators smooth out the notching characteristics of the Kalman filter providing better stability margins with only a slight degradation in RMS performance. This example clearly demonstrates the utility of the adjustment procedure.

2.3 Digital Design

The techniques described above do not explicitly address a digital mechanization of flight control designs. They are, of course, all applicable to digital system design and analysis lacking only in a transformation from continuous to discrete space. In fact the most common design scenario for a digital flight control law has evolved using continuous system techniques. The steps generally followed are

1. Design the feedback structures using continuous techniques to achieve performance and sensitivity goals (i. e., stability margins) for the continuous plant-controller.
2. Choose a sample time with a Nyquist frequency well above the control frequencies and discretize the continuous compensators using appropriate algorithms such as Z-transform, Tustin's method, or Prewarped Tustin's method.
3. Choose a first or second order continuous prefilter for each sensor to eliminate the impact of aliasing from unmodeled high frequency dynamics such as structural modes or high band sensor noise. This is typically chosen conservatively low, i. e., well below the Nyquist frequency.
4. Select a control command output continuous postfilter (also thought of as an actuator prefilter) with an output hold device to reduce the effects of digital quantization but obtain minimum phase loss at the control frequencies.

Steps 2, 3, and 4 provide a sufficient scenario to implement a digital representation yielding the desired flight control goals of step 1.

The major difficulty with this approach is that these steps all contribute phase lag to the system. This presents little problem if the sample rate is sufficiently higher than the stability crossover frequencies. Lowering the sample rate results in stability difficulties and performance reduction. The net result is a design technique which dictates high sample rates. This represents the state of the art in digital design techniques for production aircraft systems today.

2.3.1. Low Sample Rate Design

It has been claimed that designing directly with discrete plant models will produce lower sample rates and minimum compensation and still meet the same design goals as analog conversion techniques. This has led to a number of design techniques and tools which do result in low sample rates [2.24], [2.25]. The direct digital design technique described in reference [2.24] is based on an optimization approach formulated to match a modeled transient response at discrete time points. The feedback control law, gains and compensation parameters, are designed to force the closed loop response of a discretized plant, (including pre and post filters) to best fit a desired response transient at the discretized points. This technique was utilized by Peled to examine prefilter and sample rate selection [2.26]. As an example of the technique, a direct digital design was performed for a digital feedback around a simple integrator which attempted to match a desired closed loop exponential response.

Shown in Figure 16 the optimization technique results in parameter selections for K , α , and β , for a fixed sample time, T , and prefilter bandwidth, a . These parameters are synthesized to fit the discrete points generated at the sample instances of a unit step response of a continuous feedback control design (Figure 16-a). Details are given in reference [2.26], with a summary provided in reference [2.27].

The key point for discussion is not the optimization but what it produced. Examining the plant to be operated on

$$\frac{D(z)}{E(z)} = \frac{z-1}{z} \cdot z \cdot \left[\frac{1}{s^2 \left(\frac{s}{a} + 1 \right)} \right]$$

$$= \frac{J_1(T) (z - \beta_0)}{(z-1) (z - \alpha_1)}$$

where as shown in reference [2.28]

$$J_1(T) = T + \frac{e^{-aT}}{a} - \frac{1}{a}$$

$$\alpha_1 = e^{-aT}$$

$$\beta_0 = \frac{1 - \alpha_1 - aT\alpha_1}{1 - \alpha_1 - aT}$$

The inclusion of an extra discrete zero, β_0 , along with the prefilter pole, α_1 , form the basis for the selection of the compensator parameters in Figure 16-b, α_c and β_c .

In almost all cases examined in reference [2.26], i. e., choices of T and a, α_c was optimized to cancel β_0 and β_c optimized to cancel α_1 . The effect of this cancellation is characterized by lead compensation near the Nyquist frequency and results in total system phase enhancement.

2.3.2 F-8 Design Example

The compensation structure suggested by this technique was used to develop a low sample rate design for the NASA Digital Fly-by-wire F-8C CCV aircraft. The F-8 digital system operates at 53.33 Hz due to a remote augmented vehicle (RAV) implementation. Analysis determined that the system could operate at 20 Hz with no significant degradation in aircraft stability and performance characteristics and with no phase enhancement applied through direct digital design techniques. F-8 Flight tests had indicated unsatisfactory performance at 6.7 Hz. Application of phase enhancement through direct digital design permitted a 4 Hz sample rate [2.28]. A comparison of the continuous and low sample rate control structure block diagrams is shown in Figure 17. Table 4 presents a comparison of pitch axis stability margins for the continuous design and the low sample rate design at four flight conditions. A comparison of frequency response plots for FC#1 is shown in Figures 18 and 19. Transient response comparisons are given in Figures 20 and 21.

These results have not been verified in man in the loop simulation or flight test, however they do indicate lower sample rates are achievable based on analytical design criteria. A limiting factor not discussed but which also must be recognized is the effect of output quantization in the actuator command signals. Smoothing techniques will generally provide adequate performance in this area.

3.0 CONCLUSIONS AND RECOMMENDATIONS

Because of the number of control inputs and close dynamic coupling of future aircraft, and requirements that the flight control system provide the stabilizing influence on the vehicle, efficient and reliable control system design and analysis techniques are essential to satisfactory aircraft performance. Several techniques have been discussed in this chapter. Modal control techniques permit the designer to handle a large number of inputs and provide an approach to achieve a desired, within constraints, system response. A technique based on asymptotic regulator properties reduces the weight selection difficulties associated with optimal regulator design in a root locus equivalent design approach. We have shown how to design in stability margins for Kalman filters in the loop with the robust estimator technique. The most powerful technique of all, however, is the use of singular values in analyzing the stability characteristics of multivariable systems. Further research is required in this area particularly in transforming it into a synthesis and design technique. Questions exist on the possible conservative nature of the stability margins computed with singular value analyses. Research is currently being done in this area. We firmly believe that stability margins may one day be specified for multivariable systems based on singular value analysis.

More complex design issues which arise when subsystems are integrated in design have not been addressed in this chapter. Tight pointing and tracking requirements for today's fighter aircraft will result in overlapping bandwidths between the flight and fire control systems. Design criteria for the two systems are not always homogenous and are often conflicting. New techniques are needed to handle multiple dissimilar design criteria.

In the singular value analysis discussion, techniques for analyzing the effect of nonlinearities were described. While these can be a powerful tool, much work still needs to be done in treating system nonlinearities.

Finally, digital control is still in its infancy. Designers are still trying to make digital systems look like their analog counterparts. Work is ongoing today in the area of finite state machines to try and discover the real power of digital structures for control application.

REFERENCES

- 2.1 H.H. Rosenbrock, "Design of multivariable control systems using the inverse Nyquist array," Proc. IEEE, Vol. 116, pp. 1929-1936, 1969.
- 2.2 H.H. Rosenbrock, Computer-aided Control System Design, Academic Press, London, 1974.

- 2.3 A.G.J. MacFarlane and B. Kouvaritakis, "A design technique for linear multivariable feedback systems," In. J. Control, Vol. 25, pp. 837-874, 1977.
- 2.4 A.G.J. MacFarlane and I. Postlethwaite, "Characteristic frequency functions and characteristic gain functions," Int. J. Control, Vol. 26, pp. 265-278, 1977.
- 2.5 J.D. Simon and S.K. Mitter, "A theory of modal control," Inform. & Contr., Vol. 13, pp. 316-353, 1968.
- 2.6 B.C. Moore, "On the flexibility offered by state feedback in multivariable systems beyond closed loop eigenvalue assignment," IEEE Trans. AC-21, pp. 685-692, 1976.
- 2.7 B.C. Kuo, Automatic Control Systems, Prentice-Hall, 1967.
- 2.8 J.W. Brewer, Control Systems, Prentice-Hall, 1974.
- 2.9 I.M. Horowitz, Synthesis of Feedback Systems, Academic Press, 1963.
- 2.10 J.H. Wilkinson, The Algebraic Eigenvalue Problem, Clarendon Press, 1965.
- 2.11 G.E. Forsythe and C.B. Moler, Computer Solutions of Linear Algebraic Systems, Prentice-Hall, 1967.
- 2.12 C.A. Harvey and J.C. Doyle, "Optimal Linear Control (Characterization and Loop Transmission Properties of Multivariable Systems)," ONR Report CR215-238-3, 1978.
- 2.13 A.G.J. MacFarlane and I. Postlethwaite, "The Generalized Nyquist Stability Criterion and Multivariable Root Loci," Int. J. Control, Vol. 23, No. 1, pp. 81-128, January 1977.
- 2.14 G. Stein and A.H. Henke, "A design procedure and handling quality criteria for lateral-directional flight control systems," AFFDL-TR-70-152, May 1971.
- 2.15 C.A. Harvey and G. Stein, "Quadratic weights for asymptotic regulator properties," IEEE Trans. AC-23, pp. 378-387, 1978.
- 2.16 A.J. Ostroff, D.R. Downing and W.J. Road, "A technique using a nonlinear helicopter model for determining terms and derivations," NASA Technical Note TN D-8159, NASA Langley Research Center, May 1976.
- 2.17 R.H. Hoheuemser, and S. Yin, "Some Applications of the Method of Multiblade Coordinates," J. Am. Helicopter Soc., July 1972.
- 2.18 M.G. Safonov, "Tight Bounds on the Response of Multivariable Systems with Component Uncertainty," 1978 Allerton Conference.
- 2.19 G. Stein, "Generalized Quadratic Weights for Asymptotic Regulator Properties," IEEE Trans. AC-24, pp. 559-566, 1979.
- 2.20 R.E. Kalman, "When is a Linear System Optimal?" J. Basic Engrg., Vol. 86, pp. 51-60, 1964.
- 2.21 M.G. Safonov and M. Athans, "Gain and phase margin for multiloop LQG regulators," IEEE Trans. AC-22, pp. 173-176, 1977.
- 2.22 J.C. Doyle, "Guaranteed margins for LQG regulators," IEEE Trans. AC-23, pp. 756-757, 1978.
- 2.23 J.C. Doyle and G. Stein, "Robustness with observers," IEEE Trans. AC-24, pp. 607-611, 1979.
- 2.24 P.H. Whitaker, "Development of a Parameter Optimization Technique for the Design of Automatic Control Systems," NASA CR-143844, May 1977.
- 2.25 R.F. Whitbeck, and L.F. Hofmann, "Analysis of Digital Flight Control Systems with Flying Qualities Applications," AFFDL-TR-78-115, September 1978.
- 2.26 U. Peled, "A Design Method with Application in Prefilter Design and Sampling-Rate Selection in Digital Flight Control Systems," Dept. of Aero/Astro, Stanford Univ., Stanford, CA 94303 SUDAAR Rept, 512.
- 2.27 U. Peled, and J.F. Powell, "The Effect of Prefilter Design on Sample Rate Selection in Digital Flight Control Systems," AIAA paper 78-1308, 1978.
- 2.28 T.B. Cunningham, "A Low Sample Rate Design for the F-8 Aircraft," 3rd. Digital Avionics Systems Conference, Ft. Worth, Texas, 6, 7, 8 November 1979.

TABLE 1. AIRCRAFT CONTROL SYSTEMS EARLY TO CURRENT OPERATIONAL SYSTEMS

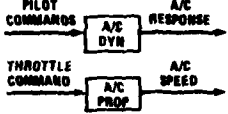
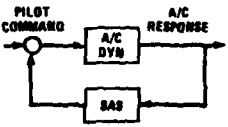
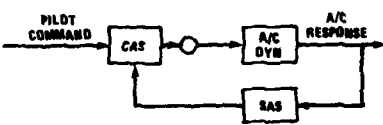
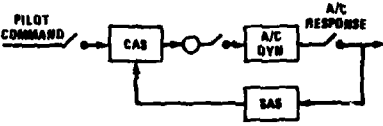
APPLICATION	REQUIREMENTS	CHARACTERIZATION	DESIGN & ANALYSIS
4 DOF STATICALLY STABLE AIRCRAFT	STABLE AND CONTROLLABLE AIRFRAME		AIRFRAME STABILITY AND CONTROL
↓	+ IMPROVED A/C STABILITY CHARACTERISTICS		+ STABILITY ANALYSIS TECHNIQUES BODE PLOTS NYQUIST PLOTS NICHOLS PLOTS ROOT LOCUS TRANSIENT RESPONSE ANALYSIS-SIMULATION
	+ IMPROVED A/C RESPONSE		+ MULTIVARIABLE CONTROL TECHNIQUES???
↓			+ DIGITAL SYSTEM STABILITY ANALYSIS Z-PLANE W-PLANE

TABLE 2. AIRCRAFT CONTROL SYSTEMS CURRENT EXPERIMENTAL SYSTEMS AND PROJECTED

APPLICATION	CURRENT REQUIREMENTS	CHARACTERIZATION	DESIGN & ANALYSIS
CCV	STABLE AND CONTROLLABLE CLOSED LOOP AIRCRAFT SYSTEM		CLASSICAL STABILITY ANALYSIS TECHNIQUES, MULTIVARIABLE CONTROL TECHNIQUES?, TRANSIENT RESPONSE ANALYSIS-SIMULATION
CCV + 6DOF	IMPROVED MANEUVERABILITY CAPABILITY		MULTIVARIABLE CONTROL TECHNIQUES?
	INTEGRATE WITH GUIDANCE FIRE CONTROL PROPULSION CONTROL WEAPON DELIVERY STRUCTURAL CONTROL		MULTIVARIABLE CONTROL TECHNIQUES
	FOR IMPROVED PERFORMANCE AND RELIABILITY AT LOWER POWER, SIZE, WEIGHT AND COST		MULTIVARIABLE OPTIMIZATION TECHNIQUES

TABLE 3. ROBUSTNESS SUMMARY FOR DAST EXAMPLE

Controller	q	RMS		Gain Margin				Phase Margin				Bandwidth Hz
		δ	δ̇	Db	Hz	Db	Hz	Deg	Hz	Deg	Hz	
State	.0	1.804	164.9	-8.1	9.90	-	—	-63.7	7.05	+82.3	15.25	23.2
Kalman	.0	2.330	186.2	-5.3	10.28	+6.4	21.87	-42.5	8.26	+32.4	13.64	59.8
Robust	.000001	2.733	196.8	-6.6	9.85	20.0	75.28	-45.4	7.46	+66.2	13.56	19.3
Robust	.00001	3.066	212.0	-7.3	9.87	21.5	103.56	-53.3	7.23	+72.9	14.23	11.1
Robust	.0001	3.534	240.2	-7.7	9.90	24.9	149.65	-57.9	7.16	+76.3	14.64	21.8

TABLE 4. PITCH AXIS STABILITY MARGINS

Flight Conditions	1		5		9		17	
	Cont.	4 hz						
Gain Margin (db)	>40	7.0	>40	7.3	>40	6.4	>40	6.1
Phase Margin (deg)	78°	63°	72°	50°	81°	90°	80°	48°

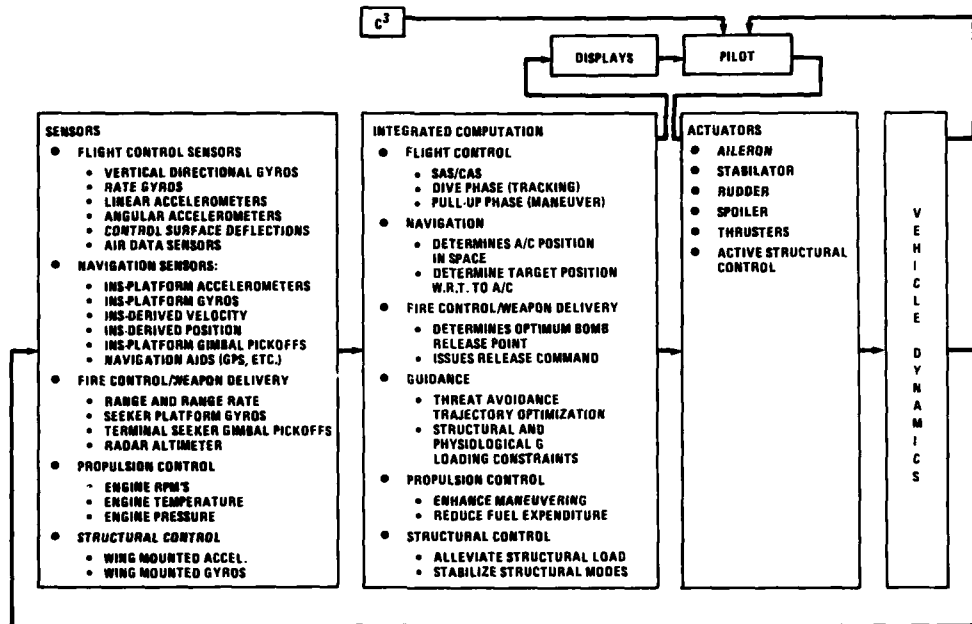


Figure 1. Integrated System Representation

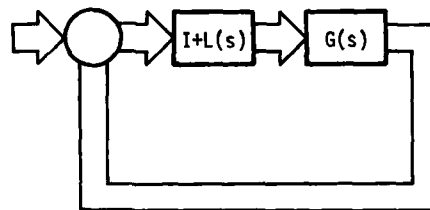


Figure 2. Linear Feedback System with Multiplicative Perturbation

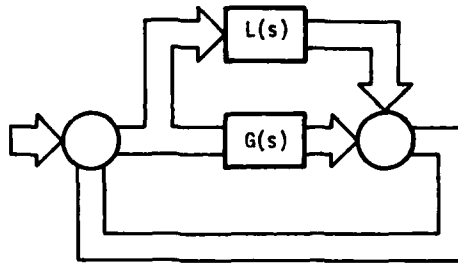


Figure 3. Linear Feedback System with Additive Perturbation

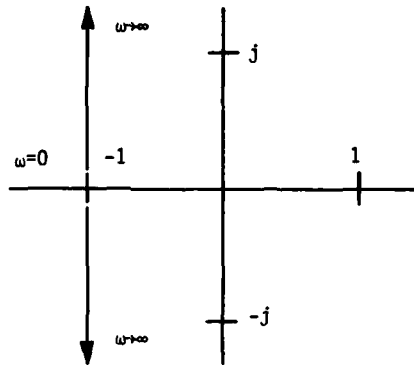


Figure 4. Z-Plot for the First Example

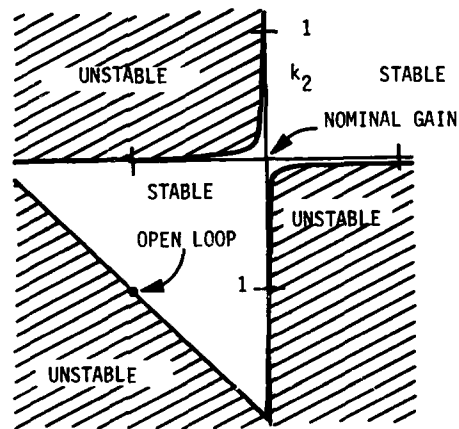


Figure 5. Stability Domain for the First Example

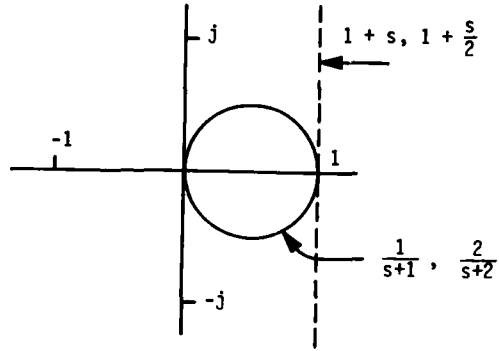


Figure 6. Nyquist and Inverse Nyquist Diagram for the Second Example

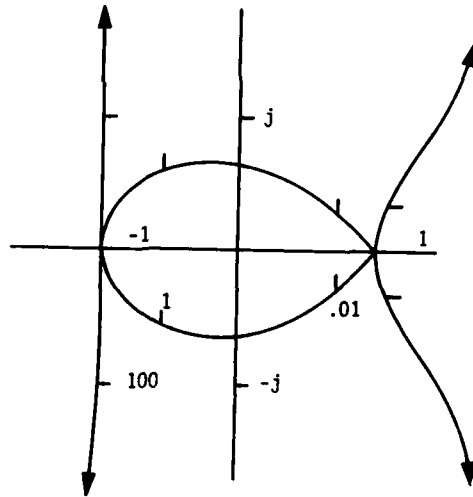


Figure 7. Z-Plot for the Second Example

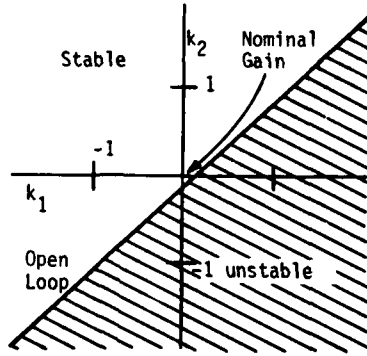


Figure 8. Stability Domain for the Second Example

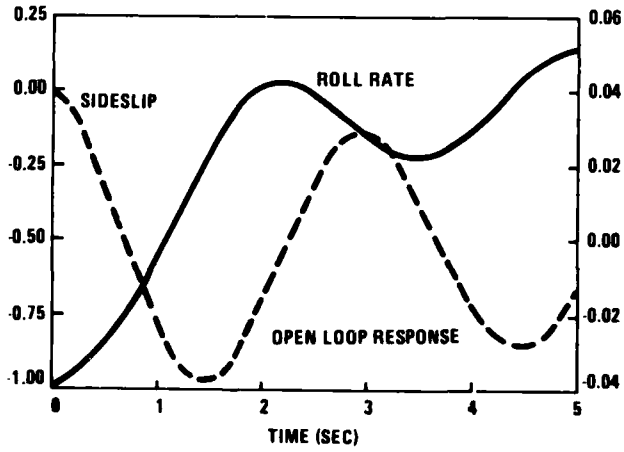


Figure 9. F-4 Lateral-Directional Open-Loop Response

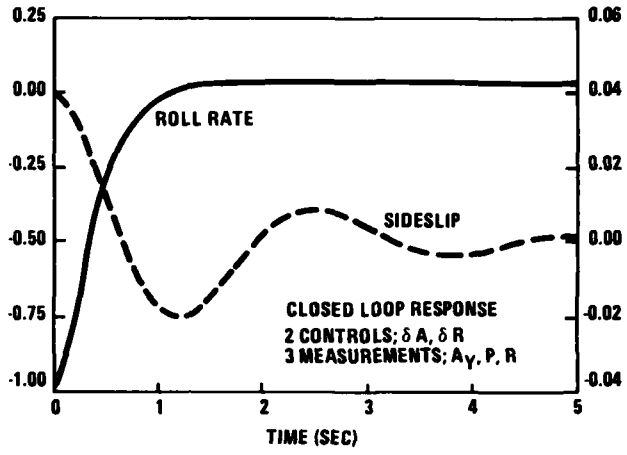


Figure 10. F-4 Lateral-Directional Closed-Loop Response

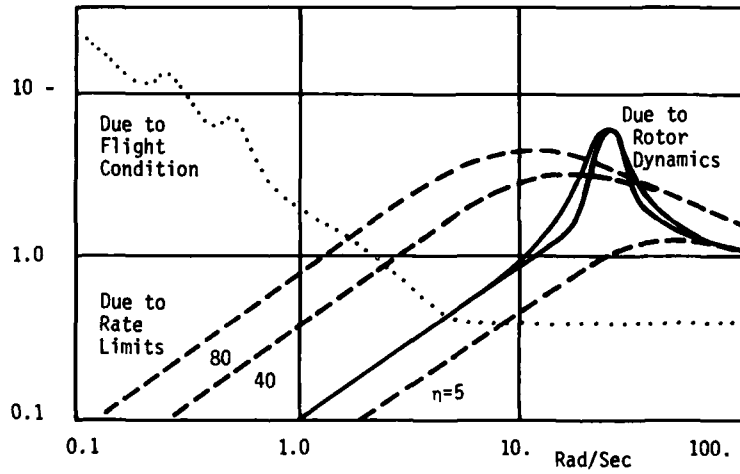


Figure 11. $\sigma(L)$ Bound

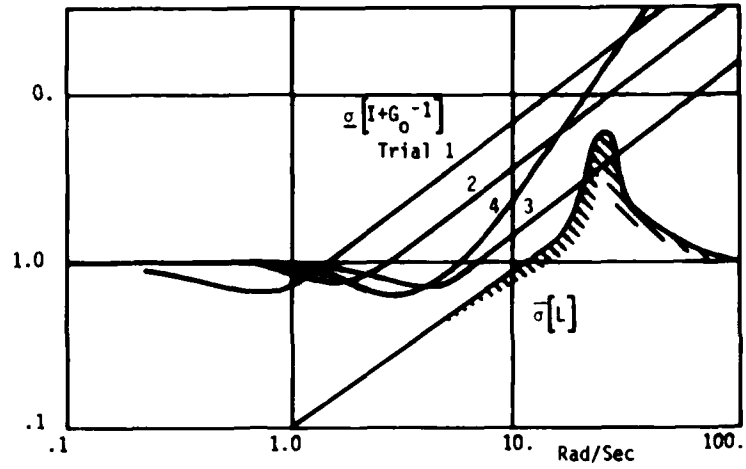


Figure 12. Trial Designs for Pitch Control at Hover

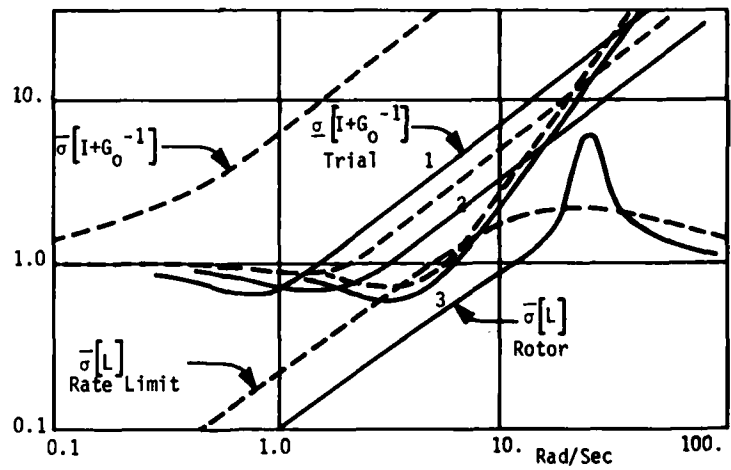


Figure 13. Trial Designs for Pitch and Vertical Velocity Control

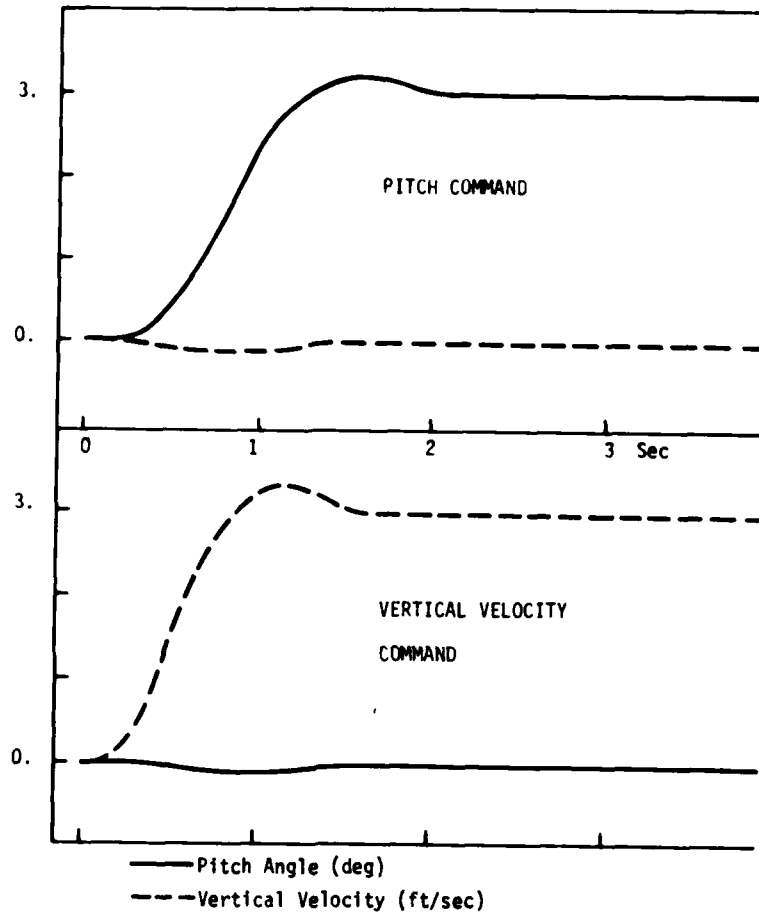


Figure 14. Transient Responses (Trial 3)

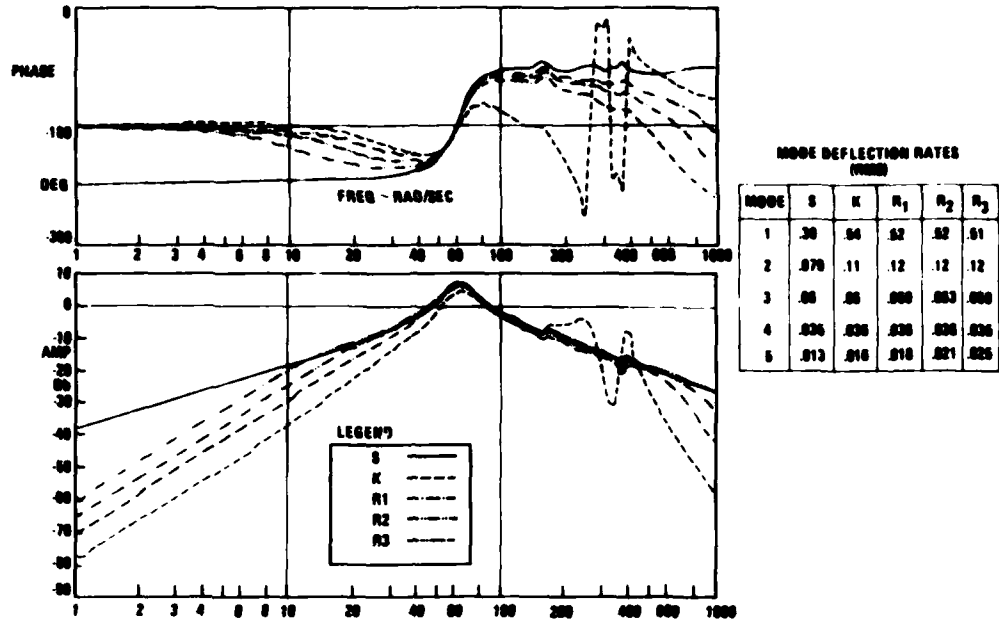


Figure 15. Robust Estimator Characteristics for DAST Example

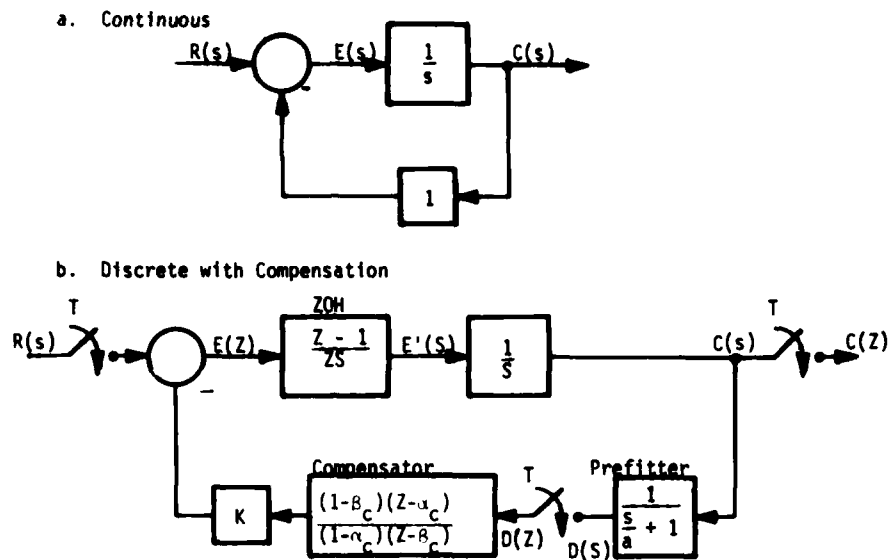


Figure 16. Peled's First Order Example

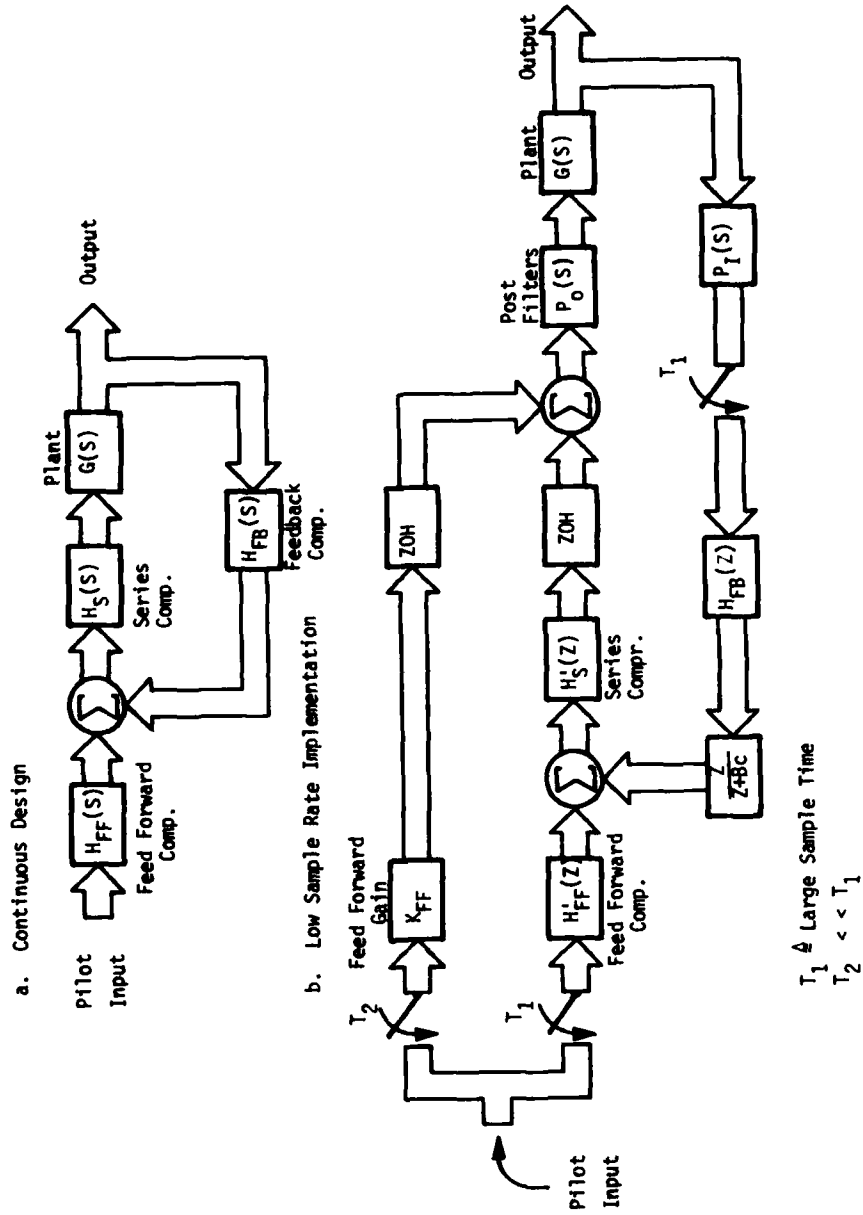
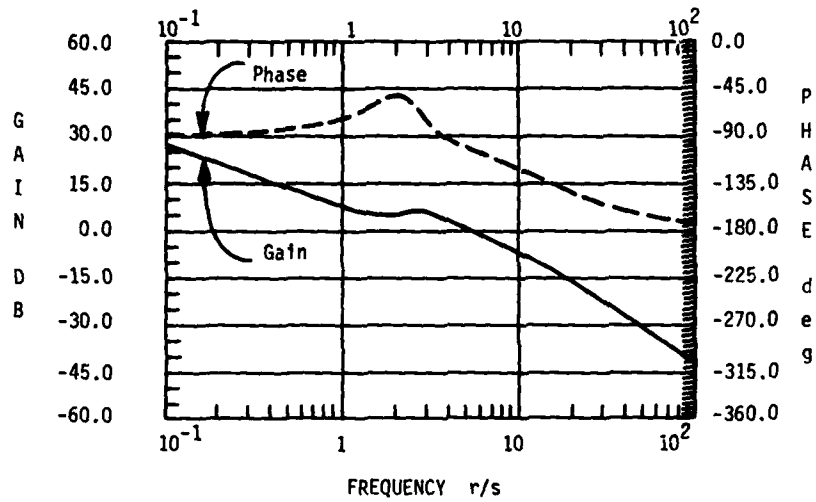


Figure 17. Low Sample Rate Control Implementation



Flight Condition #1

Gain Margin = 59 db
 Phase Margin = 78°
 Cross Over Frequency = 5.2 rad/sec.

Figure 18. Pitch Axis Open-Loop Response (continuous)

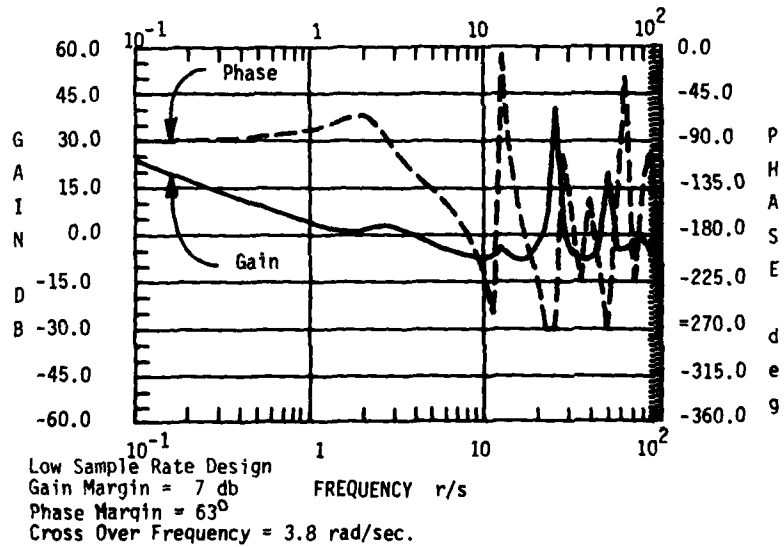


Figure 19. Pitch Axis Open-Loop Frequency Response (low sample rate)

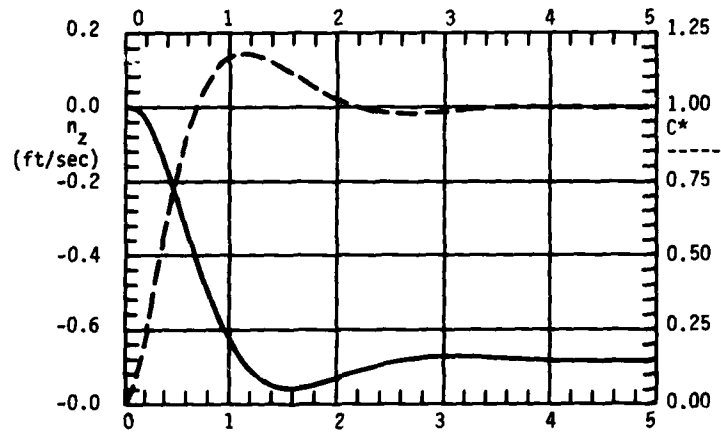


Figure 20. Pitch Axis Transient Response (continuous)

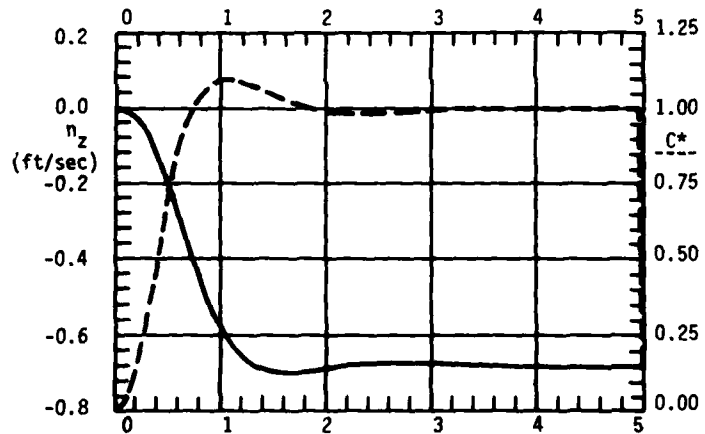


Figure 21. Pitch Axis Transient Response (low sample rate)

PRACTICAL DESIGN AND REALIZATION OF A
DIGITAL ADAPTIVE FLIGHT CONTROL SYSTEM *)

by

V. Krebs and U. Hartmann

Bodenseewerk Gerätetechnik GmbH
Postfach 11 20, D 7770 Überlingen
Federal Republic of Germany

SUMMARY

A new approach for the design and the practical realization of a digital adaptive command- and stability system is proposed. The control law for the longitudinal motion of the aircraft is obtained by state vector feedback using the MIL-F-8785 B handling qualities requirements. The design principle is based on decoupling of the angle of attack and pitch rate on the one hand and the pole allocation method for the eigenvalues of the control system on the other hand. Since the necessary gain factors contain unknown and variable aircraft parameters an on-line fading-memory least squares algorithm for the estimation of these parameters is used.

Only conventional aircraft sensors (rate gyros and accelerometers) and an airborne digital computer are necessary. Hybrid simulations of the complete system as well as flight test results demonstrate the efficiency of the concept.

1. INTRODUCTION

Advanced high performance aircraft show drastic changes of their dynamic characteristics which are caused by a variety of aerodynamic and configuration parameters. Therefore we are faced with the need for proper adaptation of the control loops. A usual approach to solve the adaptation problem is to measure a few of these parameters and to preprogram the controller gains as a function of them. Generally this is a tedious task and in some cases it is difficult to meet the handling qualities requirements.

Therefore we observe efforts to solve these problems via self-adaptive solutions since more than two decades (/1/,/2/). In the development of a self-adaptive flight control system -by reason of simplicity in the sequel called only "adaptive control system"- three basic questions must be answered:

- How can we satisfy the handling qualities requirements? This is the basic concern because the adaptive approach has to provide better results than the programmed approach or at least the same ones with considerable less expense. The resulting handling qualities have to be documented and verified, therefore an easily understood design process is an obvious need.
- How can we identify the essential parameters of the aircraft model? In fact the parameter estimation is another essential part of the design process. Only a limited number of parameters should be required by the adaptation mechanism because the difficulties of parameter identification increase significantly with the number of parameters to be identified.
- How can we provide software and hardware reliability? Early attempts in the history of adaptive flight control have used analog hardware, but the problems of a rather complex signal processing and of pre- and inflight-testing could not be solved with this technology. The advent of powerful microprocessors has now changed these basic technical aspects of the problem: The digital hardware allows the reliable realization of complex signal processing algorithms and detailed testing procedures. Nevertheless a remarkable part of the reliability problems has been shifted to the software field. Strong efforts have to be carried out that no software malfunction deteriorates the reliability figures of the whole system.

The approach presented in this contribution has been evolved during some years (/3/,/4/,/5/). Recently flight tests have been carried out which demonstrated the proper function of the adaptive control system. The paper describes shortly the design principle and the identification process of the system. In a further chapter the realization of the adaptive controller and some typical data of interest will be documented. Finally significant results so far obtained in digital and hybrid simulations as well as in flight tests are discussed.

*) This work was supported by the ministry of defense of the Federal Republic of Germany under grant T/R 421/70002/72400.

2. DESIGN PRINCIPLE

The design approach of the adaptive control system is based on the principles of state vector feedback and pole assignment and has been described in detail (/4/). In the following we will give a short introduction to the basic ideas using well known root locus techniques. By reason of clarity the actuator dynamics will be considered negligible in treating the aircraft dynamics. Actually the realization of the adaptive control system took account of the actuator dynamics (Chapter 5).

Basically we are following two main steps in the design procedure of the control system. First we are decoupling the angle of attack and the pitch motion of the aircraft.

For this purpose in aircraft with static stability a positive feedback of the angle of attack is required. In the dynamics of the controlled aircraft we find therefore motions with varying angle of attack and elevator deflection but without any change in pitch, i.e. the influence of the angle of attack is completely compensated. In the second step we have to satisfy the handling qualities requirements concerning the frequency and the damping of the short period mode. This will be done by using a proper feedback of pitch angle and pitch rate.

Following this approach it should be noted that the feedback gain of the angle of attack on the one hand and the gains of pitch angle and pitch rate on the other hand are completely independent: The angle of attack gain depends only on the aerodynamic characteristics of the aircraft whereas the pitch angle and pitch rate gains depend on both, the aerodynamic characteristics and the handling qualities requirements.

This will be shown using the basic linearized state vector equation

$$\dot{\underline{x}}(t) = \underline{A} \underline{x}(t) + \underline{B} \cdot \Delta \eta \quad (1)$$

of the longitudinal motion of aircraft. With the state vector definition

$$\underline{x} = [\Delta \theta, \Delta q, \Delta \alpha, \Delta u]^T$$

$\Delta \theta$ = pitch angle
 Δq = pitch rate
 $\Delta \alpha$ = angle of attack
 Δu = forward velocity
 $\Delta \eta$ = elevator deflection

we have in general the following system matrices

$$\underline{A} = \begin{bmatrix} 0 & 1 & 0 & 0 \\ a_{21} & a_{22} & a_{23} & a_{24} \\ a_{31} & a_{32} & a_{33} & a_{34} \\ a_{41} & a_{42} & a_{43} & a_{44} \end{bmatrix}, \quad \underline{B} = \begin{bmatrix} 0 \\ b_{21} \\ b_{31} \\ b_{41} \end{bmatrix} \quad (2)$$

and the feedback law

$$\Delta \eta = \underline{k}^T \underline{x} = [K_\theta, K_q, K_\alpha, K_u] \cdot \underline{x} \quad (3)$$

It can be shown (/4/) that the forward velocity Δu has only a negligible influence on the short period mode of the aircraft. Furtheron the relation between pitch angle and pitch rate is purely kinematic. Therefore we proceed to a simplified state vector equation describing only the short period mode of the aircraft dynamics

$$\begin{bmatrix} \dot{\Delta q} \\ \dot{\Delta \alpha} \end{bmatrix} = \begin{bmatrix} a_{22} & a_{23} \\ a_{32} & a_{33} \end{bmatrix} \cdot \begin{bmatrix} \Delta q \\ \Delta \alpha \end{bmatrix} + \begin{bmatrix} b_{21} \\ b_{31} \end{bmatrix} \cdot \Delta \eta \quad (4)$$

and the corresponding transfer functions (b_{31} is usually very small, $a_{32} \approx 1$)

$$\frac{\Delta q}{\Delta \eta}(s) = \frac{b_{21}(s+s_0)}{C(s)} \quad (5)$$

$$\frac{\Delta \alpha}{\Delta \eta}(s) = \frac{b_{31}(s+s_0)}{C(s)} \quad (6)$$

$$\text{with } s_q = \frac{b_{31} a_{23} - b_{21} a_{33}}{b_{21}}, \quad s_\alpha = \frac{b_{21} a_{32} - b_{31} a_{22}}{b_{31}}$$

and the characteristic equation

$$C(s) = s^2 - (a_{22} + a_{33})s + a_{22} a_{33} - a_{23} a_{32} \quad (7)$$

Fig. 1 shows the locations of poles and zeros in the case of the DO 28D aircraft (Altitude = 2000 m, VTAS = 70 m/s). In Fig. 1.a we see the effect of the positive angle of attack feedback, which cancels in the closed loop the zero of the $\Delta q/\Delta \eta$ -transfer function at $\sigma = -1.59$ (Fig. 1.b). This can be interpreted as a decoupling of the angle of attack $\Delta \alpha$ and Δq in Fig. 2. Finally we obtain the required handling qualities, i.e. the damping and the frequency of the short period mode by proper feedback gains K_θ and K_q (Fig. 1.c).

The necessary feedback gains can be readily calculated from the condition of decoupling of $\Delta \alpha$ and $\Delta \dot{q}$ and from the handling qualities requirements. Using equation (4) we obtain immediately

$$a_{23} \Delta \alpha + b_{21} \Delta \eta = 0$$

or

$$\Delta \eta = - \frac{a_{23}}{b_{21}} \cdot \Delta \alpha = K_\alpha \cdot \Delta \alpha \quad (8)$$

The differential equation of the decoupled short period mode are now

$$\dot{\Delta \theta} = \Delta q \quad (9)$$

$$\dot{\Delta q} = a_{22} \Delta q + b_{21} (K_\theta \theta + K_q \Delta q)$$

which yield the characteristic equation

$$s^2 - (a_{22} + b_{21} K_q) s - b_{21} K_\theta = 0 \quad (10)$$

Comparing equation (10) with the desired characteristic equation

$$s^2 + 2\zeta_{sp} \omega_{sp} s + \omega_{sp}^2 = 0 \quad (11)$$

where ζ_{sp} and ω_{sp} are the damping and the frequency of the short period mode as prescribed by the MIL-F 8785 B requirements (/6/), we obtain immediately

$$K_q = \frac{-2\zeta_{sp} \omega_{sp} - a_{22}}{b_{21}}, \quad K_\theta = \frac{-\omega_{sp}^2}{b_{21}} \quad (12)$$

Equations (8) and (12) establish a direct relationship between the dynamic parameters of the aircraft, the handling qualities requirements and the feedback gains. It should be noted that only three dynamic parameters of the aircraft - a_{22} , a_{23} and b_{21} - are necessary.

By reasons of reliability and costs we are interested to avoid pitch attitude and angle of attack sensors in stability augmentation systems of high performance aircraft. This can easily be done by integrating the signal of a pitch rate gyro and by substituting the angle of attack signal by the signal of a normal accelerometer, using the fact that the relation between the normal acceleration a_z and the angle of attack is approximately given by

$$a_z = Z_\alpha \cdot \alpha \quad (13)$$

if the normal force due to an elevator deflection can be neglected. Fig. 3 shows the simplified dynamics of the longitudinal control system where the factor b_{31} - which is usually sufficient small - has been neglected. It should be noted that the closed loop of the pitch rate control system provides exactly a steady state one to one response of the q/q_c -transfer function. By prefilters it is possible to shape the pitch rate response in an appropriate manner according to the requirements of the C^* -criterion /7/ or the load factor control system.

For practical realizations we are interested in a discrete time version of the control system. As the sampling frequency of the control system should be high in comparison with the typical time constants of the aircraft, we are looking for a discrete time approximation of the control law. This control law should be immediately suited for the automatic adaption. For this purpose we start with a discrete time version of the state equation (4), include the above mentioned relation between angle of attack and normal acceleration (13) and obtain (Δ symbols are dropped)

$$\begin{bmatrix} q(k+1) \\ a_z(k+1) \end{bmatrix} = \begin{bmatrix} \varphi_{11} & \varphi_{12} \\ \varphi_{21} & \varphi_{22} \end{bmatrix} \begin{bmatrix} q(k) \\ a_z(k) \end{bmatrix} + \begin{bmatrix} h_1 \\ h_2 \end{bmatrix} \cdot \eta(k) \quad (14)$$

The feedback law is put up in the form

$$\eta(k) = K_{\theta}^* \dot{\theta}(k) + K_q^* q(k) + K_{a_z}^* a_z(k) . \quad (15)$$

The condition for decoupling the pitch rate q from the normal acceleration can be used in the first equation of (14) with the feedback law (15)

$$q(k+1) - (\varphi_{11} + h_1 K_q^*) q(k) - h_1 K_{\theta}^* \dot{\theta}(k) = (\varphi_{12} + h_1 K_{a_z}^*) a_z(k) = 0 . \quad (16)$$

Thus the feedback of the normal acceleration is given by

$$K_{a_z}^* = - \frac{\varphi_{12}}{h_1} . \quad (17)$$

With the sampling period T we express

$$q(k+1) = q(k) + \dot{q}(k) \cdot T$$

and obtain as characteristic equation of (16)

$$Ts^2 + (1 - \varphi_{11} - h_1 K_q^*) \cdot s - h_1 K_{\theta}^* = 0 \quad (18)$$

and by comparison with the desired characteristic equation (11)

$$K_{\theta}^* = - \frac{T \cdot \zeta_{sp}^2}{h_1} , \quad K_q^* = \frac{1 - \varphi_{11} - 2 \cdot \zeta_{sp} \cdot \omega_{sp} T}{h_1} . \quad (19)$$

Therefore the identification process must deliver the three coefficients

$$\varphi_{11}, \varphi_{12}, h_1$$

of the measurement equation

$$q(k+1) = \varphi_{11} q(k) + \varphi_{12} a_z(k) + h_1 \dot{q}(k) \quad (20)$$

whereas the natural frequency ω_{sp} and the damping ratio ζ_{sp} are derived from the handling qualities requirements.

The natural frequency ω_{sp} is determined in the MIL-specifications by the so called load factor sensitivity (/6/). An evaluation shows that the load factor sensitivity can be well approximated by a power function of the dynamic pressure q_c (/12/).

$$\omega_{sp} = g \cdot q_c^p \quad (21a)$$

The required damping ratio of the aircraft does not depend on the flight case. Therefore we chose a constant damping ratio of

$$\zeta_{sp} = 0.7 . \quad (21b)$$

3. IDENTIFICATION ALGORITHM

In section 2 it has been pointed out that realization of the adaptive stabilization concept requires knowledge of three coefficients φ_{11} , φ_{12} and h_1 of the discrete state-space equation (14). The estimation algorithm to be used should show the following properties:

- minimum variance unbiased estimates
- recursive form since on-line identification is necessary
- identification of time variable parameters (due to different flight conditions)
- convergence independent of choice of the initial conditions of the estimator
- easy programming on a process computer.

We apply a least-squares approach in state-space representation with exponentially weighting of past data to ensure parameter tracking. Though this method gives biased estimates /8/ it has the advantage of a very simple structure. Moreover its efficiency has been proven already in wide-spread successful applications. Other algorithms which yield unbiased estimates like the generalized least squares method /9/ are too complex or give no practical improvement. Moreover we remember that the mathematical model (14) is an approximation, hence our demands for accuracy of the estimates should not be emphasized too much.

The structure of the process with unknown parameters is given in state-space form by

$$\underline{x}(k+1) = \underline{A} \underline{x}(k) + \underline{H} \underline{u}(k); \quad (22)$$

$$\underline{y}(k) = \underline{x}(k) + \underline{n}(k), \quad (23)$$

where \underline{x} is the $n \times 1$ state vector, \underline{A} is the $n \times n$ transition matrix, and \underline{H} is the $n \times m$ input matrix. Measurements of the input $\underline{u}(k)$ ($m \times 1$ vector) and noisy measurements $\underline{y}(k)$ of the state $\underline{x}(k)$ are available at discrete time instants k ($k = 0, 1, 2, \dots$). The model of the process is then

$$\underline{y}(k+1) = \hat{\underline{A}}(k) \underline{y}(k) + \hat{\underline{H}}(k) \underline{u}(k) + \underline{e}(k) \quad (24)$$

where " $\hat{}$ " indicates that the matrices $\hat{\underline{A}}$ and $\hat{\underline{H}}$ contain parameter estimates (Fig. 4).

The method of least squares means that we minimize the quadratic error

$$E = \underline{e}^T(k) \underline{e}(k) \rightarrow \text{Min.} \quad (25)$$

for each k , where

$$\underline{e}(k) = \underline{y}(k+1) - \hat{\underline{A}}(k) \underline{y}(k) - \hat{\underline{H}}(k) \underline{u}(k). \quad (26)$$

This leads to

$$\frac{\partial E}{\partial \hat{\underline{A}}(k)} = -2 \underline{e}(k) \underline{y}^T(k) \stackrel{!}{=} \underline{0} \quad (27a)$$

and

$$\frac{\partial E}{\partial \hat{\underline{H}}(k)} = -2 \underline{e}(k) \underline{u}^T(k) \stackrel{!}{=} \underline{0} \quad (27b)$$

Now we obtain the adjustment mechanism for the model parameters applying the gradient method, i.e. the rate of change in the parameter estimates is chosen proportional to the gradient to the cost functional E (see for the scalar case /10/, p.203):

$$\frac{\hat{\underline{A}}(k+1) - \hat{\underline{A}}(k)}{T} \approx \frac{d\hat{\underline{A}}(k)}{dt} \sim - \frac{\partial E}{\partial \hat{\underline{A}}(k)} \quad (28a)$$

$$\frac{\hat{\underline{H}}(k+1) - \hat{\underline{H}}(k)}{T} \approx \frac{d\hat{\underline{H}}(k)}{dt} \sim - \frac{\partial E}{\partial \hat{\underline{H}}(k)} \quad (28b)$$

Equations (27) and (28) yield the iterative estimation procedure

$$\hat{\underline{S}}(k) = \hat{\underline{S}}(k-1) + \underline{m}(k-1) \{ \underline{y}^T(k) - \underline{m}^T(k-1) \hat{\underline{S}}(k-1) \} \quad (29)$$

with

$$\hat{\underline{S}}(k) = \begin{bmatrix} \hat{\underline{A}}^T(k) \\ \hat{\underline{H}}^T(k) \end{bmatrix}, \quad \underline{m}(k) = \begin{bmatrix} \underline{y}(k) \\ \underline{u}(k) \end{bmatrix} \quad (30)$$

and the proportionality-matrix $\underline{\Gamma}$, comparing Eq. (29) with the usual recursive least squares approach for single input-single output systems, we see that we may equate

$$\underline{z} = \underline{P}(k) \quad (31)$$

where $\underline{P}(k)$ is a matrix with decreasing norm evolving according to

$$\underline{P}(k) = \underline{P}(k-1) - \frac{\underline{P}(k-1)\underline{m}(k-1)\underline{m}^T(k-1)\underline{P}^T(k-1)}{\underline{m}^T(k-1)\underline{P}(k-1)\underline{m}(k-1) + 1}; \quad \underline{P}(0) = \underline{P}_0 \quad (32)$$

Tracking of time-variable parameters is ensured, if we provide an exponential weighting of past data in the estimation algorithm (29) - (32), i. e. new measurements influence the updating of the parameter estimates in a stronger way than older ones. This yields (7/17, p. 240)

$$\underline{P}(k) = f \cdot \left[\underline{P}(k-1) - \frac{\underline{P}(k-1)\underline{m}(k-1)\underline{m}^T(k-1)\underline{P}^T(k-1)}{\underline{m}^T(k-1)\underline{P}(k-1)\underline{m}(k-1) + \frac{1}{f}} \right]; \quad \underline{P}(0) = \underline{P}_0 \quad (33)$$

with the weighting factor

$$f \gg 1, \quad f \approx 1.$$

4. APPLICATION OF THE ESTIMATION ALGORITHM TO FLIGHT TEST DATA

Before implementing the identification algorithm in the adaptive flight control system, extensive tests of the estimator have been carried out using flight test data of the business jet HFB 320 "HANSA". These tests gave information about the following items

- bias in sensor signals
- determination of the weighting factor f in Eq. (33).
- influence of input-signals to the quality of the parameter estimates

The problem of signal-bias may be solved either by including an additional bias parameter b_1 in the estimation equation (29) or by digital prefiltering of the sensor signals using a lead-type filter. The identification results with both methods are given in Fig. 5 and Fig. 6.

The input to the aircraft is the deflection of the elevator, commanded by the pilot - Fig. 5a. The three parameter estimates as well as the estimate b_1 of the bias-term is given in Fig. 5b, while Fig. 5c shows the reconstruction of the output q (rate of pitch) by

$$\hat{q}(k+1) = \hat{\varphi}_{11}q(k) + \hat{\varphi}_{12}a_z(k) + \hat{h}_1(k) - \hat{b}_1(k)$$

in comparison to the measured output to verify the estimation as theoretical values of the parameters are not available. Since real flight test data have been used all adverse effects of the sensors (noise, nonlinearities) and the airframe (vibrations, structural bending modes) are included.

Fig. 6 contains the corresponding results after lead-filtering of all measured sensor signals. The estimates converge in both cases in the same time (about 3s, Fig. 5b, 6b). Though the estimation with the bias parameter included is slightly more exact than lead-filtering (Fig. 5c, 6c), the latter method has been selected for application in the adaptive flight control system to reduce the computational burden.

The effect of the weighting factor is demonstrated in Fig. 6d. A smaller factor $f \gg 1$ yields smoother parameter estimates, since the present data have less influence in the algorithm. On the other hand the estimator is now unable to follow fast parameter variations. The absolute value of f obviously depends on the signal to noise ratio. Suitable values are in the range of 1,01 - 1,15.

Finally we discuss the importance of the input signal type to the quality of the identification. The input signal (elevator deflection) has to excite all eigenfrequencies of the system; that is why binary or three-valued uncorrelated noise (Fig. 7a or 5a) is well suited. Moreover the power-spectrum of the input signal should be sufficiently large in view of the signal/noise-ratio and the problem of linear dependent measurements. Figure 7 illustrates the estimator dynamics with elevator deflections which are about ten times smaller than in Fig. 5. Now the settling time of the parameter estimates is 7 seconds, more than twice as long as in Fig. 5.

5. REALIZATION OF THE ADAPTIVE FLIGHT CONTROL SYSTEM

For hybrid simulations and flight tests an experimental adaptive flight control system has been realized using a 16-bit minicomputer. A STOL-aircraft DO 28 D was readily available for the flight tests. This aircraft is not typical for the application of an adaptive control system because of its limited flight envelope. Since the main concern during this phase of the study was only to verify the proper function of the adaptive control system in the real world, the aircraft was indeed very useful.

During the realization phase of the experimental adaptive control system the following items turned out to be of importance:

Actuating system: Usually the hydraulic actuating system of high performance aircraft is very fast. Earlier simulation results indicated that in cases where the actuator bandwidth is three to four times wider than the aircraft bandwidth it is possible to neglect the actuator dynamics in calculating the adaptive controller gains. In case of the DO 28 aircraft an electric actuator has been used with a bandwidth of only 1 Hz. Therefore it turned out to be necessary to introduce a compensation network in order to reduce the phase shift of the actuator (see. Fig. 8).

Safety considerations: In case of an experimental adaptive control system a potential malfunction of the identification process has to be taken into account. Errors of the estimated parameters may result in significant increased controller gains thus leading to stability problems of the closed loop. To avoid these stability problems the computed gains of the adaptive controller have been limited to safe, precalculated values. These limitations varied according to the dynamic pressure $q_c = p_t - p_s$. The adaptive control system contained also a set of preprogrammed controller gains (dependent on the dynamic pressure) for comparison and evaluation purposes.

Identification algorithm: The identification algorithm has been programmed according to table 1 with the following definitions (k =index of sampling instant):

State vector (2x1)	$\underline{x}_k = [q_k, az_k]^T$
Output signal (1x1) (only first element of \underline{y}_k is required)	$y_{1,k} = q_k + \text{Noise}$
Input vector (1x1)	$u_k = \eta_k$
Measurement vector (3x1)	$\underline{m}_k = [q_k, az_k, \eta_k]^T$
Weighting matrix (3x3)	\underline{P}_k (initiated with $P_1(i,j) = 0, i \neq j$ $P_1(i,i) = P_0, \text{ for } i = 1, 2, 3$)
Parameter matrix (3x1) (only first column of $\underline{\hat{S}}_k$ is required)	$\underline{\hat{S}}_{1,k}$ (initiated with precalculated values, e.g. for the take-off flight condition)

The block diagram of the complete adaptive control system is shown in Fig. 8 where the main functions of the control system are clearly separated.

Description	Instruction	Number of instructions				Comments
		Load/Store	Add/Sub	Mult.	Div.	
Store old measurements	$\underline{m}_{k-1} \rightarrow \underline{m}_k$	6	-	-	-	
Correction of last measurements	$\underline{m}_{k-1} \leftarrow \underline{E} \underline{m}_{k-1} + (I - \underline{E}) \underline{m}_k$	8	2	2	-	Weighting of discrete time values of continuous time variables (\underline{E} -correction matrix, I -Identity matrix)
Instrumental vector	$\underline{h} = \underline{P}_{k-1} \underline{m}_{k-1}$	18	6	9	-	
Factor	$q = \underline{m}_{k-1}^T \underline{h} + 1^{-1}$	6	3	3	-	Fading memory factor $f = 1.025$
Corrective weighting matrix	$\Delta \underline{P} = -q^{-1} \underline{h} \underline{h}^T$	14	-	12	1	
Corrected weighting matrix	$\underline{P}_k = f (\underline{P}_{k-1} + \Delta \underline{P})$	12	6	6	-	
Corrective parameter matrix	$\Delta \underline{\hat{S}} = \underline{P}_k \underline{m}_{k-1} (\underline{y}_k - \underline{m}_{k-1}^T \underline{\hat{S}}_{k-1})$	24	9	12	-	
Corrected parameter matrix	$\underline{\hat{S}}_k = \underline{\hat{S}}_{k-1} + \Delta \underline{\hat{S}}$	6	3	-	-	

Table 1: Identification algorithm break-down

Programming considerations: After a detailed analysis of the adaptive control system a sampling rate of 10 Hz has been adopted. The equations of the control system have been programmed on a 16-bit airborne minicomputer (ROLM 1602) using fixed point arithmetic throughout. To increase the accuracy of the identification process the critical parts of the program have been written in double-word arithmetic. Table 2 shows the memory space and the computation time required for the adaptive control system.

Program	Memory space (16-bit-words)	Computation time (ms)
Identification	535	11.3
Control	400	0.9
Operating System	1994	not applicable
Total experimental Control System	2929	12.2

Table 2: Computational requirements of the experimental adaptive control system

Hardware of the experimental control system: Fig. 9 shows a blockdiagram of the test equipment of the experimental adaptive control system including the computer and the aircraft and actuator dynamics. The actuator and the clutch is engaged or disengaged by the pilot. To provide a smooth engagement of the control system the actual value of the elevator deflection at the instant of engagement has been stored in the computer. With the control system engaged the pilot had the possibility of control wheel steering (CWS). Furtheron provisions were made to introduce different test and disturbance signals (q_c , n_c , Δn_D).

6. RESULTS

The properties of the digital adaptive stabilizing system first have been tested by digital and hybrid simulations using the longitudinal dynamics of the Mc Donnell/Douglas F-4 "Phantom" aircraft. This aircraft is well suited for the adaptive stabilizing concept because its flight conditions span a wide envelope with drastic changes in the open loop dynamics /12/.

Later on flight tests with the complete adaptive system have been carried out using the DO 28 - D "Skyservant" of the Bodenseewerk.

The simplified block-diagram of the adaptive control system is given in Fig. 10. As mentioned above the C^* -criterion requires the application of a pre-filter with positive phase characteristic. It should be carefully observed that the introduction of the dynamic pressure $p_t - p_s$ is not required for the adaption of the control laws. It is only used to match the desired handling qualities - especially the eigenfrequency of the closed loop-according to equation (21).

Extensive digital simulations of the adaptive system with complete fourth order longitudinal dynamic equations yielded good results (/12/) under fast parameter variations and in atmospheric disturbances which have been simulated using the Dryden form of a continuous random gust model. This gust model is defined and specified in the MIL-F-8785 requirement /6/.

As discussed in the preceding paragraph the adaptive system has been implemented on a 16-bit airborne computer. The results of hybrid simulations (the longitudinal aircraft dynamics was reproduced by an analogue computer) of the complete digital adaptive command- and stability system are given in Fig. 11. The aircraft is disturbed by wind-gusts Fig. 11h. A rapid change in the velocity from Mach 0,2 to Mach 1,0 and back to Mach 0,2 - as indicated on Fig. 11a - yields a considerable change in the parameters and consequently a change in the estimates \hat{p}_{11} , \hat{p}_{12} and \hat{h}_1 (Fig. 11e - 11g). The rate of convergence of the estimation algorithm may be demonstrated even better by using another Mach number versus time function given in Fig. 12a. See the estimates Fig. 12e-12g.

The flight tests with a DO28-D STOL aircraft have been carried out to verify the whole system. Actually a business aircraft like the DO28 with a small flight envelope does not require an adaptive flight control system at all. However the flight tests demonstrated the efficiency of the system under the following circumstances, which are different from the simulations:

- modelling errors of plant and actuator due to nonlinearities
- influence of noise and structural bending modes on sensor-signals
- drift of sensors
- real turbulence

As discussed in more detail by Krebs (/13/) the adaptive system generally works well for different flight conditions including power approach.

The atmospheric turbulence generally yields sufficient excitation for the parameters to be identified. During periods of quiescent flight however, no parameter tracking is possible and the parameter estimates have to be locked. Otherwise the parameter estimates diverge thus increasing the closed loop gains. Due to this fact a certain self-excitation of the whole system occurs and the resulting pitch rate q , normal acceleration a_z , and elevator deflection η lead to acceptable parameter estimates, though. This may be demonstrated in the simulation as well as in the flight test data (Fig.13 and 14).

7. CONCLUSIONS

The simulations as well as the flight test results with the adaptive flight control system suggest the following conclusions:

- The development and introduction of digital adaptive control systems for advanced high performance aircraft is possible using today's digital technology. Both, the handling qualities requirements and hardware reliability can be met.
- Some problems arise with regard to the parameter identification during quiescent flight but may be surmounted by special provisions like locking of the parameter estimates, setting the weighting factor f equal to one, or introducing a test signal. The latter method is discussed e.g. in /14/.
- The question whether scheduled controller gains or self-tuning of the gains is superior can not be answered definitely. It requires further research activities and flight tests with high performance aircraft including comparison of both methods.

REFERENCES

- /1/ Gregory P.C.
(Editor) Proceedings of the self adaptive flight control systems symposium. Wright-Patterson Air Force Base Ohio (1959). WADC Techn.Rep. 59-49, ASTIA Doc.No.AD 209 389
- /2/ — Mini Issue on NASA's Advanced Control Law Programm for the F-8 DFBW Aircraft. IEEE Transactions on Automatic Control, Vol AC-22 (1977), pp 752-806
- /3/ Hartmann, U. Ein Beitrag zum Entwurf digitaler selbstadaptiver Flugregelungssysteme. Dissertation. Technische Universität Hannover (1974)
- /4/ Hartmann,U.
Lonn,E. Anwendung der Polfestlegung beim Entwurf von Stabilisierungssystemen am Beispiel der Flugzeuglängsbewegung. Zeitschrift für Flugwissenschaften und Weltraumforschung, Vol. 1 (1977), pp. 135-147
- /5/ Hartmann,U.
Krebs,V. Command and stability systems for aircraft: A new digital adaptive approach. IFAC VII World Congress, Techn.Session 29.4., Preprints pp 1243-1249
- /6/ — Military Specification, Flying Qualities of Piloted Airplanes MIL-F-8785 B (ASG), 07.Aug. 1969
- /7/ Tobie, H.N.
Elliott, E.M.
Malcolm, L.G. A new Longitudinal Handling Qualities Criterion.National Aerospace Electronics Conference, Dayton, Ohio 16.-18.May 1966
- /8/ Krebs, V.
Thöm, H. Parametererkennung nach der Methode der kleinsten Quadrate — Ein Überblick. Regelungstechnik und Prozessdatenverarbeitung 22 (1974), pp 1-10
- /9/ Clarke, D.W. Generalized-least-squares estimation of the parameters of a dynamic model. IFAC symp. Identification in autom. Control systems, Prague (1967), paper 3.17
- /10/ Isermann, R. Experimentelle Analyse der Dynamik von Regelungssystemen-Identifikation I. Bibliographisches Institut, Mannheim (1971)
- /11/ Eykhoff, P. System Identification. John Wiley, New York (1974)
- /12/ Hartmann, U. Untersuchung über die Auslegung digitaler adaptiver Stabilisierungssysteme. Bodenseewerk Gerätetechnik GmbH, TB 000 D 996/75 (1975)
- /13/ Krebs, V. Fluglerprobung eines digitalen adaptiven und eines parameterunempfindlichen Regelungssystems. Bodenseewerk Gerätetechnik GmbH, TB 1145/77 (1977)
- /14/ Stein, G.
Hartmann, G.L.
Hendrick, R.C. Adaptive Control Laws for F-8 Flight Test. IEEE Transactions on Automatic Control, Vol. AC-22 (1977), pp 758-767
- /15/ Heffley, R.K.
Jewell, W.F. Aircraft Handling Qualities Data. National Aeronautics and Space Administration Washington, D.C. Report NASA CR-2144

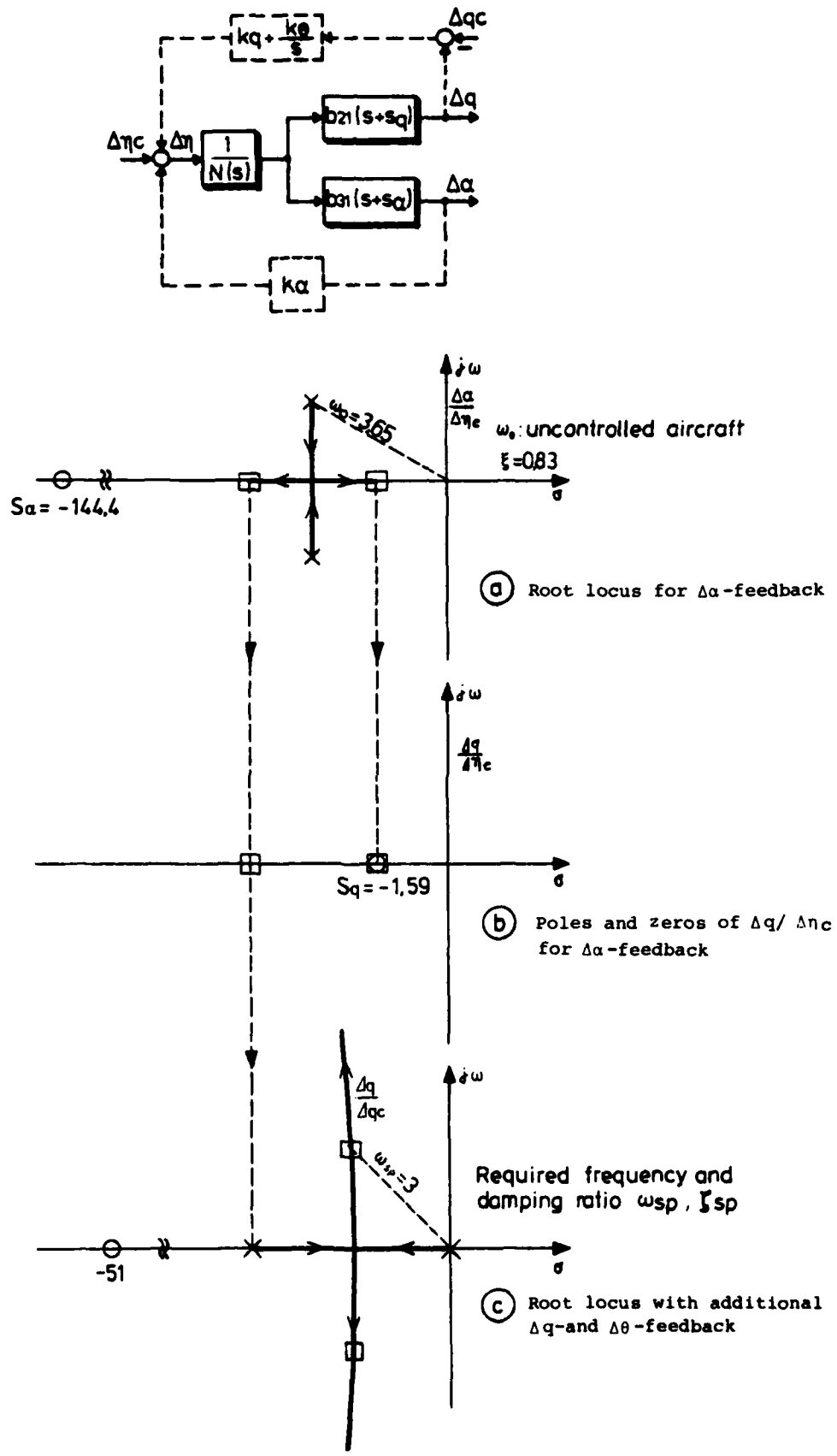


Fig. 1: Block-diagram and root-locus of the control-system

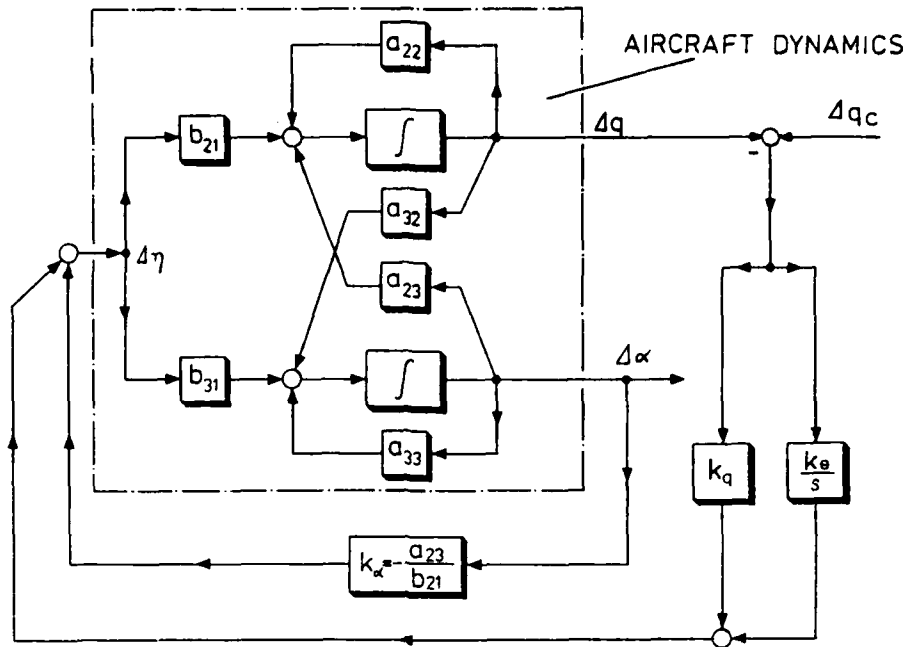


Fig. 2: Block-diagram of the command- and stability system

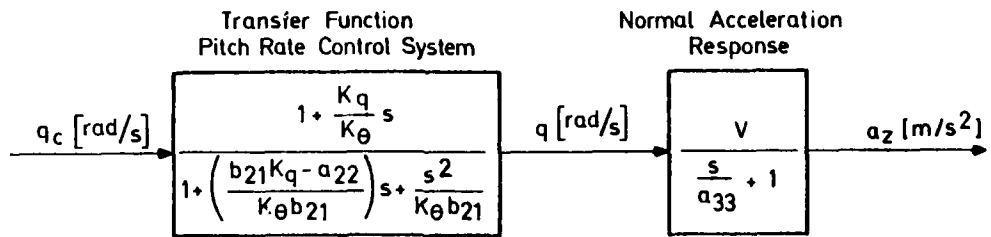


Fig. 3: Simplified dynamics of the longitudinal control system

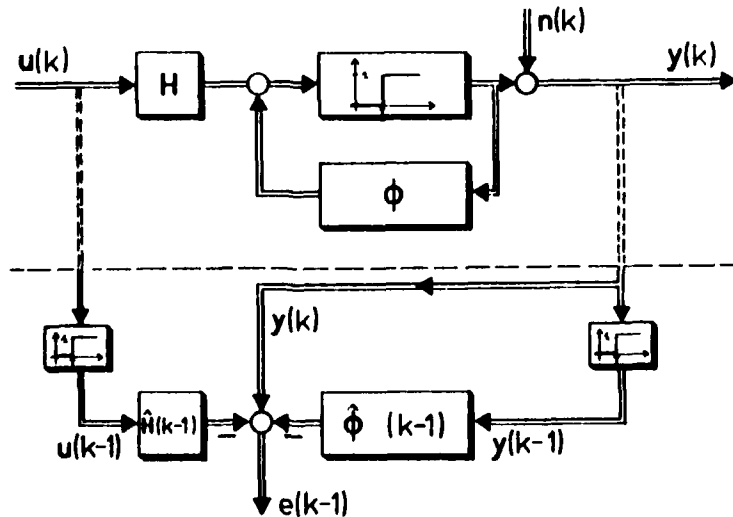


Fig. 4: Configuration of the parameter estimation

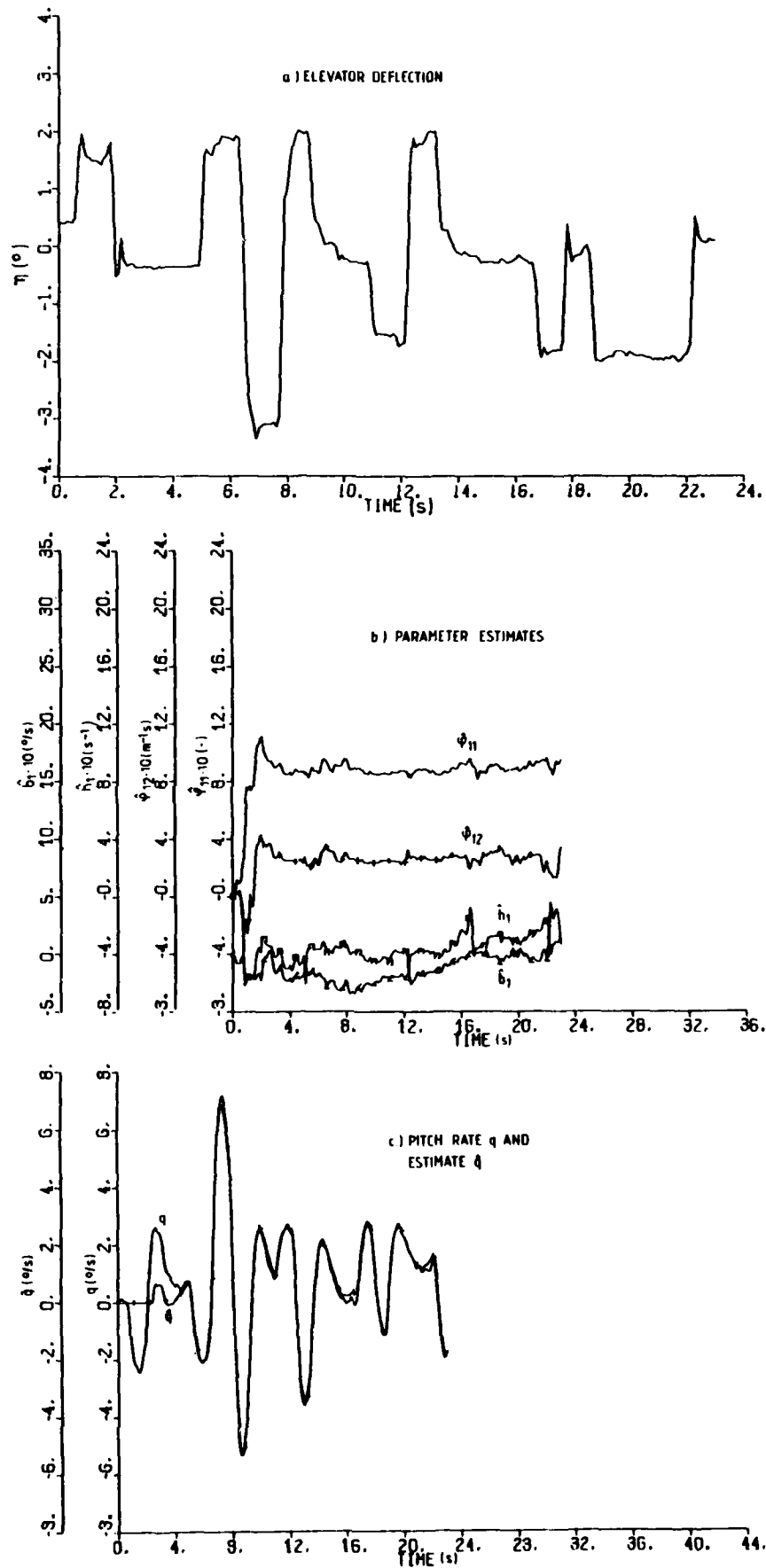


Fig. 5: Identification of HFB 320 parameters - bias estimation; $V=98m/s$, weighting factor $f=1.15$

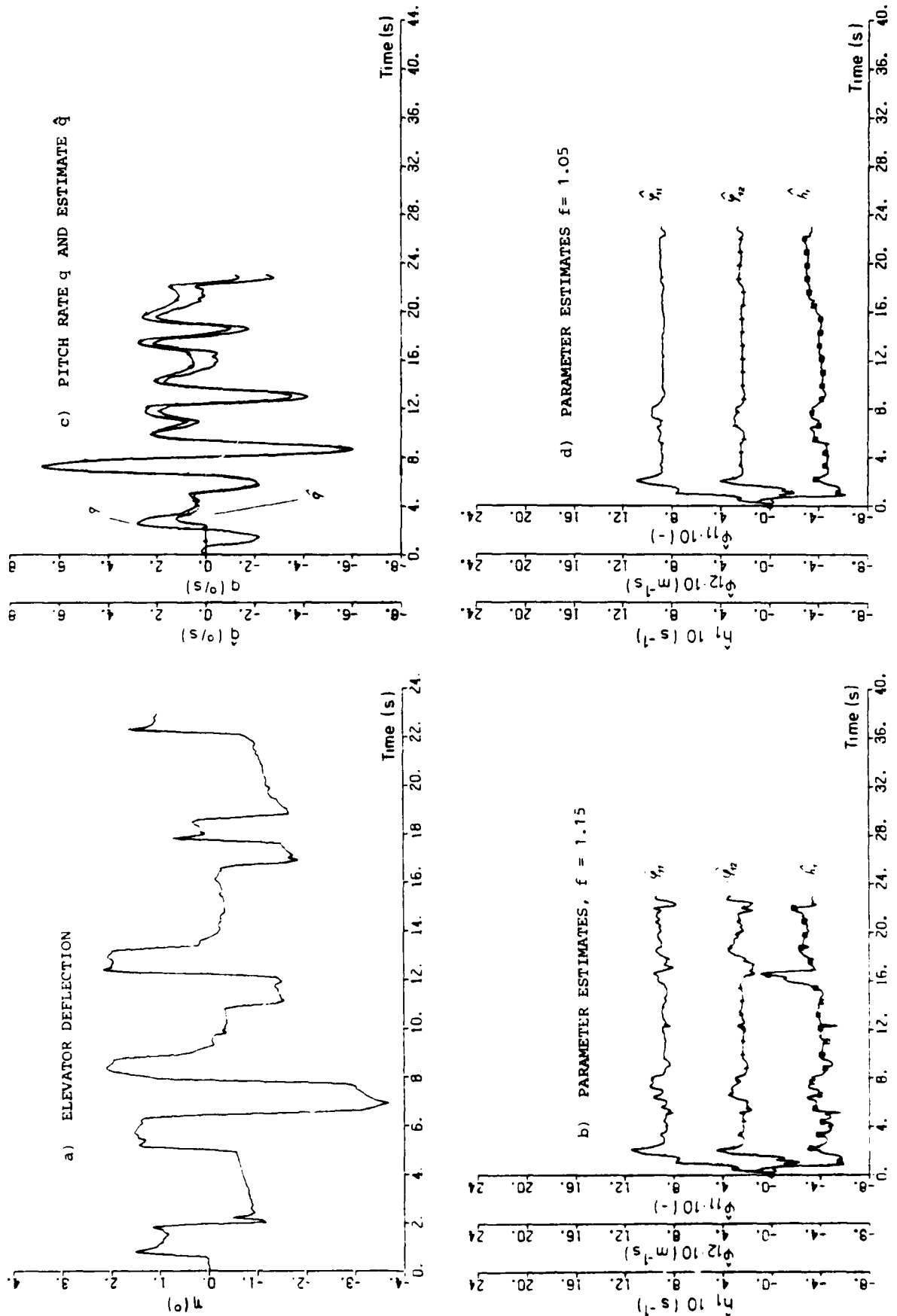


Fig. 6: Identification of HFB 320 parameters - lead filtering of sensor signals; $V = 98$ m/s, weighting factor $f=1.15/1.05$

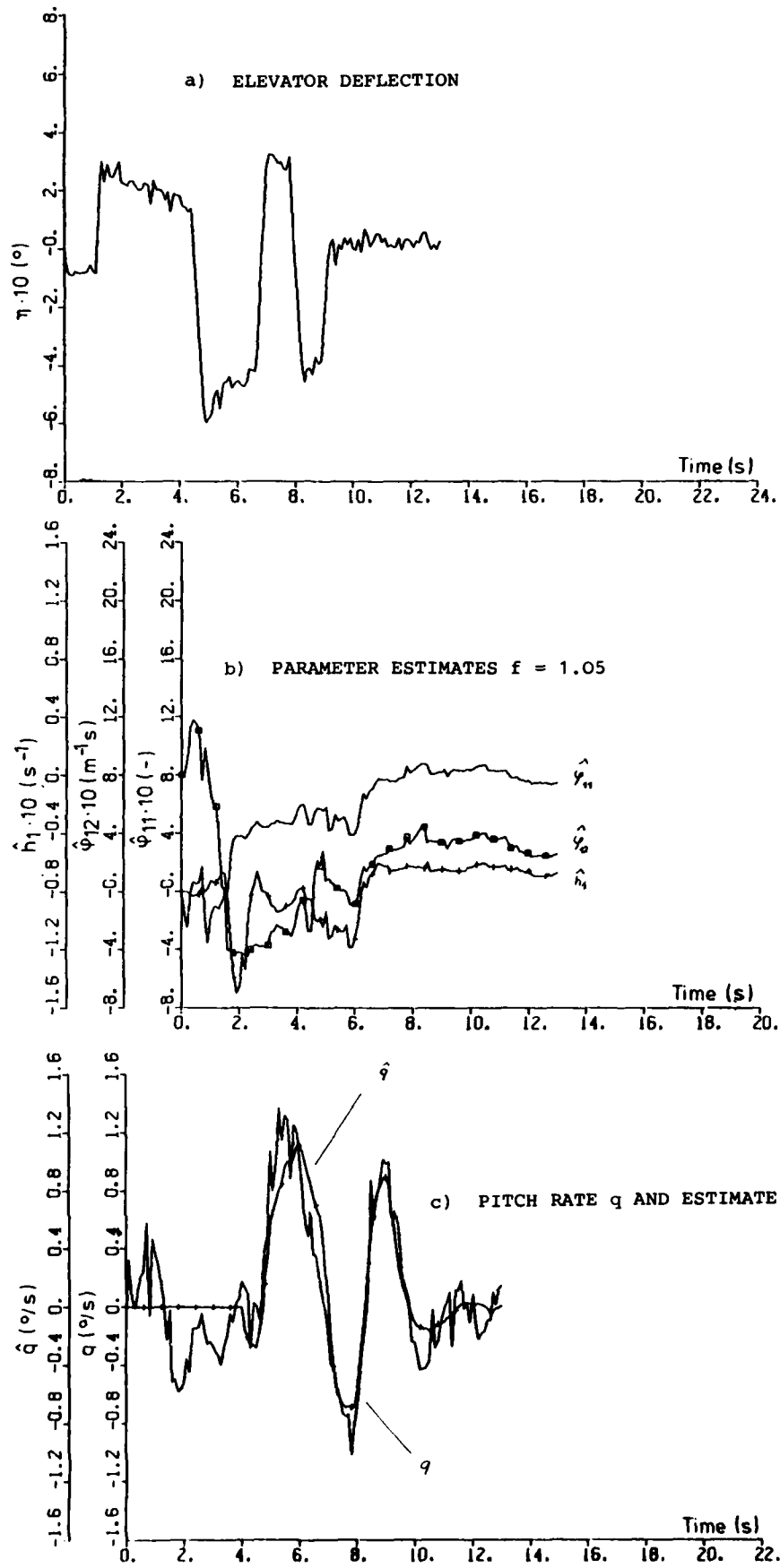


Fig. 7: Identification of HFB 320 parameters- influence of input signal, $V = 79$ m/s, weighting factor $f=1.05$, lead filtering of sensor signals

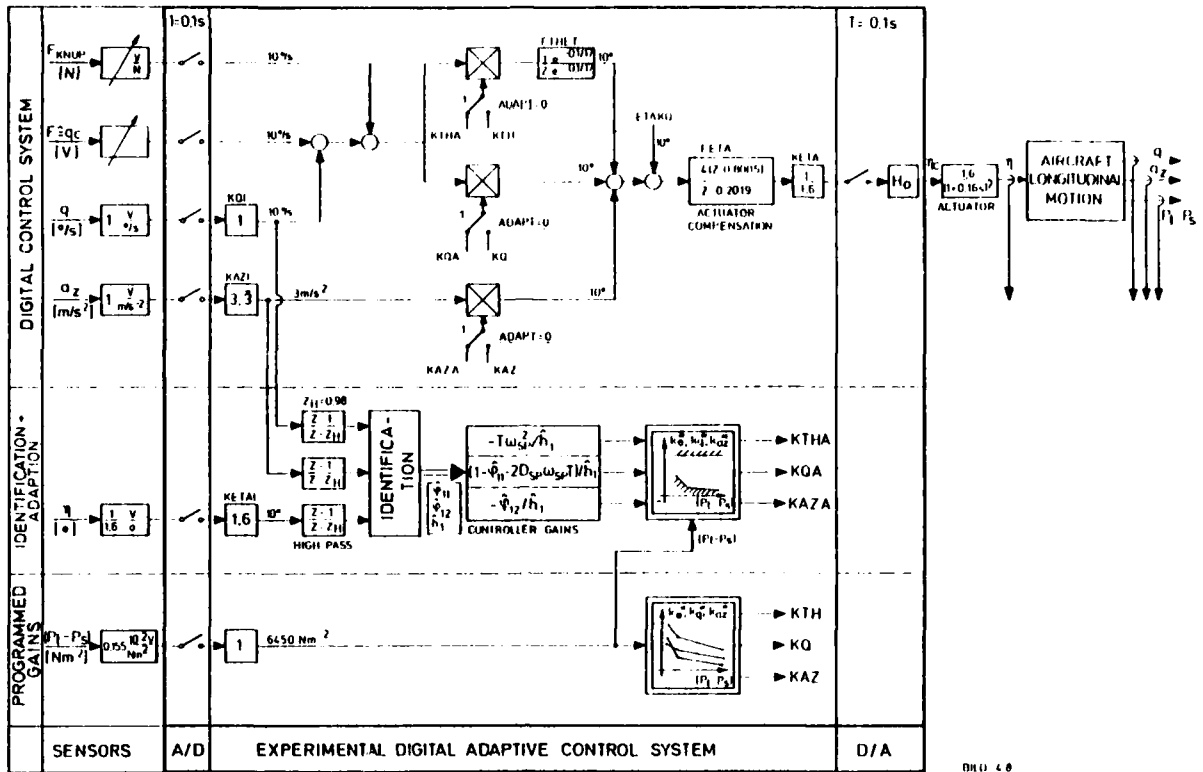


Fig. 8: Block diagram of the complete experimental digital adaptive control system

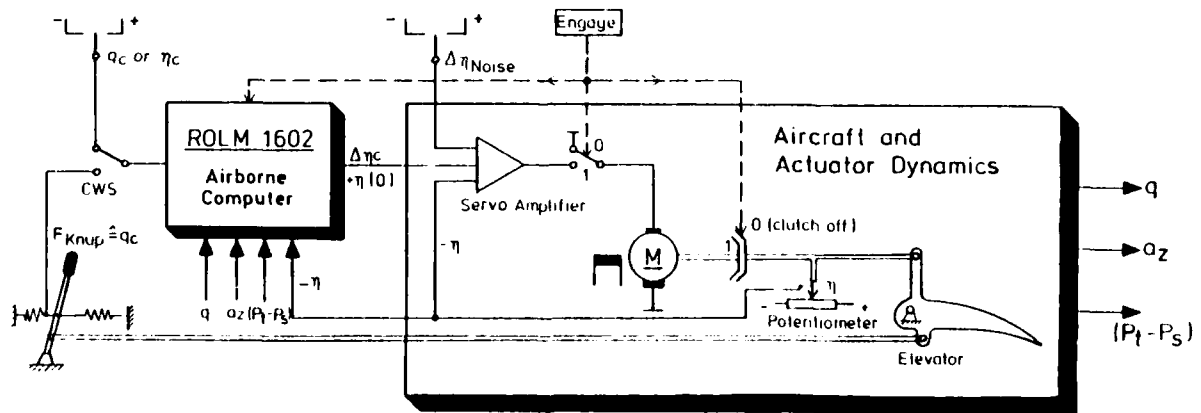


Fig. 9: Block diagram of the test equipment of the adaptive control system

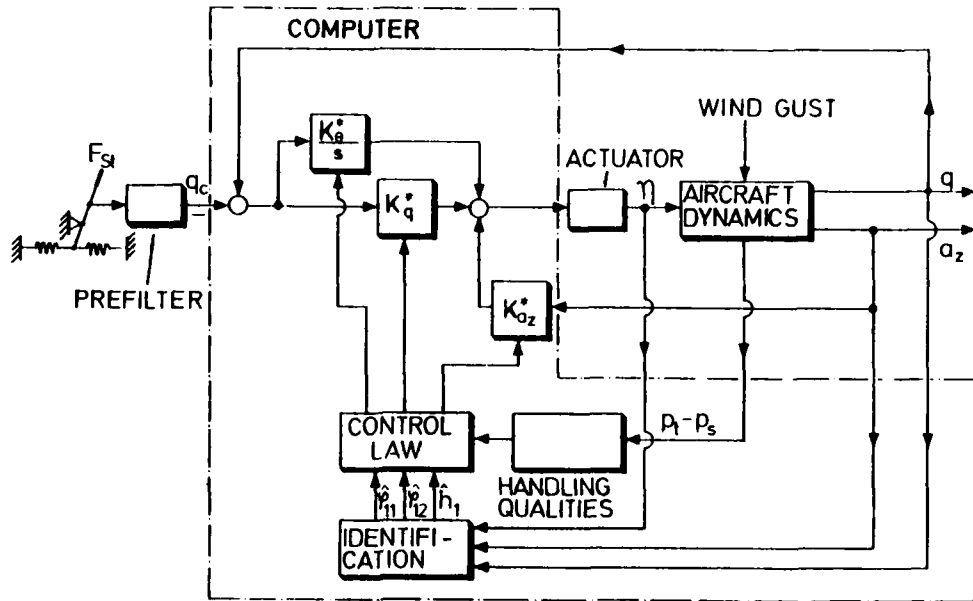


Fig. 10: Signal flow graph of the digital adaptive command-and stability system

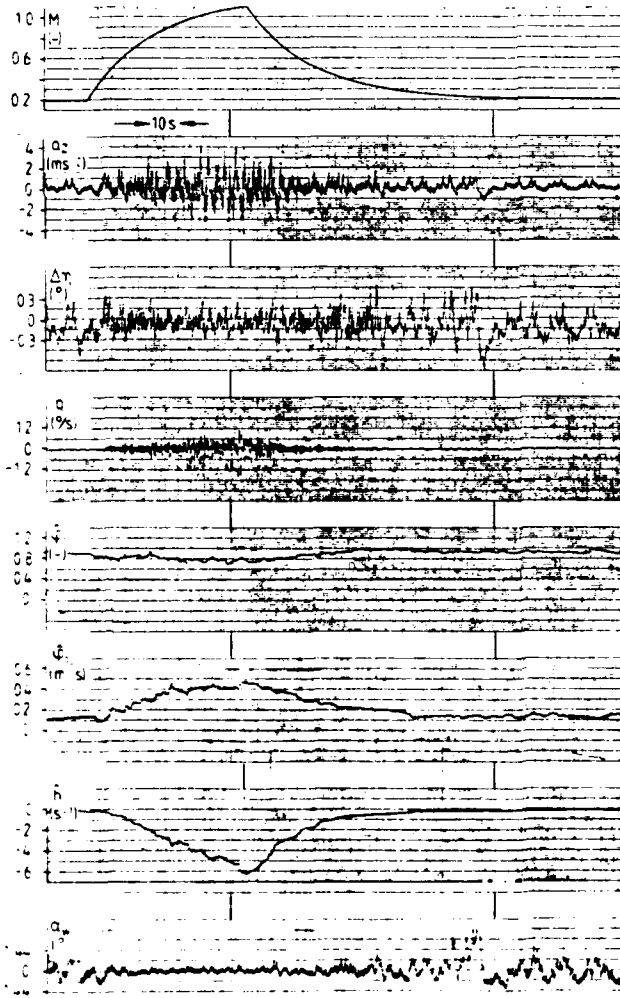


Fig. 11: Digital adaptive command- and stability system for F-4 "PHANTOM" - hybrid simulation with exponential Mach number history.

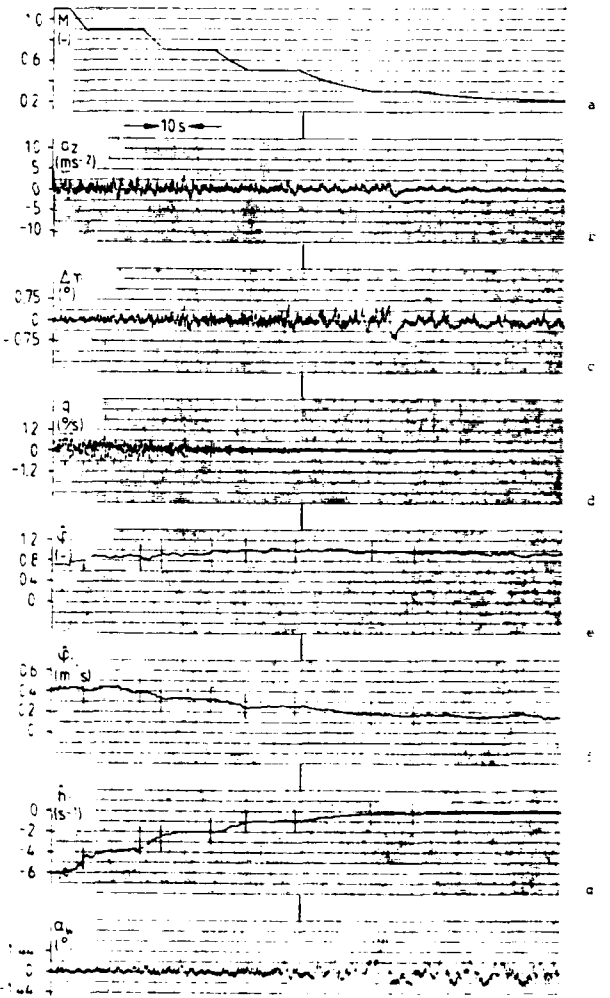


Fig. 12: Digital adaptive command- and stability system for F-4 "PHANTOM" - hybrid simulation with stepwise Mach number history.

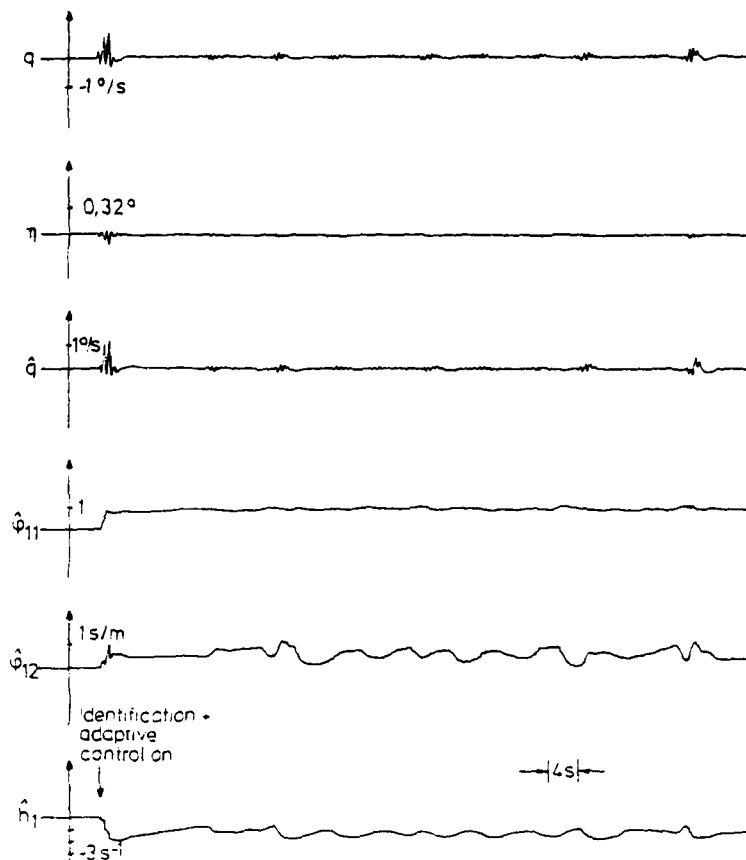


Fig. 13: Hybrid simulation of digital adaptive control system with DO 28 - aircraft in quiescent flight; $V = 70$ m/s, $f = 1.03$, $H = 2000$ m

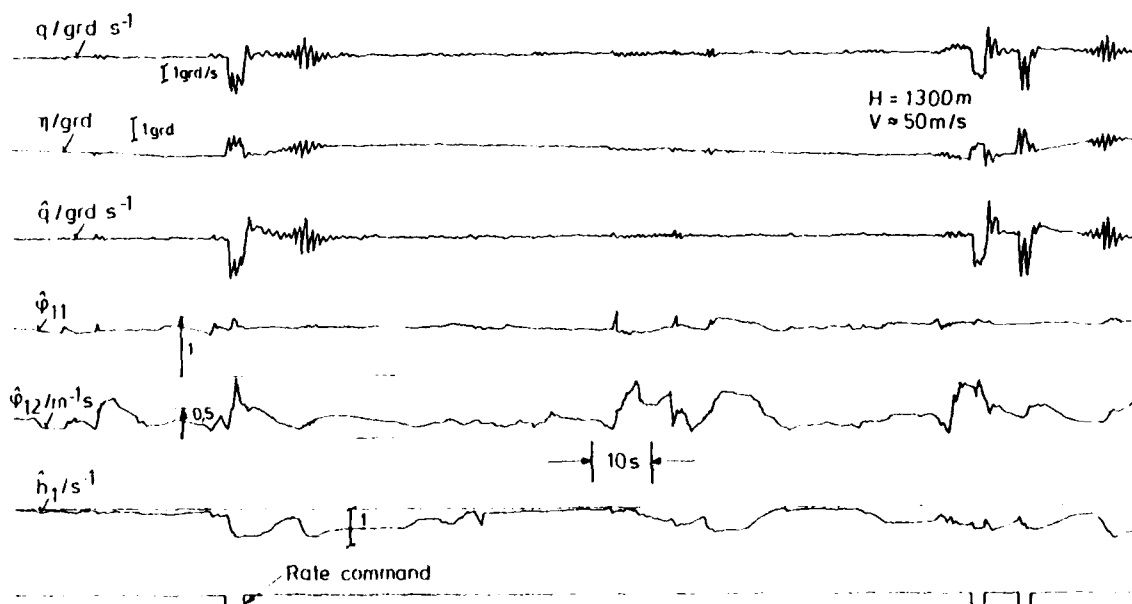


Fig. 14: Flight test results of digital adaptive control system with Do 28-aircraft in quiescent flight. $V = 50$ m/s, $f = 1.03$, $H = 1300$ m

APPENDIX

The development and the verification of the adaptive flight control system has been carried out using unclassified data on the F-4 fighter aircraft which is considered to be a typical aircraft for the application of an adaptive control system. Handling qualities data on this aircraft have been published in great detail /15/. During the work the following flight conditions have been considered:

No.	Flight Condition	Airspeed (m/s)	Altitude (m)
1	Power Approach	70.1	0
2	Low altitude, supersonic	374.3	0
3	High altitude, subsonic	178.0	10670.
4	High altitude, supersonic	634.3	13720.

In these flight conditions the dynamics of the aircraft is described by the following system matrices (Eq. 1)

Flight condition 1

$$\underline{A} = \begin{bmatrix} 0. & 1. & 0. & 0. \\ 00419 & -.462 & -.369 & .00166 \\ -.0284 & .979 & -.454 & -.00253 \\ -9.61 & -14.21 & 9.14 & -.0418 \end{bmatrix} \quad \underline{B} = \begin{bmatrix} 0. \\ -1.46 \\ -.029 \\ 1.83 \end{bmatrix}$$

Flight condition 2

$$\underline{A} = \begin{bmatrix} 0. & 1. & 0. & 0. \\ -.00013 & -3.13 & -72.1 & .0108 \\ .00014 & 1. & -2.11 & .00006 \\ -9.81 & 1.96 & -1.76 & -.0674 \end{bmatrix} \quad \underline{B} = \begin{bmatrix} 0. \\ -63.5 \\ -.21 \\ -.411 \end{bmatrix}$$

Flight condition 3

$$\underline{A} = \begin{bmatrix} 0. & 1. & 0. & 0. \\ .00127 & -.444 & -1.8 & .00142 \\ -.009 & .987 & -.298 & -.00038 \\ -9.68 & -29.1 & .662 & .0003 \end{bmatrix} \quad \underline{B} = \begin{bmatrix} 0. \\ -4.99 \\ -.0411 \\ 1.21 \end{bmatrix}$$

Flight condition 4

$$\underline{A} = \begin{bmatrix} 0. & 1. & 0. & 0. \\ -.00002 & -.372 & -42.8 & .0044 \\ -.00038 & 1. & -.484 & 0. \\ -9.81 & -15.5 & 1.67 & -.0155 \end{bmatrix} \quad \underline{B} = \begin{bmatrix} 0. \\ -17.7 \\ -.042 \\ .65 \end{bmatrix}$$

To examine the parameter tracking capabilities of an adaptive control system it can be of interest to use a state space description of aircraft dynamics with time varying parameters. In the following simplified, time-varying system matrices are provided, which are dependent on the Mach number:

Elements of the A-matrix

$$a_{11} = 0.$$

$$a_{12} = 1.$$

$$a_{13} = 0.$$

$$a_{14} = 0.$$

$$a_{21} = 0.$$

$$a_{22} = \frac{\bar{q}}{V} \cdot \frac{S l_{\mu}^2}{I_y} (C_{mq} + C_{m\dot{\alpha}})$$

$$a_{23} = \bar{q} \cdot \frac{S l_{\mu}}{I_y} \left\{ C_{m\alpha} - \frac{l_{\mu}}{V} C_{m\dot{\alpha}} \left[\frac{\bar{q}}{V} \cdot \frac{S}{m} (C_{A\alpha} + C_W) \right] \right\}$$

$$a_{24} = \frac{\bar{q}}{V} \cdot \frac{S l_{\mu}}{I_y} \left\{ (2C_m + MC_{mM}) - l_{\mu} C_{m\dot{\alpha}} \left[\rho \cdot \frac{S}{m} (C_A + \frac{1}{2} MC_{AM}) \right] \right\}$$

$$a_{31} = 0.$$

$$a_{32} = 1.$$

$$a_{33} = - \left[\frac{\bar{q}}{V} \cdot \frac{S}{m} (C_{A\alpha} + C_W) \right]$$

$$a_{34} = - \left[\rho \frac{S}{m} (C_A + \frac{1}{2} MC_{AM}) \right]$$

$$a_{41} = -g$$

$$a_{42} = 0.$$

$$a_{43} = \bar{q} \frac{S}{m} (C_A - C_{W\alpha})$$

$$a_{44} = -2 \frac{\bar{q}}{V} \cdot \frac{S}{m} \cdot (C_W + \frac{1}{2} MC_{WM})$$

Elements of the B-Matrix

$$b_{11} = 0.$$

$$b_{21} = \bar{q} \frac{S l_{\mu}}{I_y} \left[C_{m\eta} - \frac{l_{\mu}}{V} \cdot C_{m\dot{\alpha}} \cdot \left(\frac{\bar{q}}{V} \cdot \frac{S}{m} C_{A\eta} \right) \right]$$

$$b_{31} = - \frac{\bar{q}}{V} \cdot \frac{S}{m} \cdot C_{A\eta}$$

$$b_{41} = - \bar{q} \cdot \frac{S}{m} \cdot C_{W\eta}$$

In the equations the following symbols have been used:

Symbol	Description	Unit
\bar{q}	Dynamic pressure $q = \frac{1}{2} \rho V^2$	N/m^2
ρ	Air density	kg/m^3
V	True airspeed	m/s
S	Reference wing area	m^2
l_{μ}	Reference chord	m
m	Mass	kg
I_y	Moment of inertia about y-axis	kgm^2
g	Acceleration due to gravity	m/s^2
M	Mach number	-
C_{Ai}	Nondimensional lift derivatives	-
C_{Wi}	Nondimensional drag derivatives	-
C_{mi}	Nondimensional pitching moment derivatives	-

For sea level we obtain the following numerical values

Expression	Value	Unit
$\rho \cdot \frac{S}{M}$	$3.416 \cdot 10^{-3}$	m^{-1}
$\sqrt{\bar{q}} \cdot \frac{S}{M}$.581 M	s^{-1}
$\bar{q} \cdot \frac{S}{M}$	197.7 M^2	ms^{-2}
$\bar{q} \cdot \frac{Sl_{\mu}}{I_y}$	102.9 M^2	s^{-2}
$\sqrt{\bar{q}} \cdot \frac{Sl_{\mu}}{I_y}$.3026 M	$m^{-1} \cdot s^{-1}$
$\sqrt{\bar{q}} \cdot \frac{Sl_{\mu}^2}{I_y}$	1.479 M	s^{-1}

Values of the nondimensional derivatives

	Mach number				
	.206	.8	.9	1.	1.1
C_A	.915	.079	(-)	(-)	.0404
$C_{A\alpha}$	2.8	3.26	(-)	(-)	3.26
C_{AM}	0	0	.25	(-)	-.12
$C_{A\eta}$.24	.34	(-)	(-)	.328
C_W	.242	.0175	(-)	(-)	.0416
$C_{W\alpha}$.555	.085	(-)	(-)	.031
C_{WM}	0.	0.	0.	.4	.02
$C_{W\eta}$	-.14	0.	(-)	(-)	0.
$C_{m\alpha}$	-.098	-.275	(-)	(-)	-.594
$C_{m\dot{\alpha}}$	-.475	-.49	(-)	(-)	-.57
C_{mq}	-1.	-1.17	(-)	(-)	-1.35
C_{mM}	0.	-.037	-1.	(-)	.0323
$C_{m\eta}$	-.322	-.49	(-)	(-)	-.511

(-) denotes: actual values can be computed by linear interpolation.

CONTROL LAW DESIGN FOR TRANSPORT AIRCRAFT FLIGHT TASKS

by
 Volkmar Adam
 Hagen Leyendecker
 Deutsche Forschungs- u. Versuchsanstalt
 für Luft- u. Raumfahrt
 Flughafen
 3300 Braunschweig
 Federal Republic of Germany

Summary

The manufacturers Bodenseewerk Gerätetechnik, MBB, VFW-Fokker and the research institution Deutsche Forschungs- u. Versuchsanstalt für Luft- u. Raumfahrt have developed and flight-tested an integrated digital flight control system for future transport aircraft. The primary objective of the program was, both to improve the manual control of the aircraft assisted by control systems, and to develop new control and display systems. In addition, automation is to be provided for longer flight phases which are to be optimized with respect to fuel consumption, flight time, or other criteria. This paper describes some aspects of the control law design and flight test experience with the integrated digital flight control system.

Nomenclature

a	speed of sound	p	roll rate
a_y	lateral acceleration	p_H	static pressure
C_D	drag coefficient	q	dynamic pressure
C_D/C_L	drag/lift ratio	q	pitch rate, rad/s
C_L	lift coefficient	r_s	thrust pitch moment arm
$C_{L(*)}$	lift coefficient due to the variable(*), e.g. C_{L_α}	S	wing reference area
$C_{l(*)}$	rolling moment coefficient due to the variable(*), e.g. C_{l_p}	s	Laplace operator
$C_{m(*)}$	pitching moment coefficient due to the variable(*), e.g. C_{m_q}	U_w	horizontal wind speed
CWS	control wheel steering	v	indicated air speed as an element of the state vector
EPR	engine pressure ratio	V_{IAS}	indicated air speed
F	thrust	V_K	velocity of aircraft mass center
Fl	angle of flaps	V_{TAS}	true air speed
g	acceleration due to gravity	W	aircraft weight
GCS	guidance and control system	W_w	vertical wind speed
\dot{h}	vertical speed, m/s	\underline{x}	state vector
i_x	dimensionless moment of inertia about x-axis	Y	flight path angle
$K_{F(*)}$	feedback of the variable(*) to the thrust, e.g. K_{F_v}	$\delta_a, \delta_e, \delta_r$	angles of aileron, elevator, and rudder, rad
$K_{\delta_a(*)}$	feedback of the variable(*) to the aileron, e.g. $K_{\delta_a\phi}$	δ_{ap}, δ_{ep}	pilot's commands via control wheel
$K_{\delta_e(*)}$	feedback of the variable(*) to the elevator, e.g. $K_{\delta_e\theta}$	$\Delta(*)$	deviation from a reference flight, e.g. $\Delta\delta_e$
$K_{\delta_r a_y}$	lateral acceleration feedback to the rudder	$\epsilon\dot{h}, \epsilon V, \epsilon\phi$	control error signals
l_μ	length of mean aerodynamic chord	θ	pitch attitude, rad
M	Mach number	ϕ	bank angle
m	aircraft mass	ρ_H	air density
n	normal load factor	ω_N	undamped natural frequency
		ξ	damping ratio
		Subscripts:	
		c	commanded
		o	reference flight
		sp	short period mode

1.0 Introduction

In the past, the increasing operational requirements placed on the flight control system of transport aircraft have led to systems of more complexity with a large number of components. This resulted in increasing weight, volume, energy consumption and costs and paved the way for digital flight control systems. The advantage of digital systems compared to former analog developments becomes obvious, if the following is considered:

- Integration of a great deal of single functions in a limited number of computers.
- Simple implementation of complex algorithms.
- High flexibility due to definition of system characteristics by software.
- Good self-checking capability.

Airlines thus expect the digital flight control system which will be used in the next generation of transport aircraft to provide a reduction in cost and a further improvement in performance, in particular when provision of additional operating modes and automatic functions is desired.

The increasing air traffic density in the Terminal Maneuvering Area and the size of the aircraft in use today place high requirements on the ability of the pilot and on the quality of the control and sensor system. For the coming near terminal operational procedures, the pilot should be able, with the minimum possible work load, to achieve a precision level in aircraft guidance close to that of an automatic system. Thus, an important development objective is both to improve the manual control of the aircraft assisted by control systems, and to develop new control and display systems. In addition, automation is to be provided for longer flight phases which are to be optimized with respect to fuel consumption, flight time, or other criteria. The development of such functions becomes more and more important as fuel prices rise.

In order to gather experience with regard to the above-mentioned operational aspects, an integrated digital flight control system for future transport aircraft has been developed and flight-tested with a HFB 320 (figure 1) as part of a research project sponsored by the Federal Minister of Research and Technology.

2.0 The guidance and control system

The flight control system includes a guidance and control system modes concept (GCS modes concept) with a hierarchical structure corresponding to the degree of automation. The three levels of the hierarchy are control wheel steering, automatic modes, and automatic functions (figure 2). The basic GCS mode is the control wheel steering mode, which considerably simplifies flying the aircraft. By control wheel deflections, the pilot can intervene at any time and command changes for the longitudinal motion in the pitch attitude, or in the rate of vertical speed, respectively, if thrust control is active. In the lateral motion he can command changes in the bank angle. The primary automatic modes and functions are immediately switched off and the control system calculates control surface deflections for stabilization of the required new flight condition. This results in high maneuverability with reduced pilot work load.

The modes for altitude and heading hold are automatically engaged when the pilot has approximately reached stationary straight and level flight condition via control wheel steering. All other GCS modes are selected and engaged on the control unit of the flight control system. In addition to well-known autopilot modes for altitude change, heading change and VOR navigation, the autothrottle mode is implemented for preselection of aircraft speed. By further, newly developed GCS modes, aerodynamic variables are controlled, too. For example, the pilot selects a multiple of the stall speed. Automatically the actual aircraft configuration with respect to weight, flap position, etc. is taken into account by the control law computation. Furthermore, a climb maneuver can be initiated with maximum flight path angle or with maximum vertical speed on the pilot control unit of the control system. In addition, automatic functions can be selected, which permit automatic execution of longer flight phases. These functions are making use of the ordinary GCS modes and include automatic approach or automatic overshoot in the case of a missed approach, transition from cruising flight to the approach flight condition with minimum fuel consumption and transition with time control.

The management of the GCS mode concept is performed by the GCS management logic. The software of the flight control system is divided into three sections: Computation of command inputs, controller outputs, and computation of total control variables. Each of these sections includes several modules which can be activated individually. Corresponding to its logic state with respect to the engaged GCS modes, the GCS management logic selects the respective modules of the three sections. Figure 3 demonstrates, for example, which modules of the three sections are engaged when AUTOLAND is switched on together with the compatible GCS mode speed change (VC).

3.0 The sensor system

All sensor signals required by the flight control system are provided by the sensor system in a filtered form suitable for flight control. The signal quality of the various sensors corresponds to the expected standard for future transport aircraft. Filtering of the measured analog signals is carried out on the analog side as the digital controller does not permit high frequency filtering due to its sample time.

An air data and navigation calculation program processes the signals of the static pressure sensor, of the inertial sensor system, and of the radio navigation receivers. The vertical acceleration signal is integrated twice and is slowly slaved to pressure altitude signal, resulting in very smooth altitude and vertical speed signals.

The long-term errors of the inertial navigation system are reduced aiding with a reference position. The reference position can be calculated either from the signal of a MLS station or from those of a VOR-DME station. If the reference signal fails during a turn at low altitude due to shadowing of the antennas on the aircraft, a very precise continuous flight path can still be maintained. This means that navigation signals of a constant quality corresponding to the short-term accuracy of the platform are available in all GCS modes which are used in the Terminal Maneuvering Area.

4.0 Dimensioning of the flight control system

In accordance with the hierarchical structure of the flight control system, dimensioning of the controller consists of step-by-step development of a coupled multivariable feedback system. All essential sensor and command inputs act on the controls available to the flight control system. These controls are rudder, aileron and elevator. The throttle

of the engines is used additionally in some GCS modes. If the selected controller structure (figure 4) is applied strictly, the design of the system eigenmodes can be separated from the gain determination of the command feedforward loop and the disturbance compensating loops.

Well-damped eigenvalues must be achieved for all flight conditions and for every conceivable combination of GCS modes. This also provides an improved response to gust in case of no direct feedforward gust alleviation system. Disturbances resulting from configuration changes of the aircraft, for example extension and retraction of flaps or landing gear, can be modeled with a good degree of accuracy and can therefore also be compensated by open loop control.

Various methods are used to determine the gains of the flight control system and to schedule them to flight condition parameters. It should be emphasized that the classical methods such as the time vector method (ref. [1]) and the root locus method have proved to be as useful as modern numerical design methods such as solving the Riccati equation or automatic parameter optimization by minimizing a cost function (ref. [2, 3]).

The methods were used with equal priority and their results have supplemented and supported each other. As the control system gains and the system dynamics after minimization of a cost function do not necessarily comply with the engineer's ideas, gain modification "by hand" together with a nonlinear simulation still plays an important part in the development of a multivariable feedback system. The design engineer has a fairly wide decision range in which there is more than one satisfying combination of possible structures and corresponding gains for achieving good closed loop response.

In contrast to the feedback loop design, the feedforward open loop control is determined explicitly. High control accuracy is strongly dependent on the precision of the control surface positioning with respect to the dynamic feedforward open loop control signal. On the one hand, the command model must not exceed the flight-mechanical capabilities of the aircraft, on the other hand, all knowledge of the aircraft dynamic behavior during stationary and instationary flight phases must be taken into account for the open loop control. If the error because of undesired stimulation of the eigenmodes is reduced, then unnecessary deflections of the controls would also be reduced. This is, for example, the case when aileron and rudder are to be deflected at the begin of a turn, or when elevator and thrust increase is needed during a steady turn.

In the first design step, feedback of the complete state vector was considered. The physical effects of the various control loops were then examined both by analytical methods and by simulation. An important design objective was to reduce the number of feedback loops to the really necessary ones without loss in performance. A further design objective was to maintain the existing structure and gain factors of the basic inner control loops when further loops were added by activation of other GCS modes. The design was carried out iteratively, i.e. the effects of each modification step was checked by simulation. Also the pilot rating was included in the evaluation process to define the modifications for the next iteration step. The following chapters describe how the final determination of the control structure and gains was carried out for the basic modes, such as the control wheel steering modes. A detailed presentation of all intermediate steps has been omitted.

4.1 Feedforward open loop control laws

A criterion for the quality of a control system is the activity of the controls. This is particularly true for the throttle activity. Therefore, open loop control laws are determined on the basis of good knowledge about the aircraft behavior resulting from deflections of the controls. Thus, necessary adjustments for command changes and known disturbance effects are rapidly carried out with reduced control activity. The following examples demonstrate how the open loop control laws are developed.

4.1.1 Compensation of secondary effects of thrust control

In addition to the desired effects, the controls have undesirable secondary effects, too. For example, an increase in thrust not only changes the resultant longitudinal force, but also provides a component in lift direction and generates a pitch moment. The only really important secondary effect of the HFB 320 thrust control is the resultant pitch moment. Therefore, a compensation by proportional elevator deflection was carried out. Pitch moment balance indicates:

$$\Delta \delta_e = \frac{-r_s}{C_{m\delta_e} \mu \bar{q} S} \Delta F \quad (1)$$

As the thrust cannot be measured directly, it must be determined approximately from the engine pressure ratio EPR:

$$\Delta F = \Delta EPR \cdot K_{FEPR} \frac{\bar{q} + P_H}{P_0} \quad (2)$$

where K_{FEPR} is a constant and the second term takes into account changes in air density and Mach number. Thus, elevator deflection due to thrust changes can be expressed by:

$$\Delta \delta_e = K_{\delta_e F} \frac{\bar{q} + P_H}{P_0} \left(\frac{\bar{q}}{\bar{q}_0} \right) \Delta EPR \quad (3)$$

with the constant factor

$$K_{\delta_e F} = - \frac{C_{m\delta_e} \cdot K_{FEPR}}{C_{m\delta_e} \cdot l_{\mu} \bar{q}_0 \cdot S} \quad (4)$$

4.1.2 Thrust setting

According to the GCS modes control concept, the throttle is used for control of speed, and either altitude or vertical speed. The linearized force equations in x- and z-direction provide the following expression for the thrust setting:

$$\frac{\Delta F}{W} = \frac{\dot{V}_K}{g} + \frac{\dot{H}}{g} + \left(\frac{C_D}{C_L} - \frac{W_w}{V_{TAS}} \right) \cdot n \quad (5)$$

Since V_{TAS} is the control variable for speed, V_K must be substituted by:

$$V_K = V_{TAS} + U_w \quad \text{with} \quad V_{TAS} = V_{IAS} \cdot \sqrt{\frac{\rho_0}{\rho_H}} \quad (6a, 6b)$$

Thus, the following relation results for the thrust setting:

$$\Delta F = W \cdot \left[\frac{V_{TAS}}{g} \sqrt{\frac{\rho_0}{\rho_H}} + \frac{\dot{H}}{V_K} + \left(\frac{C_D}{C_L} - \frac{W_w}{V_{TAS}} \right) n + \frac{U_w}{g} \right] \quad (7)$$

The weight W of the aircraft is a multiplicative factor for all of the various input variables and is therefore of great importance for open loop control of the thrust. Determination of the weight from the takeoff weight minus the weight of fuel consumed during the flight is necessary, but sufficient with respect to the measurement accuracy.

The thrust law shows that further variables determine the thrust required for changes in speed. First, the thrust is immediately be adjusted in proportion to the acceleration command. Secondly, the drag-lift ratio C_D/C_L has to be taken into account. During cruise flight condition the drag-lift ratio is relatively constant. Therefore, changes can be ignored in this case. But during landing approach with changing flap position or landing gear extension the effect of changes in the drag-lift ratio on the speed error becomes significant, due to the decrease in aerodynamic efficiency. An approximate thrust correction as a function of the flap position at an average angle of attack is therefore provided.

During climb and descent, the thrust requirement depends on the flight path angle $\gamma = H/V_K$. In some of the GCS modes a continuous command function for altitude rate (\dot{H}) is generated, resulting in corresponding changes of the thrust setting. During a turn maneuver the normal load factor n changes, too. The necessary thrust increase depends on

$$\Delta n \approx \frac{\phi^2}{2}$$

It becomes obvious that the open loop thrust control can be easily performed, because the variables needed for a suitable thrust setting can be derived within the computer. In principal, this is also true when, in addition, the remaining terms of the required thrust setting with respect to wind disturbances (W_w, U_w) are considered. For the control system presented in this paper, these terms are neglected for open loop thrust setting.

4.1.3 Open loop for steady turn maneuvers

The position of the controls required to maintain the steady turn is defined by the steady state condition with respect to the aerodynamic moments about the three axes. Since the deflections of aileron and rudder are very small, it is sufficient to consider the elevator angle only. The change in elevator control surface deflection required in a steady turn is the following (ref. [4]):

$$\Delta \delta_e = - \frac{C_{m\alpha} \cdot W}{C_{m\delta_e} \cdot C_{L\alpha} \bar{q} \cdot S} (n-1) - \frac{C_{m\alpha}}{C_{m\delta_e}} \cdot \frac{l_{\mu}}{V_{TAS}^2} \cdot g \cdot n \left(1 - \frac{1}{n^2} \right) \quad (8)$$

$$\text{with the normal load factor } n = \frac{1}{\cos \phi} \quad (9)$$

The expression for $\Delta \delta_e$ can be simplified for bank angles less than 30° and by introduction of the dynamic pressure ratio \bar{q}_0/\bar{q} :

$$\Delta \delta_e = K_{\delta_e \phi^2} \cdot \phi^2 \cdot \frac{\bar{q}_0}{\bar{q}} \quad (10)$$

with $K_{\delta_e \phi^2}$ as a multiplicative constant:

$$K_{\delta_e \phi^2} = \frac{C_{m\alpha}}{C_{m\delta_e}} \cdot \frac{l_{\mu}}{V_0^2} \cdot g - \frac{C_{m\alpha} \cdot W}{2 C_{m\delta_e} C_{L\alpha} \bar{q}_0 \cdot S} \quad (11)$$

4.2 Design experiences

4.2.1 Longitudinal motion

The design requirements with respect to flying quality characteristics are based on specified areas for eigenvalues of the aircraft in the root locus plot (ref. [5]). Therefore, the root locus method is mainly used for the dimensioning of the control behavior in the basic GCS mode, the control wheel steering mode. If the number of closed control loops is small, the coupling effects of the gains remain clear and are easily represented. The design can be carried out in a simple, straightforward manner.

For the longitudinal motion of the aircraft, the requirements for the short-period natural frequency ω_N and the damping ratio ξ , are specified in ref. [5]. Figure 5 shows that the experimental aircraft HFB 320 meets the frequency requirements even in the uncontrolled case. Also the damping ratio ξ of the short-period mode meets the requirements of ref. [5]. In addition to these requirements, a design goal is defined for the relative damping of the short-period mode as $\xi = 0.7$ for all flight conditions. Furthermore, the damping of the phugoid mode needs improvement. Figure 6 shows the control structure for the control wheel steering mode (CWS- θ).

In addition to the feedback gains $K_{\delta_{eQ}}$ and $K_{\delta_{e\theta}}$, which are determined at first, three further feedback loops are always active to compensate for effects during a turn maneuver, for the lift change when flaps are extended, and for the pitch moment due to thrust changes. The compensating task of these feedback loops is strongly alleviated by the open loop control as described in chapter 4.1.

The complete range of flight operation was analyzed using the time vector method and the root locus method, both showing the interactions of $K_{\delta_{eQ}}$ and $K_{\delta_{e\theta}}$ with respect to damping and frequency of the two eigenvalue pairs of the longitudinal motion. Figure 7 provides an example of the investigations described here. The $K_{\delta_{eQ}}$, $K_{\delta_{e\theta}}$ combination shown in figure 7, ensures together with adaptive elevator control as a function of the dynamic pressure that the relative damping of the short-period mode is located between 0.7 and 0.82 in all flight conditions examined, and that the eigenfrequency ω_N is increased slightly compared with that of the uncontrolled aircraft (figure 5). At the same time, the relative damping of the phugoid mode is always greater than 0.70. Figure 8 shows a simulation result of the control wheel steering mode CWS- θ in turbulent air.

The turbulence model used corresponds to ref. [5], for clear air turbulence at an altitude of 500 feet. The pitch command input is derived from a typical pull-up maneuver, with a constant pitch rate of $q_C = 2^\circ/\text{s}$ at the beginning, then being reduced asymptotically to zero as the required new pitch attitude is approached.

The response of the uncontrolled aircraft to gust disturbances is shown on the right-hand side of figure 8. The comparison with the response of the controlled aircraft demonstrated the effect of the $K_{\delta_{eQ}}$, $K_{\delta_{e\theta}}$ combination, particularly on the stabilization of the pitch attitude. Figure 9 shows simulation results in turbulent air for four different flight conditions. Satisfactory results were obtained by constant gains and dynamic pressure adaption throughout the entire flight envelope investigated (figure 6). As operation of the flight control system for both without and with an integrated auto-throttle system is planned, it was also possible to test a second control wheel steering mode CWS-H (figure 10) in the experimental system.

In accordance with the hierarchical and modular structure of the flight control system, all loops of the pitch damper and the control wheel input with the gain $K_{\delta_{eQ}}$ act on the elevator. A vertical speed command H_C is generated from the control wheel signal by multiplication with the true airspeed signal and integration with respect to time. The vertical speed error signal activates the elevator by a proportional gain $K_{\delta_{eH}}$ and by integration with the gain $K_{\delta_{eH}}$. A signal for adjustment of the thrust is generated from the difference between the command signal H_C and the vertical speed existing when the mode was engaged.

As this CWS mode must also comply with the flying quality requirements described above, the root locus method is again suitable for design. However, the relationship of the four gains $K_{\delta_{eQ}}$, $K_{\delta_{e\theta}}$, $K_{\delta_{eH}}$, and $K_{\delta_{eH}}$ would have become difficult to read if the values were not related to the $K_{\delta_{eQ}}$, $K_{\delta_{e\theta}}$ combination previously determined. Figure 11 shows that the eigenfrequency ω_N of the short-period mode is reduced slightly by the gains $K_{\delta_{eH}}$ and $K_{\delta_{eH}}$, but still complies well with the requirements of figure 5. The selected $K_{\delta_{eH}}$, $K_{\delta_{eH}}$ combination (figure 11) also requires dynamic pressure adaption for the elevator, as shown by analysis for the examined flight envelope.

In parallel to these investigations by use of the root locus method, a linear optimization method by solving the Riccati equation was used. If physically reasonable weighting coefficients K_i are used, the cost functional

$$J = \int_0^{\infty} [K_1 \dot{q}^2(t) + K_2 \dot{H}^2(t) + K_3 H^2(t)] dt = \text{MINIMUM} \quad (12)$$

provides gains which correspond to the results of the root locus method. For good dynamic behavior, which is influenced not only by the pole position but also by the corresponding eigenvectors, cautious changes of the eigenvalues from those of the uncontrolled system are favorable.

Figure 12 shows a typical simulation result with the control structure of figure 10. The open loop control of the thrust in this example is rather weak, which means that the speed decreases during the climb and returns gradually to the initial value after the climb maneuver is completed. As the correct open loop control depends almost exclusively on the actual aircraft weight, the pilot must expect a change in the speed behavior, depending on whether the open loop control provides too much or too little thrust for the climb. However, the very slow return to the initial value of speed always occurs.

This behavior results from the pole near the origin (figure 11), which has previously received little attention. As the speed is the major element in the corresponding set of eigenvectors and the position of the pole changes only slightly with varying weighting coefficients in the cost functional, the gain K_{Fv} must be of great importance for this eigenvalue. Figure 13 clearly shows, in comparison with figure 12, how the climb speed control operates with and without speed feedback loop.

Root locus graph examinations show that the speed feedback to the thrust has a significant effect on the position of the problematic pole near to the origin over the entire flight envelope, while the other two pairs of poles, already set up by the above-mentioned four feedback loops to the elevator, remain at about the same position.

It is clear that the speed must be fed back to the thrust in order to provide satisfactory dynamic behavior for the CWS-H mode. This means one step towards speed control.

The optimization method by solving the Riccati equation was applied to the coupled multivariable system with the state vector $\underline{x} = (\theta, q, \dot{H}, H, v)$ and the two controls elevator and thrust. With selected weighting coefficients K_i , the cost functional

$$J = \int_0^{\infty} [K_1 q^2(t) + K_2 \theta^2(t) + K_3 \dot{H}^2(t) + K_4 H^2(t) + K_5 v^2(t)] dt = \text{MINIMUM} \quad (13)$$

provides the gains $K_{\delta_{eq}}, K_{\delta_{\theta}}, K_{\delta_{\dot{H}}}, K_{\delta_{H}}$ which were determined from the root locus graph examination and, on the basis of the complete state vector feedback, the gains $K_{Fv}, K_{\delta_{ev}}, K_{Fq}, K_{F\theta}, K_{FH}$, and $K_{F\dot{H}}$ which were previously not considered.

This design method again shows the importance of the gain K_{Fv} , in that a variation of the weighting coefficient K_5 results almost exclusively in a change of the gain K_{Fv} . In contrast to this, variation of the other weighting coefficients change all feedbacks in a manner which cannot be predicted.

By detailed simulation, it becomes evident that the gain $K_{\delta_{ev}}$ will better be determined by a physical consideration than by using the result of the optimization run. Flying with constant glide path angle, the elevator must be deflected when a speed change is commanded. Provided that the x-force balance is achieved by the thrust during the phase of acceleration, the required control surface deflection can be derived from the condition that changes of aerodynamic z-force and pitch moment must be approximately zero. The combination of the two equations results in the following relationship:

$$\frac{\Delta \delta_e}{\Delta V_{IAS}} = \frac{C_{L\alpha}}{C_{m\alpha} C_{L\delta_e} - C_{L\alpha} C_{m\delta_e}} \left[\left(\frac{F}{W} \frac{r_s}{l_M} - \frac{C_{m\alpha}}{C_{L\alpha}} \right) \frac{2W}{V_{IAS} \bar{q} S} + \left(C_{mM} - \frac{C_{m\alpha}}{C_{L\alpha}} C_{LM} \right) \frac{1}{a} \right] \quad (14)$$

In the speed range 130-230 kts the neutral point position defined by $C_{m\alpha}/C_{L\alpha}$ has the most important influence on the required elevator deflection during speed change. This term must thus be realized within the control structure. As the aerodynamic derivatives in equation (14) are approximately constant in the flight regime investigated the gain is easily determined.

The other four gains $K_{Fq}, K_{F\theta}, K_{F\dot{H}}$, and K_{FH} have little effect on the closed loop behavior and are thus not so important. From a physical point of view, the small effect of the two gains $K_{F\dot{H}}$ and K_{FH} in an altitude control loop is surprising. An energy consideration of the aircraft provides a certain amount of clarification.

As mentioned previously a particularly important criterion in flight control system design is a low throttle activity. On the other hand, increasing the thrust is the only possibility of supplying additional energy to the aircraft, i.e. it is not possible to fly without any activity of the thrust. Minimization of the thrust activity is achieved if the thrust is used only for modification of the total energy and if the exchange of potential and kinetic energy is controlled by the elevator. A controller which controls altitude H and indicated air speed V_{IAS} can, therefore, be named an energy controller.

If small deviations from a reference steady flight condition are considered, the linearized form of the change in total energy can be expressed by

$$\Delta E = m \cdot g \cdot \Delta H + m \cdot V_K \cdot \Delta V_K, \quad (15)$$

whereby the mass is regarded as constant for short times.

Since the controller is intended to control V_{IAS} , the appropriate substitution of V_K must be carried out with the equations (6a, 6b). This then results in

$$\Delta E = m \cdot g \cdot \Delta H + m \left(\Delta V_{IAS} \sqrt{\frac{\rho_0}{\rho_H}} + \Delta U_W \right) V_K \quad (16)$$

If the energy is to remain constant, then any change in the wind U_W will cause a deviation in the speed and the altitude. In addition, any change of altitude at a constant wind speed will result in speed error. In case of flight in higher altitude (corresponding to the change in the density) or with higher velocity V_K , deviation from the speed V_{IAS} causes increasing altitude errors. Conversely, it can be said that speed control will be satisfactory if it is possible to achieve good altitude maintenance with the elevator at high altitudes and high speeds. A controller which is intended to control the total energy by means of the thrust must be designed in accordance with the structure in figure 4. In addition to the open loop control of the thrust defined in chapter 4.1 proportional and integrated speed feedback must be provided. If the potential

and kinetic energies are regarded as command inputs, then the two paths must be connected together with appropriate weight:

$$\Delta F \sim \frac{\Delta E}{V_K} = W \cdot \left(\frac{\Delta H}{V_K} + \frac{\Delta V_{AS}}{g} \sqrt{\frac{\rho_0}{\rho_H}} + \frac{\Delta U_w}{g} \right) \quad (17)$$

The speed feedback loop is therefore dependent on the aircraft weight and the air density. Parameter investigations have shown that a constant gain K_{FV} is sufficiently satisfying throughout the operational envelope considered. The altitude feedback loop is dependent on the velocity V_K ; the thrust control becomes weaker as the velocity increases. This explains why the gain K_{FH} has a noticeable effect only in the case of the aircraft flying at low speeds. However, simulations of flight with the GCS modes VC and ALT HOLD engaged and with simultaneous flap setting show that inclusion of K_{FH} provides an additional reduction in the thrust activity. The controller structure implemented in the flight control system, divided into pitch damper, altitude controller, and speed controller, is shown in figure 14.

The open loop control for the speed controller consists of the gain K_{FV} . It is interesting to see that $K_{\delta_{ov}}$ is the only connection to the elevator from speed control. The nonlinear expression K_{FFI} , compensates changes in drag during flap setting. The effects of these gains are described in chapter 4.1.

The gains K_{FV} and K_{FV} are important with regard to compensation of disturbances and errors remaining from unprecise open loop control. If the thrust reaches its limits, the integrating path is disconnected, and this results in a speed error. Altitude control via the elevator still operates satisfactorily.

4.2.2 Lateral motion

The control structure for the lateral motion is much alike that one of the longitudinal motion. Also similar design steps are carried out starting with the basic GCS mode, the control wheel steering mode CWS ϕ . These investigations show that the lateral oscillation, the Dutch roll mode, can be damped either by lateral acceleration ($K_{\delta_{ay}}$) or yaw rate feedback to the rudder. The control structure is shown in figure 15. The two gains $K_{\delta_{\phi p}}$ and $K_{\delta_{\phi}}$ (figure 15) are required for bank angle control. They have virtually no effects on the Dutch roll mode. The gain $K_{\delta_{\phi}}$ is of no major importance for bank angle control, because the gain $K_{\delta_{\phi}}$ already has an integrating characteristic. However, it must be provided in the controller for trimming of the aileron after the controller has been switched on. The integrating gain is kept very small such that it causes no significant change in the dynamic behavior.

Therefore, only the two gains $K_{\delta_{\phi p}}$ and $K_{\delta_{\phi}}$ are further considered. The rolling moment equation together with the two gains, leads to the characteristic equation

$$I_x s^2 \cdot (C_{lp} + C_{l\delta_a} K_{\delta_{\phi p}}) s - C_{l\delta_a} K_{\delta_{\phi}} = 0 \quad (18)$$

If the resulting poles are always to have a relative damping $\xi \geq 0.7$, then the following relationship applies:

$$|K_{\delta_{\phi}}| \leq \frac{(C_{lp} + C_{l\delta_a} K_{\delta_{\phi p}})^2}{2 I_x |C_{l\delta_a}|} \quad (19)$$

This relationship has been evaluated to select a constant gain combination such that the relative damping is always greater than 0.7 and the eigenfrequency of the root pair is sufficiently high. As no side-slip sensor is used, the side-slip angle cannot be controlled.

Even in turns with a bank of 25° the side-slip angle is always less than 1° for the HFB 320 aircraft. An open loop control gain $K_{\delta_{r\phi c}}$ can reduce the side-slip in turn even further. If required, the pilot can deflect the rudder directly with the pedals, thus achieving a required side-slip angle, for example during an approach. In order to permit intervention in the above bank angle control loop by the control wheel steering CWS ϕ , the deflection of the control wheel corresponds to a roll rate command p_c . Figure 16 shows simulation results of the bank angle controller for four flight conditions, the gains $K_{\delta_{\phi p c}}$, $K_{\delta_{\phi p}}$, $K_{\delta_{\phi}}$, $K_{\delta_{\phi}}$, and $K_{\delta_{r\phi c}}$ being constant.

5.0 Flight tests

A flight test program was conducted, using the DFVLR experimental aircraft HFB 320. The objective was to test the algorithms for control and command computation, the GCS modes management logic and the pilot interface hardware during flight.

Because of intensive ground tests of the system by use of an elaborated nonlinear simulation no major deviation in the control performance did show up during the flight tests. Nearly all simulation results were confirmed. No essential modification of any of the control system gains or structures was necessary during the flight tests. Within 60 flight hours all control system functions and modes were tested and approved in the speed range of 130 through 230 kts.

The following figures show some flight test results. Only those flight phases were selec-

ted referring to GCS modes already presented. Figure 17 shows a climb maneuver by use of the mode CWS-H with speed control automatically engaged. The pilot's activity on the control column is plotted in the upper trace. The integral of the control wheel deflection presents the commanded vertical speed. The relief for the feedback control on thrust due to speed errors, achieved by the open loop control gain K_{FF} , becomes obvious regarding the speed deviation which is always less than 2 kts, as well as the thrust activity. The mode ALT ACQ offers another possibility of automatic altitude change. The pilot enters commands for altitude and vertical speed via keying in the corresponding value and using the RATE V/S switch on the control unit, respectively.

Two different flight phases are shown in figure 18: A descent maneuver with 1900 ft/min and 40° flap extension and a following climb maneuver with 1000 ft/min climb rate with a flap retraction from 40° to 20°. The maximum altitude deviation of about 20 ft occurs during the nonlinearly curved sections of the flight path. The flap retraction causes no remarkable deviation of speed and altitude.

Speed changes can be commanded if the mode VC is used. Figure 19 shows two deceleration phases, from 230 kts to 170 kts and, after 25 seconds, further down to 150 kts. The commanded deceleration is preset in the computer (1kt/s). The maximum speed error occurs during the deceleration phase. Its value is about 2 kts and the maximum altitude error is 15 ft.

These speed reductions are combined with a commanded heading change of 180° initiated by use of the mode HDG ACQ. The turn maneuver is carried out with a maximum bank angle of 25°. As the transition to the commanded heading is performed by controlling with a function of V_{TAS} , nearly no overshooting occurs.

Figure 20 is chosen to demonstrate the effectiveness of open loop control. The extension of flaps nearly causes no deviation of speed and altitude, although the drag is strongly dependent on the flap position. The nonlinear gain K_{FF} provides the adjustment of the thrust whereas the gain K_{dF} compensates the pitch moment due to thrust. The control loops for maintaining speed and altitude are effectively relieved.

6.0 Summary

The increasing operational requirements placed on flight control systems can be achieved economically only by use of digital technology and by construction in the form of an integrated system. Such systems also provide new possibilities in control design. Knowledge of aircraft parameters and dynamics can be exploited to develop nonlinear powerful algorithms for improvement of the control accuracy. Experience with the experimental systems have shown that in spite of a high degree of complexity in the software structure the modular structure of the software with well defined interface signals permit flexible execution of the modifications and effective testing of these modifications. The control system can be extended step-by-step by new GCS modes and additions of further control and controller modules.

Because of the fact that the control system is designed as a coupled multivariable system and that the controller structure has nonlinear feedforward open loop control, the requirements with respect to good closed loop response is achieved. Careful design of command input models matched to the flight-mechanical capabilities of the aircraft is important. If high quality sensor signals are available, for example those provided by integrated navigation and inertial attitude sensor system, then precise flight control throughout the entire flight envelope is possible.

References

- [1] Doetsch, K.H. The Time Vector Method for Stability Investigations. ARC R. & M. 2945, August 1953.
- [2] Kalman, R.E. Englar, T.S. A User's Manual for the Automatic Synthesis Program. NASA-CR-475, June 1966.
- [3] Jacob, H.G. An Engineering Optimization Method with Application to STOL Aircraft Approach and Landing Trajectories. NASA TN D-6978, September 1972.
- [4] Etkin, B. Dynamics of Flight. John Wiley & Sons, London, January 1962.
- [5] Anon. Flying Qualities of Piloted Aircraft. MIL-F-8785 B, August 1969.
- [6] Adam, V. Onker, P. Evaluation of a new Flight Path Command Control Concept. ICAS Paper No. 76-55, October 1976.
- [7] Adam, V. Leyendecker, H. Erhöhung der Führungsgenauigkeit durch den Einsatz eines integrierten digitalen Flugführungssystems. DGLR/DGON-Symp., Paper No. 79-041, April 1979.

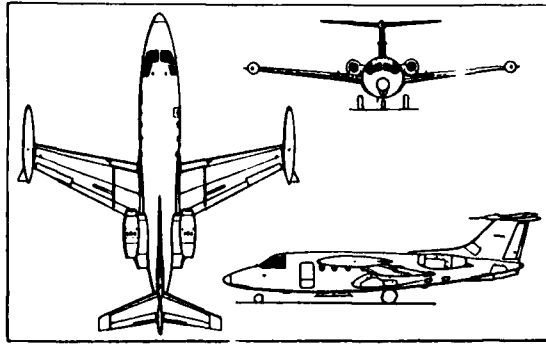


Figure 1: Three-view drawing of the experimental aircraft HFB 320 "Hansa"

CONTROL WHEEL STEERING

- o CWS-θ PITCH ATTITUDE
- o CWS-H VERTICAL SPEED
- o CWS-B BANK ATTITUDE

AUTOMATIC MODES

- o ALT HOLD ALTITUDE HOLD
- o ALT ACQ ALTITUDE ACQUIRE
- o HDG HOLD HEADING HOLD
- o HDG ACQ HEADING ACQUIRE
- o NAV VOR-NAVIGATION
- o VC SPEED COMMAND
- o VS MULTIPLE OF STALLING SPEED
- o VX MAXIMUM FLIGHT PATH ANGLE
- o VY MAXIMUM VERTICAL SPEED

AUTOMATIC FUNCTIONS

- o HOLDING AUTOMATIC FLIGHT OF HOLDING PATTERNS
- o AUTOLAND AUTOMATIC APPROACH AND LANDING
- o GO AROUND AUTOMATIC GO AROUND
- o TMA 1 3D-NAVIGATION
- o TMA 2 4D-NAVIGATION

Figure 2: Guidance and control modes concept

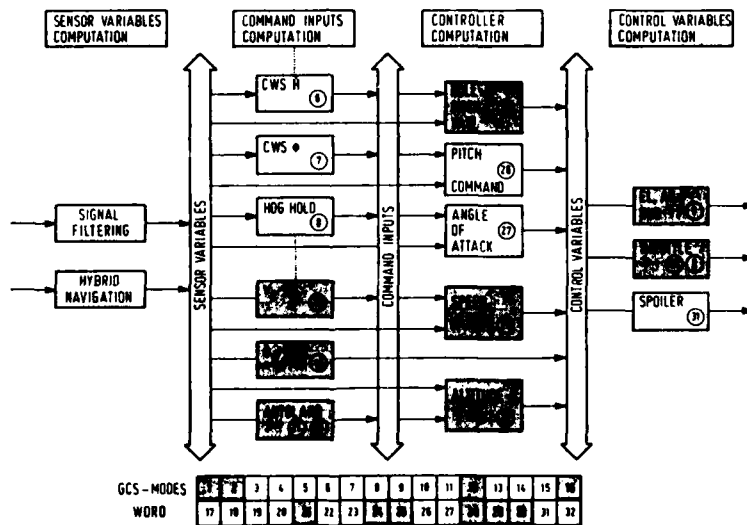


Figure 3: Connection of modules by the GCS-modes word for AUTOLAND with speed command (VC)

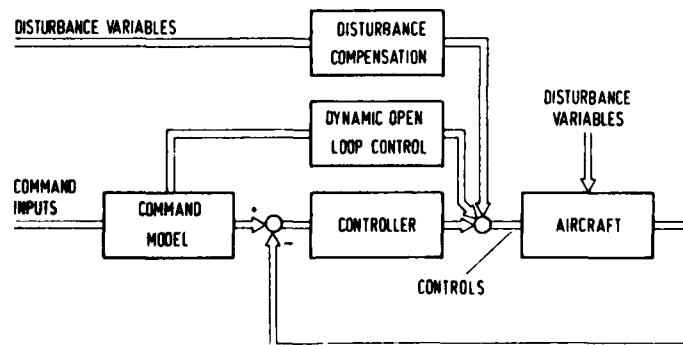


Figure 4: Block diagram of the flight control system

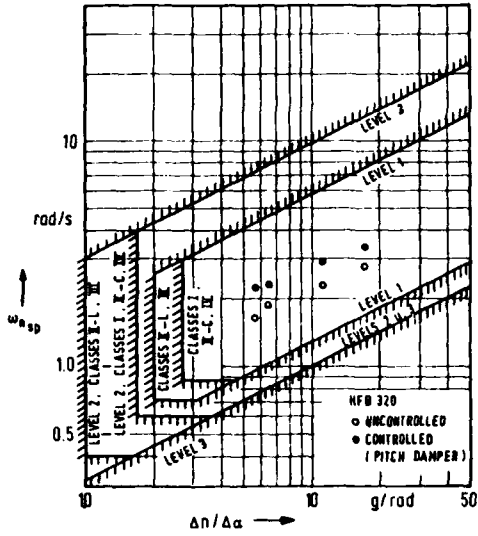


Figure 5: Short-period frequency requirements

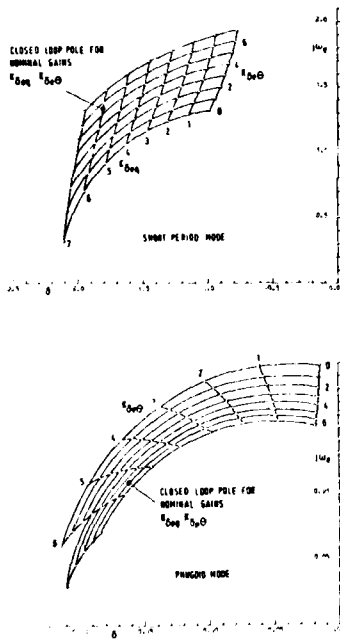


Figure 7: Root locus for pitch attitude and pitch rate feedback. IAS = 126 kts, H = 0 ft

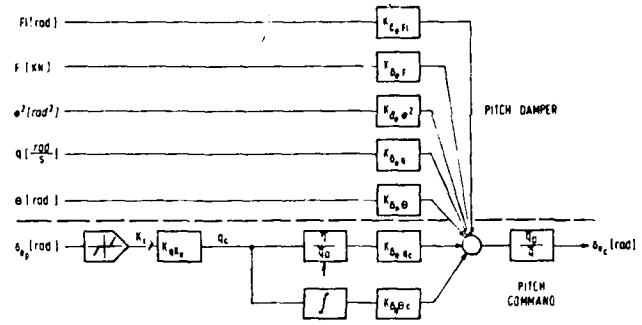


Figure 6: Functional diagram of control wheel steering CWS- θ for longitudinal control

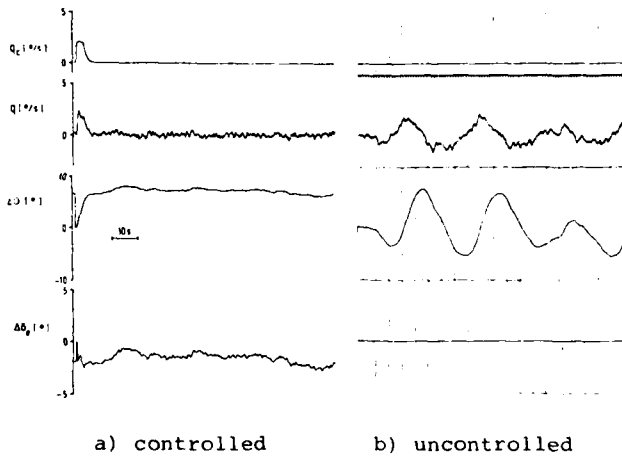


Figure 8: Simulation results for CWS- θ . IAS = 126 kts, H = 0 ft

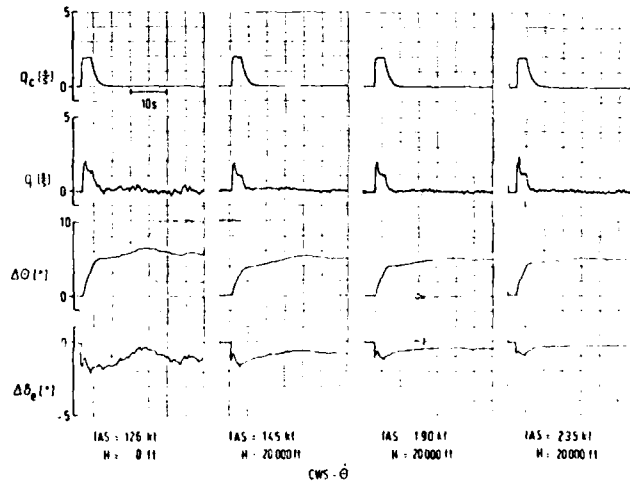


Figure 9: Simulation results for CWS- θ at four flight conditions

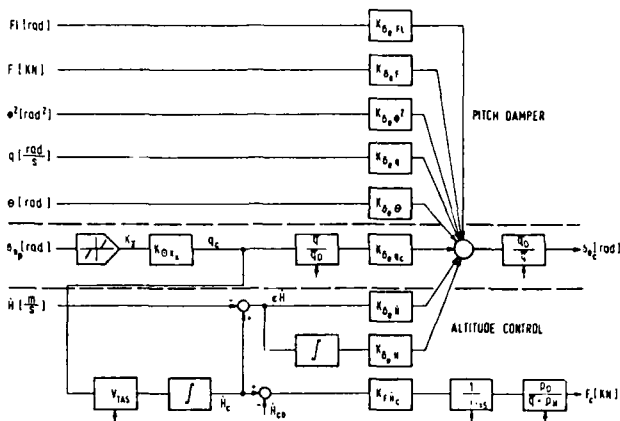


Figure 10: Functional diagram of control wheel steering CWS-H for longitudinal control

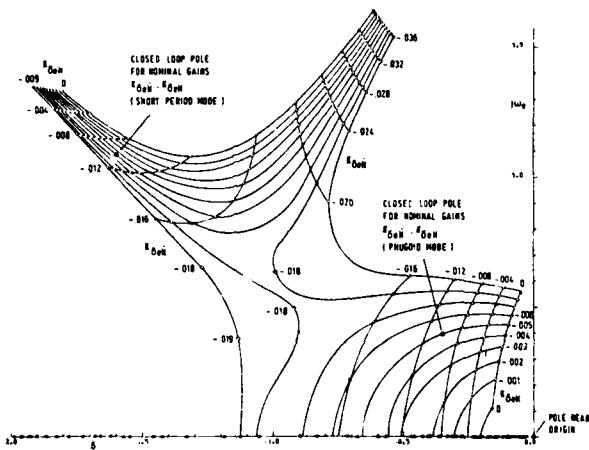


Figure 11: Root locus for \dot{H} , H-feedback with pitch attitude and pitch rate loop closed. IAS = 126 kts, H = 0 ft

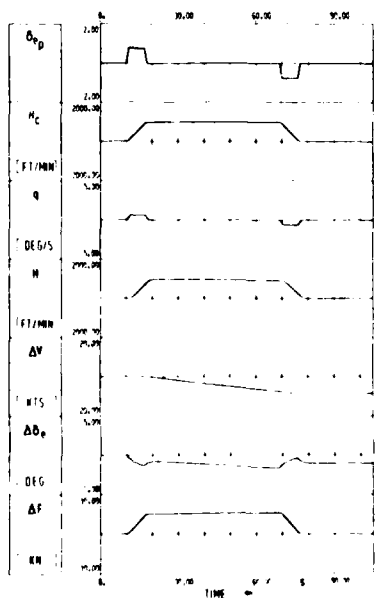


Figure 12: Simulation result of control wheel steering CWS-H without speed feedback

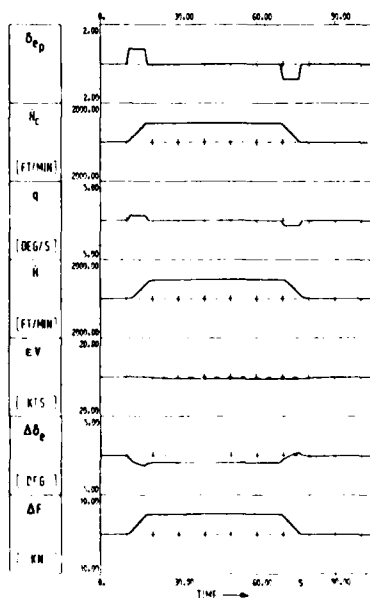


Figure 13: Simulation result of control wheel steering CWS-H with speed feedback to the thrust

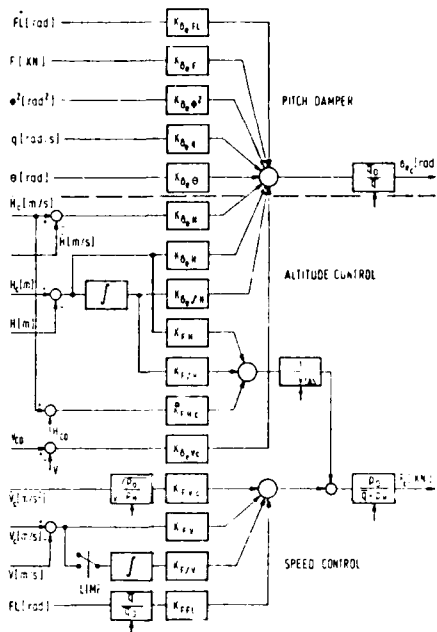


Figure 14: Functional diagram for longitudinal control

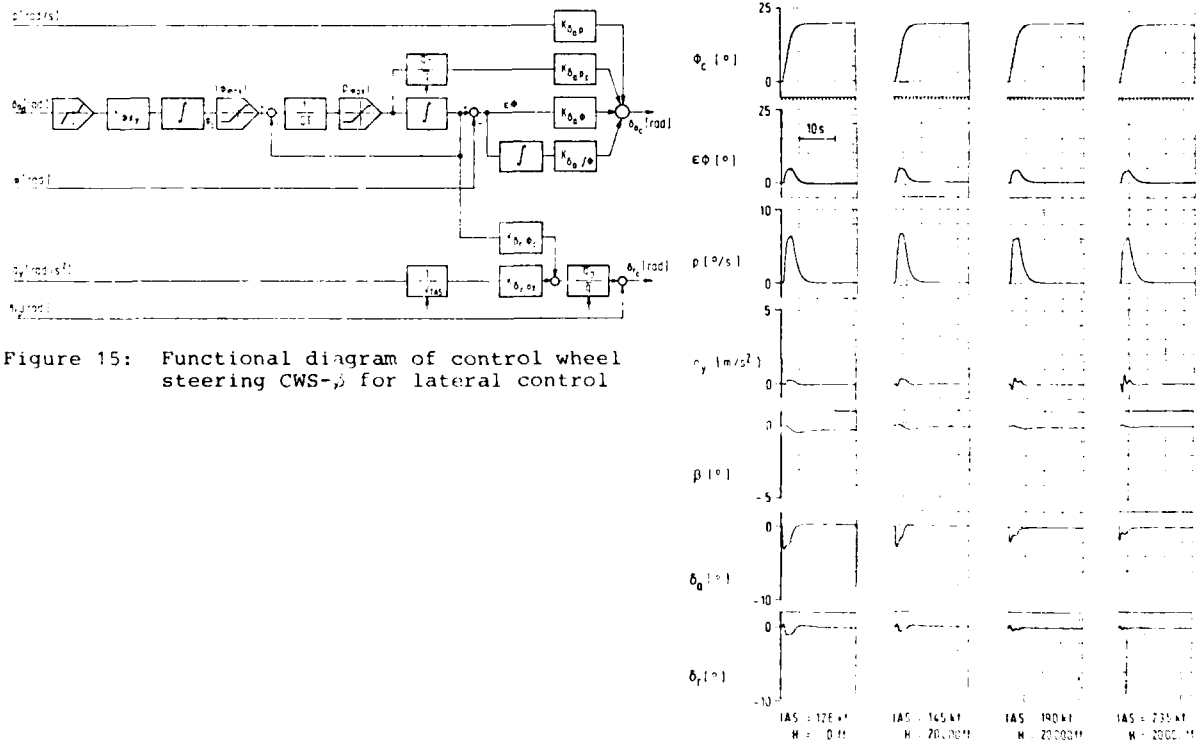


Figure 16: Simulation results for CWS- ϕ at four flight conditions

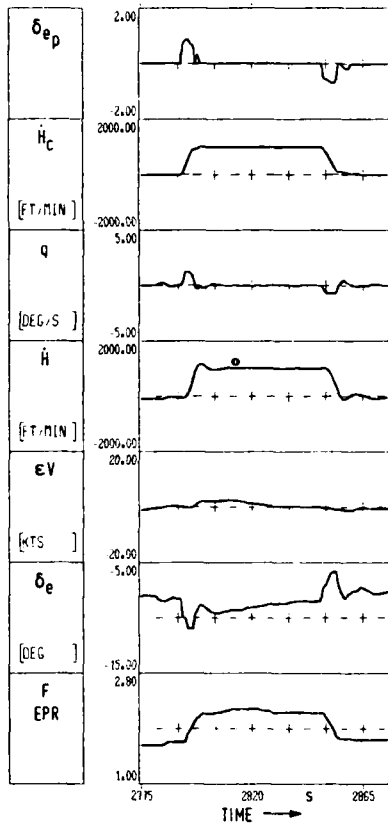


Figure 17: Flight test result with the control wheel steering mode CWS-H

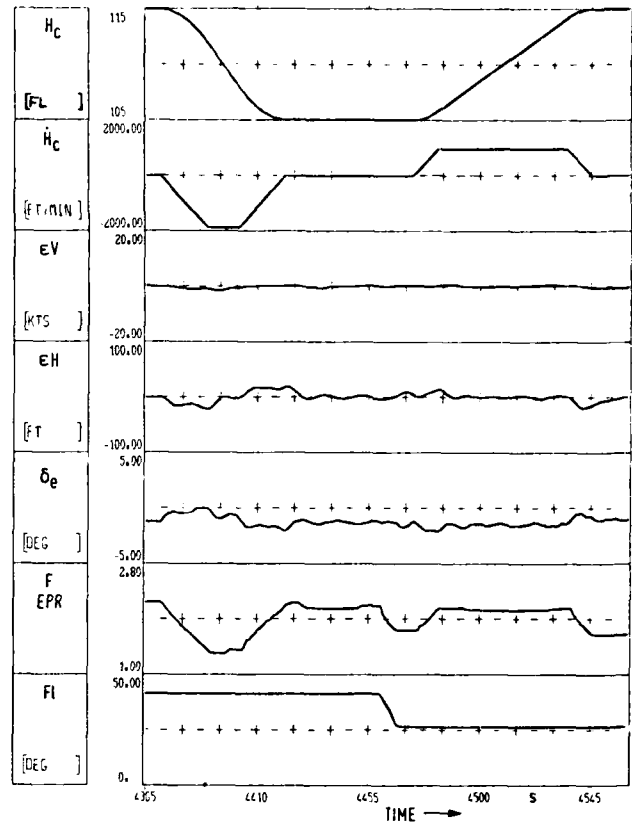


Figure 18: Flight test result with the GCS-mode altitude acquire (ALT ACQ), speed hold engaged

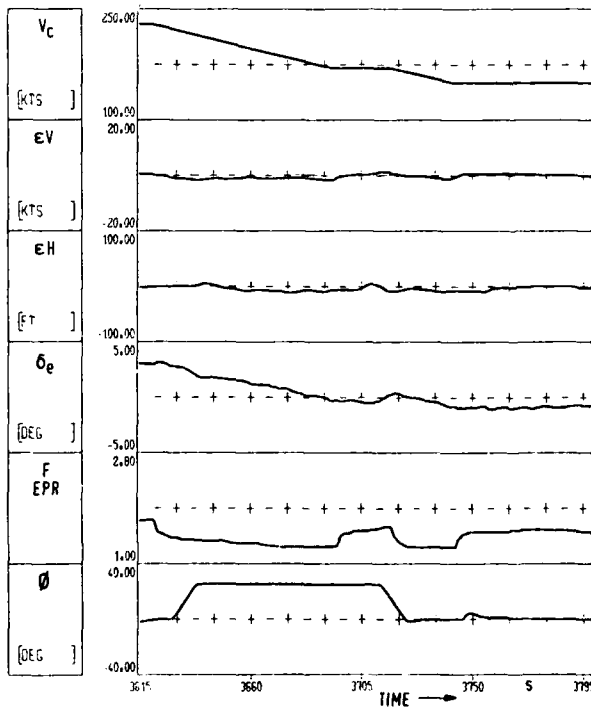


Figure 19: Flight test result with the GCS-modes speed command (VC) and heading acquire (HEAD ACQ), altitude hold engaged

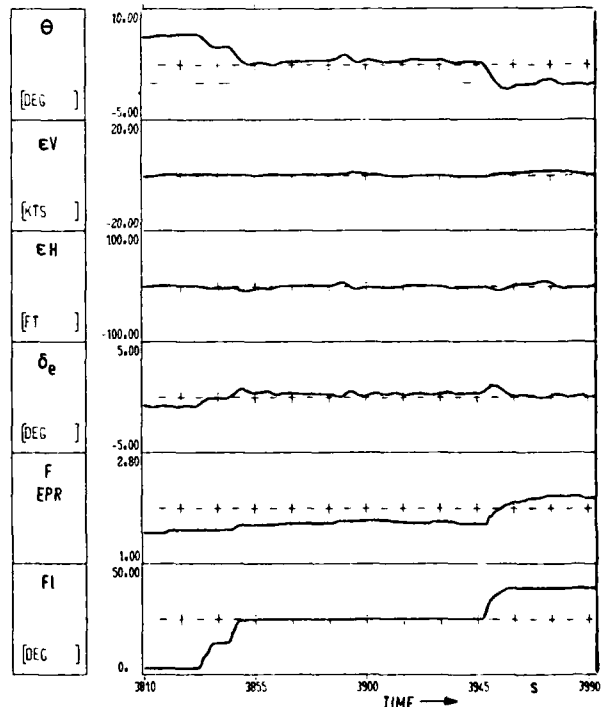


Figure 20: Flight test result with the GCS-modes altitude hold (ALT HOLD) and speed hold (SPEED HOLD) during flap setting

CONTROL DESIGN OF FLEXIBLE SPACECRAFT

by
 Robert E. Skelton
 School of Aeronautics and Astronautics
 Purdue University
 West Lafayette, Indiana 47907
 USA

SUMMARY

When compared to other large scale systems, flexible spacecraft have some peculiarities which can make control more difficult. In this discussion emphasis is placed upon the time domain and suboptimal Linear Quadratic Gaussian (LOG) methods, with special attention given to the effects of modeling errors. These effects are discussed in light of the model reduction problem, stability, and control design. Stability, controllability and observability computations are reduced to their simplest form possible to provide insight and to facilitate the location of sensors and actuators. The techniques of modal cost analysis are used to identify the critical parameters and the critical modes of the structure. In the final stage of design, component cost analysis reveals which states of the optimal dynamical controller should be deleted to produce a reduced controller which is compatible with the on-line computer software limitations.

CONTENTS

	Page
1.0 Introduction	1
2.0 Models of Space Structures	2
3.0 Model Error Effects	4
4.0 Stability and Performance In the Presence of Modeling Errors	5
4.1 Stability and Modeling Errors	5
4.2 Performance and Modeling Errors	6
5.0 Position and Rate Feedback: Colocated Position Sensors with Actuators (Perfect)	8
6.0 Rate Feedback: Colocated Rate Sensors with Actuators (Perfect)	9
6.1 Rate Feedback Design by Approximate Pole Assignment	11
6.2 Rate Feedback Design by Optimal Control	13
7.0 Component Cost Analysis and Order Reduction	15
7.1 Performance Objectives	16
7.2 Modal Cost Analysis	17
7.3 Component Cost Analysis as a Spacecraft Control Design Procedure	21
7.4 The CCA Design Algorithm	22
8.0 Conclusions	26
9.0 References	27

1.0 INTRODUCTION

Flexible structures and their dynamics have been studied well over a century. However, only recently has there been an interest in the active control of flexible structures. Such interest was piqued in the 1960's by a flexibility-induced instability in USA's first satellite [1], and more recently by sophisticated requirements for precision controlled structures in space for astronomy, communication networks, near-earth scientific studies, and space solar power alternatives, [2]. The rapid development of computers and control theory in the 1960's has encouraged active control applications for other structures as well, such as flutter suppression in aircraft [3], and active damping of bridges and tall buildings [4]. This is not to say that active control is needed in every structure, however, and there is no clear means to make the decision of when and how much control effort is needed in a structure. There is a need to study the dynamical properties of the mechanical system with a view toward discerning what improvements in performance can easily be made by redesigning the structure and what improvements must be left for active control functions. This *beneficial* interaction of the dynamics and control disciplines in the development of a rational design methodology has not yet occurred to any mature degree. Usually the structure designs and the control designs occur sequentially. This luxury cannot be afforded in the future, as stringent requirements force us to provide better coordination between structure design, control design, and controller software design.

Some of the reasons that the control of flexible spacecraft can be a difficult task are briefly described by the following three problems.

(i) The Model Error Problem

The space structure is usually constructed of lightweight materials, and thus the assembled structure is very lightly damped. This uniqueness of light damping for the space structure makes the control design extremely sensitive to modeling errors, since the slightest perturbation of truncated modes by control action can shift these eigenvalues into the right half plane. Also there is the usual uncertainty in the computation of the modal data. This problem is especially critical for spacecraft since modal data uncertainties cannot be removed before flight, due to the difficulty of testing the extremely lightweight structure in a 1-g environment.

(ii) The Limited Controller Software Problem

The practical limitations of memory and speed of on-board computers mean that only controllers of constrained dimension can be considered. These constraints can severely reduce the performance capabilities of the controlled system due again to the effect of modeling errors imposed by the controller order constraints. (An infinite dimensional system controlled by finite controllers immediately suggests that "optimal" state feedback solutions are not going to be realized). Thus, limited software serves only to compound the model error problem by constraining the order of the controller and by adding delays in the feedback loop.

(iii) The Performance Requirement Problem

Of course the model error problem and the limitations of software pose no serious threat to the mission if the performance requirements are quite lenient. Thus, the degree to which (i) and (ii) pose problems is directly related to the severity of the performance requirements. Therefore, early researches on the subject have sought to help with the tradeoffs between performance and modeling errors (including those induced by controller software limitations).

The aim of this chapter is to describe some preliminary approaches to cope with these problems. The organization of the chapter is as follows. Section 2.0 describes the form of the dynamical model. Section 3.0 describes some of the model error effects in general terms. Section 4.0 presents results on stability, controllability and observability of flexible spacecraft, and Sections 5.0 and 6.0 assume perfect position and rate sensors. Section 7.0 treats the more general LOG problem with application of component cost analysis [5], and Section 8.0 offers some concluding remarks.

2.0 MODELS OF SPACE STRUCTURES

Those portions of the structure resembling beams, plates, and membranes might reasonably be idealized as a material continuum. The resulting partial differential equations (PDEs) contain all the modal data over an infinite spectrum, [6]. Other parts of the structure might contain trusses or complicated connections which require a finite element formulation of the model, resulting in a set of ordinary differential equations (ODEs), [7]-[9]. Also, the dynamics of actuators and sensors are usually described by ODEs. This combination of distributed-parameter models (PDEs) and lumped-parameter models (ODEs) must eventually be reduced to a finite set of ODEs. The discretization of the PDEs must be accomplished so that the frequency spectrum over which each of the subsystems (actuators, sensors, sub-structure 1, sub-structure 2, etc.) are modeled is consistent. Otherwise, troublesome dynamical interactions between subsystems might be unintentionally concealed at the outset. Thus, each of the substructure models might be truncated prior to the assembly of the composite model of Fig. 1,

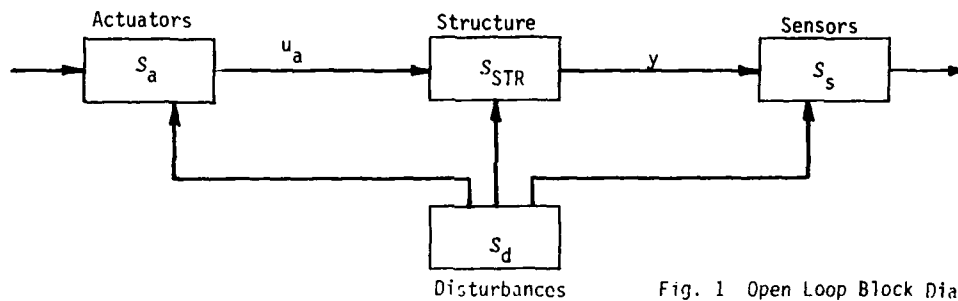


Fig. 1 Open Loop Block Diagram

$$\left. \begin{aligned} M'\ddot{q} + C'\dot{q} + G'\dot{q} + K'q &= B'u_a \\ y &= \begin{pmatrix} P'q \\ R'\dot{q} \end{pmatrix} \end{aligned} \right\} \text{structures, } S_{STR} \quad (2.1a)$$

$$\left. \begin{aligned} \dot{x}_a &= A_a x_a + B_a u + w_a \\ u_a &= C_a x_a + v_a \end{aligned} \right\} \text{actuators, } S_a \quad (2.1b)$$

$$\left. \begin{aligned} \dot{x}_s &= A_s x_s + B_s y + w_s \\ z &= C_s x_s + v \end{aligned} \right\} \text{sensors, } S_s \quad (2.1c)$$

where the inertia or "mass" matrix $M' = M'^T > 0$ is positive definite and symmetric, the stiffness matrix $K' = K'^T \geq 0$ is positive semidefinite and symmetric, the internal energy dissipation due to damping is $\dot{q}^T C' \dot{q}$ and $C' = C'^T \geq 0$ is positive semidefinite and symmetric, and any gyroscopic term is due to $G' = G'^T$, which is skew-symmetric. The disturbance models assumed for w_a, v_a, w_s, v are all zero-mean white noise processes. The dimensions of the vector are $x_s \in R^S, x_a \in R^a, q \in R^N, u_a \in R^m, u \in R^m, y \in R^N, z \in R^N$.

One strategy for truncating each of the sub-structure models before constructing the composite structural model (2.1a) is to use the momentum "completeness" indices of Hughes [10]. The subsystems might typically be truncated to 100 modes and the composite system S_{STR} might therefore have several hundred configuration variables q . For further model reductions *after* the composite system (2.1) is constructed, "completeness" of the model will be judged by criteria more closely related to the specific control task than the momentum criteria of [10]. Such methods will be discussed in Section 7.

The coordinate transformation

$$q = Tn \quad (2.2a)$$

is often made to put the structural subsystem S_{STR} in the modal coordinates

$$\ddot{n} + Z_1 \dot{n} + Z_2 n = Bu_a, \quad B \triangleq T^T B' \quad (2.2b)$$

$$y = \begin{bmatrix} P_r n \\ K_e n \end{bmatrix}, \quad P \triangleq P' T \quad (2.2c)$$

$$R \triangleq R' T \quad (2.2d)$$

$$Z_2 \triangleq T^T K' T, \quad Z_1 \triangleq T^T [C' + G'] T \quad (2.2e)$$

Let the first n_r elements of q and n be associated with rigid-body (zero frequency) modes of the structure. Then these matrix partitions apply

$$Z_2 \triangleq T^T K' T \triangleq \text{block diag. } [0 \quad \omega^2], \quad \omega^2 \triangleq \text{diag } [\omega_1^2, \dots, \omega_N^2] = T_e K' T_e \quad (2.2f)$$

$$T^T M' T = I, \quad T = [T_r \quad T_e] \quad (2.2g)$$

$$T^T C' T = \text{block diag } [0 \quad \Delta], \quad \Delta \geq 0 \quad (2.2h)$$

$$T^T G' T = \begin{bmatrix} G'_{rr} & G'_{re} \\ G'_{er} & G'_{ee} \end{bmatrix} \quad (2.2i)$$

$$n^T = [n_r^T \quad n_e^T] \quad (2.2j)$$

$$P = [P_r \quad P_e] \quad (2.2k)$$

$$R = [R_r \quad R_e] \quad (2.2l)$$

$$B^T = [B_r^T \quad B_e^T] \quad (2.2m)$$

where the zero in (2.2h) holds if the rigid modes are undamped, and $G'_{rr} = -G'_{rr}{}^T$, $G'_{er} = -G'_{er}{}^T$, $G'_{ee} = -G'_{ee}{}^T$. Now (2.2) becomes

$$\ddot{n}_r + G'_{rr} \dot{n}_r + G'_{re} \dot{n}_e = B_r u_a \quad (2.3a)$$

$$\ddot{n}_e + G'_{er} \dot{n}_r + G'_{ee} \dot{n}_e + \Delta \dot{n}_e + \omega^2 n_e = B_e u_a \quad (2.3b)$$

$$y = \begin{pmatrix} P_r n_r + P_e n_e \\ R_r \dot{n}_r + R_r \dot{n}_e \end{pmatrix} \quad (2.3c)$$

$$y = \begin{pmatrix} P_r n_r + P_e n_e \\ R_r \dot{n}_r + R_r \dot{n}_e \end{pmatrix} \quad (2.3d)$$

There are N nearly elastic modes with frequencies

$$\{\omega_1 \leq \omega_2 \leq \dots \leq \omega_N\}, \quad (2.4)$$

and eigenvectors

$$T_e = [t_1, t_2, \dots, t_N] \quad (2.5)$$

From (2.2) or (2.3) state variable models are readily constructed, but note that such models rely on accurate modal data ω_j, t_j . $T^T G' T$ represents the gyroscopic terms due to the presence of spinning rotors on the structure or spinning structures. Since the absence of a precise theory of damping makes C' difficult to characterize, [7], the term $\Delta \dot{n}_e$ often is *arbitrarily* added to represent energy-dissipative forces internal to the structure. The arbitrary assumption of "modal damping", ζ_j , gives to Δ the form

$$\Delta = \text{diag } [2\zeta_1 \omega_1, \dots, 2\zeta_N \omega_N] \quad (2.6)$$

and ζ_i , $i = 1, 2, \dots, N$ perhaps are the least accurately known parameters in the model. Modal damping on the order of $\zeta_i = 0.005$ is typically assumed [11] for space structures. Uncertainties in the mass and stiffness matrices M and K , lead to incorrect eigenvectors t_i . This renders uncertain the mode shapes and mode slopes at actuator locations (in B_e) and at sensor locations (in P_e , R_e) on the elastic portions of the structure. Also the structure of the matrix ω^2 is altered by errors in T . The uncertainty in the frequencies ω_i and eigenvectors t_i tends to increase with mode number i . It is plausible, then, that a reasonable model for uncertainties in each of these parameters

$$\{\omega_i, B_{ei} \triangleq t_i^T B^T, P_{ei} \triangleq P^T t_i, R_{ei} \triangleq R^T t_i\} \quad (2.7)$$

is a variance of the form

$$\sigma_i^2 = i\sigma_0^2 \quad (\sigma_0^2 \triangleq \text{variance associated with parameters of mode 1}) \quad (2.8)$$

for some constant σ_0 . Thus, for all appropriate elements jk of the i th rows of B_e , and the i th columns of P_e , R_e ,

$$\sigma_i^2 \triangleq E(\omega_i - \bar{\omega}_i)^2 = E(B_{ei} - \bar{B}_{ei})_{jk}^2 = E(P_{ei} - \bar{P}_{ei})_{jk}^2 = E(R_{ei} - \bar{R}_{ei})_{jk}^2 \quad (2.9)$$

where E denotes expected value, and the overbar denotes mean value. The uncertainty in the arbitrarily assumed modal damping ζ_i is quite large, but it is not known whether this increases with frequency. When the need arises (in later sections) we will arbitrarily assume

$$E(\zeta_i - \bar{\zeta}_i)^2 = \mu\sigma_0^2 \quad (2.10)$$

for some $\mu \gg 1$. Of course, more appropriate statistical models might be developed for particular structures. The above models are offered only to help put into perspective the relative degree of uncertainty of the parameters of the dynamic models. Such assumptions are *not* employed in later Sections of this chapter, save Section 7.0.

3.0 MODEL ERROR EFFECTS

Let the composite model (2.1) be written in state form

$$\begin{aligned} \dot{x} &= Ax + Bu + Dw + f, \quad x^T \triangleq (n^T, \bar{n}^T, x_a^T, x_s^T) \\ z &= Mx + v + g, \quad w^T = (w_a^T, w_s^T, v_a^T) \end{aligned}, \quad x \in \mathbb{R}^n, \quad n = 2n_q + a + s \quad (3.1)$$

where nonlinearities f and g might be added to the model for performance evaluation purposes, but might be ignored during control design. The associated parameters (A, B, D, M) may be deduced from (2.1), (2.2). There may be several stages of model simplification between the most general model used for simulation and performance evaluation before flight, and the model upon which the control design is based. To simplify the discussion we discuss only two models. In this section model (3.1) will represent the physical system (admittedly in this case, the state x is infinite-dimensional and the parameters A, B, D, M are not precisely known). The reduced model used for controller design is

$$\begin{aligned} \dot{x}_R &= A_R x_R + B_R u + D_R w_R, \quad x_R \in \mathbb{R}^r \\ z_R &= M_R x_R + v_R \end{aligned} \quad (3.2)$$

and we postpone to Section 7 the discussion of how (3.2) might be derived. Our current interest concerns the characterization of the differences between any two models (3.2) and (3.1). In order to match identically the measurements $z(t)$ actually obtained from the physical system, one could define vector functions of time $e_x(t)$, $e_z(t)$ as those which drive the state and measurement equations in such a way

$$\begin{aligned} \dot{x}_R &= A_R x_R + B_R u + D_R w_R + e_x(t) \\ z &= M_R x_R + e_z(t) \end{aligned} \quad (3.3)$$

that $z(t)$ matches the actual measurements. Such model error vectors have been shown [12] to be composed of four parts

$$\begin{pmatrix} e_x \\ e_z \end{pmatrix} \triangleq e = e_\Delta + e_t + e_d + e_n \quad (3.4)$$

where e is due only to parameter errors, e_t is due to errors in model order, e_d is due to neglected disturbances and e_n is due to neglected nonlinearities. Of course, neither of these e_Δ , e_t , e_d , e_n can be known *a priori*. Parameter adaptive control and identification methods [13]-[15] strive to drive $e_\Delta(t)$ to zero. Such methods can be effective when e_Δ is the dominant source of error in (3.4). Terms contributing to e_t depict the coupling between retained and truncated equations in the (infinite dimensional) model underlying the physical system. Much attention [16]-[18] has been devoted to the reduction of the "spillover" terms e_t , (and their corresponding closed loop consequences, to be illustrated in Section 3.1). Such approaches can be effective if e_t happens to be the dominating term in (3.4). Orthogonal filters [19], [20] make fewer assumptions about $e(t)$, save that it is square integrable. This more general characterization of model error has the potential advantage of simultaneously accommodating errors of the type (3.4), but the method also has disadvantages in the design stage. The method requires the selection and storage of a set of independent functions (to be used for fitting the actual error function) and the choice of these functions is not unique. One choice is to use elements of the state transition matrix for a higher order model as in [21]. Another choice is to use orthogonal functions as in [19].

Having described the *nature* of the modeling errors, we wish now to be more explicit about their *effects*. These effects will now be described, first in terms of stability and then in terms of a quadratic performance metric.

4.0 STABILITY AND PERFORMANCE IN THE PRESENCE OF MODELING ERRORS

4.1 Stability and Modeling Errors

Let

$$\begin{aligned} u &= G_R \hat{x}_R \\ \dot{\hat{x}}_R &= A_R \hat{x}_R + B_R u + K_R(z - M_R \hat{x}_R) \end{aligned} \quad (4.1)$$

describe the dynamical controller used to control the system (3.1). G_R is usually chosen to stabilize $[A_R + B_R G_R]$ and K_R is usually chosen to stabilize $[A - K_R M]$, although the controller poles, $\lambda_j[A_R + B_R G_R - K_R M]$, $j = 1, \dots, r$, should also be stable [22]. There is no unique relationship between the parameters of the controller (4.1) and the evaluation model of the system (3.1). The controller parameters (A_R, B_R, M_R) may or may not be related to some reduced order model obtained from (3.1). For example, the simpler model (A_p, B_p, M_p) might have been derived directly from physical laws, but using an *idealization** of the system that was simpler than the idealization that led to (3.1). For these reasons the phrase "parameter errors" has no unique meaning. In fact, none of the terms in the decomposition (3.4) are unique. Nonetheless we may present a precise characterization of results by introducing an arbitrary coordinate transformation,

$$x = \begin{bmatrix} \Omega_R & \Omega_T \end{bmatrix} \begin{bmatrix} x_R \\ x_T \end{bmatrix}, \quad \begin{bmatrix} \Omega_R & \Omega_T \end{bmatrix}^{-1} = \begin{bmatrix} \Psi_R \\ \Psi_T \end{bmatrix}, \quad (4.2)$$

We define parameter errors by

$$\begin{aligned} \Delta A &\triangleq \Psi_R A \Omega_R - A_R \\ \Delta B &\triangleq \Psi_R B - B_R \\ \Delta M &\triangleq M \Omega_R - M_R \end{aligned} \quad (4.3)$$

(Note: We do not intend to calculate either the exact system model (3.1) or the transformation (4.2). The present discussion serves only to provide insight into the character of the actual modeling errors.) The system (3.1) may now be written in the form

$$\dot{x}_R = A_R x_R + B_R u + e_x, \quad z = M_R x_R + e_z \quad (4.4a)$$

$$\dot{x}_T = \Psi_T A \Omega_R x_R + \Psi_T A \Omega_T x_T + \Psi_T B u + \Psi_T f \quad (4.4b)$$

where the model error vectors e_x and e_y are given by (3.4) and

$$\begin{aligned} e_\Delta &= \begin{bmatrix} \Delta A \\ \Delta M \end{bmatrix} x_R + \begin{bmatrix} \Delta B \\ 0 \end{bmatrix} u \\ e_t &= \begin{bmatrix} \Psi_R A \Omega_T \\ M \Omega_T \end{bmatrix} x_T \end{aligned} \quad (4.5)$$

$$e_d = \begin{bmatrix} \Psi_R w - w_R \\ v - v_R \end{bmatrix}, \quad e_n = \begin{bmatrix} \Psi_R f \\ g \end{bmatrix}$$

Augmenting the controller (4.1) to the system (3.1) or (4.4), and defining $\tilde{x}_R \triangleq x_R - \hat{x}_R$, the controlled system becomes

$$\begin{bmatrix} \dot{\tilde{x}}_R \\ \dot{x}_T \\ \dot{\hat{x}}_R \end{bmatrix} = \begin{bmatrix} A_R + \Delta A - K_R(M_R + \Delta M) & \Psi_R A \Omega_T - K_R M \Omega_T & \Delta A + \Delta B G_R - K_R \Delta M \\ \Psi_T A \Omega_R & \Psi_T A \Omega_T & \Psi_T A \Omega_R + \Psi_T B G_R \\ K_R M \Omega_R & K_R M \Omega_T & A_R + B_R G_R \end{bmatrix} \begin{bmatrix} \tilde{x}_R \\ x_T \\ \hat{x}_R \end{bmatrix} +$$

*By *idealization* we mean the set of hypotheses within which the dynamical system is assumed to move. For example, different idealizations of the same system might include: an elastic material continuum, a set of connected rigid bodies, a rigid body, etc.

$$\begin{bmatrix} \psi_R(w + f) - K_R(v + g) \\ \psi_T(w + f) \\ -K_R(v + g) \end{bmatrix} \quad (4.6a)$$

$$y = \begin{pmatrix} y \\ u \end{pmatrix} = \begin{bmatrix} C_R & C_T & C_R \\ 0 & 0 & G_R \end{bmatrix} \begin{pmatrix} \dot{x}_R \\ x_T \\ \dot{x}_R \end{pmatrix} \quad (4.6b)$$

where $y = Cx$ represents those variables we wish to control in the sense that

$$y_{MS} = \lim_{t \rightarrow \infty} E \|y\|_Q^2 = \lim_{t \rightarrow \infty} E v^T Q v, \quad Q = \begin{bmatrix} Q & 0 \\ 0 & R \end{bmatrix}, \quad Q > 0, R > 0 \quad (4.7)$$

is used as a performance metric. ((4.7) is discussed further in Section 7). Certain remarks can be made concerning the eigenvalues of the closed loop system (4.6). Let the integers i, j, k have the range $\{i = 1, \dots, n, x \in R^n\}$, $\{j = 1, \dots, r, x_R \in R^r\}$, $\{k = 1, \dots, n-r\}$, and denote eigenvalues of a matrix $[\cdot]$ by $\lambda_i[\cdot]$.

Theorem 1:

(a) The eigenvalues of the closed loop system (3.10) go to

$$\lambda_i[A] \text{ and } \lambda_j[A_R - K_R M_R]$$

$$\text{as } \|B G_R\| \rightarrow 0.$$

(b) The eigenvalues of the closed loop system (3.10) go to

$$\lambda_i[A] \text{ and } \lambda_j[A_R + B_R G_R]$$

$$\text{as } \|K_R M\| \rightarrow 0.$$

(c) The eigenvalues of the closed loop system (3.10) are

$$\lambda_j[A_R - K_R M_R], \quad \lambda_j[A_R + B_R G_R], \quad \lambda_k[\psi_T A \Omega_T]$$

if

$$\psi_R A \Omega_T = 0, \quad \psi_T A \Omega_R = 0 \quad (4.8)$$

$$\Delta A = 0, \quad \Delta B = 0, \quad \Delta M = 0 \quad (4.9)$$

and either

$$\psi_T B = 0 \text{ or } M \Omega_T = 0 \quad (4.10)$$

The proof of (c) follows by substituting the appropriate zero matrices into (4.6a). The proofs of (a) and (b) are given in [23]. These results may be physically interpreted as follows:

- (a),(b) When the controller gains are "small enough", [control gain G_R as in (a), or filter gain K_R as in (b)] and the open loop system is stable, the modeling errors will not destabilize the system.
- (c) Condition (4.8) implies a choice of coordinates in which the open loop system is dynamically uncoupled between the x_R and x_T variables. (Modal coordinates are a special case of this). Condition (4.9) means no parameter errors ($e_A = 0$). The first condition in (4.10) is equivalent to no "control-spillover" and the second condition in (4.10) is equivalent to no "observation-spillover", in the sense of Balas [6]. The eigenvalues $\lambda_i[\psi_T A \Omega_T]$, $i = 1, \dots, n-r$, represent the eigenvalues of the truncated states x_T . Stability is guaranteed in this case (c), if the truncated modes are stable ($\text{Re } \lambda_i < 0$).

Thus, since stringent performance requirements (such as large Q in (4.7)) usually lead to larger control gains G_R , it is evident that the severity of the model error problem (in terms of stability) hinges upon the performance requirements.

4.2 Performance and Modeling Errors

We cite here the performance available with and without modeling errors. If one chooses G_R and K_R in (4.1) to be optimal for the model (A_R, B_R, M_R) with noise intensities W_R and V_R respectively for the zero-mean white noise processes $w_R(t)$ and $v_R(t)$, and if there were no model errors $e(t) = 0$, then the tradeoff between the optimal output performance

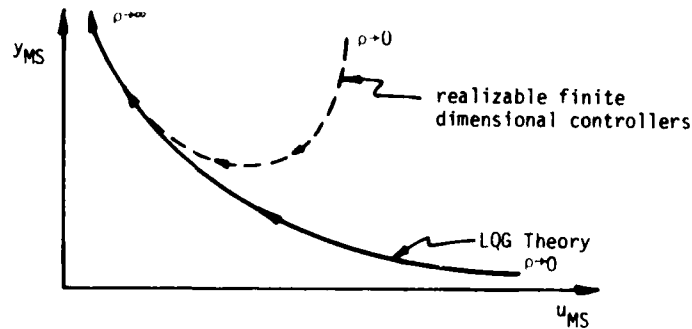
$$y_{MS} \hat{=} \lim_{t \rightarrow \infty} E \|y\|_Q^2, \quad Q > 0 \quad (4.11)$$

and the optimal input performance

$$u_{MS} \hat{=} \lim_{t \rightarrow \infty} E \|u\|_{R_0}^2, \quad R = R_0 > 0 \quad (4.12)$$

(where ρ is an arbitrary weighting scalar chosen by the designer) would be "hyperbolic" in the sense of Fig. 2.

Fig. 2
PERFORMANCE
vs.
CONTROL EFFORT



The output of the reduced model is $y_R = C_R x_R$. Under the assumptions of controllability of (A_R, B_R) and observability of both (A_R, C_R) , and (A_R, M_R) , [24]

$$G_R = -\frac{1}{\rho} R_0^{-1} B_R^T K \quad , \quad 0 = K A_R + A_R^T K + C_R^T Q C_R - G_R^T R G_R \quad (4.13)$$

$$K_R = P M_R^T V_R^{-1} \quad , \quad 0 = P A_R^T + A_R P + D_R^T W R D_R^T - K_R V_R K_R^T \quad (4.14)$$

and small ρ leads to large control gains. In the presence of inevitable modeling errors, Fig. 2 illustrates the eventual (and perhaps rapid) degradation in output performance with increasing control authority (decreasing ρ), a result not predicted, of course, by the standard LQG theory since the theory relies upon the absolute fidelity of the mathematical model. Means to combat such model error effects is the subject of the remainder of the chapter.

For any performance metric of the form (4.7), the relationship between stability of (4.6a) and the value of (4.7) is established as follows. Denote the plant matrix in (4.6a) by A , and the output matrix in (4.6b) by C , and ignore nonlinearities f and g . Then (4.6a) has the form

$$\dot{x} = Ax + Dw \quad (4.15a)$$

$$y = Cx \quad , \quad V_{MS} \triangleq \lim_{t \rightarrow \infty} E \|y\|_Q^2 \quad , \quad Q > 0 \quad (4.15b)$$

If the matrix pair (A, C) is observable and (A, D) is distorbable then V_{MS} is finite only if A is stable, [22]. Thus, relative stability information is contained in the magnitude of V_{MS} , and we have the result:

Proposition 1:

If observability and distorbability are properties of the closed loop system (4.6), then V_{MS} serves both as a stability margin and a quadratic performance metric.

Thus, the calculation

$$V_{MS} = \text{tr } PC^TQC \quad , \quad 0 = PA^T + AP + DWD^T \quad (4.16)$$

provides an acceptable performance evaluation if the triple (A, C, D) is distorbable, observable. There are three problems which prevent the use of proposition 1 in *guaranteeing* stability of physical systems.

- (1) the "physical" system (4.6) purports to represent is infinite dimensional.
- (2) observability and distorbability tests are impossible to do with precision on a digital computer, even for a finite-dimensional model.
- (3) even if we had reliable computations for observability, distorbability, the physical system is never observable in the following sense.

Proposition 2: Unobservability of physical systems

As mathematical models increase in complexity, describing more and more completely the dynamical details of the physical process, the model eventually includes unobservable states with respect to any finite dimensional output vector y .

Proposition 2 explains the sense in which physical systems are never completely observable. This proposition is intuitively verified by imagining that microscopic phenomena such as molecular motions are not going to be observable in the rate gyro measurements. Even though one may not be interested in such trivial examples as molecular motions, the useful point of propositions 1 and 2 is that as far as stability is concerned there is no clear way to know when minute motions become "nontrivial". Thus, the propositions serve to remind us that one can never *guarantee* stability of the physical system. This point may be made from another view. Since stability is a *mathematical* property of a *mathematical* model, interpretations of stability for the underlying *physical system* must be accompanied by precise statements of the type of modeling errors ignored. Thus, "stability guarantees" refer only to properties of the assumed model, and these comments must be kept in mind when reading the "stability" results of this (or any other) report.

5.0 POSITION AND RATE FEEDBACK: COLOCATED POSITION SENSORS WITH ACTUATORS (PERFECT)

In this section we ignore the dynamics of sensors and actuators, x_a and x_s in (2.1), to cite the stability properties of flexible structures which are either passive (no active feedback control) or which use measurement feedback with perfect (infinite bandwidth) sensors and actuators. The appropriate model for this case is (2.2), where the control u_a and the noise-free measurements z are given by

$$u_a = - [G_p \ G_r] z \quad , \quad z = \begin{pmatrix} \dot{y} \\ R \dot{\eta} \end{pmatrix} \quad (5.1)$$

Thus, z in (5.1) describes what we mean by the phrase "perfect" sensors (no phase shifts or time delays). Substituting (5.1) into (2.2b) gives the system under study with measurement feedback using perfect sensors,

$$\ddot{\eta} + [Z_1 + BG_r R] \dot{\eta} + [Z_2 + BG_p P] \eta = 0 \quad (5.2)$$

For convenience in notation we separate the symmetric and skew-symmetric parts of the matrices and rewrite (5.2) as

$$\ddot{\eta} + (Z_s + Z_{sk}) \dot{\eta} + [K_s + K_{sk}] \eta = 0 \quad (5.3a)$$

where

$$Z_s \triangleq T^T C^T T + \frac{1}{2} (BG_r R + R^T G_r^T B^T) \quad (5.3b)$$

$$Z_{sk} \triangleq T^T G^T T + \frac{1}{2} (BG_r R - R^T G_r^T B^T) \quad (5.3c)$$

$$K_s \triangleq T^T K^T T + \frac{1}{2} (BG_p P + P^T G_p^T B^T) \quad (5.3d)$$

$$K_{sk} \triangleq \frac{1}{2} (BG_p P - P^T G_p^T B^T) \quad (5.3e)$$

The following results are available by minor extensions of the work in [25].

Theorem 2:

Measurement feedback with perfect sensors and actuators leads to the system (5.3) which is asymptotically stable under these conditions:

$$Z_s \geq 0 \quad (5.4a)$$

$$K_{sk} = 0 \quad (5.4b)$$

$$K_s > 0 \quad (5.4c)$$

$$\text{The system } \begin{cases} \ddot{\rho} + Z_{sk} \dot{\rho} + K_s \rho = 0 \\ y = Z_s \rho \end{cases} \text{ is completely observable.} \quad (5.4d)$$

By first putting (5.2) in the form (5.3) with the additional assumption $K_{sk} = 0$, Theorem 4 of [23] directly applies as a proof of this result. [25] also shows that under the given conditions (5.4a)-(5.4c) the fourth condition (5.4d) is both *necessary* and *sufficient*. This necessary condition gives a very tidy statement of what active control is *required* to stabilize the system. Note that condition (5.4b) suggests that the position sensors be colocated with the actuators (e.g. translational displacement sensor colocated with a force actuator, or rotational displacement sensor colocated with a torque actuator), and that $G_p = G_p^T > 0$. This yields $P = B^T$ and hence (5.4b) is satisfied. Condition (5.4a) is satisfied if rate sensors are colocated with the actuators (translational rate sensors colocated with force actuators and rotational rate sensors colocated with torque actuators), and $G_r = G_r^T > 0$. Hence, $R = B^T$ in this case. Condition (5.4d) can be tested with minimum computation by employing the simple criteria for observability developed in [25]. Toward this end we define the matrices T_s and T_{sk} by

$$T_s^T K_s T_s = \Omega^2 = \text{diag} [\Omega_1^2, \Omega_2^2, \dots, \Omega_N^2] \quad (5.5a)$$

$$T_s^T T_s = I \quad (5.5b)$$

$$T_{sk}^T T_{sk} = I \quad (5.5c)$$

$$T_{sk}^T \begin{bmatrix} 0 & \Omega \\ -\Omega & -Z_{sk} \end{bmatrix} T_{sk} = \begin{bmatrix} 0 & 0 \\ 0 & S \end{bmatrix} \quad (5.5d)$$

$$S \triangleq \text{block diag} \left\{ \dots \begin{bmatrix} 0 & -s_1 \\ s_1 & 0 \end{bmatrix} \dots \right\}, \quad i = 1, \dots, p \quad (5.5e)$$

$$p = \text{no. nonzero eigenvalue of } \Theta^2 \triangleq \begin{bmatrix} 0 & \Omega \\ -\Omega & -Z_{sk} \end{bmatrix}^2 \quad (5.5f)$$

$$Z_{sk} \hat{=} T_s^T Z_{sk} T_s, \quad \frac{2(N-p)}{2p} \begin{bmatrix} T_{sk1} \\ T_{sk2} \end{bmatrix} \hat{=} T_{sk} \quad (5.5g)$$

Define the columns of the matrix $Z_s^T T_s$ by

$$[r_1^a, r_1^b, \dots, r_p^a, r_p^b] \hat{=} Z_s^T T_s \quad (5.5h)$$

We can now cite a special case of theorem 2, where condition (5.4d) is replaced by an explicit numerical computation.

Corollary 2.1

Assume that

(1) All position sensors (perfect) are colocated with actuators.

$$(2) \quad G_p = G_p^T > 0 \quad (5.6a)$$

$$(3) \quad Z_s \geq 0 \quad (5.6b)$$

$$(4) \quad K_s > 0 \quad (5.6c)$$

(5) the p nonzero eigenvalues of G^* are distinct. Under these conditions the system (5.3) is asymptotically stable if and only if

$$(6) \quad \text{either } \|r_i^a\|^2 > 0 \text{ or } \|r_i^b\|^2 > 0 \text{ for all } i = 1, \dots, p. \quad (5.6e)$$

The assumptions (1) and (2) guarantee condition (5.4b). Condition (5.4d) is satisfied if and only if (5.6e) holds. (This is proved by the more general corollary 4.1 of [25] where assumption (5) is not required)

6.0 RATE FEEDBACK: COLOCATED RATE SENSORS WITH ACTUATORS (PERFECT)

The stability conditions of corollary 2.1 greatly simplify under two additional conditions; (i) no gyroscopic terms ($G^* = 0$) and (ii) collocation of rate sensors with actuators. In this case $Z_{sk} = 0$, and the observability test (3.22d), which was reduced to (5.6e) under the conditions in corollary 2.1, now further simplifies to the following.

Corollary 2.2

Assume that

(1) All position and rate sensors (perfect) are colocated with actuators, $P = B^T$, $R = B^T$.

$$(2) \quad G_p = G_p^T > 0, \quad G_r = G_r^T > 0 \quad (6.1a)$$

$$(3) \quad G^* = 0 \quad (6.1b)$$

$$(4) \quad \text{rank } B_r = n_r \quad (6.1c)$$

Then the system (5.3) is asymptotically stable if and only if

$$\text{rank } [Z_s^T T_{s_i}] = n_i \quad (6.2)$$

where n_i is the multiplicity of frequency ω_i and T_{s_i} is the corresponding set of columns of T_s , where,

$$T_s = [T_{s_1}, T_{s_2}, \dots, T_{s_0}] \quad , \quad \sum_{i=1}^0 n_i = N$$

The proof of this corollary is provided by noting that (5.4d) becomes in this case

$$\ddot{z} + K_s \dot{z} = 0, \quad y = Z_s \dot{z} \quad (6.3)$$

whose observability condition (6.2) is obtained from (5.5h) by omitting the additional transformation T_{sk} which was required in (5.5) due to the presence of gyroscopic terms. Note from (2.2f) that $T_s^T A^T$ is singular. Hence, to satisfy (5.4c) and (5.6c) position sensors are required and must be located so that the rigid body modes are observable ((6.1c) is satisfied [25]). Further discussion of the number and type of actuators (and colocated sensors) required for controllability appears in [26].

Finally we cite the stability condition when only rate feedback is utilized. In this case we assume no gyroscopic terms $G^* = 0$ so that the control

$$u_a = -G_r z, \quad z = R_r \dot{r}_r + R_e \dot{r}_e \quad (6.4)$$

substituted into (2.4) yields

$$\ddot{r}_r + B_r(G_r R_r \dot{r}_r + B_r R_e \dot{r}_e) = 0 \quad (6.5a)$$

$$\ddot{r}_e + B_e(G_r R_r \dot{r}_r + [B_e(G_r R_e + \lambda)] \dot{r}_e + \omega_e^2 r_e) = 0 \quad (6.5b)$$

With rate-only feedback it is clear from (6.5a) that the rigid body coordinates n_r are not stabilized. Hence, we concentrate on the simpler task of improving the stability of the elastic coordinates n_e . We choose actuators so that the rigid body modes are uncontrollable. Hence $B_r = 0$, and with collocation with sensors $B_r^T = R_r^T = 0$, $B_e = R_e^T$. The system of interest is therefore

$$\ddot{n}_r = 0 \quad (6.6a)$$

$$\ddot{n}_e + [B_e G_r B_e^T + \Delta] \dot{n}_e + \omega^2 n_e = 0 \quad (6.6b)$$

Note that conditions (5.4a)-(5.4c) are automatically satisfied by (6.6b). Thus by theorem 2 the necessary and sufficient condition for asymptotic stability of (6.6b) is given by appropriate interpretation of (5.4d). This leads to

Corollary 2.3

For nongyroscopic systems with collocated rate sensors (perfect), located so that $B_r = 0$, the measurement of feedback control

$$u_a = -G_r z, \quad z = B_e^T \dot{n}_e, \quad G_r = G_r^T > 0 \quad (6.7)$$

gives to (3.21) these properties: $n_r(t)$ is unstable, $\dot{n}_r(t)$ is stable. Furthermore, $n_e(t)$ is asymptotically stable if and only if the system

$$\ddot{\delta} + \omega^2 \delta = 0, \quad y = [\Delta + B_e G_r B_e^T] \delta \quad (6.8a)$$

is completely observable, or equivalently, if and only if

$$\text{rank} [\Delta_i + [B_e G_r B_e^T]_i] = n_i, \quad i = 1, \dots, N_Q, \quad \sum_{i=1}^{N_Q} n_i = N - n_r \quad (6.8b)$$

where n_i is the multiplicity of frequency ω_i , and $[\cdot]_i$ denotes the corresponding columns of the matrix $[\cdot]$.

Also, n_r is the number of rigid modes and N_Q is the number of distinct frequencies ω_i .

Set $B_r = R_r^T = 0$ in (6.5). The proof is then immediate by interpreting corollary 2.2 for the system (6.6b) in lieu of the system (5.3). Thus $\omega^2 > 0$ satisfies the equivalent of (6.1c) and $T_s = I$ since

ω^2 is already diagonal. Hence (6.2) reduces to (6.8b). #

Proceeding from the proof of the most general corollary 2.1 to the most specific corollary 2.3 note that the form of the proofs and results are basically the same, except that two transformations, T_s and T_{sk} , were required in (5.5h), and, T_s , was required in (6.2), and none in (6.8).

Now we turn to questions of modeling errors. Noting that the stability conditions (6.9b) are already independent of the modal frequencies, we can also make them independent of the assumed modal damping by requiring

$$\text{rank} [B_e G_r B_e^T]_i = n_i, \quad i = 1, \dots, N_Q, \quad G_r = G_r^T \quad (6.9)$$

This is a sufficient condition for stability which we now use as a design criterion to replace the necessary condition (6.8b). This condition (6.9) can be replaced by

$$\text{rank} [B_{e_i}] = n_i, \quad i = 1, \dots, N_Q \quad (6.10)$$

provided $G_r > 0$. Further insight is available by noting that since ω^2 is positive definite and $B_e G_r B_e^T$ is positive semidefinite, the observability condition (3.32a) is equivalent to either observability or controllability of the matrix pair $(\omega^2, \Delta + B_e G_r B_e^T)$. The diagonal property of ω^2 is utilized to get the equivalent condition (6.8b). Hence, (6.8b) is the test for controllability or observability of the matrix pair $(\omega^2, \Delta + B_e G_r B_e^T)$ and (6.9), or equivalently (6.10) is the test for controllability or observability of the pair $(\omega^2, B_e G_r B_e^T)$. This point of view makes it clear that the system is stable with respect to $n_e(t)$

for any positive definite rate feedback gain G_r . All elastic modes which are controllable will be asymptotically stable. Note that this condition is independent of the actual modal damping and frequencies. Now consider the manner in which the test (6.10) depends upon the modal data. For a system with distinct frequencies and torque actuators B_{e_i} is a row matrix whose j th element is the i th mode slope at the location

of the j th actuator. Thus, the test (6.10) depends upon the mode shapes. However, the test is "almost" independent of mode shapes in the sense that the rank test is satisfied for any error in mode shapes except the binary error possibility $B_{e_i} = 0$ when it should be $B_{e_i} \neq 0$, or vice-versa. The actual magnitude $\|B_{e_i}\|$

is irrelevant, from the theoretical view. Therefore we may call the test (6.10) "almost" robust with respect to modal data, but is it robust with respect to model order errors? That is, if (6.10) is satisfied for a design model of N modes, is it satisfied for an evaluation model of $N_p \gg N$ modes? To answer this question simply consider the fact that the larger model leads to the sufficient stability condition

$$\text{rank} [B_{e_i}] = n_i, \quad i = 1, \dots, N_p \quad (6.11)$$

where B_{e_i} , $i = N_{Q+1}, \dots, N_p$ are associated with the truncated modes (modes not considered in the test (6.9)), and $N_p > N_Q$ is the number of distinct frequencies in the N_p mode model. Condition (6.11) is just the controllability condition for all N_p modes. We summarize these results in the following theorem.

Theorem 3

If $G' = 0$

(no gyroscopic terms)

(6.12a)

$$B_r = R_r^T = 0 \quad (\text{uncontrollable rigid modes}) \quad (6.12b)$$

$$B_e = R_e^T \quad (\text{colocated rate sensors}) \quad (6.12c)$$

$$G_r = G_r^T > 0 \quad (\text{positive definite rate measurement feedback gain}) \quad (6.12d)$$

then all elastic modes $n_{e_i}(t)$ which are actually controllable, i.e.

$$\text{rank } B_{e_i} = n_i, \quad (B_{e_i} = \text{actual mode shapes, slopes}) \quad (6.13)$$

are asymptotically stable regardless of uncertainties in modal damping, modal frequencies or mode shapes.

In view of this result it seems desirable to choose enough actuators (and colocated sensors) to make all modes controllable. Clearly from (6.13) the lower bound on the number of actuators required for complete controllability is $\max\{n_i, i = 1, 2, \dots\}$. Theorem 2 of [25] proves that the rigid body modes are controllable if and only if

$$\text{rank } B_r = n_r \quad (6.14)$$

Hence the number of actuators m required to stabilize the complete system (3.29) is

$$m \geq \max\{n_r, n_1, n_2, \dots, n_Q\} \quad (6.15)$$

where n_r is the number of rigid modes and n_i is the multiplicity of frequency ω_i . If all frequencies are distinct

$$m \geq \max\{n_r, 1\}, \quad (6.16)$$

subject, of course, to the conditions (6.13).

This Section has shown stability conditions for any control gain $G_r = G_r^T > 0$. The next two Sections show two ways to pick G_r . The first is by pole assignment and the second is by solving a least squares optimal problem.

6.1 Rate Feedback Design by Approximate Pole Assignment

There are formal pole assignment methods (for example see [27]) which may be used for general linear systems. However, our present problem is so special that an easier approach can be taken. The peculiarities of large flexible structures which suggest the use of these simpler methods are:

- (1) the open loop system contains an infinite number of *very lightly damped* modes
- (2) the rate feedback objective might be to simply add a *small* amount of damping to these modes

Thus, because we are asking only for *small* perturbations in the pole locations we might use first order perturbation methods. Toward this end let us cite known results in the perturbation of eigenvalues and eigenvectors of time-invariant linear systems.

Theorem 4

If (λ_i, e_i) is the i th eigenvalue, eigenvector of the $n \times n$ matrix A with distinct eigenvalues and $(\lambda_i + \Delta\lambda_i, e_i + \Delta e_i)$ is the i th eigenvalue, eigenvector of the matrix $[A + \Delta A]$, then to first order approximation,

$$\Delta\lambda_i = [F \Delta A E]_{ij}, \quad FE = I, \quad FA = \Delta F, \quad AE = EA \quad (6.17)$$

where F and E are, respectively, the matrix of left and right eigenvectors of A , and

$$[\Delta e_1, \Delta e_2, \dots, \Delta e_n] = \Delta E = EH \quad (6.18)$$

where the matrix H has elements

$$H_{ij} = \frac{1 - \delta_{ij}}{\lambda_j - \lambda_i} [F \Delta A E]_{ij}, \quad (i, j = 1, 2, \dots, n) \quad (6.19)$$

Proof:

The eigenvalues and eigenvectors of any matrix $[A + \Delta A]$ satisfy (assume distinct eigenvalues),

$$[A + \Delta A][E + \Delta E] = [E + \Delta E][\Lambda + \Delta\Lambda], \quad [\Lambda + \Delta\Lambda] = \text{diag} [\lambda_i + \Delta\lambda_i] \quad (6.20)$$

or

$$AE + A\Delta E + \Delta AE + \Delta A\Delta E = EA + E\Delta\Lambda + \Delta E\Lambda + \Delta E\Delta\Lambda \quad (6.21)$$

Deleting the products of assumed small perturbations, the last term on each side of equation (6.21) disappears. Solve (6.21) for $\Delta\Lambda$ to get

$$\Delta\Lambda \approx F\Delta AE + FA\Delta E - F\Delta EA + FAE - FE\Lambda \quad (6.22)$$

Or, using the facts $FA = \Delta F$, $FAE = \Lambda$, $FE = I$,

$$\Delta\Lambda = FAE + \Delta F\Delta E - F\Delta EA \quad (6.23)$$

The eigenvectors e_i span the n -space. Hence the perturbation of the eigenvector can also be written as a linear combination of the e_i . Thus for some matrix H with zero diagonal elements,

$$\Delta E = EH \quad , \quad H_{ij} = 0 \quad (6.24)$$

Substituting (6.24) into (6.23) gives, for the i th element of (6.23)

$$\Delta \lambda_i = [\Delta \Lambda]_{ii} = [F \Delta A E]_{ii} \quad (6.25)$$

and for the ij th element of (6.23), $i \neq j$

$$0 = [F \Delta A E]_{ij} + [AH]_{ij} - [HA]_{ij} \quad (6.26)$$

Solving (6.26) for H_{ij} yields (6.19) directly. #

As an application of theorem 4 to the rate feedback design problem of Section 6.1, let

$$A = \begin{bmatrix} 0 & I \\ -\omega^2 & 0 \end{bmatrix} \quad , \quad \Delta A = \begin{bmatrix} 0 & 0 \\ 0 & -B_e G_r B_e^T \end{bmatrix} \quad (6.27)$$

Then,

$$E = \begin{bmatrix} I & | & \cdot \\ \hline j\omega & | & -j\omega \end{bmatrix} \quad , \quad F = \begin{bmatrix} I & | & -j\omega^{-1} \\ \hline I & | & j\omega^{-1} \end{bmatrix} \quad (6.28)$$

and theorem 4 gives the real number

$$\Delta \lambda_i = -[B_e G_r B_e^T]_{ii} \quad (6.29)$$

Write b_i^T as the i th row of B_e . Then

$$\Delta \lambda_i = -b_i^T G_r b_i = -\|b_i\|_{G_r}^2 \quad (6.30)$$

The new pole locations are, to first order approximation

$$\lambda_i + \Delta \lambda_i = \begin{cases} -\|b_i\|_{G_r}^2 + j\omega_i & , \quad i = 1, \dots, N \\ -\|b_i\|_{G_r}^2 - j\omega_i & , \quad i = N+1, \dots, 2N \end{cases} \quad (6.31)$$

The damping factors associated with these new poles are

$$\zeta_i = \omega_i^{-1} \|b_i\|_{G_r}^2 \sqrt{1 - \zeta_i^2} \approx \omega_i^{-1} \|b_i\|_{G_r}^2 \quad (6.32)$$

where the second equality holds under the usual assumption of small damping. Thus, if one has sufficient knowledge to know which modes should be damped and the amount of damping needed in each mode, then one can choose G_r to approximately satisfy (6.32) for $i = 1, \dots, N$. This is equivalent to satisfying

$$\text{diag}[\zeta_d \omega - B_e G_r B_e^T] = 0 \quad (6.33)$$

for a desired $\zeta_d \triangleq \text{diag} [\zeta_1 \zeta_2 \dots \zeta_N]_d$. One may find approximate solutions by solving

$$\min_{G_r} \text{tr} (\zeta_d \omega - B_e G_r B_e^T)^2 \quad (6.34)$$

which has the solution (assuming that the number of modes N is equal to or greater than the number of actuators)

$$G_r = (B_e^T B_e)^{-1} B_e^T \zeta_d \omega B_e (B_e^T B_e)^{-1} \quad (6.35)$$

Thus the approximate expressions (5.38) and (5.35) reveal that the damping ζ_i obtained by (6.35) is

$$\zeta_i \omega_i = [B_e (B_e^T B_e)^{-1} B_e^T \zeta_d \omega B_e (B_e^T B_e)^{-1} B_e^T]_{ii} \quad (6.36a)$$

or

$$\zeta_i = \omega_i^{-1} \|b_i\|_{G_r}^2 \quad , \quad G_r \triangleq (B_e^T B_e)^{-1} B_e^T \zeta_d \omega B_e (B_e^T B_e)^{-1} \quad (6.36b)$$

The first order perturbation in eigenvectors is given by (6.18), and can be readily calculated for the present problem using (6.27), (6.28). The form of the results (6.32) implies that ζ_i is not negative for any b_i . Therefore the only significance of errors in the assumed mode shapes and mode slopes within the vectors b_i , $i=1,2,\dots,N$ is that a damping different from the expected damping will be experienced, in accordance with (6.32) for the actual b_i .

Similar problems are treated in more detail in [20]. Also see [29] - [30] for other interpretations of the rate feedback problem.

6.2 Rate Feedback Design by Optimal Control

In Section 5.1 stability conditions were established for any positive definite rate feedback gain G_r . In Section 6.1 a pole-assignment strategy was suggested for choosing G_r . In this Section we find the G_r which is optimal for a linear regulator problem. The problem is stated as follows. Find the control u which minimizes

$$V[u] = y_{MS} + \rho u_{MS}, \quad u = -G_r z, \quad z = \delta_e^T \dot{\eta}_e + v \quad (6.37)$$

where y_{MS} and u_{MS} are defined in (4.11), (4.12), subject to the constraint of measurement feedback control. The necessary conditions for this constrained output feedback problem are (from [31]),

$$K(A - BG_r M) + (A - BG_r M)^T K + M^T G_r^T R G_r M + C^T Q C = 0 \quad (6.38a)$$

$$L(A - BG_r M)^T + (A - BG_r M)L + D W D^T = 0, \quad W \triangleq E \left\{ \begin{pmatrix} w(t) \\ v(t) \end{pmatrix} \begin{pmatrix} w(t) \\ v(t) \end{pmatrix}^T \right\} \quad (6.38b)$$

$$-R G_r M L M^T + B^T K L M^T = 0 \quad (6.38c)$$

where for the special problem throughout Section 5,

$$A \triangleq \begin{bmatrix} 0 & I \\ -\omega^2 & -\Delta \end{bmatrix}, \quad B \triangleq \begin{bmatrix} 0 \\ B_e \end{bmatrix}, \quad D \triangleq \begin{bmatrix} 0 \\ D_e \end{bmatrix}, \quad \rho \triangleq [D, -B G_r M] \quad (6.39)$$

$$M \triangleq [0, B_e^T], \quad C^T Q C \triangleq \begin{bmatrix} 0 & 0 \\ 0 & Q_e \end{bmatrix}$$

$$\dot{x} = Ax + Bu + Dw, \quad y = Cx, \quad z = Mx + v, \quad x^T = (\eta_e^T, \dot{\eta}_e^T)$$

For the present problem the output vector y and the control u in (4.11), (4.12) are

$$y = [0, I] \begin{pmatrix} \eta_e \\ \dot{\eta}_e \end{pmatrix}, \quad y_{MS} = \lim_{t \rightarrow \infty} E [\dot{\eta}_e^T Q_e \dot{\eta}_e] \quad (6.40)$$

$$u = -G_r z, \quad z = [0, B_e^T] \begin{pmatrix} \eta_e \\ \dot{\eta}_e \end{pmatrix} + v$$

where Q_e is some weighting matrix to be chosen. In this stochastic version of the problem we have added white noise disturbances w, v to the plant and measurements of the previous Section. The model is the same as (2.1a) except that $u_a = u + w$ where w is a zero-mean white noise with intensity W , representing noise propagating into the structure from various electrical, mechanical sources within the actuators and their power sources.

If it happens (for reasons to be apparent) that the partitions of K in (6.38a) turn out to be

$$\text{where } K_{12} = 0, \quad K_{22} = \alpha I, \quad \alpha > 0 \quad (6.41a)$$

$$K = \begin{bmatrix} K_{11} & K_{12} \\ K_{12}^T & K_{22} \end{bmatrix} \quad (6.41b)$$

then substitution of (6.41) into the necessary conditions (6.38) yields

$$G_r = \alpha R^{-1}, \quad u = -G_r z, \quad \rho R_0 \triangleq R \quad (6.42)$$

and K_{11} and α satisfy

$$K_{11} = \alpha \omega^2 \quad (6.43)$$

$$-\alpha (L + \alpha B_e R^{-1} B_e^T) + \alpha^2 B_e R^{-1} B_e^T + Q_e = 0 \quad (6.44)$$

Thus, if Q_e is chosen by the designer to have the value

$$Q_e = \alpha^2 B_e R^{-1} B_e^T + 2\alpha \Delta \quad (6.45)$$

then (6.44) is satisfied. In summary, we have shown that if the K which satisfies (6.38a) has the property (6.41) and if Q_e is selected by (6.45) then the control (6.42) is the optimal measurement feedback control. Now we must show whether (6.41) is indeed satisfied. To pursue this question we now consider the optimal control problem without the measurement feedback constraint. The control which is optimal for the linear regulator problem

$$V = \lim_{t \rightarrow \infty} E (\dot{\eta}_e^T Q_e \dot{\eta}_e + u^T R u) \quad (6.46)$$

subject to

$$\dot{x} + Ax + u^T R u = Bu + Dw \quad (6.47)$$

is

$$u = -R^{-1} [0 \quad B_e^T] K \begin{pmatrix} n_e \\ \dot{n}_e \end{pmatrix} \quad (6.48)$$

$$-(KA + A^T K) + KBR^{-1}B_e^T K - C^T Q C = 0 \quad (6.49)$$

where A, B, C^TQC are defined in (6.39). The partitioned parts of (6.49) are

$$2K_{12}\omega^2 + K_{12}B_e R^{-1}B_e^T K_{12}^T = 0 \quad (6.50a)$$

$$-K_{11} + K_{12}\Delta + K_{22}\omega^2 + K_{12}B_e R^{-1}B_e^T K_{22} = 0 \quad (6.50b)$$

$$-K_{12}^T + K_{22}\Delta - K_{12} + \Delta K_{22} + K_{22}B_e R^{-1}B_e^T K_{22} - Q_e = 0 \quad (6.50c)$$

We now wish to use a theorem due to A. Yousuff, [32].

Theorem 5

For the optimal control problem (6.46), (6.47), any choice of Q_e in (6.46) of the form

$$Q_e = \Delta Q + \hat{Q}\Delta + \hat{Q}B_e R^{-1}B_e^T \hat{Q} \quad (6.51)$$

where \hat{Q} is any selected positive definite diagonal matrix, leads to the optimal control

$$u = -R^{-1}B_e^T K_{22} \dot{n}_e \quad (6.52)$$

where $K_{22} = \hat{Q}$ is the unique solution of

$$K_{22}B_e R^{-1}B_e^T K_{22} + \Delta K_{22} + K_{22}\Delta = Q_e \quad (6.53)$$

By comparing (6.53) with (6.50c) one can see that the choice of Q_e given by (5.56) leads to

$$K_{12} + K_{12}^T = 0 \quad (6.54)$$

Then either

$$K_{12} = -K_{12}^T \quad \text{or} \quad K_{12} = 0 \quad (6.55)$$

Yousuff [32] has shown that $K_{12} = 0$ is the correct solution of (6.54) if and only if K_{22} is diagonal. The condition for diagonal K_{22} is (6.51). Hence, $K_{12} = 0$ is the correct solution of (6.55) and (6.50a). See [33] for earlier results very similar to (6.51). By choosing $\hat{Q} = \alpha I, \alpha > 0$ the optimal control (6.52) becomes

$$u = -\alpha R^{-1}B_e^T \dot{n}_e \quad (6.56)$$

Thus the optimal state feedback problem (6.46) - (6.49) shows that the control gain is independent of the disturbance w , and the optimal measurement feedback problem (6.37) - (6.42) shows the control to be independent of the disturbance v . These results are summarized as follows.

Theorem 6

For nongyroscopic flexible structures with collocated (and perfect) actuators and rate sensors the control policy

$$u = -G_r z, \quad z = B_e^T \dot{n}_e + v, \quad G_r = G_r^T > 0 \quad (6.57)$$

where G_r is an arbitrary symmetric positive definite matrix, is both the optimal output feedback control and the optimal state feedback control for the problem

$$v = \lim_{t \rightarrow \infty} [\dot{n}_e^T Q_e \dot{n}_e + u^T G_r^{-1} u] \quad (6.58a)$$

$$Q_e = B_e G_r B_e^T + 2\Delta \quad (6.58b)$$

$$\ddot{n}_e + \Delta \dot{n}_e + \omega^2 n_e = R_e u + D_e w \quad (6.58c)$$

To prove Theorem 6 substitute, from (6.42), $R^{-1} = \frac{1}{\alpha} G_r$ into (6.45) and (6.46). Then divide (6.46) by α to get the form (6.58a). #

It should be emphasized that the solution (6.57) is independent of the disturbances w, v and the stochastic and deterministic problems have the same solution.

Theorem 6 has two possible uses: (1) the inverse optimal control problem reveals what performance criteria has been minimized for any given positive definite gain G_r . (2) Alternately, one may find for any given weighting Q_e the choice of \hat{Q} in (6.51) (i.e. $\min ||Q_e - \Delta \hat{Q} - \hat{Q} B_e R^{-1} B_e^T \hat{Q}||$) to yield the best rate-only feedback solution to a given

$$\begin{aligned} M\ddot{q} + Kq &= Bu, \quad M = I, \quad K = \begin{bmatrix} 1 & 0 \\ 0 & 10 \end{bmatrix}, \quad B = \begin{pmatrix} 1 \\ 1 \end{pmatrix} \\ z &= B^T \dot{q} \end{aligned} \quad (6.59)$$

For a desired damping of $\zeta_1 = \zeta_2 = 0.1$ a first order root perturbation method might be used. Hence, (6.35) yields the measurement feedback gain

$$G_r = 1.1/4 \quad (6.60)$$

and (6.36b) reveals the damping $\zeta_1 = \frac{1.1}{4}$, $\zeta_2 = \frac{1.1}{20}$. Theorem 6 shows that (6.60) is the gain which minimizes the performance criterion

$$V = \lim_{t \rightarrow \infty} \dot{q}^T \begin{bmatrix} 1 & 1 \\ 1 & 1 \end{bmatrix} \dot{q} + \frac{4}{1.1} u^2 = V = \lim_{t \rightarrow \infty} \varepsilon (G_r z^2 + G_r^{-1} u^2) \quad (6.61)$$

Example 2:

For all problems described by the deterministic version of Theorem 6 show that the closed loop system is described by

$$\ddot{\eta}_e + D_e \dot{\eta}_e + \omega_e^2 \eta_e = 0, \quad D_e \stackrel{\Delta}{=} (\Delta + B_e G_r B_e^T) \quad (6.62)$$

$$\min_u V = \lim_{t \rightarrow \infty} 2\dot{\eta}_e^T D_e \dot{\eta}_e \quad (6.63)$$

and that the cost of regulating $\dot{\eta}_e(t)$ (corresponding to the first term in (6.58a)) is always greater than the cost of control (corresponding to the second term in (6.58a)) by the amount $\lim_{t \rightarrow \infty} 2\dot{\eta}_e^T \Delta \dot{\eta}_e$. To show this, substitute (6.57) and (6.58b) into

$$V_y \stackrel{\Delta}{=} \lim_{t \rightarrow \infty} \dot{\eta}_e^T Q_e \dot{\eta}_e, \quad V_u \stackrel{\Delta}{=} \lim_{t \rightarrow \infty} u^T G_r^{-1} u \quad (6.64)$$

to get

$$V_y = V_u + \lim_{t \rightarrow \infty} 2\dot{\eta}_e^T \Delta \dot{\eta}_e \quad (6.65)$$

Hence, if the open loop system is undamped the cost of control V_u and the cost of output regulations V_y are equal.

Example 3:

Under what condition does rate feedback control minimize the kinetic energy of a purely elastic structure ($\Delta=0$)? Answer: The first term in (6.58a) represents kinetic energy if $Q_e = I$. However, from (6.58b) this can never happen for a finite number of actuators and an infinite number of modes in the structure, since $B_e G_r B_e^T$ must be nonsingular to achieve $Q_e = I$. Consequently, for a finite number of modes, the necessary condition for kinetic energy to be minimized by rate feedback is to have as many actuators as modes as in [39]

7.0 COMPONENT COST ANALYSIS AND ORDER REDUCTION

In Section 3.0 general model errors were defined and in Sections 4.0 and 5.0 conditions for stability in the presence of only parameter errors were discussed. In this Section our attention is focused on errors of model order. In Sections 5.0 and 6.0 dynamics of sensors and actuators were neglected. We first continue that assumption to first consider how one might reduce the dimension of the model (2.1a) before considering the more general treatment of the composite model (2.1). Thus in Section 7.1 only the open loop system is considered and the inclusion of actuator/sensor dynamics are postponed to Section 7.3.

The central idea of the model reduction methods to be discussed in this Section is to exploit the precise statement of the optimal control problem in order to predict which system components will make the largest contributions in the total quadratic performance criterion. These components are retained and the balance are discarded from the model. A "component" of the system can be any subset of coordinates designated by the analyst. For example, all of those coordinates associated with a particular substructure (antenna, solar panel, etc.) might be called one "component" for the purpose of assigning a value to the component for its contribution in the total performance criterion. The general ideas of such "component cost analysis" (CCA) are described in [5]. As another example, each modal coordinate might be designated as a "component". In this event the procedure becomes modal cost analysis (MCA), and the result is that the contribution of each mode is determined for the given quadratic performance criterion. MCA has been applied to models of flexible structures in [34] - [37], and the next Section is drawn largely from these references. We now proceed to make these several notations more precise.

7.1 Performance Objectives

The performance of the dynamical system must be judged by a specific criterion. One may require specific pole locations, focusing only on stability, but that leaves the question of eigenvectors and output performance imprecisely specified. Stability is clearly not a sufficient design goal. The Linear Quadratic Gaussian (LQG) problem has the advantage that poles and zeros are involved in the design specification and that the motion of specific variables of interest can be penalized directly by inserting these variables into the cost function to be minimized. On the other hand, these specified variables may be regulated satisfactorily while other variables become unbounded. The earlier *Proposition 1* states that observability is sufficient to prevent this situation but it may not be known whether all the potentially unstable motions are observable in the selected variables for minimization. Thus, in oversimplified terms, the "classical" approach is to "design for stability" (and then we must check for performance), whereas the LQG approach is to "design for performance" (and then we must check for stability). Insights into the best of both methods are required for successful designs. In this section the LQG methods are presented.

We define by the vector y the collection of all variables we wish to directly control. For example, if attitude control of the rigid body [described by η_r in (2.3a)] is the objective then one might choose $y \triangleq \eta_r$. Alternately, if vibration suppression is the only objective, then $y \triangleq \dot{\eta}_e$ might be chosen, as in the case of Section 6.0. The choice of a weighting matrix Q in (4.11) is often dictated by energy considerations. As an illustration the choices $\{Q \triangleq I, y \triangleq \dot{\eta}_e\}$ lead to $y^T Q y \triangleq$ kinetic energy in elastic modes. The potential energy in elastic modes is characterized by the choice $\{Q \triangleq \omega^2, y = \eta_e\}$. The expected value operator E is required in (4.11) due to the presence of random "noisy" disturbances in the actuators and sensors (2.1). The control mean-square effort u_{MS} is added to the performance metric as in (6.37), where the scalar ρ is an arbitrary weighting scalar which trades off control performance y_{MS} versus control effort u_{MS} . In practice, ρ must be chosen so that u_{MS} does not exceed the physical bounds of the actuators or structure load design constraints.

If the model (2.1) chosen for evaluation of candidate control policies were perfectly reliable then the performance evaluation using the performance criterion (6.37) might be acceptable. But alas, (2.1) is also subject to modeling errors and the straightforward evaluation of (6.37) subject to (2.1), together with any specified control policy, conceals the very real problem of uncertainties in the model (2.1). The uncertainty of the actual parameters in (2.1) usually prompts repeated simulations of (2.1) using different parameters. Controllers which perform "well" in each simulation might be acceptable. To make this situation more tractable one might choose to evaluate controllers on the basis of the first order sensitivity of performance with respect to parameter errors [in addition, of course, to the nominal performance (6.37)]. The following is one way to characterize this objective. Let p be the vector of v parameters considered uncertain in (2.1). The new performance metric is

$$V = y_{MS} + \rho u_{MS} + (y_p)_{MS} \quad (7.1)$$

where

$$y_{MS} \triangleq \lim_{t \rightarrow \infty} E \|y\|_Q^2 \quad (7.2)$$

$$u_{MS} \triangleq \lim_{t \rightarrow \infty} E \|u\|_{R_0}^2 \quad (7.3)$$

$$(y_p)_{MS} \triangleq \lim_{t \rightarrow \infty} E \|y_p\|_{Q'}^2 = \lim_{t \rightarrow \infty} E \sum_{i=1}^v \sigma_i^2 \left\| \frac{\partial y}{\partial p_i} \right\|_Q^2 \quad (7.4)$$

$$y_p^T \triangleq \left(\frac{\partial y^T}{\partial p_1}, \dots, \frac{\partial y^T}{\partial p_v} \right), \quad Q' \triangleq \text{diag} [\sigma_1^2 Q, \dots, \sigma_v^2 Q]$$

and ρ is an arbitrary weighting scalar to be chosen by the evaluator. Thus $(y_p)_{MS}$ is a mean squared measure of the first order effects of parameter variations on the variables we wish to control, y . Of course, to compute v one must have a model for y_p . By using the notation

$$[\cdot]_p \triangleq \begin{bmatrix} \frac{\partial [\cdot]}{\partial p_1} \\ \vdots \\ \frac{\partial [\cdot]}{\partial p_v} \end{bmatrix}, \quad [\cdot] \triangleq \text{block diag} \{[\cdot], \dots, [\cdot]\} \quad (v \text{ times}) \quad (7.5)$$

the complete model (3.1) and its sensitivity may be written [36]

$$\begin{pmatrix} \dot{x} \\ \dot{x}_p \end{pmatrix} = \begin{bmatrix} A & 0 \\ A_p & \tilde{A} + \tilde{J} \end{bmatrix} \begin{pmatrix} x \\ x_p \end{pmatrix} + \begin{bmatrix} B \\ B_p \end{bmatrix} u + \begin{bmatrix} D \\ D_p \end{bmatrix} w + \begin{pmatrix} f \\ f_p \end{pmatrix} \quad (7.6)$$

$$\begin{pmatrix} y \\ y_p \end{pmatrix} = \begin{bmatrix} C & 0 \\ C_p & \tilde{C} \end{bmatrix} \begin{pmatrix} x \\ x_p \end{pmatrix}, \quad J \triangleq \frac{\partial f}{\partial x}$$

$$V = y_{MS} + u_{MS} + (y_p)_{MS} = \lim_{t \rightarrow \infty} E \|y\|_Q^2 \quad (7.7)$$

$$y^T = (y^T, u^T, y_p^T), \quad Q = \begin{bmatrix} Q & 0 & 0 \\ 0 & \rho R_0 & 0 \\ 0 & 0 & Q' \end{bmatrix}$$

We will assume in what follows that the uncertain parameters are the modal damping factors ζ_i , squared modal frequencies ω_i , mode shapes and slopes at actuator locations B_{ij} . Other parameters can be added to the list.

$$p^T \triangleq (c_1, \dots, c_N; \omega_1^2, \dots, \omega_N^2; B_{e1}, \dots, B_{eN}) \quad (7.8)$$

where we have assumed distinct frequencies for convenience, so that B_{ei} is a row matrix. The variance

$$\sigma_i^2 \triangleq E(p_i - \bar{p}_i)^2, \quad \bar{p}_i \triangleq \text{nominal value} \quad (7.9)$$

is selected as the weighting for each sensitivity in the quadratic term

$$y_p^T Q' y_p = \sum_{i=1}^N \sigma_i^2 \left| \frac{\partial y}{\partial p_i} \right|_Q^2 \quad (7.10)$$

Thus, the less certain is a particular parameter, the greater is the importance of reducing its effect in the control system performance. Hence, a larger weighting in V , by the choice of σ_i^2 as a weighting gives V this property. From (2.8), (2.9),

$$\sigma_{\omega_i^2}^2 = E(\omega_i^2 - \bar{\omega}_i^2)^2 = i\sigma_0^2, \text{ for } i = 1, \dots, N \quad (7.11)$$

and the variance associated with uncertainties is the i th mode shapes or slopes at the j th actuator locations are

$$\sigma_{B_{ei}}^2 = E(B_{ei} - \bar{B}_{ei})^2 = i\sigma_0^2, \quad j = 1, \dots, m_a$$

where m_a is the number of actuators. Now Q' in (7.3) may be written

$$Q' = \text{diag} [\mu\sigma_0^2 Q, \dots, \mu\sigma_0^2 Q \mid \sigma_0^2 Q, \dots, N\sigma_0^2 Q \mid \sigma_0^2 Q, \dots, N\sigma_0^2 Q]$$

corresponding to the partitions of p in (7.8).

Finally, the objective of component cost analysis is to decompose V into "component costs" V_i ,

$$V = \sum_{i=1}^{n_c} V_i \quad (7.12)$$

where n_c is the number of components in the system and V_i is in the *in situ* contribution of component i . We choose in the next section to define "components" of the open loop system as "modal" coordinates, and its sensitivities. In Section 7.3 we choose to define a "component" of the closed loop system as a state of the dynamical controller. In each case we intend to assign a relative importance to each component by determining its ranking in the manner

$$V_1 \geq V_2 \geq V_3 \geq \dots \geq V_{n_c} \quad (7.13)$$

and truncate components with small component costs V_i from the system. The next two Sections give the necessary mathematics.

7.2 Modal Cost Analysis

Ignoring the sensor and actuator dynamics in this section, and considering the nongyroscopic system, (2.3) becomes (6.39), rewritten here,

$$\ddot{\eta}_e + \Delta \dot{\eta}_e + \omega^2 \eta_e = B_e w_a, \quad \eta_e \in R^N \quad (7.14a)$$

$$E w_a(t) = 0, \quad E w_a(t) w_a^T(\tau) = W_a \delta(t-\tau) \quad (7.14b)$$

$$V \triangleq y_{MS} = \lim_{t \rightarrow \infty} E \|y\|_Q^2 \quad (7.14c)$$

where only the noisy part of the control forces $u_a = u + w_a$ are considered in this section. When N is small enough for closed loop control calculations we will *not* ignore the effects of u in model reduction decisions. However, we now presume that N is very large (7.14a) and u cannot yet be computed.

Our immediate objective is to ascertain the contribution of each mode of the system in the overall cost value V . We presume at this point to be dealing with a system of very high order whose control inputs $u(t)$ are not yet known. Yet to ignore the source of excitation *altogether* would be a mistake since the *final* judgement of the quality of the model is *in the presence of actuator activity*. Until more is known about $u(t)$, (after control design considerations) we assume that $u = u_w(t)$ is a white noise of random disturbances being propagated through the actuators due to electronic noise in the electrical or magnetic amplifier devices, etc. A white noise disturbance $w(t)$ has already been included in the model (7.6). The consideration of the control and its effect in the model reduction process will be postponed to the next Section. To proceed we now need the following definitions.

Definition: Let x_i be any subset of n_i state variables of the linear system

$$\dot{x} = Ax + Dw, \quad Ew(t) = 0, \quad Ew(t)w^T(\tau) = W\delta(t-\tau) \quad (7.15a)$$

$$y = Cx$$

$$x^T = (\dots x_i^T \dots), \quad x_i \in R^{n_i}, \quad x \in R^{n_x}, \quad n_x = \sum_{i=1}^n n_i$$

$$V \triangleq \lim_{t \rightarrow \infty} E Y, \quad Y \triangleq y^T Q y$$

x_i will be called the i th "component" of the system and the "component cost" associated with component x_i is defined by

$$V_i \triangleq \frac{1}{2} \lim_{t \rightarrow \infty} E \frac{\partial Y}{\partial x_i} x_i, \quad \frac{\partial Y}{\partial x_i} \triangleq \left(\frac{\partial Y}{\partial x_i}, \dots, \frac{\partial Y}{\partial x_i n_i} \right) \quad (7.15b)$$

It is easy to verify that the total cost value V is the sum of all component costs

$$V = \sum_{i=1}^n V_i \quad (7.15c)$$

and that the component costs may be computed by

$$V_i = \text{tr}[C^T Q C X]_{ii} \quad (7.16a)$$

$$0 = XA^T + AX + DWD^T \quad (7.16b)$$

where $[C^T Q C X]_{ii}$ denotes the $n_i \times n_i$ matrix partition of $C^T Q C X$. The above analysis (7.15)-(7.16) of a linear system is called component cost analysis (CCA), [5]. The "components" of a system might be defined from physical or mathematical considerations. From physical considerations x_i might represent any physical component of the system such as the states associated with:

- (a) a substructure of the flexible spacecraft (an antenna, a solar panel, a rigid body, etc.)
- (b) an electrical or electromechanical element in the system (actuators, sensors, amplifiers, filters, etc.)

From mathematical considerations x_i might represent any mathematical component of the state in any transformed (non-physical) coordinates. One such example which is common is to define the "components" to be "modes" of the systems. In this case the "component costs" (7.14) are called "modal costs" [5]. We choose to now examine system (7.6), (7.7) using such modal cost analysis (MCA). To begin our modal cost analysis of (7.6) we define the system components as follows. The vector x is rearranged and decomposed according to

$$x_i \triangleq \begin{pmatrix} n_i \\ \dot{n}_i \end{pmatrix} \quad i=1, \dots, N \quad (7.17a)$$

and the vector x_p is rearranged and decomposed according to

$$x_x \triangleq \frac{\partial x_j}{\partial p_i} = \begin{pmatrix} x_{p_i} \end{pmatrix}_j \quad \begin{matrix} j=1, \dots, N \\ i=1, \dots, (2N+Nm_a) \\ \alpha=N+1, \dots, (2N+Nm_a) \end{matrix} \quad (7.17b)$$

where the p_i are defined by (7.8). Generally, one must compute the component costs by first solving (7.16) on a computer. However, due to the simple form of A resulting from the "modal" components defined in (7.17), the eqs. (7.16) can be solved analytically. The results for the control problem (7.1) - (7.4) with $p = 0$ and

$$y = \begin{pmatrix} n \\ \dot{n} \end{pmatrix}, \quad Q = \begin{bmatrix} I & 0 \\ 0 & \beta I \end{bmatrix} \quad (7.18a)$$

$$\ddot{n}_i + 2\zeta_i \omega_i \dot{n}_i + \omega_i^2 n_i = d_i^T w \quad (7.18b)$$

are (see [37] for proofs):

$$V(x_i) = (4\zeta_i \omega_i^3)^{-1} (1 + \beta \omega_i^2) d_i^T W d_i \quad i=1, \dots, N \quad (7.19a)$$

which represents the modal cost for each mode of the structure, and,

$$V(\omega_i^2) = \sigma_{\omega_i}^2 (32\zeta_i^3 \omega_i^7)^{-1} (1 + 4\zeta_i^2 + \beta \omega_i^2) d_i^T W d_i \quad (7.19b)$$

which represents the cost associated with the uncertainty in the squared modal frequencies ω_i^2 and,

$$V(\zeta_i) = \sigma_{\zeta_i}^2 (8\zeta_i^3 \omega_i^3)^{-1} (1 + \beta \omega_i^2) d_i^T W d_i \quad (7.19c)$$

which represents the cost associated with the uncertainty in modal damping ζ_i and,

$$V(\delta e_{ij}) = \sigma_{\delta e_{ij}}^2 (4\zeta_i \omega_i^3)^{-1} (1 + \beta \omega_i^2) W_{ij} \quad \begin{matrix} i=1, \dots, N \\ j=1, \dots, m_a \end{matrix} \quad (7.19d)$$

which represents the cost associated with the uncertainty in the i th mode shape at the location of actuator j . The variances $\sigma_{\zeta_i}^2$, $\sigma_{\omega_i^2}^2$, $\sigma_{\delta e_{ij}}^2$ are given by (7.9)-(7.11). From (7.15) the total cost is

$$V = \sum_{i=1}^N [V(x_i) + V(\omega_i^2) + V(\zeta_i) + \sum_{j=1}^{m_a} V(\delta e_{ij})] \quad (7.19e)$$

Due to the fact that the component costs (7.19) are given in explicit form, they may be computed for a large number of modes and a large number of parameters. If we had to rely on numerical methods for solving (7.16) we would be faced with the task of solving (7.16b) for a system of order $2N(1+(2+m_a)N)$. Unfortunately, this is indeed the situation when control objectives *different* from (7.18a) are required.

Example:

Consider the system with small damping,

$$\begin{aligned} \ddot{q} + 2\zeta\omega\dot{q} + \omega^2 q &= D w, \quad \bar{D}^T = (1, 1), \quad W = 1 \\ \bar{\zeta}_i &= 0.005 \quad i = 1, 2, \quad \zeta = \text{diag} [\zeta_1, \zeta_2] \\ \bar{\omega}_1 &= 1, \quad \bar{\omega}_2 = 10, \quad \omega = \text{diag} [\omega_1, \omega_2] \end{aligned} \quad (7.20)$$

$$V = \lim_{t \rightarrow \infty} E \dot{q}^T \dot{q}.$$

choosing $\beta = 0$ in (7.18a) we find from (7.19)

$$V(x_1) = 50, \quad V(x_2) = 0.05 \quad (7.21)$$

indicating that mode 1 is more important to performance than mode 2. Choosing $\sigma_{\omega_0}^2 = 10$, then (7.19b) reveals

$$V(\omega_1^2) = 25 \times 10^4, \quad V(\omega_2^2) = 0.05 \quad (7.22)$$

indicating that ω_1 is a more critical parameter than ω_2 . Choosing $\nu = 100$ in (7.9) leads to

$$V(\zeta_1) = 10^8, \quad V(\zeta_2) = 2 \times 10^5 \quad (7.23)$$

indicating that the damping in mode 1 is more critical than damping in mode 2. Finally,

$$V(D_1) = 50, \quad V(D_2) = 0.1 \quad (7.24)$$

indicating that the mode shape of mode 1 at the location of disturbing force w is more critical than the mode shape of mode 2 at the location of the disturbing force. The parameters, *in order* of their importance are therefore, $(\zeta_1, \zeta_2, \omega_1, D_1, D_2, \omega_2)$.

Modal Costs for Kinetic Energy Performance Metric

Consider a kinetic energy performance metric,

$$V = \lim_{t \rightarrow \infty} E \dot{q}^T \dot{q} \quad (7.25)$$

Eqs. (7.13) and (7.18a) can give this result by letting β be much larger than 1 and then normalizing the cost by dividing by β . The results (7.19) reduce to

$$V(x_i) = (4\zeta_i \omega_i)^{-1} d_i^T W d_i \quad x_i^T \triangleq (q_i, \dot{q}_i) \quad (7.26a)$$

$$V(\omega_i^2) = \sigma_{\omega_i^2}^2 (32\zeta_i^3 \omega_i^5)^{-1} d_i^T W d_i \quad (7.26b)$$

$$V(\zeta_i) = \sigma_{\zeta_i}^2 (8\zeta_i^3 \omega_i)^{-1} d_i^T W d_i \quad (7.26c)$$

$$V(\delta e_{ij}) = \sigma_{\delta e_{ij}}^2 (4\zeta_i \omega_i)^{-1} W_{ij} \quad j=1, \dots, m_a \quad (7.26d)$$

Example:

Consider again (7.20) with the kinetic energy metric (7.25). Then

$$\begin{aligned}
 V(x_1) &= 50, & V(x_2) &= 5 \\
 V(\omega_1^2) &= 25 \times 10^4, & V(\omega_2^2) &= 5 \\
 V(\zeta_1) &= 10^8, & V(\zeta_2) &= 10^7 \\
 V(D_1) &= 50, & V(D_2) &= 5
 \end{aligned}$$

The parameters, in order of their importance are therefore, $(\zeta_1, \zeta_2, \omega_1, D_1, \omega_2, D_2)$, where the last two parameters are equally important. In general, the parameters which are found to be most critical will depend upon the specific performance criterion chosen.

When the system parameters are certain ($\sigma_i = 0$ in (7.1)-(7.3)), it is possible to solve for explicit modal cost expressions *without* the special restrictions (7.18). The necessary assumption in what follows is that the modal damping ζ_i is very small. Theorem 7 deals with the theory for deterministic problems and theorem 8 treats stochastic problems.

Theorem 7

For the system

$$\begin{aligned}
 \ddot{n}_i + 2\zeta_i \omega_i \dot{n}_i + \omega_i^2 n_i &= 0, & \{n_i(0), \dot{n}_i(0)\} & \text{specified, } i=1, \dots, N \\
 y &= \sum_{i=1}^N (p_i n_i + r_i \dot{n}_i)
 \end{aligned} \tag{7.27}$$

the cost function

$$V \triangleq \int_0^\infty y^T Q y dt = \sum_{i=1}^N V_i \tag{7.28}$$

decomposes into the modal costs V_i given by

$$\begin{aligned}
 V_i &= \frac{1}{2} \frac{\partial V}{\partial x_i(0)} x_i(0) = \frac{1}{4\zeta_i \omega_i} [\|p_i\|_Q^2 + \omega_i^2 \|r_i\|_Q^2] [n_i^2(0) + \frac{\dot{n}_i^2(0)}{\omega_i^2}] \\
 x_i^T &= (n_i, \dot{n}_i).
 \end{aligned} \tag{7.29}$$

in the limit as $\zeta_i \omega_i \rightarrow 0$.

Theorem 8

For the system

$$\begin{aligned}
 \ddot{n}_i + 2\zeta_i \omega_i \dot{n}_i + \omega_i^2 n_i &= b_i^T u_W + d_i^T w, & w & \sim N(0, W), & u_W & \sim N(0, U) \\
 y &= \sum_{i=1}^N (p_i n_i + r_i \dot{n}_i)
 \end{aligned} \tag{7.30}$$

where u_W and w are zero mean uncorrelated white noises with intensities U and W , the cost function

$$V \triangleq \lim_{t \rightarrow \infty} E(y^T Q y) = \sum_{i=1}^N V_i \tag{7.31}$$

decomposes into the modal costs V_i given by

$$\begin{aligned}
 V_i &= \lim_{t \rightarrow \infty} \frac{1}{2} E \left(\frac{\partial Y}{\partial x_i} x_i \right) = \frac{1}{4\zeta_i \omega_i} [\|p_i\|_Q^2 + \omega_i^2 \|r_i\|_Q^2] [\|b_i\|_U^2 + \|d_i\|_W^2] \frac{1}{\omega_i^2} \\
 V &= y^T Q y
 \end{aligned} \tag{7.32}$$

The proof of theorem 7 may be found in [38] and the proof of theorem 8 may be found in [39]. The value of (7.32) is that both disturbance and control points of excitation are considered in the subsequent model reduction decisions. The intensity U of the actuator excitations depends upon the relative bandwidth of the actuators. In the absence of better data we would use

$$U = \omega_{BW}^2 I, \quad (\omega_{BW} \triangleq \text{actuator bandwidth}) \tag{7.33}$$

Of course, the *real* purpose for including $b_i^T u_w$ in (7.30) is to anticipate some sort of excitation through the actuators, *prior* to the actual design of the control law.

The output (7.27) is slightly more general than the *separable* outputs defined in (2.2c). However, most problems seem to fit nicely into the format of (2.2c). To interpret (7.27) in the spirit of (2.2c), simply make the substitutions

$$p_i \rightarrow \begin{pmatrix} p_i \\ 0 \end{pmatrix}, \quad r_i \rightarrow \begin{pmatrix} 0 \\ \lambda_i \end{pmatrix} \quad (7.34)$$

in which case the form of the result (7.32) does not change, merely the interpretation of p_i and r_i as p_i and λ_i . According to modal costs (7.32) the importance of a mode is determined basically by the product of three properties of the mode,

$$V_i = (\text{time constant})(\text{observability})(\text{disturbability} + \text{controllability}) \quad (7.35)$$

where mode i is: unobservable in position if and only if $\|p_i\| = 0$, unobservable in rate outputs if and only if $\|r_i\| = 0$, undisturbable from w if and only if $\|d_i\| = 0$, and uncontrollable from u_w if and only if $\|b_i\| = 0$. By substitution of (7.18a) and $U = 0$ into (7.32) the result (7.19a) is obtained as a special case of (7.32). The expressions (7.29) and (7.32) are general modal costs for matrix-second-order systems which have no gyroscopic terms.

7.3 Component Cost Analysis as a Spacecraft Control Design Procedure

The results of Sections 6.0 and 7.0 are now combined to form a design algorithm for flexible spacecraft control. The reader should be advised that at this time of rapid developments of both theory and practice that any such algorithms are ad hoc at best and new theories may allow considerable improvement in these procedures. However, in the interest of stimulating such improvements the following algorithm is suggested. Each step in the algorithm is discussed and motivated in some detail.

Definitions and Assumptions:

- A1. The system under consideration has the form (2.1) with $G' = 0$ and (2.6) holds.
- A2. Rate sensors are collocated with the m actuators. An actuator applies a force between two points in the structure, and a sensor measures the time rate of change of the resulting rectilinear displacement. Alternatively, an actuator applies a torque between two points in the structure, and a sensor measures the time rate of change of the resulting angular displacement.
- A3. n_r of the m actuators are located so that rigid modes are controllable.
- A4. There are n_r inertially-referenced position sensors located so that rigid modes are observable.
- A5. The number of elastic modes calculated for the structure is N .
- A6. The largest Liapunov equation of the form (7.16b) which can be solved reasonably accurately on the available off-line computer has dimension $2N_L \times 2N_L$.
- A7. The largest Riccati equations of the types (4.13), (4.14) which can be solved reasonably accurately on the available off-line computer has dimension $N_R \times N_R$.
- A8. The largest controller (4.1) which can be accommodated in the on-line computer has dimension N_C , where $N_C \leq N_R \leq 2N_L \leq 2N$.
- A9. The highest bandwidth of the available actuators is ω_{BW} .
- A10. The parameters considered uncertain are given by (7.8), and these uncertainties are modeled by (7.9).
- A11. We have in mind the performance measure

$$V = \lim_{t \rightarrow \infty} E \left\{ \alpha y^T Q y + \beta \dot{y}^T \dot{Q} \dot{y} + \rho u^T R_0 u + \sum_{i=1}^v \sigma_i^2 \left(\alpha \frac{\partial y^T}{\partial p_i} Q \frac{\partial y}{\partial p_i} + \rho \frac{\partial u^T}{\partial p_i} R_0 \frac{\partial u}{\partial p_i} \right) \right\} \quad (7.36)$$

where for (7.8), $v = 2N_e + N_e m$, $N_e \triangleq \frac{1}{2} N_R - n_r$.

To illustrate the design procedure we use the simple example

$$\begin{aligned} \ddot{n}_r &= B_r u + D_r w, \quad n_r \in R^1 \\ \ddot{n}_e + 2\zeta \omega \dot{n}_e + \omega^2 n_e &= B_e u + D_e w, \quad n_e \in R^4 \end{aligned} \quad (7.37)$$

$$y = P_r n_r + P_e n_e, \quad z_p = M_{pr} n_r + v_p, \quad z_r = M_{re} \dot{n}_e + v_r$$

where

$$\begin{aligned} \zeta &= 0.005, \quad \omega = \text{diag} [1, 2, 5, 10], \quad M_{pr} = 10, \quad B_r = 1, \quad D_r = 10, \quad P_r = 1, \quad Q = 100, \\ \beta &= 1, \quad E u(t) u^T(\tau) = U \delta(t-\tau), \quad U = 1, \quad E w(t) w^T(\tau) = W \delta(t-\tau), \quad W = 100, \quad E v_p(t) v_p^T(\tau) = V_p \delta(t-\tau), \end{aligned}$$

$$V_p = 10, \quad E v_r(t) v_r^T(\tau) = V_r \delta(t-\tau), \quad V_r = 0.1, \quad P_e = (0.1, 1.0, 0.01, 1.0), \quad B_e^T = (0.1, 0.01, 1.0, 0.1), \\ D_e^T = (0.01, 0.1, 0.01, 0.001),$$

and we take, for illustrative purposes only,

$$N = 4, \quad n_r = 1, \quad m = 1, \quad N_L = 3, \quad N_R = 6, \quad N_C = 2.$$

The measurements z_p and z_r respectively represent position of the rigid body and a rate measurement. It may be readily verified that all the assumptions (A1 - A11) are satisfied.

7.4 The CCA Design Algorithm

Step I: The Preliminary Model Reduction:

Set $\beta = \rho = \alpha_i = 0$ in (7.36) and use MCA (7.32) to reduce the number of vehicle modes from $(N + n_r)$ to $(N_L + n_r')$, where n_r' is the number of rigid body modes surviving the MCA truncation.

Purpose of STEP I: Reduce the number of modes to a tractable number, but do so with knowledge of $y^T Q y$, the primary control objective.

Example of STEP I: For (7.37), using (7.32) we have

$$V(n_p) = \infty, \quad V(n_1) = 1.00, \quad V(n_2) = 625.00, \quad V(n_3) = 40.40, \quad V(n_4) = 0.50 \quad (7.38)$$

Hence, by the modal cost rule for truncation (7.13), mode 4 is truncated and the retained modes, listed in order of their modal cost (their predicted importance in the problem) are (n_r, n_2, n_3, n_1) . The reduced model is

$$\ddot{n}_r = B_r u + D_r w \quad (7.39a)$$

$$\ddot{n}_e' + 2\zeta\omega' n_e' + \omega'^2 n_e' = B_e' u + D_e' w \quad (7.39b)$$

$$y = P_r n_r + P_e' n_e', \quad z_p = M_{pr} n_r + v_p, \quad z_r = M_{re}' n_e' + v_r$$

where

$$\omega' = \text{diag}[2, 5, 1], \quad D_e'^T = (0.10, 0.01, 0.01)$$

$$B_e'^T = (0.01, 1.00, 0.10), \quad P_e' = (1.00, 0.01, 0.10)$$

STEP II: Rate Feedback Design:

Set $u = u_0 + u_r$ where

$$u_r = -G_r z_r, \quad G_r = (B_e'^T B_e')^{-1} B_e'^T (P_e'^T Q P_e' \beta - 2\zeta\omega') B_e' (B_e'^T B_e')^{-1} \quad (7.40)$$

where β is chosen large enough so that $P_e'^T Q P_e' \beta - 2\zeta\omega' > 0$.

Purpose of STEP II: It follows from theorem 6 that the control (7.40) is the control which is both the optimal measurement z_r feedback control and the optimal state feedback control for

$$V = \lim_{t \rightarrow \infty} E \{ \dot{n}_e'^T [2\zeta\omega' + B_e' G_r B_e'^T] \dot{n}_e' + u_r^T G_r^{-1} u_r \} \quad (7.41)$$

subject to (7.39b). Furthermore, such a control increases the relative stability of all controllable modes and, of course, does not move others. Hence, the system is stable in the presence of almost all modal data uncertainties. However, this promise is only valid for those modes within the actuator, sensor bandwidths. The main purpose of STEP II is to increase the damping of those modes that MCA has identified as critical to the cost function, and to do this for a larger number of modes than the subsequent outer control loop u_0 can be optimized for. This allows a control spillover "cushion" in the sense that the control spillover from u_0 will have to push those residual poles (truncated in the u_0 design but present in the u_r design of STEP II) further to the right to destabilize them. Now, in order to be sure that STEP II has provided "spillover protection" for the same modes for which such protection will be needed later, it is important that the design of u_r and u_0 be "coordinated" to the extent that they are both concerned with the regulation of the output vector y . The rate feedback design minimizes rates, so choosing u_r to minimize \dot{y} is the rational thing to do. Hence, we may interpret STEP II in the spirit of (7.36) by setting $\alpha = \alpha_i = 0$ with $u = u_r$. To match this objective as closely as possible with (7.41), we set

$$\rho R_0 = G_r^{-1}, \quad B P_e^T Q P_e^T = 2\zeta\omega' + B_e' G_r B_e'^T \quad (7.42)$$

and find the G_r which comes closest (in a least squares sense) to satisfying the second equation in (7.42). The result is (7.40).

Example of STEP III: From (7.39), (7.40)

$$G_r = 7.82 \quad (7.43)$$

The system (7.39) is now described by

$$\ddot{n}_r + B_r G_r B_e'^T \dot{n}_e' = B_r u_0 + D_r w \quad (7.44a)$$

$$\ddot{n}_e' + [2\zeta\omega' + B_e' G_r B_e'^T] \dot{n}_e' + \omega'^2 n_e' = B_e' u_0 + D_e' w \quad (7.44b)$$

$$y = P_r n_r + P_e' n_e', \quad z_p = M_{pr} n_r + v_p, \quad z_r = M_{re}' n_e' + v_r$$

STEP III: Second Stage of Model Reduction:

Put (7.44b) in the state form

$$\dot{x} = A_0 x + B_0 u_0 + D_0 w \quad (7.45)$$

$$y = C_0 x$$

$$z = M_0 x + v \quad z^T = (z_p^T, z_r^T)$$

where the $2N_L$ components of x are n_{e_i}' , \dot{n}_{e_i}' $i = 1, \dots, N_L$ arranged in any order. Compute

$$V_i = [C_0^T Q C_0 X_0]_{ij}, \quad Q = X_0 A_0^T + A_0 X_0 + D_0 W D_0^T \quad (7.46)$$

and delete from (7.44b) those modes with the smaller component costs defined by

$$V(n_{e_j}', \dot{n}_{e_j}') \triangleq V(n_{e_j}') + V(\dot{n}_{e_j}') \quad (7.47)$$

where $V(n_{e_j}')$ and $V(\dot{n}_{e_j}')$ are computed from (7.46). The number of equations retained in (7.44b) is $(\frac{1}{2}N_R - n_r)$.

Purpose of STEP III: STEP III must reduce the model (7.44) to "Riccati-solvable" dimension N_R to prepare for design of the control u_0 .

Example of STEP III: From (7.44b) - (7.47) we have

$$V(n_{e_1}', \dot{n}_{e_1}') = 0.60, \quad V(n_{e_2}', \dot{n}_{e_2}') = 609.20, \quad V(n_{e_3}', \dot{n}_{e_3}') = -0.02 \quad (7.48)$$

indicating that the equation for $n_{e_3}'(t)$ is to be truncated from (7.44b). The model now is put into the form

$$\begin{aligned} \dot{x} &= Ax + Bu_0 + Dw \\ y &= Cx \\ z &= Mx + v \end{aligned} \quad (7.49)$$

where $x^T = (n_r, \dot{n}_{e_2}', \dot{n}_{e_1}', n_r, \dot{n}_{e_2}', \dot{n}_{e_1}')^T$.

STEP IV: Design of the Outer Loop u_0 .

Set $\sigma_1 = 0 = \beta$, $\rho R_0 = G_r^{-1}$ in (7.36) to get the optimal controller

$$u_0 = G\hat{x}, \quad \dot{\hat{x}} = A\hat{x} + b u_0 + F(z - M\hat{x}) \quad (7.50)$$

$$G = -G_r B^T K, \quad 0 = KA + A^T K - KBG_r B^T K + C^T Q C \alpha$$

$$F = XM^T V^{-1}, \quad 0 = XA^T + AX - XM^T V^{-1} M X + DWD^T$$

Purpose of STEP IV: The value of $R = G_r^{-1}$ has been established earlier. Now the optimal controller for (7.49) has been computed in (7.50), assuming certain parameters, $\sigma_i = 0$.

Those modes of the structure that are observable in y are also observable in \dot{y} . It is in this sense that the rate feedback controller of STEP II (which focused on the $y^T Q \dot{y}$ term in (7.36)) and the optimal controller of STEP II (which focused on $y^T Q y$ term) are "coordinated".

Example of STEP IV: The essential data from (7.50) is

$$G = (-3.16E-01, -4.41E-02, -5.77E-01, -8.16E-01, -4.41E-03, 2.62E-01)$$

$$C = (1.00E+00, 1.00E+00, 1.00E-01, 0, 0, 0), \quad \alpha = 7.82 E-03^*$$

$$M = \begin{bmatrix} 1.00E+01 & 0 & 0 & 0 & 0 & 0 \\ 0 & 0 & 0 & 0 & 1.00E-02 & 1.00E-01 \end{bmatrix}$$

$$A = \begin{bmatrix} 0 & 0 & 0 & 1 & 0 & 0 \\ 0 & 0 & 0 & 0 & 1 & 0 \\ 0 & 0 & 0 & 0 & 0 & 1 \\ 0 & 0 & 0 & 0 & -7.82E-02 & -7.82E-01 \\ 0 & -4 & 0 & 0 & -2.08E-02 & -7.82E-03 \\ 0 & 0 & -1 & 0 & -7.82E-03 & -8.82E-02 \end{bmatrix}, \quad D = \begin{bmatrix} 0 & 0 & 0 \\ 0 & 0 & 0 \\ 0 & 0 & 0 \\ 1 & 1.0E+01 & -7.82E+00 \\ 1.0E-02 & 1.0E-01 & -7.82E-02 \\ 1.0E-01 & 1.0E-02 & -7.82E-01 \end{bmatrix}$$

$$B = \begin{bmatrix} 0 \\ 0 \\ 0 \\ 1.00E+00 \\ 1.00E-02 \\ 1.00E-01 \end{bmatrix}, \quad F = \begin{bmatrix} 2.51E+00 & 6.35E-02 \\ 2.51E-02 & 6.30E-04 \\ 2.60E-03 & 6.78E-05 \\ 3.16E+01 & 1.62E+00 \\ 3.12E-01 & 1.66E-02 \\ 3.23E-02 & 3.36E-01 \end{bmatrix}$$

STEP V: Controller Reduction

The optimal system of STEP IV is

$$\begin{aligned} \dot{\hat{x}} = \begin{pmatrix} \dot{x} \\ \dot{\hat{x}} \end{pmatrix} &= \begin{bmatrix} A & BG \\ FM & A+BG-FM \end{bmatrix} \begin{pmatrix} x \\ \hat{x} \end{pmatrix} + \begin{bmatrix} D & 0 \\ 0 & F \end{bmatrix} \begin{pmatrix} w \\ v \end{pmatrix} = Ax + Dw \\ y = \begin{pmatrix} y \\ u \end{pmatrix} &= \begin{bmatrix} C & 0 \\ 0 & G \end{bmatrix} \begin{pmatrix} x \\ \hat{x} \end{pmatrix} = Cx \end{aligned} \quad (7.51)$$

which is now to be evaluated by criterion (7.36). First we show the simpler case of known parameters ($\sigma_i = 0$).

*Multiplying (7.36) by $1/\alpha$ yields a parameter ρ/α to be selected to achieve an acceptable control effort. The best value of α is therefore determined from Fig. 2 as that choice which corresponds to the lowest point on the dotted curve of Fig. 2. This point is found by trial and error, first picking an α then truncating the controller to the desired order N_c , and repeating this process for a new α . Thus, the above value of α was found after several passes through STEP V.

STEP VA: Controller Reduction with Certain Parameters ($\sigma_i = 0$)

Delete from the controller

$$\begin{aligned} \dot{\hat{x}} &= [A+BG-FM]\hat{x} + Fz, \quad \hat{x} \in R^{N_R} \\ u_0 &= G\hat{x} \end{aligned} \quad (7.52)$$

those states (\hat{n}_i, \hat{n}_i) with the smallest component costs $V(\hat{n}_i, \hat{n}_i) = V(\hat{n}_i) + V(\hat{n}_i)$ defined by

$$V_i = [C^T Q C X]_{jj}, \quad 0 = XA^T + AX + DWD^T, \quad Q = \text{block diag}[Q, G_r^{-1}]. \quad (7.53)$$

for $j = i + N_r, i=1, \dots, N_r$, where $V_i = V(\hat{n}_i)$ and $V_{i+1} = V(\hat{n}_i)$ if \hat{x} has the form $\hat{x}^T = (\dots, \hat{n}_i, \hat{n}_i, \dots)$. This yields the reduced controller.

$$\dot{\hat{x}}_R = A_R \hat{x}_R + F_R z, \quad u_0 = G_R \hat{x}_R, \quad \hat{x}_R \in R^{N_C} \quad (7.54)$$

where A_R is obtained by deleting the indicated rows and columns of $[A+BG-FM]$, F_R is obtained by deleting the same rows of F , and G_R is obtained by deleting the same columns of G .*Purpose of STEP VA:* Reduce the order of the controller (7.52) to the order N_C acceptable by on-line software limitations.*Example of STEP VA:* The calculation (7.53) reveals that the *cost-ordered* components of the controller are

$$\hat{x}^T = (\hat{n}_r, \hat{n}_r, \hat{n}_{e_2}, \hat{n}_{e_2}, \hat{n}_{e_1}, \hat{n}_{e_1}) \quad (7.55)$$

Hence, if only 4 components of the controller are to be retained they would be

$$\hat{x}_R^T = (\hat{n}_r, \hat{n}_r, \hat{n}_{e_2}, \hat{n}_{e_2}) \quad (7.56)$$

and if only 2 components of the controller are to be retained, they would be

$$\hat{x}_R^T = (\hat{n}_r, \hat{n}_r) \quad (7.57)$$

The corresponding reduced controller dynamics are deduced from (7.52) in the manner described above.

STEP VB: Controller Reduction with Uncertain Parameters ($\sigma_i > 0$)Delete from the controller (7.52) those states \hat{x}_i with the smallest component costs $V_i \triangleq V(\hat{x}_i, \hat{x}_i)$ computed by

$$V_i = \sum_{k=0}^{\infty} [C_{\delta}^T Q_{\delta} C_{\delta} X_{\delta}]_{jj}, \quad 0 = X_{\delta} A_{\delta}^T + A_{\delta} X_{\delta} + D_{\delta} W D_{\delta}^T \quad (7.58)$$

for $j = (i + N_r + 2N_r k), i = 1, \dots, N_r$, where

$$A_{\delta} = \begin{bmatrix} A & 0 \\ A_p & \tilde{A} \end{bmatrix}, \quad D_{\delta} = \begin{bmatrix} D \\ D_p \end{bmatrix}, \quad C_{\delta} = \begin{bmatrix} C & 0 \\ C_p & \tilde{C} \end{bmatrix} \quad (7.59)$$

$$Q_{\delta} = \text{block diag}[Q, \sigma_1^2 Q, \dots, \sigma_v^2 Q]$$

and where Q is defined by (7.53).*Purpose of STEP VB:* The component costs (7.58) represent the sum

$$V_i = V(\hat{x}_i) + \sum_{k=1}^{\infty} V((\hat{x}_i)_{pk}) \quad (7.60)$$

where the total cost is given by (7.36) with $\beta = 0$. By use of (7.59) and (7.51) the total cost may be written

$$V = \text{tr}[C_{\delta}^T C_{\delta} X_{\delta}] = \sum_{i=1}^{N_R} V(\hat{x}_i, \hat{x}_{ip}) + \sum_{i=1}^{N_R} V(x_i, x_{ip}) \quad (7.61)$$

where V_i in (7.58) picks out the first terms in (7.61) due to \hat{x}_i . The remaining terms in (7.61) are due to the states x_i and their sensitivities, which are not needed for this design but may be computed from the remaining terms in (7.58). The particular range of indices in the V_i computation of (7.58) are due to the choice of coordinates represented by (7.59). Of course, any other choice of coordinates may be chosen with an attendant change in the range of indices jj in (7.58) to identify those variables of the augmented state vector x representing controller dynamics and their sensitivities, \hat{x}_i and \hat{x}_{ip} . STEP VB allows sensitivity considerations to influence the controller reduction, whereas, STEP VA assumes the parameters are known a priori. There is an additional computational burden in STEP VB and for this step assumption A8 must be changed to

$$N_C \leq 2N_R \leq 2N_L \leq 2N$$

due to the fact that (7.58) decomposes into $(v+1)$ Liapunov equations each of which is $2N_R \times 2N_R$ [37].

Example of STEP VB: Assume uncertain frequencies ω_1, ω_2 . Hence

$$p^T = (\omega_1, \omega_2), \quad \bar{p}^T = (1, 2)$$

$$\sigma_1^2 = E(\omega_1 - \bar{\omega}_1)^2 = \sigma_0^2 = 100$$

$$\sigma_2^2 = E(\omega_2 - \bar{\omega}_2)^2 = i\sigma_0^2 = 2(100) = 200$$

Carrying out the computations (7.58) we find that the controller states arranged in their cost-order, are

$$\hat{x}^T = (\hat{\eta}_{e1}, \hat{\eta}_{e1}, \hat{\eta}_r, \hat{\eta}_r, \hat{\eta}_{e2}, \hat{\eta}_{e2}) \quad (7.62)$$

Hence if only a fourth order controller is desired we would choose

$$\hat{x}_R^T = (\hat{\eta}_{e1}, \hat{\eta}_{e1}, \hat{\eta}_{r1}, \hat{\eta}_{r1}) \quad (7.63)$$

If only a second order controller is desired we would choose

$$\hat{x}_R^T = (\hat{\eta}_{e1}, \hat{\eta}_{e1}) \quad (7.64)$$

Controller (7.64) would lead to instability since the rigid body mode has been truncated. By comparing (7.55), (7.56) and (7.57), respectively, with (7.62), (7.63) and (7.64), the influence of parameter sensitivity on the reduced controller design can clearly be seen. For example, (7.55) indicates that $(\hat{\eta}_{e2}, \hat{\eta}_{e2})$ are more important than $(\hat{\eta}_{e1}, \hat{\eta}_{e1})$ in the nominal optimal controller (7.52), whereas (7.62) indicates that, from parameter sensitivity consideration, $(\hat{\eta}_{e1}, \hat{\eta}_{e1})$ is more important.

8.0 Conclusions

In this chapter we have outlined in some detail many of the critical problems associated with the control of lightly damped flexible structures. Underlying all of the practical problems of

- high performance
- assembly in space, configuration changes
- on-line controller software design
- lack of test data

is the central problem of modeling errors. To justify the expense of a space structure, the performance requirements will necessarily be very severe. On the other hand, the absence of economical tests precludes the availability of reliable data before flight. Thus, a greater burden of responsibility is placed upon analytical methods in the design without the benefit of test data for a system nearly unstable without control. This is the triple jeopardy faced by all flexible space structure designs.

Some precise statements have been verified concerning the performance of such structures in the presence of controllers based upon erroneous models. The modeling error can always be classified into four categories: (1) parameter errors, (2) model order errors, (3) disturbance errors and (4) neglected nonlinearities. Section 4 (theorem 1, part (c)) has shown the class of parameter errors (i.e. yielding *either* no control or no observation spillover) which allow the controlled system to be stable in the presence of all model order errors. Sections 5 and 6 have shown the class of model order errors (i.e. infinite bandwidth sensors, actuators) which allow the controlled system to be stable in the presence of all parameter errors (theorem 3). Section 6 has shown such properties of rate measurement feedback control as damping and inverse optimal control solutions. Section 7 has provided a systematic approach to model order reduction, controller order reduction and parameter sensitivity using component cost analysis (CCA). Finally, a design algorithm is offered which has these properties:

1. Provides damping for a larger number of modes than the optimal attitude controller controls. This rate measurement feedback design, with colocated rate sensors and actuators, provides control spillover protection for the truncated controller.
2. Coordinates the rate feedback design with the attitude control design by use of a similar cost function.
3. Provides model reduction and controller reduction decisions which are systematically connected to the mathematical statement of the control objectives and the disturbance models.

There are many possible versions of the CCA design algorithm. Some versions would require more computation with some attendant improvement in performance. For example, other choices of coordinates besides "modal" coordinates may provide better reduced models in Section 7. However, in the interest of clarity, the procedures have been explained with some economy of detail.

Flexible space structure control is indeed a fitting challenge to the best of available control and estimation theories - what an excellent example with which to test the worth of powerful theories. And, conversely, out of such challenging examples come pointed needs for new theory.

Acknowledgements

My insights into this problem have been deepened by many colleagues with whom I have been privileged to associate. Some having direct influences on my work in this chapter will be mentioned. Peter Hughes has influenced my thoughts on stability and the tidy relationships with observability. Mark Balas and I have had many stimulating conversations on modeling errors and "spillover" problems. Mike Lyons and Jean Aubrun have shown me the value of "two-stage" designs using rate feedback in the first stage. The references clearly show the close relationship with the work of Arbel and Gupta on inverse optimal control. Finally, my students Ajmal Yousuff and Ramakrishna Yedavalli have made considerable contributions both in the analysis and the numerical work.

References

- [1] Pilkington, W. C., "Vehicle Motions as Inferred From Radio Signal Strength Records," External Publication No. 551, Jet Propulsion Laboratory, Pasadena, CA, September 5, 1958.
- [2] AIAA/NASA Proceedings, Conference on Advanced Technology for Future Space Systems, Hampton, VA, May 8-10, 1979.
- [3] Nissim, E., "Flutter Suppression and Gust Alleviation Using Active Controls," NASA TN D-8212, 1976. Also see, J. Guidance and Control, Vol. 2, No. 5, September-October, 1979, pp. 395-401.
- [4] Nordell, W. J., "Active Systems for Blast-Resistant Structures," Technical Report R-611 Naval Civil Engineering Laboratory, Post Hueneme, CA, February 1969.
- [5] Skelton, R. E., "Cost Decomposition of Linear Systems with Application to Model Reduction," to appear, International J. Control. Also see JACC 1979, pp. 56-62.
- [6] Balas, M. J., "Some Trends in Large Space Structure Control Theory: Fondest Hopes; Wildest Dreams" to appear, IEEE Trans. Auto. Control.
- [7] Zienkiewicz, O., The Finite Element Method in Engineering Science, McGraw-Hill, NY, 1971.
- [8] Oden, J. T., and Reddy, J., An Introduction to the Mathematical Theory of Finite Elements, Wiley, NY, 1976.
- [9] Likins, P. W., "Finite Element Appendage Equations, for Hybrid Coordinate Dynamic Analysis," NASA Technical Report 32-1525, Jet Propulsion Laboratory, October 15, 1971.
- [10] Hughes, P. C., "Modal Identities for Elastic Bodies, with Application to Vehicle Dynamics and Control," J. Applied Mechanics, Vol. 47, No. 1, March 1980, pp. 177-184.
- [11] Garg, S. C., Hughes, P. C., Miller, R. A., and Vigneron, F. R., "Flight Results on Structural Dynamics from Hermes," J. Spacecraft, Vol. 16, No. 2, March-April 1979.
- [12] Skelton, R. E. and Likins, P. W., "Techniques of Modeling and Model Error Compensation in Linear Regulator Problems," Control and Dynamic Systems, Vol. 14, Academic Press, 1978. Ed. C. T. Leondes.

- [13] Mehra, R. K., and Lainiotis, D. G., System Identification: Advances and Case Studies, Academic Press, 1976.
- [14] Eykhoff, P., System Identification, Parameter and State Estimation, Wiley, 1974.
- [15] Johnson, C. R., "Approaches to Adaptive Digital Control Focusing on the Second Order Modal Descriptions of Large, Flexible Spacecraft Dynamics," Proceedings of the Second VPI&SV/AIAA Symposium on Dynamics and Control of Large Flexible Spacecraft, Blacksburg, VA, June 1979, pp. 301-316. Also see IEEE Trans. Auto. Control, AC-25, No. 4, Aug. 1980, pp. 697-702.
- [16] Balas, M. J. "Feedback Control of Flexible Systems," IEEE Trans. Auto. Control, AC-23, 1978, pp. 673-679.
- [17] Sesak, J. R., "Control of LSS via Singular Perturbation Optimal Control," AIAA Conf. on Large Space Platforms, Los Angeles, CA, 1978.
- [18] Sesak, J. R., Likins, P. W., and Coradetti, T., "Flexible Spacecraft Control by Model Error Sensitivity Suppression," Proceedings of the Second VPI&SV/AIAA Symposium on Dynamics and Control of Large Flexible Spacecraft, Blacksburg, VA, June 1979, pp. 349-368.
- [19] Skelton, R. E., "Adaptive Orthogonal Filters for Compensation of Model Errors in Matrix-Second-Order Systems," to appear J. Guidance and Control.
- [20] Skelton, R. E. and Likins, P. W., "Orthogonal Filters for Model Error Compensation in the Control of Nonrigid Spacecraft," J. Guidance and Control, Vol. 1, 1978, pp. 41-49.
- [21] Potter, J. E. and Ginter, S. D., "A New Concept in Adaptive Structural Control," Proceedings of the Second VPI&SV/AIAA Symposium on Dynamics and Control of Large Flexible Spacecraft, Blacksburg, VA, June 1979, pp. 331-348.
- [22] Johnson, C. D., "State Variable Design Methods May Produce Unstable Feedback Controllers," Int. J. Control, Vol. 29, No. 4, April 1979, pp. 607-620.
- [23] Skelton, R. E., "Application of Disturbance Accommodating Control in the Model Error Problem," J. of Interdis. Model. & Simul., Vol. 3, No. 1, 1980, pp. 47-62.
- [24] Kwakernaak, H., and Sivan, R., Linear Optimal Control Systems, Wiley, 1972.
- [25] Hughes, P. C., and Skelton, R. E., "Stability, Controllability and Observability of Matrix-Second-Order Systems," Proceedings JACC, June 1979, pp. 56-62.
- [26] Hughes, P. C., and Skelton, R. E., "Controllability and Observability for Flexible Spacecraft," J. Guidance and Control, Vol. 3, No. 5, September-October 1980, pp. 452-460.
- [27] Fallside, F., Editor, Control System Design by Pole-Zero Assignment, Academic Press, 1977.
- [28] Aubrun, J., "Theory of the Control of Structures by Low-Authority Controllers," J. Guidance and Control, Vol. 3, No. 5, September-October 1980, pp. 444-452.
- [29] Balas, M., "Direct Velocity Feedback Control of LSS", J. Guidance and Control, May-June 1979, Vol. 2, No. 3, pp. 252.
- [30] Lin, J. G., Hegg, D. R., Lin, Y. H., and Keat, J. E., "Output Feedback Control of Large Space Structures: An Investigation of Four Design Methods," Proceedings of the Second VPI&SV/AIAA Symposium on Dynamics and Control of Large Flexible Spacecraft, Blacksburg, VA, June 1979, pp. 1-18.
- [31] Levine, W. and Athans, M., "On Determination of the Optimal Constant Output Feedback Gains for Linear Multivariable Systems," IEEE Trans. Auto. Control, AC-15, 1970, pp. 44-48.
- [32] Yousuff, A., and Skelton, R., "Rate Feedback of Flexible Structures," to appear. Also see Yousuff, A., "Order Reduction of Dynamical Systems," Ph.D. Dissertation, Purdue University, School of Aeronautics and Astronautics, West Lafayette, IN.
- [33] Gupta, N. K., and Arbel, A. "Robust Inverse Optimal Control for Flexible Structures," J. Optimization Theory & Applications, to appear, 1980.
- [34] Skelton, R. E., and Hughes, P. C., "Modal Cost Analysis for Linear Matrix-Second-Order Systems," J. Dynamic Systems, Measurement and Control, to appear, 1980.
- [35] Skelton, R. E., Hughes, P. C., "Flexible Space Structure Model Reduction by Modal Cost Analysis," Proceedings of the Second VPI&SV/AIAA Symposium on Dynamics and Control of Large Flexible Spacecraft, Blacksburg, VA, June 1979, pp. 641-661.
- [36] Skelton, R. E., "On Cost-Sensitivity Controller Design Methods for Uncertain Dynamic Systems," Journal of Mathematical Sciences, Vol. XXVII, No. 2, April 1979, pp. 181-205.
- [37] Skelton, R. E., and Yedavalli, R. K., "Modal Cost Analysis of Flexible Space Structures with Experimental Modal Data," IEEE Control and Decision Conference, Albuquerque, NM, December 1980.
- [38] Skelton, R. E., "Component Cost Analysis of Large Scale Systems," Control and Dynamic Systems, Vol. XVIII, Academic Press, 1981.
- [39] Skelton, R. E., "Optimal Control of Damped Flexible Gyroscopic Systems," paper 78-103, International Astronautical Congress, Dubrovnik, Yugoslavia, October 1978. Also see J. Guidance and Control, vol. 3, No. 2, March 1980, pp. 140-150.

OPTIMUM CLIMB AND DESCENT TRAJECTORIES FOR AIRLINE MISSIONS

Heinz Erzberger
Research Scientist
Ames Research Center, NASA, Moffett Field, California 94035

SUMMARY

The characteristics of optimum fixed-range trajectories whose structure is constrained to climb, steady cruise, and descent segments are derived by application of optimal control theory. The performance function consists of the sum of fuel and time costs, referred to as direct operating cost (DOC). The state variable is range to go and the independent variable is energy. In this formulation a cruise segment always occurs at the optimum cruise energy for sufficiently large range. At short ranges (400 n. mi. and less), a cruise segment may also occur below the optimum cruise energy. The existence of such a cruise segment depends primarily on the fuel flow vs thrust characteristics and on thrust constraints. If thrust is a free control variable along with airspeed, it is shown that such cruise segments will not generally occur. If thrust is constrained to some maximum value in climb and to some minimum in descent, such cruise segments generally will occur. The algorithm has been implemented in a computer program that can be incorporated in an airline flight planning system or can serve as a basis for an onboard implementation. The various features of the program are described and the characteristics of the optimum trajectories are illustrated with a set of example trajectories for an aircraft model representative of the Boeing 727-100.

NOMENCLATURE

c_f	fuel cost factor, dollars/kg (dollars/lb)	T	thrust, kg (lb)
c_t	time cost factor, dollars/hr	T_{up}, T_{dn}	climb and descent thrusts, respectively
D	drag force	t	time
D_v, D_{v^2}	first and second partial derivatives of drag with respect to airspeed	t_c	time at end of climb
d_c	cruise distance	t_d	time at start of descent
d_f	desired distance to fly	t_f	total mission time
d_{up}, d_{dn}	total climb and descent distances, respectively	V	true airspeed
E	total aircraft energy in units of altitude	V_c	cruise speed
E_c	cruise or maximum energy	V_{up}, V_{dn}	climb and descent airspeeds
$E_{c_{opt}}$	optimum cruise energy	V_w	wind speed along flightpath
E_i, E_f	initial and final energy	$V_{w_{up}}, V_{w_{dn}}$	wind speeds in climb and descent segments, respectively, functions of altitude
\dot{E}	rate of change in energy	W	aircraft weight in kg (lb)
g	acceleration of gravity	W_f	total mission fuel, kg (lb)
H	Hamiltonian, dollars per unit of energy	W_i	initial aircraft weight, kg (lb)
h	altitude, m (ft)	W_{ref}	reference weight in climb fuel relation
I_{up}, I_{dn}	components of the Hamiltonian	\dot{W}_f	fuel flow rate, kg/hr (lb/hr)
J	value of performance function, dollars/kg (dollars/lb)	x	distance flown, n. mi.
KLAS	indicated airspeed, knots	x_{up}, x_{dn}	climb and descent distances, running variables
K_{up}, K_{dn}	operands under the minimization operator in H	β	parameter defining direction of control perturbations
K_l	constant in climb fuel relation	γ	flightpath angle, radian
L	lift force	γ_{up}, γ_{dn}	climb and descent flightpath angles, respectively, radian
P	integrand of cost function or cost per unit time	ΔR	length of control perturbation
S_{FC}	thrust specific fuel consumption per hr	$\Delta T, \Delta V$	thrust and speed perturbations relative to cruise conditions
$S_{FC}^{(.)^n}$	n th partial derivatives of S_{FC} with respect to $(.)$	$\lambda(E_c)$	cruise cost at cruise energy E_c , dollars/n. mi.

Index categories: Flight Operations; Guidance and Control; Navigation; Communication; Trajectory Control.

δ throttle setting δ_{up}, δ_{dn} throttle settings in climb and descent, respectively ψ costate variable	λ cruise cost per unit distance λ_{opt} optimum cruise cost over all energies, per unit distance
---	---

INTRODUCTION

The continuing rise in airline operating costs due to escalating fuel prices and other inflationary factors has stimulated interest in techniques for trajectory optimization. Recent work has focused on the derivation of simplified algorithms for computing trajectories with specified range. Such an algorithm was described in Ref. 1. The trajectories calculated by this algorithm, unlike those obtained by classical performance optimization, minimize an integral performance measure such as total mission fuel cost.

Another problem that has received attention recently concerns the optimality of steady-state cruise flight. Steady-state cruise is generally not optimum for minimum fuel performance (Ref. 2), but the performance penalty of steady-state cruise is unknown because the actual nonsteady or cyclic optimum cruise has not been computed to date. However, if the steady-state cruise satisfies first-order necessary conditions, Speyer (Ref. 2) shows, in an example, that the performance improvement of a particular (though nonoptimum) cyclic cruise is about 0.1%. This improvement, if representative of the optimum cyclic cruise, is not economically significant. Nevertheless, the determination of the optimum cyclic cruise poses an interesting and unsolved problem.

Even if economically significant, cyclic cruise could not be used in airline operation because it is incompatible with existing air traffic control procedures, disconcerts passengers, and decreases engine life. Optimum trajectories, to be compatible with typical airline practice, should consist of a climbout, a steady-state cruise, and a descent. Thus, at least for commercial airline applications, the optimum trajectory must be selected from a set of trajectories that is limited *a priori* to such types.

A formulation of the trajectory optimization problem that constrains the admissible trajectories to those containing climb, steady cruise, and descent was given in Ref. 1. In this formulation, energy height was used as the independent or timelike variable in climb and descent, thus forcing energy to change monotonically in these segments. It was shown that the use of energy as the independent variable eliminates the integration of a separate adjoint differential equation, thus simplifying the numerical solution of the optimal control problem. Therefore, this formulation is also adopted here.

An evaluation of the constrained optimum trajectories by airline operators indicated an interest in the additional constraint of setting the thrust to some maximum during climb and to idle during descent to reduce pilot workload of flying the trajectories. An examination of this procedure raised the following questions that are investigated here. How do the constraints on thrust and, more generally, the aerodynamic and propulsion characteristics affect the structure of the trajectories? Under what condition is the constrained thrust procedure optimum? What performance penalty is incurred by the constraint on thrust?

The avionics and aircraft industry is currently developing onboard performance computer systems to assist the flight crew in minimizing fuel consumption and operating costs. Because of its modest computational requirements, the algorithm described herein can be implemented in an onboard computer. This paper briefly describes a computer implementation of the algorithm and also discusses the characteristics of several optimum trajectories computed for the Boeing 727-100 aircraft.

OPTIMAL CONTROL FORMULATION

As stated in the Introduction, we assume at the outset that the optimum trajectories have the structure shown in Fig. 1. This structure consists of climb, cruise, and descent segments, with the aircraft energy increasing monotonically in climb and decreasing monotonically in descent. Neglecting flightpath-angle dynamics and weight loss due to fuel burn, the point mass equations of motion for flight in the vertical plane are

$$(1/g)(dV/dt) = [(T - D)/W] - \sin \gamma \quad (1)$$

$$dh/dt = V \sin \gamma \quad (2)$$

$$dx/dt = V \cos \gamma + V_w \quad V + V_w \quad (3)$$

with the constraint $L = W \cos \gamma$. The along-track wind component V_w may be a function of altitude, but accelerations due to wind shears as well as the vertical wind component can be neglected in this analysis. In airplanes, unlike rockets, the rate of change of weight due to fuel burn introduces negligible dynamic effects in the trajectory optimization. Nevertheless, the effect of weight loss on a trajectory is important but can be accounted for without adding another state variable by techniques described in the section on computer implementation. If energy is defined as

$$E = h + (1/2g)V^2 \quad (4)$$

then the familiar relation for the rate of change in energy is obtained by differentiating Eq. (4) with respect to time and substituting the right-hand sides of Eqs. (1) and (2) in place of dV/dt and dh/dt , respectively:

$$\dot{E} = dE/dt = [(T - D)/W]V \quad (5)$$

The cost function to be minimized is chosen as the direct operating cost of the mission and consists of the sum of the fuel cost and the time cost:

$$J = c_f W_f + c_t t_f \quad (6)$$

where c_f and c_t are the unit costs of fuel and time, respectively. Setting $c_t = 0$ results in the familiar minimum fuel performance function. In integral form, the cost function becomes

$$J = \int_0^{t_f} (\dot{W}_f c_f + c_t) dt \equiv \int_0^{t_f} P dt \quad (7)$$

It is assumed that the time to fly, t_f , is a free variable, but the distance to fly is a specified quantity d_f . Following the formulation in Ref. 1, we now write the total mission cost as the sum of the costs for the three segments of the assumed trajectory (illustrated in Fig. 1);

$$J = \underbrace{\int_0^{t_c} P dt}_{\text{climb cost}} + \underbrace{(d_f - d_{up} - d_{dn})\lambda}_{\text{cruise cost}} + \underbrace{\int_{t_d}^{t_f} P dt}_{\text{descent cost}} \quad (8)$$

where λ designates the cost of cruising at a given energy E_c . Next, we transform the integral cost terms in Eq. (8) by changing the independent variable from time to energy, using the transformation $dt = dE/\dot{E}$:

$$J = \int_{E_i}^{E_c} (P/\dot{E})|_{\dot{E}>0} dE + (d_f - d_{up} - d_{dn})\lambda + \int_{E_f}^{E_c} (P/|\dot{E}|)_{\dot{E}<0} dE \quad (9)$$

where E_i and E_f are the given initial climb and final descent energies, respectively. The transformation uses the assumption that the energy changes monotonically in climb and descent. This places strict inequality constraints on \dot{E} , as shown in Eq. (9). Also in Eq. (9), the integration limits have been reversed in the descent cost term. In this formulation the cost function is of mixed form, containing two integral cost terms and a terminal cost term contributed by the cruise segment.

With the change in independent variable from time to energy, the state equation (Eq. (5)) is eliminated, leaving Eq. (3) as the only state equation. Furthermore, we note that the performance function (Eq. (9)) depends on the distance state x only through the sum of the climb and descent distances $d_{up} + d_{dn}$. Therefore, the state equation for the distance is rewritten in terms of this sum as:

$$d(x_{up} + x_{dn})/dE = (v_{up} + v_{w_{up}})/\dot{E}|_{\dot{E}>0} + (v_{dn} + v_{w_{dn}})/|\dot{E}|_{\dot{E}<0} \quad (10)$$

Here the transformation $dt = dE/\dot{E}$ was used again. Also, Eq. (10) provides for independence in the choice of climb and descent speeds v_{up} and v_{dn} and the wind velocities $v_{w_{up}}$ and $v_{w_{dn}}$. Wind velocities in climb and descent are allowed to be independent of each other; generally, different wind conditions will prevail in physically different locations of climb and descent. The wind velocities can also be altitude-dependent. The effect of altitude-dependent winds on the optimum trajectories is discussed in Ref. 3.

Necessary conditions for the minimization of Eq. (9), subject to the state equation (Eq. (10)) are obtained by application of optimum control theory (see, e.g., Ref. 4, p. 71). Then the following relations are obtained for the Hamiltonian and costate equations, respectively:

$$H = \min_{\substack{v_{up}, v_{dn} \\ \pi_{up}, \pi_{dn}}} \left\{ \left(\frac{P}{\dot{E}} \right)_{\dot{E}>0} + \left(\frac{P}{|\dot{E}|} \right)_{\dot{E}<0} + \psi \left[\frac{v_{up} + v_{w_{up}}}{\dot{E}|_{\dot{E}>0}} + \frac{v_{dn} + v_{w_{dn}}}{|\dot{E}|_{\dot{E}<0}} \right] \right\} \quad (11)$$

$$d\psi/dE = -[\partial H/\partial(x_{up} + x_{dn})] = 0 \quad (12)$$

The right-hand side of the Hamiltonian equation is minimized with respect to two pairs of control variables, one pair applicable to climb (v_{up} and π_{up}), the other pair to descent (v_{dn} and π_{dn}). Since each term under the minimization operator in Eq. (11) contains only one of the two pairs of control variables, the minimization simplifies into two independent minimizations, one involving climb controls, the other, descent controls. Also, since the right-hand side of the costate equation (Eq. (12)) is zero, ψ is constant.

TRANSVERSALITY CONDITIONS

The transversality conditions are additional necessary conditions that depend on the end-point constraints of state variables (Ref. 4). The basic constraint in this problem is that the range of the trajectory be d_f . However, d_f is a parameter in the transformed cost function, Eq. (9), and not a state variable. The final value of the state variable $d_{up} + d_{dn}$ is, in this formulation, subject only to the inequality constraint $d_{up} + d_{dn} \leq d_f$. This constraint is, of course, necessary for a physically meaningful result. This inequality constraint can be handled by solving two optimization problems, one completely free ($d_{up} + d_{dn} < d_f$), the other constrained ($d_{up} + d_{dn} = d_f$), and then choosing the trajectory with the lowest cost. Physically, the comparison is between a trajectory with a cruise segment and one without a cruise segment. Considering first the free terminal state case, $d_{up} + d_{dn} < d_f$, we obtain the following relation for the final value of the costate ψ :

$$\psi(E_C) = \frac{\partial(d_f - x_{up} - x_{dn})\lambda}{\partial(x_{up} + x_{dn})} \Big|_{E=E_C, x_{up}=d_{up}, x_{dn}=d_{dn}} = -\lambda \quad (13)$$

This is the transversality condition for the free final state problem with terminal cost (Ref. 4). It shows that the constant costate value is the negative of the cruise cost.

Next, consider the case of no cruise segment. Then, the middle term of Eq. (9) drops out and the performance function contains only the integral cost terms. This is the case of the specified final state $d_f = d_{up} + d_{dn}$; the corresponding transversality condition yields $\psi(E_C) = \psi_f$. In practice it is not necessary to compute the constrained terminal state trajectory if a valid free terminal state trajectory exists, i.e., one for which $d_f > d_{up} + d_{dn}$, since the addition of a terminal constraint can only increase the cost of the trajectory. Therefore, this case is not considered further here.

In both cases the choice of costate determines a particular range. Since the functional relationship between these variables cannot be determined in closed form, it is necessary to iterate on the costate value to achieve a specified range d_f .

The last necessary condition applicable to this formulation is obtained by making use of the fact that the final value of the timelike independent variable E is free. Its final value is the upper limit of integration E_C in Eq. (9). Application of results in Ref. 4 provides the following condition:

$$\left(H + \left\{ \partial[(d_f - d_{up} - d_{dn})\lambda(E)] / \partial E \right\} \right)_{E=E_C} = 0 \quad (14)$$

which, when evaluated and simplified, becomes

$$\left\{ H + [d_c(d\lambda/dE)] \right\}_{E=E_C} = 0 \quad (15)$$

where d_c is the cruise distance.

Condition (15) has the following physical interpretation. The value of the Hamiltonian H evaluated at cruise energy E_C is (after substituting Eq. (13) into (11)) the minimum increment in the sum of climb cost and descent cost to make a unit increment in cruise energy. The product $d_c(d\lambda/dE)_{E=E_C}$ is the increment in cruise cost resulting from a unit change in cruise energy. Condition (15) requires the optimum trajectory to be such that the sum of these two increments be zero for a given cruise distance d_c and cruise energy E_C .

DEPENDENCE OF OPTIMUM TRAJECTORIES ON RANGE

Equation (15), together with knowledge of the salient characteristics of the cruise cost λ and the Hamiltonian H , can be used to determine the structural dependence of the optimum trajectories on range.

Cruise cost at a cruise energy E_C and cruise speed V_C is computed from the relation

$$\lambda(E_C, V_C) = [P(T, E_C, V_C)] / (V_C + V_W) \quad \text{with constraints} \quad \begin{cases} T = D \\ L = W \end{cases} \quad (16)$$

where the denominator is the ground speed in the flightpath direction. Examination of the term containing λ in the relation for the performance function (9) shows that the value for λ should be as small as possible at each cruise energy to minimize the total cost J . Therefore, the cruise-speed dependence of λ is eliminated by minimizing the right side of Eq. (16) with respect to V_C :

$$\lambda(E_C) = \min_{V_C} P(T, E_C, V_C) / (V_C + V_W) \quad (17)$$

In this paper, λ and V_C are always assumed to be the optimum cruise cost and cruise speed, respectively, at a particular cruise energy E_C .

Except in high wind shear, the cruise cost as a function of cruise energy exhibits the roughly parabolic shape shown in Fig. 2. For subsonic transport aircraft, the minimum of the cruise cost with respect to energy occurs close to the maximum energy boundary. This characteristic of the cruise cost prevails for essentially all values of the performance function parameters c_f and c_t . The quantities defining the optimum cruise conditions are $E_{C_{opt}}$ and λ_{opt} . In Eq. (15), the derivative of the cruise cost function multiplies the cruise distance. Except under extreme wind shear conditions, the derivative is monotonic and crosses the zero axis at $E_C = E_{C_{opt}}$.

By distributing the minimization operator in Eq. (11) and substituting Eq. (13) in Eq. (11), H can be decomposed into climb and descent components as follows:

$$H[E, \lambda(E_C)] = I_{up} + I_{dn} \quad (18)$$

where

$$I_{up} = \min_{V_{up}} \left[\frac{P - (V_{up} + V_{W_{up}})}{E - \dot{E}_0} \right], \quad I_{dn} = \min_{V_{dn}} \left[\frac{P - (V_{dn} + V_{W_{dn}})}{E - \dot{E}_0} \right] \quad (19)$$

In the preceding section, the Hamiltonian, evaluated at $E = E_C$, was interpreted as the cost penalty to achieve a unit increase in cruise energy. Extensive numerical studies of Eq. (18) for several comprehensive models of subsonic turbofan aircraft show $H[E_C, \lambda(E_C)] \geq 0$ for $E_C < E_{C_{opt}}$. Moreover, the minimum cost penalty for increasing energy I_{up} is always positive and that for decreasing I_{dn} is negative, but the sum has never been found negative for models of currently used turbofans. While these characteristics have been established for several aircraft models, they are not intended to imply a generalization to all aircraft since no physical laws prevent H from being negative.

Consider first the case where $H[E_C, \lambda(E_C)] > 0$. Then Eq. (15) can be solved for the cruise distance d_C :

$$d_C = -H[E_C, \lambda(E_C)] / (d\lambda/dE)_{E=E_C} \quad (20)$$

Since $d\lambda/dE < 0$, but approaches zero as $E_C \rightarrow E_{C_{opt}}$, the cruise distance must increase without limit as $E_C \rightarrow E_{C_{opt}}$. Our numerical studies have shown that the value of H tends to decrease as E_C increases, but not enough to change this trend. Figure 3 shows the resulting family of trajectories, assuming $H > 0$ for all values of E_C . In this case, interestingly, nonzero cruise segments occur at short ranges and at energies below the optimum cruise energy $E_{C_{opt}}$. Optimum cruise is approached asymptotically at long range.

Consider next the case where $H[E_C, \lambda(E_C)] = 0$. Then $d_C = 0$, i.e., no cruise segment is present for $d\lambda/dE < 0$. However, Eq. (15) shows that d_C can be nonzero $d\lambda/dE = 0$. This implies that, for $H = 0$, cruise flight is optimum only at the optimum cruise energy $E_{C_{opt}}$. Figure 4 shows the family of trajectories for this case.

THRUST OPTIMIZATION FOR MINIMUM FUEL TRAJECTORIES

Evaluation of the Hamiltonian equation would be simplified if one of the two pairs of control variables, airspeed or thrust, could somehow be eliminated *a priori* from the minimization. Since the pair of throttle settings, π_{up} and π_{dn} , is thought to be near its limit, we shall look for conditions where extreme settings of the throttle are optimum. The remainder of this paper examines only the minimum fuel case $c_f = 1$ and $c_t = 0$, with winds set to zero to simplify the derivation. However, the results can be extended to the more general cost function.

For minimum fuel performance, the two terms in the Hamiltonian Eq. (19) become

$$I_{up} = \min_{\pi_{up}, V_{up}} K_{up}, \quad I_{dn} = \min_{\pi_{dn}, V_{dn}} K_{dn} \quad (21a)$$

where

$$K_{up} = \left[\frac{\dot{W}_f - \lambda V_{up}}{(T - D)V_{up}/W} \right]_{T(\pi_{up}) > D}; \quad K_{dn} = \left[\frac{\dot{W}_f - \lambda V_{dn}}{|T - D|V_{dn}/W} \right]_{T(\pi_{dn}) < D} \quad (21b)$$

An accurate model for thrust and fuel flow generally includes the functional dependencies, $T(\pi, V, h)$ and $\dot{W}_f(\pi, V, h)$. In addition, these functions must be corrected for nonstandard temperatures and bleed losses.

In previous work on aircraft trajectory optimization (Ref. 5), a simpler model for fuel flow and thrust was used:

$$\dot{W}_f = TS_{FC}(V, h); \quad T_{min}(V, h) < T < T_{max}(V, h) \quad (22)$$

The critical assumption in Eq. (22) is independence of the specific fuel consumption S_{FC} from thrust. The virtue of this model lies in the insight it yields into the minimum fuel problem. If Eq. (22) is substituted into Eqs. (21b), one obtains

$$K_{up} = \frac{S_{FC}W}{V_{up}} \left[\frac{T_{up} - (\lambda/S_{FC})V_{up}}{T_{up} - D} \right]_{T_{up} > D}; \quad K_{dn} = \frac{S_{FC}W}{V_{dn}} \left[\frac{T_{dn} - (\lambda/S_{FC})V_{dn}}{|T_{dn} - D|} \right]_{T_{dn} < D} \quad (23)$$

For any fixed values of V_{up} or V_{dn} , the operand functions for the minimization of K_{up} and K_{dn} are hyperbolas with poles at $T = D$. The numerator zero must be to the left of the pole on the thrust axis for energies less than cruise energy. Figure 5 is a typical plot of these functions. Clearly, maximum thrust minimizes K_{up} and idle thrust minimizes K_{dn} for any $E < E_C$, proving that the limiting values of thrust are optimum for this propulsion model throughout the climb and descent trajectories. This result also implies that the departure from the extreme thrust values found for the more general propulsion model is directly attributable to the nonlinear dependence of fuel flow on thrust. Conversely, the need for throttle setting optimization can be determined *a priori* from the fuel flow vs thrust dependence for a particular engine. Such data are found in the engine manufacturer's performance handbook.

EVALUATION OF HAMILTONIAN AT CRUISE

We have seen in a preceding section that the value of the Hamiltonian computed at cruise energy E_C determines the structure of the trajectories near cruise. Here we shall relate the existence of cruise below $E_{C_{opt}}$ to specific engine and aerodynamic model parameters by substituting truncated Taylor series expansions of fuel flow and drag as functions of airspeed and thrust into the expression for the Hamiltonian. The location of the minimum with respect to the controls as well as the value of H can then be determined as functions of the Taylor series coefficients at $E = E_C$.

How should one pick the point in the control space about which to make the expansion? Computational experience in Refs. 1 and 3 has shown that the minimum is in the neighborhood of the optimum cruise speed and throttle setting, corresponding to the given cruise energy. This suggests that the cruise controls should be picked for the expansion point.

The fuel flow and drag functions expanded to second order about the cruise controls $T = T_c, V = V_c$ are

$$\begin{aligned} \dot{W}_f = & T_c S_{FC} + (T_c S_{FC_T} + S_{FC}) \Delta T + T_c S_{FC_V} \Delta V + (1/2) (2S_{FC_T} + T_c S_{FC_{T^2}}) \Delta T^2 \\ & + (T_c S_{FC_{TV}} + S_{FC_V}) \Delta V \Delta T + (1/2) T_c S_{FC_{V^2}} \Delta V^2 + \text{higher-order terms} \end{aligned} \quad (24)$$

$$D = D(V_c, E_c) + D_V \Delta V + (1/2) D_{V^2} \Delta V^2 + \text{higher-order terms} \quad (25)$$

The subscripts to S_{FC} and D designate the partial derivatives with respect to the subscripted variable. Note that the expansion allows for a general fuel flow model in which specific fuel consumption can be thrust-dependent.

Before substituting Eqs. (24) and (25) into the expression for H , we observe that H is singular at cruise with $T = T_c$ and $V = V_c$, because both numerator and denominator are identically zero at that point. Figure 6 plots the loci of the numerator and denominator zeros of K_{up} and K_{dn} in the control space at $E = E_c$. It is proved in the Appendix that the locus of numerator zeros is tangent to the locus of denominator zeros at the optimum cruise controls. For $E < E_c$, the two loci have no points in common. The two loci can be tangent but cannot cross since, otherwise, controls would exist that would make the Hamiltonian infinitely negative, a result ruled out as physically meaningless.

Upon substituting Eqs. (24) and (25) into (21) using the tangency condition (A4) derived in the Appendix, the following expressions for K_{up} and K_{dn} at cruise energy are obtained:

$$\left. \begin{array}{l} K_{up} \\ \text{or} \\ K_{dn} \end{array} \right\} = \frac{W}{(V_c + \Delta V)} \left\{ \frac{\begin{array}{l} (T_c S_{FC_T} + S_{FC}) \Delta T - (D_V S_{FC} + T_c S_{FC_T} D_V) \Delta V \\ + (1/2) (2S_{FC_T} + T_c S_{FC_{T^2}}) \Delta T^2 + (T_c S_{FC_{TV}} + S_{FC_V}) \Delta V \Delta T \\ + (1/2) T_c S_{FC_{V^2}} \Delta V^2 \end{array}}{|\Delta T - D_V \Delta V - (1/2) D_{V^2} \Delta V^2|} \right\} \quad (26)$$

Terms above second order have been neglected since we are investigating a small neighborhood of the cruise point. Expression (26) represents K_{up} if the quantity under the absolute value sign is positive and K_{dn} if it is negative.

Since the cruise point at $\Delta T = 0$ and $\Delta V = 0$ gives the undefined value of 0/0 for Eq. (26), it is necessary to evaluate the limit as ΔT and ΔV approach zero. If the limit exists, it must be independent of the direction from which the cruise point is approached. To compute the limit and investigate the neighborhood of the cruise point, a polar coordinate system centered at the cruise point is used to define control perturbations. Let ΔR and β define control perturbations ΔT and ΔV as follows:

$$\Delta T = (D_V + \beta) \Delta V \quad (27)$$

$$\Delta V = \frac{\Delta R}{\sqrt{1 + (\beta + D_V)^2}}, \quad \Delta T = \frac{\Delta R (\beta + D_V)}{\sqrt{1 + (\beta + D_V)^2}} \quad (28)$$

The parameter β defines a direction relative to the reference direction of the line $\Delta T = D_V \Delta V$. The reference direction $\beta = 0$ is excluded from the control space since it is along the direction of the locus of $T = D$ at the cruise point.

After substituting Eqs. (28) into (26) and taking the limit of the resulting expressions as $\Delta R \rightarrow 0$, one obtains for any $\beta \neq 0$:

$$K_{up}]_{\text{limit}} = (W/V_c) (S_{FC} + T_c S_{FC_T}), \quad K_{dn}]_{\text{limit}} = (-W/V_c) (S_{FC} + T_c S_{FC_T}) \quad (29)$$

The limit is thus well defined since it is independent of the approach direction in each region. However, it remains to be shown that the limit value is in fact the minimum of Eq. (26) with respect to the perturbation controls. This question is investigated for two cases, one for which S_{FC} is independent, and the other, dependent on thrust.

Case (A): S_{FC} Independent of Thrust

Along the direction defined by $\Delta V = 0$, i.e., along the thrust direction, Eq. (23) can be used directly to determine the dependence of the functions on T_{up} and T_{dn} under the minimization operator. Since at $V = V_c$, $D(V_c, E_c) = T_c = (\lambda/S_{FC})V_c$, Eq. (23) reduces to

$$K_{up} = (W/V_c)S_{FC}, \quad K_{dn} = (W/V_c)S_{FC} \quad (30)$$

showing that, at the cruise speed V_c , these functions are independent of thrust. This result is not restricted to small perturbations relative to the cruise thrust. Along other directions, the truncated Taylor series form (Eq. (26)) must be used. After setting the zero all thrust-dependent derivatives and substituting Eqs. (28) into (26), the following expression is obtained.

$$K_{up} \text{ or } K_{dn} = \frac{WS_{FC}}{(V_c + \Delta V)} \left[\begin{array}{c} \pm 1 + \frac{(2S_{FCV}(|\beta| + D_V) + T_c S_{FCV_2})\Delta R}{2|\beta|S_{FC}\sqrt{1 + (\beta + D_V)^2}} \\ 1 - \frac{D_{V_2}\Delta R}{2|\beta|\sqrt{1 + (\beta + D_V)^2}} \end{array} \right] \quad (31)$$

where the positive sign applies to K_{up} and the negative sign to K_{dn} . The characteristics of these functions depend on the drag and specific fuel consumption derivatives. The drag derivatives D_V and D_{V_2} are both positive since the aircraft will certainly operate on the "front" side of the thrust-required curve. The dependence of S_{FC} on speed for a typical, currently in-service turbofan engine at cruise energies exhibits a slight upward curvature above Mach 0.4 (as shown in Fig. 7), implying that both S_{FCV} and S_{FCV_2} are positive in the range of interest between Mach 0.4 and 0.9. The slight curvature of S_{FC} indicates that a quadratic function can accurately model the Mach number dependence of S_{FC} in the Mach range of interest and not just in a small neighborhood of the expansion point. Also, at typical cruise conditions, one finds that $D_{V_2} > (2S_{FCV}D_V + T_c S_{FCV_2})$. Therefore, for any β , the denominator of Eq. (31) goes to zero before the numerator does as ΔR is increased from an initial value of zero. Moreover, the slope of the operand function with respect to ΔR increases as $\beta \rightarrow 0$. The effect of ΔV can be neglected since $V_c \gg \Delta V$.

These observations lead to the conclusion that the functions in Eq. (31) slope upward in all directions as ΔR increases, except in the direction parallel to the thrust axis, along which the slope is level. Figure 8 shows a family of plots of the operand functions as β varies over its range. The limiting values of these functions at the cruise point $(\pm W/V_c)S_{FC}$ are therefore also the global minimums, and the value of the Hamiltonian, which is the sum of the two components, is zero. At the cruise energy, furthermore, the optimum climb and descent speeds are equal to the optimum cruise speed. The optimum climb and descent thrusts at that point are arbitrary since the Hamiltonian is independent of them.

By applying these results to Eq. (29), it now follows that the structure of the optimum trajectories near cruise is given by the family of trajectories in Fig. 4. Specifically, no cruise segment occurs except at optimum cruise energy $E_{c,opt}$.

By combining results from this and the preceding section, the important result follows that, for the assumed engine model, optimum trajectories, corresponding optimum controls, and performance are not affected by constraining the thrust to extreme values in the climb and descent segments.

Case (B): S_{FC} Thrust-Dependent

A complete investigation of the neighborhood of the cruise point analogous to Case (A) requires estimates of the various thrust-dependent derivatives in Eq. (26). However, understanding of this case can be obtained by examining the functions in Eq. (26) only along the thrust direction, i.e., for $\Delta V = 0$. Under that assumption, Eq. (26) simplifies to:

$$\left. \begin{array}{c} K_{up} \\ \text{or} \\ K_{dn} \end{array} \right\} = (WS_{FC}/V_c) \left[\pm 1 + \left(T_c S_{FC_T} / S_{FC} \right) + (|\lambda T| / 2S_{FC}) \left(2S_{FC_T} + T_c S_{FC_{T^2}} \right) \right] \quad (32)$$

where the plus sign and $\Delta T > 0$ are chosen for K_{up} and the negative sign and $\Delta T < 0$ for K_{dn} .

This simplified approach focuses attention on the derivatives S_{FC_T} and $S_{FC_{T^2}}$, which are crucial for this case. The characteristics of these derivatives can be deduced from plots of S_{FC} vs thrust (Fig. 9). These plots, and those in Fig. 7, were derived from the operating instructions manual of a typical in-service turbofan (Ref. 6). Obviously, the assumption of a thrust-independent S_{FC} is grossly violated for this engine since, at low thrust values, the S_{FC} curves approach infinity; i.e., they become undefined. However, at typical climb or cruise thrusts, corresponding to the upper half of the thrust range, the variation in S_{FC} is only about 5%.

Fuel flow is also plotted in Fig. 9. The dashed line through the origin gives the best constant S_{FC} approximation to the fuel flow function. Comparison indicates an excellent match at high thrust, but an error of as much as 1200 lb/hr (550 kg/hr) at low thrust. For some applications the assumption of a constant S_{FC} could be adequate if fuel flow errors at very low or idle thrust settings can be tolerated.

For the upper two thirds of the thrust range, quadratic functions provide good fits to the S_{FC} curves. Therefore, one can use the second-order Taylor series expansion at the cruise point to estimate S_{FC} for fairly large deviations of thrust from cruise thrust.

The thrust in climb or cruise is typically larger than the thrust at which SFC is a minimum in Fig. 9. Both SFC_T and SFC_{T_2} will therefore be greater than zero and so will the coefficient of ΔT in Eq. (32). It follows that the slope of Eq. (32) as a function of Δt is greater than zero for K_{up} and less than zero for K_{dn} . In other words, along the thrust direction these functions have a strong minimum at the cruise point whereas in Case (A) they were level along this direction. Along other directions, the investigation of Case (A) has shown a positive slope. Thus, if thrust is an unconstrained control variable along with airspeed, so that the cruise point lies in the interior of the control region, then the optimum climb and descent thrusts and airspeeds will converge toward the optimum cruise thrust and airspeed as the climb and descent energies approach the cruise energy. It should be noted that this holds for all cruise energies, including those less than the optimum cruise energy, $E_{C_{opt}}$. Since the Hamiltonian is again zero at the cruise energy, it follows that the structure of the optimum trajectories as a function of range is identical to that of Case (A) and is illustrated by Fig. 4. Computer calculations for this case in Ref. 1, using a similar engine model, showed that the thrust is either maximum or idle for about three-fourths of the energy range between initial and cruise energies and then departs from the extremum values so as to converge smoothly to the value at cruise as cruise energy is approached.

Consider now the case where thrust is constrained to some maximum in climb and is idle in descent. In that case, the minimum at the cruise point is not accessible since it does not lie in the region of permissible controls. Also, unlike Case (A), the thrust dependence of K_{up} and K_{dn} in Eq. (23) does not disappear along the thrust direction at $V = V_C$. Therefore, it is unlikely that at the minimum the sum of the two terms will be zero. The Hamiltonian is, in fact, greater than zero at any cruise energy. In order to show this, note in Fig. 9 that, as thrust decreases, SFC increases without bound. It follows that I_{dn} will be less negative than it would be if SFC were thrust-independent and therefore will be insufficient to cancel I_{up} at cruise energy, resulting in a positive value for the Hamiltonian. This was shown earlier to give rise to nonzero cruise segments below the optimum cruise energy. Thus, the structure of the optimum trajectories for the constrained thrust case is given by the family of trajectories in Fig. 3.

COMPUTER IMPLEMENTATION

(a) Algorithm Description

The climb and descent profiles are generated by integrating the state equation (10) from the initial energy E_i to the maximum or cruise energy E_C . For this purpose, Eq. (10) is separated into its climb and descent components, which are then modified to include the effect of nonzero flightpath angles as follows:

$$\left. \begin{aligned} dx_{up}/dE &= \left(V_{up} + V_{w_{up}} \right) \cos \gamma_{up} / \dot{E} \\ dx_{dn}/dE &= \left(V_{dn} + V_{w_{dn}} \right) \cos \gamma_{dn} / |\dot{E}| \end{aligned} \right\} \quad (33)$$

Flightpath angles are not defined within the reduced dynamics of the energy state model. Nevertheless, during the integration of the trajectory, the flightpath angles for climb and descent, γ_{up} and γ_{dn} , can be computed by using increments of altitude and distance from two successive energy points. The use of these computed flightpath angles in Eq. (33) slightly increases the accuracy of the climb and descent distance integrations.

At each energy in the integration the optimum airspeeds and thrust settings are obtained as the values that minimize the two components of the Hamiltonian in Eq. (19). The minimization of the Hamiltonian is carried out by the Fibonacci search technique (Ref. 7). It has the advantage of using the least number of function evaluations of all known search techniques to locate the minimum with prescribed accuracy and also is well suited to handle tabular data. Fibonacci search is basically a one-variable minimization procedure. It is adapted here to two variables by applying the technique to one variable at a time while holding the other variable fixed. Convergence to the minimum is achieved by cycling between the two variable several times. Prior to a search over a given control variable, the limits of the regions for K_{up} and K_{dn} , which consist of the $T = D$ locus and the dashed line with shaded border in Fig. 6, are computed to keep the search interval as small as possible.

As previously explained, the choice of λ in the Hamiltonian determines the range of the trajectory, but the exact functional dependence between λ and range cannot be determined explicitly for the various weights, wind profiles, and other parameter changes encountered in real time operation. An iterative procedure is therefore used and is explained in part (b) of this section.

An important part of the algorithm involves accounting for the weight change due to fuel burn. The effect on the optimum trajectory of the change in weight was not included explicitly in the theory for reasons previously stated. Two methods are used to correct the optimum trajectories for the weight change. The first merely integrates the fuel flow and updates the weight in the calculation of \dot{E} during climb and descent. This ensures that updated values of aircraft weight are used in the integration of Eqs. (33) to generate the climb and descent trajectories.

The second method modifies the value of λ used in the Hamiltonian. This modification involves using the estimated weight of the aircraft at the end of climb, i.e., at energy E_C , to compute the value of λ rather than the weight at takeoff. It is important to use the weight at E_C rather than the weight at some other energy, to compute λ because the sensitivity of the optimum controls to changes in λ increases as the aircraft energy approaches E_C . The fuel consumption for the entire climb trajectory, F_{up} , is estimated at the start of climb from the empirical relation:

$$F_{up} = K_1 (E_C - E_i) W_1 / W_{ref} \quad (34)$$

where K_1 is an aircraft-dependent constant and W_{ref} is a typical initial climb weight. This relation estimates the climb fuel weight to about 10% accuracy, which is adequate for this purpose. Similarly, the weight at the end of cruise, if a cruise segment is present, is used to compute λ for the descent optimization. The cruise fuel consumption, F_C , is determined from the relation:

$$F_c = \bar{W} d_c / \bar{V}_g \quad (35)$$

where \bar{W} is the average fuel flow rate and \bar{V}_g the average ground speed during cruise. The calculation of the average quantities is described in Ref. 8.

The computer implementation includes both the free and constrained thrust cases. For the constrained thrust case, the cruise distance is computed from Eq. (20). However, because $d\lambda/dE \rightarrow 0$ as $E_c \rightarrow E_{c\text{opt}}$, there is a practical limit to the use of Eq. (20), determined by the numerical accuracy of computing $d\lambda/dE$ for E_c in the neighborhood of $E_{c\text{opt}}$. A practical limit for E_c is that value for which $\lambda = 1.01\lambda_{\text{opt}}$. The total range of the trajectory obtained for this value of λ is referred to as d_{max} . All trajectories requiring longer ranges than d_{max} are assumed to cruise at $E_{c\text{opt}}$ and contain cruise segments of length $d_c = d_f - d_{\text{up}} - d_{\text{dn}}$, where d_{up} and d_{dn} are computed for $\lambda = 1.01\lambda_{\text{opt}}$. In the free thrust case, numerical difficulties can arise in minimizing Eq. (19) as $E_c \rightarrow E_{c\text{opt}}$. The value of $1.01\lambda_{\text{opt}}$ has also been found to serve as a practical criterion for computing the longest range without a cruise segment at $E_{c\text{opt}}$.

(b) Simplified Flow Chart

A computer program of the algorithm has been implemented in FORTRAN IV and is described in detail in Ref. 8. The program contains one main program and 38 subroutines. There are approximately 2400 FORTRAN instructions in the program. In this paper, the organization and major elements of the program are outlined with reference to the simplified flow chart shown in Fig. 10.

After reading aircraft lift, drag, and propulsion data, performance function parameters, and wind and temperature data, the optimum cruise speeds and costs and $d\lambda/dE$ are computed for a range of cruise energies and cruise weights using Eq. (17). Cruise weight is incremented in steps of about 5% of average gross weight. Cruise energy is incremented in 1000-ft steps from 5000 energy-feet to the maximum or ceiling energy. The results are stored in what is referred to as cruise performance tables. At each weight the cruise performance vs energy will show a dependence as in Fig. 2. The tables also contain a variety of other quantities such as fuel flow, thrust setting, Mach number, etc., that are needed to fly the trajectories. In addition, at each weight the optimum cruise energy $E_{c\text{opt}}$ and the optimum cruise cost λ_{opt} are computed and stored in separate tables. Since these tables contain extensive amounts of data and are time consuming to compute, they can be permanently saved on a mass storage medium.

After reading in additional input data, two optimum trajectories referred to as the minimum and maximum range trajectories are synthesized. The minimum range trajectory is obtained by choosing the largest value of λ (called λ_{max}) stored in the cruise performance tables at the gross weight of interest. The maximum range trajectory is obtained by choosing the smallest λ , namely, $1.01\lambda_{\text{opt}}$, as explained in part (2). Values of λ at given weights are computed by interpolating between data points in the cruise tables. The corresponding ranges d_{max} and d_{min} can now be compared with d_f to decide on the type of trajectory required. If $d_f > d_{\text{max}}$, the trajectory will always contain a segment of cruise at optimum cruise energy $E_{c\text{opt}}$. No iteration on λ is required in this case since the specified range d_f is obtained by choosing a cruise segment of length $d_c = d_f - d_{\text{up}} - d_{\text{dn}}$. The optimum altitude and Mach number in the cruise segment are updated every 100 n. mi. to account for the loss of weight due to fuel burn. This is the well-known climb-cruise technique.

If $d_{\text{min}} \leq d_f \leq d_{\text{max}}$, the maximum energy will fall below $E_{c\text{opt}}$ and iteration with respect to λ is required. Here the approximately known inverse relationship between λ and d_f , illustrated in Fig. 11 for a Boeing 727-100, is incorporated in heuristic to minimize the iteration. Thus, the first estimate of λ is computed from

$$\lambda = (A/d_f) + B \quad (36)$$

The constants A and B are chosen to yield λ_{max} and $1.01\lambda_{\text{opt}}$ when d_f is set to d_{min} and d_{max} , respectively. Then the trajectory is synthesized to yield the actual range d . If d is not sufficiently close to d_f , constants A and B are updated by using a pair of ranges and the corresponding pair of λ 's computed in preceding syntheses. The ranges included in this pair are selected so they enclose the desired range and lie closest to it. A new estimate of λ is now computed and the synthesis is repeated. Typically, after two iterations the actual range will have converged to within 5 n. mi. of the specific range and iteration is terminated.

The optimum climb and descent trajectory is specified by storing the range, time, fuel, Mach number, thrust setting, and altitude as a function of energy height in 500 energy-feet increments.

The computer implementation of the algorithm described here was designed for off-line use primarily as a benchmark for evaluating various non- or suboptimum trajectories. Various simplifications are possible to reduce the computer complexity for onboard implementation. For example, the iteration loop to achieve a specified range need not be mechanized. This approach was used in a piloted simulation of the algorithm (Ref. 9). In that study, the pilot played an active part in closing the loop on range.

RESULTS

The computer-implemented version of this algorithm was used to compute and to study the characteristics of several types of optimum trajectories. This section presents a summary of the results. A more complete discussion, including the effects of winds, nonstandard temperatures, and gross weight changes, can be found in Ref. 8. The aerodynamic and propulsion models used in these calculations are representatives of the Boeing 727-100 aircraft equipped with JT8D-7A engines. The time and fuel cost parameters in the performance function Eq. (7) were chosen to be \$500/hr and 6.23 cents/lb, respectively. Inflation has increased these

parameters since their selection in early 1978. However, because the trajectories actually depend only on the ratio of the parameters, the trajectories continue to be useful, especially for comparing minimum fuel and DOC cases.

Figure 10(a) shows the altitude vs range for 100, 200, and 1000 n. mi. range minimum DOC trajectories. The aircraft takeoff weight for these trajectories is 150,000 lb. Winds are assumed to be zero and atmospheric conditions are for a standard day. For the 200-n. mi. range, both the constrained thrust (solid line) and the free thrust (dashed line) trajectories are shown. Also, for the 200-n.mi. range, Fig. 10(b) shows the corresponding altitude vs airspeed profiles.

Below 10,000 ft altitude, all trajectories are essentially identical in both climb and descent profiles. At 10,000 ft both the climb and descent profiles are interrupted by short segments of almost level flight. These are the result of the 250 KIAS speed limit imposed on the trajectory below 10,000 ft by U.S. air traffic control rules. Thus, when the aircraft reaches 10,000 ft in climb, the aircraft accelerates to the unconstrained optimum climb speed (see Fig. 12(b)). Similarly, a deceleration occurs in descent at this altitude.

The constrained thrust trajectories for the 100- and 200-n. mi. ranges contain short cruise segments below the optimum cruise altitude of 31,000 ft. Optimal cruise altitude is used for ranges longer than about 250 n. mi. For the relatively long range flight of 1000 n. mi., the optimum cruise altitude increases at a rate of approximately 2.5 ft/n. mi. of cruise distance due to fuel burnoff.

The free thrust trajectory for the 200-n. mi. range does not contain a cruise segment. However, the difference between the constrained and free thrust profiles is slight and is noticeable only above 25,000 ft. Below this altitude the optimum thrust values are identical for both types, namely, maximum in climb and idle in descent. Above this altitude the thrust reduces gradually in climb for the free thrust case; it continues to reduce during the initial descent and reaches idle thrust at 20,000 ft. Differences in the speed profiles also are noticeable only above about 24,000 ft. As expected, the difference in operating costs between the two types of trajectories is slight, amounting to an additional \$8 saving for the 200-n. mi. free thrust trajectory.

Minimum fuel trajectories, obtained by setting the time cost parameter in the performance function to zero, are shown in Fig. 13. In comparison with the minimum DOC trajectories, the minimum fuel trajectories for a given range climb to a higher altitude and use a substantially lower airspeed above 10,000 ft. Also, above 10,000 ft the flight-path angle of the minimum fuel trajectories is steeper in climb and shallower in descent. As before, differences in the altitude profiles between the constrained and unconstrained thrust trajectories are apparent only near the top of the climb. The penalty in fuel consumption due to the 250 KIAS speed restriction below 10,000 ft was found to be 66 lb. This penalty increases with an increase in gross weight but is essentially independent of range.

Table 1 summarizes several important numerical values for the trajectories calculated. Comparison of tabulated figures shows that the fuel saved by flying the minimum fuel instead of the minimum DOC trajectory is about 1,000 lb for the 1,000-n. mi. range, or about 1 lb/n. mi. However, the associated time and cost penalties are 16 min and \$80, respectively. If the price of fuel continues to increase more rapidly than the cost of time, as was the case in 1979, the optimum DOC and fuel trajectories will converge, resulting in smaller fuel and cost differences between them.

For the 200-n. mi.-range minimum fuel trajectories, the differences in fuel consumption between the constrained and free thrust cases is 23 lb. This relatively small difference would seem to justify the use of the simpler-to-mechanize and computationally faster constrained thrust mode, especially in an onboard computer implementation. However, as was pointed out in the preceding theory sections, this difference is aircraft- and propulsion-model dependent and therefore should be checked whenever there is a change in model characteristics.

CONCLUSIONS

The approach presented here has established the structure of optimum trajectories for airline operations and has yielded an efficient computer algorithm for calculating them. The algorithm can be incorporated in an airline flight planning system or can be used to determine the performance penalty of simplified onboard algorithms. The latter application is important at this time in view of the current effort by industry to develop onboard performance management systems.

Two pairs of opposing assumptions, constrained vs free thrust and dependence vs independence of specific fuel consumption on thrust, played pivotal roles in determining the characteristics of the optimum trajectories. If the assumption of specific fuel consumption independent of thrust is justified, constrained thrust trajectories are identical in structure and performance to free thrust trajectories. However, when the realistic dependence of specific fuel consumption on thrust is taken into account, there will be a difference, though slight for the example studied, in both performance and structure between constrained and free thrust cases. The actual differences in performance depend on the propulsion and aerodynamic models as well as other factors and must be determined for each aircraft model by computer calculation.

APPENDIX

It is to be proved that the loci of $\dot{W}_f - \dot{V} = 0$ and $T - D = 0$ are tangent at the cruise point, assuming that the cruise point at $T = T_C$, $V = V_C$ is a minimum of the cruise cost \dot{W}_f/V along the locus $T - D = 0$. This is equivalent to proving that the cruise point lies on both loci and that the slopes of the loci are identical at that point.

That the cruise point satisfies $\dot{W}_f - \lambda V = 0$ follows from the sequence of relations below:

$$\left. \begin{aligned} (\dot{W}_f - \lambda V) \\ T=T_C \\ V=V_C \end{aligned} \right\} = V \left. \begin{aligned} \left(\frac{\dot{W}_f}{V} - \lambda \right) \\ T=T_C \\ V=V_C \end{aligned} \right\} = V_C \left\{ \left. \begin{aligned} \left(\frac{\dot{W}_f}{V} \right) \\ T=T_C \\ V=V_C \end{aligned} \right\} - \lambda \right\} = V_C (\lambda - \lambda) = 0$$

To prove that the slopes are identical, compute the gradient of $\dot{W}_f - \lambda V$:

$$\nabla(\dot{W}_f - \lambda V) = \hat{i} \left[TS_{FCV} - \frac{TS_{FC}}{V} \right]_{\substack{T=T_C \\ V=V_C}} + \hat{j} \left[TS_{FCT} + S_{FC} \right]_{\substack{T=T_C \\ V=V_C}} \quad (A1)$$

The perpendicular unit vectors \hat{i} and \hat{j} point in the speed and thrust directions, respectively. Now write λ as a function of the perturbation ΔV :

$$\lambda = [(T_C + D_V \Delta V) S_{FC}(T_C + D_V \Delta V, V_C + \Delta V)] / (V_C + \Delta V) \quad (A2)$$

Since, by assumption, λ has a minimum at $V = V_C$, set the derivative of λ with respect to ΔV equal to zero. This yields the following relation:

$$\lambda = D_V S_{FC} + T_C \left(S_{FCT} D_V + S_{FCV} \right) = T_C S_{FC} / V_C \quad (A3)$$

Next compute the gradient of $(T - D)(V/W)$ at the cruise point:

$$\left. \begin{aligned} (T - D)(V/W) \\ T=T_C \\ V=V_C \end{aligned} \right\} = (V_C/W) [\hat{i}(-D_V) + \hat{j}] \quad (A4)$$

The slope of Eq. (A1) relative to the \hat{i} direction is given by

$$\text{Slope} = \frac{(T_C S_{FCV} + S_{FC})}{[T_C S_{FCV} - (T_C S_{FC} / V_C)]} \quad (A5)$$

After substituting Eq. (A3) in place of $T_C S_{FC} / V_C$ in Eq. (A5), the slope simplifies to $-1/D_V$, which is identical to the slope of Eq. (A4).

REFERENCES

1. Erzberger, H., McLean, J. D., Barman, J. F.: Fixed-Range Optimum Trajectories for Short Haul Aircraft. NASA TN D-8115, Dec. 1975.
2. Speyer, J. L.: Nonoptimality of the Steady-State Cruise for Aircraft. AIAA J., Vol. 14, Nov. 1976, pp. 1604-1610.
3. Barman, J. F., and Erzberger, H.: Fixed Range Optimum Trajectories for Short-Haul Aircraft. J. Aircraft, Vol. 13, Oct. 1976, pp. 748-754.
4. Bryson, A. E., Jr., and Ho, Y-C.: Applied Optimal Control. Blaisdell, Waltham, Mass., 1969, ch. 2.
5. Schultz, R. L., and Zagalsky, N. R.: Aircraft Performance Optimization. J. Aircraft, Vol. 9, Feb. 1972, pp. 108-114.
6. Specific Operating Instructions, JT8D-7 Commercial Turbofan Engines, Pratt and Whitney Aircraft, East Hartford, Connecticut, Jan. 1969.
7. Cooper, L., and Steinberg, D.: Introduction to Methods of Optimization. W. B. Saunders Co., 1970, pp. 147-151.
8. Lee, Homer Q., and Erzberger, Heinz: Algorithm for Fixed Range Optimal Trajectories. NASA TP 1565, Jan. 1980.
9. Bochem, J. H., and Mossman, D.C.: Simulator Evaluation of Optimal Thrust Management/Fuel Conservation Strategies for Airbus Aircraft on Short Haul Routes. Final Report, prepared by Sperry Flight Systems, Phoenix, Ariz. NASA Contractor Report NAS 2-9174, May 1977 - April 1978.

TABLE 1. CHARACTERISTICS OF EXAMPLE OPTIMUM TRAJECTORIES

Thrust mode	Range, n. mi.	Time, hr/min/sec	Cost, \$/n. mi.	Fuel, lb/n. mi.	Cruise Altitude/ft	Climb Distance/n. mi.	Descent Distance/n. mi.
Minimum Direct Operating Cost Trajectories (150,000 lb Takeoff weight)							
CT ¹	100	20:06	3.58	30.405	14899	43.15	52.66
CT	200	33:02	3.00	25.774	26970	101.42	77.85
FT ²	200	33:00	2.98	25.331	27827	116.00	84.00
CT	1000	2:13:07	2.28	18.779	30819	135.76	85.38
Minimum Fuel Trajectories (150,000 lb Takeoff weight)							
CT	100	21:26	3.60	29.247	17531	37.73	54.12
CT	200	37:03	3.07	24.38	27226	80.06	83.21
FT	200	37:06	3.06	24.268	28011	101.93	98.07
CT	1000	2:29:14	2.36	17.763	33185	121.07	103.51

¹CT = Constrained thrust.

²FT = Free thrust.

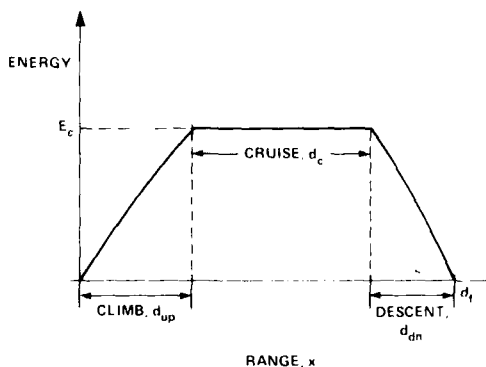


Fig. 1. Assumed structure of optimum trajectories.

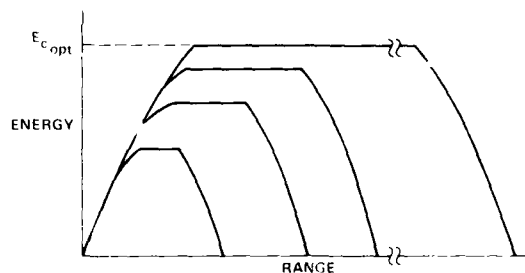


Fig. 3. Energy vs. range, $H = 0$ at E_c .

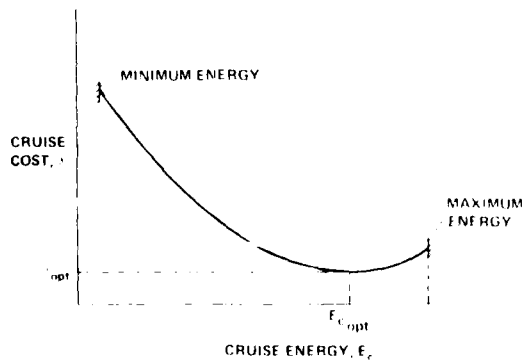


Fig. 2. Cruise cost function.

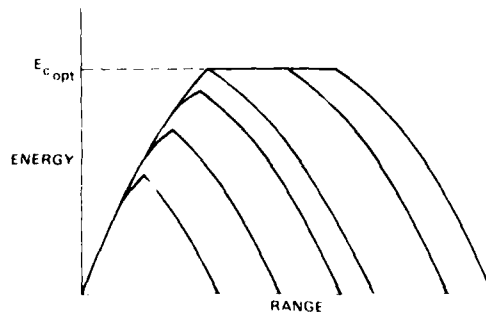


Fig. 4. Energy vs. range, $H = 0$ at E_c .

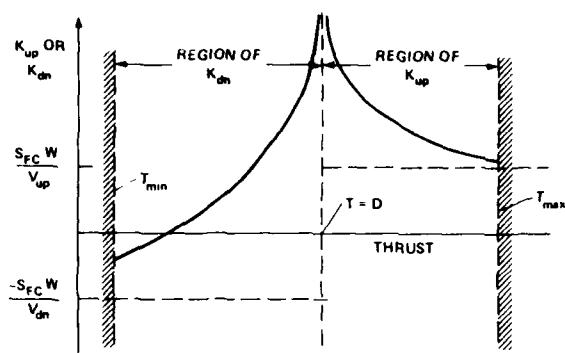


Fig. 5. Illustrating dependence of K_{up} and K_{dn} on thrust.

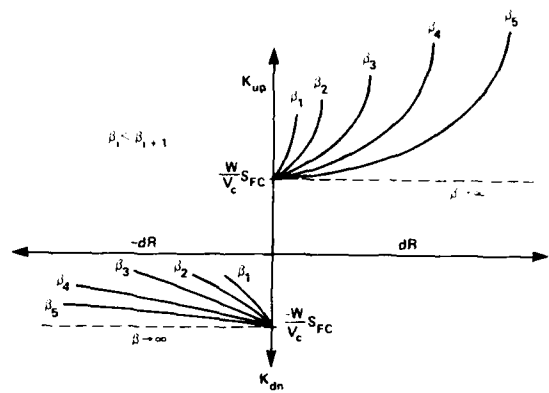


Fig. 8. Dependence of operand function on dR and β at cruise energy E_C .

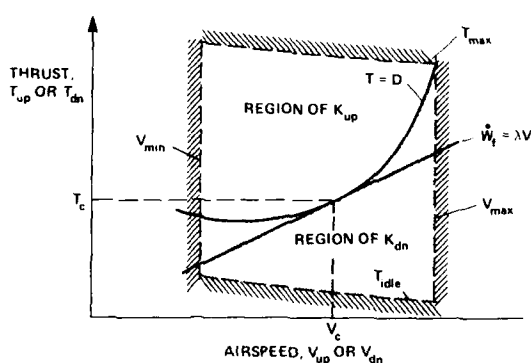


Fig. 6. Loci of $T = D$ and $\dot{W}_f = \lambda V$ in control space at $E = E_C$.

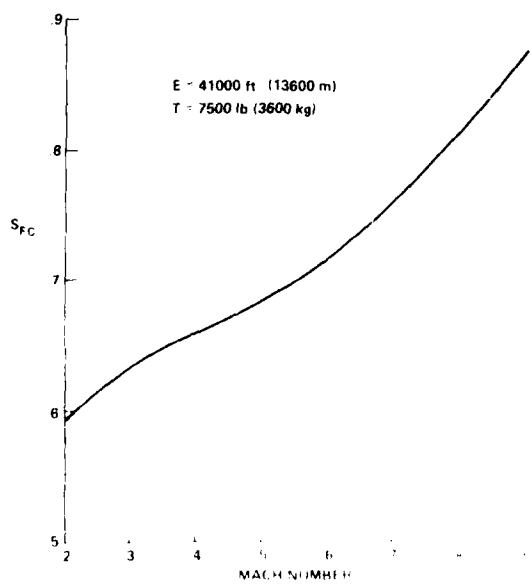
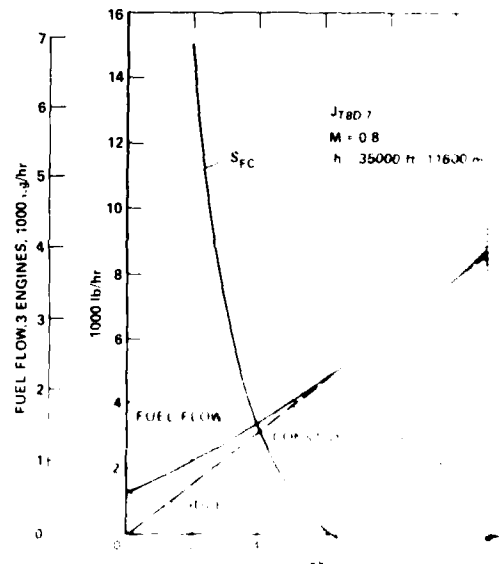


Fig. 7. S_{FC} dependence on Mach number.



AD-A106 937

ADVISORY GROUP FOR AEROSPACE RESEARCH AND DEVELOPMENT--ETC F/G 1/4
THEORY AND APPLICATIONS OF OPTIMAL CONTROL IN AEROSPACE SYSTEMS--ETC(U)
JUL 81 P KANT

UNCLASSIFIED

AGARD-A6-251

NL

3x3
21
20-247

END
DATE
FILMED
12-81
DTIC

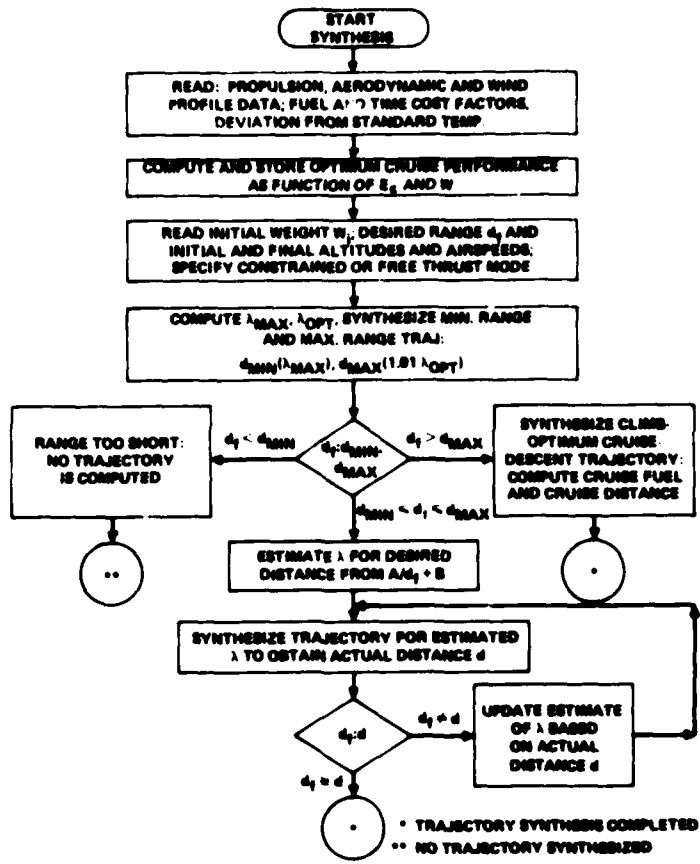


Fig. 10. Flow chart for computer algorithm.

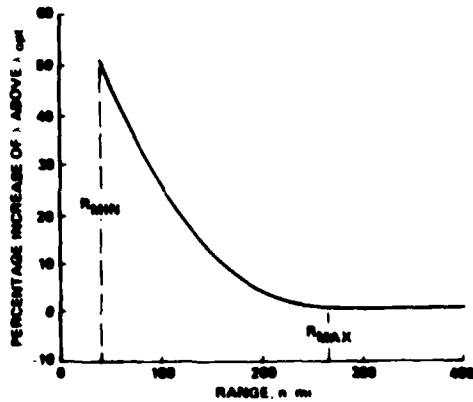
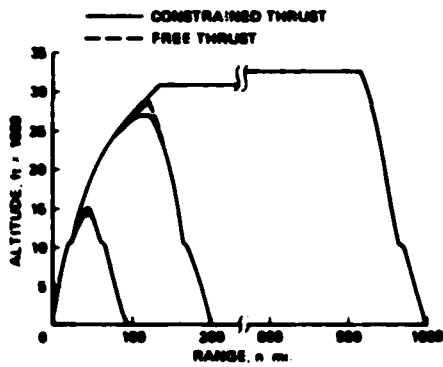
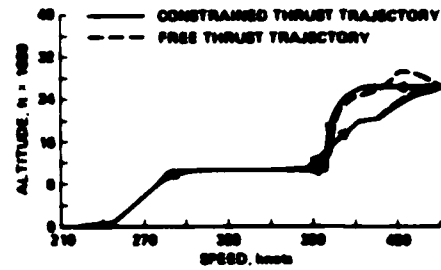


Fig. 11. Typical cruise cost vs range relationship.

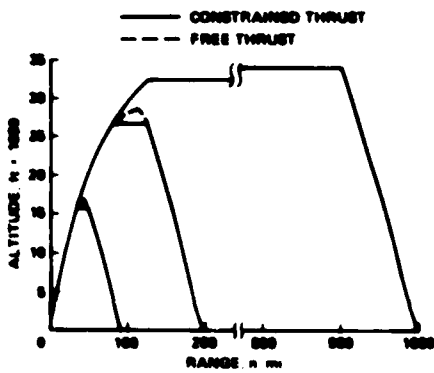


(a) Altitude-range profiles.

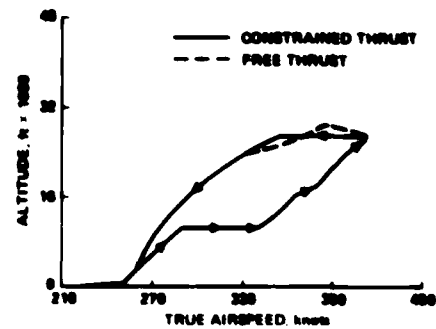


(b) Airspeed-altitude profiles for 200 n.m. range.

Fig. 12. Minimum DOC trajectories.



(a) Altitude-range profiles.



(b) Airspeed-altitude profiles for 200 n.m. range.

Fig. 13. Minimum fuel trajectories.

APPLICATION OF NONLINEAR SYSTEMS INVERSES TO AUTOMATIC FLIGHT CONTROL DESIGN -
SYSTEM CONCEPTS AND FLIGHT EVALUATIONS

by
George Meyer and Luigi Cicolani
Ames Research Center, NASA
Moffett Field, California, U.S.A. 94035

SUMMARY

A practical method for the design of automatic flight control systems for aircraft with complex characteristics and operational requirements, such as the powered lift STOL and V/STOL configurations, is presented. The method is effective for a large class of dynamic systems requiring multi-axis control which have highly coupled nonlinearities, redundant controls, and complex multidimensional operational envelopes. It exploits the concept of inverse dynamic systems, and an algorithm for the construction of inverses is given. A hierarchical structure for the total control logic with inverses is presented. The method is illustrated with an application to the Augmentor Wing Jet STOL Research Aircraft equipped with a digital flight control system. Results of flight evaluation of the control concept on this aircraft are presented.

SYMBOLS

A_{ba}	transformation of vectors from frame a to frame b	$\bar{r}, \bar{r}_c, \delta \bar{r}$	actual, commanded, error position vectors
$\bar{a}, \bar{a}_c, \delta \bar{a}_c$	actual, commanded, corrective, and total acceleration vectors	S_w	wing area
\bar{b}	aircraft specific force model error compensation	T_H, T_C	hot, cold thrusts of AMJSRA propulsion system
C_L, C_D, C_{Y_B}	aerodynamic and thrust coefficients	u_a, u_p	control vectors for aircraft moments and power/configuration system
C_{N_B}, C_{N_r}		$\bar{v}, \bar{v}_c, \delta \bar{v}$	actual, commanded, error velocity vectors
C_{L_q}, C_J		V_a, V_e	true, equivalent airspeeds
\bar{f}_c	commanded applied specific force	α	angle of attack
f_z	aircraft specific force model	β	sideslip
K_r, K_v, K	control law gains	γ, γ_a	inertial and air mass-referenced flight-path angles
L_x, L_y, L_z	single axis rotation transformations	δ	stagnation pressure ratio
M	Mach number	δ_f	flap angle
m	aircraft mass or reference trajectory leg number	$\bar{\epsilon}$	acceleration error vector
N_H	engine power, % reference RPM	θ	pitch angle or stagnation temperature ratio
P_1, P_2	power/configuration position, rate states	ν	engine exhaust nozzle angle
Q	dynamic pressure	ϕ, ϕ_v	roll angles about \bar{i}_b, \bar{i}_p

INTRODUCTION

The aerodynamic characteristics and operational requirements of modern aircraft present the control system designer with problems that are increasingly difficult to solve with the standard control system design methods. For example, these aircraft can have force and moment generation processes with strong, multi-axis, highly coupled nonlinearities. In addition, anticipated operational capabilities require that these aircraft be precisely controlled over a substantial portion of the flight envelope that encompasses the range of nonlinear aerodynamics. Consequently, the nonlinearity is an essential part of the control design problem. This paper is concerned with the method of attacking such problems. A method for the design of an automatic control system for such aircraft is developed in the first part of the paper, and an application to a powered lift STOL aircraft is presented in the second part; the latter part includes results obtained from flight evaluation of the automatic control system over the aircraft's operational flight envelope.

The automatic control arrangement for which this new design method will be described is shown schematically in Fig. 1. The flightpath that the aircraft will be commanded to fly is defined by the path-command generator labeled ATC. Air traffic control is a primary example of a system that prescribes flightpaths to be flown either automatically or manually. The control system (CS) transforms the desired path r^* and aircraft state x into an appropriate control u that forces the aircraft (AC) to fly a flightpath r that approaches the commanded path, even in the presence of disturbances w . The disturbances will be assumed to be generated by a deterministic environment EN. Thus, we are concerned with a deterministic servo problem. The input r^* is at least a three-dimensional function of time; the state x is at least 12-dimensional (position, velocity, attitude, and angular velocity in three axes), and the equation of motion of the aircraft,

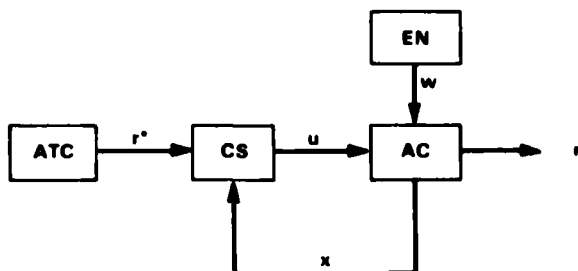


Fig. 1 Model of the fully automatic mode.

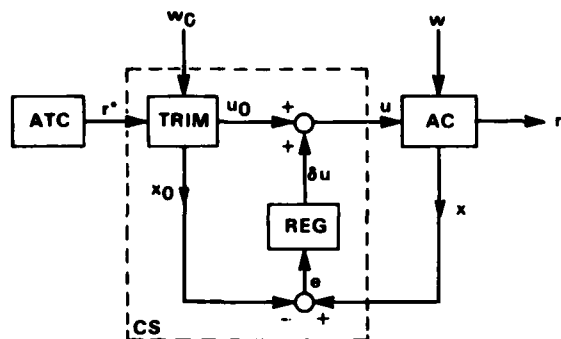


Fig. 2 Conventional control system configuration.

$$\left. \begin{aligned} \dot{x} &= f(x, u, w) \\ r &= h(x) \end{aligned} \right\} \quad (1)$$

can be strongly nonlinear and highly coupled.

CONTROL SYSTEM DESIGN METHODS

Current Design Practice

The general approach to control design for such a nonlinear system is to separate the control system synthesis into two parts, as shown in Fig. 2. The total control u is considered to be composed of the trim control u_0 and the perturbation control δu . The TRIM logic defines the nominal control positions required for the aircraft to fly the reference flightpath r^* . In other words, a solution (x_0, u_0) is computed to the equation of motion, assuming a disturbance w_0 , so that the output r will coincide with the input r^* :

$$\left. \begin{aligned} \dot{x}_0 &= f(x_0, u_0, w_0) \\ r^* &= h(x_0) \end{aligned} \right\} \quad (2)$$

Ideally, if the model of the aircraft were exact and there were no unaccounted disturbances, the trim control u_0 would make the aircraft follow the specified flightpath. However, practical considerations dictate that a regulator REG be synthesized to correct for various uncertainties by means of feedback, such as illustrated in Eq. (3).

$$\delta u = k(e, x_0) \quad (3)$$

Once the reference operating condition (x_0, u_0) has been defined, a perturbation analysis is undertaken to define the regulator. The equations of motion (1) are expanded about the trim condition: $x = x_0 + \delta x$, $u = u_0 + \delta u$, $w = w_0 + \delta w$, and only the linear terms are retained,

$$\left. \begin{aligned} \delta \dot{x} &= \left. \frac{\partial f}{\partial x} \right|_0 \delta x + \left. \frac{\partial f}{\partial u} \right|_0 \delta u + \left. \frac{\partial f}{\partial w} \right|_0 \delta w \\ \delta r &= \left. \frac{\partial h}{\partial x} \right|_0 \delta x \end{aligned} \right\} \quad (4)$$

The designer is fortunate if the partial derivatives in Eq. (4) can be considered to be invariant, because the well-developed theory of linear systems can then be brought to bear on the design problem.

Two approaches are commonly used in cases when the matrices in Eq. (4) are not constant. One approach is to try to design the control system to be, in some sense, insensitive to parameter variations. Primary emphasis is placed on the regulator performance near the design point. Reference 1 gives several effective techniques for synthesizing a constant gain feedback such that the closed-loop system behavior is acceptable for all values of the parameters within specified limits.

Adaptive control provides the second approach. Here the intent is to solve problems in which the variations in the plant parameters are not known a priori; of course, the method is also applicable in cases in which the variations, although known a priori, are intentionally ignored to simplify the problem. Effective techniques are given in Ref. 2 for the synthesis of adaptation schemes that adjust the open-loop and closed-loop gains so as to adapt to variations in the perturbation model of the controlled process.

Both of these approaches can be expected to yield good control near the target. One meets severe difficulties, however, when the nonlinearities of the process are strong and the required operating range is wide. It may then be necessary to select a large set of operating points to adequately cover the entire operational flight envelope, design a perturbation servo for each condition, and design a scheduling algorithm that will tie all these individual designs into a total system. Since the resulting complexity would make the task of validating the overall system performance difficult for the aircraft configurations being considered in the present paper, we took a fundamentally different approach.

Concept Using Nonlinear System Inverses

Consider again the usual approach to control design shown in Fig. 2. Conceptually, the source of the difficulty for the design is the complexity of the feedback control algorithm. However, the trim logic represents an inverse of the aircraft response to control inputs, and the combined relationship of the input to the trim logic to the aircraft's response is, ideally, an identity. Therefore, the relationship is used to advantage by closing the feedback loop in front of the trim logic, as shown in Fig. 3. As a result, because of the invariance of the feedback control response ($\delta r_0 \rightarrow e$), the design of the regulator becomes much simpler; however, the design of the trim logic becomes the central issue. Applications of this concept

have shown that the total complexity of the control system can be reduced. Furthermore, a better balance between the open-loop (a priori) and closed-loop (a posteriori) control is a consequence of the method.

The approach is illustrated with the help of the following example, after which a formal description is given.

EXAMPLE APPLICATION

Consider the process to be controlled as that shown in Fig. 4. The state space is four-dimensional but two-axis, so that the state $x = (x_1, x_2)$ and both x_1 and x_2 are two-dimensional. The output $r = x_1$ is the position vector in two dimensions. The velocity $\dot{r} = \dot{x}_1$ is generated by x_2 through two-dimensional rotation, given by the matrix E whose angle a is a function of the distance $\|x_1\|$ from the position origin. The control u is two-axis, and the state equation is

$$\dot{x} = \begin{pmatrix} 0 & E(a) \\ 0 & 0 \end{pmatrix} x + \begin{pmatrix} 0 \\ I \end{pmatrix} u + \begin{pmatrix} 0 \\ I \end{pmatrix} w \quad (5)$$

where 0 and I are 2×2 zero and identity matrices, respectively. It may be noted that the nonlinearity E is between the integrators, and that the sign of $\partial \dot{x}_1 / \partial x_2 = E$ may change without passing through zero.

Let the reference path be given by the function $r^*(t)$ with velocity $\dot{r}^*(t)$ and acceleration $\ddot{r}^*(t)$. The trim condition is,

$$\begin{aligned} x_{10} &= r^* \\ a_0 &= a(\|r^*\|) \\ x_{20} &= E^T(a_0) \dot{r}^* \\ u_0 &= E^T(a_0) \ddot{r}^* - \frac{\partial a}{\partial \|x_1\|} \frac{(r^*)^T \dot{r}^*}{\|r^*\|} \begin{pmatrix} 0 & 1 \\ -1 & 0 \end{pmatrix} E^T(a_0) \dot{r}^* - w_0 \end{aligned}$$

The perturbation model is

$$\delta \dot{x} = \left(\begin{array}{c|c} \frac{1}{\|r^*\|} \frac{\partial a}{\partial \|x_1\|} \begin{pmatrix} 0 & 1 \\ -1 & 0 \end{pmatrix} \dot{r}^* (r^*)^T & E(a_0) \\ \hline 0 & 0 \end{array} \right) \delta x + \begin{pmatrix} 0 \\ -I \end{pmatrix} \delta u + \begin{pmatrix} 0 \\ I \end{pmatrix} \delta w \quad (6)$$

Consider two special cases in which the reference is constant ($\dot{r}^* = 0$). When the position r^* is such that the corresponding angle $a = 2n\pi$, the perturbation model is

$$\delta \dot{x} = \begin{pmatrix} 0 & I \\ 0 & 0 \end{pmatrix} \delta x + \begin{pmatrix} 0 \\ I \end{pmatrix} \delta u + \begin{pmatrix} 0 \\ I \end{pmatrix} \delta w$$

But when r^* is such that $a = (2n + 1)\pi$, one has

$$\delta \dot{x} = \begin{pmatrix} 0 & -I \\ 0 & 0 \end{pmatrix} \delta x + \begin{pmatrix} 0 \\ I \end{pmatrix} \delta u + \begin{pmatrix} 0 \\ I \end{pmatrix} \delta w$$

Since there is a sign change in the (1,2) block, a fixed-gain control system that must be stable for this range of positions cannot be designed. Also, due to the nature of the perturbation model, an adaptive scheme that ignores the details of $\partial \dot{x} / \partial x$ is likely to be difficult to verify.

On the other hand, the scheme based on system inversion is very direct. Thus, let $y_1 = x_1$ and consider the string of integrators

$$\left. \begin{aligned} \dot{y}_1 &= y_2 \\ \dot{y}_2 &= v \end{aligned} \right\} \quad (7)$$

which is related to the given system (5) by the nonsingular transformation,

$$\begin{aligned} W: \quad x_1 &= y_1 & T: \quad y_1 &= x_1 \\ x_2 &= E^T(a) y_2 & y_2 &= E(a) x_2 \end{aligned} \quad (8)$$

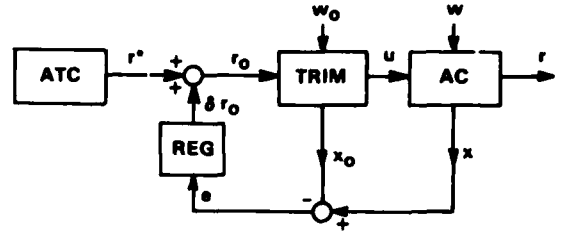


Fig. 3 Control system configuration with feedback closed ahead of TRIM.

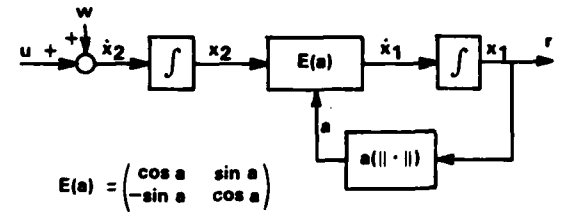


Fig. 4 Block diagram of example system.

The controls transform according to

$$\left. \begin{aligned} v &= E(a) \left[\frac{\partial a}{\partial \|x_1\|} \frac{x_1^T E(a) x_2}{\|x_1\|} \begin{pmatrix} 0 & 1 \\ -1 & 0 \end{pmatrix} x_2 + u + w \right] \\ u &= E^T(a) \left[-\frac{\partial a}{\partial \|x_1\|} \frac{y_1^T y_2}{\|y_1\|} \begin{pmatrix} 0 & 1 \\ -1 & 0 \end{pmatrix} y_2 + v \right] - w \end{aligned} \right\} \quad (9)$$

The y -coordinate description (Eq. (7)) of the system is fully equivalent to the natural (x -coordinate) description (Eq. (5)).

A configuration of the complete control system is shown in Fig. 5. There are four subsystems: command generator, regulator, trimmap, and the plant. The generator is initialized at $t = t_0$ to coincide with the transformed plant state (y_1, y_2). Note that if there are no modeling errors ($\delta r^* = 0$), then the combined map $r^* \rightarrow r$ along the path ABCD in Fig. 5 is an identity for all $t \geq t_0$; consequently, the map $r^* \rightarrow u$ along ABC is an inverse of the plant. In addition, the regulator sees a pair of two-axis integrators (Eq. (7)) as in path BA, and not the complicated perturbation model described above by Eq. (6), which would have to be considered had the feedback been introduced at point C (as is commonly done). Therefore, the design of the regulator is easy. Gain scheduling to stabilize the feedback is not necessary; it is provided automatically by the trimmap. Of course, the regulator can be scheduled for other reasons if desired, such as to account for operational limitations of the plant.

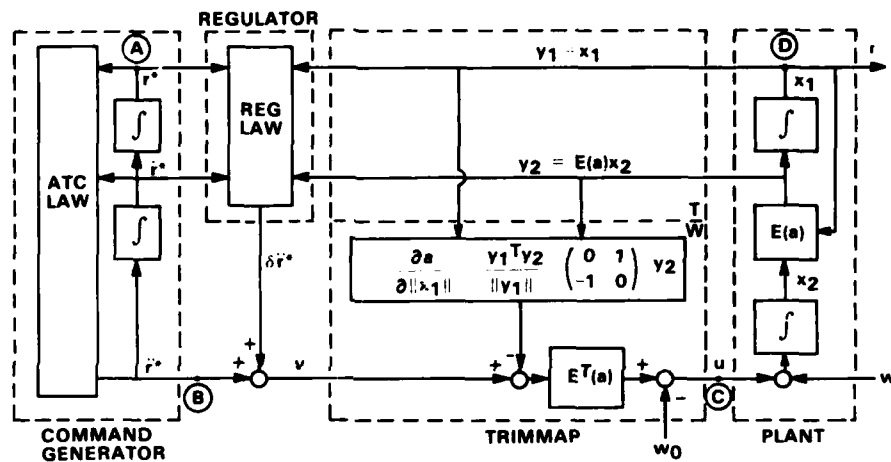


Fig. 5 Exact model following by a nonlinear plant.

It may be noted that the resulting control logic (Fig. 5) has the structure of a model follower. Reference 3 gives conditions for which exact model following is possible when both the model and the plant are linear and constant. The example in this section shows that exact model following may be possible even when the model is linear but the plant is not.

GENERALIZATION — BLOCK-TRIANGULAR SYSTEMS

Consider next the possibility of extending the procedure followed in the preceding example to more general situations. Let the system state equation have the form

$$\dot{x} = f(x, u, t) \quad (10)$$

where the state x is n -dimensional; the control u is m -dimensional; and f may be nonlinear and time-dependent. Suppose that, as in the example, there is a nonsingular transformation

$$T(x, u, t) = (y, v), \quad w(y, v, t) = (x, u) \quad (11)$$

such that the new variables (y, v) satisfy the system $S_0(m, k)$ defined by k m -dimensional columns of scalar integrators

$$\dot{y} = \begin{pmatrix} 0 & I & 0 & \dots & 0 \\ 0 & 0 & I & \dots & 0 \\ \dots & \dots & \dots & \dots & \dots \\ 0 & 0 & 0 & \dots & I \\ 0 & 0 & 0 & \dots & 0 \end{pmatrix} y + \begin{pmatrix} 0 \\ 0 \\ \dots \\ 0 \\ I \end{pmatrix} v \quad (12)$$

where 0 and I are m by m and the integer $k = n/m$. The relation is shown schematically in Fig. 6. The system (Eq. (7)) in the example is the special case $S_0(2, 2)$. The complete control logic shown in Fig. 5 generalizes to that shown in Fig. 7.

A servo is designed for the transformed system (Eq. (12)). The matrices A_0 and B_0 are the first and second matrices, respectively, in Eq. (12). This servo is used as a model reference. The integrators in

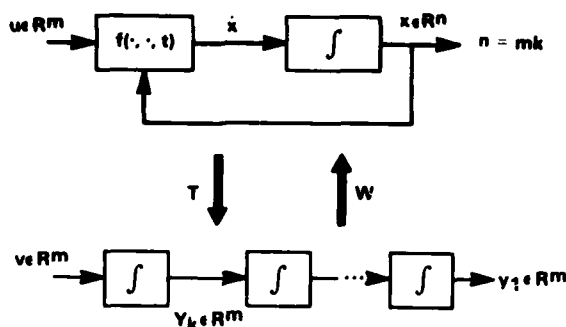
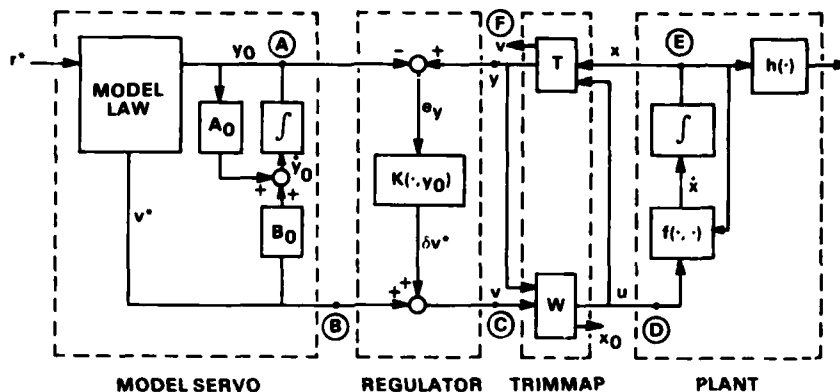
Fig. 6 Transformation into canonical system $S_0(m,k)$.

Fig. 7 Structure of the complete control system.

the model servo are initialized at $t = t_0$ to coincide with the transformed plant state y . If there are no modeling errors ($\delta v^* = 0$), then the combined map $y_0 \rightarrow y$ along the path ABCDEF in Fig. 6 is an identity for all $t \geq t_0$. The nonlinear, time-dependent plant can track exactly the model servo in terms of the transformed plant variables y .

The regulator sees the map $v_0 \rightarrow y$ along CDEF which has the model dynamics,

$$\dot{e}_y = A_0 e_y + B_0 \delta v^* \quad (13)$$

So, the design of the regulator law

$$\delta v^* = K(e_y, y_0, t) \quad (14)$$

is considerably simplified. No gain scheduling is needed for stabilization; that function is provided automatically by the trimmap (W,T). However, the regulator law can depend on the reference y_0 in order to match the regulator dynamics with the operational requirements associated with various flight conditions. The regulator law, just as the model servo law, can be dynamic, including, for example, integral feedbacks; it can also be nonlinear, including, for example, limiters and rate limiters.

A further useful property of the structure is that it makes practical the techniques of insensitive control and adaptive control discussed previously because the trimmap removes gross nonlinearity of the plant. The remaining nonlinearity, due to improper modeling, and other disturbances are much more likely to be tractable with these techniques than in the case of the original plant.

An effective sensitivity analysis can be developed for this structure. Thus, a Liapunov function $V(y)$ can be constructed in the Y space where the plant dynamics are $S_0(m,k)$, and then transformed into the natural plant state space X where the effects of disturbances on the derivative of $V(x)$ can be investigated in the usual manner (Ref. 4). Alternatively, the disturbance $w(x,t)$ defined in X can be mapped into an equivalent disturbance $w(y,t)$ in Y , and its effect on the derivative of $V(y)$ investigated.

Consider now the problem of existence and construction of the required transformations. The problem is currently understood in the case of linear systems. Time-invariant linear systems are treated in Refs. 5 and 6; time-varying linear systems are treated in Ref. 7. The problem for the nonlinear systems has been recently attacked from the point of view of differential geometry. References 8 and 9 discuss systems of the type

$$\dot{x} = f(x) + \sum_{i=1}^m u_i g_i(x), \quad f(0) = 0$$

and provide conditions for invertibility.

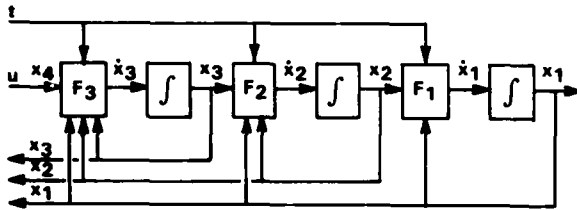


Fig. 8 Block lower triangular system
 $S(m,k)$, $k = 3$.

We consider systems of the type shown schematically in Fig. 8. The system is strictly m -axis in the sense that dimension of x_i equals m for all integrator columns i from 1 to k . The system is triangular in the sense that the only feed forward permitted is from x_{i+1} to \dot{x}_i , and each F_i is invertible with respect to the pair (x_{i+1}, \dot{x}_i) . Such an inverse of F_i will be denoted by G_i . The case shown is for $k = 3$. The associated state equation is

$$\left. \begin{aligned} \dot{x}_1 &= F_1(x_1, x_2, t) \\ \dot{x}_2 &= F_2(x_1, x_2, x_3, t) \\ \dot{x}_3 &= F_3(x_1, x_2, x_3, x_4, t), \quad x_4 = u \end{aligned} \right\} \quad (15)$$

with the obvious generalization to other k . We call the system block-triangular because of the form of the state equation in the case when the functions F_i are linear. Thus, for $k = 4$, the equation is

$$\dot{x} = \begin{pmatrix} A_{11}(t) & A_{12}(t) & 0 & 0 \\ A_{21}(t) & A_{22}(t) & A_{23}(t) & 0 \\ A_{31}(t) & A_{32}(t) & A_{33}(t) & A_{34}(t) \\ A_{41}(t) & A_{42}(t) & A_{43}(t) & A_{44}(t) \end{pmatrix} x + \begin{pmatrix} 0 \\ 0 \\ 0 \\ B_4(t) \end{pmatrix} u \quad (16)$$

where the upper off-diagonal blocks $A_{i, j+1}(t)$, $i = 1, k-1$ and $B_k(t)$ are nonsingular, all entries above and to the right are zero, and all blocks are m by m .

Since the structure of the system (Eq. (15)) is a generalization of the state equation of the example, one might attempt to construct the transformation (T, W) by applying the simple scheme (Eq. (7)) used in the example. Thus, let

$$\left. \begin{aligned} y_1 &= x_1 \\ y_2 &= \dot{y}_1 \\ y_3 &= \dot{y}_2 \\ y_4 &= \dot{y}_3 \end{aligned} \right\} \quad (17)$$

Then the transformation $y = T(x, t)$ is defined, assuming that all required partial derivatives exist, by

$$\left. \begin{aligned} y_1 &= x_1 \\ y_2 &= F_1(x_1, x_2, t) \\ y_3 &= \frac{\partial F_1}{\partial x_1} F_1 + \frac{\partial F_1}{\partial x_2} F_2 + \frac{\partial F_1}{\partial t} \\ y_4 &= \frac{\partial^2 F_1}{\partial x_1^2} F_1 F_1 + \dots + \frac{\partial^2 F_1}{\partial x_2 \partial t} F_2 + \frac{\partial^2 F_1}{\partial t^2} \end{aligned} \right\} \quad (18)$$

The equation for y_4 contains 16 terms. Thus, unless F_i is simple, one quickly gets bogged down in high-order partial derivatives. Moreover, the prospect of inverting Eq. (18) to obtain the backward map $x = W(y, t)$ may not always be attractive!

A computationally more practical approach to be given next is based on the observation that the time derivatives of x_1 may be obtained by first integrating the state equation (15) over a small interval of time, and then differentiating the resulting time history of x_1 the required number of times.

It will be assumed that the functions F_i are such that a simple Euler scheme is adequate for the integration of Eq. (15), that is, with time step D ,

$$\left. \begin{aligned} x_1(n+1) &= x_1(n) + F_1[x_1(n), x_2(n), t(n)] \times D \\ x_2(n+1) &= x_2(n) + F_2[x_1(n), x_2(n), x_3(n), t(n)] \times D \\ x_3(n+1) &= x_3(n) + F_3[x_1(n), x_2(n), x_3(n), x_4(n), t(n)] \times D \\ t(n+1) &= t(n) + D \end{aligned} \right\} \quad (19)$$

The discrete version $S_0^D(m, 3)$ of $S_0(m, 3)$ is given by Eq. (20). Then the transformation

$$\left. \begin{aligned} y_1(n+1) &= y_1(n) + y_2(n) \times D \\ y_2(n+1) &= y_2(n) + y_3(n) \times D \\ y_3(n+1) &= y_3(n) + y_4(n) \times D \\ t(n+1) &= t(n) + D \end{aligned} \right\} \quad (20)$$

exists and can be constructed together with its inverse as follows.

The diagram in Fig. 9 shows the construction of the forward transformation taking $x(n)$ into $y(n)$ when $k = 3$. The generalization to other values of k is obvious. The procedure is to construct the future values of x_1 from the present state $x(n)$, identify them with the future values of y_1 , and then construct the present state $y(n)$ from the future values of y_1 and the Euler version of $S_0(m,3)$. The first row $[x_1(n), x_2(n), x_3(n), x_4(n), t(n)]$ is given. (For convenience of exposition, $x_4(n) = u(n)$.) Euler integration (Eq. (19)) gives the second row. This row is used to compute the next row and so on until the column $[x_1(n), x_1(n+1), x_1(n+2), x_1(n+3)]$ is obtained. These are the future values of x_1 . The arrows in the diagram indicate the flow of the computation, and F denotes that the direct functions F_i are being used.

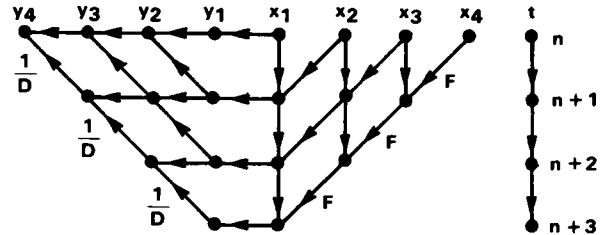


Fig. 9 Algorithm for the direct map $T(x,t) = y$.

Having thus obtained the future values of x_1 , we proceed to identify them with the future values of y_1 , thereby filling the y_1 column of the left triangle in the diagram. Since the transformed system is $S_0^*(m,3)$, column y_2 can be constructed by differencing,

$$\left. \begin{aligned} y_2(n) &= [y_1(n+1) - y_1(n)]/D \\ y_2(n+1) &= [y_1(n+2) - y_1(n+1)]/D \\ y_2(n+2) &= [y_1(n+3) - y_1(n+2)]/D \end{aligned} \right\} \quad (21)$$

This column is then used to compute the next column and so on until the row $[y_1(n), y_2(n), y_3(n), y_4(n)]$ is obtained, which was the required quantity.

The algorithm for the inverse of this transformation is shown in Fig. 10. The primary change is that the arrows along the diagonals have been reversed, and the corresponding functions have been inverted. The first row, $[t(n), y_1(n), y_2(n), y_3(n), y_4(n)]$ of the left triangle is given. Euler integration using Eq. (20) gives the next row. This row is used to compute the next row and so on until the column $[y_1(n), y_1(n+1), y_1(n+2), y_1(n+3)]$ is obtained. The entries are the future values of y_1 , which are identified with the future values of x_1 , thereby filling the x_1 column of the right triangle. The coordinates x_2 are defined by the relative inverse of \dot{x}_1 ,

$$\left. \begin{aligned} \dot{x}_1(n) &= [x_1(n+1) - x_1(n)]/D \\ x_2(n) &= G_1[x_1(n), \dot{x}_1(n), t(n)] \\ \dot{x}_1(n+1) &= [x_1(n+2) - x_1(n+1)]/D \\ x_2(n+1) &= G_1[x_1(n+1), \dot{x}_1(n+1), t(n+1)] \\ \dot{x}_1(n+2) &= [x_1(n+3) - x_1(n+2)]/D \\ x_2(n+2) &= G_1[x_1(n+2), \dot{x}_1(n+2), t(n+2)] \end{aligned} \right\} \quad (22)$$

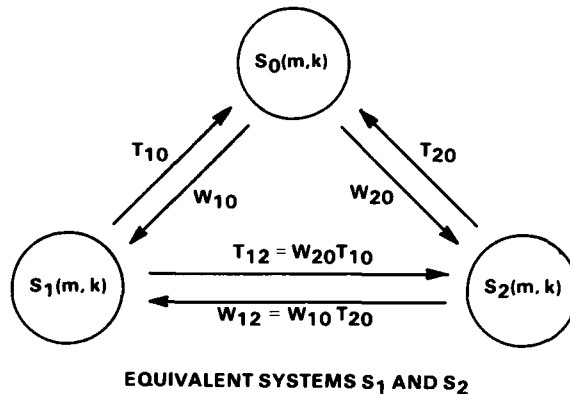
Column x_3 is obtained similarly, but using $G_2(x_1, x_2, \dot{x}_2, t)$. Column x_4 is obtained using $G_3(x_1, x_2, x_3, x_3, t)$. Thus, the row $[x_1(n), x_2(n), x_3(n), x_4(n)]$ is computed, which was the required object.

Several comments may be made at this point concerning the algorithm and systems to which it applies.

1. The calculations involved are well suited for digital computers and practical systems where the nonlinearities F_i may be given in multidimensional tabular form, rather than in sufficiently differentiable analytic form.

2. The transformations T and W are static, that is memoryless. Derivatives of measurement noise are not involved since the future of y_1 is computed from the present state x .

3. All block-triangular systems $S(m,k)$ with the same number m of axes and the same number k of integrator columns are equivalent as can be seen from the following sketch:



Hence, for example, exact model following is possible between two different nonlinear systems as long as both are block-triangular and have the same (m,k) .

4. According to Ref. 5, a constant-coefficient linear system need not be block-triangular to be transformable into $S_0(m,k)$, but then the correspondence between x_1 and y_1 will be lost. Nevertheless, the wider class of systems is useful for designing servos for $S_0(m,k)$ by means of, for example, pole-placement, eigenvector control, quadratic optimization, and Liapunov theory, and then transforming the design as well as analysis into the given system $S_1(m,k)$.

5. All time-varying systems of the type given by Eq. (16) for any m and k are equivalent to constant linear systems.

6. Systems with redundant paths can be made effectively block-triangular by treating the resolving constraints as added states. An example is shown in Fig. 11. Here $\dot{x}_1 = f_1(x_1, z_1, z_2, t)$. Many pairs (z_1, z_2) generate a given \dot{x}_1 .

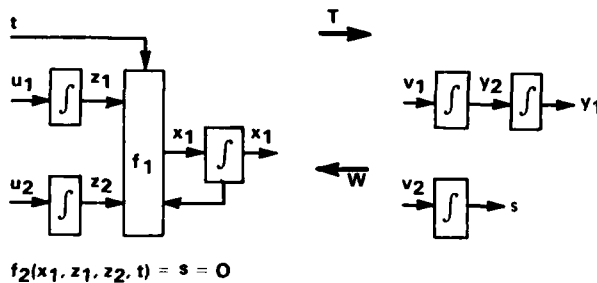


Fig. 11 Example of redundancy.

In general, a constraint $f_2(x_1, z_1, z_2, t) = 0$ must be designed to resolve this redundancy. Let $s = f_2(x_1, z_1, z_2, t)$. By construction, $F = (f_1, f_2)$ is invertible. Hence, the given state (x_1, z_1, z_2) and the canonic state $(y_1, y_2; s)$ are linked by a nonsingular transformation. The coordinates (y_1, y_2, s) serve as the states of the model $S_0(m,2)$, and s corresponds to the state of the (decoupled!) constraint model $S_0(m^*,1)$, where m^* is the dimension of the redundancy. A stable regulator designed for $S_0(m^*,1)$ will in this case force the system to satisfy the required constraints $s = 0$.

BLOCK-TRIANGULAR MODEL OF AIRCRAFT

We will consider the aircraft to be a rigid body so that the state of the aircraft is given by the position and velocity vectors of the center of mass and by the attitude and angular velocity of the body fixed axes. Position and velocity will be represented by their runway (inertial) coordinates, r_r and v_r , respectively; attitude and angular velocity will be represented as in Ref. 10 by the direction cosine matrix A_{br} and angular rates ω_b , respectively. The propulsion subsystem, including any thrust deflection, the flap deployment system, landing-gear deployment system, direct-force devices, and other similar subsystems will be represented by a power-configuration subsystem assumed to be m_p -axis and second order with m_p -axis control u_p and $2m_p$ -dimensional state (p_1, p_2) . The aerodynamics will be assumed to depend on only the rigid body state, the propulsion-configuration state, the position of the control surfaces u_a , and environmental variables, such as wind and temperature. A block diagram of the model is shown in Fig. 12. The complete system state $x = (r_r, v_r, A_{br}, \omega_b, p_1, p_2)$ has dimension $12 + 2m_p$. The combined control $u = (u_a, u_p)$ and w represents the atmospheric and other disturbances. The state equation is given by

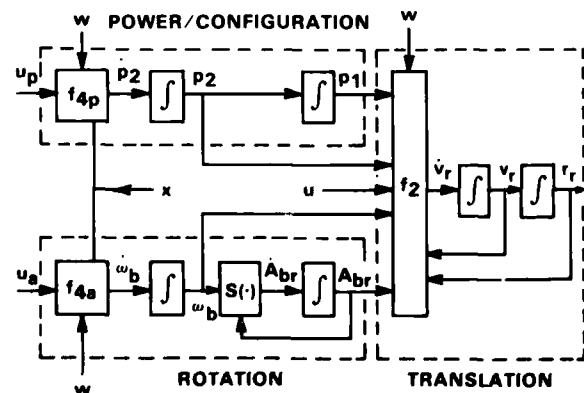


Fig. 12 Model of aircraft.

$$\dot{r}_r = v_r \tag{23a}$$

$$\dot{v}_r = f_2(x, u, w, t) \tag{23b}$$

$$\dot{A}_{br} = S(\omega_b)A_{br} \tag{23c}$$

$$\dot{\omega}_b = f_{a,b}(x, u_a, w, t) \tag{23d}$$

$$\dot{p}_1 = p_2 \quad (23e)$$

$$\dot{p}_2 = f_{4p}(x, u_p, w, t) \quad (23f)$$

Equations (23a) and (23c) are the universally valid kinematic equations for translation and rotation of a rigid body. In Eq. (23b), f_2 represents the total specific force acting on the aircraft, including gravitational, aerodynamic, and propulsive forces. In Eq. (23d) f_{4a} represents the total moment including that contributed by gyroscopic effects, aerodynamics, and propulsion. The power-configuration variable p_1 represents such quantities as throttle position, thrust deflection angle, and flap position. Usually, at least portions of the power-configuration subsystem will have a built-in servo structure. Examples of components of u_a are aileron, elevator, and rudder positions.

It may be noted from the block diagram (Fig. 12) that variables p_2 , u , and ω_b feed forward, in parallel with (A_{br}, p_1) , into the force generation process f_2 . Hence, the model is not explicitly block-triangular. Now, p_2 represents such physical quantities as throttle rate, thrust deflection rate, flap rate, collective rate in the helicopter, and mast angle rate in a tilt-rotor, all of which do not couple strongly, if at all, into the generation of the force. So, the p_2 feed forward can be deleted from the model without affecting its accuracy substantially. The u feed forward represents such effects as lift due to elevator, side force due to rudder, side force due to the tail rotor in the helicopter, and ω_b feed forward represents such effects as C_{Lq} and C_{Yr} . Although these effects do not conform to the triangular structure, they are not ignorable. Some effects associated with steady-state moment balance can be removed. The remainder will be represented as independently generated disturbances d in the force generation process as shown in Fig. 13, and the regulator must therefore correct for the associated errors.

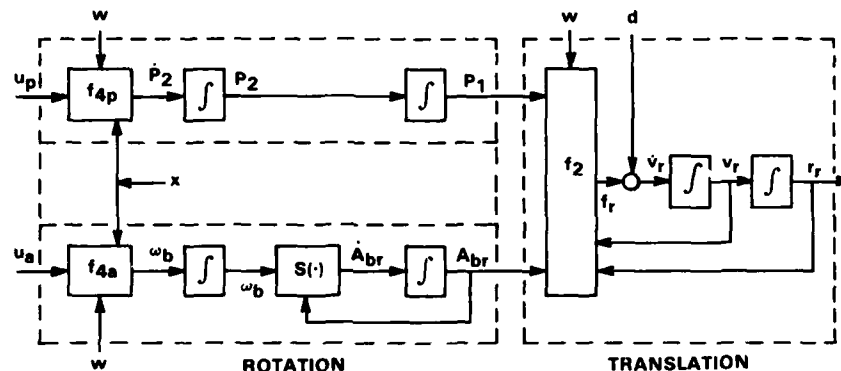


Fig. 13 Lower triangular model of aircraft.

In any case, the kinematic equations are always invertible,

$$\begin{aligned} v_r &= \dot{r}_r \\ \omega_b &= \text{skew}(\dot{A}_{br} A_{br}^T) \\ p_2 &= \dot{p}_1 \end{aligned} \quad (24)$$

Furthermore, both f_{4a} and f_{4p} are usually invertible with respect to angular acceleration ω_b and power-configuration variable \dot{p}_2 , respectively, since these quantities are generally subject to direct control. Thus, for example, aileron, elevator, and rudder control the moment vector acting on the aircraft directly and one-to-one for any fixed state, x .

Finally, consider the force generation process, f_2 in Fig. 13,

$$f_2(r_r, v_r, A_{br}, p_1, w, t) = f_r \quad (25)$$

Here, the inverse of interest is one that would specify (A_{br}, p_1) in terms of the total specific force vector f_r ,

$$(A_{br}, p_1) = g_2(r_r, v_r, f_r, w, t) \quad (26)$$

In general, there are more degrees of freedom in A_{br} and p_1 combined than in f_r , which has exactly three. Hence, constraints must be imposed to resolve the redundancy. For example, suppose that $p_1 = (\text{throttle, flap})$, then the dimension of (A_{br}, p_1) is 5. The degrees of freedom of the redundancy is two, and it can be resolved, for example, by selecting flap to give maximum lift margin, and constraining the attitude to zero sideslip angle β . It should be noted that the redundancy must be resolved regardless of what design approach one takes. In our approach, the redundancy problem is made quite explicit and much more tractable, as will be seen in the second part of the paper.

Once the constraints have been designed, f_2 becomes invertible, and the complete model becomes effectively block-triangular. A time history of the position vector r_r can be pushed back through the model to obtain the required controls and intermediate states. That is, the model is equivalent to $S_0(3,4)$ with the four three-axis integrator states defined by the three-axis position, velocity, acceleration, and acceleration rate vectors. The control is the second time-derivative of acceleration. The structure shown in Fig. 7 applies. The transformed variable at point F is defined by $y = (r, v, a, \dot{a})$, and the transformed control at point C is defined by $v = \ddot{a}$. The model states at point A are $y = (r_0, v_0, a_0, \dot{a}_0)$, and model control at point B is $v^* = \ddot{a}_0$. Thus, the structure specializes to that shown in Fig. 14. The regulator operates on the complete state error, and generates the corrective second derivative of acceleration.

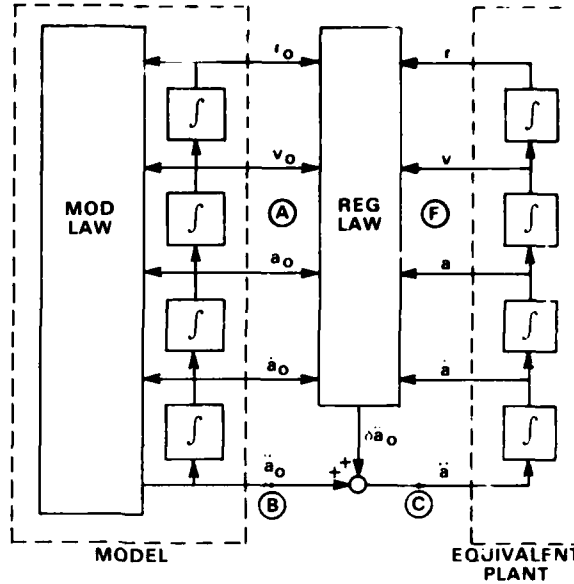


Fig. 14 Centralized form of control system.

DECENTRALIZED CONTROL STRUCTURE

Although the coarse centralized structure shown in Fig. 14 is useful for design purposes, a finer, decentralized structure is normally needed for actual implementation. Such a structure may be deduced as follows. Let the model shown in Fig. 14 be divided into an ATC subsystem, which specifies the required flightpath, and a trajectory command generator (TCOM) which defines how the aircraft is to respond to it. Thus, TCOM acts as a model reference. Its internal structure (Fig. 15) consists of a linear acceleration servo and a generally nonlinear trajectory regulator whose output is a corrective acceleration δa^* . The output of TCOM is r_o , v_o , and a_c ; the latter is shown in the figure as simply the sum of a^* and if desired it may be a nonlinear function.

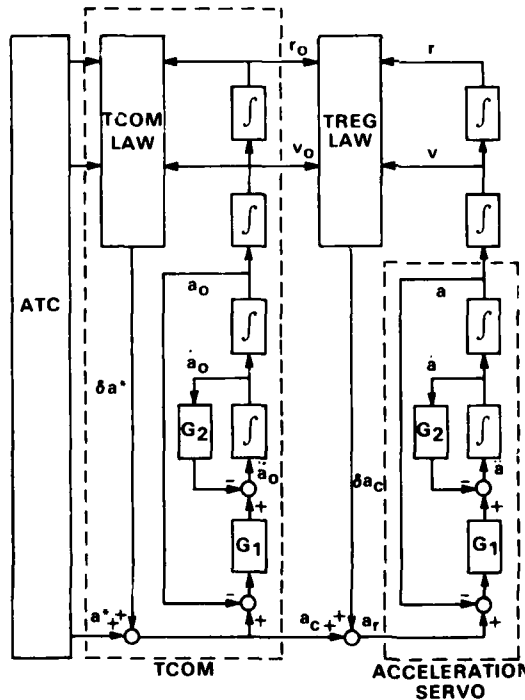


Fig. 15 Acceleration servo separated.

and attitude A_{br} . Then Eqs. (24) are used to construct the model states of power-configuration and rotation subsystems denoted in the figure as PCOM and RCOM, respectively.

Model followers are again designed by constructing regulators PREG and RREG, which provide feedback to their respective subsystems. Finally, the inverses PTRIM and MTRIM of f_{bp} and f_{ba} , respectively, are constructed to compute the control signals u_p and u_a which drive the actual plant, as shown in Fig. 18.

The complete control logic has a hierarchic structure. At the top of the hierarchy is the ATC, which defines the reference flightpath; at the bottom are the servo actuators driving the controls u_p and u_a . Information flow and processing are of two types, namely, open loop and closed loop. Thus, considering the open loop, the ATC command enters the trajectory command generator (TCOM), where it is transformed into

The identical acceleration servo structure is separated from the regulator law. The remainder is the trajectory regulator (TREG), whose output is corrective acceleration δa_c , and the acceleration servo is constructed for the plant as shown. The result is that \ddot{a}_o and \ddot{a} in Fig. 15 coincide with \ddot{a}_o and \ddot{a} in Fig. 14. Therefore, the effects are equivalent, but the decentralization is increased.

The acceleration servo can itself be synthesized as a model follower, as shown in Fig. 16. Thus, the acceleration servo in Fig. 15 is identified with the acceleration command generator (ACOM) in Fig. 16. Feedback to control disturbances is provided by the acceleration regulator (AREG).

Next consider the inverse map of the form in Fig. 10, which transforms the ACOM variables ($\ddot{a}_n, \ddot{a}_m, \ddot{a}_m$) into power-configuration variables ($\dot{p}_2, \dot{p}_2, \dot{p}_1$) and rotation variables ($\dot{\omega}_b, \dot{\omega}_b, A_{br}$) of aircraft model in Fig. 13. This map is shown schematically in Fig. 17. Future values of model acceleration vector a_m provided by ACOM are transformed using force trim (FTRIM) defined by Eq. (26) into the future values of power-configuration variables

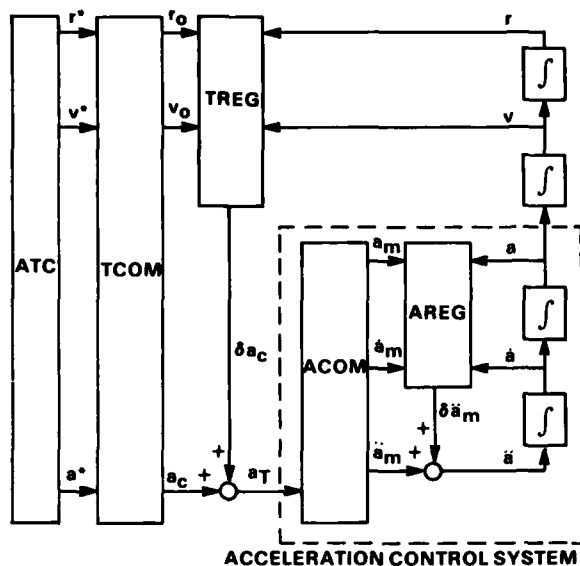


Fig. 16 Acceleration model follower.

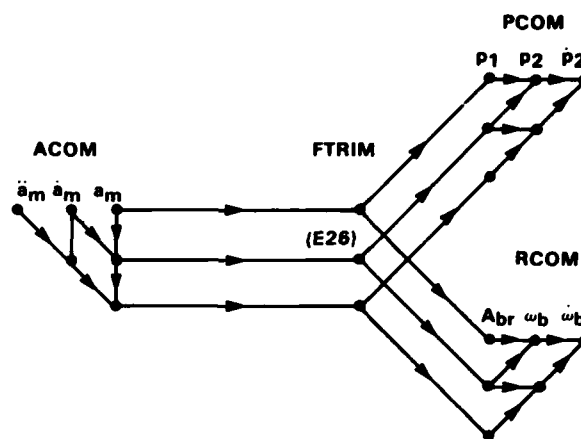


Fig. 17 Inverse force map.

executable flightpath having sufficient smoothness and meeting the required constraints. TCOM is the model reference for the translational motion of the aircraft such that exact model following is possible. The output is the flightpath and its derivatives.

In the open-loop flow, the acceleration vector is passed down the hierarchy to the acceleration command generator (ACOM) and then to the force trim (FTRIM) where the a priori information concerning the total force generation process is used, together with a variety of constraints, to compute the power-configuration variable p_1 and attitude A_{br} that will result in the required acceleration vector.

These commands are passed down the hierarchy to the power-configuration and rotation servos. The rotation command generator computes an executable rotation and corresponding angular acceleration vector. The angular acceleration vector is passed down the hierarchy to the moment trim (MTRIM) where the a priori information concerning the moment generation process is used to compute the controls u_a that will produce the requested angular acceleration. The other branch from FTRIM is passed to the propulsion-configuration command generator PCOM and then to the corresponding trim algorithm PTRIM, whose output is the control u_p .

In the absence of all disturbances and with an accurate representation of the aircraft, perfect model following would occur at all levels in the hierarchy. In the real situation, there will be modeling errors, such as those imposed by the assumptions noted previously and those deriving from imperfect knowledge of the aerodynamic characteristics and the environment. The control of these effects is achieved by means of feedbacks which enter at various levels in the hierarchy. Thus, the commanded flightpath, which is computed in TCOM, is compared with the measured flightpath; the difference, namely the path error, is used in the trajectory regulator TREG to compute the corrective acceleration vector, which is added to the primary acceleration commanded by TCOM. By construction, the trajectory error dynamics are driven only by disturbances and are decoupled from TCOM, thereby achieving decentralization. The regulator law can be parameterized by signals from TCOM or ATC to account for changing operational requirements. Propulsion-configuration and rotation regulators PREG and RREG function similarly.

The symmetry about the boundary separating the plant from the control logic may be noted. The relation between TCOM output r_0 and the plant output r_r is, except for disturbances, an identity, as are the relations between $(p_1, p_2; A_{br}, \omega_b)_m$ and $(p_1, p_2; A_{br}, \omega_b)_o$ at lower levels of the hierarchy. Most of the control is done open loop by means of generators and trimmaps. The disturbances are controlled by means of regulators, which would be unloaded if there were no disturbances.

This design method was applied to several aircraft of increasing complexity. The first complete flight control system tested in flight was for the DHC-6; results of the test are given in Ref. 11. Methods for providing pilot inputs to this design were investigated in Ref. 12. Next, the method was applied to control an A-7 for carrier landing and tested in manned simulation. The results are given in Refs. 13 and 14. The method is currently being applied to the UH-1H helicopter, with a flight test scheduled in the summer of 1980. In addition, the method was tested on the Augmentor Wing Jet STOL Research Aircraft (AWJSRA). The remaining part of the present paper describes the application and evaluation of the system on the AWJSRA, including a description of the aircraft, the flight control system, and the results of the flight evaluations of the system.

AUGMENTOR WING AIRCRAFT

The augmentor wing jet STOL research aircraft (AWJSRA) (Fig. 19; Refs. 15-17) is a modified de Havilland C-8A in which aerodynamic lift is augmented by exhausting compressed cold air from the engine through a jet flap (Fig. 20); the flow from each engine is split and ducted to both wings for engine-out lift symmetry; the amount of augmentation depends on both flap setting and engine power. Further, hot flow from the engine core is exhausted through controllable nozzles which permit deflection of the "hot" thrust from 6° to 98° relative to the fuselage centerline. The special flap permits low landing airspeeds, of the order of 60 to 70 knots, and the thrust deflection permits steep approaches at path angles down to -7.5° .

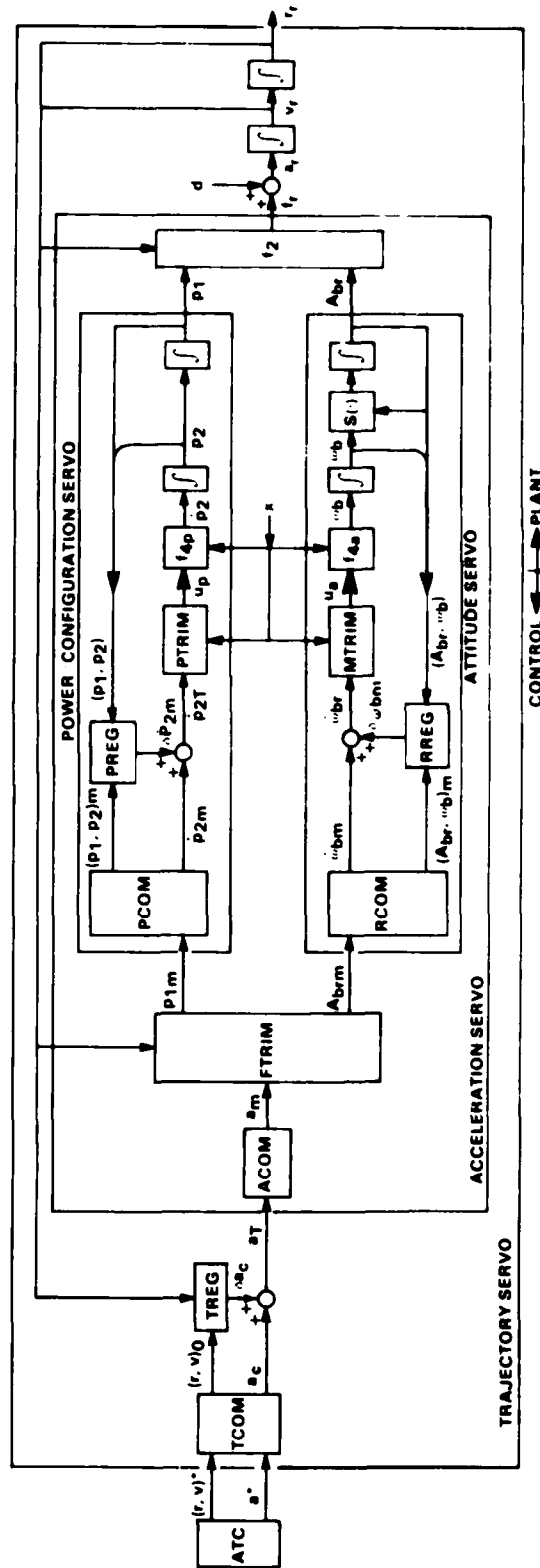


Fig. 18 Decentralized structure of the flight control system.

The force balance equations governing the AMJSRA's rigid body motion are

$$\ddot{\mathbf{a}} = (\mathbf{m}\ddot{\mathbf{g}} + \ddot{\mathbf{A}} + \ddot{\mathbf{T}})/\mathbf{m} \quad (27)$$

where $\ddot{\mathbf{A}}$, $\ddot{\mathbf{T}}$, and $\ddot{\mathbf{g}}$ are the aerodynamic and thrust forces and gravity. The right-hand side of Eq. (27) constitutes the force model, \mathbf{f} , in Fig. 18. The aircraft forces can be represented as

$$\left. \begin{aligned} \ddot{\mathbf{A}} &= -Q S_w (C_D \ddot{\mathbf{i}}_s + C_L \ddot{\mathbf{k}}_s) \\ \ddot{\mathbf{T}} &= T_H [\cos(\alpha + \delta) \ddot{\mathbf{i}}_s - \sin(\alpha + \delta) \ddot{\mathbf{k}}_s] - \dot{m}_e v_a \ddot{\mathbf{i}}_s \end{aligned} \right\} \quad (28)$$

where $\{\ddot{\mathbf{i}}_s, \ddot{\mathbf{j}}_s, \ddot{\mathbf{k}}_s\}$ are wind-tunnel stability axes and $\ddot{\mathbf{T}}$ has been separated into the vectored hot thrust T_H and the inlet ram drag $\dot{m}_e v_a$. Lift and drag coefficients and engine output parameters are required for the definition of \mathbf{f} ; these are all nonlinear scalar functions available as tabulated data from simulation models (Refs. 18, 19), and can be expressed in terms of their independent variables as

$$\left. \begin{aligned} C_L &= C_L(\alpha, \delta, \nu, C_J) \\ C_D &= C_D(\alpha, \delta, \nu, C_J) \\ C_J &= T_c / Q S_w \\ T_c &= T_c(N_H, \nu, \delta, M) \\ T_H &= T_H(N_H, \nu, \delta, M) \\ \dot{m}_e &= \dot{m}_e(N_H, \nu, \delta) \end{aligned} \right\} \quad (29)$$

The dependence of aerodynamic forces on propulsion is given in terms of the cold-thrust coefficient C_J , where T_c is the potential thrust from isentropic expansion of the compressed cold air used for lift augmentation. The lift-drag polars, including the tail contribution for trimmed pitching moment, are shown in Fig. 21 for the extreme flap settings. The sensitivity of (C_L, C_D) to (α, C_J) is seen to vary considerably with flap setting. At minimum flap, the behavior is conventional, with little dependence of C_L on engine power or of drag on angle of attack at low α ; at maximum flap, both sensitivities are greatly increased and result in significant control cross-coupling. The engine parameters (Fig. 22) depend on the engine power (rpm normalized by a reference value) and the atmospheric temperature and pressure ratios and Mach number, (θ, δ, M) .

The independent variables of the aircraft model, Eqs. (27)-(29), consist of control variables, $(\delta, \nu, \alpha, \nu, N_H)$, and the remaining path and environmental variables that define the flight condition. The control domain over which the model is defined is bounded by servo limits and the available model data, as noted in Table 1. Further, solutions of Eqs. (27)-(29), given the current flight condition, are required in both the usual control system design (Fig. 2) and the present one (Figs. 3, 18). The flight envelope of the system is the set of flight conditions for which Eqs. (27)-(29) can be solved, and the operational flight envelope is the set for which this can be done within constraints associated with the type of operation (assumed to be passenger operations here) and with the specific aircraft. An outer bound on the flight conditions of interest for the AMJSRA control system design is given in Table 2. The applied specific force, $f = (\ddot{\mathbf{a}} - \ddot{\mathbf{g}})/g$, is introduced in Table 2 in order to reduce the number of path variables needed to define the flight condition. The ranges for speed and atmospheric parameters in Table 2 are constricted compared to current jet transports because the aircraft was designed and operated principally for low-speed, low-altitude flight research in a terminal area. The range of specific forces includes CTOL and STOL passenger operations, but is smaller than for VTOL or fighter aircraft operations. Not all flight conditions encompassed

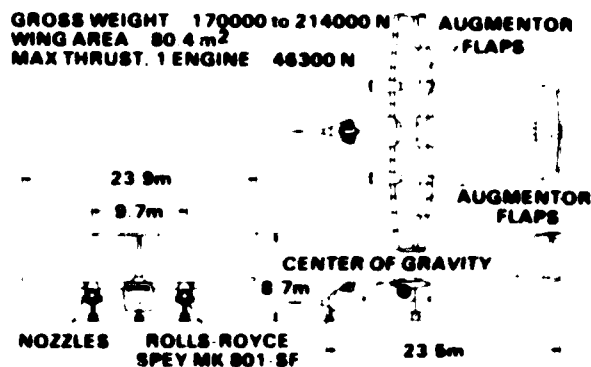


Fig. 19 Augmentor wing jet STOL research aircraft (AMJSRA).

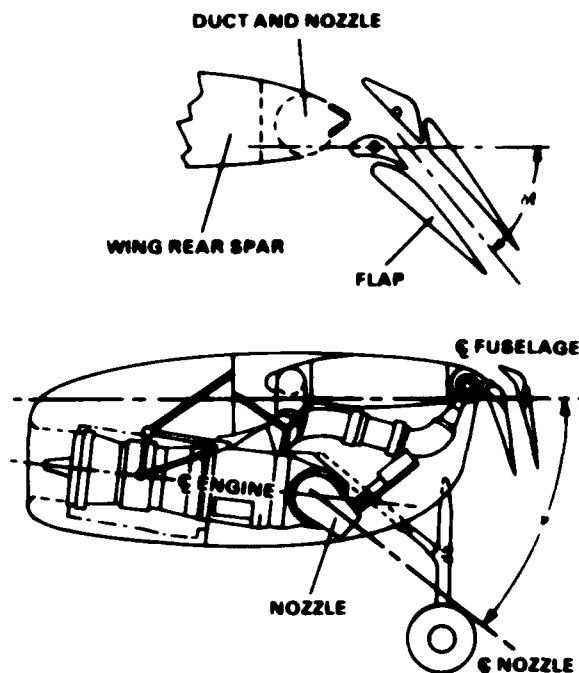


Fig. 20 Augmentor jet flap and propulsion system.

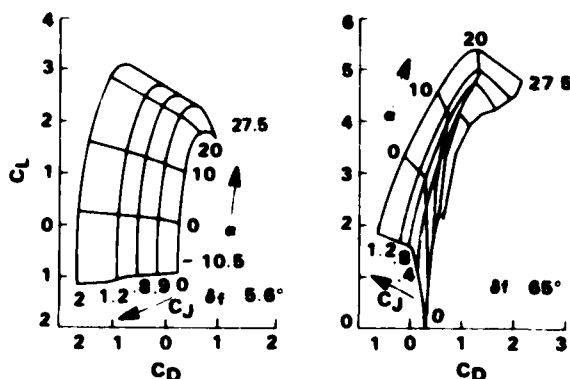


Fig. 21 AMJSRA lift-drag polars.

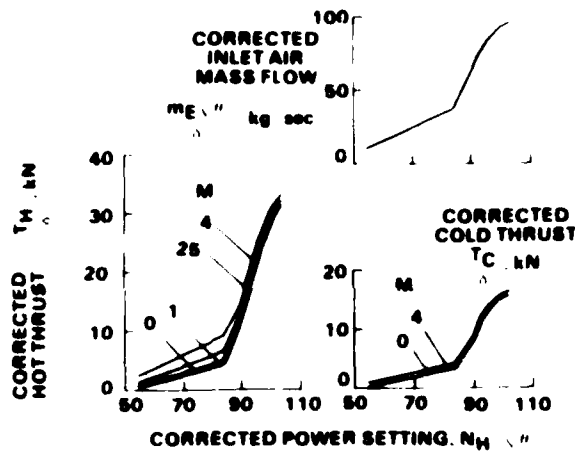


Fig. 22 AWSRA static engine model - one engine.

by the limits in Table 2 are operationally acceptable for quasi-steady flight; only those for which the system control commands satisfy the operational constraints on controls usage are acceptable. The constraints applicable to the AWSRA are listed in Table 3; these are limits on functions of the controls which reflect various servo limits and safety considerations, such as the flap structural placard, time to recover from engine-out, nozzle structural limit, lift reserve, angle-of-attack reserve, and control-margin reserve for regulator usage. These limits can be fixed or dependent on configuration or flight condition. Further discussion of these constraints, which are unique to the AWSRA research flight operations, or of constraints for powered lift aircraft generally, is omitted here (cf. Refs. 20, 21), but the length and complexity of the constraint list for this application is typical of aircraft operations generally.

TABLE 3. OPERATIONAL CONSTRAINTS ON CONTROLS USAGE - AWSRA

Control function	Steady flight limits	Regulator limits
Flap	$5.6^\circ \leq \delta_f \leq \delta_{f_{max}}(v_e)$	
Power	$N_{H_{min}}(\delta_f) \leq N_H \leq N_{H_{max}}(v_e, \delta)$	$N_{H_{min}}(\delta_f) \leq N_H \leq N_{H_{max}}(v_e, \delta)$
Nozzle	$6^\circ \leq v \leq 98^\circ$	$6^\circ \leq v \leq 98^\circ$
Lift margin	$LM \geq LM_{min}(\delta_f)$	
Pitch	$-10^\circ \leq \mu \leq 15^\circ$	
Angle of attack		$-10.5 \leq \alpha \leq \alpha_{max}(v_e)$
Control margin	$CM \geq 0.25 \text{ g}$	
Elevator	$-17 \leq \delta_e \leq 7$	
Roll angle	$-25 \leq \delta \leq 25$	$-30^\circ \leq \delta \leq 30^\circ$

The next three sections of this paper describe an application of the proposed control structure to the AWSRA. That structure applies to all aircraft; it partitions the automatic control logic into a hierarchy of similar structures consisting of command generators (feed-forward commands), regulators (state feedback) and trimmaps (plant inverses) which govern translational and rotational dynamics and the control servos. The trajectory and attitude command generators and regulators govern the aircraft kinematics and are largely independent of the specific aircraft being controlled. Design issues of interest in these elements are the enforcement of operational constraints and the desired transient response dynamics on the kinematics. The force and moment trimmaps govern control usage based on descriptions of the aircraft, including any special features, such as propulsion-dependent aerodynamic forces and moments, control nonlinearities, and novel or redundant controls. Design issues of interest in the force trimmap are the enforcement of operational constraints on controls, configuration management over the flight envelope, methods of solving the force balance equations, and compensation of model errors. The discussion is focused on the outer-loop elements where the crucial design issues are addressed. Descriptions of attitude and power control subsystems, omitted here, will be included in future reports. The attitude control closely parallels that described in Ref. 10 and 11.

The AWSRA application was begun at an early stage in the development of the control structure presented in the first part of this paper (cf. Ref. 10). Consequently, the flight system elements described next contain some simplifying approximations of the structures outlined in Figs. 15-18, but these have only minor effects on performance in the passenger operational domain. The principal approximation was the assumption that the acceleration response dynamics were fast compared to those of the trajectory commands and could therefore be neglected. However, it is apparent from the earlier discussion that these dynamics can be made simple through appropriate design of the inner-loop command generators and their model readily implemented in a practicable flight system, as outlined in Figs. 15-17, to achieve the full capability of the proposed structure for model following.

Several reference frames are required in the following development. Path axes are introduced along with runway, wind-tunnel stability, and body axes. These are defined briefly in the appendix along with related transformations and notational rules for vectors and transformations.

TABLE 1. DOMAIN OF AIRCRAFT MODEL DEFINITION

Control	Minimum	Maximum
δ_f , deg	5.6	72
v , deg	6	98
N_H , %	0	min(103.5, 104.7√6)
α , deg	-10.5	27.5

TABLE 2. LIMIT OF DESIGN FLIGHT ENVELOPE

Variable	Minimum	Maximum
v_e , knots	45	160
$\dot{\delta}_f$, $\dot{\delta}_s$, g	-0.35	0.35
$\dot{\delta}_f$, $\dot{\delta}_s$, g	-1.5	-0.5
μ , deg	-30	30
m , kg	17300	24500
δ	0.9	1.1
δ	0.7	1.0

TRAJECTORY COMMAND SYSTEM

A flyable reference trajectory is generated in two steps. First, a coarse reference trajectory (r_p^*, v_p^*, a_p^*) , is generated by ATC; it consists of any sequence of straight line and circular arc legs with arbitrary discontinuities in position, velocity, or acceleration vectors at the leg junctions. In the present application, the coarse reference is defined from a stored set of parameters S , which suffice to define each leg. This contains the leg length s_f , initial position, reference airspeed V_{af} , flightpath angle, initial course angle, and the inverse radius of curvature:

$$S = \left\{ \left(s_f^{(m)}, r_r^{(m)}(0), v_{af}^{(m)}, \gamma^{(m)}, v_{v_0}^{(m)}, 1/R^{(m)} \right), m = 1, \dots, M \right\}$$

where m is the leg number. Given the current leg number, path length, and wind estimate these parameters suffice to define (r_p^*, v_p^*, a_p^*) . Leg number and path length are reset at each leg switch. In operational practice, the commanded and actual trajectories are required to satisfy a number of constraints on the kinematics, such as angular velocity and acceleration limits for passenger comfort, speed and flightpath angle safety margins, aircraft acceleration and jerk limits, and airspace restrictions, which are denoted formally here as a list of constraint functions, λ_k :

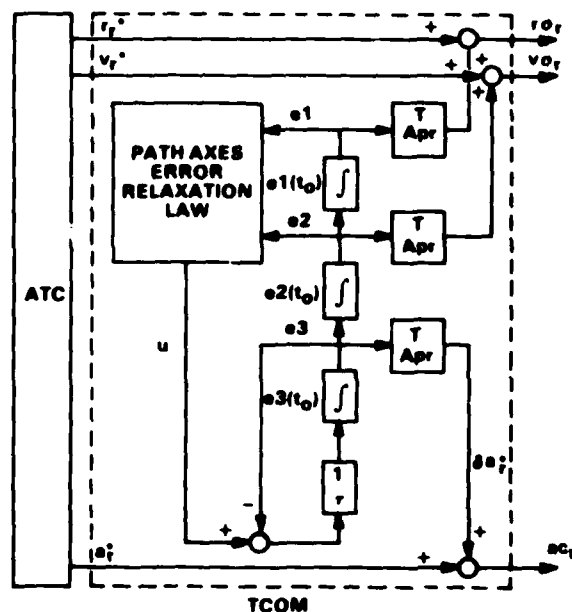
$$\lambda_k(r_r, v_r, a_r, \dot{a}_r) \geq 0; \quad k = 1, \dots, K \quad (30)$$

These constraints are not satisfied by the coarse reference at the discontinuous leg junctions, but it is assumed that each leg is selected a priori within these constraints. The use of a stored reference path suffices for the present demonstration, but we note that algorithms are available (e.g., Ref. 22) that can automatically synthesize a coarse reference subject to such constraints and couple the present control system to an advanced 4-D terminal area air traffic control system.

Next, transition maneuvering, which carries the aircraft from one leg to the next and satisfies Eq. (30), is generated in TCOM. These transitions are formulated as motion relative to the coarse reference and added to the coarse reference to form the flyable command, (r_{or}, v_{or}, a_{or}) . For this experiment, TCOM was formulated as a relaxing regulator (Refs. 10, 23) as shown in Fig. 23, rather than as a servo as applied in the DHC-6 (Ref. 11). In Fig. 23, the states e_1, e_2 are the relative position and velocity, u is the control, and e_3 is the relative acceleration command obtained by filtering u to limit jerk. The transition maneuver is generated by initializing a model of the dynamics with the leg junction discontinuities at the time of each leg switch and then relaxing these initial offsets to zero by driving the dynamics with an appropriate control law. This system and its control law have the following features: (1) the transitions are generated in each path axis independently; (2) the control law is linear for small relative offsets and saturates at large offsets to impose operational constraints on the maneuver kinematics; (3) the time of initiating the transition is selected to minimize maneuver activity; and (4) the transitions are initialized adaptively to correspond to the estimated state.

Path axes are used to synthesize the three-dimensional maneuver since accelerations along these axes independently control speed, course angle, and flightpath angle, and the maneuvers of interest can be generated by superposition of these single-axis maneuvers. The Coriolis acceleration due to rotation of the path axes is neglected in the system of Fig. 23; however, angular velocities are low in passenger operations and little tracking error resulted from this approximation of the kinematic model. The control law has a third-order linear domain with saturation or nulling as needed to limit the relative acceleration or velocity excursions about their reference values during the transition. The linear domain dynamics and saturation limits selected for the ANJSRA control law are listed in Fig. 23.

The time of initiating the transition to the next leg, t_0 , is selected by switching logic (not indicated in Fig. 23) designed to (1) minimize initial jerk magnitude in the case that the transition starts in the linear domain or (2) prevent control reversals between saturation limits if transition starts in the nonlinear domain. These initialization criteria minimize the initial or extreme control rates, eliminate unnecessary position, velocity, and acceleration overshoot of the new leg of the coarse reference trajectory, and minimize the maneuver time in the case of nonlinear transitions. Further, the transition is initiated independently on each path axis in the general case of multi-axis maneuvers.



RELAXATION LAW PARAMETERS			
AXIS	LONGITUDINAL	LATERAL	NORMAL
LINEAR DYNAMICS (ρ, ω_n) τ sec	(.7, .23 rps) 4	(.7, .18) 7	(.7, .28) 2
LIMITS $ u _{max} - 9$ $ e2 _{max} - m/sec$.03 max (.065 Va, 2)	.15 max (.13 Vec, 8)	.06 max (.06 Vec, 2)

Fig. 23 Trajectory command generator.

The initial conditions for the transition maneuvers are adaptive, that is, the integrators are loaded such that the commanded state equals the estimated state and the total acceleration command to the trimmap is continuous:

$$e_1(t_0) = A_{pr}(\hat{r}_r - r_r^*)$$

$$e_2(t_0) = A_{pr}(\hat{v}_r - v_r^*)$$

$$e_3(t_0) = A_{pr}(a_r - a_r^*)$$

This initialization rule unloads the trajectory regulator at each leg switch and permits use of the transition dynamics for initial path capture and for recapture from large error conditions, such as at switches between navigation aids where large shifts in estimated position can occur.

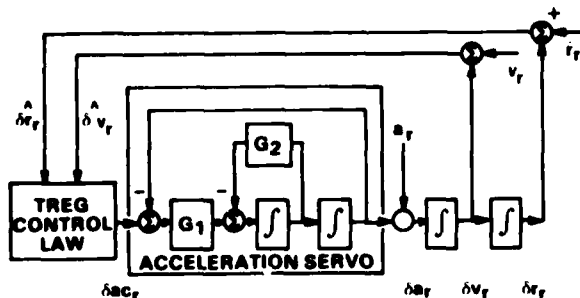
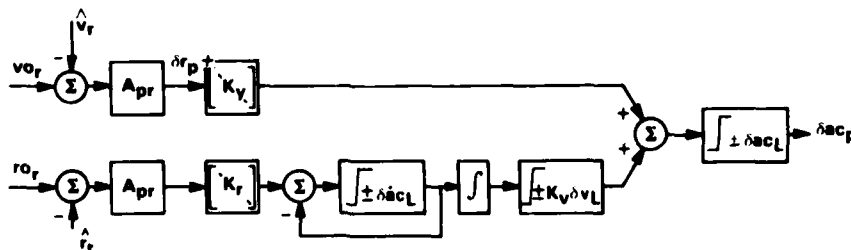


Fig. 24 Translational perturbation dynamics and regulator.

Acceleration response dynamics of the plant are neglected in the system of Fig. 23 on the assumption that these dynamics were much faster ($\omega_n = 2$ rps) than those of the transition dynamics. Experience in the AWJSRA tests showed good maneuver following was usually achieved, but with occasional noticeable tracking errors during lateral maneuvering as a result of this simplification.

The trajectory regulator (TREG) controls the translational perturbation dynamics, which are governed by the system shown in Fig. 24, where $\hat{r}, \hat{v}, \hat{a}$ are disturbances due to navigation errors and uncompensated model and measurement errors and wind disturbance. The desired linear domain dynamics and limiting can be imposed on the kinematic perturbations through an appropriate control law.

The regulator control law for the AWJSRA (Fig. 25) has the following features: (1) each path axis is independently regulated, (2) acceleration response dynamics and Coriolis accelerations are neglected, and (3) the control law is linear for small errors and saturates at larger errors to limit velocity excursions, acceleration authority, and jerk (control rate). Path axes are again the natural reference frame in which to decouple and control the kinematics. The approximations made are consistent with those made in the transition dynamics and they are justified by the low authority and bandwidth of the regulator control law.



CONTROL LAW PARAMETERS

AXES	(ρ, ω_n)	δv_L (m/sec)	δa_{CL} (g)	$\delta \dot{a}_{CL}$ (g/sec)
LONGITUDINAL	(.7, .18)	1.4	.05	.06
LATERAL	(.7, .14)	5.	.1	.065
NORMAL	(.7, .32)	2.1	.1	.1

Fig. 25 Trajectory regulator - AWJSRA.

Parameter values selected for the control law are listed in Fig. 25. In the linear domain, second-order perturbation dynamics, (ρ, ω_n), are imposed on ($\delta r_p, \delta v_p$) by calculating the gains as

$$(k_r, k_v) = (\omega_n^2, 2\rho\omega_n)$$

The authority limits, δa_{CL} , are modest here but have been satisfactory in current tests at modest levels of external disturbances. Position error feedback is both rate- and magnitude-limited (by $\delta a_{CL}, k_v \delta v_L$) in order to satisfy limits at which engine and aerodynamic forces can be varied and to limit the velocity excursions used to relax large position errors to δv_L .

It was also useful to treat the longitudinal position and velocity control specially. The longitudinal position error was erased (up to a limit of 12 m/sec) by resetting the reference trajectory path length in preference to regulating the longitudinal position error. (That is, the normal regulation that drives $\hat{r} \cdot \hat{i}_p$ to $\bar{r} \cdot \hat{i}_p$ is reversed. For brevity, Fig. 25 shows only the normal regulation). This reduces the longitudinal control and the velocity excursions that would otherwise be required to regulate position error.

Further, the longitudinal inertial velocity error is replaced by the airspeed error calculated from the airspeed sensor output. These two modifications resulted in good airspeed control and largely eliminated any dependence of the longitudinal control on the available navigation filter, whose estimation error transients would have introduced unacceptably large longitudinal axis disturbances.

FORCE TRIMMAP

The function of the force trimmap is to compute the control values that will generate those aerodynamic and engine forces required to produce the commanded acceleration. This requires a partial inverse of the plant model, Eqs. (27)-(29), which maps the acceleration command a_r into variables that are controlled by the inner loops (configuration, power, attitude). The element, ACOM, seen in Fig. 18 is omitted in the AWJSRA system; this is equivalent to neglecting the acceleration servo dynamics and is consistent with similar approximations in the trajectory command system.

The general structure of the trimmap algorithm, shown in Fig. 26, is derived next. Details of the specific aircraft are isolated in the basic trimmap element and the remainder of the structure applies to all aircraft.

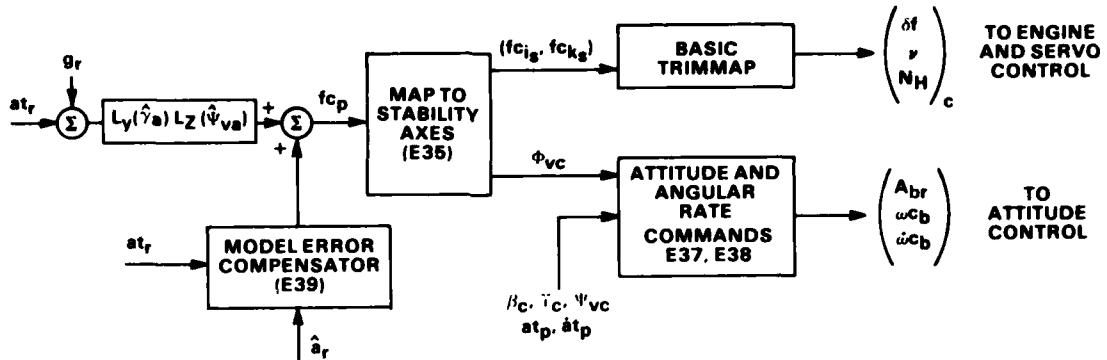


Fig. 26 Force trimmap - flow diagram.

The acceleration command is assumed given in runway axis components and can be transformed to the wind-tunnel stability axes, which are convenient for the solution of Eqs. (27)-(29). First, the applied specific force command in path axes is obtained using the transformation

$$f_{c_p} = L_Y(\hat{\gamma}_a) L_Z(\hat{\psi}_{va})(a_r - g_r) \quad (31)$$

Expressions for the path-axis components of an acceleration vector can be derived in terms of the velocity vector's spherical coordinates, (V, γ, ψ_v) with the result:

$$\bar{a} = \dot{v}\bar{i}_p + V\dot{\psi}_v \cos \gamma \bar{j}_p + V\dot{\gamma} \bar{k}_p \quad (32)$$

These components separately control speed, heading angle, and flightpath angle changes in the aircraft trajectory. Using this form in the expansion of Eq. (31) yields the specific force components as:

$$\begin{pmatrix} f_{c1p} \\ f_{c2p} \\ f_{c3p} \end{pmatrix} = \begin{pmatrix} \dot{v} + \sin \hat{\gamma}_a \\ v_c \dot{\psi}_v \cos \hat{\gamma}_a \\ v_c \dot{\gamma}_c - g \cos \hat{\gamma}_a \end{pmatrix} \quad (33)$$

Next, the transformation to stability axes is

$$f_{c_s} = L_Z(-\beta_c) L_X(\phi_{vc}) f_{c_p} \quad (34)$$

Equation (34) contains five unknowns but this can be reduced to three after noting that β_c is specified independent of the trajectory (usually zero except in decrabbed crosswind landings) and that the side force then follows from β_c and the assumed yaw moment equilibrium of the aircraft as:

$$f_{c_{j_s}} = \frac{Q S_w}{mg} \left(C_{y_\beta} - \frac{b}{l_v} C_{N_\beta} \right) \beta_c \quad (35a)$$

Equation (34) can now be solved to give the roll angle command, ϕ_{vc} , and the specific force commands along the longitudinal and normal stability axes:

$$\left. \begin{aligned}
 f_{c_{i_s}} &= (f_{c_{i_p}} - f_{c_{j_s}} \sin \beta_c) / \cos \beta_c \\
 f_{c_{k_s}} &= -\sqrt{f_{c_{i_p}}^2 + f_{c_{j_p}}^2 - f_{c_{j_s}}^2} \\
 \phi_{vc} &= \tan^{-1}(f_{c_{j_p}} / -f_{c_{k_p}}) + \Sigma
 \end{aligned} \right\} \quad (35b)$$

where

$$\left. \begin{aligned}
 f_{c_{j_s}}^* &= (f_{c_{j_s}} - f_{c_{i_p}} \sin \beta_c) / \cos \beta_c \\
 \Sigma &= \sin^{-1}(f_{c_{j_s}}^* / \sqrt{f_{c_{j_p}}^2 + f_{c_{k_p}}^2})
 \end{aligned} \right\}$$

Equation (35) is the map to stability axes seen in Fig. 26. The specific force commands, $f_{c_{i_s}}$, $f_{c_{k_s}}$ are inputs to the basic trimmap whose function is to solve the lift and drag trim equations. For the AWJSRA, Eqs. (27)-(29) yield these equations as:

$$\begin{pmatrix} f_{c_{i_s}} \\ f_{c_{k_s}} \end{pmatrix} = \frac{T_H}{mg} \begin{pmatrix} \cos(\alpha + v) \\ -\sin(\alpha + v) \end{pmatrix} - \dot{m}_e v_a \begin{pmatrix} 1 \\ 0 \end{pmatrix} - \frac{QS_w}{mg} \begin{pmatrix} C_D \\ C_L \end{pmatrix} \quad (36)$$

The solution of Eq. (36) and the design of the basic trimmap are discussed in the next section.

The trimmap outputs are commands to the inner-loop elements controlling attitude, power, nozzle, and flap. The attitude control is formulated to control the Euler parameters of the transformation between commanded and actual body axes (Refs. 10, 11, 14) and utilizes the commanded body axis transformation as well as angular rate and acceleration commands. A transformation identity is given in the appendix:

$$A_{br}(\phi, \theta, \psi) = L_y(\alpha) L_z(-\beta) L_x(\phi_v) L_y(\gamma) L_z(\psi_v)$$

from which A_{br} can be computed from the five angles $\{\alpha, \beta, \phi_v, \gamma_a, \psi_{v_a}\}$ which are independently defined by the trajectory, the trim solution, and β_c . The required angular velocity can be calculated from the commanded rates of these five independent angles oriented along their respective rotation axes:

$$\bar{\omega}_c = \dot{\alpha}_c \bar{j}_b + \dot{\beta}_c \bar{k}_s + \dot{\phi}_{vc} \bar{i}_p + \dot{\gamma}_c \bar{j}_p + \dot{\psi}_{vc} \bar{k}_r \quad (37)$$

Expressions for body axes components ω_{cb} are omitted here but can be obtained from Eq. (37) using the transformations given in the appendix by Eqs. (A2)-(A5). The angular rates $\{\dot{\gamma}_c, \dot{\psi}_{vc}, \dot{\phi}_{vc}\}$ are functions of the trajectory acceleration and jerk which can be calculated from Eqs. (32)-(35). Similarly, expressions for angular acceleration commands can be obtained from the derivatives of Eq. (37) and Eqs. (32)-(35). Although these computations are too extensive to present in this discussion, they can be simplified after neglecting second-order effects and easily implemented in the flight computer. The more recent alternative formulation of the attitude commands in Fig. 17 as three successive values of A_{br} is equivalent to the present formulation, but is expected to be computationally more efficient and exact in its digital implementation.

For convenience, the model error compensation is included in the trimmap structure and is described next. The trimmap uses a model, $\hat{f}_2^{(T)}$, of the aircraft acceleration as a function of control variables and other trajectory, environment, and aircraft variables. Denote the difference between $\hat{f}_2^{(T)}$ and the actual relation as \tilde{f}_2 . This difference results from numerous sources, including errors in static-force model data, parameter measurement errors in flight, control and attitude offsets and lags, and simplifying approximations or software programming faults in the trimmap; the difference varies in flight with maneuvering and configuration. This difference results in acceleration tracking errors which can be measured in flight and integrated to estimate and compensate the model error; the compensation, b , is:

$$\left. \begin{aligned}
 \epsilon_p &= A_{pr}(a_{tr} - \hat{a}_r) \\
 b_p &= [-k] \int_{t_0}^t \epsilon_p dt
 \end{aligned} \right\} \quad (38)$$

The acceleration error \tilde{f}_2 will include the effects of external disturbances and acceleration measurement errors in addition to $\hat{f}_2^{(T)}$. Neglecting these for the moment, the steady-state behavior of the system for constant \tilde{f}_2 is

$$(\epsilon_p, b_p, \delta r_p, \delta v_p) \rightarrow (0, -\tilde{f}_2, 0, 0) \quad (39)$$

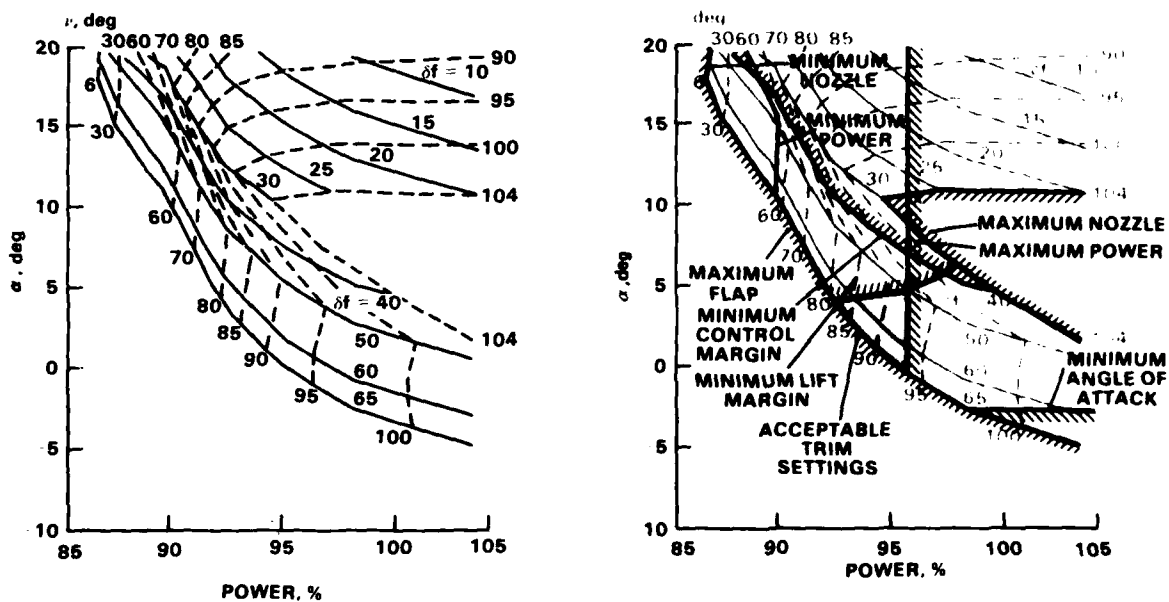
Equation (38) with integrator authority limits of 0.1g to 0.2g was used in the actual trimmap, and Eq. (39) shows that steady-state trajectory tracking performance is independent of model errors for errors within the compensator's authority limit. If $|\hat{f}_2^{(T)}|$ exceeds these limits then the trajectory regulator automatically provides additional compensation at the cost of a steady-state position error and reduced margin to regulate other disturbances. Let $|\hat{f}_2^{(T)}|$ be the model error in excess of the integrator limit and then the system steady state is

$$(\delta a_p, \delta r_p, \delta v_p) + (-\ddot{r}_2, -[k_r^{-1}]\ddot{r}_2, 0) \tag{40}$$

Finally, if $|\ddot{r}_2(T)|$ exceeds the combined authority of the model error compensator and trajectory regulator, then the system diverges from the commanded trajectory.

BASIC TRIMMAP

The function of the basic trimmap is to solve the trim equations, Eqs. (36), for a unique control command, $(\delta f_c, \alpha_c, v_c, N_{H_c})$, given the commanded or measured values of the variables defining the flight condition, $\{v_e, f_{c_s}, f_{k_s}, \theta, \delta, m\}$. Equation (36) is nonlinear with tabulated functions, Eq. (29), and lacks closed-form solutions, but it is readily solved numerically. In addition, the number of unknown controls exceeds the number of equations by two so that arbitrarily many solutions can exist at a given flight condition. This is seen in Fig. 27a, which shows all solutions at a typical glide slope condition. Not all of these are acceptable as trimmap outputs; only those that satisfy the operational constraints on controls usage for quasi-steady flight previously listed in Table 3 are acceptable. The solutions that remain after imposing these constraints are shown in Fig. 27b for the glide slope case. The result, a severe reduction of the usable solutions, is in general the result at all flight conditions. The basic trimmap must, therefore, resolve the trim solution redundancy, subject to constraints on controls usage at all points within the operational flight envelope.



(a) Trim solutions - glide slope.

(b) Acceptable trim solutions - glide slope.

Fig. 27 AWJSRA trim solution redundancy. ($v_e = 65$ knots, $f_{i_s} = -.130$, $f_{k_s} = -.991$, $m = m_0$, $\theta = 1$, $\delta = 1$)

Basic Trimmap Structure

The logical structure of the AWJSRA basic trimmap, shown in Fig. 28, consists of two principal elements: a configuration schedule and a trim solution algorithm. First, the trim solution that optimizes the configuration subject to the controls usage constraints is calculated off-line for the entire flight envelope, and solutions for two of the controls are stored in the flight computer as the configuration schedule. In flight, the configuration schedule commands these two controls as a function of the feed-forward reference trajectory from TCOM. Because the reference trajectory is a sequence of steady flight conditions and

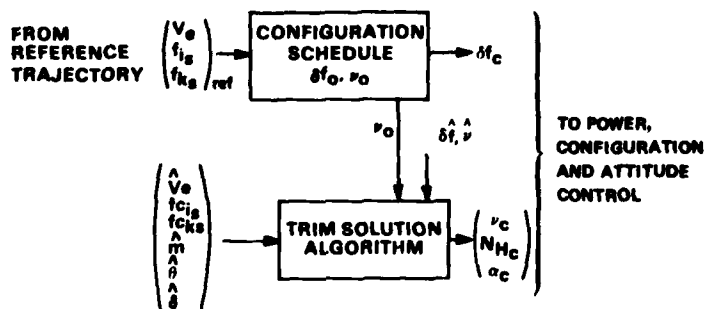


Fig. 28 Basic trimmap structure - AWJSRA.

the maneuvering between these flight conditions, the configuration schedule maintains an optimum configuration at each steady flight condition and coordinates configuration variations during the reference trajectory maneuvering. Secondly, the remaining two controls (termed regulator controls) are calculated in the trim solution algorithm by solving the trim equations at the current flight condition and actual configuration (the actual configuration may lag the commanded one in flight). The specific force command inputs include the feedback from the trajectory regulator and model error compensator, and, therefore, the two regulator controls will differ from their nominal values associated with the reference trajectory and configuration schedule to the extent that the feedback is nonzero. Further, the control margin available from the two regulator controls becomes insufficient at some boundary of the flight envelope, but this boundary can be expanded by designing the trim algorithm to use a configuration control for regulation when necessary as described below. The structure in Fig. 28 using a configuration schedule and a trim algorithm applies to other aircraft as well; for example, for CTOL aircraft, the flap is scheduled and angle of attack and throttle regulate the trajectory.

Several ways of partitioning the AWJSRA controls into regulator and configuration controls were considered; the partition normally used is shown in Fig. 28. Only the flap's response is too slow for its use in path regulation and any pair from $\{\alpha, N_H, v\}$ or all three can be used. The pair $\{\alpha, N_H\}$ is used in CTOL aircraft and can also be used satisfactorily for the AWJSRA throughout its range of configurations. However, the use of all three controls increases the available control margin and operational flight envelope compared to any single pair, so the trim algorithm is designed to vary the nozzle when the primary regulator controls saturate. This arrangement leaves flap and nozzle as the scheduled controls. Alternatively, $\{\alpha, v\}$ can be selected as the primary regulator controls with scheduled flap and power. This regulator pair has greater control margin and orthogonality of its perturbation force outputs in the low-speed, steep-descent STOL regime; it was included in the flight system as a selectable option, but will not be discussed in detail here.

Configuration Schedule

The configuration schedule results from optimization of the configuration at all flight conditions subject to the operational constraints given in Table 3. In general, fuel, noise, or control characteristics can be optimized. For the AWJSRA, control characteristics were optimized in two steps. First, the flap was maximized to obtain maximum lift margin which depends strongly on flap; this is favorable for fuel flow at low speeds but was modified in the high-speed regime to trade excess lift margin for reduced fuel flow. Secondly, the nozzle was scheduled to maximize the regulator control margin for $\{\alpha, N_H\}$, which depends strongly on nozzle setting. (Control margin refers to the envelope of specific forces that can be generated by moving the regulator controls over their permitted ranges for regulator usage (noted in Table 3). It measures the margin of that envelope from the specific force for the reference flight condition and combines both longitudinal- and normal-axis margins in a single scalar measurement; see Ref. 20.) This criterion approximately minimizes sensitivity of the primary regulator pair. For simplicity, the schedules were optimized at standard values of the parameters $\{\theta, \delta, m\}$, (denoted p_0), corresponding to an average weight and standard day sea level conditions. This reduces the computational requirements for the stored schedule at the cost of a small reduction in the operational envelope of the system. The reduction is small because of the narrow range of values for these parameters in the AWJSRA design envelope (Table 2). The resulting flap and nozzle schedules were stored in the flight computer as fitted functions; they are illustrated in Fig. 29a by contour plots on a graph of (v_e, f_{i_s}) for the case that f_{k_s} is $-1 g$ (reference values of f_{k_s} depart very little from this in passenger operations). The corresponding solutions for $\{\alpha, N_H\}$ are shown in Fig. 29. One effect of the scheduling criteria is that the configuration varies with flight condition in such a way that the corresponding steady-state values of $\{\alpha, N_H\}$ remain approximately centered in their allowed ranges until one of the configuration controls reaches a limit. Thus, during transitions between steady flight conditions the configuration changes while the regulator controls change very little, except as required in response to path tracking errors.

The flight envelope achieved by the trimmap-aircraft combination is defined by the selected configuration schedule and is reduced from the envelope of the aircraft alone as a result of any approximations that underlie the stored schedule. The flight envelopes for the present schedule are shown in Fig. 30; the inner boundary shows the limits of equivalent airspeed and longitudinal specific force within which operationally acceptable steady flight is achieved and the outer boundary shows the limits within which trim solutions exist. (Note that the longitudinal specific force reduces to $\sin \gamma$ in Eqs. (33) and (35) for the case of steady flight with zero sideslip, and is sometimes called the equivalent flightpath angle. The use of $V_e - f_{i_s}$ plots to illustrate flight envelopes here simply generalizes the more familiar $V_e - \gamma$ plots for present purposes. Further, the flight envelope is a six-dimensional volume of flight conditions, Fig. 30 shows the two-dimensional cut of this volume which is of most immediate interest.) The region between the two boundaries is the envelope-abuse region in which solutions exist but violate one or more of the constraints in Table 3, as noted in the figure. In practice, this region is a safety buffer for the automatic control because the aircraft may be carried into it unexpectedly by disturbances, particularly during approaches that exploit the minimum V_e, γ boundaries, as does the typical STOL approach shown in Fig. 30. Consequently, the configuration schedule should provide an adequate envelope-abuse region and can be optimized there after selectively relaxing the constraints of Table 3. In the present work, the schedule was optimized within the operational envelope only and the fitted scheduling functions simply extended analytically into the abuse region, but this resulted in the adequate buffer region seen in Fig. 30. Finally, the flight envelope of the AWJSRA alone is shown in Fig. 30 by a dashed line; a comparison with that of the trimmap-aircraft combination shows only a modest loss of envelope as a result of design approximations.

Trim Algorithm

The trim algorithm remains to be described. A flow diagram is shown in Fig. 31; it is constructed from trim routines that assume one of $\{v, \alpha, N_H\}$ is given and solve for the remaining two controls. The fixed-nozzle mode is used initially with the nozzle command specified from the configuration schedule. If a solution fails to exist or exceeds the permitted ranges of $\{\alpha, N_H\}$ for regulation control usage, the algorithm defaults to a different mode which changes the nozzle command from its scheduled value as necessary. If no solution exists for any mode (as a result of inaccurate limiting of the coarse reference trajectory) then the most recent solution is retained. Note that the other control pairs could also have been used in the

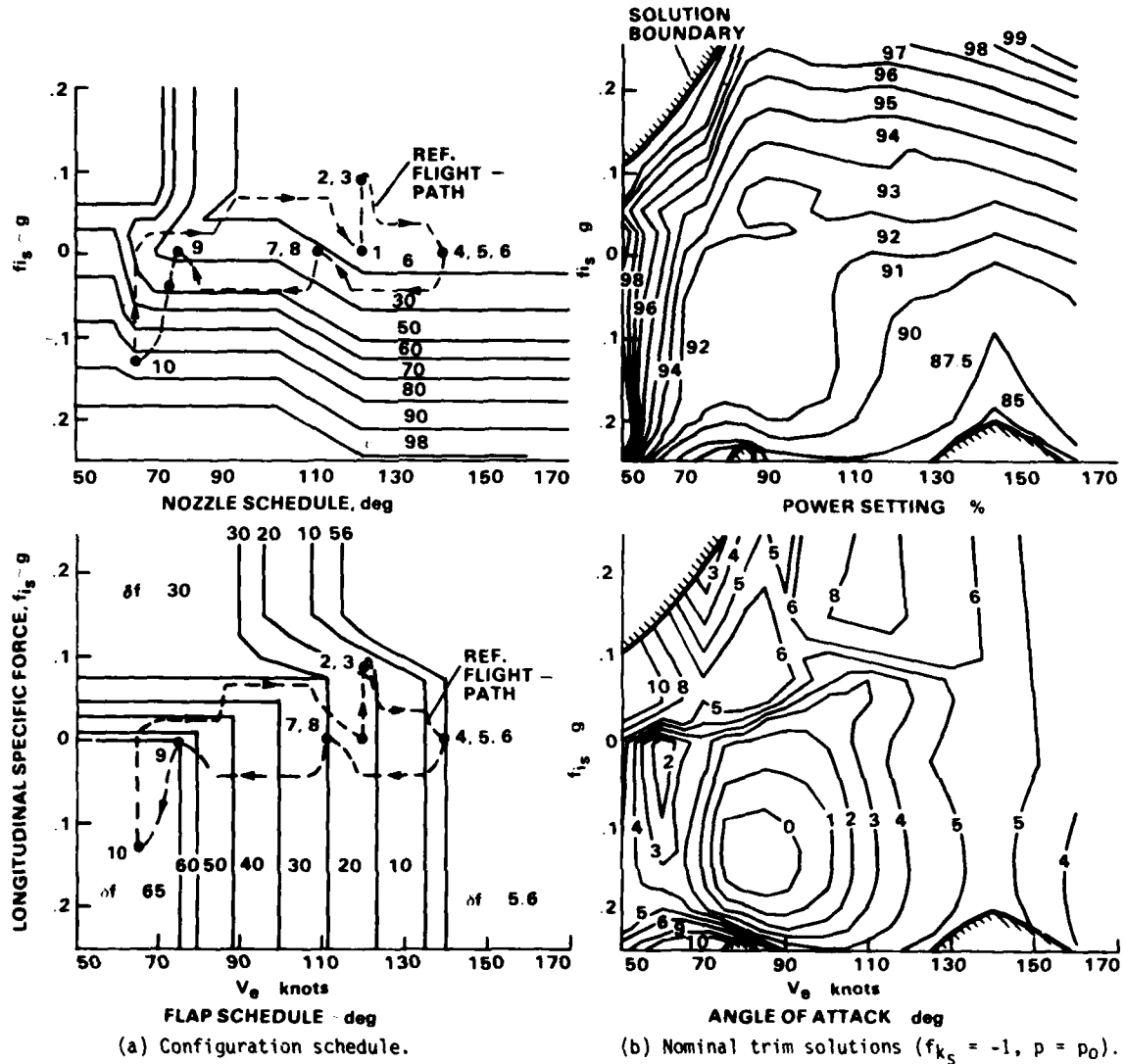


Fig. 29 Configuration schedule and nominal control settings.

neighborhood of the reference flight condition; for example, engine power can be scheduled and the fixed-power mode interchanged with the fixed-nozzle mode in Fig. 31.

The modes required in the trim algorithm were formulated using stored tables of C_L , C_D , T_H , T_C , and \dot{m}_e , and on-line numerical solution of the force balance equations by an exhaustive grid-search method. In the grid-search method, a piecewise linear model is constructed by calculating the specific force output at the grid points used in the data tables for the unknown controls; these linear models can be solved piece by piece until the piece containing the solution is found or the grid is exhausted. Solution existence is thus determined in a number of steps, not exceeding a known upper bound, and uniqueness is determined from properties of the model with selection based on engineering considerations in cases of multiple solutions. For the AWJSRA, a minor region of multiple solutions occurred but posed no significant design question. For conventional aircraft, much simpler models and routines can be used, including closed-form or tabulated solutions (Refs. 11, 14). For VTOL aircraft, such as the tilt rotor, model complexity and nonlinearity may be increased with the result that more powerful solution routines would be necessary.

The accuracy of the trim algorithm force model is measured as the maximum specific force difference over the flight envelope between the trimmap model and the a priori model (apparent accuracy) or between the trimmap model and the actual aircraft (true accuracy), and measured separately for the longitudinal and normal axes. This accuracy is of interest because of its effects on performance and on flight computational requirements. Small but variable model errors disturb the system, larger errors result in position offsets and reduced regulator control margin, and sufficiently large errors cause divergence from the reference path. Control forces of the order of 0.1 g are significant in passenger operations and authority limits for the path and modal error compensators are set at this level. On the other hand, acceleration errors of the order of 0.01 g would result in negligible tracking error transients and reserve the model error compensator authority for the unknown errors of the a priori model. Consequently, 0.01 g is sufficient apparent accuracy and is also an appropriate accuracy goal for the identification of aircraft models to be used in control system design and testing. Further, the trade-off between computational requirements and model accuracy can be of concern, depending on the flight computer and model complexity; for the AWJSRA work, interest centered on meeting a computational time limit in the fixed-nozzle routine with a model of acceptable accuracy. There, a two-dimensional search for $\{\alpha_c, N_H\}$ is required and the available time limited the model's α, N_H grids to five values each. Algorithms were developed and applied to obtain the most accurate tabulated model given the desired table size and a priori model. This resulted in a trimmap model with apparent longitudinal- and

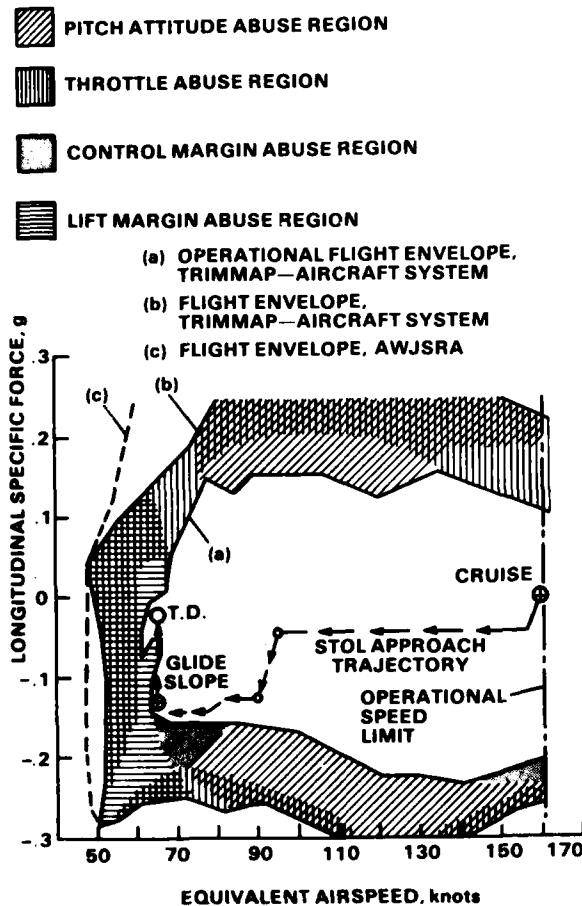


Fig. 30 Configuration schedule: operational flight envelope and envelope abuse region ($f_{k_s} = -1$, $p = p_0$).

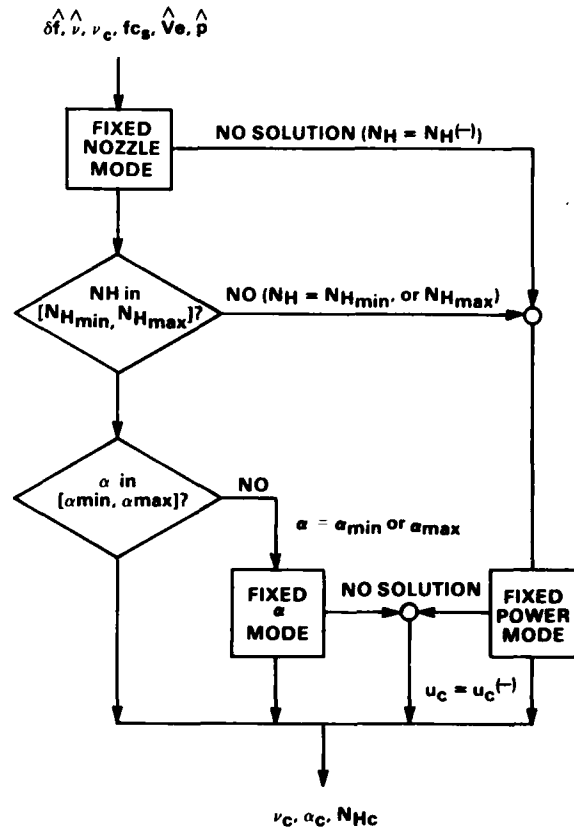


Fig. 31 Trim algorithm - scheduled nozzle algorithm.

normal-axis accuracies of (0.03 g, 0.06 g) within the computational limits imposed. Flight results from the compensator, shown later, measure the true accuracy.

AWJSRA FLIGHT TEST RESULTS

Flight tests of the AWJSRA application of the proposed control design method illustrate the feasibility of the method and the performance achieved by it. The AWJSRA application is termed the "Full Flight Envelope Autopilot" (FFEAP). This aircraft is equipped with the STOLAND digital flight control system developed at Ames Research Center; STOLAND is an integrated hardware and software system (Refs. 24, 25). The hardware includes a Sperry 1819A flight computer and associated control servos, navigation receivers and other sensors, cockpit-display instruments, flight-data recorders, and interfaces for automatic or manual control. The software contains input-output, navigation and display logic, and a hierarchy of manual, assisted-manual, and fully-automatic control modes. The FFEAP was implemented in this structure as a replacement of the existing STOLAND automatic control mode.

Development of the FFEAP proceeded using a sequence of increasingly detailed simulations of the aircraft (Ref. 26); first, the outer-loop logic (ATC, TCOM, TREG, FTRIM) was tested in a simplified simulation in which aircraft forces and the translational degrees of freedom are accurately represented, but all lower levels of the hierarchy (rotational, power, and servo control loops) are represented by the simple response dynamics imposed on the combined control logic and plant dynamics by the innerloop command generators of Fig. 18. Results from this stage of the work are reported in Refs. 20 and 23. Secondly, the inner-loop elements were integrated and tested in a complete simulation of aircraft dynamics on a general purpose scientific computer, with aircraft and engine models taken from the manned laboratory simulation. Finally, the control logic was implemented in the STOLAND system and tested in a manned simulation; this step integrated the control logic with navigation, display, and interface logic.

The final FFEAP flight program was 7,000 words in length; its implementation (Ref. 27) was facilitated by coding and debugging efficiencies inherent in the proposed method. The separation of kinematic from force and moment control allows the kinematic control to be formulated vectorially with identical logic in each of the three translational axes and the three rotational axes; hence, the design, coding, and debugging of one axis suffices for all three axes. Further, commands are generated by the logic for all aircraft and servo states and near-exact tracking is expected in the absence of disturbances so that a comparison of commanded and actual states, beginning at the lowest level of the hierarchy, permits rapid and systematic detection of software faults and significant model errors. The entire program was debugged using 50 hr on the simulator over a period of 3.5 months, beginning from an initial compiled program.

Computational requirements for the proposed method were a feasibility issue in view of the complex models and trim solution algorithms required for the AWJSRA trimmaps. The memory and speed of the 1819A and the available storage and time limits for the FFEAP logic within the STOLAND system are noted in Fig. 32. To meet the time constraint, it was necessary to attend to software efficiencies, limit the search grid of the trim solution algorithm, and execute the outer-loop trajectory control at a slower rate (0.25 sec proved acceptable for the AWJSRA) than the inner loops or the computer's cycle time (0.05 sec). Requirements for the FFEAP were 7,000 words and 31% of the computer cycle time; these are compared in Fig. 32 with requirements for the conventionally designed STOLAND automatic control, which are similar in magnitude. The requirements for the DHC-6 application were much smaller owing to the reduced trimmap complexity; there, the entire automatic control system of Fig. 18 is contained in a 2,500 word program, and this is expected to be representative for conventional aircraft. The available computational power of digital avionics systems will expand greatly in the near future so that the computational constraints of this experiment are only of special interest here, but the results above demonstrate that the system of Fig. 18, using extensive static and dynamic plant models to achieve specified design performance over the full flight envelope, can be achieved in CTOL and STOL aircraft with programs of modest size and with computer requirements that are comparable with those of conventional designs.

The manned simulation and flight tests utilized a standard closed-circuit reference path which is shown in Fig. 33; it includes cruise, transition, approach, go-around, and climb-out segments. Normally, the FFEAP was engaged in the vicinity of way point 7 after which the aircraft was flown automatically through its speed range from 140 knots to the landing airspeed on the approach half and then accelerated to 120 knots for the climb-out. The path descends at -7.5° on the glide slope with climb-out at 5° . An alternative view of the reference path is shown in the configuration schedule plots (Fig. 29) as the locus of flight conditions along the path; the numbered dots locate final flight condition on each leg. The locus is seen to carry the aircraft through the range of configurations and much of its flight envelope.

Estimates and measurements of a number of variables were required as inputs to the automatic control. Estimates of inertial position, velocity, air velocity, and acceleration were required in the outer loop; they were provided by complementary filter navigation logic similar to that of Ref. 28. This system had independent filters for the x,y,z runway axes with navaid and position-dependent gain scheduling, and utilized body-mounted accelerometer and attitude gyro measurements in combination with TACAN or MLS position-measuring navigation aids, baroaltimeter, and pitot-static airspeed measurements. MLS provides precision azimuth and range for the final approach; the MLS coverage limit and the transmitter locations for TACAN and MLS at the test site are indicated in Fig. 33. The navigation filter was also treated to avoid large estimation error transients at switches between TACAN and MLS by reinitializing the filter's position estimate at each switch, and the magnitude of the position jumps at those points was reduced by using MLS to calibrate the TACAN biases. Navigation accuracy was good on the final approach using MLS and for the vertical axis generally; on TACAN, however, it was inadequate for longitudinal control and provided the principal disturbance of the system lateral control. In addition, the trimmap and inner loops required measurements from total temperature and pressure sensors, attitude and angular rate gyros, and sensors for engine power, throttle, and nozzle position, and all control surface positions.

Performance results are illustrated in Fig. 34 with data from one circuit of the reference path in a recent flight test under conditions of low turbulence and winds. The leg number is included with the time histories for easy correlation of control activity with transition maneuvers and other events.

The trajectory commands are shown in Fig. 34a as path-axis components of acceleration, and as airspeed and flightpath angle commands. These illustrate the design features of TCOM previously described. For example, in the turn entries and exits of legs 8, 3, and 5, the lateral acceleration makes rate-limited changes to new steady-state values with little or no overshoot, and the corresponding lateral position and velocity commands (not shown) have no overshoot. Airspeed changes (legs 7, 9, 1) and flightpath angle changes (legs 10, 1, 2, 4) are made with limited acceleration and jerk and no overshoot of the velocity or position states. The adaptive transition initialization results in a jump in the command to the estimated state at

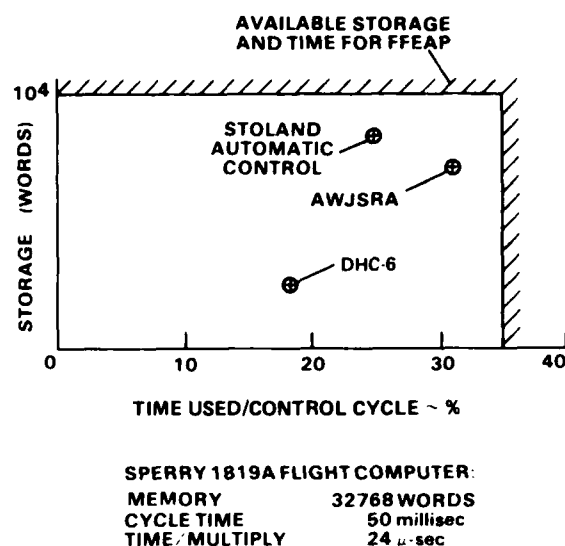


Fig. 32 Computational requirements in flight computer.

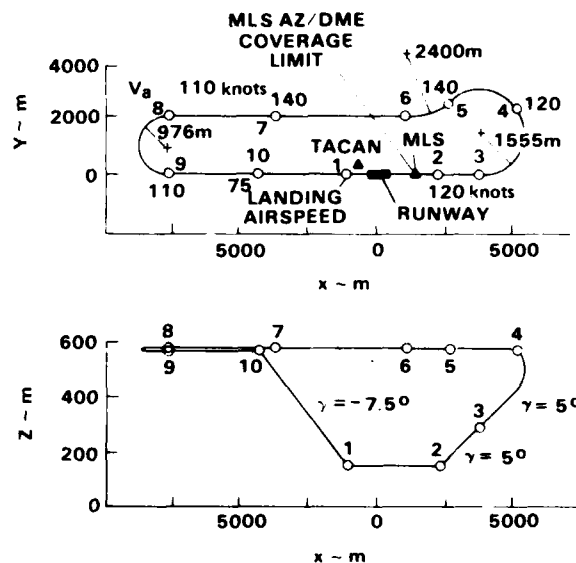
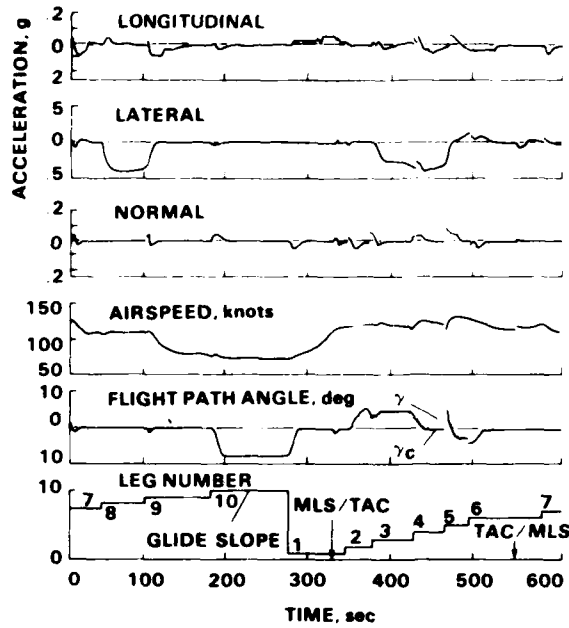
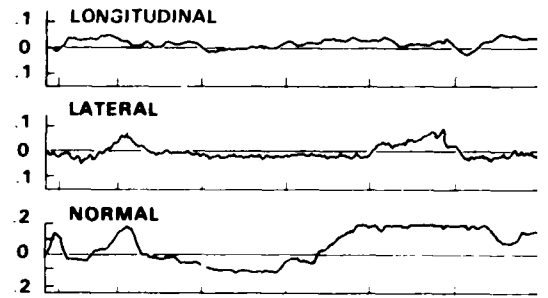


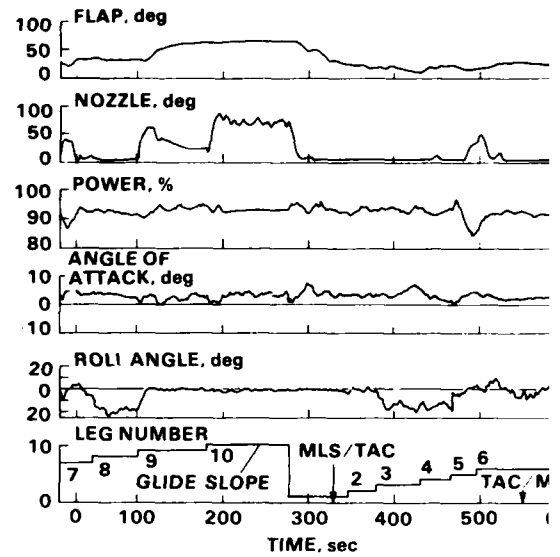
Fig. 33 Reference flightpath.



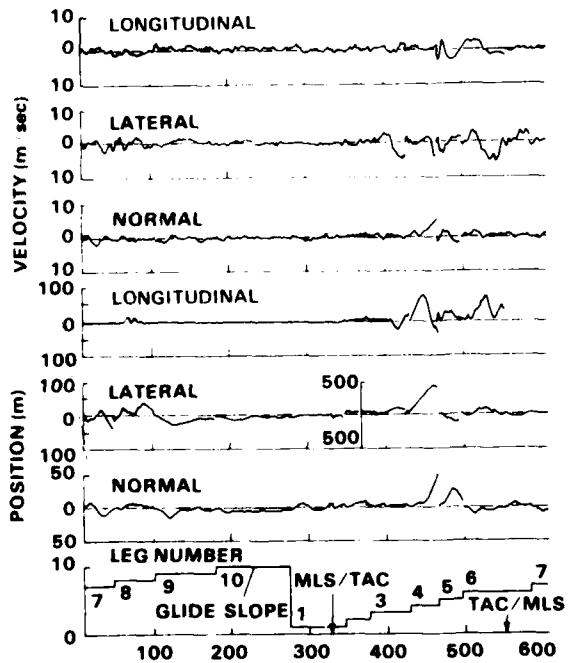
(a) Trajectory commands.



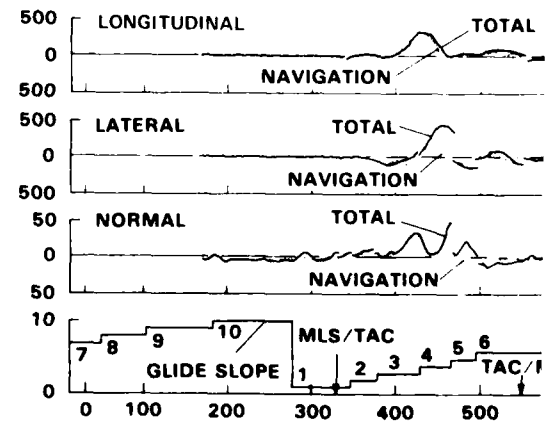
(c) Model error compensation, g.



(d) Force control commands.



(b) Apparent trajectory tracking errors.



(e) Navigation and total system errors - m.

Fig. 34 Representative time histories of AWJSRA operation with FFEAP along the reference path.

the start of each maneuver. Tracking errors were small for the cases noted above and the command jumps were negligible. However, on leg 4, a large flightpath angle error develops (as seen by the departure of the estimated from the commanded value of γ) due to excessive uncompensated model error which is discussed later. Also, a recovery transition command is initiated at the switch to leg 5, which begins with a jump of the command to the estimated flightpath angle and limits the acceleration and flightpath angle overshoot used to relax the initial offsets. Similarly, a noticeable excursion in airspeed command occurs during leg 5 as part of a transition that relaxes significant longitudinal tracking errors at the switch to leg 5. The maneuvering required at switches between TACAN and MLS is minor and reflects the success of the TACAN bias estimation logic in this test.

Figure 34b shows the path-axis components of the apparent trajectory errors as estimated in flight and entered in the feedback. These errors result from external disturbances and estimation and control errors. Turbulence levels and related error transients were low for this test. Estimation and measurement error effects were larger and entered the system as state and acceleration estimation errors that excited the path regulator, and as attitude and control measurement errors that excited the model error compensator. Control errors for the proposed system can all be viewed as plant modeling errors; their effects include low-frequency state- and acceleration-error transients associated with maneuvers and configuration changes, and path divergence if the acceleration model error persistently exceeds the system's compensation authority.

On the longitudinal axis, the principal sensor is the airspeed transducer, with errors which are uniform over the flight envelope and which result in a background of airspeed tracking error below 1.5 m/sec. The Coriolis accelerations, which were neglected in TCOM's kinematic model, result in kinematically incompatible longitudinal velocity and acceleration commands. The effect of this modeling error can be seen as speed error excursions at the turn exits from legs 8 and 4, but is otherwise negligible here and in passenger operations generally. Noticeable longitudinal position excursions occur on legs 8, 3, 4, 5, and 6; they result from large navigation errors.

The principal lateral axis excitation is navigation error; during periods of large position measurement errors (legs 7 and 8 in MLS coverage and throughout TACAN usage), lateral tracking errors are noticeably larger than during the straight-in approach section (legs 9, 10) where MLS provides excellent accuracy. Exceptional excursions in excess of 400 m occur on legs 4 and 5 due to a severe navigation error transient there. The feedback error is nulled at each leg switch as a result of initializing TCOM's transition maneuver adaptively. This has the effect of adding corrective authority; however, tracking errors continue to develop due to continued navigation error.

For the normal axis, turbulence is usually the principal disturbance but its levels were low here and estimation errors are also small for most of the test. This condition resulted in good normal position and speed tracking accuracy, of the order of 5 m and 1 m/sec, respectively, throughout the test, except during legs 4 and 5 where normal velocity error temporarily diverges due to excess (uncompensated) static force model error. Moderate position excursions also occur during path capture and the transitions to legs 9 and 1 due to angle-of-attack estimation error transients and force-model error variations with configuration changes.

The corrective acceleration command (not shown) was usually well within authority limits (0.05 g to 0.1 g) except during the large errors of legs 4 and 5, where all axes saturate. Thus, the transient response for the position and velocity regulation was in the linear domain for most of the flight independent of any nonlinearity in the control activity commanded by the trimmap.

The force-model error compensation (Fig. 34c) shows good longitudinal model accuracy and moderate lateral axis excursions in turns which are due to the combination of lift-model error and roll angle. However, large normal-axis errors were encountered which reached -0.1 g on the glide slope and exceeded the 0.2 g compensator authority during the climb-out at low flap settings (legs 3, 4, 5). Simulator results show good agreement on the glide slope but much smaller model error (0.05 g) at low flap settings.

The large error during climb-out appears to be due to an unfavorable combination of large C_L model error at low flap and angle of attack estimation error. This angle is estimated from gyro angles (using Eq. (A6)) and subject to maneuver-dependent gyro errors (cf. Ref. 29). Lift sensitivity to angle-of-attack error is significant, in excess of 0.1 g/deg here. The consequence of saturated compensation is that position errors develop and engage the state feedback in compensating the model error (Eq. (40)) during legs 3, 4, and 5. Further, this feedback was also saturated on leg 4, leaving the system with no further authority to compensate the remaining normal acceleration error (of the order of 0.03 g) and path divergence occurred, as previously noted. No control was saturated, however, and adequate control capability was present in the aircraft but was unexploited by the present compensator design. Subsequently, recovery occurred when some of TCOM's authority was added in the transition to leg 5 and some of the model error subsided. Other normal-axis model-error transients occurred during capture and leg 8 and the transitions to legs 9 and 1; they are due to gyro errors and model-error variations with configuration.

The simulation model for the DHC-6 was significantly more accurate and Ref. 11 shows measured normal-axis errors below 0.1 g throughout the test path. Model errors in excess of 0.2 g suggest very coarse identification of the plant or accuracy of the on-line measurements, and usually can be improved without exceptional effort. However, the design of the compensator logic for large model errors and methods of using the system of Fig. 18 to measure and reduce such errors systematically remains as a topic for further development.

Flight results for the measured instantaneous acceleration error (not shown) indicate good acceleration tracking throughout the test, with a background of random error below 0.025 g (including measurement error and gust effects), but with normal axis excursions in association with the configuration changes, gyro error transients, and the excess model-error event as previously noted.

Figure 34d shows the control command histories. The configuration controls (normally flap and nozzle) vary as scheduled with TCOM's maneuver commands to maintain an optimized configuration for any output of TCOM. Except on the glide slope, power and α are used for path regulation in the plane of symmetry; local

mean values are approximately constant in midrange independent of maneuvering and flight condition, as intended in the configuration optimization; excursions from these values are dependent on the output of TREG. On the glide slope, the scheduled power algorithm was selected and nozzle shows modest higher frequency activity to control path errors. Roll angle controls lateral forces and varies normally for turns with regulation activity superposed on that. This activity is low during the straight-in approach but noticeably higher elsewhere due to increased lateral-axis navigation errors. Inner-loop performance data are omitted, but flight results showed excellent accuracy in tracking the attitude and servo commands throughout the test so that inner-loop control errors other than those due to sensor errors were a negligible disturbance source.

In this test, the automatic control system used all controls, sometimes simultaneously, to execute a variety of multi-axis maneuvers and to regulate disturbances. This usage is more complex than in manual control where reference paths tend to be a sequence of single-axis maneuvers with associated infrequent discrete configuration changes. The control activity of the automatic system for each axis taken separately was considered acceptable by the pilots, both in this test and in prior simulation experience with increased turbulence. Control activity for all axes collectively was also monitored in the research flights without difficulty; this was facilitated by the organization of the controls into configuration and regulator pairs. More generally, the establishment of monitor work-load constraints and their effect on automatic control usage for redundantly controlled STOL aircraft, such as the AWJSRA, remains an open issue.

Figure 34e shows system position tracking performance as measured by radar. Path-axis components of both navigation and total system errors are shown, but results for the initial legs of the test are absent due to failure of radar coverage there. In general, results show good system performance except on legs 3 and 4, where a large y-axis navigation filter error transient occurs and the model error saturated the system compensation authority.

Large longitudinal navigation errors in excess of 400 m develop in legs 3 and 4, but with little excitation of additional control error. This results from special treatment of the longitudinal control in which the reference trajectory is reset to null the apparent position error (up to a limit of 12 m/sec), and the airspeed sensor is used to compute speed error in preference to using the navigation filter output. In contrast, lateral axis navigation errors due to the y-filter transient rise to 200 m during leg 4 and, together with related excursions in lateral velocity, wind, and acceleration estimation errors of the order of 12 m/sec, and 0.15 g, excite the control strongly and the total system errors exceed 400 m. Normal-axis system error peaks show an excursion of the order of 30 m on leg 3 and a second excursion on leg 4 to 50 m; the first is due to the projection of the y-filter error transient on the normal path axis and excites little added control error because the apparent normal-axis errors remained small, as seen in Fig. 34b. In contrast, the state navigation error is small on leg 4 - it was saturation of the model error compensation in the control system, as previously discussed, that caused the observed system error excursion.

CONCLUDING REMARKS

The concept of inverse dynamic systems provides an effective means for simplifying the control system design process when the aircraft has complex equations of motion and a flight envelope with multiple operational constraints. For a large class of practical systems, a transformation can be constructed that transforms the natural representation of the system into an equivalent linear, constant-coefficient reference model, thereby making the well-developed and powerful tools of linear control theory directly applicable, even when the natural representation is highly nonlinear. Furthermore, the complete control logic is separable into command generators that provide open-loop control, regulators that provide control of uncertainties by means of feedback, and trimmaps that contain detailed information concerning the complete force and moment generation processes of the aircraft and provide envelope limits and control redundancy management.

One result is that the design of regulators is significantly simplified because the control law sees a globally constant-coefficient system. In effect, the trimmaps provide gain scheduling automatically to counteract the changes in the natural perturbation model. Any additional scheduling of the regulator law to account for operational constraints is facilitated by the simplicity of the equivalent system.

A second result is that the design of the reference command generators is simplified by the transformation because of the simplicity of the effective system. The introduction of limiters and rate limiters, for example, in order to shape the reference flightpath to fit the flight envelope is greatly facilitated by the linearity of the effective system.

A third result is that a hierarchy can be established for the complete system in such a way that each level can be designed and tested independently of other levels. Such local autonomy allows multiple sampling-rate designs and the implementation of the complete code within a distributed, asynchronous microcomputer network. In addition, the overall complexity of the control logic can be reduced because greater use of the available a priori information can result in much greater reduction in complexity of the feedback logic.

A fourth result is that details of the force and moment models and their partial inverses are confined to the transformation algorithms at each level of the hierarchy. These models are generally available from aircraft simulations and are nonlinear but algebraic, rather than dynamic.

The proposed design approach has been applied and tested in several aircraft. Detailed descriptions of some elements of the system from the Augmentor Wing Jet STOL Research Aircraft application and results of the flight evaluation of this system have been presented. This information illustrates the design approach in a complex, redundantly-controlled, powered-lift aircraft. A trajectory command generator was derived which is capable of generating reference trajectories with optimized multi-axis maneuvering between any steady flight conditions and of satisfying a variety of safety, passenger comfort and aircraft capability constraints on the kinematics. Near exact tracking of the maneuver commands was usually achieved in the flight results in the absence of other disturbances (external disturbances or estimation and trimmap model error transients). All departures from exact tracking due to simplifying approximations in the command generator's kinematic model are removable without practical difficulty.

Design of the trajectory regulator is inherently simple in that it models the perturbation kinematics, and the desired kinematic transient behavior and constraints can then be imposed explicitly. Invariant kinematic transient dynamics were imposed over the AWJSRA flight envelope and achieved independent of any details of controls usage or configuration. Although this result is dependent on sufficiently accurate modeling of the acceleration perturbation response dynamics, these dynamics are relatively fast for the AWJSRA and were neglected without significant loss of performance.

The force trimmap is the central element of the system; it requires a partial inverse of the system model, which can be complex, and its design affects system performance significantly. Part of the inversion requires only analytical closed-form relations and is valid for all aircraft; the remainder utilizes a configuration schedule and a trim solution algorithm in which details of the specific aircraft appear. The configuration schedule defines an optimum configuration within operational constraints on controls usage at all points in the flight envelope; thus, it coordinates aircraft configuration variations with any maneuver commands from the trajectory command generator. Its design also defines the performance of the system for configuration-dependent parameters of interest (e.g., fuel or noise on any given trajectory, and the system's operational flight envelope). In the trim solution algorithm, both mathematical and performance design issues arose. Efficient algorithms, using a sufficiently accurate model, were required for solving the nonlinear trim equations. Piecewise linear tabulated-data models and an exhaustive grid search algorithm were used and efficiency and accuracy were a function of table size. This method is generally useful for moderately nonlinear aircraft. Further it was necessary to exploit all available controls, including the redundant nozzle control, in order to maximize the control margin at every flight condition and the system's flight envelope.

Flight results with the AWJSRA system operating over a complex test path were presented. Good tracking performance was normally achieved at all levels of the hierarchy (trajectory, acceleration, attitude, power, and servos); with one exception, this indicated that satisfactory modeling accuracy of the aircraft at all levels was obtained from the available simulation data. The larger trajectory error excursions observed were due in part to disturbance by navigation error transients and in part to control-system model errors, principally in the static-force model. With one exception, these latter effects were of moderate size, and steady-state performance was unaffected by model errors within the trimmap compensation authority, which corresponded to relatively coarse models (0.1 g to 0.2 g). The time histories of trajectory and compensator errors provide information for updating the force trimmap or the underlying simulation model.

In summary, flight test results to date have demonstrated in a realistic airborne computation, control, and navigation environment that the proposed method can yield effective automatic flight control systems for CTOL and STOL aircraft.

APPENDIX

REFERENCE FRAMES AND TRANSFORMATIONS

It is useful to define the reference frames and related notation used in the AWJSRA development. Subscripts indicate the axis frame to which a vector is referred, $(\)_a$, and transformations of a vector from frame a to frame b are denoted A_{ba} . The frames used here are runway (r), path (p), wind-tunnel stability (s), and body (b). Unit vectors defining the axes of frame a are denoted $(\hat{i}_a, \hat{j}_a, \hat{k}_a)$, and the components of a vector along these axes are denoted $(\)_{i_a}, (\)_{j_a}, (\)_{k_a}$. For brevity, transformations will be defined as a sequence of single-axis rotations, using the notation L_x, L_y, L_z where the subscript indicates the axis of rotation and

$$\{L_x(\sigma), L_y(\sigma), L_z(\sigma)\} = \left\{ \begin{bmatrix} 1 & 0 & 0 \\ 0 & \cos \sigma & \sin \sigma \\ 0 & -\sin \sigma & \cos \sigma \end{bmatrix}, \begin{bmatrix} \cos \sigma & 0 & -\sin \sigma \\ 0 & 1 & 0 \\ \sin \sigma & 0 & \cos \sigma \end{bmatrix}, \begin{bmatrix} \cos \sigma & \sin \sigma & 0 \\ -\sin \sigma & \cos \sigma & 0 \\ 0 & 0 & 1 \end{bmatrix} \right\} \quad (A1)$$

The aircraft body axes are located with respect to runway or inertial axes by the standard Euler angle transformation:

$$A_{br} = L_x(\phi)L_y(\theta)L_z(\psi) \quad (A2)$$

Path axes are a convenient frame in which to define and control the aircraft translational kinematics; these are, respectively, along the path tangent or velocity vector and perpendicular to the tangent in the horizontal and vertical planes. The transformation from runway axes depends only on the angles defining the velocity vector direction,

$$A_{pr} = L_y(\gamma)L_z(\psi_v) \quad (A3)$$

where ψ_v is the heading angle of the velocity vector. Where path axes are based on the velocity vector with respect to the air mass, the angles are denoted γ_a and ψ_a . The transformation from path axes to wind-tunnel stability axes is obtained by first rotating about the tangent vector through the angle ϕ_v and then about the normal axis through the sideslip angle:

$$A_{sp} = L_z(-\beta)L_x(\phi_v) \quad (A4)$$

Wind-tunnel stability axes are convenient for use in solving the force-balance equations used in the force trimmap since aircraft lift and drag forces are aligned with its axes. The transformation from stability axes to body axes is

$$A_{bs} = L_y(\alpha) \quad (A5)$$

Equations (A3)-(A5) provide a transformation from runway to body axes that is equivalent to Eq. (A2):

$$A_{br}(\phi, \theta, \psi) = A_{bs}(\alpha) A_{sp}(\beta, \phi_v) A_{pr}(\gamma_a, \psi_{v_a}) \quad (A6)$$

Aircraft attitude depends in Eq. (A6) on angles locating the velocity vector (γ_a, ψ_{v_a}) and controlling the aerodynamic force (ϕ_v, β, α). Expressions for any three angles in terms of the remaining five can be given from Eq. (A6).

REFERENCES

1. Vinkler, Aharon; and Wood, Lincoln, J.: A Comparison of Several Techniques for Designing Controllers of Uncertain Dynamic Systems. Proceedings of The 1978 IEEE Conference on Decision and Control, San Diego, 1979.
2. Landau, Yoan D.: Adaptive Control. Marcel Dekker, Inc., New York, 1979.
3. Erzberger, Heinz: Analysis and Design of Model Following Systems by State Space Techniques. Proceedings of the Joint Automatic Control Conference, Ann Arbor, 1968.
4. Kunceovich, Vsevolod; and Luchak, Michael: Synthesis of Automatic Control Systems by Means of Lyapunov Functions. Nauka, Moscow, 1977.
5. Luenberger, David, G.: Canonical Forms for Linear Multivariable Systems. IEEE Transactions on Automatic Control, vol. AC-12, no. 3, June 1967.
6. Sain, Michael K.; and Massey, James L.: Invertibility of Linear Time-Invariant Dynamical Systems. IEEE Transactions on Automatic Control, vol. AC-14, no. 3, June 1969.
7. Silverman, Leonard M.: Inversion of Multivariable Linear Systems. IEEE Transactions on Automatic Control, vol. AC-14, no. 3, June 1969.
8. Krener, Arthur J.: On the Equivalence of Control Systems and the Linearization of Nonlinear Systems. SIAM J. on Control, vol. 11, no. 4, July 1973.
9. Brockett, Roger W.: Feedback Invariants for Nonlinear Systems. IFAC Congress, Helsinki, 1978.
10. Meyer, George; and Cicolani, Luigi: A Formal Structure for Advanced Automatic Flight Control Systems. NASA TN D-7940, 1975.
11. Wehrend, William R., Jr.; and Meyer, George: Flight Tests of the Total Automatic Flight Control System (TAF COS) Concept on a DHC-6 Twin Otter Aircraft. NASA TP-1513, 1980.
12. Wehrend, William R., Jr.: Pilot Control through the TAF COS Automatic Flight Control System. NASA TM-81152, 1979.
13. Smith, G. Allan; and Meyer, George: Total Aircraft Flight Control System Balanced Open- and Closed-Loop Control with Dynamic Trimmings. 3rd Avionics Conference, Dallas, 1979.
14. Smith, G. Allan; and Meyer, George: Application of the Concept of Dynamic Trim Control to Automatic Landing of Carrier Aircraft. NASA TP-1512, 1980.
15. Skavdahl, H.; and Patterson, D. M.: The Development of an Augmentor Wing Jet STOL Research Aircraft. NASA CR-114504, 1972.
16. Quigley, H. C.; Innis, R. C.; and Grossmith, S.: A Flight Investigation of the STOL Characteristics of an Augmented Jet Flap STOL Research Aircraft. NASA TM X-62334, 1974.
17. Whitley, D. C.; and Cook, W. L.: Comparison of Model and Flight Test Data for an Augmentor Wing STOL Research Aircraft. AGARD CP-187, Flight/Ground Testing Facilities Correlation, Apr. 1976.
18. Rumsey, P. C.; and Spitzer, R. E.: Simulator Model Specification for the Augmentor Wing Jet STOL Research Aircraft. NASA CR-114434, 1971.
19. Cleveland, W. B.; Vomaska, R. F.; and Sinclair, S. R. M.: Augmentor Wing Jet STOL Research Aircraft Digital Simulation Model. NASA TM X-62149, 1972.
20. Cicolani, L. S.; Sridhar, B.; and Meyer, G.: Configuration Management and Automatic Control of an Augmentor Wing Aircraft with Vectored Thrust. NASA TP-1222, 1979.
21. Mefley, R. K.; Stapleford, R. L.; and Rumald, R. C.: Airworthiness Criteria Development for Powered Lift Aircraft. NASA CR-2791 (FAA-RD-76-195), 1977.
22. Pecsvaradi, T.: Four Dimensional Guidance Algorithms for Aircraft in an Air Traffic Environment. NASA TN D-7829, 1975.
23. Cicolani, L. S.; and Weissenberger, S.: A Nonlinear Command Generator for a Digital Flight Control System. NASA TP-1221, 1978.
24. Neuman, F.; Watson, D. M.; and Bradbury, P.: Operational Description of an Experimental Digital Avionics System for STOL Airplanes. NASA TM X-62448, 1975.

25. Grgurich, J.; and Bradbury, P.: STOLAND Final Report. NASA CR-137972, 1976.
26. Cicolani, L. S.; and Meyer, G.: Digital Simulation of a V/STOL Aircraft for Autopilot Research. Large Scale Dynamic Systems, NASA SP-371, 1974.
27. Goka, T.; and Schueller, M.: Implementation of the FFEAP on the NASA-Ames STOLAND-AWJSRA Digital Avionics Computer. Analytical Mechanics Associates Report 79-14, Oct. 1979.
28. Neuman, F.; and Warner, D. N.: A STOL Terminal Area Navigation System. NASA TM X-62348, 1974.
29. Warner, D. N.; and Moran, F. J.: Flight Test of Navigation and Guidance Sensor Errors Measured on STOL Approaches. NASA TM-81154, 1979.

MANAGEMENT OF REDUNDANCY IN FLIGHT CONTROL SYSTEMS USING OPTIMAL DECISION THEORY

by
Raymond C. Montgomery
Aero-Space Technologist
NASA Langley Research Center
Hampton, Virginia 23665

SUMMARY

This chapter addresses the problem of using redundancy that exists between dissimilar systems in aircraft flight control. That is, using the redundancy that exists between a rate gyro and an accelerometer--devices that have dissimilar outputs which are related only through the dynamics of the aircraft motion. Management of this type of redundancy requires advanced logic so that the system can monitor failure status and can reconfigure itself in the event of one or more failures. In this chapter an optimal decision theory is tutorially developed for the management of sensor redundancy and the theory is applied to two aircraft examples. The first example is the space shuttle and the second is a highly maneuvering high performance aircraft--the F8-C. The examples illustrate the redundancy management design process and the performance of the algorithms presented in failure detection and control law reconfiguration.

I. INTRODUCTION

Reliable sensor and actuator systems are particularly critical to high performance aircraft that rely on feedback to augment aircraft stability. One technique for assuring reliable operating is to provide redundant systems together with the logic for managing them. In the past, for sensor components, this has been accomplished using duplication of components and a simple voting process to manage the redundancy. Redundancy provided in that way can be termed "hardware" or "duplicative" redundancy since it owes its existence to hardware duplication. Redundancy also exists between dissimilar components. However, to use that type of redundancy, one must be aware of the dynamic behavior of the system and the interactions between system components. Such redundancy is more properly termed "analytical" redundancy since it owes its existence to analytical knowledge of the systems behavior. Unfortunately, analytical redundancy management involves real time modeling of the vehicle dynamics and a vast amount of logic. For that reason its use to this time has been confined to research vehicles.

For control surfaces the former option of hardware redundancy is not normally available. This is because, in aircraft, the effects on vehicle motion are usually different for two different surfaces. Thus, if redundancy is used, one must necessarily rely on "analytical" redundancy management since the components involved are necessarily dissimilar. The past resolution of this problem has seldom been to use redundant control surfaces but to obtain the system reliability level required by making the actuator essentially "fail proof." Developing analytical redundancy management technology to the point that it is a dependable tool of the control system designer has obvious advantages to the aerospace community in terms of survivability potential. To accomplish that objective, however, continued research will be needed. The purpose of this chapter is to explain the theoretics of analytical redundancy management from a tutorial point of view and to illustrate its use with examples using the dynamics of the space shuttle and the dynamics of the F8-C aircraft. Herein, a particular method has been selected for exposition--a moving window technique of sensor analytical redundancy management that was originally developed for the space shuttle and was later studied for the F8-C. This work was reported in references 2 and 3. This chapter contains pertinent extracts of these references as required to tutorially develop the analytical redundancy management method selected. For the interested reader, reference 1 provides an excellent survey of failure detection which is one aspect of the analytical redundancy management field.

II. THE THEORETICS OF ANALYTICAL REDUNDANCY MANAGEMENT

Consider the equations of motion of an aircraft to be represented by the nonlinear differential equation

$$\dot{x} = f(x, u) \quad (1)$$

where x is an n -dimensional state vector and u is an m -dimensional control vector. For aircraft, the function $f(x, u)$ is a continuous vector function that is differentiable in x and u . For the purpose of designing a redundancy management system controlled by a digital computer, a difference equation representation of the aircraft dynamics is useful. It can be considered to be of the form

$$x(k+1) = \phi[x(k), u(k)] + w(k)$$

where $x(k) \triangleq x(k\tau)$, $u(t)$ in equation (1) is equal to $u(k)$ for $k\tau < t < (k+1)\tau$, and τ is the cycle time for the digital control system. The term $w(k)$ represents the error in integration of (1) and any unmodelled dynamic effects (e.g. atmospheric turbulence). We shall consider $w(k)$ to be a white stationary Gaussian random process with zero mean and covariance matrix W so that $E[w(k)w^T(j)] = W\delta_{kj}$. For colored noise the model state is assumed to be extended so that the process $w(k)$ is essentially white

Sensors y will be considered to measure the vector function

$$y(k) = h^0[x(k), u(k)] + v^0(k)$$

for the unfailed state H_0 . The sequence $v^0(k)$ represents the measurement error and is considered to be a zero mean white Gaussian process for the purpose of design. For the failure states H_i , $1 \leq i \leq M-1$, it is assumed that the sensors' outputs are the same as those for the unfailed states except for y_1 , whose output is assumed to be a Gaussian process with unknown mean. Hence, for each of the $M-1$ failure states H_i the sensor outputs are

$$H_i: y(k) = h^i[x(k), u(k)] + v^i(k), 1 \leq i \leq M-1$$

where

$$E[v^i(k)] = m_i$$

$$E[v^i(k)v^{i^T}(j)] = V_v^i \delta_{kj}$$

The quantity m_i is an unknown parameter vector representing the mean of $v^i(k)$. It is also convenient to introduce a dummy hypothesis H_M with a priori probability $P_{H_M} = 0$ with $H_M: y(k) = v^0(k)$.

We shall be concerned with selecting the most probably failure state H_i based on a finite set of measurements, $Y(k) = [y(1), y(2), \dots, y(k)]$. To do this, a cost function is constructed of the form

$$\beta = \sum_{i=0}^M \sum_{j=0}^M P_{H_j} C_{ij} \int_{Z_i} P_{Y|H}(\alpha|H_j) d\alpha \quad (2)$$

subject to

$$\sum_{i=0}^M P_{H_i} = 1$$

and where the sets Z_i , $0 \leq i \leq M$, are disjoint and their union represents the entire observation space. In equation (2): P_{H_i} = a priori probability of H_i occurring; C_{ij} = cost weight for selecting H_j when H_i is true; and, $P_{Y|H}(\alpha|H_i)$ is the conditional probability density of measurement sequence α given H_i . The symbol \int_{Z_i} implies that the integral is carried out over the set Z_i that represent decision regions in the observation space so that when $Y \in Z_i$ we will assume that H_i is true. Of course, that is a possibility that an error might exist in the decision process. That is, $Y \in Z_i$, but H_j is true. The function β is selected so that it represents the cost of making an incorrect decision. This function is then minimized analytically by selecting the zones Z_i . The terms in equation 2 may be interpreted in the following way. Each of the integral terms represents the probability that a measurement sequence is in Z_i and hypothesis H_j is true. Hence, each integral term represents the probability of selecting H_i when H_j is true. These terms are multiplied by the a priori probability of H_j occurring, P_{H_j} , and design weighting constants C_{ij} to obtain the total cost function referred to in reference 2 as the Bayesian risk function. Therefore, the function β represents the cost of assigning any decision structure, Z_i . We shall assume that the cost weights C_{ij} assigned for making a correct decision are zero ($C_{ii} = 0, i = 0, \dots, M$) and that the cost of making an incorrect decision is positive ($C_{ij} \geq 0, i \neq j$). The weights to be used in designing the failure detection scheme can be selected by conducting a failure mode and effects analysis. That is, by simulating of the system in a given failure state, say H_i , and examining the response characteristics corresponding to a control system selection of state H_j . This type of simulation is illustrated in examples to follow.

The problem, then, is to select boundaries of Z_i which will result in minimum cost. The general solution to the problem is represented most easily in terms of likelihood ratios Λ_i , where

$$\Lambda_i(\alpha) = P_{Y|H}(\alpha|H_i) / P_{Y|H}(\alpha|H_M), i = 0, \dots, M-1$$

The cost function β of equation (2) may be rewritten as

$$\beta = \sum_{i=0}^M \int_{Z_i} \psi_i(\alpha) d\alpha$$

where

$$\psi_i(\alpha) = \sum_{j=0}^M P_{H_j} C_{ij} P_{Y|H}(\alpha|H_j)$$

This function is minimized by selecting i at each point α in the observation space such that $\psi_i(\alpha)$ is the smallest of the $M+1$ possible values $\psi_k(\alpha)$, $0 \leq k \leq M$. Hence,

$$Z_i = \{\alpha | \psi_i(\alpha) = \min_{0 \leq k \leq M} \psi_k(\alpha)\}$$

Dividing each ψ_i by the probability density of $Y(k)$ under H_M gives an equivalent test term, $\tau_i(\alpha)$, for making the decision in terms of the likelihood ratios:

$$\tau_i(\alpha) = \sum_{j=0}^{M-1} P_{H_j} C_{ij} \Lambda_j(\alpha)$$

Then

$$Z_i = \{\alpha | \tau_i(\alpha) = \min_{0 \leq k \leq M-1} \tau_k(\alpha)\}$$

Consider now the problem of mechanizing the preceding test. That is, the problem of determining the likelihood ratios $\tau_i(\alpha)$ for the hypothesis

$$H_i: y(k) = h^i[x(k)] + v^i(k), \quad i=0, 1, \dots, M-1, \quad k=0, 1, \dots, K$$

By the chain rule for probability densities,

$$p[Y(k)|H_i] = p[y(k)|Y(k-1), H_i] \cdot p[Y(k-1)|H_i] = p[y(1)|H_i] \prod_{j=2}^k p[y(j)|Y(j-1), H_i]$$

Since under hypothesis H_i , $y(j) = h^i[x(j)] + v^i(j)$ and h is nonlinear, the probability density $p[y(j)|Y(j-1), H_i]$ is not Gaussian. However, the first two moments can be expressed by

$$E\{y(j)|Y(j-1), H_i\} = \hat{h}^i[x(j)] + m_i$$

where

$$\hat{h}^i[x(j)] = E\{h^i[x(j)]|Y(j-1), H_i\}$$

and $m_i = E\{v^i\}$; and

$$\text{var}(y(j)|Y(j-1), H_i) = V_h^i(j|j-1) + V_v^i$$

where

$$V_h^i(j|j-1) = E\{[h^i(x(j)) - \hat{h}^i(x(j))][h^i(x(j)) - \hat{h}^i(x(j))]^T | Y(j-1), H_i\}$$

If it is assumed that the density $p[y(j)|Y(j-1), H_i]$ is Gaussian, then the first two moments give the pseudo-Bayes density function

$$p[y(j)|Y(j-1), H_i] = ((2\pi)^N \det[V_h^i(j|j-1) V_v^i])^{-1/2} \cdot \exp\{-1/2[y(j) - \hat{h}^i(x(j)) - m_i]^T [V_h^i(j|j-1) + V_v^i]^{-1} [y(j) - \hat{h}^i(x(j)) - m_i]\}$$

where $N = \dim(y)$. McLendon (Ref. 4) shows that, when the variance $V_h^i(j|j-1)$ is small compared to V_x^i the pseudo-Bayes assumption can be justified analytically.

Then the likelihood ratio becomes, after some simplification,

$$\Lambda_i(K) = \prod_{j=1}^K \frac{\{\det(V_v^0)\}^{1/2}}{\{\det[V_h^i(j|j-1) + V_v^i]\}^{1/2}} \cdot \exp \frac{1}{2} \sum_{j=1}^K \left\{ \left[y(j)^T V_v^{0-1} y(j) - \{y(j) - \hat{h}^i[x(j)] - m_i\}^T \cdot [V_h^i(j|j-1) + V_v^i]^{-1} \{y(j) - \hat{h}^i[x(j)] - m_i\} \right] \right\}$$

In order to calculate this likelihood ratio, one must have values for $\hat{h}^i[x(j)]$ and $V_h^i(j|j-1)$. Since h is nonlinear, these cannot be computed exactly; however, expanding $\hat{h}^i[x(j)]$ in a Taylor series to first order about $\hat{x}^i(j|j-1) = E\{x(j)|Y(j-1), H_i\}$ gives $\hat{h}^i[x(j)] = h[\hat{x}^i(j|j-1)]$ and

$$V_h^i(j|j-1) = (\partial \hat{h}^i / \partial x)[\hat{x}^i(j|j-1)] V_x^i(j|j-1) \cdot (\partial \hat{h}^i / \partial x)[\hat{x}^i(j|j-1)]^T$$

where $V_x^i(j|j-1)$ is the variance of $\hat{x}^i(j|j-1)$. In reference 2 for linear systems $\hat{x}^i(j|j-1)$ was obtained using a linear discrete Kalman filter. For the nonlinear problem, however, a nonlinear estimator is required. The result can be obtained only approximately for the nonlinear case using an approximate conditional-mean filter (Ref. 5). Consider H_i , and define

$$\hat{x}^i(k+1) \triangleq E\{x(k+1)|Y(k+1), H_i\}$$

$$\hat{x}^i(k+1|k) = \phi[\hat{x}^i(k), u(k)]$$

and

$$r^i(k) \triangleq y(k) - h[\hat{x}^i(k), u(k)] - \tilde{m}_i(k)$$

where $\tilde{m}_i(k)$ is the maximum likelihood estimate of m_i over the observation sequence. With these definitions, the filter algorithm is

$$\hat{x}^i(k+1) = \hat{x}^i(k+1|k) + K^i(k+1)r^i(k+1)$$

The gain matrix $K^i(k)$ can be calculated using

$$K^i(k+1) = V_x^i(k+1|k) (\partial \hat{h}^i / \partial x)[\hat{x}^i(k+1|k), u(k+1)] [V_y^i(k+1)]^{-1}$$

$$V_y^i(k+1) = (\partial \hat{h}^i / \partial x)[\hat{x}^i(k+1|k), u(k+1)] \cdot V_x^i(k+1|k) (\partial \hat{h}^i / \partial x)[\hat{x}^i(k+1|k), u(k+1)]^T \cdot u(k+1) + V_v^i$$

where $V_x^i(k+1|k)$ is the prediction error covariance given by

$$V_x^i(k+1|k) = (\partial \phi / \partial x)[\hat{x}^i(k), u(k)] V_x^i(k) (\partial \phi / \partial x)[\hat{x}^i(k), u(k)]^T + W$$

and $V_x^i(k)$ is the filter error covariance satisfying

$$V_x^i(k+1) = [I - K^i(k+1)] \cdot (\partial h / \partial x)[\hat{x}^i(k+1), u(k)] V_x^i(k+1|k)$$

Hence, for each H_i there is a filter algorithm, as indicated previously, required to accomplish the decision process. The structure of the optimal decision logic that might be implemented in a digital flight control system is indicated in figure 1. To simplify the decision process, we may take $C_{ij} = 1$, $i \neq j$. In this case the optimal decision process involves selecting for each measurement sequence $Y(K)$ the hypothesis corresponding to maximizing

$$\ln P_{H_i} = \ln \prod_{j=1}^K \frac{1}{y} |V_y^i(j)| - \frac{1}{2} \sum_{j=1}^K r^i(j)^T V_y^{i-1}(j) r^i(j)$$

where K is the total number of measurements taken to make the decision and is indicative of the window size in a moving window.

III. APPLICATION OF ANALYTIC REDUNDANCY MANAGEMENT TO AIRCRAFT

This section will illustrate the application of the theory explained in the last section using two examples. The first example will emphasize the selection of the weights C_{ij} of the Bayesian risk function to give the reader a feel for the importance of this necessary step in the process. To do this we will use the space shuttle as an example vehicle with linear models and linear simulation. Next, the performance of the analytic redundancy management system will be illustrated for a high-performance, highly maneuvering aircraft--the F8-C aircraft--in high performance roll maneuvers. The later example illustrates the necessity for including nonlinear kinematics in the analytical model.

Example 1. To obtain insight into the process of Bayesian risk weight selection, consider the space shuttle orbiter configuration at a Mach number of 5 and an altitude of 120,000 ft. Taking the state to be defined as $x = (p, \dot{p}, r, \beta)^T$ and the only effective control $u = \delta_a$ the aircraft equations of motion can be written as

$$\dot{x} = \begin{bmatrix} -0.0580 & 0 & 0.0170 & -5.791 \\ 1.0 & 0 & 0.5773 & 0 \\ -0.0029 & 0 & -0.0085 & -0.7438 \\ 0.5 & 0.0055 & -0.8660 & -0.0009 \end{bmatrix} x + \begin{bmatrix} 2.256 \\ 0 \\ 0.0553 \\ 0 \end{bmatrix} u + w$$

The noise process w is considered to be a Gaussian zero-mean process with a covariance matrix $W = \text{diag}[.005, 0, 2.02, .000003]$.

For illustration, consider that the vehicle has three sensors: a roll-rate gyro, a yaw-rate gyro, and a sideslip indicator. To design the bank of Kalman filters for this case the output matrixes are selected so that all sensor information is included for H_0 and the i th sensor is deleted from the output for H_i . There will, therefore, be four hypotheses to consider, as follows

$$H_0: y = \begin{bmatrix} 1 & 0 & 0 & 0 \\ 0 & 0 & 1 & 0 \\ 0 & 0 & 0 & 1 \end{bmatrix} x + v_0; \quad H_1: y = \begin{bmatrix} 0 & 0 & 0 & 0 \\ 0 & 0 & 1 & 0 \\ 0 & 0 & 0 & 1 \end{bmatrix} x + v_1; \quad H_2: y = \begin{bmatrix} 1 & 0 & 0 & 0 \\ 0 & 0 & 0 & 0 \\ 0 & 0 & 0 & 1 \end{bmatrix} x + v_2; \quad H_3: y = \begin{bmatrix} 1 & 0 & 0 & 0 \\ 0 & 0 & 1 & 0 \\ 0 & 0 & 0 & 0 \end{bmatrix} x + v_3$$

Note that, with the above construction of the output matrices, sensor i cannot corrupt the state estimate of the Kalman filter conditioned under H_i . Variances of the measurement error are taken, consistent with current technological capability, to be

$$v_v^0 = \text{diag} [(0.05)^2, (0.01)^2, (0.01)^2]$$

Failure covariances are assumed to be larger than the unfailed ones. (The failure detection performance of the resulting system has, however, been successfully demonstrated for both statistical failures--increased variances--and for hardover failures. This capability is a direct result of not assuming a zero-mean measurement error in the failure states.) The values of v_v^1 , v_v^2 and v_v^3 used are

$$v_v^1 = \text{diag} (0.025, 0.0001, 0.0001)$$

$$v_v^2 = \text{diag} (0.0025, 0.001, 0.0001)$$

$$v_v^3 = \text{diag} (0.0025, 0.0001, .01)$$

For each hypothesis the state is observable but, given the measurement errors and uncertainties in the vehicle equations of motion, each hypothesis has a different capability of estimating the state of the aircraft. Hence, embedded in the theory is the consideration of the capability of any given sensor group, corresponding to each hypothesis, to estimate the state of the aircraft. This is reflected in the error covariance matrix elements of each hypothesis. As an example, $E[(\hat{p}-p)^2]$ under each hypothesis is indicated as the (1,1) element of the error covariance matrix and is 0.00075, 0.0015, 0.00082, 0.00087 for H_0 , H_1 , H_2 and H_3 , respectively. As expected, H_0 has the smallest value of $E[(\hat{p}-p)^2]$, indicating that this hypothesis, if true, can produce the best estimate of p . Also indicated, however, is the fact that H_1 produces the worst estimate. Again, this is expected since H_1 corresponds to deletion of roll-rate gyro information.

Figure 1 illustrates the unaugmented step response of the space shuttle to an aileron input. This aircraft is a nonminimum phase system indicated by roll reversal. Also, it possess a large coupling of the Dutch roll into the aileron response. Digital feedback was employed at a cycle time of 0.1 sec using

feedback gains $(-4.9, 0.4, 14.5, -6)$ for $(p, \dot{\theta}, r, \delta)$, respectively, to the aileron. The gains were selected to be constrained to a control system operating with only roll control. Figure 2 shows the response of the closed-loop aircraft to the same pilot step input when state variable feedback (perfect measurement of each state) is employed. The noise apparent in the δ_a trace is a result of analog to digital conversion error only. The nonminimum phase characteristic still is present in the response indicated by the roll reversal. This could be eliminated resulting in considerable improvement in flying qualities if yaw control were available. Figure 3 illustrates the same step response using noisy measurements and accepting H_0 . No actuators and sensors have been failed in figure 3. Figure 4 is an illustration of a failure modes and effects simulation analysis to determine the weights C_{ij} appropriate for the design. In figure 4 the responses of the system are indicated for the case where H_2 is true and forcing the system to accept each hypothesis at different times. The failure mode considered in figure 4 is an increase in measurement noise. Note that at the start of the record H_0 is selected and produces poor characteristics, as can be seen by comparing the H_0 true portion of the roll-rate trace of figure 4 with that of figure 3. Had there been no failure, those traces would be almost identical. When H_1 is selected at approximately 5 sec, poor characteristics are still produced. However, when H_2 is selected at approximately 10 sec the system moves to a normal operation, only to return to its poor characteristics when H_3 is selected at approximately 15 sec. This figure illustrates the effect of accepting hypothesis H_i when H_j is true. Simulations of this type can aid the designer in selecting the C_{ij} terms in the Bayesian risk function.

Example 2. The theory was also applied to the design of a failure detection system for the F8-C digital fly-by-wire aircraft. The purpose of this example is to illustrate the effects of nonlinearities in the system. The system was designed to detect failures in the roll rate gyro, yaw rate gyro and sideslip indicator. Sensors for longitudinal motions were used, but the system was not designed to recover from failures of those sensors. The longitudinal sensors were total airspeed, angle of attack, and pitch rate. This section is devoted to items that need to be considered in designing an analytical redundancy management system and results obtained from a real time, piloted, six-degree-of-freedom simulation of the F8-C aircraft on which the system was tested. Figure 6 indicates the performance of a failure detection logic based on a linearization of the aircraft dynamics as was done in the space shuttle example previously but using the full six-degree-of-freedom dynamics in simulation. The aircraft is subject to an aileron input at reference time $t = 0$. The resulting maneuver is seen by the redundancy management system as a failure in the sensors because of disagreement of the bank of filters in the bank angle estimate. Note the difference in $\dot{\theta}$ as the system switches from H_2 to H_1 . This poor performance indicates that for highly maneuvering aircraft it is important to represent the kinematics of the vehicle correctly.

In selection of the model of the aircraft dynamics used in the failure it was considered that the aircraft stability derivatives were not sufficiently well known to justify the scheduling of such data as functions of flight condition and configuration changes. However, it was felt that the representation of the aircraft's kinematic equations was well understood and could be scheduled more conveniently as a function of aircraft configuration. Therefore, in an effort to use as simple a model as possible and provide an accurate representation of the aircraft dynamics, the model selected was one in which linear aerodynamics were assumed but the kinematic relations were included as nonlinear functions. The term "linear aerodynamics" is meant to imply that the aerodynamic force and moment coefficients, X, Y, Z, L, M, N, are assumed to be linear functions of estimated angle of attack, sideslip angle angular velocities, and control positions. The model selected was

$$\dot{u} = rv - qw + X/m - g \cdot \sin\theta + T \cdot \cos\theta_T$$

$$\dot{v} = pw - ru + Y/m + g \cdot \cos\theta \cdot \sin\phi$$

$$\dot{w} = qu - pv + Z/m + g \cdot \cos\theta \cdot \cos\phi + T \cdot \sin\theta_T$$

$$\dot{p} = [(I_y - I_z)qr + L]/I_x$$

$$\dot{q} = [(I_z - I_x)pr + M + T r_T]/I_y$$

$$\dot{r} = [(I_x - I_y)pq + N]/I_z$$

$$\dot{\theta} = q \cdot \cos\phi - r \cdot \sin\phi$$

$$\dot{\phi} = p + (q \cdot \sin\theta \cdot \sin\phi + r \cdot \sin\theta \cdot \cos\phi)/\cos\theta$$

where the aerodynamic forces and moments are given by

$$V = (u^2 + v^2 + w^2)^{1/2}$$

$$\alpha = \tan^{-1} w/u$$

$$\beta = \sin^{-1} v/V$$

$$(X, Y, Z) = 1/2 \rho V^2 S (C_x, C_y, C_z)$$

$$(L, N) = 1/2 \rho V^2 S b (C_l, C_n)$$

$$M = 1/2 \rho V S \bar{c} C_m$$

The representation of aerodynamic force coefficients was selected as

$$C_x = C_{x_0} + C_{x_\alpha} + C_{x_{\delta_f}} \delta_f + C_{x_{\delta_e}} \delta_e$$

$$C_y = C_{y_\beta} \beta + C_{y_{\delta_r}} \delta_r$$

$$C_z = C_{z_0} + C_{z_\alpha} \alpha + C_{z_{\delta_f}} \delta_f + C_{z_{\delta_e}} \delta_e$$

$$C_l = C_{l_\beta} \beta + C_{l_p} (pb/2V) + C_{l_r} (rb/2V) + C_{l_{\delta_a}} \delta_a + C_{l_{\delta_r}} \delta_r$$

$$C_m = C_{m_0} + C_{m_\alpha} \alpha + C_{m_q} (qc/2V) + C_{m_{\delta_e}} \delta_e + C_{m_{\delta_f}} \delta_f$$

$$C_n = C_{n_\beta} \beta + C_{n_p} (pb/2V) + C_{n_r} (rb/2V) + C_{n_{\delta_a}} \delta_a + C_{n_{\delta_r}} \delta_r$$

The specific aerodynamic coefficients used in the model were taken from a linearization of the F8-C aerodynamics at 20,000 ft alt and 0.6 Mach number. Note that the model assumes principal axes, whereas the sensors are body axis mounted. This introduces a modeling error that should be accounted for in the selection of the statistics of the process error $w(k)$. The preceding equations represent the continuous-time process model. The use of this model in a digital control system requires a discrete model representation. Euler's method was used to generate the discrete model difference equations using a time interval of $\tau=0.03125$ sec. Hence, for example, the preceding roll-rate equation becomes

$$p[(k+1)\tau] = p(k\tau) + \tau \cdot \dot{p}(k\tau)$$

Again, this is a source of error in modeling of the aircraft dynamics and should be included in assigning the statistics of $w(k)$.

In designing the redundancy management logic (Fig. 5), the gradients $\partial\phi/\partial x$ and $\partial h/\partial x$ were held constant, and steady-state results were used in the bank of filters and decision functions. The covariance W of $w(k)$ was computed using the techniques of reference 2.

The unfailed noise level for the sensors corresponded to a measurement error with $V_v^0 = \text{diag}(0.001, 0.001, 0.001)$ whereas the failure mode sensor variances were taken as

$$V_v^1 = \text{diag}(0.01, 0.001, 0.001)$$

$$V_v^2 = \text{diag}(0.001, 0.01, 0.0001)$$

$$V_v^3 = \text{diag}(0.0001, 0.0001, 0.01)$$

The single-stage prediction $\hat{x}^1(k+1|k)$ for each filter is obtained by using the last estimate $\hat{x}^1(k|k)$ of that filter and the control surface positions and computing the prediction $\hat{x}^1(k+1|k)$ from the nonlinear model just described. Figure 6 indicates the performance of the decision logic for failures that occur during maneuvering transients induced by aileron inputs that result in rapid rolling.

The system also tested with hardover failures of the zero output, maximum output, and minimum output types. The detection logic behaved similarly to the tests performed under increased noise types of failures. An exception was the zero output case. In that case, the failure detection logic was not able to detect failures until the system was excited with some input, since the sensor output was supposed to be zero until some input causes an output. Failures of this type, if required to be detected during a nonmaneuvering state, would have to be handled using built-in test equipment.

IV. CONCLUSION

The use of analytical redundancy management has been addressed for the aircraft flight control problem. A specific technique of examining failure modes using Bayesian decision theory to process a moving window of sensor data has been examined in detail. The theoretical methodology has been tutorially developed and selection of constant parameters required for the decision logic has been illustrated for two aircraft flight control examples. The logic required to implement an analytical redundancy management system dwarfs that required for a simple voting test using hardware duplication yet it offers the promise, if developed to a useful technology stage, of dealing with redundant actuators. This capability can be used to improve the survivability of future aircraft guarding against such problems as failure to remove control surface locks-- a problem known to be the cause of several aerospace disasters. Hence, there is motive for developing the technology even though the cost of implementation may be currently high.

V. REFERENCES

1. Wilsky, A. S.: A Survey of Design Methods for Failure Detection in Dynamic Systems. Automatica, Vol. 12, 1976, pp. 601-611.
2. Montgomery, R. C.; and Caglayan, A. K.: Failure Accomodation in Digital Flight Control Systems by Bayesian Decision Theory. Journal of Aircraft, Vol. 13, No. 2, February 1976, pp. 69-75.
3. Montgomery, R. C.; and Price, D. B.: Failure Accomodation in Digital Flight Control Systems Accounting for Nonlinear Dynamics. Journal of Aircraft, Vol. 13, No. 2, February 1976, pp. 76-82.
4. McLendon, J. R.; and Sage, A. P.: Computational Algorithms for Discrete Detection and Likelihood Ratio Computation. Information Sciences, Vol. 2, 1970, pp. 273-298.
5. Sage, A. P.; and Melsa, J. L.: Estimation Theory, McGraw-Hill, New York, 1971, pp. 420-495.

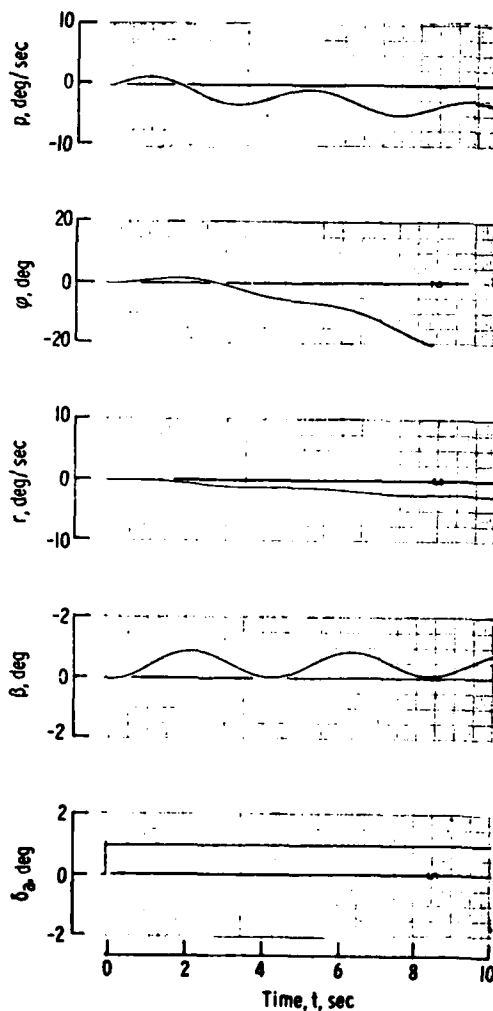


Figure 1.- Response of unaugmented aircraft to aileron step.

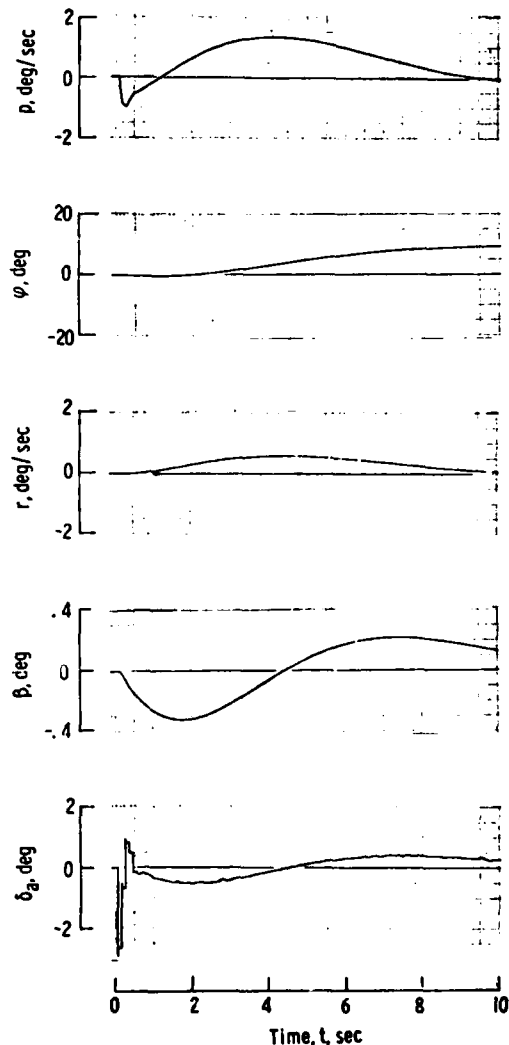


Figure 2.- Response of aircraft to step pilot input when digital state variable feedback (with no measurement noise) is used.

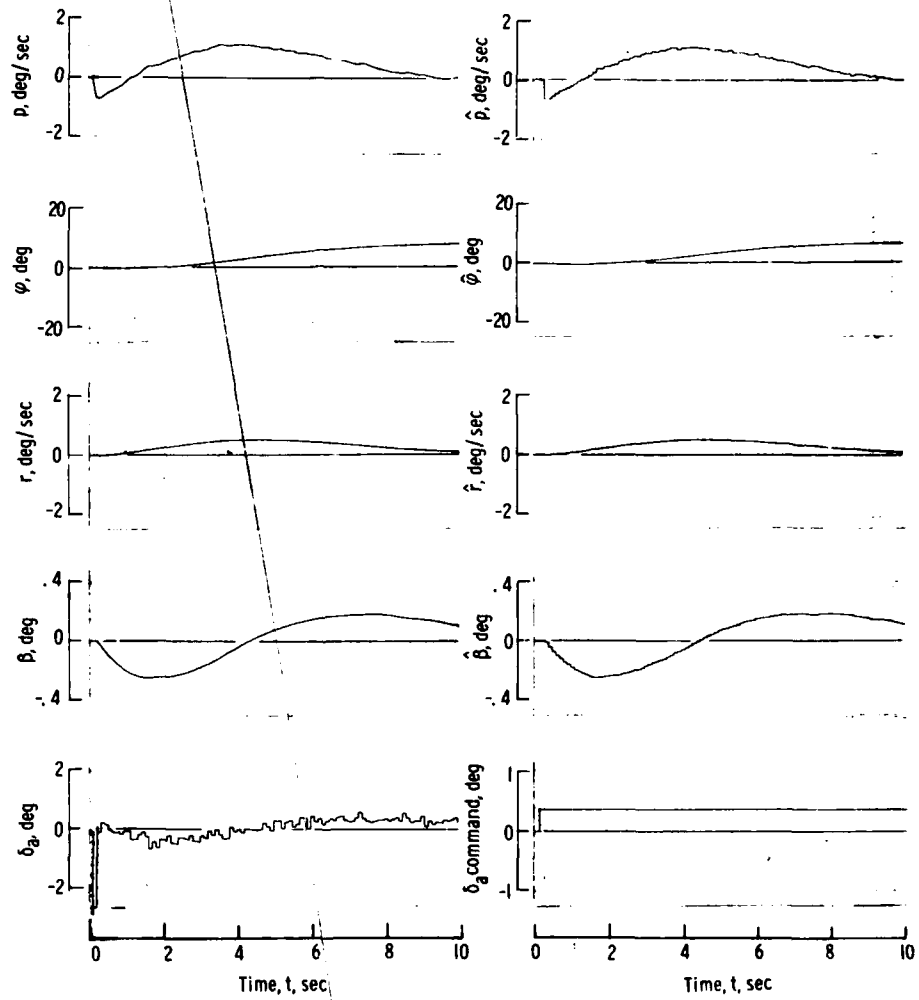


Figure 3.- Response of closed-loop system with noisy measurements under normal operation.

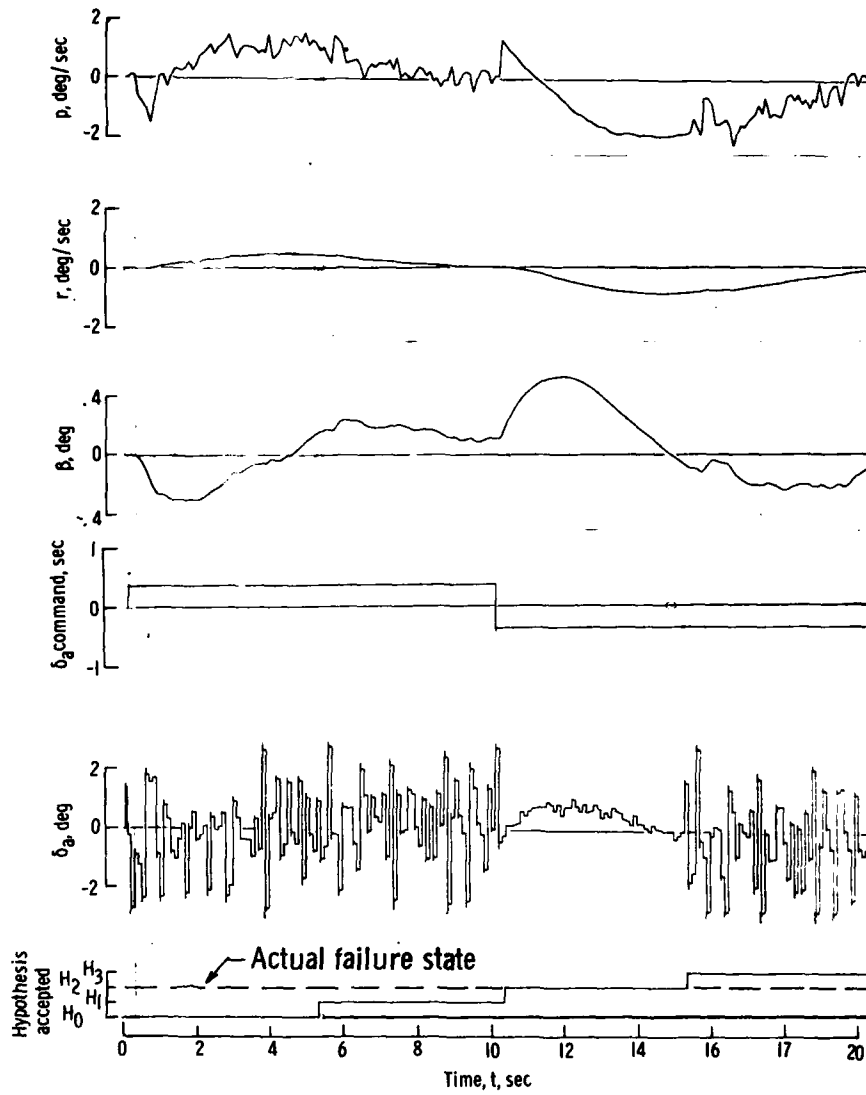


Figure 4.- Response of closed-loop system demonstrating effects of accepting hypothesis H_0, H_2, H_3 , when H_2 is true.

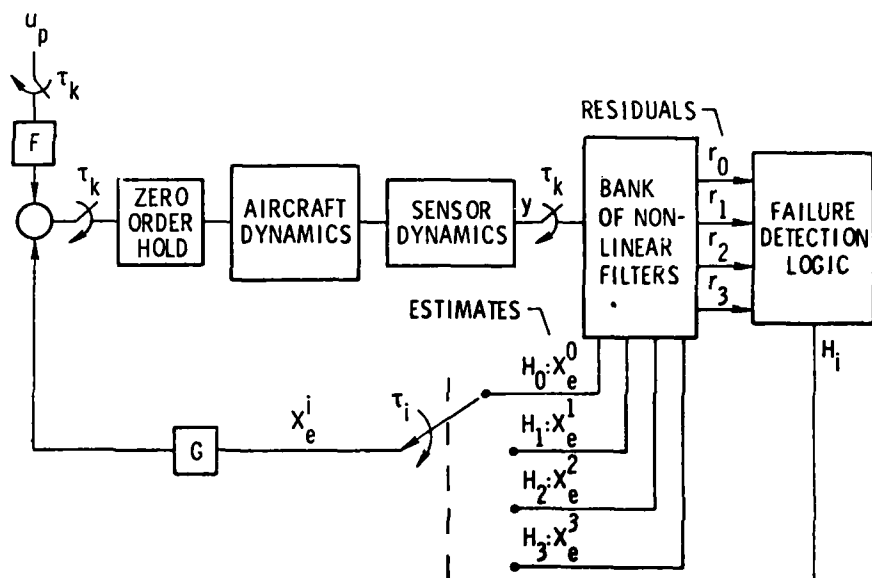


Figure 5.- Analytical redundancy management scheme block diagram.

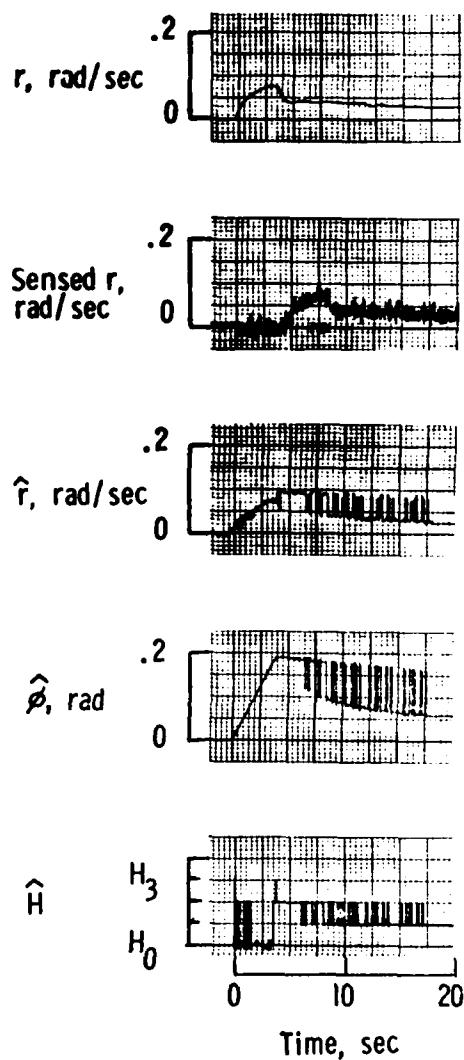


Figure 6.- Performance of the failure detection system using a linear process model.

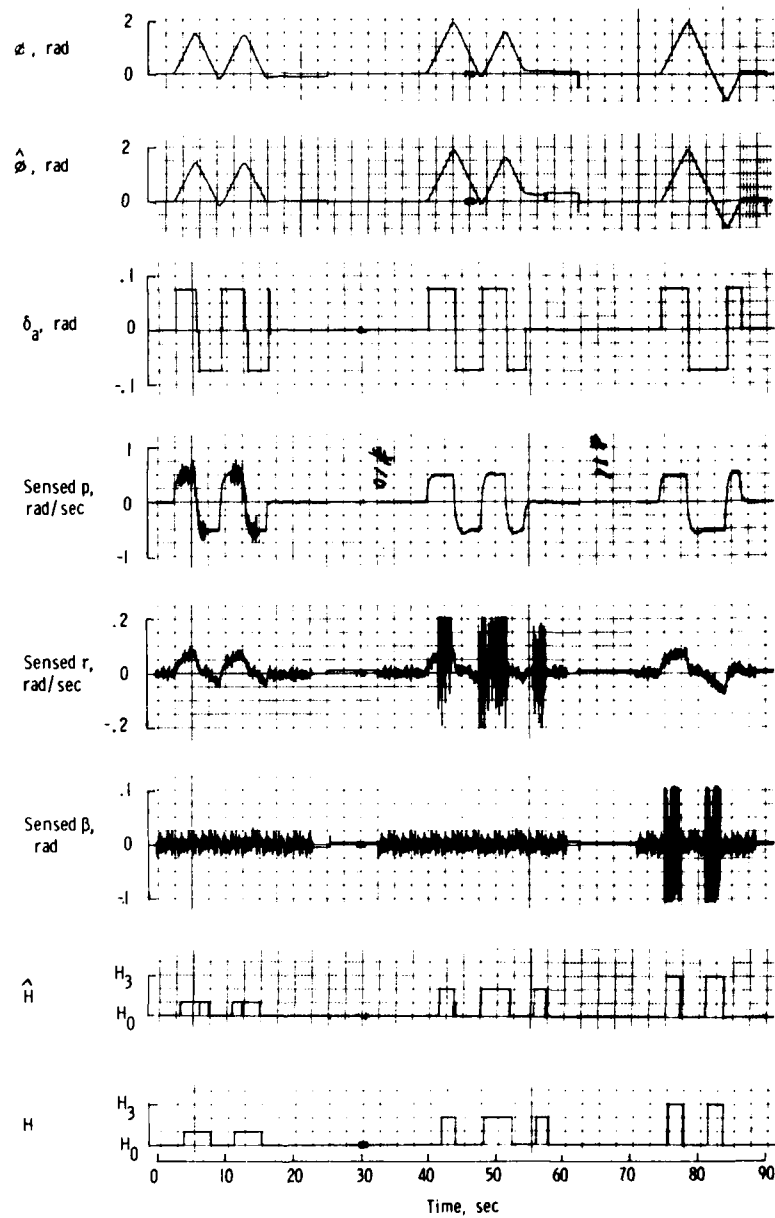


Figure 7.- Performance of the failure detection system under increased noise mode failures with maneuvering transients introduced by aileron inputs.

OPTIMAL CONTROL IN THE
LUNAR MODULE DIGITAL AUTOPILOT

by

William S. Widnall
Associate Professor
Department of Aeronautics and Astronautics
Massachusetts Institute of Technology
Cambridge, Massachusetts 02139
USA

SUMMARY

The Apollo lunar module (LM) digital autopilot was a first generation computer-based automatic control system. The use of a digital computer permitted the implementation of a controller structure and control algorithms that would have been difficult to synthesize using analog controller technology. Optimal control theory has recommended a cascade synthesis for controller design: an observer or estimator of the state followed by memoryless control laws. This structure was utilized in the LM autopilot. The state estimator had some similarities to a Kalman filter, but the variable gains were chosen to minimize nonlinear measurement quantization effects. The memoryless reaction control system (RCS) laws employed parabolic switching curves as suggested by minimum time/fuel control theory for a double integral plant. The memoryless thrust vector control (TVC) law was the first application of the minimum time control law for a triple integral plant.

LIST OF SYMBOLS

c	= conversion factor having dimension of time
c_1, c_2, c_3	= constants for stored mass properties
CSM	= command and service modules
F	= thrust of the throttleable descent engine
I, I_q, I_r	= moment of inertia about the Q or R axis
IMU	= inertial measurement unit
K_ω, K_α	= gains used in the state estimator
L	= distance from descent engine gimbal plane to vehicle center of mass
LM	= lunar module
m	= spacecraft mass
$n, n - 1$	= present, previous sample
n_p, n_u, n_v	= number of RCS jets selected to torque about the P, U, and V axes
R	= thrust vector actuator drive rate (0.2 deg/sec)
RCS	= reaction control system
t	= time at present sample instant
T	= autopilot sample period (0.1 sec)
t_j	= same as $t_p, t_u,$ or t_v
t_p, t_u, t_v	= jet torquing durations commanded by the P, U, and V RCS control laws—the sign gives the sign of the torque desired
u_q, u_r, u	= thrust vector rotation command signal for the Q or R axis (1, 0, or -1)
u_{opt}	= thrust vector rotation command signal for time-optimal control
v_e	= assumed rocket exhaust velocity
x_1, x_2, x_3	= components of a nondimensional attitude state vector
α_j	= magnitude of the angular acceleration that will result from firing the RCS jets for one axis
α_{pp}	= magnitude of the P-axis angular acceleration that will result from firing one P-RCS jet
$\alpha_{qu}, \alpha_{ru}, \alpha_{u'u}$	= magnitudes of the Q, R, and U' components of angular acceleration that will result from firing one U-RCS jet
$\alpha_q, \alpha_r, \alpha$	= Q and R components of the estimated vehicle bias angular acceleration vector
$\dot{\alpha}_q, \dot{\alpha}_r, \dot{\alpha}$	= magnitude of the Q or R axis rate of change of angular acceleration that will result from commanding thrust vector rotation
δ	= angle by which the U' and V' axes are skewed away from the U and V axes
$\delta\alpha, \delta\omega$	= correction to a component of the estimated angular acceleration, angular velocity, based on the unexplained attitude
$\Delta\alpha_q, \Delta\alpha_r$	= estimated changes in the Q and R bias angular accelerations due to thrust vector rotation commands in the last control interval
$\Delta\omega_p, \Delta\omega_q, \Delta\omega_r$	= estimated changes in the P, Q, and R angular velocities due to RCS jets commanded during the last control interval
$\Delta\theta_p, \Delta\theta_q, \Delta\theta_r$	= changes in P, Q, and R components of vehicle attitude (small angles)
Δt	= sample period of the powered flight guidance equations (2 sec)
Δv	= measured change in velocity due to thrusting

θ_e	= attitude error
$\theta_o, \theta_i, \theta_m$	= outer, inner, and middle gimbal angles of the IMU
$\theta_{do}, \theta_{di}, \theta_{dm}$	= desired outer, inner, and middle gimbal angles
θ_{db}	= attitude error deadband size in the RCS control laws
$\theta_p, \theta_q, \theta_r$	= P, Q, and R components of the unexplained attitude (small angles)
θ_{max}	= threshold value that must be exceeded by a component of the unexplained attitude before an attitude measurement is incorporated
ω	= estimated vehicle angular velocity vector
ω_d	= desired angular velocity vector
ω_e	= angular velocity error
$\omega_p, \omega_q, \omega_r$	= components of the estimated vehicle angular velocity

INTRODUCTION

The lunar module (LM) digital autopilot provides attitude control of the spacecraft during both coasting and powered flight. It is designed to control the three spacecraft configurations shown in Fig. 1: LM descent, LM ascent, and commanded and service modules (CSM) docked.

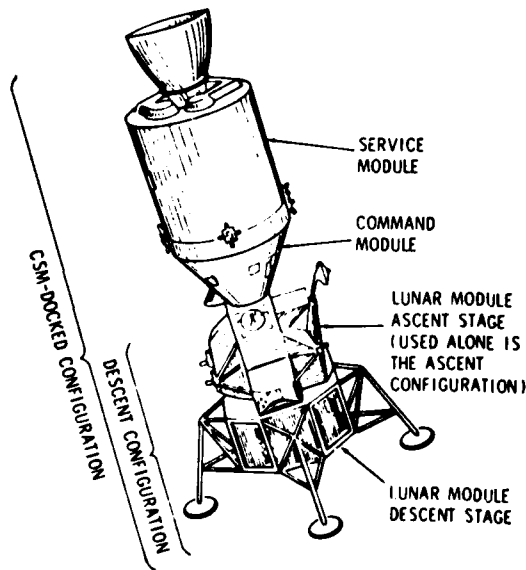


Fig. 1 Spacecraft configurations controlled by the lunar module autopilot.

Torques for attitude control may be generated by the reaction control system (RCS) and by the descent propulsion system. The RCS employs 16 jets mounted in clusters of four on outriggers equally spaced around the LM ascent stage. Each jet has a thrust of 450 newtons. The descent propulsion system has a single engine that can be throttled from a maximum thrust of 45,000 newtons down to 12% of the maximum thrust. This engine is mounted in a gimbal system with actuators which can change the angle of the thrust vector relative to the spacecraft center of mass at the constant rate of 0.2 deg/sec. The ascent propulsion system has a single 16,000-newton engine, which is mounted rigidly to the ascent stage. During ascent, attitude control must be maintained by use of the RCS jets alone.

The autopilot is an integral part of the LM primary navigation, guidance, and control system.^{1,2} Most logical functions of this system are programmed in the general purpose on-board digital computer, which has 36,864 words of fixed memory for program storage, and 2048 words of erasable memory. The word length is 15 data bits plus a parity bit. It utilizes fixed decimal point arithmetic. The memory cycle time is $12 \mu\text{sec}$. The execution of most instructions requires either two or three memory cycles.

The preliminary design of the autopilot is presented by Chery and O'Connor.^{3,4} A history of the development of the autopilot is presented by Cox.⁵ A summary of the final design of the autopilot, as flown in the first lunar landing mission Apollo 11, is presented by Widnall.⁶ The complete design details are presented in Ref. 7.

Insights from optimal control theory were useful in formulating the structure of the autopilot, the state estimator, the RCS control laws, and the thrust vector control law.

STRUCTURE OF THE AUTOPILOT

A control structure that has been popularized by optimal control theory is the cascade synthesis: the combination of a state estimator followed by a memoryless control law. In the case of the LQG problem (the control of a linear plant with a quadratic cost performance index and with Gaussian noises disturbing the plant and corrupting the measurements) Joseph and Tou⁸ proved that the optimal control of the plant is accomplished by the cascade combination of a Kalman filter and the deterministic state feedback optimal regulator. The Kalman filter is a linear estimation algorithm. The optimal regulator is a linear memoryless control law. Part of the appeal of the cascade synthesis is that the estimator and the control law can be independently designed. Changes in the driving noise and measurement noise assumptions lead to changes in the optimal filter gains but do not affect the control gains. Changes in the quadratic cost weightings on state deviations or control effort lead to changes in the control gains but do not affect the filter gains.

This appealing separation of the controller design problem into an estimation problem and a deterministic state feedback control problem was utilized in the LM autopilot. The

control law design problem was further divided into an RCS control law design problem and a thrust vector control law design problem. Thus three major subsections of the autopilot were identified, each of which could be designed somewhat independently: (1) the attitude state estimator, (2) the RCS control laws, and (3) the thrust vector control laws.

To reduce the order of the control law synthesis problems, it was assumed that independent control laws could be implemented for the different spacecraft axes. The RCS control laws were divided into three separate channels, termed P, U, V. The locations and orientations of the RCS jets are such that if the spacecraft center of gravity lies near the geometric center of the 16 RCS jets (such as in the ascent configuration), then eight "P jets" thrusting only in the Y or Z directions produce torques about the P axis only (Fig. 2), four "U jets" thrusting in the + X direction produce torques about the U axis only, and four "V jets" thrusting in the - X direction produce torques about the V axis only.

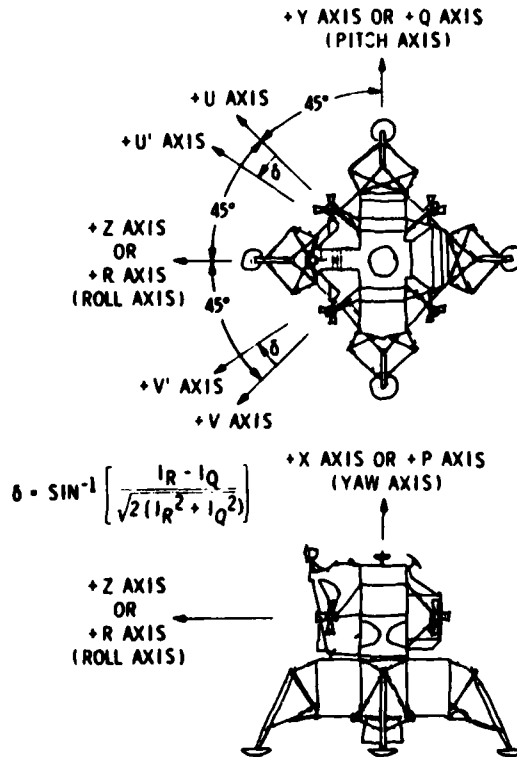


Fig. 2 The control axes of the LM.

The velocity-change information is also used every 2 sec (Δt) to update the estimates of spacecraft mass and thrust:

$$m(t) = m(t - \Delta t) - \Delta v m(t - \Delta t) / v_e \quad (1)$$

$$F = m(t) \Delta v / \Delta t \quad (2)$$

These estimates are inputs to the autopilot adaptive loop. The control effectiveness of the RCS jets about the P, Q, and R axes is calculated according to

$$\alpha_j = c_1 + c_2 / (m + c_3) \quad (3)$$

A separate set of constants is appropriate for each axis and for the descent and ascent configurations. The values so calculated for the orthogonal angular acceleration components α_{qu} and α_{ru} are then resolved onto the U' axis to determine $\alpha_{u'u}$. Because of the inertia symmetry, the value of $\alpha_{u'u}$ can be used also for V axis computations.

The effectiveness of the thrust-vector control signals in the descent configuration is calculated according to

$$\dot{\alpha}_q = FLR / I_q, \quad \dot{\alpha}_r = FLR / I_r \quad (4)$$

where F is calculated by Eq. (2), I_q and I_r are calculated as being inversely proportional

The descent engine may be gimballed under computer control about the pitch (Q) axis and the roll (R) axis. Therefore, the descent-engine trim-gimbal control laws were separated into two channels (Q and R). The computation of the proper trim-gimbal drive for each channel is based on independent single-plane control laws.

The basic sample interval of the autopilot is 0.1 sec. Every 0.1 sec, whatever computer job is in progress is interrupted and control is transferred to the autopilot computations. Typically, it requires 0.025 sec to complete the autopilot computations. In addition to the main autopilot computations there is a subprogram that is executed every 2 sec in powered flight to adapt the autopilot gains as a function of the estimated decreasing vehicle mass and the estimated bias angular acceleration due to the thrusting main engine.

The most complex interaction between the guidance equations and the autopilot, and between subsections within the autopilot occurs during descent-engine powered flight (Fig. 3). The spacecraft velocity-changes due to thrusting are measured by the three integrating accelerometers of the inertial measurement unit (IMU). The velocity-change information is sampled every 2 sec by the computer and is used by the navigation equations to determine the present velocity and position. The guidance equations then compute the desired new thrusting attitude. In addition to commanding the desired thrusting attitude, the guidance equations can command changes in the thrust level of the throttleable descent engine.

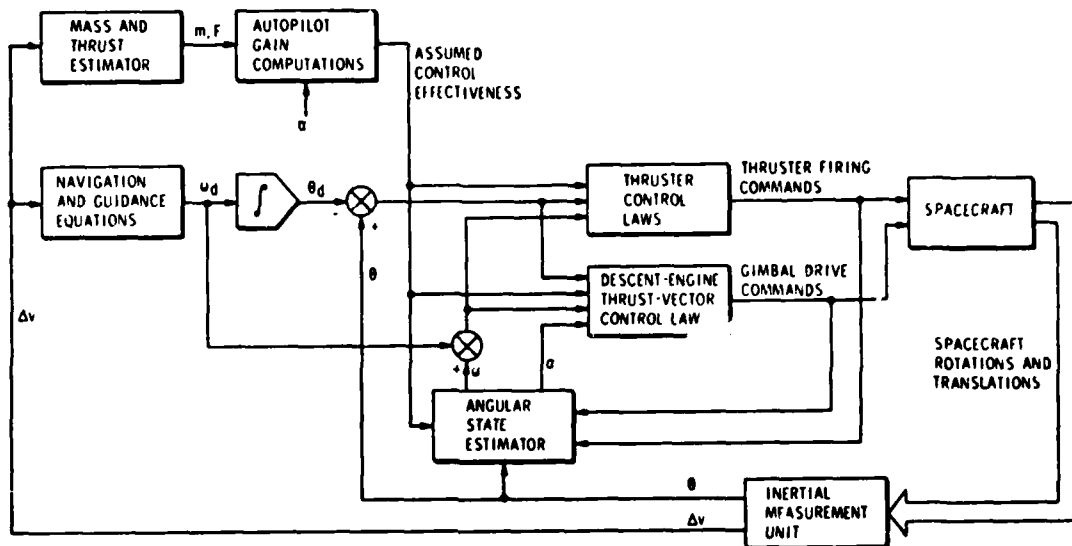


Fig. 3 Information flow in the autopilot during descent-engine powered flight.

to α_{qu} and α_{ru} , and L is calculated as

$$L = c_4 + c_5/(m + c_6) \quad (5)$$

ATTITUDE STATE ESTIMATOR

The Kalman filter⁹ or the Luenberger observer^{10,11} is a linear estimator. Inputs to the estimator are the physical measurements and the known control actions. The estimator uses a linear mathematical model for the plant to predict the response to the known control actions. Predicted values for the measurements are formed from the predicted state vector. The difference between an actual measurement and the predicted measurement is multiplied by a gain vector and the resulting vector is used to adjust the state estimate. In a Kalman filter, the optimal time varying gain vector is obtained from statistical considerations, taking into account the initial estimation error covariance, the plant state driving noise density, and the measurement noise variance. In the Luenberger observer the gain vector is usually chosen to be constant. The gains might be chosen by estimation error pole placement techniques.

The fundamental structure of a Kalman filter or Luenberger observer has been utilized in the LM autopilot attitude state estimator. This includes the modeling of the spacecraft response to the known control actions and the correcting of the state vector according to the difference between the actual measurement and the predicted measurement. However nonlinear logic is used to determine the gain vector, to overcome the severe effect of measurement quantization.

The basic measurements of the vehicle attitude state available to the autopilot are the gimbal angles of the inertial measurement unit, which are sampled every 0.1 sec. To separate any bias angular acceleration due to the main engine from the angular acceleration due to RCS jet firings, the state estimator needs additional inputs from the RCS control laws containing the jet-firing information. Including jet-firing information as well as thrust-vector-command information gives an added benefit; the basic attitude inputs may be filtered as required, without necessarily introducing large lags into the estimates of angular velocity and bias angular acceleration.

The estimated changes in the P, Q, and R angular velocities due to RCS jets selected during the last control interval are computed as

$$\begin{aligned} \Delta \dot{\omega}_p &= \alpha_{pp} t_p n_p \\ \Delta \dot{\omega}_q &= \alpha_{qu} (t_u n_u - t_v n_v) \\ \Delta \dot{\omega}_r &= \alpha_{ru} (t_u n_u + t_v n_v) \end{aligned} \quad (6)$$

The estimated changes in the Q and R bias angular acceleration due to thrust vector rotation commands in the last control interval are computed as

$$\Delta\alpha_q = \dot{\alpha}_q T u_q, \quad \Delta\alpha_r = \dot{\alpha}_r T u_r \quad (7)$$

The IMU gimbal angles observed during the previous execution of the estimator computations have been stored. The present gimbal angles are now sampled, the change in gimbal angles is computed, and the change is transformed to a change in body angles. The difference between the measured change in attitude and the predicted change in attitude is called the unexplained change in attitude. This is computed and added to the previous total unexplained attitude to form the present total unexplained attitude:

$$\theta_p(n) = \theta_p(n-1) + \Delta\theta_p - [\omega_p(n-1)T + \Delta\dot{\omega}_p T/2] \quad (8a)$$

$$\theta_q(n) = \theta_q(n-1) + \Delta\theta_q - [\omega_q(n-1)T + \alpha_q(n-1)T^2/2 + \Delta\dot{\omega}_q T/2] \quad (8b)$$

$$\theta_r(n) = \theta_r(n-1) + \Delta\theta_r - [\omega_r(n-1)T + \alpha_r(n-1)T^2/2 + \Delta\dot{\omega}_r T/2] \quad (8c)$$

The quantities in brackets may be identified as components of the predicted attitude change. Note that the predicted attitude change due to gimbal drive commands has been neglected, and the exact expression for the attitude change due to jet firings has been approximated by a simpler term.

The unexplained attitude is used to update the estimates of angular velocity and angular acceleration. But first, logic is applied to reject the measurement quantization noise. Since the probability distribution of this noise is not Gaussian but is rectangular, the noise may be largely rejected by a nonlinear filter logic which is applied independently to the P, Q, and R axes in the state estimator. For each axis, if the component of the unexplained attitude is less than a threshold value $\theta_{max} = 0.14$ deg, then the unexplained attitude is assumed to be largely due to the attitude measurement quantization noise. In this case, the corrections $\delta\omega$ and $\delta\alpha$ to the estimates of angular velocity and bias angular acceleration for that axis are set to zero. The unexplained attitude is not zeroed. However, for each axis where the unexplained attitude exceeds the threshold, it is assumed that the estimated angular velocity and angular acceleration for that axis are in need of corrections. Nonzero corrections $\delta\omega$ and $\delta\alpha$ are computed as

$$\delta\omega = K_\omega \theta(n)/T, \quad \delta\alpha = K_\alpha \theta(n)/T^2 \quad (9)$$

and then the unexplained attitude $\theta(n)$ for that axis is reset to zero.

The estimates of the angular velocity and the bias angular acceleration are now updated to the present sample instant as

$$\omega_p(n) = \omega_p(n-1) + \Delta\dot{\omega}_p + \delta\omega_p \quad (10a)$$

$$\omega_q(n) = \omega_q(n-1) + \alpha_q(n-1)T + \Delta\dot{\omega}_q + \delta\omega_q \quad (10b)$$

$$\omega_r(n) = \omega_r(n-1) + \alpha_r(n-1)T + \Delta\dot{\omega}_r + \delta\omega_r \quad (10c)$$

$$\alpha_q(n) = \alpha_q(n-1) + \Delta\alpha_q + \delta\alpha_q \quad (11a)$$

$$\alpha_r(n) = \alpha_r(n-1) + \Delta\alpha_r + \delta\alpha_r \quad (11b)$$

Note that bias angular acceleration about the P axis is assumed to be zero, and the estimated rate-change term due to trim-gimbal activity in the last control interval has been neglected. In periods of coasting flight, it is assumed that the Q and R components of bias angular acceleration are also zero. Accordingly, the final step in the state estimator sets α_q and α_r to zero during periods of coasting flight.

The dynamic characteristics of the state estimator are strongly determined by the choice of filter gains K_ω and K_α . The gains selected for the different vehicle configurations are given in Ref. 7. The engineering considerations which were used for determining the estimator gains are as follows: The sampled measurements of vehicle attitude do not contain significant noise. Therefore the attitude gain selected (for incorporating the

measurement error into the estimate of attitude) was unity. That is, the best estimate of vehicle attitude is taken to be the measured attitude. The rate gain K_{ω} (for incorporating the measurement error into the estimate of angular velocity) should be set as high as possible to obtain fast accurate tracking of the vehicle angular velocity. Accordingly a high rate gain is used in the lunar-module-alone configuration. In this case the angular velocity estimate is similar to that obtained by a simple attitude back-difference. However, the high rate gain cannot be used in the docked configuration, or the angular velocity due to bending mode oscillations is contained unattenuated in the estimated angular velocity. This bending mode noise would lead to degraded control action by the thruster control laws and the descent-engine thrust vector control law. Therefore, in the docked configuration a substantially lower value of rate gain is used to filter the bending mode oscillations, thus yielding a better estimate of the rigid body angular velocity.

The proper choice of the acceleration gain, K_{α} , for incorporating the measurement error into the estimate of angular acceleration, is a balance between the need to filter unwanted disturbances such as due to propellant slosh or bending and the need to have reasonable transient control. Various parameters for the thruster control laws are computed every 2 sec in the adaptive loop as a function of the present estimate of bias angular acceleration. If the bias-acceleration estimates followed the sinusoidal disturbances due to slosh or bending, the resulting fluctuations in the autopilot parameters would produce unpredictable performance. Therefore a low value for the acceleration gain is desired. However, if the value selected is too low in descent engine powered flight the proper control response to the angular-acceleration, due to thrust-vector misalignment at ignition or at a throttle change, would be delayed by the slow build-up of the acceleration estimate. Extensive simulations were used to demonstrate that these compromises were made satisfactorily in selecting the filter gains. It was not necessary to implement a higher-order filter having explicit estimation of bending or slosh modes, with the attendant difficulties associated with the uncertain parameters. It was not necessary to implement gains that varied as a function of time-since-ignition or time-since-thrust-change.

RCS CONTROL LAWS

In the LQG optimal control problem, the optimal state feedback regulator turns out to be a linear memoryless function of the estimated state of the plant. The LM autopilot follows the insight that the control laws should be memoryless functions of the estimated state. However linear control action is not possible. The reaction control system (RCS) jets have only two control levels: on or off. The thrust vector gimbal drive rate has only three values: plus on, zero, or minus on. It might have been possible to approximate the action of a LQ optimal regulator by utilizing pulse width modulation to achieve an average control level less than the full on level. However this design approach was not taken. In the case of the RCS control laws, the high total number of firings under pulse width modulation might have increased the chances of a jet failure. Furthermore optimization criteria other than quadratic cost had greater appeal.

The RCS control law that was developed for coasting flight has a strong resemblance to the optimal control law for the minimization of a linear combination of time and fuel for the double integral plant. Athans and Falb¹² show that the optimal nonlinear state feedback control law has the switching curves and optimal trajectory shown in Fig. 4. The switching curve γ is made up of two parabolic arcs, which are realizable trajectories of the plant and are a function of the control effectiveness. The Γ_k switching curve is also comprised of parabolic arcs. However these arcs are not trajectories of the plant. They are a function of the relative weight k that has been placed on minimizing settling time as opposed to minimizing fuel. If k is chosen to be large, the Γ_k switching curve is close to the γ switching curve. If k is chosen to be small, the Γ_k switching curve is close to the x_1 axis. Note that this optimal controller requires only two control-on periods to bring any initial state error to zero. Although number of control actions was not mentioned in the performance index, the optimal controller appears to minimize the required number of control actions.

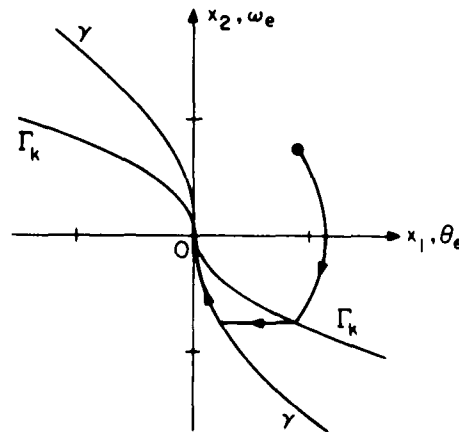


Fig. 4 Time and fuel optimal controller for a double integral plant.

One implementation of the theoretical optimal controller would require continuous monitoring of the state estimate to determine the exact instant for changing the control command. This approach is not possible with digital control. Within the computational capacity of the LM guidance computer, the fastest repetition rate that is possible for the autopilot calculations is 10 cps. However, in the lightest ascent configuration, two RCS jets torquing can produce an angular acceleration of about 50 deg/sec². The simplest form of RCS control law would turn-on and turn-off the RCS jets only at the control sample instants. However, if this approach were used, the angular velocity of the lightest ascent configuration would be controlled to an accuracy of only 5 deg/sec.

This is clearly unacceptable. To overcome this difficulty, the assumed control effectiveness of the RCS jets is used to determine the exact jet firing durations that are required to deliver a desired change in angular velocity.

For automatic control in the LM-alone case, a subroutine is programed which calculates the required jet torquing time t_j for one axis as a function of: (1) the attitude error θ_e and the angular velocity error $\dot{\omega}_e$, (2) the parameters, as calculated in the adaptive loop, that determine the curvature and position of phase plane parabolas, and (3) the preference for 1-jet or 2-jet firings to obtain the required torque impulse. By successive calls to this subroutine, with the appropriate input information for each axis, the jet firing times for each axis are determined.

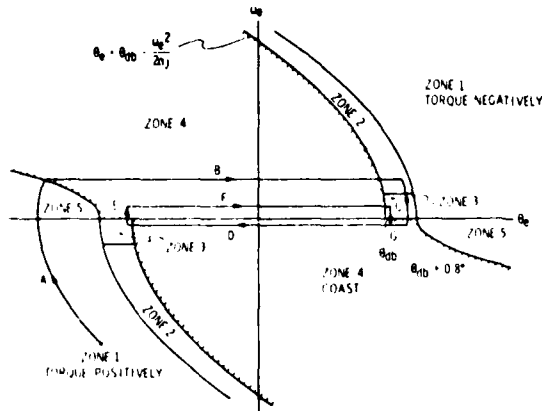


Fig. 5 RCS control law for LM-alone coasting flight.

not have been chosen without rescaling the fixed-point arithmetic calculations. The intercepts of the parabolas with the θ_e axis are a function of the deadband θ_{db} selected by the astronaut or by the automatic maneuver program. Available attitude error deadbands are 0.3, 1.0, and 5.0 deg.

This phase plane design is such that the control action in response to any initial condition will transfer the state toward the origin with at most two major pulses. This is illustrated by segment A-B-C of the sample trajectory in Fig. 5. After the acquisition of the deadzone, the vehicle state is held in a minimum impulse limit cycle, as shown by segment D-E-F-G. The state traverses the deadzone, and its direction is reversed by a single firing of one RCS jet each time a zone 3 is encountered.

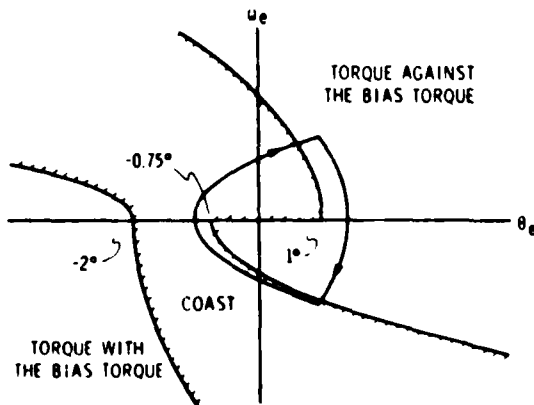


Fig. 6 RCS control law for LM-alone powered flight with a large bias torque.

The actual control logic applied by the subroutine in coasting flight is illustrated by the phase plane diagram in Fig. 5. There are several noticeable departures from the theoretical optimal control law. The most obvious is the introduction of an attitude deadband so that once the initial state error has been reduced to near zero, there will not be frequent jet firings. The phase plane above the θ_e axis is divided into five zones. The boundaries of these zones are parabolas. The steepness of the parabolas bounding zone 2 are identical to that of the estimated vehicle phase plane trajectory when the jets are torquing. The jet acceleration magnitude which determines this parabola was calculated in the adaptive loop. The parabola separating zone 4 and zone 5 is not a trajectory of the vehicle. It is flat to keep control angular velocities low, but is not so flat that a large θ_e can persist. The flatness selected corresponds to an acceleration of 1.4 deg/sec². A smaller acceleration could

The control logic applied by the subroutine in powered flight is illustrated by the phase plane diagram shown in Fig. 6. The intercepts of the various parabolas are shifted as a function of the magnitude of the estimated bias angular acceleration. The intercept locations shown in Fig. 6 are typical for powered ascent with a large ascent engine thrust vector misalignment. The steepness of the four parabolas are based on four different angular accelerations. The upper left parabola is based on the minimum acceleration $\alpha_{min} = 1.4$ deg/sec² as in coasting flight. The upper right parabola is based on the net acceleration possible with the jets firing against the bias torque. The lower right parabola is based on the bias angular acceleration alone (no jets firing), however, it is steepened by a factor $\frac{1}{2}$ to improve the probability that the trajectory would not recross the switch curve into the torquing zone causing an unnecessary small pulse.

A typical phase plane trajectory is shown superimposed on the phase plane logic in Fig. 6. The phase plane design is such that the vehicle is controlled with a low-frequency limit cycle in which the jets are commanded to fire a single pulse in opposition to the bias torque once each cycle.

The autopilot must perform the same basic control functions in the CSM-docked case as in the LM-alone case. However, a separate subroutine was developed for the CSM-docked case. A problem peculiar to the docked configuration is that the vehicle has three low-

frequency bending modes associated with the relatively weak docking adapter connecting the vehicles. To guarantee that the RCS jets not not be fired at the bending frequency, jet inhibition logic was designed for the CSM-docked case.¹³

In addition to the RCS control laws provided to follow the automatic attitude commands, separate control laws are provided to follow manual attitude commands, as inputed to the computer by the rotational hand controller.¹⁴

An interesting performance problem existed with an earlier autopilot design, in which the orthogonal P-U-V axes were used for the application of the single-axis phase-plane RCS control laws. Figure 7 (from Ref. 15) shows the U-axis jet firings as telemetered to the ground during a short portion of ascent-stage-only powered flight in Apollo 9. One can see evidence of the low-frequency limit cycle, in agreement with the design intent, in which the bias torque from the thrusting ascent engine is balanced by torque pulses from one U-axis jet. (The U-axis jet selected is the one that can provide the desired sign torque by thrusting in the same direction as the ascent engine.) However, note in addition to the four substantial RCS pulses there are five useless small pulses.

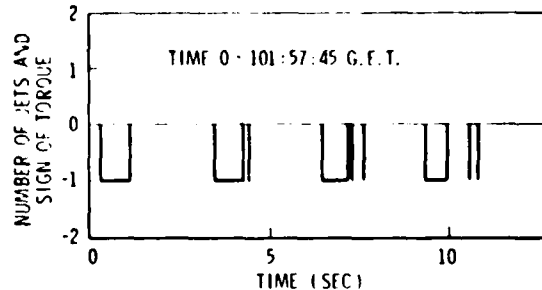


Fig. 7 Typical U-axis jet firings during Apollo 9 ascent powered flight.

These multiple jet firings are caused by inertia cross-coupling effects. The mass distribution in the LM is such that the principal axes of the moment of inertia are aligned closely with the Q and R axes, not the U and V axes. As a result, applying a torque with a V-axis jet produces an angular acceleration not only along the V axis but also along the U axis. The magnitude of this cross-coupled acceleration is such that in the worst case the angular acceleration vector is about 15° away from the applied torque vector. During the same interval of time shown in Fig. 7 a similar low-frequency limit cycle existed about the V axis. The V-axis pulses were occurring slightly delayed with respect to the U-axis major pulses. Hence at the end of a major U-axis pulse, the V-axis jet was still firing. This V-axis torque produced a cross-coupled angular acceleration along the U axis. This in turn caused the U-axis phase-plane trajectory to leave the coast zone and return to the torquing zone. The result is unwanted small pulses. This cross-coupling effect had been anticipated before flight as a result of detailed autopilot performance simulations.^{16,17}

To decouple the RCS control channels and thereby reduce the number of RCS firings, a nonorthogonal set of control axes called U' and V' was introduced.¹⁸ The U' and V' axis directions are uniquely determined by the requirement that the U' direction shall be orthogonal to the angular acceleration induced by applying either a V-axis torque or a P-axis torque, and the V' direction shall be orthogonal to the angular acceleration induced by applying either a U-axis torque or a P-axis torque. The U' and V' axes are skewed symmetrically with respect to the LM R axis as shown in Fig. 2. The sines and cosines of the angle δ , by which the U' and V' axes are skewed away from the U and V axes toward the R axis, are

$$\sin \delta = (I_R - I_Q) / [2(I_R^2 + I_Q^2)]^{1/2} \quad (12a)$$

$$\cos \delta = (I_R + I_Q) / [2(I_R^2 + I_Q^2)]^{1/2} \quad (12b)$$

By resolving the attitude error vector and the angular velocity error vector onto the U' and V' axes and by utilizing the U' and V' components for the purpose of determining U and V jet torquing requirements, the two control channels have been decoupled.

MINIMUM TIME THRUST VECTOR CONTROL LAW

It was originally expected that the autopilot would be designed to estimate the misalignment of the descent-engine thrust vector relative to the spacecraft center-of-mass and then command the engine-gimbal actuators so as to null this misalignment. In such a design, attitude-maneuvering and attitude-hold capabilities would be provided by utilizing the small thrusters of the reaction control system. However, minimizing the propellant expenditure of these attitude thrusters was an essential design consideration. Furthermore, the probability of thruster failure would be reduced if the number of thruster firings was also minimized. It was noted that torques for attitude control could be developed without a propellant-expenditure penalty by using the descent engine, because the descent engine in powered flight would be firing continuously. Therefore, an attitude control law was sought that would utilize the descent engine in such a way as to permit attitude control without the assistance of the attitude thrusters. Because the actuator drive rate was so slow (0.2°/sec), there was no hope of eliminating entirely the need for occasional thruster activity. Rapid attitude maneuvers, such as were required at certain critical instants in a lunar landing, would demand torque from the

small thrusters. During less critical intervals, on the other hand, the guidance command would be slowly varying. During these intervals it was hoped that a thrust-vector attitude control law could maintain the attitude errors sufficiently small so as not to require the assistance of the thrusters. Accordingly, the control law was sought which would provide the fastest possible response time—that is, the optimal (minimum-time) control law. It is known that the desired time-optimal controller would have the property that the actuators would always be commanded to drive one way or the other. At no time would a command not to drive be issued. Inasmuch as no limitations on actuator activity could be identified, this characteristic was considered acceptable.

About either of the two spacecraft axes that could be under thrust-vector control, the differential equation relating the gimbal-drive control signal, u , to the deviation of the vehicle attitude, θ , from the desired attitude, θ_d , is

$$\frac{d^3\theta_e}{dt^3} = \frac{FLR}{I} u \quad (13)$$

where $\theta_e = \theta - \theta_d$ is the attitude error, F is the thrust of the descent engine, L is the distance from the engine hinge point to the spacecraft center-of-mass, R is the available actuator drive-rate magnitude and I is the moment-of-inertia of the spacecraft for that axis. The control signal u from the computer, because of the digital interface, can take on only the values $+1$, 0 , and -1 . These relationships are illustrated in Fig. 8. Note that for equation (13) to be true, the third derivative of the desired attitude must be zero. This restriction, however, does not exclude the most likely guidance commands: a constant attitude-hold command or a constant pitch-rate command. Note also that equation (13) ignores the dynamics of bending and propellant slosh.

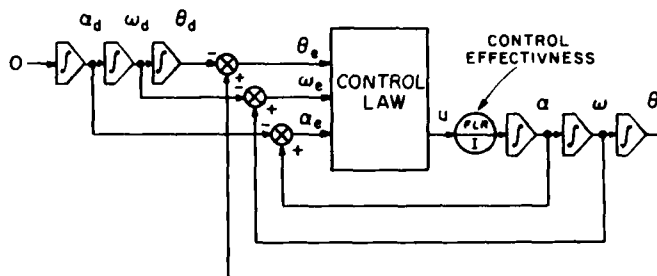


Fig. 8 The assumed dynamics of the desired attitude θ_d and the vehicle attitude θ .

As the descent engine expends its propellant, the spacecraft mass decreases. The moment arm, L and the inertia, I , vary with the mass; hence they are time-varying. The descent-engine thrust, F , is throttleable, to make possible a soft-landing, and it is commanded to deliver varying thrust levels by the guidance equations. Thus, the control effectiveness FLR/I is a time-varying coefficient. However, L and I can vary only slowly, and large discontinuities in the thrust F are commanded at only a few discrete points in a lunar-landing trajectory. Therefore, for the purpose of control-law derivation, we can assume that FLR/I is constant.

The first and second derivatives of the attitude error, θ_e , are the angular velocity error, ω_e and the angular acceleration error, α_e . An important assumption is that these state variables θ_e , ω_e and α_e are all available to the controller with no measurement noise or estimation error. Under these assumptions, the time-optimal feedback control law can be derived. It is a feedback law, rather than an open-loop law, in the sense that the control signal u is given as an explicit function of the present state (α_e , ω_e , θ_e). This control law will drive any initial state to zero in the minimum time.

Extensive general results appear in the literature on optimal control for linear time-invariant systems. Time-optimal controls have been found for a number of second-order systems and for a few third-order systems. However, the time-optimal controller for the triple-integral plant, of which the thrust-vector control problem is an example, could not be found in the literature. Therefore, it was necessary to derive the time-optimal controller for the triple-integral plant. The derivation of Widnall is presented in Refs. (19) and (20) and is summarized briefly in the Appendix. In terms of the variables of the thrust-vector control problem, it is found that the optimal control signal, u_{opt} , may be determined as a function of the present state (α_e , ω_e , θ_e) by the following sequence of calculations, which constitutes the minimum-time control law:

$$c = \left(\frac{I}{FLR}\right)^{1/3}$$

$$x_1 = c^2 \alpha_e, \quad x_2 = c \omega_e, \quad x_3 = \theta_e \quad (14)$$

$$s_1 = \text{sign}(x_1), \quad s_2 = \text{sign}(x_2 + \frac{1}{2}s_1 x_1^2)$$

$$u_{opt} = -\text{sign}\left[x_3 + \frac{1}{3}x_1^3 + s_2 x_1 x_2 + s_2 \left(s_2 x_2 + \frac{1}{2}x_1^2\right)^{3/2}\right]$$

The parameter c has the dimension of time. It is used to convert the state $(a_e, \omega_e, \theta_e)$ into a nondimensional state (x_1, x_2, x_3) . The optimal control signal, u_{opt} , is then given in terms of the nondimensional state.

The sequence of calculations of the optimal control law given by equation (14) is executed easily by the autopilot program stored in the lunar-module computer. If a digital computer were not available, implementation of the optimal control law by analog techniques would be a formidable engineering task.

A distinct design advantage of the optimal control law over a linearized switching law is the validity of the control law for all values of the state variables and the control effectiveness. To synthesize a linearized switching law, the designer must base his choice of gains on some assumption about the maximum values of the state variables. Large values for the initial conditions call for low control gains, otherwise the closed-loop response exhibits gross overshoot. But if conservative low gains are selected, the closed-loop response will be needlessly slow for small values for the initial conditions. These design considerations apply throughout the full range of control effectiveness. In this Apollo application, the control effectiveness has more than a two order-of-magnitude variation from the heaviest docked configuration at low thrust to the lightest LM-alone descent configuration at high thrust.

In theory, if using the optimal control law, any initial angular state of the spacecraft will be driven to zero with at most two control reversals. For example, the theoretical response of the control system to an initial thrust misalignment, but with zero initial angular velocity and attitude error, is shown in Fig. 9.

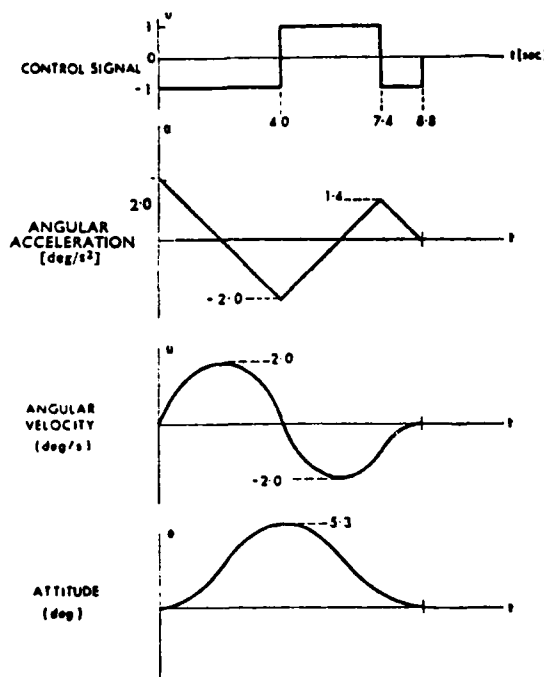


Fig. 9 Minimum time recovery from an initial thrust misalignment (control effectiveness = $1^\circ/\text{sec}^3$)

first-order system having an exponential response with a 0.1 sec time constant. The simulation assumed that the angular state was available with no estimation error. Furthermore, structural-bending and propellant-slosh dynamic effects were not simulated. These tests were performed with a control effectiveness of $\text{FLR}/I = 1.0^\circ/\text{sec}^3$. This is about the largest control authority possible; it corresponds to the lunar-landing configuration with maximum thrust and nearly empty descent propellant tanks.

The initial test results were quite disappointing.²¹ The delays in the control loop due to sampling, i.e., missing the optimal switching time by up to 0.2 sec, plus the finite actuator response time, resulted in a poor initial transient response—showing a large overshoot of the desired zero attitude error—and an unacceptably large limit cycle in the steady-state response. The limit cycle attitude excursions exceeded 8° peak to peak.

The most elegant solution to this problem would have been to find the minimum-time control law for the sampled-data triple-integral plant. Extensive general results exist

To achieve the theoretical optimal performance with the minimum-time control law of Eq. (14), the angular state of the vehicle must be continuously supplied and the optimal control action must be continuously computed. In this way, control reversals take place at the exact instant when the switching surface is reached. In the application under consideration, however, the control law was to be implemented in a digital autopilot where the angular state could be estimated and the optimal control action could be computed, only at discrete sample instants. To approximate continuous feedback control, it is of course desirable to sample and take control action, as frequently as possible. However, the total autopilot computational load, including the control law, must stay below a certain fraction of the total computer capacity, about 25 per cent, so that the remaining capacity is adequate for the navigation, guidance, display, and other computations. These considerations determined a feasible sample rate of 5 optimal-control-law evaluations per second for both axes under thrust vector control. That is, the optimal control action could be calculated every 0.2 sec. The gimbal-drive control signals, u , would be held constant between these control determinations.

To test the effect of the finite sample rate upon the closed-loop performance, a simple single-plane simulation of the vehicle was programmed and flown under the action of the proposed control law. The sample interval of 0.2 sec was simulated. In addition, the response characteristic of the gimbal-drive actuator was simulated by a

concerning the theory of minimum time discrete regulators,²² The optimal control law has been found for the sampled-data double-integral plant^{23,24}. However, the control law for the triple integral plant has not been presented in the literature. An attempt to derive the desired control law was not successful.

An engineering solution to the problem of overshoot and unacceptably large limit cycles was to utilize the continuous control law but with a reduced gain.²⁵ If the switch curve programmed in the control law is based upon an assumed control effectiveness, which is less than the actual control effectiveness, then the exact switching time becomes less critical. The state trajectory will still overshoot the switching surface. However, the excess actual control effectiveness permits the subsequent trajectory to converge back toward the switching surface. By staying close to the switching surface, the trajectory will not overshoot the origin by a large amount.

This proposed solution to the problem was simulated for the triple-integral plant, again utilizing the single-axis rigid-body simulation with sampling and actuator lag. The actual control effectiveness in the simulation was FLR/I equal to $1.0^\circ/\text{sec}^2$. The initial angular state was $\theta_0 = 0$, $\dot{\theta}_0 = 0$, and $\ddot{\theta}_0 = 2^\circ/\text{sec}^2$. The results shown in Table 1 were obtained for various choices of assumed control effectiveness employed in the control law. Settling time in Table 1 is defined as the time to reach zero angular acceleration with angular velocity and attitude simultaneously near zero. No meaningful settling time is identified in the full-gain case, because the limit cycle is comparable in amplitude to the initial conditions.

Control-law assumed control effectiveness as a fraction of the actual control effectiveness	Limit-cycle amplitude ($^\circ$, peak to peak)	Settling time	
		(sec)	(% of the theoretical minimum)
1.00	8.1	--	--
0.75	0.9	9.7	110
0.50	0.5	10.1	115
0.40	0.3	10.5	119
0.30	0.15	10.9	124
0.20	0.07	12.9	146
0.10	0.03	16.5	188

The results given in Table 1 clearly show that reducing the control-law gain can reduce significantly the expected limit-cycle amplitude. The required settling time increases as the gain is reduced. However, the increase in settling time is not large until very small values of control-law gain are used.

Based on these simulation results, the gain-reduction approach was selected as the solution to the problems introduced by sampling and actuator response delay. A 0.3 reduction in gain was implemented for all spacecraft configurations and weights. That is, the first expression in the minimum-time control law given in Eq. (14) was modified to become

$$K = 0.3 \text{ FLR/I}$$

$$c = K^{-1/3} \quad (15)$$

where K is the control effectiveness assumed by the control law.

The structure of the autopilot including the interrelationships of the state estimator, the RCS thruster control laws, and the descent-engine thrust vector control laws was discussed earlier and was illustrated in Fig. 3. The estimated vehicle angular state is compared with the angular state commanded by the guidance equations. Attitude errors and angular-velocity errors are computed. These errors plus the estimated angular acceleration form the inputs to the control laws. During descent engine powered flight, gimbal-drive commands for both axes under thrust-vector control are computed according to the optimal control law of Eq. (14) with the reduced gain of Eq. (15). Attitude control about the third axis is maintained by firing the small thrusters. The nonlinear logic, discussed earlier, operating on the attitude error and angular-velocity error, controls these thruster firings. In general, the thrusters are commanded to fire only when the errors exceed certain deadbands. In the lunar-module-alone configuration, the small thrusters also will fire about the two axes nominally under thrust-vector control, if the errors exceed the deadbands. In the docked configuration, simulation results showed that if the small thrusters were permitted to assist the thrust-vector control, they would be commanded to fire for excessively long periods. The impingement of the thruster exhaust on the descent stage would then cause a dangerous level of heating. Therefore, the autopilot for the docked configuration was modified so that during powered flight the small thrusters would not be commanded to fire about the two axes under thrust-vector control. This placed the entire burden for control on the optimal thrust vector control law.

The primary tool for testing the digital autopilot was a detailed simulation of the

vehicle and of the guidance computer.²⁶ The exact coded instructions of the digital autopilot were executed in this simulation. The test results¹⁷ showed that the optimal control law could successfully control the attitude in both the lunar-module-alone configuration and the docked configuration. The important disturbances were shown to be the thrust misalignment at ignition and the unsymmetrical compliance of the engine-gimbal structure in response to thrust-magnitude changes.

PERFORMANCE IN FLIGHT

A dramatic demonstration of the attitude-control capability of the minimum-time thrust-vector control law was given during the flight of Apollo 9. The mission was the first manned flight of a lunar module and took place in earth orbit. The previous flight test of a lunar module was unmanned and, due to a premature engine cut-off, failed to demonstrate a long-duration period of thrusting with the descent-propulsion-system engine. Therefore, for Apollo 9, a primary flight-test objective was to obtain a long period of powered flight using the descent engine. In addition, the engine-throttling capability was to be tested. If the lunar module was to perform such a long burn while not docked to the command module, the orbits of the lunar module and the command module would become substantially different, creating a rescue problem should difficulties develop in the lunar module. Furthermore, the different low-altitude earth orbits would make tracking coverage difficult. Therefore, the mission planners decided to conduct the long-burn test of the descent engine while the two spacecrafts were in the docked configuration. Should problems develop, the crew could immediately transfer to the command module. Also the greater the mass of the combined vehicles permitted less orbital change for the same duration of thrusting, thereby helping the tracking problem.

The planned main-engine thrust profile is shown in Fig. 10. Simulation of the autopilot performance on the digital simulator produced the predicted system performance shown in Fig. 11. The attitude errors about the three spacecraft axes are shown. The P axis

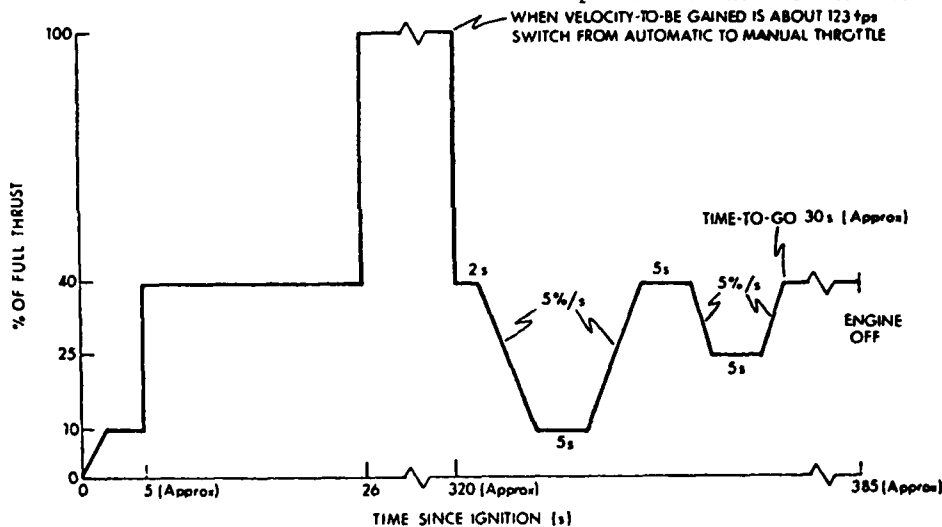


Fig. 10 Planned descent-engine thrust profile for the Apollo 9 docked burn.

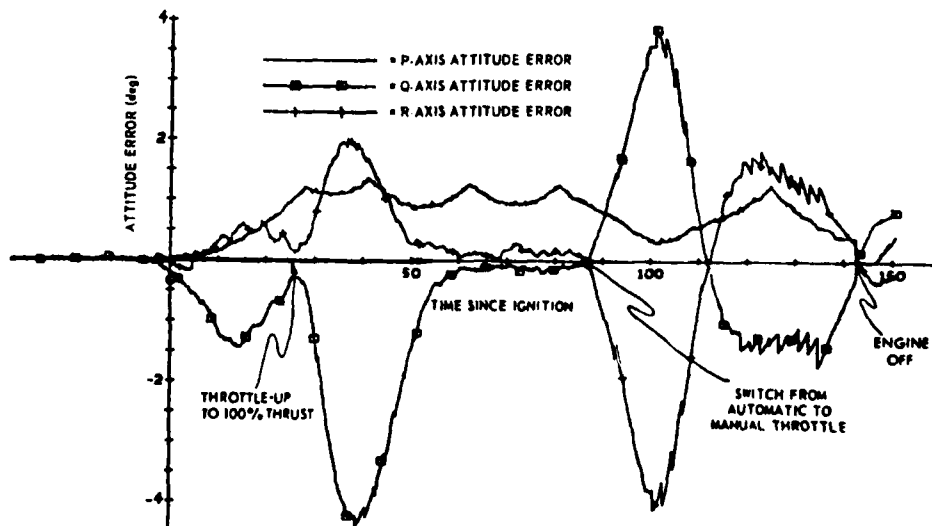


Fig. 11 Predicted attitude errors during the Apollo 9 docked burn.

is the axis being controlled by the small thrusters. The Q and R axes are the two spacecraft axes being controlled by the minimum-time thrust-vector control law. During the initial 26 sec after ignition at 10 and 40 per cent thrust, there is a mild attitude transient during which the angular-state estimator and the thrust-vector control law discover the state deviations due to the small thrust misalignment at ignition and take action to restore the angular state to zero. At throttle-up to 100 per cent 26 sec after ignition, the compliance of the structure where the engine is mounted causes a shift in thrust-vector direction when the thrust level is changed. The change in thrust from 40 to 100 per cent thrust was assumed to produce a 0.4° shift in thrust-vector direction relative to the center-of-mass about both axes. The angular-state estimator soon discovers the new bias angular acceleration due to the thrust misalignment, and the minimum-time control law automatically responds to the updated state estimates. The attitude transient induced by the thrust misalignment at throttle-up produces a peak attitude error of 4° . The control law returns the attitude error, angular velocity error, and angular acceleration to nearly zero. The total transient from throttle-up to steady state lasts about 30 sec.

In the flight plan, a long 5-min period at 100 per cent thrust exists for most of the burn. This period was noticeably shortened in the simulation, to save computer time. No significant change from the steady-state behavior shown in Fig. 11 would be expected in a full-length burn simulation. The end of the planned burn was to include a period of manual throttling to test further the variable-thrust performance of the engine. The simulation results predicted similar attitude transients when the thrust was reduced from 100 to 40 per cent, but of the opposite sign. During the last 30 sec at constant 40 per cent thrust, the control law is not sufficiently fast to reduce the attitude error to zero. Because the vehicle is not at this time perfectly aligned with the remaining velocity-to-be-gained, the guidance equations are commanding a change in the desired attitude. The discontinuities in desired attitude every 2 sec can be seen in Fig. 11 through their effect on the attitude error. The actual vehicle attitude is changing somewhat faster than the desired attitude, so the attitude errors are reducing. In the last 4-6 sec, the guidance equations stop changing the desired attitude and the attitude errors are seen to move smoothly toward zero.

The Apollo 9 mission was flown in March 1969. The docked burn utilizing the descent engine was conducted as planned. The astronauts' comments during the burn indicated that the control was quite satisfactory. Astronaut Schweickart commented that he felt some low-frequency oscillations, probably propellant sloshing, but it did not prevent satisfactory performance. Subsequent analysis²⁷ of the telemetered data produced the plots of attitude error shown in Fig. 12. As discussed in Ref. 27, the initial throttle-up transients in flight may bear little resemblance to the predicted transients. This is

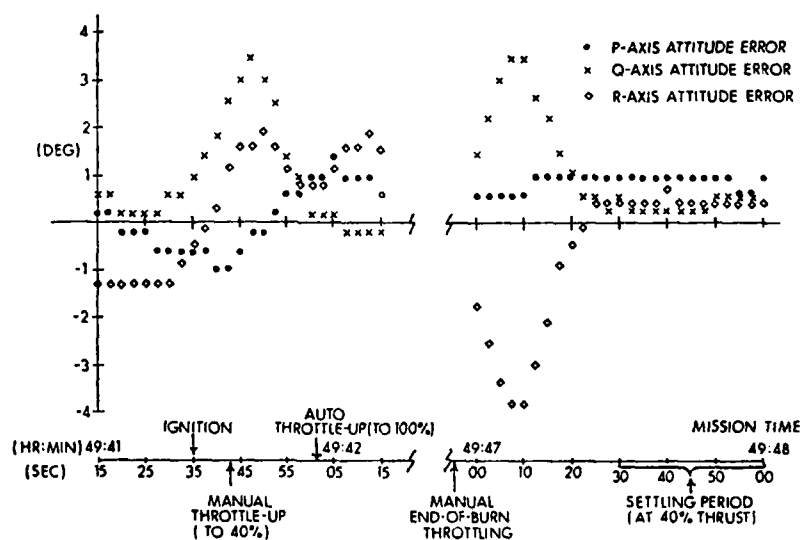


Fig. 12 Actual attitude errors during the Apollo 9 docked burn.

because the throttle-up transient errors are strongly influenced by the random engine misalignment at ignition. The predicted and actual end-of-burn transients, on the other hand, are quite similar. After the long period at 100 per cent thrust, the engine thrust vector is aligned quite close to the center-of-mass. The only significant disturbance is the deterministic thrust-misalignment angle introduced at throttle-down by the structural compliance.

The LM autopilot continued to fly with dramatic success in the several Apollo missions, including the lunar landings. Telemetered data plus comments from the astronauts confirmed that the autopilot performed in flight in close agreement with the intended performance.

During the first lunar landing (Apollo 11) the autopilot followed first the automatic and later the manual attitude commands, changing from a nearly horizontal thrusting attitude at ignition to a vertical (upright) attitude at touchdown. During the first four minutes of the powered descent after the initial transient, the thrust-vector attitude control law was successful at following the slowly changing attitude commands without the assistance of the U or V RCS jets. Later, a propellant slosh oscillation developed with amplitude sufficiently large to exceed the deadbands in the RCS control laws. Small RCS firings were commanded to limit the slosh oscillation amplitude. The slosh oscillation at 0.5 Hz may be seen in the pitch angular velocity shown in Fig. 13

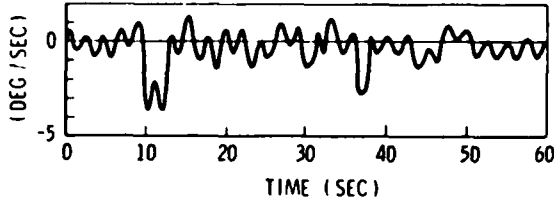


Fig. 13 Pitch-rate during a portion of the lunar landing powered descent.

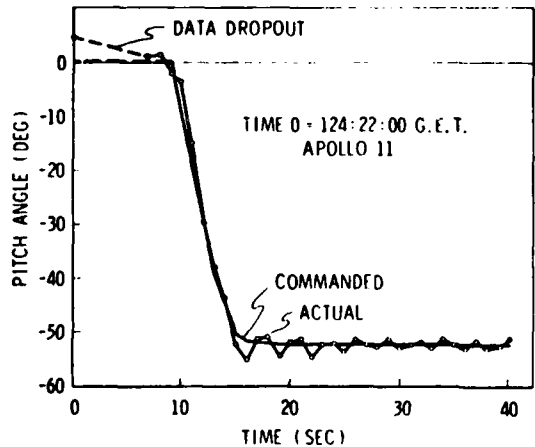


Fig. 14 Pitch guidance command and response, initial phase of powered ascent.

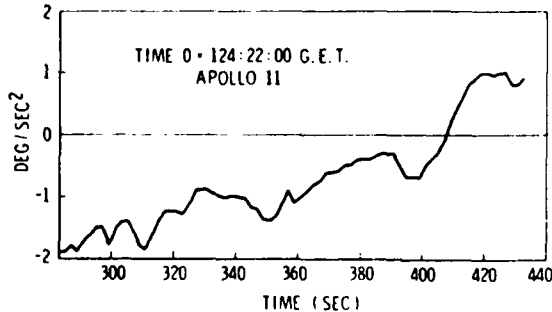


Fig. 15 V' component of estimated bias angular acceleration during final phase of powered ascent.

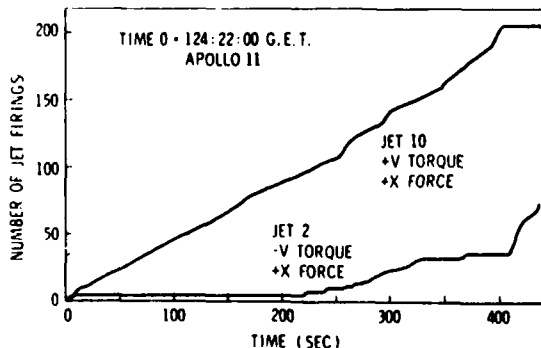


Fig. 16 Total V-axis RCS jet firings during powered ascent.

from Ref. 15. The automatic guidance was landing the spacecraft among numerous boulders, so Armstrong switched from automatic to manual attitude commands and pitched the Eagle upright to extend the trajectory beyond the rock field.²⁸

The pitch attitude following liftoff from the lunar surface is shown in Fig. 14 from Ref. 15. After 10 sec of vertical rise, the automatic guidance commanded a pitch-over of 50 deg at a rate of 10 deg/sec. Note the rapid response provided by the RCS control laws. The actual attitude follows closely the desired attitude. After the pitch-over maneuver, the typical ascent low-frequency attitude limit cycle can be seen.

As the ascent propellant is expended, the center of mass moves from behind the thrust vector ($-Z$ direction) at liftoff to slightly ahead of the thrust vector ($+Z$ direction) at cutoff. This causes a time-variation in the bias angular acceleration components along both the U' and V' axes. The V' component of the bias angular acceleration as computed by the state estimator during the last 150 sec of powered ascent is shown in Fig. 15 from Ref. 15. The autopilot adapted its critical parameters in the RCS control laws in response to this varying estimated bias acceleration. The accumulated number of firings of the V axis RCS jets for the entire powered ascent is shown in Fig. 16 from Ref. 29. After liftoff and the initial pitchover, it is evident that attitude control about the V axis was maintained for about 200 sec by firing the $+V$ jet only. Later the limit cycle amplitude increased until firings from both the $+V$ jet and the $-V$ jet were required to maintain attitude control. Although the $-V$ torque firings produce angular acceleration in the same direction as the bias angular acceleration of the ascent engine, nevertheless both the $+V$ torque and $-V$ torque are generated by upward forcing ($+X$) jets and hence, represent no loss in Δv . This period of $+V$ and $-V$ torquing may be related to propellant slosh oscillations.²⁹ Near the end of the powered ascent after the bias angular acceleration has reversed sign, no further firings are commanded of the $+V$ jet and attitude control is maintained about the V axis by the $-V$ jet alone. With the nonorthogonal control axes, no unnecessary small pulses were seen.

CONCLUSIONS

The separate synthesis of the attitude state estimator and the memoryless control laws, a structure suggested by optimal control theory, proved to be a practical design approach. Separate control laws were designed for the RCS jets and for the descent engine thrust vector. The control laws were further subdivided into separate channels. The axes chosen for application of the separate RCS control laws were non-orthogonal. This design effectively

eliminated performance problems that existed because the torque vectors of the RCS jets were not parallel to the principal axes of inertia of the vehicle.

The attitude state estimator had a structure similar to that of a Kalman filter or a Luenberger observer in that the modeled response of the vehicle to known control commands was used to eliminate estimation lag. However the estimator gains were not the Kalman gains but were set in a novel manner to minimize the nonlinear quantization effects. The attitude state estimator computed the angular velocity and angular acceleration of the vehicle, based on measurement of vehicle attitude and assumed control response. The success of this state estimator demonstrates that rate gyros are not required sensors for an autopilot. They may be eliminated to achieve an increase in over-all system reliability.

The RCS control laws in the LM-alone case employed parabolic switch curves in their phase plane logic. This form was suggested by the minimum time/fuel control law for the double integral plant. The critical parameters in the RCS control laws were adapted in response to the varying mass of the spacecraft and the bias angular acceleration due to the thrusting main engine. The control law design permitted rapid response to commands with a minimum of jet firings. Satisfactory control was possible even in the lightest ascent configuration because the RCS control laws computed the exact firing time required to achieve a desired rate change.

A third-order minimum time control law was used to control the vehicle attitude by means of the thrusting descent engine. The minimum-time continuous control law for the triple-integral plant was derived. This control law was then successfully integrated into the digital autopilot. Although the angle of the thrust vector relative to the center-of-mass could only be commanded to change at the slow rate of $0.2^\circ/\text{sec}$, the time-optimal control law permitted satisfactory attitude control, often without the assistance of the small thrusters. This achieved a saving in the propellant expenditure and number of firings required by the thrusters. Within the knowledge of this author, this was the first successful application of a third-order minimum-time control law to a significant control problem.

This design experience with the minimum time thrust vector control law provides a valuable lesson for future spacecraft designers. In particular, the designer may not need to specify high-power, high-speed actuators when the spacecraft is to be controlled by gimbaling the thrusting engine. If the uncontrolled vehicle is unstable (for example, many boosters are aerodynamically unstable), then rapid actuation is required. (This is because for an unstable plant with bounded control the set of initial states from which the origin can be reached is larger if the maximum control is larger. Hence a faster actuator reduces the probability that a random disturbance can lead to loss of control.) If rapid attitude maneuvers must be controlled using the thrust vector, then rapid actuation again may be required. But where the vehicle is at least neutrally stable and there are no rapid-maneuver requirements which must be met solely by torque from the thrust vector, low-power low-speed actuators may meet the mission requirements. This permits a significant saving in spacecraft weight and reduces the power that must be supplied to drive the actuators. To obtain the maximum performance with slow actuators, the control-system engineer should explore the use of a time-optimal control law.

APPENDIX. SUMMARY OF DERIVATION OF THE TIME OPTIMAL CONTROLLER FOR THE TRIPLE INTEGRAL PLANT.

Triple integral plant. The differential equation may be transformed into a non-dimensional set of first-order equations

$$\begin{aligned} \dot{x}_1 &= u \\ \dot{x}_2 &= x_1 \\ \dot{x}_3 &= x_2 \end{aligned} \tag{A.1}$$

It is desired to derive a control law having the property that any initial state will be transferred to the origin of the state space in the minimum time. The available control is bounded

$$-1 \leq u \leq +1 \tag{A.2}$$

Applicable theorems. Several theorems are available for the problem of time-optimal control of linear time-invariant systems:

Existence: A control can easily be constructed for any initial state which will transfer the state of system (A.1) to the origin. Then by Theorem 13 of Ref. 30, since there exists for the system at least one control taking the state from the initial state to the origin, an optimal control also must exist. (If system (A.1) had been unstable, then a bounded control for all initial states could not have been found.)

Uniqueness: It can be shown that the state of system (A.1) is completely controllable. Since it is completely controllable, it follows from Theorem 11 of Ref. 30 that the optimal control is unique.

Necessary conditions: The characteristic values of system (A.1) are real (there is a triple root at zero). It follows from Theorem 10 of Ref. 30 that the following

necessary conditions must be met for a control $u(t)$ to be optimal:

1. The control $u(t)$ must be piecewise-constant, taking on the values +1 or -1 only.
2. The control can change values at most twice (that is, there can be no more than three intervals of constancy).

A control law satisfying the necessary conditions. Define V_1 to be the set of all states from which the origin can be reached in positive time by applying the single constant control $u = +1$ or $u = -1$. It can be shown that states in V_1 are on the curve given by

$$\left. \begin{aligned} x_2 &= -\frac{1}{2} s_1 x_1^2 \\ x_3 &= \frac{1}{6} x_1^3 \end{aligned} \right\} -\infty < x_1 < \infty \quad (\text{A.3})$$

where

$$s_1 = \text{sign}(x_1). \quad (\text{A.4})$$

If the state is in V_1 , a constant control which carries the state to the origin is

$$u = -\text{sign}(x_1). \quad (\text{A.5})$$

Define V_2 to be the set of all states from which the origin can be reached in positive time by applying either a control sequence $(-1, +1)$ or a control sequence $(+1, -1)$. It can be shown that states in V_2 are on the surface given by

$$x_3 = -\frac{1}{3} x_1^3 - s_2 x_1 x_2 - s_2 (s_2 x_2 + \frac{1}{2} x_1^2)^{3/2} \quad (\text{A.6})$$

where

$$s_2 = \text{sign}(x_2 + \frac{1}{2} s_1 x_1^2). \quad (\text{A.7})$$

If the state is in V_2 , a constant control which carries the state to V_1 is

$$u = -\text{sign}(x_2 + \frac{1}{2} s_1 x_1^2). \quad (\text{A.8})$$

Define V_3 to be the set of all states from which the origin can be reached in positive time by applying either a control sequence $(+1, -1, +1)$ or a control sequence $(-1, +1, -1)$. It can be shown that if the state is in V_3 , a constant control which carries the state to V_2 is

$$u = -\text{sign} \left[x_3 + \frac{1}{3} x_1^3 + s_2 x_1 x_2 + s_2 (s_2 x_2 + \frac{1}{2} x_1^2)^{3/2} \right] \quad (\text{A.9})$$

Equations (A.5), (A.8) and (A.9), taken together, constitute a control law which meets the necessary condition that any initial state is transferred to the origin with no more than two control reversals.

The optimal control. It can be shown that if at any instant the control specified by the above control law is not applied, then more than two control reversals will be required to reach the origin. Hence no other control exists that satisfies the necessary condition. Therefore the above control is the optimal control.

In a practical application, it is improbable that the control reversal will be executed so that the state trajectory is transferred precisely onto the surface V_2 . Even if the improbable occurred and the control was reversed precisely on the analytic surface V_2 , the ensuing trajectory would soon wander off the analytic surface, because the actual plant is not described perfectly by the assumed differential equation. Therefore it is necessary to implement only Eq. (A.9). The control given by Eq. (A.9) will bring the state sufficiently close to the origin.

REFERENCES

1. Miller, J.E. ed., Space Navigation Guidance and Control, AGARDograph 105, 1966, Technivision Ltd., Maidenhead, England.
2. Hoag, D.G., "Apollo Navigation, Guidance and Control Systems: A Progress Report," April 1969, National Space Meeting of the Institute of Navigation, Houston, Texas.
3. Cherry, G.W. and O'Connor, J., "Design Principles of the Lunar Excursion Module Digital Autopilot," R-499, July 1965, M.I.T. Instrumentation Lab., Cambridge, Mass.
4. Cherry, G.W., "Design Principles for an Integrated Guidance and Control System for the Lunar Excursion Module," AIAA Fourth Manned Space Flight Meeting, Oct. 1965, St. Louis, Mo.
5. Cox, K.J., "A Case Study of the Apollo Lunar Module Digital Autopilot," IEEE Case Studies in System Control, 69-C41-AC, Aug. 1969, Boulder, Colo.
6. Widnall, W.S., "Lunar Module Digital Autopilot," Journal of Spacecraft and Rockets, Vol. 8, No. 1, Jan. 1971, pp. 56-62.

7. Widnall, W.S. et al., "Digital Autopilot," Sec. 3 (Rev. 1) of "Guidance System Operations Plan for Manned LM Earth Orbital and Lunar Missions Using Program LUMINARY 1A," R-567, June 1969, M.I.T. Instrumentation Lab., Cambridge, Mass.
8. Joseph, P.D., and Tou, J.T., "On Linear Control Theory," AIEE Transactions, Applications and Industry, Vol. 80, Sept. 1961, pp. 193-196.
9. Kalman, R.E., "A New Approach to Linear Filtering and Prediction Problems," Journal of Basic Engineering, March 1960, pp. 35-45.
10. Luenberger, D.G., "Observing the State of a Linear System," IEEE Trans. on Military Electronics, Vol. MIL-8, No. 2, April 1964, pp. 74-80.
11. Luenberger, D.G., "Observers for Multivariable Systems," IEEE Trans. on Automatic Control, Vol. AC-11, No. 2, April 1966, pp. 190-197.
12. Athans, F., and Falb, P.L., Optimal Control, An Introduction to the Theory and its Applications, McGraw-Hill, New York, 1966, pp. 703-710.
13. Kalan, G.R., "Improvement of the Bending Stability of the LM Autopilot in the CSM-Docked Configuration," SAD 18-69, April 1969, M.I.T. Instrumentation Lab., Cambridge, Mass.
14. Stengel, R.F., "Manual Attitude Control of the Lunar Module," Journal of Spacecraft and Rockets, Vol. 7, No. 8, Aug. 1970, pp. 941-948.
15. Delashmit, W.H. and Lee, R., "Apollo DAP Postflight Analysis Summary," EG-70-10, March 1970, NASA/MSC, Houston, Texas.
16. Croston, R.C., Raney, J.L., and Goekler, W.B., "Digital Autopilot for the LM Mission Simulator," IAF Congress, Oct. 1968, New York.
17. Widnall, W.S., Keene, D.W., Weissman, P.S., Goss, R.D., Jones, J.E., and Work, C.C., "LM Digital Autopilot Simulation Results Using Program SUNDANCE," E-2377, Jan. 1969, M.I.T. Instrumentation Lab., Cambridge, Mass.
18. Goss, R.D., "Nonorthogonal Axis System for LM Digital Autopilot," SAD 12-69, March 1969, M.I.T. Instrumentation Lab., Cambridge, Mass.
19. Widnall, W.S., "Derivation of the Optimum Control Program for Steering the LEM Using the Gimbaled Descent Engine," SGA 3-66, Jan. 1966, M.I.T. Instrumentation Lab., Cambridge, Mass.
20. Widnall, W.S., "The Minimum-Time Thrust-Vector Control Law in the Apollo Lunar-Module Autopilot," Automatica, Vol. 6, No. 5, Sept. 1970, pp. 661-672.
21. Goss, R.D., Undocumented simulation results, M.I.T. Instrumentation Laboratory, Cambridge, Mass., Jan. 1966.
22. Desoer, C.A., Polak, E., and Wing, J., "Theory of Minimum Time Discrete Regulators," Proceedings of the 2nd IFAC Congress, Automatic and Remote Control, 1964.
23. Nelson, W.L., "Optimal Control Methods for On-Off Sampling Systems," Trans. ASME, J. Bas. Engng 84, No. 1, 1962.
24. Polak, E., "Minimum Time Control of Second Order Pulse-Width-Modulated Sample-Data Systems," Trans. ASME, J. Bas. Engng 84, No. 1, 1962.
25. Widnall, W.S., "Increasing the Stability of Nonlinear Bang-Bang Control Programs Through Gain-Reduction," Informal Memo, M.I.T. Instrumentation Laboratory, Cambridge, Mass., Jan. 22, 1966.
26. Widnall, W.S., Glick, F.K., Henize, J., and Drane, L.W., "The Digital Simulation for the Verification of Program SUNBURST," M.I.T. Instrumentation Laboratory Report E-2146, Cambridge, Mass., July 1967.
27. Jones, J.E., "Post-Flight Analysis of the Digital Auto-Pilot Performance in the SUNDANCE Mission D Docked DPS Burn (Apollo 9)," Post-Flight Data Analysis Memo No. 21, M.I.T. Instrumentation Laboratory, Cambridge, Mass., June 4, 1969.
28. Stengel, R.F., "The Manually-Controlled Landing of Eagle," SAD 28-69, Aug. 1969, M.I.T. Instrumentation Lab., Cambridge, Mass.
29. Goss, R.D., Private communication, Sept. 23, 1969, M.I.T. Instrumentation Lab., Cambridge, Mass.
30. Pontryagin, L.S., Boltyanskii, V.G., Gamkrelidze, R.V., and Mishchenko, E.F., The Mathematical Theory of Optimal Processes, MacMillan, New York, 1964 (or Interscience, New York, 1962).

APPLICATION OF OPTIMAL CONTROL TECHNIQUES
TO TACTICAL MISSILE GUIDANCE

by
Charles F. Price
THE ANALYTIC SCIENCES CORPORATION
One Jacob Way
Reading, Massachusetts 01867
United States of America

SUMMARY

This paper illustrates the application of optimal control theory to the design of guidance laws for tactical missiles. A survey of applications reported in the open literature is presented. Case studies are developed using several different linear-quadratic-gaussian formulations of stochastic optimal control problems. A new guidance law is presented which explicitly accounts for target parameter uncertainty. Simulation results and parameter sensitivity studies are presented which provide performance comparisons between the optimal guidance techniques and conventional proportional guidance.

1.

INTRODUCTION

1.1 BACKGROUND

Tactical missile guidance offers a number of opportunities for applying optimal control techniques to achieve practical performance benefits. First, the basic guidance objective is to intercept the target with as small a miss distance as possible, a condition which is readily expressed as a mathematical performance index. Usually implicit in this objective is the requirement to achieve as large an operational envelope as possible -- that is, intercepts should be possible from a wide variety of launch conditions. Consequently, the missile energy must be efficiently managed.

The missile typically is propelled by a rocket engine having a fixed thrust schedule and uses aerodynamic controls for effecting guidance maneuvers; however, concepts for thrust vectored control and throttleable or segmented-burn engines have also been considered. Such controls provide the means to implement guidance laws which yield efficient trajectories, as well as accurate intercepts.

A missile trajectory may consist of several phases during which different guidance modes are active. A typical sequence is: the post-launch phase which consists of a preprogrammed flight path to achieve safe separation from the launch platform and to orient the missile in the general direction of the target; a mid-course phase during which the missile either flies a preplanned course toward the target, or receives guidance signals from the launch platform, without the missile itself directly sensing the target position; and a terminal phase during which the missile senses the target position directly with its own active or semi-active sensor, and flies a homing guidance law designed to null the intercept miss distance.

Although the overall objective is miss distance minimization, the guidance laws used during intermediate phases are generally more concerned with operational constraints. For instance, midcourse guidance usually steers the missile so that the missile seeker can acquire the target at the appropriate range, and so that the missile velocity is adequate at the beginning of the terminal phase. Although such constraints can, in principle, be incorporated within a global trajectory optimization problem, the guidance laws for each phase have typically been developed separately.

This paper is primarily concerned with the terminal guidance phase where target dynamic characteristics can have an important effect on guidance accuracy. Potential missile targets are of many different types, but the important distinctions from the standpoint of guidance law design are those on the earth's surface and those which are airborne. Surface targets tend to operate at speeds and possess maneuvering capabilities which are significantly less than a missile's; therefore hitting the target is largely a matter of knowing where it is, and conventional missile guidance techniques (e.g., beam-riding, pursuit, and proportional) are generally quite adequate. By contrast, the much higher speeds and maneuver capabilities of air targets can cause significant miss distances against conventionally guided missiles. In this case the guidance law must know something about the target's velocity, and perhaps its acceleration as well; correct use of the higher derivatives of target motion calls for the application of optimal control methods.

1.2 A SURVEY OF GUIDANCE TECHNIQUES

The first applications of optimal control methods to the missile guidance problem dealt with simplified linear equations of motion for characterizing missile motion normal to the initial line-of-sight to the target. Minimization of quadratic penalties on the acceleration time-history and the terminal miss distance lead to a linear feedback guidance

law that is readily interpreted as a modification to conventional proportional navigation. Representative treatments of this problem are found in Refs. 1 and 2; a recent paper (Ref. 3) derives a number of different guidance laws for different types of quadratic performance indices.

Deterministic treatment of optimal guidance attempts to derive feedback guidance laws, expressed in terms of the system state variables. When accounting for the noise inherent in measurement data, the separation theorem of linear-quadratic-gaussian (LQG) stochastic control (Ref. 4) is invoked to design a stochastic guidance law consisting of a Kalman filter, which estimates the state variables, cascaded with the guidance command computation. Performance analyses of stochastic guidance laws are presented in Refs. 5 and 6.

A number of techniques have been developed for relaxing the assumption that the missile-target engagement dynamics are linear. In Refs. 5 and 6, an optimal stochastic guidance law is derived which accounts for bounded control constraints. A suboptimal stochastic guidance law is derived in Ref. 7, based upon statistical linearization, for the case where both control variables and state variables are bounded. References 8 and 9 apply singular perturbation methods to derive approximately optimal, deterministic feedback guidance laws accounting for nonlinear kinematic and aerodynamic effects.

The references listed above typically treat the target dynamics as known, either following a prescribed guidance law of its own, or maneuvering according to a specified stochastic model. Reference 10 adopts a differential game formulation wherein the target evasive and the missile pursuit strategies are jointly optimized. A similar approach is taken in Ref. 11 where a concept is developed for guiding the missile so that the target is always "reachable".

In principle, missile accelerations in three directions can be effected with both aerodynamic lift and thrust magnitude controls. Most investigations have dealt only with lift; however, Ref. 7 applies thrust control assuming a fixed proportional guidance law for generating lift, and Ref. 12 derives both thrust and lift controls for a bilinear model of the engagement dynamics.

All of the cases described above are concerned largely with air targets; against ground targets, trajectory shaping may be an important consideration so that the missile approaches at the required aspect angle. References 13 and 14 apply optimal control techniques to achieve specified constraints on the terminal intercept geometry.

Finally, when direct measurements of target position are available, all the variables needed for guidance can be estimated with appropriate filtering, and separation between the functions of filtering and control is usually justified. However, if an important position coordinate, such as target range, cannot be measured, then missile maneuvers may be required to improve estimation accuracy prior to attempting to reduce the miss distance. Applications of this so-called dual-control concept are given in Refs. 15 and 16.

The above review is not intended to be exhaustive, but provides some indication of the various applications of optimal control to the missile guidance problem. This paper demonstrates the use of optimal lift control to reduce miss distance, drawing on new material as well as upon previously published results primarily taken from Ref. 6.

2.

GUIDANCE SYSTEM MODEL

Figure 1 presents a functional diagram of a missile terminal homing guidance system. This section briefly describes the assumed mathematical models for the subsystems, which are defined by the expanded block diagram in Fig. 2.

Guidance Law - The guidance law is separated into a guidance filter which estimates the guidance state variables, and a guidance command which computes missile normal acceleration commands. The guidance law design is discussed in detail in subsequent sections. Observe that it is thought of as separate from the missile autopilot, in the sense that each can be designed separately. This is typically valid because the speed-of-response of the airframe rotational dynamics is much greater than that of the translational dynamics.

Seeker - The homing seeker measures the angular position of the line-of-sight (LOS) to the target relative to the sensor centerline by observing the direction of electromagnetic energy reflected from the target. The LOS angle measurement is corrupted by wideband noise. It is implicitly assumed here that the seeker is a radar which measures range as well as LOS angle; however, the range measurement errors are neglected. The seeker model includes the parasitic coupling of missile airframe dynamics into the LOS direction perceived by the seeker. The latter error is caused by aberration of the electromagnetic energy as it passes through the protective covering -- radome -- over the seeker, and it depends on missile attitude through the gain k_r in Fig. 2.

Missile Dynamics - The missile dynamics consist of the missile airframe dynamics and associated autopilot, which is designed so that the missile lateral acceleration follows the autopilot acceleration commands as closely as possible. Although the actual airframe dynamics are a nonlinear function velocity, angle of attack, control surface

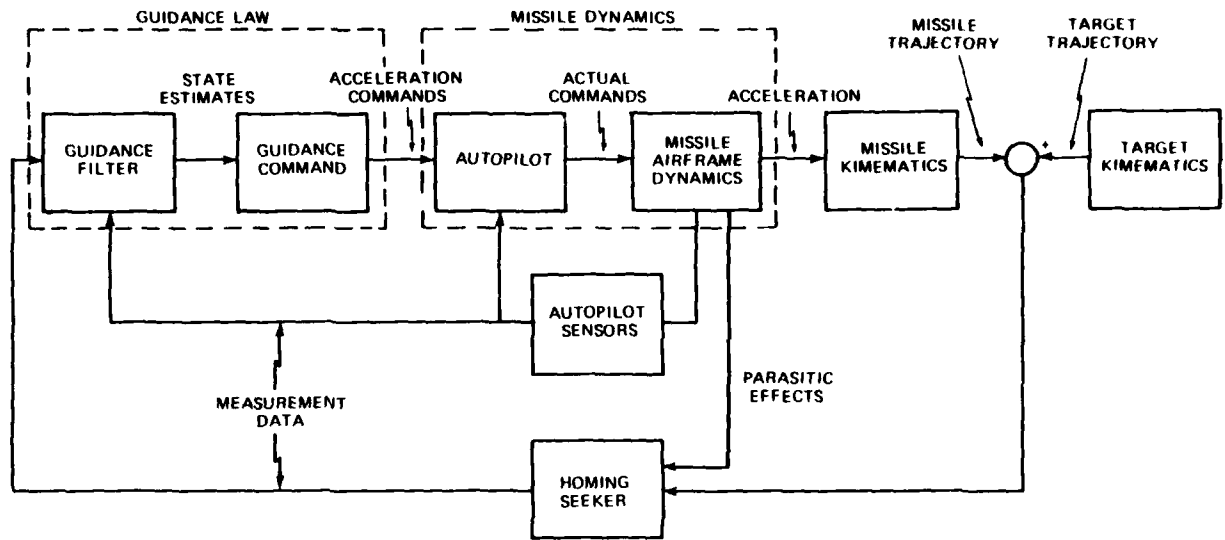


Figure 1 Terminal Guidance System Functional Diagram

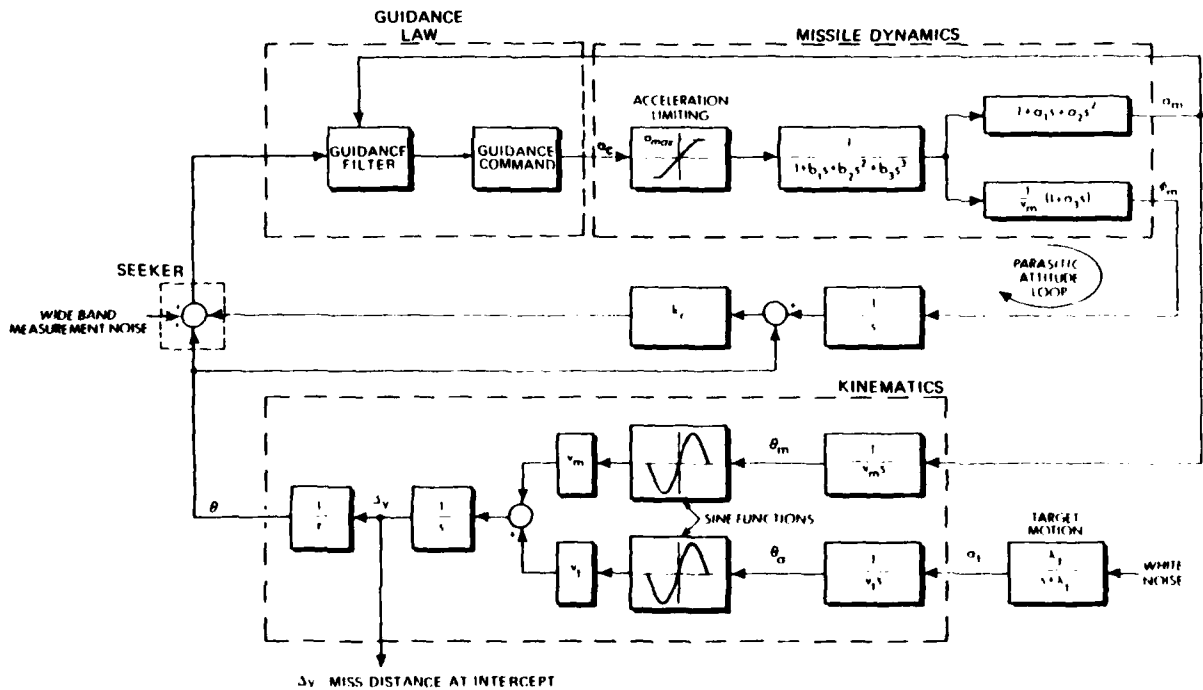


Figure 2 Detailed Model Description

deflection and altitude, a properly designed autopilot provides a nearly linear response characteristic if changes in these parameters about a nominal flight condition are small. In addition, the dynamics model includes one of the most significant guidance system nonlinearities -- acceleration input command limiting. The airframe acceleration command must be limited in an actual missile to prevent either structural failure or stalling.

Missile-Target Kinematics - The model of the interceptor-target kinematics assumes that the missile and target accelerations are normal to their respective velocity vectors. This implies that both velocities have constant magnitude but variable direction. The components of missile and target acceleration which are normal to the line-of-sight, and which control the terminal miss distance, are represented as trigonometric functions of

the appropriate orientation angles. This constitutes another important nonlinear effect included in the model.

Measurement Noise - The noise on the measurement of LOS angle is caused by a number of error sources, some of which are range dependent. Three types of noise are included in the model: receiver noise (decreases with decreasing range), target angular scintillation noise (increases with decreasing range), and range independent noise caused by the seeker servo system and possibly by amplitude fluctuations in the received signal.

Target Motion - The system model includes a randomly accelerating target, modeled as the output of a lowpass filter driven by white noise. This is statistically representative of maneuvers that are constant in magnitude, but switch sign at random times -- sometimes referred to as "jinking". The filter output has the same autocorrelation function as the jinking maneuver.

The model in Fig. 2 is referred to here as the simulation model; it is used to evaluate the performance of various guidance laws which are derived using simpler design models. The missile-target motion is restricted to a fixed plane and the effects of gravity and aerodynamic drag are neglected. The kinematic variables -- r , v_m , v_t , θ_m , θ , a_m , and a_t are defined in Fig. 3. The quantity k_r is a gain representing the aberration error -- often referred to as random slope -- which couples the missile airframe motion into the seeker measurements of LOS angle. The transfer function coefficients -- λ_t , a_1 , a_2 , a_3 , a_4 , b_1 , b_2 , and b_3 -- are assigned values to yield realistic dynamic characteristics.

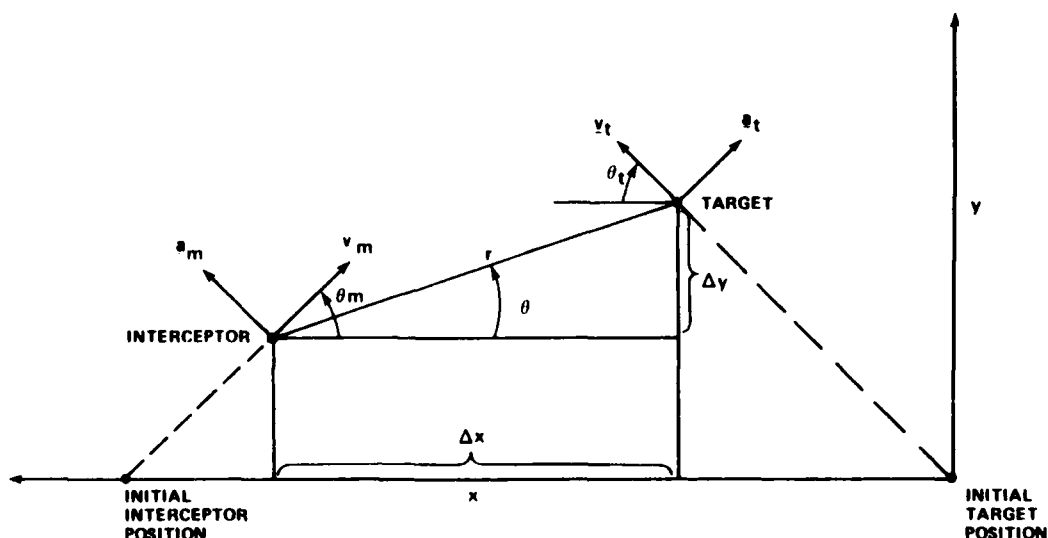


Figure 3 Definitions of Kinematic Variables

Miss distance is defined as the minimum value of r and represents the point of closest approach between the missile and target. For most normal engagements -- i.e., $\dot{\Delta x} \approx \dot{y}_d$ -- the minimum range vector is nearly perpendicular to the original LOS. Consequently, miss distance is approximated in Fig. 2 as Δy at time t_f when Δx equals zero.

3. COMPARISON OF SEVERAL OPTIMAL GUIDANCE LAWS

3.1 DESIGN MODEL ASSUMPTIONS

Development of any optimal guidance law must be based upon a mathematical model of the missile/target intercept dynamics. The simulation model shown in Fig. 2 could be used, but it is convenient to introduce several approximations in order to simplify the guidance law derivations.

The equations in Table 1 provide a simplified approximate representation of the dynamics in Fig. 2, resulting from the following assumptions:

- θ_m and θ_t are nearly constant

TABLE 1
GUIDANCE LAW DESIGN MODEL

Kinematics:	$\Delta \ddot{y} = a_t - a_m$ $\Delta \dot{x} = \text{constant}$
Target:	$\dot{a}_t = -\lambda_t a_t + \lambda_t w_t$ $E\{w_t\} = 0; \quad E\{w_t(t) w_t(t)\} = \frac{2\sigma_t^2}{\lambda_t} \delta(t-t)$
Missile Dynamics:	$\dot{a}_m = -\lambda_m a_m + \lambda_m a_c \cos \theta_m$
Discrete Measurements:	$z_{1k} = \theta_k + v_k$ $z_{2k} = \Delta v_k / r_k + v_k$ $z_{2k} = t_{go_k} - r_k / \dot{r}_k$ $z_{3k} = r_k$ $z_{4k} = a_{mk}$ $E\{v_k\} = 0$ $E\{v_k^2\} = \sigma_g^2 / r_k^2 + \sigma_r^2 r_k^2 + \sigma^2$

- The dependence of $\Delta \ddot{y}$ on θ_t is suppressed in the definition of a_t
- The dependence of $\Delta \ddot{y}$ on θ_m is accounted for in the differential equation for a_m , but the time-variation in θ_m is neglected
- The missile dynamics can be approximated as a first-order lag.
- The effect of airframe acceleration limiting is neglected
- Range, time-to-go, and missile acceleration are measured with negligible error
- The target driving noise spectral density is chosen to yield $E\{a_t^2\} = \sigma_t^2$
- The measurement noise variances σ_g^2 , σ_r^2 , and σ^2 correspond to glint, receiver and servo noise components, respectively; the receiver noise model is that associated with a semi-active radar receiver.

The equations in Table 1 can be written in the state variable form

$$\dot{\underline{x}}(t) = \underline{F}\underline{x}(t) + \underline{g} a_c(t) + \underline{w}(t) \quad (1)$$

$$z_k = \underline{h}^T \underline{x}(t_k) + v_k \quad (2)$$

where

$$\underline{x}^T = [\Delta y \quad \Delta \dot{y} \quad a_t \quad a_m]$$

$$\underline{w}^T = [0 \quad 0 \quad \lambda_t w_t \quad 0]$$

$$F = \begin{bmatrix} 0 & 1 & 0 & 0 \\ 0 & 0 & 1 & -1 \\ 0 & 0 & -\lambda_t & 0 \\ 0 & 0 & 0 & -\lambda_m \end{bmatrix}; \quad g = \begin{bmatrix} 0 \\ 0 \\ 0 \\ \lambda_m \cos \theta_m \end{bmatrix} \quad (3)$$

$$h^T = \left[\frac{1}{r} \quad 0 \quad 0 \quad 0 \right]$$

3.2 LINEAR-QUADRATIC-GAUSSIAN (LQG) GUIDANCE LAW

Based on the above model, we can formulate a general LQG guidance problem stated as:

Minimize

$$J = E \left\{ \Delta y^2(t_f) + \gamma \int_0^{t_f} a_c(t)^2 dt \right\} \quad (4)$$

subject to Eqs. 1 and 2, where γ is a penalty on the control weighting. We know from the separation theorem that the structure of the resulting guidance law is a Kalman (guidance) filter cascaded with a guidance command, the same as in Fig. 2. The Kalman filter has the form shown in Fig. 4 where the gains k_{1k} , k_{2k} , and k_{3k} are elements of the Kalman gain vector, \underline{k} , computed by

$$P_{k+1}^- = \Phi P_k \Phi + Q \quad (5)$$

$$k_{k+1} = P_{k+1}^- h_k^T (h_k^T P_{k+1}^- h_k + \sigma_v^2)^{-1} \quad (6)$$

$$P_{k+1} = P_{k+1}^- - k_{k+1} (h_k^T P_{k+1}^- h_k + \sigma_v^2)^{-1} k_{k+1}^T \quad (7)$$

where Φ and Q are the discrete dynamics and process noise matrices associated with F and w in Eq. 3; i.e.,

$$\Phi = e^{F\Delta t}$$

$$Q = \int_0^{\Delta t} e^{F(\Delta t - \alpha)} Q_c e^{F^T(\Delta t - \alpha)} d\alpha$$

$$Q_c = \begin{bmatrix} 0 & 0 & 0 & 0 \\ 0 & 0 & 0 & 0 \\ 0 & 0 & \frac{2\sigma_t^2}{\lambda_t} & 0 \\ 0 & 0 & 0 & 0 \end{bmatrix}$$

where Δt is the measurement interval. Note that the filter contains only three states because a_m is regarded as an error-free measurement. The filter is linear because the range r in the h -vector is also assumed to be known.

The guidance command is also linear, and is derived by solving the deterministic control problem obtained by eliminating all noise terms and initial condition uncertainty from the LQG problem. The latter is then solved for $a_c(t)$ as a linear function of the state x , and implemented with x replaced by its estimate $\hat{x}(t)$. Thus, the structure of the law is given by

$$a_c(t) = c^T(t) \hat{x}(t) / \cos \theta_m \quad (8)$$

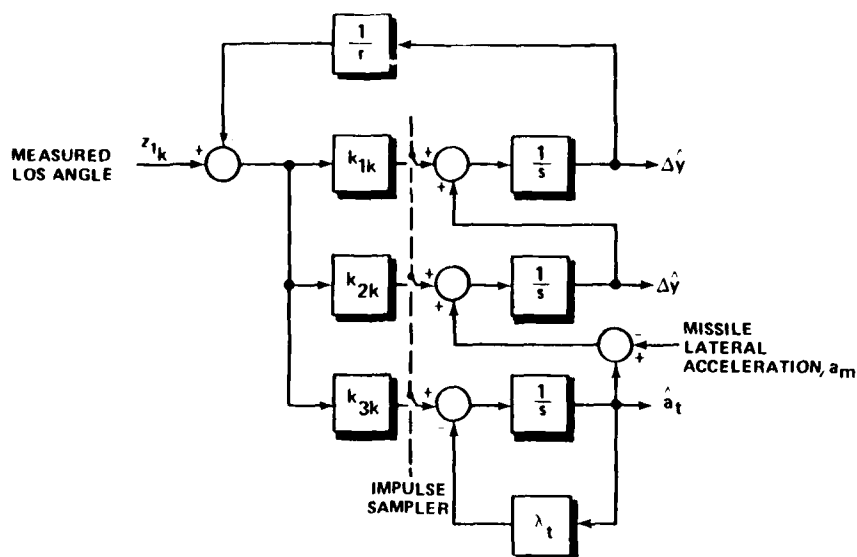


Figure 4 Kalman Filter Mechanization

where the gain vector $c(t)$ is a function of the deterministic parameters of the system. The solution for the elements of c is given by the relations

$$c_1 = \eta/t_{go}^2 \quad (9)$$

$$c_2 = \eta/t_{go} \quad (10)$$

$$c_3 = \eta \left[\frac{e^{-\lambda_t t_{go}} + \lambda_t t_{go} - 1}{\lambda_t^2 t_{go}^2} \right] \quad (11)$$

$$c_4 = -\eta \left[\frac{e^{-\lambda_m t_{go}} + \lambda_m t_{go} - 1}{\lambda_m^2 t_{go}^2} \right] \quad (12)$$

$$\eta = \frac{3t_{go}^2 |t_{go} - (1 - e^{-\lambda_m t_{go}})/\lambda_m|}{3\gamma + \frac{3}{2\lambda_m^3} (1 - e^{-2\lambda_m t_{go}}) + \frac{3t_{go}}{\lambda_m} (1 - 2e^{-\lambda_m t_{go}}) + t_{go}^2 (t_{go} - \frac{3}{\lambda_m})} \quad (13)$$

Note that in the simulation model (Fig. 2), the commanded acceleration a_c is limited by the maximum allowable acceleration, a_{max} .

The quantity η in Eqs. 9 through 13 is referred to as the navigation ratio because of its connection with conventional proportional guidance. This is illustrated by expanding a_c in Eq. 8 as follows:

$$a_c = \frac{c_1 \Delta \dot{y} + c_2 \dot{\Delta y} + c_3 \hat{a}_t + c_4 a_m}{\cos \theta_m}$$

$$= \frac{\eta}{\cos \theta_m} \left[\frac{\Delta \dot{y}}{t_{go}} + \frac{\dot{\Delta y}}{t_{go}} \right] + \frac{(c_3 \hat{a}_t + c_4 a_m)}{\cos \theta_m}$$

$$\begin{aligned} &= \frac{\eta}{\cos \theta_m} \left[\frac{r^2 \Delta \dot{y}}{r} - \frac{\dot{r} \Delta y}{r} \right] + \frac{(c_3 \hat{a}_t + c_4 a_m)}{\cos \theta_m} \\ &= -\frac{\eta \dot{r} \dot{\theta}}{\cos \theta_m} + \frac{(c_3 \hat{a}_t + c_4 a_m)}{\cos \theta_m} \end{aligned} \quad (1)$$

The first term on the right hand side of this expression has the form of proportional guidance with η as the navigation ratio. If $\lambda_m \rightarrow \infty$ and $\gamma \rightarrow 0$ in Eq. 13, then $\eta \rightarrow 3$; thus conventional proportional guidance with a navigation ratio of 3 is a limiting case of the LQG guidance law.

Another useful interpretation of Eq. 8 is that $a_c(t)$ can be written as

$$a_c(t) = \frac{\eta \hat{m}(t+t_{go})}{t_{go}^2 \cos \theta_m} \quad (1)$$

where $\hat{m}(t+t_{go})$ is the predicted miss at time $t+t_{go}$ if no control is applied. This is seen by recognizing that Eqs. 8 through 13 combine to yield

$$a_c(t) = \frac{\eta}{t_{go}^2 \cos \theta_m} \left[\Delta y + \Delta \dot{y} t_{go} + \int_0^{t_{go}} \int_0^\sigma [\hat{a}_t(t+\tau) - \hat{a}_m(t+\tau)] d\tau d\sigma \right] \quad (1)$$

where

$$\hat{a}_t(t+\tau) = \hat{a}_t(t) e^{-\lambda_t \tau}$$

$$\hat{a}_m(t+\tau) = a_m(t) e^{-\lambda_m \tau}$$

The quantities $\hat{a}_t(t+\tau)$ and $\hat{a}_m(t+\tau)$ are respectively the predicted target and missile acceleration at time $t + \tau$, assuming that w_t and a_c are zero in Table 1.

3.3 MINIMUM EXPECTED MISS DISTANCE CRITERION

The minimum expected miss distance problem formulation is based on the same model used for the LQG problem; however, the performance objective is different, and is stated as follows: Choose $a_c(t)$ to minimize

$$J = E\{\Delta y(t_f)\} \quad (1)$$

subject to Eqs. 1 and 2 and the constraint

$$a_c \leq a_{max} \quad (1)$$

Here we place no penalty on the commanded acceleration except that it is required not to exceed the upper bound imposed by the airframe. Thus, we expect this law to yield a smaller miss distance than any of the LQG laws, because the latter do not account for the acceleration constraint in their formulation; they are limited by the constraint only after the fact in the implementation in Fig. 2.

The derivation for the optimal acceleration command is presented in Ref. 5. It is found to have the same linear structure as in the LQG problem; viz.,

$$a_c(t) = \frac{\eta \hat{m}(t+t_{go})}{t_{go}^2 \cos \theta_m} \quad (1)$$

However, the four control gains are different. An analytical solution is obtained at each control stage as a result of the following steps:

- Determine the predicted terminal miss distance based on the Kalman filter estimate of the state vector at the current control computation stage, using the dynamic system model.
- Determine the value of commanded acceleration required over a single control interval to null the predicted terminal miss distance, neglecting the constraint in Eq. 18.
- Determine the actual acceleration command, a_c , by passing the above value through a saturation function that satisfies Eq. 18.

The predicted terminal miss based on a state estimate at time t is given by

$$\Delta \hat{y}(t_f) = \phi^T(t_f, t) \hat{x}(t) \quad (20)$$

where $\phi^T(t_f, t)$ is the first row of the state transition matrix $\phi(t_f, t)$ corresponding to F in Eq. 3,

$$\phi(t_f, t) = e^{F(t_f - t)}$$

The effect of a constant command a'_c , applied over an interval Δt , on the terminal miss distance is given by

$$\delta \Delta \hat{y}(t_f) = \phi^T(t_f, t + \Delta t) \int_t^{t + \Delta t} \phi(t + \Delta t, \tau) b a'_c d\tau$$

$$\Delta \rho_c(t) a'_c \quad (21)$$

The objective is to select a'_c such that

$$\delta \Delta \hat{y}(t_f) = -\Delta y(t_f) \quad (22)$$

in order to null the predicted miss distance. Substituting from Eqs. 21 and 22 leads to the result,

$$a'_c = -\frac{1}{\rho_c(t)} \cdot \phi^T(t_f, t) \hat{x}(t)$$

$$\Delta \frac{[c_1 \Delta \hat{y} + c_2 \dot{\Delta \hat{y}} + c_3 \ddot{\Delta \hat{y}} + c_4 a'_c]_m}{\cos \theta'_m} \quad (23)$$

Carrying out the computation for c_1 through c_4 shows that they are identical to the optimal LQG control gains in Eqs. 9 through 12, except that the navigation ratio η is given by

$$\eta = \frac{-t_{g0}^2}{\Delta t \left(\frac{1}{\lambda_m} - t_{g0} + \frac{\Delta t}{2} \right) - \frac{1}{\lambda_m^2} e^{-\lambda_m(t_{g0} - \Delta t)} (1 - e^{-\lambda_m \Delta t})} \quad (24)$$

As previously noted, the missile autopilot acceleration command a_c is obtained by passing a'_c given by Eq. 23 through a nonlinear saturation function which limits at $\pm a_{\max}$.

3.4 GUIDANCE LAW SUMMARY

In order to compare conventional proportional guidance with the various optimal laws suggested by the above problem formulations, a hierarchy of laws is defined in Table 2. Law A is based on proportional guidance and uses a first order low-pass guidance filter, as illustrated in Fig. 5. The filter time-constant is optimized empirically for the particular set of engagement conditions simulated. Law B is also proportional guidance, but the low-pass filter is replaced by the Kalman filter illustrated in Fig. 4. Law D is the LQG law summarized above. Law C is a suboptimal version of D obtained by ignoring the missile dynamics; this is equivalent to letting $\lambda_m \rightarrow \infty$ in Eqs. 12 and 13. Consequently, Law C has only three guidance gains, omitting the a_m term in Eq. 8. Finally, Law E is the minimum expected miss distance. Thus, the designations A, ..., E order the guidance laws with respect to increasing capability to null the intercept miss distance. The control gains and navigation ratios for each law are summarized in Tables 3 and 4.

TABLE 2
MISSILE GUIDANCE LAWS

IDENTIFYING SYMBOL	DISTINGUISHING CHARACTERISTICS	TYPE OF FILTER
A	Proportional Guidance	First-Order, Low-Pass
B	Proportional Guidance	Kalman
C	LQG Guidance; Accounts for target maneuvers	Kalman
D	LQG Guidance; Accounts for target maneuvers and missile dynamics	Kalman
E	Minimum Expected Miss Distance Guidance; Accounts for target maneuvers, missile dynamics, and missile airframe saturation	Kalman

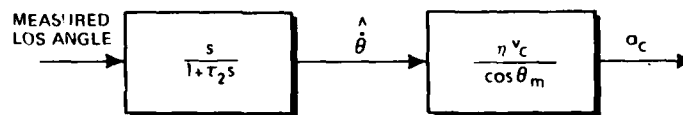


Figure 5 Guidance Law A

TABLE 3
CONTROL GAINS

CONTROL GAINS	GUIDANCE		
	B	C	D,E
c_4	0	0	Eq. 12
c_3	0	Eq. 11	
c_2	Eq. 10		
c_1	Eq. 9		

TABLE 4
NAVIGATION RATIOS

GUIDANCE LAW	NAVIGATION RATIO, η
A, B	3
C	$\frac{3t^3 g_0}{3\gamma + t^3 g_0}$
D	Eq. 13
E	Eq. 24

Both Laws C and D are of the LQC type. The principal difference between them is that in Law D, η increases with decreasing range (for small γ) and becomes large near intercept to compensate for the lag in missile acceleration caused by the missile dynamics. This behavior is illustrated in Fig. 6.

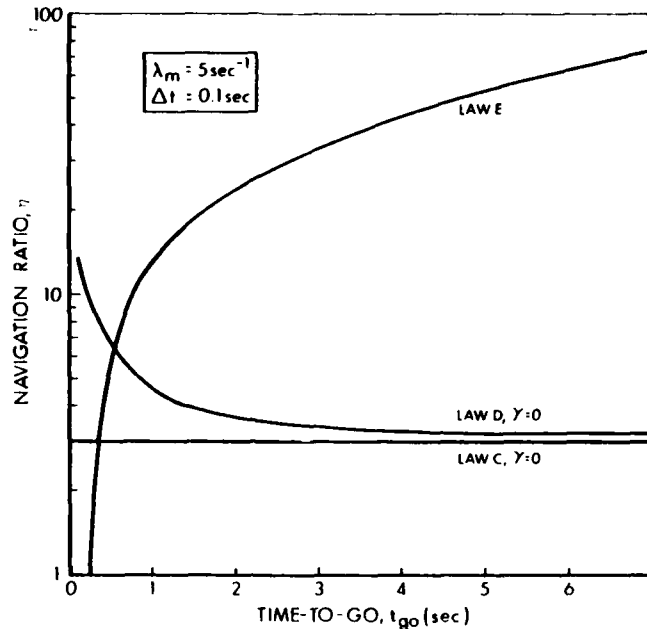


Figure 6 Comparison of Navigation Ratios

Typically, the value of η given in Eq. 22 for guidance Law E is much larger than the value from Eq. 13 for law D over most of the trajectory, as indicated in Fig. 6. This is explained by the fact that between seeker measurements, guidance Law E attempts to null the predicted miss distance completely before the next seeker measurement is processed. By contrast, the other guidance laws effectively attempt only to reduce the predicted miss distance at each stage. Law E is useful in the sense that it provides a lower bound on the miss distance that can be achieved for the assumed engagement conditions.

3.5 SIMULATION RESULTS

A new and powerful computerized approach to the direct statistical analysis of nonlinear systems has been developed in recent years (Ref. 17). This method, called the Covariance Analysis Describing Function Technique -- CADETTM -- provides for efficient computation of the mean and covariance of high-order, multiple-nonlinearity systems with multiple statistically described inputs. Although CADET is an approximate technique, experience has shown that it yields good agreement with multiple trial monte carlo results for a large class of system configurations and requires significantly less computer running time. The performance results presented here were calculated with a CADET computer program, which has been validated with a monte carlo simulation in a selected number of cases. A detailed treatment of CADET can be found in Ref. 18.

In order to compare the performance of the guidance laws listed in Table 2, nominal values were chosen for the missile-target engagement initial conditions, and for the parameters of the model in Fig. 2. These quantities are listed in Table 5. All exceptions to the nominal conditions are explicitly stated in the subsequent discussion.

All five guidance laws are compared in Fig. 7 over a range of values for the target maneuver bandwidth.* In order that Law A be fairly compared with the others, its filter time constant, τ_2 in Fig. 5, is optimized to yield the lowest value of rms miss distance for each value of λ_t . Observe that the dispersion between the various laws

*Guidance Laws B through D listed in Table 1 depend upon knowledge of the bandwidths of the target maneuver (λ_t) and the first-order design model for the autopilot (λ_m).

Unless otherwise stated in the following discussion, it is assumed that these quantities are equal to the values used in the simulation model in Fig. 2; i.e., the optimal guidance laws are matched to the simulation model.

TABLE 5
NOMINAL CONDITIONS

QUANTITY	NOMINAL VALUE SPECIFICATION
Missile Parameters $\left\{ \begin{array}{l} a_1 \\ a_2 \\ b_1 \\ b_2 \\ b_3 \end{array} \right.$	0
	0
	0.1 sec
	0
	0
Target Maneuver Bandwidth, λ_t	0.2 sec ⁻¹
RMS Target Acceleration, σ_t	300 ft/sec ²
Missile Acceleration Limit, a_{\max}	800 ft/sec ²
Radome Slope, k_r	0
Initial Mean Heading Angles, θ_m and θ_a	0
Control Effort Weighting, γ	0
Launch Range	24,000 ft
RMS Heading Error, $[E\{\theta_m^2\}]^{1/2}$	0.15 rad
Target Velocity	1000 ft/sec
Interceptor Velocity	3000 ft/sec
Noise Parameters $\left\{ \begin{array}{l} \text{Receiver, } \sigma_r/r \\ \text{Glint, } \sigma_{gr} \\ \text{Range Independent, } \sigma \end{array} \right.$	4×10^{-8} ft ⁻¹
	4 ft
	4×10^{-4} rad

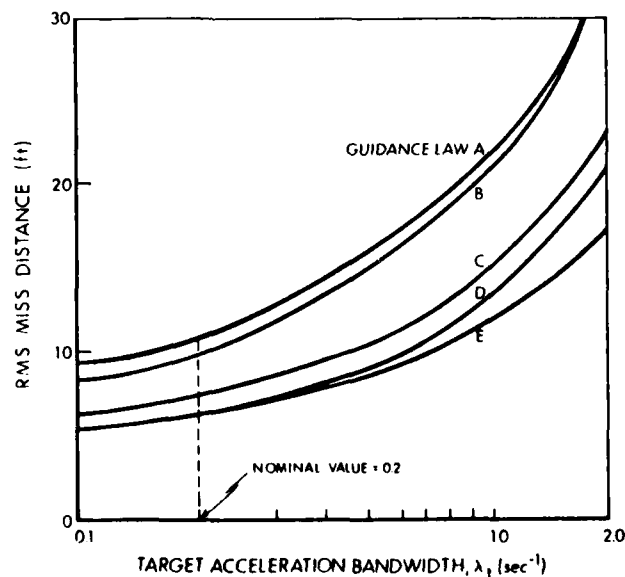


Figure 7 Guidance Law Performance Versus Target Maneuver Bandwidth

generally increases with λ_t . However, the major improvement over conventional proportional guidance is achieved through use of Law C, which includes a target acceleration term to compensate for target maneuvers. Some additional improvement is achieved by accounting for missile autopilot dynamics (Law D). Guidance Law E provides a lower bound on the achievable miss distance.

Figure 8 displays guidance law performance as a function of missile maneuver capability.* As a_{\max} approaches the target rms acceleration level (300 ft/sec^2), Laws C, D, and E offer marked improvement over proportional guidance (Law B). In addition, the difference between D and E increases; this is attributable to the fact that Law E explicitly accounts for the acceleration limit whereas D does not. Hence the former offers greater improvement over the latter as acceleration saturation becomes more significant.

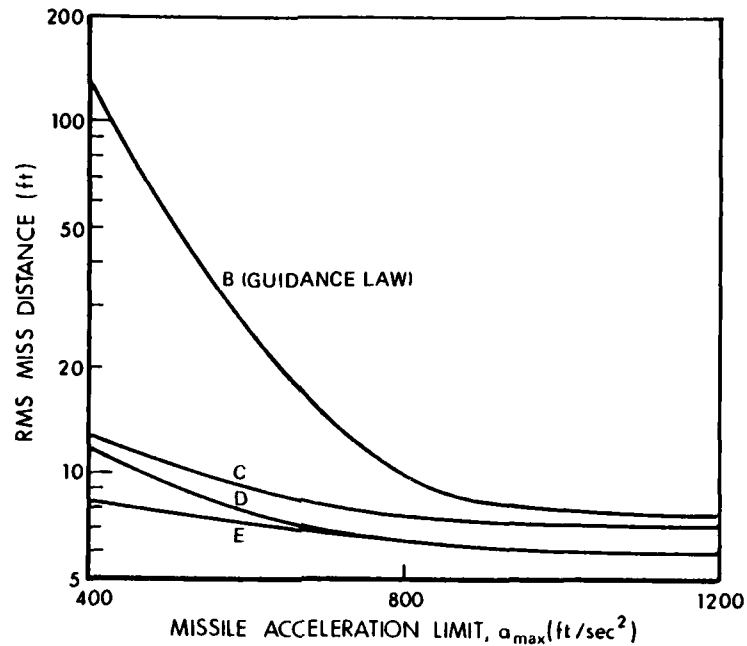


Figure 8 Guidance Law Performance Versus Interceptor Missile Maneuver Capability

The influence of the missile time-constant on miss distance is demonstrated in Fig. 9. As the latter gets larger, Laws D and E, which explicitly account for missile dynamics, offer significantly better performance than Laws B and C.

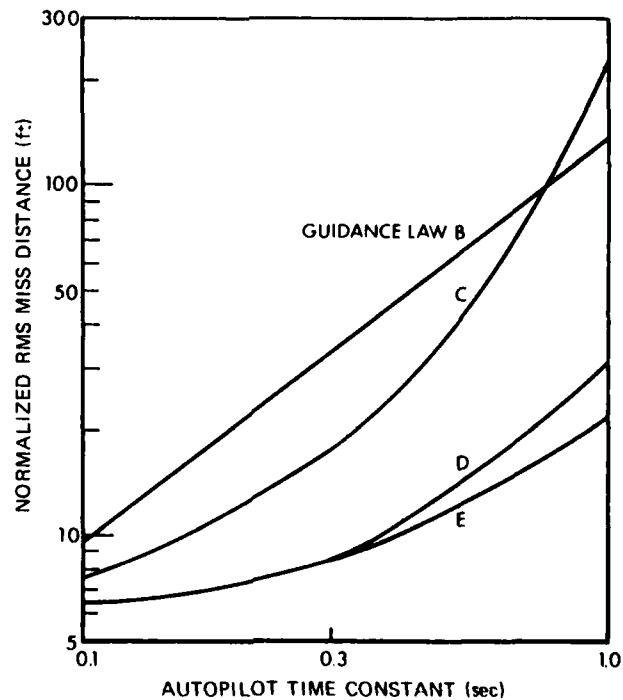


Figure 9 Guidance Law Performance Versus Interceptor Missile Time-Constant

*Law A is omitted from subsequent guidance law comparisons on the basis that it yields performance quite close to Law B when its filter time-constant is optimized for the nominal noise levels.

In all the cases treated thus far, the designs of guidance Laws D and E are matched to the truth model representation of missile dynamics, except for the kinematic nonlinearities neglected in the model in Table 1. An important remaining issue is the sensitivity of guidance law performance to variations in missile parameters from their assumed values. One potentially important error source is parasitic coupling through the seeker aberration effect represented in Fig. 2 by the constant k_r , which has heretofore been chosen as zero. Figure 10 illustrates the effect on guidance system performance when k_r is nonzero. For this case, the parameters a_1 , a_2 , b_1 , b_2 and b_3 are selected to yield missile poles at -1 rad/sec and $-7.5 \pm j15$ rad/sec, and zeros at ± 20 rad/sec. The design models for Law D and E assume the missile dynamics are first-order with time-constant (τ_m) equal to 1 sec. The value of $a_3 = 2.0$ is chosen to be representative of high altitudes, where missile-seeker coupling is most pronounced. With the exception that here $k_r \neq 0$, the above conditions are nearly the same as those in Fig. 9 when the missile time-constant = 1.0 sec.

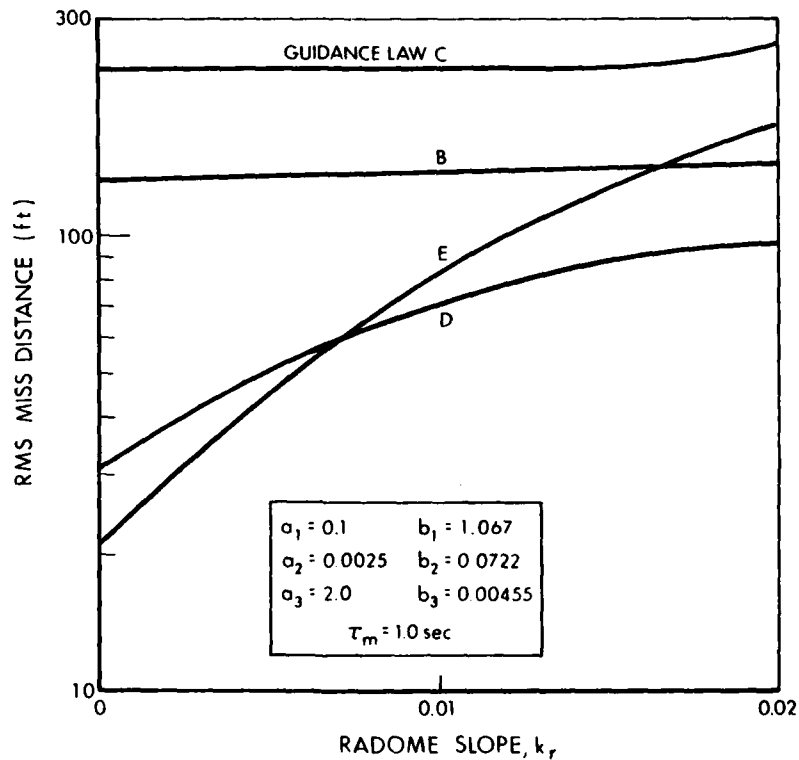


Figure 10 Guidance Law Sensitivity to Radome Error

As k_r increases, the performance advantage of Laws D and E deteriorates relative to Laws B and C. This is attributed to the fact that the high value of η associated with Laws D and E is incompatible with the parasitic attitude loop in Fig. 2, because the latter is not accounted for in the derivation of the guidance law. Generally k_r is an unknown time-varying quantity, so that it cannot be accounted for exactly. Consequently, degradation in the performance of the "high-gain" guidance laws will be experienced in situations where the effect of k_r is important -- i.e., at high altitudes.

A word of qualification is merited with respect to the results presented above. The mechanism by which the optimal guidance laws improve performance is an increase in the effective guidance gain over that associated with proportional guidance. The increased gain provides a higher commanded acceleration early in the trajectory. However, higher maneuvering acceleration is not penalty-free in practice. It results in an increase in drag, which in turn causes missile slow-down; the latter can reduce the missile acceleration capability. These effects are not included in the simulation model (Fig. 2). Nevertheless, practical experience with more detailed simulation models, including drag effects, indicates that these optimal guidance techniques continue to offer improvements over conventional methods.

4.

UNCERTAIN MODEL PARAMETERS

In all of the design approaches described in Section 3, it is assumed that the parameters of the model in Table 1 are known. Thus, the guidance problem has a linear

gaussian structure which yields a relatively simple guidance law. The model fidelity can be improved by including uncertainty in the model parameters, particularly those associated with the target, about which little specific information is available.

Incorporating parameter uncertainty in the model typically casts the guidance problem into the general category of nonlinear stochastic control problems, which usually do not have tractable solutions. In particular, the structure of the guidance law does not separate into a filter for state estimation cascaded with a guidance command computation. Indeed, a dual control effect is present wherein guidance maneuvers can be employed to improve knowledge of the model parameters. A notable example is the case where range measurements are not available, either because the missile has a passive seeker or range measurements are denied by jamming. For this situation, interceptor maneuvers normal to the line of sight are required to estimate range (Refs. 15 and 16).

A common linearization approach to the unknown parameter case carries out the following steps: assume that the guidance law separation (into filtering and control functions) principle holds; augment the model state vector with the unknown parameters; estimate the augmented state vector with an extended Kalman filter; and use the estimated parameter values in one of the guidance laws described in Section 3. This procedure is approximately optimal if the parameter uncertainty is small. However, when the uncertainty is large the linearization assumed in the extended Kalman filter will not be valid. It is expected that target parameter uncertainties will be large, not only because they are poorly known, a priori, but also because the sensor measurement errors are often too large to estimate such parameters accurately.

To illustrate how the guidance law can be affected by accounting for parameter uncertainties in its formulation, consider the model in Table 1 and assume that the target bandwidth λ_t is a random variable with a known probability density function. Assume further that perfect measurements of the state vector are available. Note that even with perfect measurements, λ_t could not be estimated without error due to the presence of the white noise term w_t in the target acceleration model.

With the above assumptions, it can be shown that the solution to the LQG problem, with the performance index in Eq. 4, is of the certainty-equivalence type (Ref. 18); viz,

$$a_c(t) = E \{ c^T(t) \underline{x}(t) / \cos \theta_m \} \quad (25)$$

where $E \{ \}$ denotes the expectation over λ_t , conditioned on the measurements taken up until time t . Because all the parameters and states in Eq. 25 except λ_t are assumed known exactly, the solution for $a_c(t)$ is the same as in Eqs. 8 through 13 except that c_3 becomes

$$c_3 = \eta E \left\{ \frac{e^{-\lambda_t t_{go}} + \lambda_t t_{go} - 1}{\lambda_t^2 t_{go}^2} \right\} \quad (26)$$

$$= \eta E \left\{ \frac{1}{2} - \frac{\lambda_t t_{go}}{6} + \frac{\lambda_t^2 t_{go}^2}{24} - \dots (-1)^n \frac{(\lambda_t t_{go})^n}{(n+2)!} \dots \right\}$$

Thus, for this case the guidance law does separate into a "filter" which propagates the probability density function for λ_t (it is not sufficient just to propagate the mean and variance of λ_t since the density is not normally distributed), and a guidance command computation where c_3 is computed from the filter output. The effect of accounting for the uncertainty in λ_t is to increase the gain c_3 above the value it would have if the true value of λ_t were its mean value $\hat{\lambda}_t$; viz.,

$$c_3 = \eta \left[\frac{1}{2} - \frac{\hat{\lambda}_t t_{go}}{6} + \frac{(\hat{\lambda}_t^2 + \sigma_\lambda^2) t_{go}^2}{24} - \dots \right] \quad (27)$$

where σ_λ^2 is the variance of λ_t .

For the purpose of comparing the conventional and modified LQG guidance laws, a simplified point-mass simulation was conducted. The simulation does not explicitly contain a guidance filter, but instead provides each guidance law with perfect position and velocity information, along with a target acceleration estimate containing a time-varying error with an rms level of 1.0 g. The autopilot/airframe dynamics are also neglected.

Table 6 summarizes the target engagement that was investigated. Note that the parameter values used in the two guidance law designs are compatible, in that the value of λ_t (time-constant in the target acceleration model) used in the conventional LQG formulation is identical to the mean value of λ_t used in the modified LQG formulation. However, note that neither of the target acceleration models are matched to the true target acceleration profile.

TABLE 6
ENGAGEMENT CONDITIONS

QUANTITY	VALUE
<u>Simulation Model</u>	
Missile parameters: a_1, a_2, b_1, b_2, b_3	0
Target maneuver bandwidth, λ_t	0
Target acceleration	10 g
Radome slope, k_r	0
Heading angles $\begin{cases} \theta_m \\ \theta_t \end{cases}$	0 180°
Range rate	1000 ft/sec
Launch range	6000 ft
<u>Measurements</u>	
Data rate	10 Hz
Position, Δy , error	0
Velocity, Δy , error	0
Acceleration, a_t , error	1-g rms
<u>Guidance Law Models</u>	
LQG	
Target maneuver bandwidth, λ_t	2 sec ⁻¹
Control effect weighting, γ	10 ⁻⁴
Modified LQG	
Target maneuver bandwidth, $\hat{\lambda}_t$	2 sec ⁻¹
Bandwidth standard deviation, σ_λ	2 sec ⁻¹
Control effort weighting, γ	10 ⁻⁴

Figure 11 illustrates the relative performance of the two laws as a function of the missile acceleration capability. Each point on both curves was determined by averaging the results of 15 monte carlo trials. Evidently, the modified LQG law offers significant improvement over the LQG law as the missile acceleration capability (relative to the 10-g target) decreases. These limited simulation results with an idealized, simplified model indicate that it may be both practical and beneficial to account for parameter uncertainty in guidance gain computations.

5.

CONCLUSIONS

This paper illustrates the application of optimal control techniques to designing missile guidance laws. One significant conclusion deduced from the examples treated is that the extent to which optimal guidance techniques yield better accuracy than conventional proportional guidance is strongly related to the comparison between the missile's acceleration capability and the target maneuver level. When the ratio is less than 3:1, the optimal laws tend to perform significantly better as a result of including a term proportional to target acceleration. Accounting for missile dynamics in the optimal laws (D and E) offers appreciable improvement over Law C (which neglects the dynamics), when the missile time-constant is greater than about 0.2 sec.

It has also been demonstrated that guidance law performance is sensitive to the design assumptions. If the actual engagement parameters (e.g., missile radome slope) are different from their assumed values, significant performance degradation is a likely result.

A new guidance law is presented in the paper which accounts for uncertainty in the target dynamics. The result is a modified LQG-type law with an increased acceleration

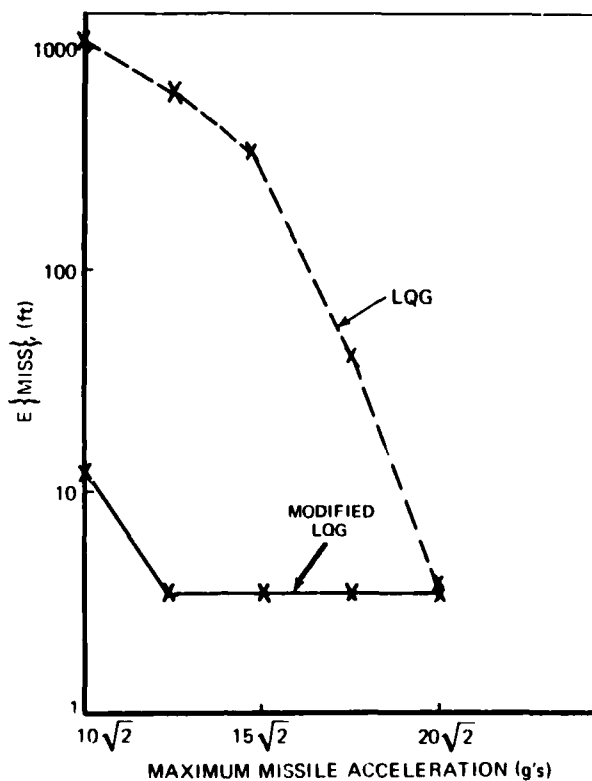


Figure 11 Relative Performance of LQG and Modified LQG Guidance Formulation

gain. This technique is shown to be better than the LQG-law when the ratio of missile capability to target acceleration is less than 2.8:1.

It has been pointed out that certain effects, such as aerodynamic drag, have been omitted in the analyses performed here. However, practical experience with detailed simulations indicates that the results presented in this paper are, in fact, a valid demonstration of many of the potential benefits in applying optimal control techniques to guidance law design.

REFERENCES

1. Garber, V., "Optimum Intercept Laws for Accelerating Targets," *AIAA Journal*, Vol. 6, No. 11, November 1968, pp. 2196-2198.
2. Stallard, D.V., "Discrete Optimal Terminal Control, with Application to Missile Guidance," *IEEE Transactions on Automatic Control*, August 1973, pp. 373-377.
3. Anderson, G.M., "Effects of Performance Index/Constraint Combinations on Optimal Guidance Laws for Air-to-Air Missiles," *Proceedings of the IEEE 1979 National Aerospace and Electronics Conference*, Vol. 2, (Dayton), May 1979, pp. 765-771.
4. Bryson, A.E., Jr., and Ho, Y.C., *Applied Optimal Control*, Blaisdell Publishing Company, Waltham, Massachusetts, 1969.
5. Devst, J.J., Jr., and Price, C.F., "Optimal Stochastic Guidance Laws for Tactical Missiles," *AIAA Journal on Spacecraft and Rockets*, Vol. 10, No. 5, May 1973, pp. 301-308.
6. Warren, R.S., Price, C.F., Gelb, A., and Vander Velde, W.E., "Direct Statistical Evaluation of Nonlinear Guidance Systems," *Proceedings AIAA Guidance and Control Conference*, (Key Biscayne), August 1973, Paper No. 73-836.

7. Kain, J.E. and Yost, D.J., "Command to Line-of-Sight Guidance - A Stochastic Optimal Control Problem," Proceedings AIAA Guidance and Control Conference, (San Diego), 1976, pp. 356-364.
8. Calise, A.J., "A Singular Perturbation Study of Optimal Thrust Control with Proportional Navigation Guidance," Proceedings 1977 IEEE Conference on Decision and Control, Vol. 1, (New Orleans), December 1977, pp. 1167-1176.
9. Sridhar, B., and Gupta, N.K., "Accurate Real-Time SRAAM Guidance Using Singular Perturbation Optimal Control," Proceedings of the IEEE 1979 National Aerospace and Electronics Conference, Vol. 2, (Dayton), May 1979, pp. 772-774.
10. Gutman, S., "On Optimal Guidance for Homing Missiles," Journal of Guidance and Control, Vol. 2, No. 4, July-August 1979, pp. 296-300.
11. Gupta, N.K., and Sridhar, B., "Reachable Sets for Missile Guidance Against Smart Targets," Proceedings of the IEEE 1979 National Aerospace and Electronics Conference, Vol. 2, (Dayton), May 1979, pp. 780-787.
12. Wei, K.C., and Pearson, A.E., "Control Law for an Intercept System," Journal of Guidance and Control, Vol. 1, No. 5, September-October 1978, pp. 298-304.
13. Sheporaitis, L.P., Balbirnie, E.C., and Liebner, G.A., "Practical Optimal Steering for Missile Terminal Guidance," Proceedings AIAA Guidance and Control Conference, (San Diego), 1976, pp. 47-56.
14. York, R.J., and Pastrick, H.L., "Optimal Terminal Guidance with Constraints at Final Time," AIAA Journal of Spacecraft and Rockets, Vol. 14, No. 6, June 1977, pp. 381-383.
15. Brown, C.M., Jr., Price, C.F., and Licata, W.H., "Inertially Aided Ranging for Guidance Systems," Proceedings AIAA Guidance and Control Conference, (Boston), August 1975, Paper No. 75-1109.
16. Casler, R.J., Jr., "Dual-Control Guidance Strategy for Homing Interceptors Taking Angle-Only Measurements," Journal of Guidance and Control, Vol. 1, No. 1, January-February 1978, pp. 63-70.
17. Gelb, A. and Warren, R.S., "Direct Statistical Analysis of Nonlinear Systems -- CADET," AIAA Journal, Vol. 11, No. 5, May 1973, pp. 689-694.
18. Gelb, A. ed., Applied Optimal Estimation, M.I.T. Press, Cambridge, Massachusetts, 1974.
19. Aoki, M., Optimization of Stochastic Systems, Academic Press, New York, New York, 1967.

ACKNOWLEDGEMENTS

The author wishes to acknowledge the contributions of Dr. Philip H. Fiske and Dr. Joseph E. Wall, Jr., while employed at TASC, to this work. The work presented here was supported by the Office of Naval Research, under Contract No. N00014-69-C-0391 and by the Air Force Armament Laboratory under contract No. F08635-77-C-0034.

DEVELOPMENT OF MULTIVARIABLE CONTROLLERS FOR AIRCRAFT TURBINE ENGINES

Ronald L. De Hoff
Senior Engineer
Systems Control, Inc. (Vt)
Palo Alto, California 94304

Stephen M. Rock
Senior Engineer
Systems Control, Inc. (Vt)
Palo Alto, California 94304

Muhammed M. Akhter
Engineer
Systems Control, Inc. (Vt)
Palo Alto, California 94304

1. INTRODUCTION

The current high performance military aircraft engine represents an extremely complex, highly tuned and expensive hardware component. Successful mission performance and, indeed, the very life of the pilot is contingent upon its proper operation. Near-future engines will be driven by aircraft requirements to a substantial increase in configuration complexity and a decrease in allowable error tolerances [1]. These factors combine to form one of the most exciting and challenging areas of control design application. Since near-term propulsion control requirements cannot be met with current design practices, the opportunity and requirement for truly practical adaptations of the many new theoretical multivariable control design methodologies are unique in this field. Hence, the propulsion control technology area has had an unparalleled level of development and test of synthesis methods over the past 10 years.

The development process for multivariable control laws for turbine engines is described. In Section 2, a model reference structure is discussed which has been shown to be a flexible framework within which digital control programs of a wide variety of function and complexity can be formulated. In Section 3, the development of the plant reference model is discussed and trade-offs between accuracy and complexity presented. The techniques used to produce optimized, feed-forward state, control and output trajectories are presented in Section 4. The well-known methods of regulator synthesis using quadratic performance functions are briefly reviewed in Section 5, and the results of several successful applications of this methodology are summarized in Section 6.

2. MODEL REFERENCE CONTROL STRUCTURE

The model reference structure for multivariable controls is well known from process control applications [2,3]. Utilization of this architecture permits implementation of optimal regulator designs, decoupled integral loops, high response trajectory inputs and failure tolerant functional blocks (Figure 1) in a straightforward fashion. The reference point quantities, i.e., estimates of a compatible set of engine states, X_0 , outputs, Y_0 , and control values, U_0 , are desired operating values achievable by the actual system. Table 1 lists typical choices for these quantities for a low bypass, fixed geometry engine and a more complex variable geometry engine. Typically, these schedules are developed by the manufacturer during engine evolution. Pilot input (throttle or operating modes) and ambient conditions are sensed and converted to the desired steady-state operating condition. The trajectory generator produces a compatible and optimized path [5] for large requested changes. This functional block utilizes a nonlinear engine model describing the dynamic response characteristics of the engine to synthesize a path in states, outputs and controls which respects engine and actuator capabilities and operating constraints. This structure is presented in more detail in Section IV. A filter or estimator, often tolerant of actuator and sensor faults [6], is used to produce a best estimate of plant operating characteristics. Finally, an optimal regulator structure incorporating integral trim produces coordinated control actuator requests which regulate the engine behavior within acceptable and safe margins. The modeling and synthesis methods for each of these blocks are discussed in the following sections.

3. MODEL DEVELOPMENT

3.1 LINEAR MODELS

Dynamic equations modeling the engine response must be accurate, easily implemented and tractable for real-time, digital, control purposes. The regular synthesis procedures use linear design models. Simple nonlinear models developed from these are implemented to provide both feed-forward trajectories and filter update equations. This provides a significant program economy and efficiency.

The engine modeling is best attacked from basic principles. The problem can be formulated to define nomenclature. The engine dynamics are expressed in terms of a general, nonlinear equation relating n state variables, x , and m input variables, u , and p ambient variables, w , as follows:

$$\dot{x} = f(x, u, w) \quad (1)$$

Engine state variables are elements of the thermodynamic and mechanical equations modeling mass, energy and torque balance. They consist of temperatures, pressures and rotor speeds (for example, see Figure 2). Control inputs are fuel flow and geometry positions (e.g., nozzle area, variable stator angle, etc.).

The p outputs are statically related to the states and controls through the nonlinear expression:

$$y = h(x, u, w) \quad (2)$$

There are two important types of outputs, viz those that are measured and those that are not. Measured outputs typically include rotor speeds, temperatures, and pressures throughout the engine gas path. Unmeasured outputs represent engine performance and limit quantities such as thrust, fuel consumption, surge margin, and turbine inlet temperature. These quantities are related to the state variables by static thermodynamic equations which are not accurately predictive of these values and whose accuracy varies with engine build, deterioration and age.

Design models [7] are developed for engine response near a static equilibrium point (i.e., $\dot{x} = 0$) which can be characterized by steady-state values of the states, controls, and outputs, (x_0, u_0, y_0) . A linearized model is written as follows:

$$\dot{x} = F\delta x + G\delta u \quad (3)$$

$$\delta y = H\delta x + D\delta u \quad (4)$$

where, in principle,

$$F_{ij} = \left. \frac{\partial f_i}{\partial x_j} \right|_{\substack{x=x_0, \text{ etc.} \\ u=u_0}} \quad (5)$$

and

$$\delta x = x - x_0, \text{ etc.} \quad (6)$$

A modal decomposition [7,8] provides the framework for reducing arbitrary linear models to design models containing the appropriate parameterization for the control function.

The linear Eq. (3) can be transformed to block-diagonal form assuming the $n \times n$ dynamics matrix, F , has no repeated eigenvalues:

$$x = Tz \quad (7)$$

$$\dot{z} = \Lambda z + \Xi u \quad (8)$$

$$y = HTz + Du \quad (9)$$

where Λ is an $n \times n$ block diagonal matrix, T is an $n \times n$ matrix composed of the column eigenvectors of F , z is an $n \times 1$ modal coordinate vector, and Ξ is the $n \times m$ modal control distribution matrix. Also,

$$FT = T\Lambda \quad (10)$$

If the following equilibrium relationship is approximately true (within the time frame of control interest),

$$z_2 = 0 \quad (11)$$

then the following reduction can be made

$$\dot{x}_1 = F_r x_1 + G_r u \quad (12)$$

where x_1 is now the $q \times 1$ state vector, F_r is the $q \times q$ dynamics matrix, and G_r is the $q \times m$ control distribution matrix. Also

$$\begin{bmatrix} x_2 \\ y \end{bmatrix} = \begin{bmatrix} H^* \\ H_r \end{bmatrix} x_1 + \begin{bmatrix} D^* \\ D_r \end{bmatrix} u \quad (13)$$

where x_2 is treated as an additional $(n-q) \times 1$ output vector with a $(n-q) \times q$ state distribution matrix H^* and a $(n-q) \times m$ control distribution matrix D^* .

Linear models for the F100 engine have been published [8,9]. An examination of the eigensystem of these models (see Table 2) shows that many of the response roots, especially those associated with flow response, are outside actuator limits. The slower roots model rotor dynamics and a smaller effect due to heat-soak phenomena in the metal components of the engine. For design purposes, these temperature roots may often be neglected.

The characteristics of the rotor response are of the same form in all turbofan engines [10]. The rotor response is dominated by a second-order system with two real roots. Examination of typical eigenvectors at various flight points (Figure 3) shows that the faster response can be associated with the rotor speeds differentially rematching, i.e., the fan spool decelerating while the compressor accelerates. The slower root involves the collective or rigid-body response of the two shafts. The differential and collective response is characteristic in the motion of two heavily damped and heavily coupled inertia elements. (The two spools are aerodynamically coupled in the turbines.) The characteristic motion is present in all regions of the operating envelope.

It is highly desirable to provide a model in a simple form to minimize computer storage and computation requirements. Outlined below is a procedure for further simplifying the reduced order system (system order remains unchanged). The procedure is based on eliminating (setting to zero) elements in the system dynamics matrix, F [6].

The procedure is comprised of three steps:

Step 1: Identify those elements in F which have little effect on the engine's dynamic response. Specifically, let J_0 represent a measure of the system state response to initial conditions.

$$J_0 = \frac{1}{2} \int_0^{\infty} x^T A x dt \quad (14)$$

Unimportant elements, F_{ij} , are those for which

$$\frac{\partial J_0 / J_0}{\partial F_{ij} / F_{ij}} \approx 1 \quad (15)$$

That is, F_{ij} is unimportant if a 100 percent change in F_{ij} produces a small percentage change in J_0 . Define all of these elements as F_{ij}^* .

Step 2: Set all the $F_{ij}^* = 0$, and define the resultant system dynamics matrix as F .

Step 3: Modify the non-zero elements in F to minimize the mean square difference between the initial condition responses of the reduced system and the original. Specifically, find

$$F = \min \left\{ J = \frac{1}{2} \int_0^{\infty} (\hat{x} - x)^T A_z (\hat{x} - x) dt \right\} \quad (16)$$

where

$$\dot{\hat{x}} = F\hat{x} \text{ (original)}$$

$$\dot{x} = Fx \text{ (reduced)}$$

The response sensitivities can be calculated using the algorithm presented in Section 5, using the following definitions:

$$G_{eq} = I \quad (17)$$

$$H_{eq} = I \quad (18)$$

$$C_{eq} = F. \quad (19)$$

Then finding $\frac{\partial J_0}{\partial C_{eq}}$ for the system

$$\dot{\hat{x}} = F\hat{x} + G_{eq} u_{eq} \quad (20)$$

$$y_{eq} = H_{eq} \hat{x} \quad (21)$$

$$u_{eq} = C_{eq} y_{eq} \quad (22)$$

is the same as finding

$$\frac{\partial J_0}{\partial F} = \frac{J_0}{\partial F} \left|_{\Delta F=0} \right. \quad (23)$$

in the desired perturbational system:

$$\dot{\hat{x}} = (F + \Delta F)\hat{x}. \quad (24)$$

The sensitivity in Eq. (23) will be the principal calculation in the output regulator synthesis algorithm discussed below.

Example 1: Nearly Uncoupled Response

A simple second-order example is presented to clarify the procedure. Consider the system

$$\dot{\hat{x}} = \begin{bmatrix} -10 & 1 \\ 0 & -20 \end{bmatrix} \hat{x}. \quad (25)$$

The diagonal elements will dominate this response. Hence, it is desired to find an F matrix of the form

$$\hat{\hat{x}} = \begin{bmatrix} a & 0 \\ 0 & b \end{bmatrix} \hat{\hat{x}} \quad (26)$$

which most nearly matches the initial condition's response of the original system.

If specific initial conditions are chosen, the problem is easily solved in closed form. That is, $x(t)$ and $\hat{x}(t)$ may be found; then from these, J may be computed. Parameters a and b can then be chosen to minimize J (Eq. (16)).

For the case

$$x(0) = \begin{bmatrix} 1 \\ 10 \end{bmatrix} \text{ and } \dot{x}(0) = \begin{bmatrix} 1 \\ 10 \end{bmatrix} \quad (27)$$

The solution is

$$\hat{F} = \begin{bmatrix} -6.495 & 0 \\ 0 & -20 \end{bmatrix} \quad (28)$$

Note that due to the one-way coupling in the system, the F_{22} element was not affected; only the F_{11} element was altered.

Example 2: Turbine Engine Dynamics

A typical turbofan dynamics matrix consists of two rotor states, fan speed and compressor speed and several heat transfer states representing engine metal heat capacity and turbine blade heating effects [6]. Such a model was derived for a turbofan engine at a wide range of flight envelope points and sensitivities were calculated to each element of the F matrix. Figure 4 shows the range of sensitivity values and clearly indicates the choice of elements to neglect. Elements which are retained may be scheduled or held constant in a nonlinear representation using this analysis as discussed below.

The calculation also indicates that the optimal cost, $J_0 = 1.03$, i.e., setting the indicated elements to zero and performing no optimization yielded only a 1.0 percent change in J_0 . Performing the optimization reduced this already small error to 0.9 percent. This confirms the unimportance of those terms which were eliminated.

The eigenvalues of the original and reduced systems are presented for comparison in Table 3 for an operating point.

3.2 NONLINEAR MODELS

Low-order linear models are the basis for point design of control regulator logic. These dynamic models in a slightly different form can also be used within the controller program to implement transition logic, filter update equations, and fault-tolerant strategies [11]. The primary requirement for this simplification arises from the real-time, microprocessor implementation. If it is assumed that $u(t)$ is piecewise constant on an interval $[nT, (n+1)T]$, Eq. (1) can be rewritten relative to the constant value of u and the value of x which would be reached if u remained at the value [12] or,

$$\dot{x} = F_x(x_{ss}, u(n)) [x(t) - x_{ss}] \quad (29)$$

where x_{ss} must satisfy the nonlinear equilibrium relationship

$$0 = f(x_{ss}, u(n), \dots) \quad (30)$$

or, equivalently,

$$x_{ss} = g(u(n), \dots) \quad (31)$$

where $g(u(n), \dots)$ is the reference schedule of the states given the control input levels [4].

For a set of operating variables, z (e.g., rotor speeds, ambient conditions, and control inputs), terms of the following form are created to match each selected element of the dynamic equations (17):

$$t_j(z) = \prod_{i=1}^q z_i \quad (32)$$

The set of coefficients, a_j , which minimize the following cost function are found:

$$J^* = \min_{a_j, r, q} \left\{ \sum_{k=1}^N \left[p(k) - \sum_{j=1}^r a_j t_j(z(k)) \right]^2 \right\} \quad (33)$$

where the non-zero elements of the reduced dynamics matrix, $p(k)$ at each of N flight points are fit with a set of polynomial functions of the operating variables $t_j(z(k))$. The minimization is carried over the constant coefficients, a_j , the number of terms used, r , and the highest powers represented in each term, q [13,14].

The resulting dynamic matrix can be written as follows:

$$\left. \frac{\partial f}{\partial x} \right|_{x=0} = F(x) \quad (34)$$

i.e., the matrix F represents the gradient of the nonlinear function, $f(x,u)$ along the steady-state operating line. A Taylor series expansion of $f(x,u)$ matches the function at an arbitrary (x,u) to the gradient at the static operating line, $F(x)$. The results [11] indicate that to match the nonlinear dynamics to arbitrary order, the following form can be used:

$$f(x,u) = \frac{1}{2} [FF(x_k)] \quad (35)$$

For example, to match the nonlinear dynamics at arbitrary point to order $\| \delta x \|^5$, the following form can be used:

$$f(x,u) = \frac{1}{2} F(x_1) + F(x_2) + 0 (x-x_0)^5 \quad (36)$$

$$\frac{1}{2} F(x, x_{ss})$$

where

$$x_1 = x_0 + \frac{x-x_0}{q_1} \quad (37)$$

$$x_2 = x_0 + \frac{x-x_0}{q_2} \quad (38)$$

$$q_1 = 3 + \sqrt{3} \quad (39)$$

$$q_2 = 3 - \sqrt{3} \quad (40)$$

$$x_0 = g(u) \quad (41)$$

Example 3: Turbofan Engine Dynamics

The reduced parameter models discussed in Example 2 represented fifth-order engine dynamics and were parameterized with 10 nonzero elements. Curves were derived for each dynamic element using subset selection methods over the operating envelope.

The models derived for the elements of the dynamics matrix form the basis for the nonlinear model. Table 4 shows the preliminary model selected to represent engine dynamics throughout the operating envelope. Thirty-three terms are sufficient to match the linearized dynamics at all flight points. The model's accuracy is summarized in Figure 5, which shows a comparison of the actual engine time constants and those calculated from the curve-fit model of the dynamics matrix. This procedure represents a significant simplification over other linear modeling method and allows a tractable simulation of nonlinear dynamics.

4. TRAJECTORY GENERATOR

If a perfect plant model were known, and if there were no unknown disturbances, then it would be possible to control the plant using only feed-forward (open-loop) inputs. Furthermore, assuming the plant were stable, the feed-forward could simply be a change in the control set point which would produce the desired steady-state condition. However, using this strategy, transition from the current state to that commanded would occur with the dynamics characteristic of the open-loop plant. There would be no direct control over the maximum output excursions.

Another more sophisticated approach calculates an input time history that is optimal with respect to a specified performance index. Current techniques for trajectory optimization [15-17] utilize an engine simulation of varying complexity. A cost functional is derived which represents desirable trajectory attributes (e.g., maximum thrust response or minimum turbine inlet temperature rates), and a group of constraints in the trajectory are formulated to respect stability limits and other physical operating constraints. A trial trajectory is calculated which may or may not satisfy the constraints. Standard function optimization procedures can be used to derive feasible and optimal paths.

The problems with this type of procedure are threefold. First, engine transient simulations, especially for gross transitions, may poorly represent engine behavior; second, implementation of exact trajectories is inevitably impractical; and third, there is no convenient control law formulation of the optimal solution.

Reference outputs from the reference point schedules represent a group of engine variables and controls which are at equilibrium conditions and which are within physical and operating limits. These quantities are chosen to be the values of throttle setting, mode, and inlet conditions. These may instantaneously change to sample because of pilot inputs. The actual reference outputs could be discontinuous in time, but the reference values are linked directly to the regulator, moderate engine response, and saturate the actuators. To rate limit the reference points or the throttle command, a low-pass filter is used to degrade small signal response. Also, since the system response to very large inputs is nonlinear, the response achieved without some input compensation would be suboptimal (and most likely unstable). The transition generator is designed to produce an ideal reference between the current state and the state most recently requested by the reference values.

The transition generator will have the following attributes:

1. It will produce reference input trajectories which, when compared with actual engine response, i.e., the reference input trajectories, will produce reference output trajectories, which are within physical limits, and

- (3) it should exhibit optimized response for both large and small inputs.

The approach chosen for this function is to utilize the dynamic model of the engine compensated with a nonlinear feedback law and driven by the reference point schedule as the generator of this nominal path.

The trajectory generation logic is shown in Figure 6. A nonlinear, proportional override logic is used as the compensation. The critical element in the design is that the model compensation gains are generated directly from the regulator gain schedules. The procedure results in a 50 percent reduction of the gain schedule storage requirement. Operation of the trajectory generator and the initial design approach is discussed below.

For small transients, reference inputs are used as direct commands to the engine model. The model response is further compensated with output gains which are proportional to the optimal regulator gains. When no limits are exceeded by the model, the response of the model is controlled by the locally linear gains. When a model output approaches a limit, the rate limits are proportionally reduced. This has the effect of transferring the control law from the unlimited regulator to one of several specifically designed multivariable limit loops. The rate limit is proportional to the error signal from the limiting blocks. This feedback in one or more of the control channels will tend to cause the model to move smoothly onto a limit. If the proportional error signal indicates that the system can move away from the boundary, the limit is smoothly removed. The feedback gains for the limit loops are designed using output weightings on the specific engine constraints. This yields a feedback vector for the limit loop. This vector is simplified using sensitivity calculation and scheduled as a function of ambient conditions.

The large input performance of the system will tend to behave in a time-optimal fashion. This assertion is justified from optimal solution to the minimum time problem [15,16] for a linear system. Here, optimal trajectories consist of a minimum time (corresponding to a bang-bang control) trajectory to a limit, tracking the limit, and moving off the limit to the final point. The character of the trajectories generated in this method will be very similar to this type of motion without the requirement of explicit solution of nonlinear optimization problems.

Example 4: Turbofan Engine Dynamics

Trajectory generator logic was designed and demonstrated at one flight condition to demonstrate the concept. A linear model of the engine at sea level, static, intermediate power was used as the engine simulator. An "acceleration" from 90 percent intermediate power to intermediate power was performed using fuel flow as the only modulated variable.

The response of the engine to a step input is compared to the linear servomechanism response in Figure 7. It is observed that the compensated command generator produces a faster thrust response at the cost of a temperature overshoot and unacceptable surge margin loss.

The nonlinear variable rate limit design was also implemented using the $T_{4.1}$ (turbine entrance) gas temperature limit and the compressor surge margin limits as inputs to the system. The response is shown in Figure 8. It can be seen that the trajectory generated with this system provides a fast response without causing a predicted overtemperature or unacceptable surge margin loss in the model.

5. OPTIMAL REGULATOR DESIGN

Linear optimal control synthesis [15] methods are used to derive constant feedback gains for each design model. The two most common cost functionals are shown below:

$$J_1 = \frac{1}{2} \int_0^{\infty} (\delta x^T A \delta x + \delta u^T B \delta u) dt \quad (42)$$

$$J_2 = \frac{1}{2} \int_0^{\infty} (\delta y^T A^* \delta y + \delta u^T B \delta u) dt \quad (43)$$

where A is an $n \times n$ state weighting matrix, B is a $m \times m$ control weighting matrix, and A^* is a $p \times p$ output weighting matrix. The conditions on the problem for a unique solution are well known [15]. The resulting state variable feedback control law is optimal for an initial condition response near the equilibrium point. The control law is suitable for regulating the system along a trajectory which is "near" the linearization point. If the controller produces a nominal trajectory of this type, characterized by a state and control time history, $(x_n(t), u_n(t))$, then the regulating controller is written as follows:

$$u(t) = u_n(t) + C(x(t) - x_n(t)) \quad (44)$$

where C is a $m \times n$ state variable feedback matrix designed for the equilibrium point. The relationship between the control criteria and the weightings, A, A^* , and B , is established during the design by evaluating closed-loop response and sensitivity. This procedure will be discussed.

In many applications, the quantities that are to be regulated are system output variables and not system state variables. Using state variable feedback in these applications (outputs weighted in the performance index) generally involves estimation of unmeasured states (e.g., the Kalman filter) and mathematical modeling of the system's output equations (e.g., $y = Hx + Du$). If the mathematical model of the plant were well understood, this procedure would generally produce an acceptable control law. Often, modeling errors are present. Consequently, additional integral or trim control is necessary to ensure satisfaction of performance requirements.

Sometimes these difficulties can be avoided by designing a controller that feeds back functions of the output errors directly. One disadvantage of this approach is that the resulting gain matrices cannot be found as solutions to a matrix Riccati equation; they must be found by solving directly minimizing the objective function [18].

One technique of finding the minimum of J (with respect to C) involves the use of a gradient search procedure. An efficient procedure is the modified Newton-Raphson with derivative technique [19]. The algorithm requires the gradient of J with respect to C .

The gradient of J with respect to C is developed in part in Ref. 20. Summarizing briefly, let

$$y^* = Hx = y - Du \quad (45)$$

and

$$u = \bar{C} y^* \quad (46)$$

with

$$\bar{C} = C(I - DC)^{-1} \quad (47)$$

Then, from Ref. 19,

$$\frac{dJ}{dC} = (B\bar{C}H + N^T) LH^T + G^TK LH^T \quad (48)$$

where

$$F^* = F + G\bar{C}H \quad (49)$$

$$O = LF^{*T} + F^*L + X_0 \quad (50)$$

$$O = KH^* + F^{*T}K + A + H^T\bar{C}^T B\bar{C}H + N\bar{C}H + H^T\bar{C}^T N^T \quad (51)$$

and

$$X_0 = E[x(0) x^T(0)] \quad (52)$$

The gradient search may therefore be used to find a matrix \bar{C} ($u = \bar{C} y^*$) which minimizes J . The resulting \bar{C} may be transformed to C ($u = C y$) using Eq. (39).

One difficulty remains. The resulting feedback gain matrix, C , is, in general, full. That is, there is a feedback path from every output to every control. Often, unimportant or ineffective error to actuator paths can be identified and eliminated, yielding significant reduction in the number of feedback paths which must be implemented. Optimization of the resulting fixed structure gain matrix requires a slightly different formulation of the gradient. Specifically, the gradient of J with respect to C (instead of \bar{C}) must be found.

The derivation of $\frac{dJ}{dC}$ is provided in Ref. 6. The result is

$$\frac{dJ}{dC} = (I + C\bar{C}D)^T \frac{dJ}{d\bar{C}} \bar{C}^T \quad (53)$$

where

$$B = (I - DC)^{-1} \quad (54)$$

With $\frac{dJ}{d\bar{C}}$ available, the gradient search

procedure can be used to optimize specific elements in the C matrix with the remaining elements fixed (e.g., at zero).

6. SUMMARY AND APPLICATION HIGHLIGHTS

6.1 APPLICATION TO THE F100 AND VCE TURBOFANS

The theoretical methods described have been applied to two advanced turbofan engine designs. The F100 turbofan is the current engine in the F15 and F16 fighters. A digital MVCS was implemented and successfully tested in digital, hybrid and altitude engine test runs. A variable cycle engine is an advanced, highly complex turbofan concept. An MVCS [6] for this engine designed for implementation within a powerful microprocessor was designed and evaluated on a detailed digital test bed. Highlights from these applications are summarized below.

The F100 Multivariable Control Synthesis (MCVS) program [4,8,9], jointly initiated by the Air Force Aero Propulsion Laboratory and the NASA-Lewis Research Center, was aimed at demonstrating the benefits

of LQR synthesis theory in the design of a multivariable engine control system for operation throughout the flight envelope. The payoffs from the method include: (1) enhanced performance from cross-coupled controls, (2) maximum use of engine variable geometry, and (3) a systematic design procedure that can be applied efficiently to new engine systems.

Steady-state operating data [4] were taken at 309 combinations of flight condition and power lever angle. The MVCS tracked the reference point schedules well. Temperature and burner pressure limits were accommodated where required for safe operation. The integral trims held geometry variables to their respective schedules. The fan rotor speed and fan discharge pressure were held to their scheduled values through the use of integral trims on exhaust nozzle area and main burner fuel flow.

In general, steady-state performance of the F100 MVCS control was good at all points tested. The integral control action held scheduled variables close to their scheduled values. Minor reference point schedule adjustments allowed schedule matching without controls saturating or engine variables exceeding allowable limits.

Transient performance was assessed at all the flight points. Large PLA transients were run at all points where air flow constraints permitted PLA operation below 83 . Small PLA transients of 3 were run to check the regulator performance while random PLA sequences were run to verify correct gain scheduling operation.

Good transient performance was demonstrated at all flight points. The control attenuated afterburner pressure pulses occurring during afterburner lights at all but two flight points. At supersonic points, where operation was permitted only at intermediate and above, excellent suppression of afterburner disturbances was observed. The multivariable control successfully operated the engine for random PLA excursions, thereby verifying the correct functioning of regulator gain schedules and transition logic. A number of flight maneuvers were performed to check the control's performance with simultaneously varying PLA and ambient conditions. The control tracked reference point schedules well and accommodated all limits.

Programming flexibility which exists due to the modular structure of the multivariable control was demonstrated by testing two alternate control modes. A fast acceleration set of transition control rates was implemented which allowed more rapid engine accelerations. Also, the integral trim structure was changed to use engine pressure ratio instead of the fan discharge Mach number parameter normally used with the multivariable control.

Sensor and actuator failure detection logic was incorporated into the control for altitude tests and functioned well in conjunction with a backup control. All logic was programmed in 9500 words of core memory, using a 12-msec computer cycle time. These computer requirements are within the capabilities of present generation computers envisioned for use as engine-mounted digital controls.

The micro-electronic revolution has already significantly affected turbine engine controls. This capability alone would not radically alter the hydromechanical hardware on current commercial and military turbines because these systems have a long reputation for reliability and cost effectiveness. However, near-term propulsion system requirements for V/STOL and military flight applications cannot be realized with purely hydromechanical devices. The performance capability of these propulsion systems is now dependent on the control rather than the components. Practical designs integrating engine, inlet, and airframes will be necessary. Multivariable procedures must be used to accommodate dynamic and static interactions which will dominate these system configurations. Proposed V/STOL applications, for example, have propulsion system components, gas generators, fans, ducts, mechanical linkages, etc. distributed throughout the airframe. A design method to make this type of system operable is imperative.

The evolution of multivariable, electronic controls for complex turbine propulsion systems is in full swing. Next generation engines will have the hardware and the requirement. Optimal control procedures and locally linear design techniques offer a strong option to design engineers for the development of the high performance, high reliability, cost-effective systems which are needed.

REFERENCES

1. Skira, Charles A., "Future Air Force Aircraft Propulsion Control Systems," 1979 Propulsion Controls Symposium, NASA Lewis Research Center May 1979.
2. Tysgo, A., Brembo, J.C. and Lind, K., "The Design of a Multivariable Control System for a Ship Boiler" *Automatica*, Vol. 12, pp. 211-224, 1976.
3. Erzberger, H. and Lee, H., "Constrained Optimum Trajectories with Specified Range," *J. of Guidance and Control*, Vol. 3, No. 1, January-February 1980.
4. De Hoff, R.L., et al, "Multivariable Control Synthesis Program - Control Aspects of the F100 Altitude Demonstration of the Multivariable Control System," AFWAL-TR-80-2010, December 1979.
5. Akhter, M.M., Rock, S.M. and De Hoff, R.L., "Trajectory Generation Techniques for Multivariable Control of Aircraft Turbine Engines," 1979 Circuits, Systems and Computers Conference, Asilomar, November 1979.
6. Rock, S.M. and De Hoff, R.L., "Variable Cycle Engine Multivariable Control Synthesis: Interim Report - Control Structure Definition," AFAPL-TR-79-2043, February 1979.
7. Skira, C.A. and De Hoff, R.L., "A Practical Approach to Linear Model Analysis for Multivariable Turbine Engine Control Design," 1977 Proceedings of the International Forum on Alternatives for Multivariable Control, N.E.C., Chicago, 1977.

8. De Hoff, R.L., et al., "F100 Multivariable Control Synthesis Program," AFAPL-TR 77-35, June 1977.
9. Miller, R.J. and Hackney, R.D., "F100 Multivariable Control System Engine Models/Design Criteria," Pratt and Whitney Aircraft Group, Government Products Division, Report to AFAPL, Contract F33615-75-C-2048, Final Report for Period 1 June 1975 - 31 August 1976, AFAPL-TR-76-74, November 1976.
10. De Hoff, R.L., "Identification of a STOL Propulsion Plant Model from Flight Data," J. of Guidance and Control, Vol. 2, No. 3 May-June 1979.
11. De Hoff, R.L. and Rock, S.M., "Development of Simplified Nonlinear Models from Multiple Linearizations," 17th IEEE Conference on Decision and Control, San Diego, January 1979.
12. Leake, R.J. and Comiskey, J.G., "A Direct Method for Obtaining Nonlinear Analytical Models of a Jet Engine," 1977 Proceedings of the International Forum on Alternatives for Multivariable Control, NEC, Chicago, 1977.
13. Selser, G.A.F., Linear Regression Analysis, J. Wiley and Sons, New York, 1977.
14. De Hoff, R.L. and Hall, W.E., "Advanced Fault Detection and Isolation Methods for Aircraft Turbine Engines," ONR-CR-215-245-1, February 1978.
15. Bryson, A.E. and Ho, Y.C. Applied Optimal Control, Ginn Blaisdell, Waltham, Massachusetts, 1969.
16. Teren, F., "Minimum Time Acceleration of Aircraft Turbine Engines," NASA TM X-73624, June 1977.
17. De Hoff, R.L., Hall, W.E., "Design of a Multivariable Controller for an Advanced Turbofan," 1977 JACC, San Francisco, CA.
18. Merrill, W.C., "Design of Turbofan Engine Controls Using Output Feedback Regulator Theory," Presented at the 1977 JACC, San Francisco, California, June 1977.
19. Gill, P.E., Murray, W. and Pitfield, R.A., "The Implementation of Two Revised Quasi-Newton Algorithms for Unconstrained Optimization," National Physics Laboratory, NACL1, April 1972.
20. Choi, S.S. and Sirisena, H.R., "Computation of Optimal Output Feedback Gains for Linear Multivariable Systems," IEEE Transactions on Automatic Control, Vol. AC-19, No. 3, p. 257, June 1974.

Table 1: Typical Inputs, Outputs, and Controls

	SINGLE TURBOJET	PRODUCTION TURBOFAN	VCE
STATES			
COMPRESSOR SPEED	X	X	X
FAN SPEED		X	X
BLADE TEMPERATURE	X	X	X
TAILPIPE PRESSURE	X	X	X
COMBUSTOR PRESSURE	X	X	X
METAL TEMPERATURE	X	X	X
CONTROLS			
FUEL FLOW	X	X	X
COMPRESSOR GEOMETRY		X	X
FAN GEOMETRY		X	X
TURBINE GEOMETRY			X
NOZZLE AREA	X	X	X
A/B FUEL	X	X	X
BLEED	X	X	X
DUCT GEOMETRY			X
OUTPUTS			
THRUST	X	X	X
SFC	X	X	X
FAN SURGE MARGIN		X	X
COMPRESSOR SURGE MARGIN	X	X	X
ΔP/P IN FAN		X	X
ΔP/P IN COMPRESSOR	X	X	X
TURBINE INLET TEMPERATURE	X	X	X

Table 2: Eigenvalue Spectrum with Associated State Groupings from Sea Level Static, Intermediate Power Linear Models in F100 Turbofan Engines

ROOT LOCATION (SEC ⁻¹)	RESPONSE VARIABLE
-501	P _{1,5}
-191	P ₃
-50	BLC
-50	CIVV
-50	-VS
-42	T _{4HI}
-56	T _{4E}
-47 = 4.8j	T ₁
	T ₂
-20	F _J
-22	T _{2,5C}
-20 = 4.2j	T ₃
	T ₅
	T _{5C}
-10	T ₄
-4 = 3j	T ₄
	T ₄
	T ₄
-2.7	T ₄
-1.9	T ₄ 5L0
-0.57	T ₄ 0

DESIGN MODEL DYNAMICS { BANDWIDTH CONTROL } DESIGN MODEL STATES

Table 3: Comparison of Eigenvalues Between F and \hat{F}

ORIGINAL EIGENVALUES (F)	REDUCED EIGENVALUES (\hat{F})
-0.49	-0.49
-3.38	-3.50
-1.90	-1.95
-0.41	-0.39
-0.14	-0.14

*Eigenvalues normalized by collective response mode eigenvalue.

Table 4: Preliminary Nonlinear Model Structure

MATRIX ELEMENT	MODEL FORM	RMS ERROR*
F ₁₁	$a_1 P_{S3C} + a_2 P_2^2 + a_3$	1.0
F ₃₃	$b_1 P_{S3C} + b_2 N_2 T_2 + b_3$	0.3
F ₁₂	$c_1 P_2 + c_2 T_2 + c_3 N_{25} P_2 + c_4$	1.7
F ₂₁	$d_1 P_2 + d_2 P_{21} + d_3 P_{S3C} + d_4$	1.5
F ₂₂	$e_1 F_{11} + e_2 P_2^2 + e_3 N_2 P_2 + e_4$	1.2
F ₂₃	$f_1 P_2 + f_2 P_{21} + f_3 F_{33} + f_4$	1.5
F ₃₂	$g_1 P_2 + g_2 P_{21} + g_3 P_{S3C} + g_4$	1.2
F ₄₄	$h_1 F_{33} + h_2$	0.3
F ₅₃	$k_1 P_{S3C} + k_2 F_{33} + k_3$	0.4
F ₅₅	$z_1 F_{33} + z_2$	0.1

* Percentage of mean.

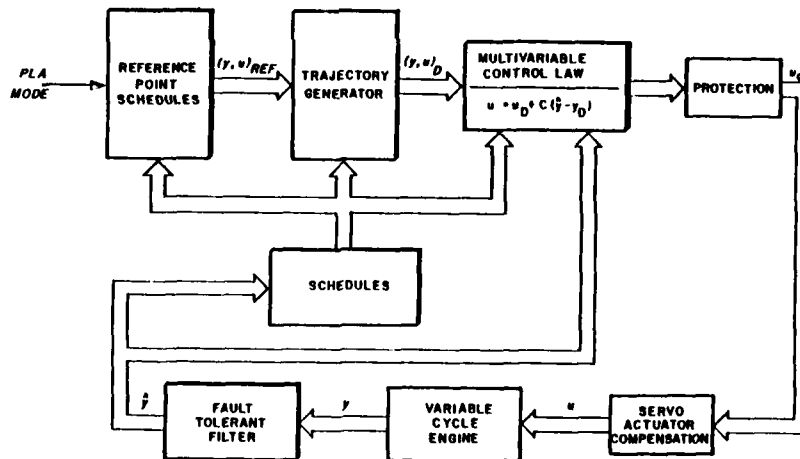


Figure 1: Multivariable Control Structure

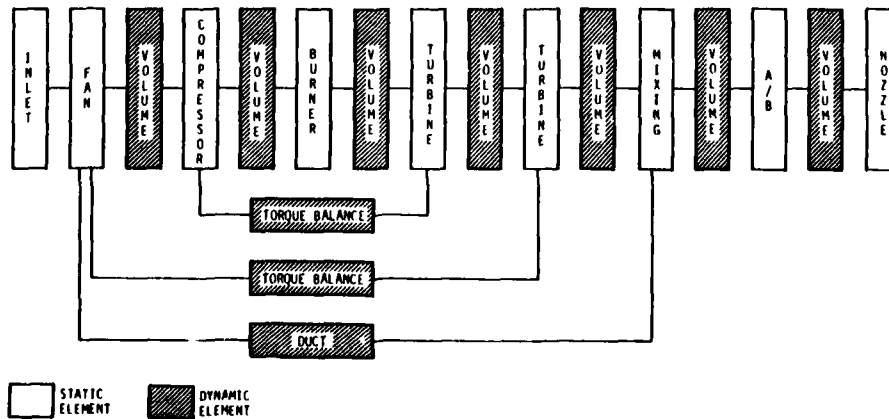


Figure 2: Schematic Flow Diagram of Typical Nonlinear Digital Simulation Calculation

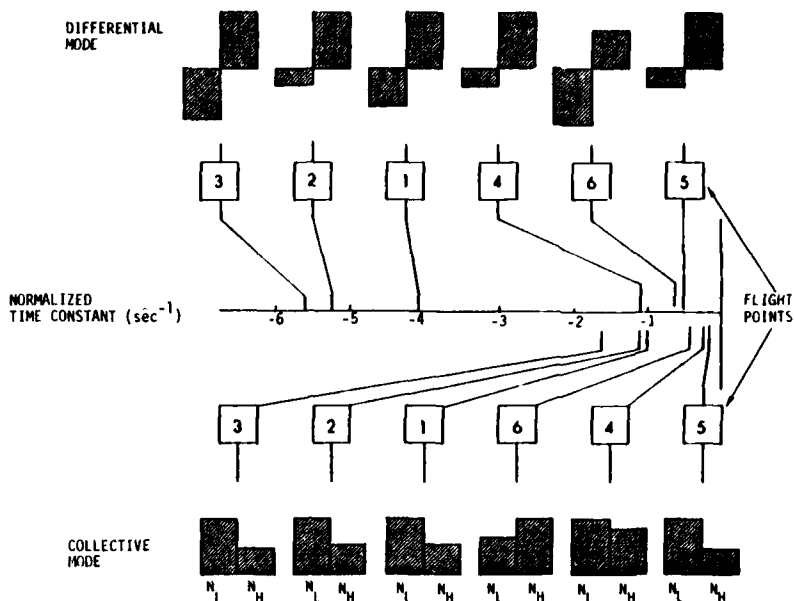


Figure 3: Differential and Collective Spool Response Time Constants at Various Flight Points Showing the Relative Magnitude of the Fan Speed, N_L , and Compressor Speed, N_H , Eigenvector Component

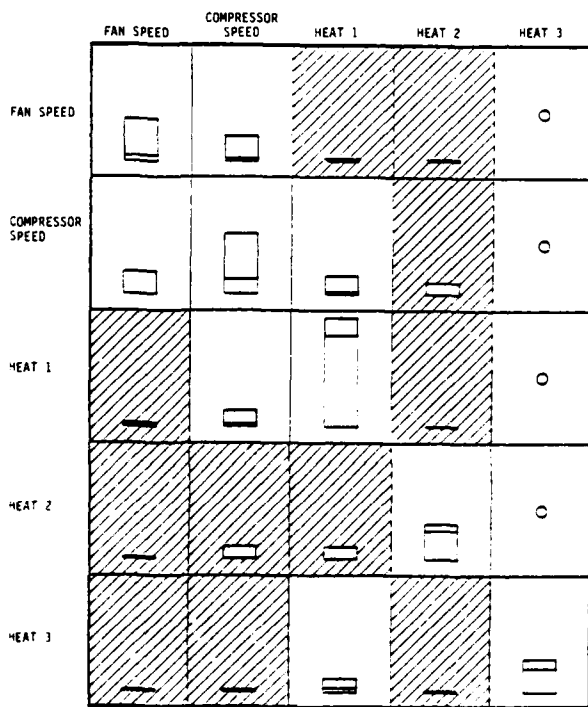


Figure 4: Sensitivity of Mean Square Response to Elements in F Matrix for a Typical Dynamics Matrix Contain Rotor Speed Roots and Three Temperature Roots Calculated Open Full Power/Flight Operating Conditions

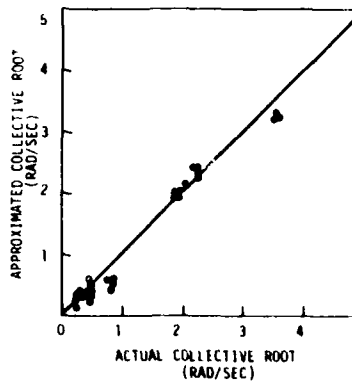
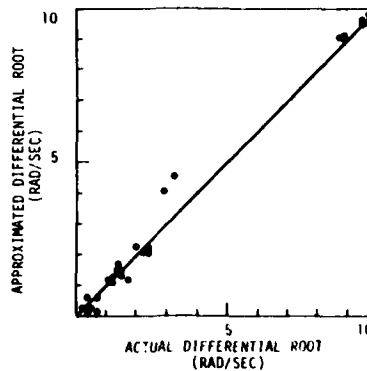


Figure 5: Comparison of Linear Eigenvalue Locations Found by Linearizing the Nonlinear Model at 28 Flight Points Spanning the Operating Envelope

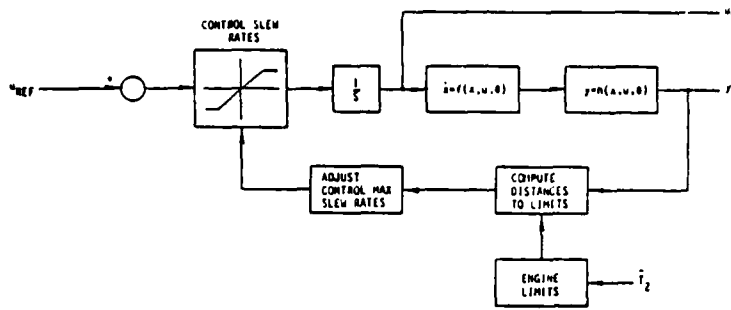


Figure 6a: Trajectory Generator Logic - Large Transient Control Loop

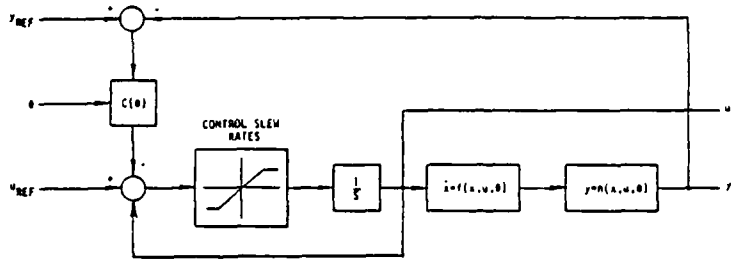
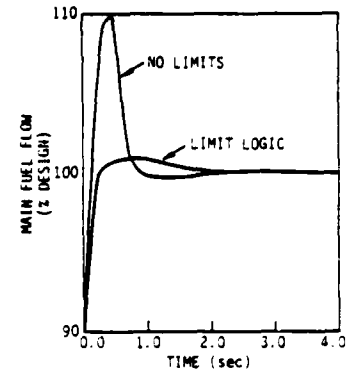


Figure 6b: Trajectory Generator Logic - Small Transient Control Loop

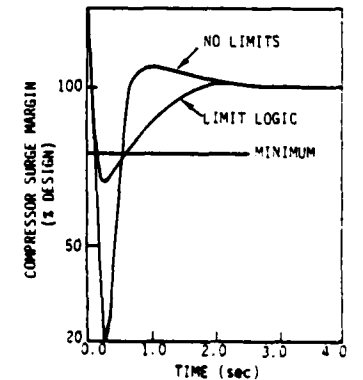
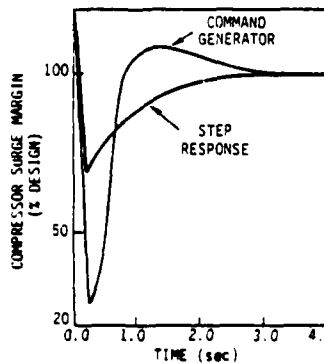
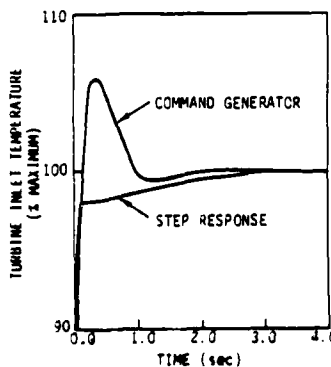
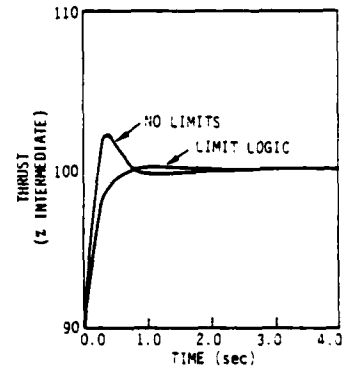
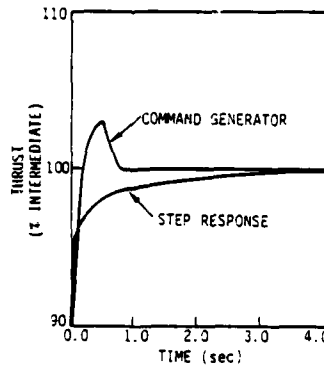
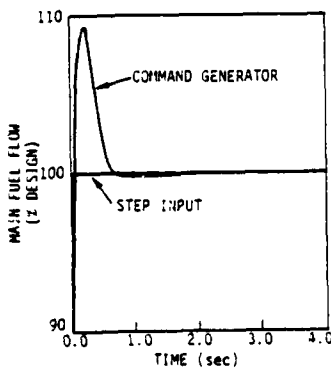
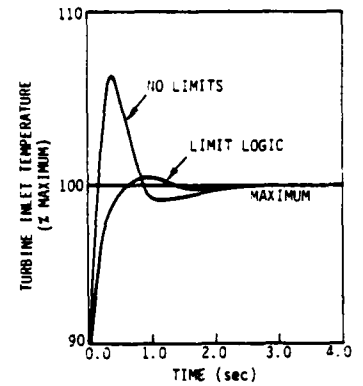


Figure 7: Comparison of Step Response and Linear Servomechanism Response for a Ten (10) Percent Acceleration to SLS, Intermediate Power

Figure 8: Demonstration of Temperature and Surge Limiting Acceleration Trajectory Using Nonlinear, Variable Rate Feedback

REPORT DOCUMENTATION PAGE

1. Recipient's Reference	2. Originator's Reference	3. Further Reference	4. Security Classification of Document						
	AGARD-AG-251	ISBN 92-835-1391-6	UNCLASSIFIED						
5. Originator	Advisory Group for Aerospace Research and Development North Atlantic Treaty Organization 7 rue Ancelle, 92200 Neuilly sur Seine, France								
6. Title	THEORY AND APPLICATIONS OF OPTIMAL CONTROL IN AEROSPACE SYSTEMS								
7. Presented at									
8. Author(s)/Editor(s)	Ir. Pieter Kant		9. Date July 1981						
10. Author's/Editor's Address	Head of Space Department National Aerospace Laboratory, Postbus 153 8300 AD Emmeloord, The Netherlands		11. Pages 292						
12. Distribution Statement	This document is distributed in accordance with AGARD policies and regulations, which are outlined on the Outside Back Covers of all AGARD publications.								
13. Keywords/Descriptors	<table> <tr> <td>Optimal control</td> <td>Multivariable flight control</td> </tr> <tr> <td>Stochastic optimal control</td> <td>Optimal decision theory</td> </tr> <tr> <td>Digital adaptive flight control</td> <td></td> </tr> </table>			Optimal control	Multivariable flight control	Stochastic optimal control	Optimal decision theory	Digital adaptive flight control	
Optimal control	Multivariable flight control								
Stochastic optimal control	Optimal decision theory								
Digital adaptive flight control									

14. Abstract

This AGARDograph addresses the advances effected in the theory and design of modern optimal guidance and control systems, in the following areas: Part I: Theory, Part II: Design Techniques, Part III: Applications and should provide an aid in the application of these modern techniques.

This AGARDograph was prepared at the request of the Guidance and Control Panel of AGARD.

<p>AGARDograph No. 251 Advisory Group for Aerospace Research and Development, NATO THEORY AND APPLICATIONS OF OPTIMAL CONTROL IN AEROSPACE SYSTEMS Edited by Ir. Pieter Kant Published July 1981 292 pages</p> <p>This AGARDograph addresses the advances effected in the theory and design of modern optimal guidance and control systems, in the following areas: Part I: Theory, Part II: Design Techniques, Part III: Applications and should provide an aid in the application of these modern techniques.</p> <p>P.T.O.</p>	<p>AGARD-AG-251</p> <p>Optimal control Stochastic optimal control Digital adaptive flight control Multivariable flight control Optimal decision theory</p>
<p>AGARDograph No. 251 Advisory Group for Aerospace Research and Development, NATO THEORY AND APPLICATIONS OF OPTIMAL CONTROL IN AEROSPACE SYSTEMS Edited by Ir. Pieter Kant Published July 1981 292 pages</p> <p>This AGARDograph addresses the advances effected in the theory and design of modern optimal guidance and control systems, in the following areas: Part I: Theory, Part II: Design Techniques, Part III: Applications and should provide an aid in the application of these modern techniques.</p> <p>P.T.O.</p>	<p>AGARD-AG-251</p> <p>Optimal control Stochastic optimal control Digital adaptive flight control Multivariable flight control Optimal decision theory</p>
<p>AGARDograph No. 251 Advisory Group for Aerospace Research and Development, NATO THEORY AND APPLICATIONS OF OPTIMAL CONTROL IN AEROSPACE SYSTEMS Edited by Ir. Pieter Kant Published July 1981 292 pages</p> <p>This AGARDograph addresses the advances effected in the theory and design of modern optimal guidance and control systems, in the following areas: Part I: Theory, Part II: Design Techniques, Part III: Applications and should provide an aid in the application of these modern techniques.</p> <p>P.T.O.</p>	<p>AGARD-AG-251</p> <p>Optimal control Stochastic optimal control Digital adaptive flight control Multivariable flight control Optimal decision theory</p>
<p>AGARDograph No. 251 Advisory Group for Aerospace Research and Development, NATO THEORY AND APPLICATIONS OF OPTIMAL CONTROL IN AEROSPACE SYSTEMS Edited by Ir. Pieter Kant Published July 1981 292 pages</p> <p>This AGARDograph addresses the advances effected in the theory and design of modern optimal guidance and control systems, in the following areas: Part I: Theory, Part II: Design Techniques, Part III: Applications and should provide an aid in the application of these modern techniques.</p> <p>P.T.O.</p>	<p>AGARD-AG-251</p> <p>Optimal control Stochastic optimal control Digital adaptive flight control Multivariable flight control Optimal decision theory</p>

<p>This AGARDograph was prepared at the request of the Guidance and Control Panel of AGARD.</p>	<p>This AGARDograph was prepared at the request of the Guidance and Control Panel of AGARD.</p>
<p>ISBN 92-835-1391-6</p>	<p>ISBN 92-835-1391-6</p>

FILMED

2-8